Springer Series on

ATOMIC, OPTICAL, AND PLASMA PHYSICS 47

Springer Series on

ATOMIC, OPTICAL, AND PLASMA PHYSICS

The Springer Series on Atomic, Optical, and Plasma Physics covers in a comprehensive manner theory and experiment in the entire field of atoms and molecules and their interaction with electromagnetic radiation. Books in the series provide a rich source of new ideas and techniques with wide applications in fields such as chemistry, materials science, astrophysics, surface science, plasma technology, advanced optics, aeronomy, and engineering. Laser physics is a particular connecting theme that has provided much of the continuing impetus for new developments in the f ield. The purpose of the series is to cover the gap between standard undergraduate textbooks and the research literature with emphasis on the fundamental ideas, methods, techniques, and results in the field.

36 **Atom Tunneling Phenomena in Physics, Chemistry and Biology**
Editor: T. Miyazaki

37 **Charged Particle Traps**
Physics and Techniques of Charged Particle Field Confinement
By V.N. Gheorghe, F.G. Major, G.Werth

38 **Plasma Physics and Controlled Nuclear Fusion**
By K. Miyamoto

39 **Plasma-Material Interaction in Controlled Fusion**
By D. Naujoks

40 **Relativistic Quantum Theory of Atoms andMolecules**
Theory and Computation
By I.P. Grant

41 **Turbulent Particle-Laden Gas Flows**
By A.Y. Varaksin

42 **Phase Transitions of Simple Systems**
By B.M. Smirnov and S.R. Berry

43 **Collisions of Charged Particles withMolecules**
By Y. Itikawa

44 **Collisions of Charged Particles withMolecules**
Editors: T. Fujimoto and A. Iwamae

45 **Emergent Nonlinear Phenomena in Bose-Einstein Condensates**
Theory and Experiment
Editors: P.G. Kevrekidis, D.J. Frantzeskakis, and R. Carretero-González

46 **Angle and Spin Resolved Auger Emission**
Theory and Applications to Atoms and Molecules
By: B. Lohmann

47 **Semiclassical Dynamics and Relaxation**
By: D.S.F. Crothers

Vols. 10-35 of the former Springer Series on Atoms and Plasmas are listed at the end of the book

D.S.F. Crothers

Semiclassical Dynamics and Relaxation

With 56 Figures

Springer

D.S.F. Crothers
Department of Applied Mathematics
and Theoretical Physics
Queen's University of Belfast, UK
University Road
Belfast BT7 1NN
E-mail: d.crothers@qub.ac.uk

ISBN: 978-0-387-74312-7 e-ISBN: 978-0-387-74313-4

Library of Congress Control Number: 2007940870

Printed on acid-free paper.

9 8 7 6 5 4 3 2 1

springer.com

I dedicate this book to the memory of my mentor and supervisor, the late Professor Sir David Bates FRS. I gratefully acknowledge my teachers: at Rainey Endowed School: the late Mr Thomas Fazackerley (applied mathematics), the late Dr Arthur Gwilliam (pure mathematics), and the late Mr James McAteer (physics), at Balliol College Oxford: the late Professor Jacobus Stephanus de Wet (applied mathematics) and the late Dr Kenneth Gravett (pure mathematics), and at Queen's University Belfast my other supervisor Professor Ron McCarroll.

I warmly acknowledge fruitful collaboration with Professors Anders Bárány, Alex Devdariani, Bill Coffey, Yura Kalmykov, Kanika Roy, and Vladimir Gaiduk. I also thank my 32 PhD students for their inspiring hard work and collaboration and my wife Eithne for her loving care. Of my 32 PhD students I particularly thank my colleagues Dr Jim McCann and Dr Francesca O'Rourke, each of whom I have collaborated with over the years. I also thank my former postdocs: Dr Narayan Deb, Dr Geoffrey Brown, Dr P.J. Cregg, Dr Lawrence Geoghegan, Dr Elaine Kennedy, Dr Arlene Loughan, Dr Pierre-Michel Dejardin, Dr Elena Bichoutskaia, and Dr Sergei Titov. I thank Miss (soon to be Dr) Carla McGrath for her wonderfully precise typing of this book in Springer-Latex. Last but not least, I profoundly thank Carla and Elizabeth (Dr O'Sullivan)for their industrious application of Springer corrections to the final version.

Preface

The eclectic choice of topics in the book reflects the author's research interests over forty four years, before which he was War Memorial Open Scholar in Mathematics at Balliol College Oxford (1960–1963). Accordingly Chapter 1 covers some good oldfashioned applied mathematics of relevance to Chapters 2–4 concerning atomic and molecular physics in the gaseous phase (single collisions at low pressures) and to Chapter 5 concerning condensed-matter physics in the liquid and solid phases (dielectrics and ferromagnetics). The five chapters are based on a set of five special lectures given to postgraduate PhD students in the Centre for Atomic, Molecular and Optical Physics, in the School of Mathematics and Physics, Queen's University Belfast, in May and June 2003. The author was appointed to a Personal Chair in Theoretical Physics at Queen's University Belfast (1985), and elected as Member of the Royal Irish Academy (1991), Fellowship of the American Physical Society (1994), Honorary Professor of Physics at St Petersburg State University (2003) and Honorary Fellow of Trinity College Dublin (2006).

A good introduction to Chapters 3 and 4 is given by Chapter 52 (Continuum Distorted Waves and Wannier Methods by D.S.F. Crothers et al) of the Springer Handbook of Atomic, Molecular and Optical Physics (ed G.W.F. Drake), 2006.

Belfast,
Northern Ireland

Derrick Crothers
April 2007

Contents

1

Mathematics for the Semiclassicist

1.1 Single-Valued Analytic Functions

$$x = \frac{1}{2}z + \frac{1}{2}z^* , \qquad y = \frac{1}{2\mathrm{i}}\,(z - z^*) \tag{1.1}$$

Consider a function f of $z = x + \mathrm{i}y$ and $z^* = x - \mathrm{i}y$. Clearly if x and y are independent, then so in general are z and z^*. Then we have, with $*$ as complex conjugate,

$$\frac{\partial f}{\partial z} = \frac{\partial x}{\partial z}\frac{\partial f}{\partial x} + \frac{\partial y}{\partial z}\frac{\partial f}{\partial y} = \frac{1}{2}\frac{\partial f}{\partial x} + \frac{1}{2\mathrm{i}}\frac{\partial f}{\partial y} \tag{1.2}$$

and

$$\frac{\partial f}{\partial z^*} = \frac{\partial x}{\partial z^*}\frac{\partial f}{\partial x} + \frac{\partial y}{\partial z^*}\frac{\partial f}{\partial y} = \frac{1}{2}\frac{\partial f}{\partial x} - \frac{1}{2\mathrm{i}}\frac{\partial f}{\partial y} \tag{1.3}$$

However, if and only if $\partial f/\partial z^* = 0$, then

$$\mathrm{i}\frac{\partial f}{\partial x} = \frac{\partial f}{\partial y} \quad \Rightarrow \tag{1.4}$$

$$\frac{\partial f}{\partial z} \equiv \frac{\mathrm{d}f}{\mathrm{d}z} = \frac{\partial f}{\partial x} = -\mathrm{i}\frac{\partial f}{\partial y} \tag{1.5}$$

and setting

$$f(z) = u(z) + \mathrm{i}v(z) \tag{1.6}$$

(where u and v are real functions of a complex variable z), we have

$$\frac{\partial u}{\partial x} + \mathrm{i}\frac{\partial v}{\partial x} = -\mathrm{i}\frac{\partial u}{\partial y} + \frac{\partial v}{\partial y} \tag{1.7}$$

$$\Rightarrow \quad \frac{\partial u}{\partial x} = \frac{\partial v}{\partial y} \quad \text{and} \quad \frac{\partial v}{\partial x} = -\frac{\partial u}{\partial y} \tag{1.8}$$

(the Cauchy–Riemann equations)

$$\Rightarrow \quad \frac{\partial^2 u}{\partial x^2} = \frac{\partial^2 v}{\partial x \partial y} = \frac{\partial^2 v}{\partial y \partial x} = -\frac{\partial^2 u}{\partial y^2} \tag{1.9}$$

since x and y are independent variables. Thus

$$\frac{\partial^2 u}{\partial x^2} + \frac{\partial^2 u}{\partial y^2} = 0 \tag{1.10a}$$

and, similarly,

$$\frac{\partial^2 v}{\partial x^2} + \frac{\partial^2 v}{\partial y^2} = 0 \tag{1.10b}$$

that is, we have the two-dimensional Laplace equations for the real and imaginary parts u and v. If f is a multivalued function such as $\ln z$, then a branch cut must be inserted on $[-\infty, 0]$ with $\arg z$ assigned to 0 on $(0, +\infty]$ to define, say, the principal branch of $\ln z$, which is then an analytic function of z for $z \notin [-\infty, 0]$, that is, a real single-valued function of a complex variable z, differentiable at each point of its domain.

To summarise, a function $f(z)$ is analytic if it is indeed a function of z and only of z, and it is single-valued and differentiable in its domain of definitiion. By contrast, the following are not analytic:

$$|z|^2 = zz^* \qquad (\forall z \neq 0) \tag{1.11a}$$

$$\arg z = -\frac{\mathrm{i}}{2} \ln \frac{z}{z^*} \qquad (\forall z) \tag{1.11b}$$

$$z^a = \exp(a \ln z) \qquad (z \in [-\infty, 0] \text{ and a noninteger}) \tag{1.11c}$$

1.2 Method of Steepest Descent and Asymptotic Methods

$$I(s) \equiv \int_{-\infty}^{(0+)} g(z) \mathrm{e}^{s f(z)} \mathrm{d}z \tag{1.12}$$

Real s ($s \gtrsim 1$), complex z, f, g ($g' \lesssim 1$), and $\arg z$ are assigned to $+\pi$ on the upper lip of the branch cut along the negative real axis and to $-\pi$ on the lower lip. Then we have

$$I(s) \approx g(z_0) \mathrm{e}^{s f(z_0)} \int_{-\infty}^{(0+)} \mathrm{e}^{-\frac{s}{2}(z-z_0)^2 f''(z_0)\, \mathrm{d}z} \tag{1.13}$$

where

$$f'(z_0) = 0 \tag{1.14}$$

On

$$\arg(z - z_0) = \alpha \tag{1.15}$$

set

$$t^2 = \mathrm{e}^{-\mathrm{i}\pi} s (z - z_0)^2 f''(z_0) \tag{1.16}$$

$$= s|z - z_0|^2 \left| f''(z_0) \right| \tag{1.17}$$

if we choose

$$\alpha = \frac{\pi}{2} - \frac{1}{2}\arg f''(z_0) \tag{1.18}$$

and let $C+$ be the straight line through z_0 in the direction $\arg(z - z_0) = \alpha$, then

$$I_{C+}(s) \ni \frac{\mathrm{e}^{\mathrm{i}\alpha}}{\sqrt{s}\,|f''(z_0)|^{1/2}} \int_0^\infty \mathrm{e}^{-t^2/2}\,\mathrm{d}t \tag{1.19}$$

Similarly for

$$\arg(z - z_0) = \alpha + \pi \tag{1.20}$$

so that

$$I_{C-}(s) \ni \frac{\mathrm{e}^{\mathrm{i}\alpha}}{\sqrt{s}\,|f''(z_0)|^{1/2}} \int_{-\infty}^0 \mathrm{e}^{-t^2/2}\,\mathrm{d}t \tag{1.21}$$

$$\Rightarrow I(s) \simeq \frac{g(z_0)\mathrm{e}^{sf(z_0)+\mathrm{i}\alpha}\sqrt{2\pi}}{\sqrt{s}\,|f''(z_0)|^{1/2}} \tag{1.22}$$

using polar coordinates,

$$\left[\int_0^\infty \mathrm{e}^{-t^2/2}\,\mathrm{d}t\right]^2 = \int_0^{\pi/2}\mathrm{d}\theta \int_0^\infty r\,\mathrm{d}r\,\mathrm{e}^{-r^2/2} \tag{1.23}$$

We may assume $\alpha \in [-\pi/2, +\pi/2]$, i.e., that C may be taken as going from left to right and that $\arg f''(z_0) \in [0, 2\pi]$; otherwise ambiguity is only resolved by appeal to global geometry.

1.2.1 Stationary-Phase Version

Suppose $f = \mathrm{i}F$ with F real,

$$\int_a^b g(x)\mathrm{e}^{s\mathrm{i}F(x)}\,\mathrm{d}x \simeq \frac{g(x_0)\mathrm{e}^{s\mathrm{i}F(x_0)\pm\mathrm{i}\pi/4}\sqrt{2\pi}}{\sqrt{s}\,\sqrt{|F''(x_0)|}} \tag{1.24}$$

according to

$$F''(x_0) \gtrless 0 \tag{1.25}$$

[with $F'(x_0) = 0$ and $x_0 \in [a, b)\,;\ b > a$]; for example

$$\Gamma(s+1) \simeq s^{s+1/2}\mathrm{e}^{-s}\sqrt{2\pi} \tag{1.26}$$

e.g., quantal interference between elastic phase shifts if the potential difference passes through a turning point.

1.3 Generalized Variation and Perturbation Theories

Referring to [8] let us consider the functional

$$J[u] = \iint_D f(x, y, u, u_x, u_y, u_{xx}, u_{xy}, u_{yy})\,\mathrm{d}x\,\mathrm{d}y \tag{1.27}$$

and set the first-order variation of J, δJ according to

$$\delta J = 0 \tag{1.28}$$

Thus we have, by integration by parts,

$$f_u - \frac{\partial}{\partial x} f_{u_x} - \frac{\partial}{\partial y} f_{u_y} + \frac{\partial^2}{\partial x^2} f_{u_{xx}} + \frac{\partial^2}{\partial x \partial y} f_{u_{xy}} + \frac{\partial^2}{\partial y^2} f_{u_{yy}} = 0 \tag{1.29}$$

In the preceding, subscripts refer to the variables with respect to which the partial derivative is taken. Then we may deduce Sil's time dependent variational principle [560]

$$L = \psi^* \left(H - \mathrm{i} \frac{\mathrm{d}}{\mathrm{d}t} \right) \psi \tag{1.30}$$

$$\delta \int_{-\infty}^{\infty} \mathrm{d}t \int \mathrm{d}\boldsymbol{r} L = 0 \tag{1.31}$$

$$H = -\frac{\hbar^2}{2m} \nabla_{\boldsymbol{r}}^2 + V(r) \tag{1.32}$$

implies that

$$\left(H - \mathrm{i} \frac{\mathrm{d}}{\mathrm{d}t} \right) \psi = 0 \tag{1.33}$$

where H is the Hamiltonian, L is the Lagrangian density, $\mathbf{r}$ is the electron coordinate with respect to an infinite nucleus, and t is the time.

Similarly we may deduce Kohn's time-independent (stationary) variational principle where $\boldsymbol{R}$ is now the internuclear coordinate and $\boldsymbol{r}_T$ and $\boldsymbol{r}_P$ are the coordinates of the electron relative to the target and projectile nucleus.

$$L = \Psi^* (H - E) \Psi \tag{1.34}$$

$$\delta \int \mathrm{d}\boldsymbol{R} \int \mathrm{d}\boldsymbol{r} L = 0 \tag{1.35}$$

$$H = -\frac{1}{2M} \boldsymbol{\nabla}_{\boldsymbol{R}}^2 - \frac{1}{2} \boldsymbol{\nabla}_{\boldsymbol{r}}^2 + V^T(r_T) + V^P(r_P) + W(R) \tag{1.36}$$

$$(H - E) \Psi = 0 \tag{1.37}$$

In the preceding V, V^T, V^P, and W are all potential energies of their respective variables. Notice that in applying (1.27) to (1.30) and (1.34) only second-order nonmixed derivatives arise, apart from first-order derivatives with respect to ψ, ψ^*, and t. This is not the case in the electromagnetic problem.

Regarding stationary perturbation theory any quantum mechanics course covers Rayleigh-Schrödinger perturbation theory. So we shall be content to outline the energy-shell continuum distorted-wave (CDW) generalized perturbation theory of Crothers [187] in terms of the CDW Neumann–Born series. We adopt the Dirac bra(c)ket notation impling integration over the electronic and internuclear collision coordinates. With E the total energy and $\xi_i^{(+)}$ and $\xi_f^{(-)}$ the initial outgoing and final ingoing CDW functions ((4.264) and (4.265) with $m = 0$) we consider the transition amplitude given by

$$A_{fi}^{+} = \langle \xi_f^{(-)} | \, (H - E)^{\dagger} \, | \Psi_i^{+} \rangle \tag{1.38}$$

where

$$\Psi_i^{+} = \left[1 + G^{+} \, (H - E) \right] \xi_i^{(+)} \tag{1.39}$$

$$G^{+} = [E - H + \mathrm{i}\epsilon]^{-1} \tag{1.40}$$

$$= G_{CDW}^{+} + G_{CDW}^{+} \, (H - H_{CDW}) \, G^{+} \tag{1.41}$$

$$= G_{CDW}^{+} \sum_{n=0}^{\infty} \{ (H - H_{CDW}) \, G_{CDW}^{+} \}^{n} \tag{1.42}$$

where

$$G_{CDW}^{+} = [E - H_{CDW} + \mathrm{i}\epsilon]^{-1} \tag{1.43}$$

because

$$B^{-1} \equiv C^{-1} + C^{-1} \, (C - B) \, B^{-1} \tag{1.44}$$

The CDW Neumann-Born series is given by

$$\begin{aligned} A_{fi}^{+} = & \langle \xi_f^{(-)} | \, (H - E)^{\dagger} \, | \xi_i^{(+)} \rangle + \langle \xi_f^{(-)} | \, (H - E)^{\dagger} \, G_{CDW}^{+} \, (H - E) \, | \xi_i^{(+)} \rangle \\ & + \langle \xi_f^{(-)} | \, (H - E)^{\dagger} \, G_{CDW}^{+} \, (H - E) \, G_{CDW}^{+} \, (H - E) \, | \xi_i^{(+)} \rangle + \cdots \end{aligned} \tag{1.45}$$

Note that $H - H_{CDW} \equiv H - E \equiv -\boldsymbol{\nabla}_{\mathbf{r}_P} \boldsymbol{\nabla}_{\mathbf{r}_T}$, which is the nonorthogonal kinetic energy of Ch 4.

Interchanging B and C in (1.44) we have

$$B^{-1} = C^{-1} + B^{-1} \, (C - B) \, C^{-1} \tag{1.46}$$

so that

$$G^{+} = G_{CDW}^{+} + G^{+} \, (H - H_{CDW}) \, C_{CDW}^{+} \tag{1.47}$$

$$= G_{CDW}^{+} + G^{+} \, (H - E) \, G_{CDW}^{+} \tag{1.48}$$

Thus we have

$$A_{fi}^{+} = \langle \xi_f^{(-)} | T | \xi_i^{(+)} \rangle \tag{1.49}$$

$$T \equiv (H - E)^{\dagger} + (H - E)^{\dagger} \, G^{+} \, (H - E) \tag{1.50}$$

$$(H - E)^{\dagger} \, G^{+} = T G_{CDW}^{+} \tag{1.51}$$

$$T = (H-E)^{\dagger} + (H-E)^{\dagger} G^{+}_{CDW} (H-E) + (H-E)^{\dagger} G^{+} (H - H_{CDW}) G^{+}_{CDW} (H-E) \tag{1.52}$$

$$= (H-E)^{\dagger} [1 + G^{+}_{CDW} (H-E)] + T G^{+}_{CDW} (H - H_{CDW}) G^{+}_{CDW} (H-E) \tag{1.53}$$

The integral equation for the transition operator [227] is thus given by iteration by

$$T = (H-E)^{\dagger} \sum_{n=0}^{\infty} \{G^{+}_{CDW} (H-E)\}^{n} \tag{1.54}$$

Notice that we have a connected kernel in that $\boldsymbol{\nabla}_{\boldsymbol{r}_P}$ connects $e^- + P$ and $\boldsymbol{\nabla}_{\boldsymbol{r}_T}$ connects $e^- + T$. The nonorthogonal kinetic energy $-\nabla_{\mathbf{r}_P} \cdot \nabla_{\mathbf{r}_T}$ connects all three particles. This convergent expansion is especially transparent due to the use of generalized nonorthogonal coordinates (see (1.30)) and the avoidance of spurious *nonlocal* potentials and operators.

1.4 Hypergeometric Series

We define

$${}_pF_q \left(a_1 - a_p;\ b_1 - b_q;\ z\right) \equiv \sum_{n=0}^{\infty} \frac{\prod_{i=1}^{p} (a_i)_n}{\prod_{j=1}^{q} (b_j)_n} \frac{z^n}{n!} \tag{1.55}$$

where the Pochhammer symbol or rising factorial is

$$(\alpha)_n = \begin{cases} \alpha(\alpha+1)\cdots(\alpha+n-1) & (n \geq 1) \\ 1 & (n=0) \end{cases} \tag{1.56}$$

Note the very useful compendium of relations between products of Pochhammer symbols ([563] appendix I, pp.239–240).

We note that

$${}_1F_0(b;;z) = (1-z)^{-b} \equiv \sum_{n=0}^{\infty} \frac{(b)_n z^n}{n!} \equiv {}_2F_1(a,b;a;z) \tag{1.57}$$

is the binomial series and

$$(1-z)^{-1} = {}_1F_0(1;;z) \tag{1.58}$$

is the geometric progression. Other well-known hypergeometric series are: the exponential

$${}_0F_0(;;z) = \mathrm{e}^z = \sum_{n=0}^{\infty} \frac{z^n}{n!} \equiv {}_1F_1(a;a;z) \tag{1.59}$$

the modified Bessel function

$$I_\nu(z) = \frac{(z/2)^\nu}{\Gamma(1+\nu)} {}_0F_1 \left(;\nu+1;+\frac{1}{4}z^2\right) \tag{1.60}$$

and the Bessel function

$$J_\nu(z) = \frac{(z/2)^\nu}{\Gamma(1+\nu)}\,{}_0F_1\left(;\nu+1;-\frac{1}{4}z^2\right) \tag{1.61}$$

$${}_1F_1(a;c;z) \equiv M(a,c,z) = \sum_{n=0}^{\infty} \frac{(a)_n z^n}{(c)_n\, n!} \tag{1.62}$$

is the regular Kummer or confluent hypergeometric function. It satisfies the ordinary differential equation (ODE) with a regular singularity at $z = 0$ and an essential singularity at $z = \infty$, given by

$$zw'' + (c - z)w' - aw = 0 \tag{1.63}$$

The Gauss hypergeometric function given by

$${}_2F_1(a,b;c;z) \equiv \sum_{n=0}^{\infty} \frac{(a)_n (b)_n}{(c)_n} \frac{z^n}{n!} \tag{1.64}$$

satisfies the ODE given by

$$z(1-z)w'' + [c - (a+b+1)z]\,w' - abw = 0 \tag{1.65}$$

It has three regular singularities at $z = 0,\ 1,\ \infty$. ${}_1F_1$ converges for all finite z and ${}_2F_1$ converges absolutely for all $|z| < 1$. When $z = 1$ $c \neq 0, -1, -2, \cdots$; Re(c – a – b) > 0 implies conditional convergence so that

$${}_2F_1(a,b;c;1) = \frac{\Gamma(c)\Gamma(c-a-b)}{\Gamma(c-a)\Gamma(c-b)} \tag{1.66}$$

Otherwise (e.g.$|z| > 1$) one needs the full suite of analytic continuations [1] (5.3:3–14) for both real and complex z. This is the advantage of ${}_2F_1$ over many other functions whose continuations are often unknown.

R.C. Forrey, ITAMP, Harvard University has a suite for complex z now rewritten in FORTRAN 90: see chyp.f on cfa – www.harvard.edu/ref/ .

Analytic continuations include:

$${}_2F_1(a,b;c;z) = (1-z)^{-a}\,{}_2F_1\,(a,c-b;c;z/(1-z)) \tag{1.67}$$

for $|\arg(1-z)| < \pi$. Equation (1.66) follows from (1.120) and the Beta function ([1] 6.2.1)

$$\begin{aligned} {}_2F_1(a,b;c;1) &= \frac{\Gamma(c)}{\Gamma(c-b)\Gamma(b)} \int_0^1 \mathrm{d}t\, t^{b-1}(1-t)^{c-a-b-1} \\ &= \frac{\Gamma(c)\Gamma(c-a-b)}{\Gamma(c-a)\Gamma(c-b)} \end{aligned} \tag{1.68}$$

and analytic continuation of (1.64) to $|1 - z| < 1$ may be derived as follows. Let

$$y_1 = {}_2F_1(a, b; c; z) \qquad (|z| < 1) \tag{1.69}$$

$$y_2 = z^{1-c}{}_2F_1(1 + a - c, 1 + b - c; 2 - c; z) \qquad (|z| < 1) \tag{1.70}$$

be two independent solutions. Set

$$z = 1 - Z \tag{1.71}$$

in the ordinary differential equation for the Gauss ${}_2F_1$:

$$Z(1 - Z)\frac{\mathrm{d}^2y}{\mathrm{d}Z^2} - \{c - (a + b + 1)(1 - Z)\}\frac{\mathrm{d}y}{\mathrm{d}Z} - aby = 0 \tag{1.72}$$

$$\therefore \quad y_5 = {}_2F_1(a, b; 1 + a + b - c; 1 - z) \qquad (|1 - z| < 1) \tag{1.73}$$

$\therefore \quad \exists A,\ B$ so that

$$y_5 = Ay_1 + By_2 \tag{1.74}$$

Map $z \to 1 - z$ and $c \to 1 + a + b - c \quad \Rightarrow$

$$\begin{aligned} {}_2F_1(a, b; c; z) =& A{}_2F_1(a, b; 1 + a + b - c; 1 - z) \\ &+ B(1 - z)^{c-a-b}{}_2F_1(c - b, c - a, 1 + c - a - b; 1 - z) \end{aligned} \tag{1.75}$$

Set $z = 1$ and assume Re (c − a − b) > 0. Equation (1.68) implies

$$A = \frac{\Gamma(c)\Gamma(c - a - b)}{\Gamma(c - a)\Gamma(c - b)} \tag{1.76}$$

Setting $z = 0$ we verify

$$B = \frac{\Gamma(a + b - c)\Gamma(b)}{\Gamma(a)\Gamma(b)} \tag{1.77}$$

using the gamma function reflection formula ([1] chapter 6). The analytic continuation is completed.

Other useful hypergeometric representations include the normalized harmonic oscillator

$$u_n(x) = \left[\frac{\alpha}{\sqrt{\pi}2^n n!}\right]^{1/2} H_n(\alpha x)\mathrm{e}^{-\alpha^2x^2/2} \quad \left(\alpha = \sqrt{\frac{m\omega}{\hbar}}\right) \tag{1.78}$$

where n is the principal quantum number, m is the mass, ω is the frequency, and $\hbar$ is Planck's reduced constant.

$$H_{2m}(x) = (-1)^m\frac{(2m)!}{m!}{}_1F_1\left(-m, \frac{1}{2}, x^2\right) \tag{1.79a}$$

$$H_{2m+1}(x) = (-1)^m\frac{(2m + 1)!}{m!}2x{}_1F_1\left(-m, \frac{3}{2}, x^2\right) \tag{1.79b}$$

More generally we have the parabolic cylinder function given by

$$D_p(z) = 2^{p/2}\mathrm{e}^{-z^2/4}\left[\frac{\sqrt{\pi}}{\Gamma((1 - p)/2)}{}_1F_1\left(-\frac{p}{2}; \frac{1}{2}; \frac{z^2}{2}\right) - \frac{z\sqrt{2\pi}}{\Gamma(-p/2)}{}_1F_1\left(\frac{1 - p}{2}; \frac{3}{2}; \frac{z^2}{2}\right)\right] \tag{1.80}$$

Others are

$$\ln(1-z) = z\,{}_2F_1(1,1;2;z) \tag{1.81}$$

$$\tan^{-1}(z) = z\,{}_2F_1\left(\frac{1}{2},1;\frac{3}{2};-z^2\right) \tag{1.82}$$

$$\cos(2az) = {}_2F_1\left(-a,a;\frac{1}{2};\sin^2 z\right) \tag{1.83}$$

$$T_n(x) = {}_2F_1\left(-n,n;\frac{1}{2};\frac{1-x}{2}\right) \tag{1.84}$$

where the T_n are Chebyshev polynomials of type 1.

Spherical harmonics are

$$Y_l^m(\theta,\phi) = \left[\frac{(2l+1)}{2}\frac{(l-|m|)!}{(l+|m|)!}\right]^{1/2} P_l^{|m|}(\cos\theta)\,\frac{\mathrm{e}^{\mathrm{i}m\phi}}{\sqrt{2\pi}} \quad (l \geq |m|) \tag{1.85}$$

where

$$P_l^{|m|}(\cos\theta) = \frac{(l+|m|)!}{(l-|m|)!}\frac{\sin^{|m|}\theta}{|m|!\,2^{|m|}}\,{}_2F_1\left(|m|-l,l+|m|+1;1+|m|;\sin^2(\theta/2)\right) \tag{1.86}$$

and

$$P_l(\cos\theta) = {}_2F_1\left(-l,l+1;1;\sin^2(\theta/2)\right) \tag{1.87}$$

Normalized eigenenergy functions for the H-like atom/ion are

$$u_{nlm}(r,\theta,\phi) = R_{nl}(r)Y_l^m(\theta,\phi) \tag{1.88}$$

where

$$R_{nl}(r) = N_{nl}\rho^l L_{n+l}^{2l+1}(\rho)\mathrm{e}^{-\rho/2} \tag{1.89}$$

$$\rho = \frac{2Zr}{na_0}$$

where

a_0 : Bohr radius
Z = charge
n = principal integer quantum number
l = azimuthal integer quantum number
m = magnetic integer quantum number

and

$$N_{nl} = -\left[\left(\frac{2Z}{na_0}\right)^3\frac{(n-l-1)!}{2n\{(n+l)!\}^3}\right]^{1/2} \tag{1.90}$$

Our associated Laguerre polynomials are

$$L_{n+l}^{2l+1}(\rho) \equiv \frac{\{(n+l)!\}^2}{(n-l-1)!(2l+1)!}\,{}_1F_1(l+1-n;2l+2;\rho) \quad (n>l) \tag{1.91}$$

which disagrees with the choice of definition of Morse and Feshbach [440].

One should note that intelligent application of the convergence ratio test is required and the invoking of a finite probability density $|u_{nlm}(r,\theta,\phi)|^2$ is insufficient to prefer r^l to r^{-l-1} when $l=0$. However, it merely requires the observation that

$$\nabla_{\boldsymbol{r}}^2 \frac{1}{r} = -4\pi\delta(\boldsymbol{r}) \tag{1.92}$$

so that for the $l=0$ case, the irregular solution does not satisfy the Schrödinger equation at $r=0$, where the right-hand side of (1.92) is infinite.

The normalization of Legendre polynomials required

$$\int_{-1}^{+1} \mathrm{d}x \left[{}_2F_1\left(-l,l+1;1;\frac{1-x}{2}\right)\right]^2 = \frac{2}{2l+1} \tag{1.93}$$

Suffice it to say that this required Saalschutz' theorem that

$${}_3F_2\,(-N,a,b;c,1+a+b-c-N;1) = \frac{(c-a)_N(c-b)_N}{(c)_N(c-a-b)_N} \tag{1.94}$$

which in turn depends on Euler's relation

$${}_2F_1\,(a,b;c;z) = (1-z)^{c-a-b}\,{}_2F_1\,(c-a,c-b;c;z) \tag{1.95}$$

Note that Saalschutz' theorem generalizes to

$${}_3F_2\,(a,b,-m;e,f;1) = \frac{(f-b)_m}{(f)_m}\,{}_3F_2\,(e-a,b,-m;e,1-f+b-m;1) \tag{1.96}$$

For completeness we note that the following well-known quantities are, in fact, hypergeometric series: Rotation matrices ([517] p.53)

$$\begin{aligned} d^j_{m_1m_2}(\beta) = {} & \left[\frac{(j-m_1)!(j+m_2)!}{(j+m_1)!(j-m_2)!}\right]^{1/2} \frac{(\cos(\beta/2))^{2j+m_1-m_2}\,(\sin(\beta/2))^{m_1-m_2}}{(m_1-m_2)!} \\ & \times {}_2F_1\left(m_2-j,-m_1-j;m_2-m_1+1;-\tan^2(\beta/2)\right) \qquad (m_2\geq m_1) \end{aligned} \tag{1.97}$$

where the ${}_2F_1$ is a Jacobi polynomial; Clebsch–Gordan coefficients

$$\begin{aligned} & C\,(j_1\ j_2\ j\,m_1\ m_2\ m) = \\ & \quad (-1)^{j_2+m_2}\left[\frac{(j+j_1-j_2)!(j_1+j_2-j)!(j-m)!(j_1-m_1)!(2j+1)}{(j-j_1+j_2)!(j_1+j_2+j+1)!(j+m)!(j_1+m_1)!(j_2-m_2)!(j_2+m_2)!}\right]^{1/2} \\ & \quad \times \frac{(j+j_2+m_1)!}{(j_1-j_2-m)!} \\ & \quad {}_3F_2\,(-j+j_1-j_2,j_1-m_1+1,-j-m;j_1-j_2-m+1,-j-j_2-m_1;1) \end{aligned} \tag{1.98}$$

Of course, pure recurrence relations à la Sister Celine's technique would be cumbersome so better to refer to more specialized texts on angular momentum and group theory.

Racah coefficients ([517] p.110 (6.7))

$$W(abcd;ef) = \Delta_R(abe)\Delta_R(cde)\Delta_R(acf)\Delta_R(bdf)(-1)^{a+b+c+d} \times \sum_\psi \frac{(-1)^\psi(\psi+1)!}{(\psi-a-b-e)!(\psi-c-d-e)!(\psi-a-c-f)!(\psi-b-d-f)!} \times \frac{1}{(a+b+c+d-\psi)!(a+d+e+f-\psi)!(b+c+e+f-\psi)!} \tag{1.99}$$

where

$$\Delta_R(abc) = \left[\frac{(a+b-c)!(a-b+c)!(b+c-a)!}{(a+b+c+1)!}\right]^{1/2} \tag{1.100}$$

Assume for the sake of argument that

$$a+b+e \geq \{c+d+e, a+c+f, b+d+f\} \tag{1.101}$$

Set

$$\psi = a+b+e+r \tag{1.102}$$

Then we have

$$W \propto {}_4F_3\,(a+b+e+2, e-c-d, b-d-f, a-c-f; 1+a+b-c-d, 1+b+e-c-f, 1+a+e-d-f; 1) \tag{1.103}$$

using

$$(\alpha-\psi)! = \frac{(-1)^\psi \alpha!}{(-\alpha)_\psi} \tag{1.104}$$

and where r is the dummy summation index.

1.5 Contour Integral Transforms

Both complex contour and real integral transforms are useful, particularly regarding asymptotic expansions and the Stokes phenomenon (see Chapter 2). The Hankel integral transform:

$$\frac{1}{2\pi \mathrm{i}} \int_{-\infty}^{(0+)} \mathrm{e}^v v^{-x} \mathrm{d}v = \frac{1}{\Gamma(x)} \quad (\arg v = 0 \text{ on positive real axis}) \tag{1.105}$$

where Γ is the gamma function. This is a valuable result both here and in Section 5.3. Setting $t = 1/s$ and applying Cauchy's residue theorem, we have (b noninteger)

$$\frac{1}{2\pi \mathrm{i}} \oint^{(0+,1+)} \left(\frac{t}{t-1}\right)^b t^{n-1} \mathrm{d}t = \frac{(b)_n}{n!} \quad (\arg t = 0 = \arg(t-1) \text{ on positive real axis}) \tag{1.106}$$

It follows that

$$
\begin{aligned}
{}_1F_1(b;1;z) &= \frac{1}{2\pi\mathrm{i}}\int^{(0+,1+)}\left(\frac{t}{t-1}\right)^b \mathrm{e}^{zt}\frac{\mathrm{d}t}{t} && (1.107)\\
&= \frac{1}{2\pi\mathrm{i}}\left[\int^{(0+)}+\int^{(z+)}\right]\left(1-\frac{z}{v}\right)^{-b}\mathrm{e}^{v}\frac{\mathrm{d}v}{v} \qquad (v=zt) && (1.108)\\
&\underset{|z|\gg 1}{\simeq} \frac{(-z)^{-b}}{\Gamma(1-b)}{}_2F_0\left(b,b;;-1/z\right)+\frac{\mathrm{e}^z z^{b-1}}{\Gamma(b)}{}_2F_0\left(1-b,1-b;;1/z\right)\\
&\qquad\qquad (\arg\pm z\in(-\pi,+\pi)) && (1.109)
\end{aligned}
$$

where we have used (1.105) and for the second integral in (1.108), $u=v-z$. The two ${}_2F_0$s in (1.109) diverge for all finite z. This is an important observation and leads to the Stokes phenomenon. The Stokes/anti-Stokes lines are the positive and negative real/imaginary axes in the complex z-plane, respectively.

At $\arg z = 0$, the second-term series in (1.109) is dominant and the subdominant first-term series is ambiguous by the factor $\exp(2\pi b\mathrm{i})$. As z crosses this Stokes line in the positive (anticlockwise) sense, $(-z)$ changes from $z\mathrm{e}^{\pi\mathrm{i}}$ to $z\mathrm{e}^{-\pi\mathrm{i}}$ so that the coefficient of the subdominant term changes by a factor of $\mathrm{e}^{2\pi b\mathrm{i}}$.

On $\arg(-z)=0$, i.e., $\arg z=\pm\pi$, the first-term/ series is dominant and as z crosses the π Stokes line in the positive sense, the subdominant second-term/ series suffers an abrupt discontinuous change, namely by a factor of $\mathrm{e}^{-2\pi b\mathrm{i}}$.

On the anti-Stokes lines, $\arg z=\pm\pi/2$, neither term/ series is exponentially dominant and no discontinuity arises. This is an illustration of the Stokes phenomenon, which repeats itself ad nauseam, upon circling the origin (at a distance), in either direction. This generalizes to

$$
{}_1F_1(a;c;z)\underset{|z|\gg 1}{\simeq}\frac{\Gamma(c)(-z)^{-a}}{\Gamma(c-a)}{}_2F_0(a,1+a-c;;-1/z)+\frac{\mathrm{e}^z z^{a-c}}{\Gamma(a)}{}_2F_0(c-a,1-a;;1/z) \tag{1.110}
$$

with principal branches understood as before. As for ${}_1F_1$, so for ${}_2F_1$, we have

$$
{}_2F_1(a,b;1;z)=\frac{1}{2\pi\mathrm{i}}\oint^{(0+,1+)}\left(\frac{t}{t-1}\right)^b(1-tz)^{-a}\frac{\mathrm{d}t}{t} \tag{1.111}
$$

where b is noninteger and $1/z$ lies outside the contour.

Nordsieck integrals [461, 157] may be evaluated using (1.107):

$$
\begin{aligned}
&\int \mathrm{d}r\frac{\mathrm{e}^{\mathrm{i}\mathbf{q}\cdot\mathbf{r}-\lambda r}}{r}{}_1F_1\left(-\mathrm{i}a_1;1;\mathrm{i}p_1 r+\mathrm{i}\mathbf{p}_1\cdot\mathbf{r}\right){}_1F_1\left(\mathrm{i}a_2;1,\mathrm{i}p_2 r+\mathrm{i}\mathbf{p}_2\cdot\mathbf{r}\right)\\
&\quad=\frac{4\pi}{q^2+\lambda^2}\left[\frac{q^2+\lambda^2}{q^2+\lambda^2+2\mathbf{p}_2\cdot\mathbf{q}-2\mathrm{i}\lambda p_2}\right]^{\mathrm{i}a_2}\left[\frac{q^2+\lambda^2}{q^2+\lambda^2+2\mathbf{p}_1\cdot\mathbf{q}-2\mathrm{i}\lambda p_1}\right]^{-\mathrm{i}a_1}\\
&\qquad\times{}_2F_1\left(-\mathrm{i}a_1,\mathrm{i}a_2;1;z=\frac{\beta\gamma-\alpha\delta}{\gamma(\alpha+\beta)}\right)
\end{aligned} \tag{1.112}
$$

One should note a sign error in Nordsieck's pair-production integral where

$$\begin{aligned} \alpha &= \tfrac{1}{2}\left(q^2+\lambda^2\right) & \gamma &= \mathbf{p}_1\cdot\mathbf{q}-\lambda p_1+\alpha \\ \beta &= \mathbf{p}_2\cdot\mathbf{q}-\mathrm{i}\lambda p_2 & \delta &= \mathbf{p}_1\cdot\mathbf{p}_2-p_1p_2+\beta \end{aligned} \tag{1.113}$$

The normalization of continuum wave functions in the Coulomb case requires

$$\int \mathrm{e}^{\mathrm{i}\mathbf{k}\cdot\mathbf{r}}{}_1F_1\left(-\frac{\mathrm{i}Z_pZ_T}{v};1;\mathrm{i}kr-\mathrm{i}kz\right)\mathrm{e}^{-\mathrm{i}\mathbf{k}'\cdot\mathbf{r}}{}_1F_1\left(\frac{\mathrm{i}Z_pZ_T}{v'};1;-\mathrm{i}k'r+\mathrm{i}k'z\right) \tag{1.114}$$

Use $-\partial/\partial\lambda$ on Nordsieck and let $\lambda\to 0+$. Set

$$\begin{aligned} &\mathbf{q}=\mathbf{k}-\mathbf{k}', \quad a_1=\tfrac{Z_pZ_T}{v}, \quad a_2=\tfrac{Z_pZ_T}{v'} \\ &p_1=k \qquad\quad \mathbf{p}_1=-\mathbf{k}, \quad p_2=-k', \quad \mathbf{p}_2=\mathbf{k}' \end{aligned} \tag{1.115}$$

In limit, $q\neq 0\Rightarrow 0$ but for $q=0$ we have, using (15.1.20) in [1]

$$\frac{8\pi\lambda}{\left(\lambda^2+q^2\right)^2}\mathrm{e}^{\pi a_1}{}_2F_1\left(-\mathrm{i}a_1,\mathrm{i}a_1;1;1\right)=\frac{(2\pi)^3\delta(\mathbf{q})\mathrm{e}^{\pi Z_pZ_T/v}}{\Gamma\left(1+(\mathrm{i}Z_pZ_T)/v\right)\Gamma\left(1-(\mathrm{i}Z_pZ_T)/v\right)} \tag{1.116}$$

Note that

$$\begin{aligned} &\frac{\gamma}{\alpha+\beta}=\frac{\lambda^2-2\mathrm{i}\lambda k}{\lambda^2+2\mathrm{i}\lambda k}=\frac{\lambda-2\mathrm{i}k}{\lambda+2\mathrm{i}k}=\frac{-4k^2-4\mathrm{i}\lambda k}{4k^2+\lambda^2} \\ &\cos-\mathrm{ve}\,,\sin-\mathrm{ve}\;(\lambda\to 0+)\Rightarrow\arg\frac{\gamma}{\alpha+\beta}=-\pi \end{aligned} \tag{1.117}$$

Real integral representations may be used, for instance,

$${}_1F_1\left(A;C;\mathrm{i}D\eta\right)=\frac{\Gamma(C)}{\Gamma(A)\Gamma(C-A)}\int_0^1 \mathrm{e}^{\mathrm{i}D\eta v}v^{A-1}(1-v)^{C-A-1}\,\mathrm{d}v \tag{1.118}$$

where v is now clearly a real dummy variable and $\mathrm{Re\,C}>\mathrm{Re\,A}>0$. A useful result is

$$\begin{aligned} \int_0^\infty \mathrm{d}u\,\mathrm{e}^{-Bu}u^{C-1}{}_1F_1(A,C,\mathrm{i}Du){}_1F_1(A',C,\mathrm{i}D'u)=\frac{\Gamma(C)B^{A+A'-C}}{(B-\mathrm{i}D)^A(B-\mathrm{i}D')^{A'}} \\ \times{}_2F_1\left(A,A';C;\frac{-DD'}{(B-\mathrm{i}D)(B-\mathrm{i}D')}\right) \end{aligned} \tag{1.119}$$

this can lead the complex formulation (see (1.117)). This can lead to ambiguities in the limit as $\mathrm{Re\,B}\to 0$ and in any case for $\mathrm{Re\,(c-b)}>0$, $\mathrm{Re\,b}>0$, $|z|<1$ we have

$${}_2F_1(a,b;c;z)=\frac{1}{2\pi\mathrm{i}}\frac{\Gamma(c)\Gamma(1-b)}{\Gamma(c-b)}\oint_1^{(0+)}\left(\frac{t}{t-1}\right)^b(1-t)^{c-1}(1-tz)^{-a}\frac{\mathrm{d}t}{t} \tag{1.120}$$

for which the conditions may subsequently be relaxed by analytic continuation. Setting $z\to z/a$ and letting $a\to+\infty$ yields a similar formula for ${}_1F_1$s upon realising that

$$\lim_{a\to+\infty}\left(1-\frac{tz}{a}\right)^{-a}=\mathrm{e}^{zt} \tag{1.121}$$

For some purposes the Barnes complex-contour integral representation is simpler to use than the preceeding Euler integrals. For irregular Kummer functions complex representations are more flexible [468]. Other useful results are

$$\int_0^{2\pi}\mathrm{e}^{\mathrm{i}m\phi+\mathrm{i}k\cos\phi}\,\mathrm{d}\phi=2\pi\mathrm{i}^m J_m(k) \tag{1.122}$$

and

$$\int_0^{\infty}\mathrm{d}t\,J_\mu(at)\mathrm{e}^{-\gamma^2t^2}t^{\mu+1}\,\mathrm{d}t=\frac{a^\mu}{(2\gamma^2)^{\mu+1}}\mathrm{e}^{-a^2/(4\gamma^2)} \tag{1.123}$$

where J is the regular Bessel function.

1.6 Combinatorics

The principle of inclusion and exclusion gives

$$\Lambda_n=\sum_{k=0}^{n}(-1)^k v_{nk} \tag{1.124}$$

$$\lambda_n=\sum_{k=0}^{n}(-1)^k u_{nk} \tag{1.125}$$

where λ_n is the number of ways of avoiding a couple in problème des ménages (cyclic) and Λ_n is the number of ways of avoiding a snap in cards (linear); v_{nk} is the number of ways of selecting k couples, the remaining $(n-k)$ being arbitrary; u_{nk} is the number of ways of selecting k snaps, the remaining $(n-k)$ being arbitrary:

$$v_{nk}=(n-k)!\,{}^{2n-k}C_k \tag{1.126}$$

$$u_{nk}=(n-k)!\left[{}^{2n-k-1}C_{k-1}+{}^{2n-k}C_k\right] \tag{1.127}$$

$$\lambda_n=2(-1)^n{}_3F_1\left(-n,n,1;\frac{1}{2};\frac{1}{4}\right) \tag{1.128}$$

$$\Lambda_n=(-1)^n{}_3F_1\left(-n,n+1,1;\frac{1}{2};\frac{1}{4}\right) \tag{1.129}$$

In the preceeding, ${}^NC_R$ is the number of ways of choosing R objects from a collection of N distinct objects, without regard to order.

Probability of snap occurring is given by

$$p_n=\frac{1}{n!}\sum_{k=1}^{n}v_{nk} \tag{1.130}$$

$$=1-\text{ the first }(n+1)\text{ terms of }{}_1F_1\left(\frac{1}{2}-n;-2n;-4\right) \tag{1.131}$$

$$p_\infty=1-{}_0F_0\,(;;-2)=1-\mathrm{e}^{-2} \tag{1.132}$$

The pure recurrence relations of Lucas are

$$\lambda_n = \Lambda_n - \Lambda_{n-1} = n\Theta_n + 2(-1)^n \tag{1.133}$$

$$\Theta_{n+1} = n\Theta_n + \Theta_{n-1} + 2(-1)^n \tag{1.134}$$

$$\Theta_4 = 0 \qquad \Theta_5 = 3 \tag{1.135}$$

1.6.1 Proof via Sister Celine's Technique

Consider

$$g_n(x) = \sum_{k=0}^{\infty} \frac{(-1)^k k!(n-k-1)!}{(2k)!(n-k)!} x^k \equiv \sum_{k=0}^{\infty} \epsilon(k,n,x) \tag{1.136}$$

so that

$$\frac{(-1)^n \lambda_n}{2n} = g_n(1) \tag{1.137}$$

$$g_{n-1}(x) = \sum_{k=0}^{\infty} \frac{(n-k)}{(n+k-1)} \epsilon(k,n,x) \tag{1.138}$$

$$xg_{n-1}(x) = \sum_{k=0}^{\infty} \frac{(-1)^k k!(n+k-2)!}{(2k)!(n-k-1)!} x^{k+1} \tag{1.139}$$

$$= \sum_{k=1}^{\infty} \frac{(-1)^{k-1}(k-1)!(n+k-3)!}{(2k-2)!(n-k)!} x^k \tag{1.140}$$

$$h_n(x) = xg_{n-1}(x) + \frac{2}{n(n-1)(n-2)}$$

$$= \sum_{k=0}^{\infty} \frac{-2(2k-1)}{(n+k-1)(n+k-2)} \epsilon(k,n,x) \tag{1.141}$$

$$g_{n-2}(x) = \sum_{k=0}^{\infty} \frac{(n-k)(n-1-k)}{(n+k-1)(n+k-2)} \epsilon(k,n,x) \tag{1.142}$$

$$g_n(x) + Ah_n(x) + Bg_{n-1}(x) + Cg_{n-2}(x) = 0 \tag{1.143}$$

$$\therefore \; 1 + \frac{B(n-k)}{n+k-1} - \frac{A2(2k-1)}{(n+k-1)(n+k-2)} + \frac{C(n-k)(n-k-1)}{(n+k-1)(n+k-2)} \equiv_k 0 \tag{1.144}$$

The numerator is quadratic in k; solving gives

$$A = n-1 \qquad B = 0 \qquad C = -1 \tag{1.145}$$

Setting $x = 1$ gives

$$g_n + (n-1)\left[g_{n-1} + \frac{2}{n(n-1)(n-2)}\right] - g_{n-2} = 0 \tag{1.146}$$

$$(n-1)\lambda_{n+1} - (n^2-1)\lambda_n - (n+1)\lambda_{n-1} - 4(-1)^n = 0 \tag{1.147}$$

$$\lambda_n = n\Theta_n + 2(-1)^n \quad \Rightarrow \tag{1.148}$$

$$\Theta_{n+1} = n\Theta_n + \Theta_{n-1} + 2(-1)^n \tag{1.149}$$

1.7 Generalized Hypergeometric Functions

These include Appell functions given by

$$F_1(a;b_1,b_2;c;x,y)=\sum_{m=0}^{\infty}\sum_{n=0}^{\infty}\frac{(a)_{m+n}(b_1)_m(b_2)_n x^m y^n}{(c)_{m+n}m!n!} \tag{1.150}$$

$$F_2(a;b_1,b_2;c_1,c_2;x,y)=\sum_{m=0}^{\infty}\sum_{n=0}^{\infty}\frac{(a)_{m+n}(b_1)_m(b_2)_n x^m y^n}{(c_1)_m(c_2)_n m!n!} \tag{1.151}$$

$$F_3(a_1,a_2;b_1,b_2;c;x,y)=\sum_{m=0}^{\infty}\sum_{n=0}^{\infty}\frac{(a_1)_m(a_2)_n(b_1)_m(b_2)_n x^m y^n}{(c)_{m+n}m!n!} \tag{1.152}$$

$$F_4(a;b;c_1,c_2;x,y)=\sum_{m=0}^{\infty}\sum_{n=0}^{\infty}\frac{(a)_{m+n}(b)_{m+n} x^m y^n}{(c_1)_m(c_2)_n m!n!} \tag{1.153}$$

and Lauricella functions given by

$$\begin{aligned}F_A^{(n)}(a,b_1-b_n,c_1-c_n,x_1-x_n)&=\sum_{m_1=0}^{\infty}\sum_{m_2=0}^{\infty}\cdots\sum_{m_n=0}^{\infty}(a)_{m_1+m_2+\cdots+m_n}\\ &\times\frac{(b_1)_{m_1}(b_2)_{m_2}\cdots(b_n)_{m_n}}{(c_1)_{m_1}(c_2)_{m_2}\cdots(c_n)_{m_n}}\,\frac{x_1^{m_1}x_2^{m_2}\cdots x_n^{m_n}}{m_1!m_2!\cdots m_n!}\end{aligned} \tag{1.154}$$

which generalizes $F_2^{(n)}$ and three similar generalizations $F_B^{(n)}$, $F_C^{(n)}$, $F_D^{(n)}$ of F_3, F_4, and F_1, respectively, in the sense of generalizing from 2 to n arguments and Pochhammer symbols in the numerator and denominator.

As a simple example of F_2 we give [159]

$$B_{jk}^{\alpha\beta}(h)= \tag{1.155}$$

$$\frac{jkj!k!}{h}\mathrm{Im}\int_0^{\infty}\mathrm{r}\exp\{-(\alpha+\beta-\mathrm{ih})\mathrm{r}\}{}_1\mathrm{F}_1(1-\mathrm{j};2;2\alpha\mathrm{r}){}_1\mathrm{F}_1(1-\mathrm{k};2;2\beta\mathrm{r})\mathrm{dr} \tag{1.156}$$

$$=\frac{jkj!k!}{h}\mathrm{Im}\left\{\frac{\Gamma(2)}{(\alpha+\beta-\mathrm{ih})^2}\,\mathrm{F}_2\left(2,1-\mathrm{j},1-\mathrm{k},2,2,\frac{2\alpha}{\alpha+\beta-\mathrm{ih}},\frac{2\beta}{\alpha+\beta-\mathrm{ih}}\right)\right\} \tag{1.157}$$

$$=\frac{jkj!k!}{h}{}_2F_1\left(1-j,1-k;2;\frac{-4\alpha\beta}{(\alpha-\beta)^2+h^2}\right)\mathrm{Im}\frac{(\alpha-\beta-\mathrm{ih})^{\mathrm{k}-1}(\beta-\alpha-\mathrm{ih})^{\mathrm{j}-1}}{(\alpha+\beta-\mathrm{ih})^{\mathrm{j}+\mathrm{k}}}\,. \tag{1.158}$$

Since j and k are positive integers, F_2 and ${}_2F_1$ are both polynomials. L'Hôspital's rule yields:

$$\begin{aligned}B_{jk}^{\alpha\beta}(0)&=(-1)^j 2(k\beta-j\alpha)jkj!k!\frac{(\alpha-\beta)^{j+k-3}}{(\alpha+\beta)^{j+k+1}}\\ &\quad\times{}_2F_1\left(1-j,1-k;2;\frac{-4\alpha\beta}{(\alpha-\beta)^2}\right)\quad(\alpha\neq\beta) &(1.159)\\ &=0\qquad(\alpha=\beta,\ |k-j|\geq 2) &(1.160)\\ &=\frac{j^2(j!)^2}{4\alpha^3}\qquad(\alpha=\beta,\ j=k) &(1.161)\\ &=\frac{-j(k!)^2}{8\alpha^3}\qquad(\alpha=\beta,\ k=j+1) &(1.162)\\ &=\frac{-k(j!)^2}{8\alpha^3}\qquad(\alpha=\beta,\ j=k+1) &(1.163)\end{aligned}$$

As a simple example of $F_A^{(4)}$ we give [179]

$$\frac{1}{m!}\int_0^\infty \mathrm{d}X\, \mathrm{e}^{-X}X^m\{{}_1F_1(-n_2;m+1;X))\}^2\left|{}_1F_1\left(\mathrm{i}/v;1;\frac{\mathrm{i}X}{y_1}\right)\right|^2 \tag{1.164}$$

$$= F_A^{(4)}(m+1;-n_2,-n_2,\mathrm{i}/v,-\mathrm{i}/v;m+1,m+1,1,1;1,1,\mathrm{i}/y_1,-\mathrm{i}/y_1) \tag{1.165}$$

Define

$$J_\mu = \int_0^\infty \mathrm{e}^{-kz}z^{\mu-1}\left[{}_1F_1(-n;\gamma;kz)\right]^2\mathrm{d}z \tag{1.166}$$

$$= \frac{\Gamma(\mu)}{k^\mu}F_2(\mu;-n,-n;\gamma,\gamma;1,1) \tag{1.167}$$

which implies that

$$J_{\gamma+p} = \frac{\Gamma(\gamma+p)}{k^{\gamma+p}}F_2(\gamma+p;-n,-n;\gamma,\gamma;1,1) \tag{1.168}$$

$$= \frac{\Gamma(\gamma+p)}{k^{\gamma+p}}\frac{(-p)_n}{(\gamma)_n}{}_3F_2(-n,\gamma+p,1+p;\gamma,1+p-n;1) \tag{1.169}$$

$$= \frac{\Gamma(\gamma+p)}{k^{\gamma+p}}\frac{n!}{(\gamma)_n}{}_3F_2(-p,1+p,-n;\gamma,1;1) \tag{1.170}$$

Thus we have [377]

$$J_{\gamma+p} = J_{\gamma-1-p}\frac{\Gamma(\gamma+p)}{\Gamma(\gamma-1-p)k^{2p+1}}$$

$$= J_{\gamma-1-p}\frac{(\gamma-1-p)\cdots(\gamma+p-1)}{k^{2p+1}} \tag{1.171}$$

This result comes from

$$F_2(a;-m,-n;c,d;1,1) = \frac{(d-a)_n}{(d)_n}{}_3F_2(-m,a,1+a-d;c,1+a-d-n;1) \tag{1.172}$$

where we have used Van der Monde's theorem,

$$(a)_{p+q} = (a)_p(a+p)_q \tag{1.173}$$

and [563]

$$(d-a-p)_n = \frac{(1+a-d)_p(d-a)_n}{(1+a-d-n)_p} \tag{1.174}$$

We may now define the normalization of the Laguerre polynomials: in Dirac notation we have

$$\langle nl|nl\rangle = 1 = N_{nl}^2 J_{\gamma+1} \tag{1.175}$$

which implies, setting $\gamma = 2l+2$ and $k = 2Z/n$, that

$$N_{nl}^2 = \frac{k^{\gamma+1}(\gamma)_{n-l-1}}{\Gamma(\gamma+1)(n-l-1)!\,{}_3F_2(-1,2,l+1-n;\gamma,1;1)} \tag{1.176}$$

$$= \frac{\left(\frac{2Z}{n}\right)^{2l+3}(n+l)!(2l+2)}{(2l+2)!(n-l-1)!(2l+1)!\,2n} \tag{1.177}$$

$$N_{nl} = \frac{\left(\frac{2Z}{n}\right)^{3/2+l}}{(2l+1)!}\left[\frac{(n+l)!}{2n\,(n-l-1)!}\right]^{1/2} \tag{1.178}$$

as in [76].

Consider now the more general matrix element ($k \neq 1$) and include r^2 from the radial part of the volume element $r^2\,\mathrm{d}r$

$$\langle nl|\, r^{k-1}\,|nl\rangle = N_{nl}^2 \int_0^\infty \mathrm{d}r\; \mathrm{e}^{-2yr} r^{k-1+2l+2}\left[{}_1F_1(1+l-n;2l+2;2yr)\right]^2 \tag{1.179}$$

$$\equiv N_{nl}^2 J_{\gamma+p} \tag{1.180}$$

with

$$\begin{aligned} p &= k \\ k &= 2y = 2Z/n \end{aligned} \tag{1.181}$$

From (1.171) we have

$$\langle nl|\, r^{k-1}\,|nl\rangle = \langle nl|\, r^{-k-2}\,|nl\rangle\, \frac{(2l+1-k)\cdots(2l+1+k)}{\left(\frac{2Z}{n}\right)^{2k+1}} \tag{1.182}$$

$$= \left(\frac{n}{2Z}\right)^{2k+1} \frac{(2l+k+1)!}{(2l-k)!}\,\langle nl|\, r^{-k-2}\,|nl\rangle \tag{1.183}$$

as given by Ojha and Crothers [464]. This generalizes to [576]

$$\begin{aligned} \langle nl'\big|\, r^{-k-2}\,|nl\rangle = {} & (-1)^{l-l'}(2/an)^{2k+1}(l+l'-k)!k!^2 \\ & \times \frac{\langle nl'|\, r^{k-1}\,|nl\rangle}{(l+l'+1+k)!(k+l-l')!(k+l'-l)!} \end{aligned} \tag{1.184}$$

for $|l-l'| \leq k \leq l+l'$.

Other generalizations of the hypergeometric functions are the Kampé de Fériet functions [258]. For instance the type of integral that occurs in the condensed-matter physics of Chapter 5 includes

$$\int_0^1 \mathrm{d}z\, \mathrm{e}^{3\alpha z^4 - 2\alpha z^2} I_0\left(\alpha(1-z^2)^2\right) \tag{1.185}$$

$$= \mathrm{e}^{-\alpha} \sum_{r=0}^{\infty}\sum_{s=0}^{\infty} \frac{(2\alpha)^r}{r!}\frac{(2\alpha)^s}{s!}\frac{\left(\frac{1}{4}\right)_r\left(\frac{3}{4}\right)_r\left(\frac{1}{2}\right)_s\left(\frac{1}{2}\right)_s}{\left(\frac{3}{4}\right)_{r+s}\left(\frac{5}{4}\right)_{r+s}} \tag{1.186}$$

$$= \mathrm{e}^{-\alpha} F_{2:0;0}^{0:2;2}\left(\begin{matrix} -- : \frac{1}{4}, \frac{3}{4}; \frac{1}{2}, \frac{1}{2}; \\ \frac{3}{4}, \frac{5}{4} : \quad -- \quad ; -- ; \end{matrix} 2\alpha,\, 2\alpha\right) \tag{1.187}$$

which converges for all finite α, where I_0 is the modified Bessel function of the first kind and zero order. Another example is

$$\int_{-1}^{+1} \mathrm{d}x\, \mathrm{e}^{\sigma x^2+\xi x} P_{2n}(x)\mathrm{d}x = \frac{2^{2n+1}(2n)!\xi^n}{(3n+1)!}$$
$$\times F^{0:0;4}_{2:0;3}\left(\begin{matrix} -- & : -- ; & \frac{n}{2}+\frac{1}{2},\ \frac{n}{2}+1,\ n+\frac{1}{2},\ n+1 \\ \frac{n}{2}+\frac{1}{2},\ \frac{n}{2}+1 & : -- ; & \frac{1}{2},\ \frac{3n}{2}+1,\ \frac{3n}{2}+\frac{3}{2} \end{matrix} ; \frac{\sigma\xi^2}{4},\ \frac{\xi^2}{4} \right) \tag{1.188}$$

The integral

$$\int_{-1}^{+1} \mathrm{d}x\, (1-x^2) P_l^{M-4}(x) P_L^M(x) \tag{1.189}$$

may be written as a terminating Kampé de Fériet function. Alternative notations include Fox functions [499].

1.8 Fourier and Laplace Transforms

1.8.1 Critical Fourier Transform Relation

$$\bar{f}(p) = \frac{1}{\sqrt{2\pi}} \int_{-\infty}^{+\infty} \mathrm{d}y\, f(y)\mathrm{e}^{-\mathrm{i}py} \tag{1.190}$$

$$\Rightarrow f(x) = \frac{1}{\sqrt{2\pi}} \int_{-\infty}^{+\infty} \mathrm{d}p\, \bar{f}(p)\mathrm{e}^{\mathrm{i}px} \tag{1.191}$$

Proof. Substitute (1.190) into (1.191):

$$\begin{aligned} f(x) &= \frac{1}{2\pi} \int_{-\infty}^{+\infty} \mathrm{d}p\, \mathrm{e}^{\mathrm{i}px} \int_{-\infty}^{+\infty} \mathrm{d}y\, f(y)\mathrm{e}^{-\mathrm{i}py} \\ &= \lim_{\epsilon\to 0+} \frac{1}{2\pi} \int_{-\infty}^{+\infty} \mathrm{d}p\, \mathrm{e}^{\mathrm{i}px-\epsilon|p|} \int_{-\infty}^{+\infty} \mathrm{d}y\, f(y)\mathrm{e}^{-\mathrm{i}py} \\ &= \lim_{\epsilon\to 0+} \frac{1}{2\pi} \int_{-\infty}^{+\infty} \mathrm{d}y\, f(y) G(y) \end{aligned} \tag{1.192}$$

where

$$\begin{aligned} G(y) &= \int_{-\infty}^{+\infty} \mathrm{d}p\, \mathrm{e}^{-\epsilon|p|+\mathrm{i}p(x-y)} \\ &= 2\mathrm{Re} \int_0^{\infty} \mathrm{dp}\, \mathrm{e}^{-\epsilon\mathrm{p}+\mathrm{ip}(\mathrm{x}-\mathrm{y})} \\ &= \frac{2\epsilon}{\epsilon^2+(y-x)^2} \end{aligned} \tag{1.193}$$

$$
\begin{aligned}
f(x) &= \lim_{\epsilon\to 0+}\left[-\frac{1}{\pi}\int_{-\infty}^{+\infty} \mathrm{d}y\, f'(y)\tan^{-1}\left\{\frac{y-x}{\epsilon}\right\}\right] \\
&= -\frac{1}{\pi}\left[\int_{-\infty}^{x} \mathrm{d}y\, f'(y)\left(-\frac{\pi}{2}\right)+\int_{x}^{\infty} \mathrm{d}y\, f'(y)\left(\frac{\pi}{2}\right)\right] \qquad (1.194)\\
&= \frac{1}{2}\int_{-\infty}^{x} \mathrm{d}y\, f'(y)-\frac{1}{2}\int_{x}^{+\infty} \mathrm{d}y\, f'(y) \\
&= \frac{1}{2}\left[f(y)\right]_{y=-\infty}^{x}-\frac{1}{2}\left[f(y)\right]_{y=x}^{+\infty} \\
&= \frac{1}{2}\left[f(x)\right]+\frac{1}{2}\left[f(x)\right]=f(x) \qquad (1.195)
\end{aligned}
$$

Note that

$$\delta(x-y)=\lim_{\epsilon\to 0+}\frac{\epsilon/\pi}{\epsilon^2+(y-x)^2}$$

is one of the representations of the Dirac delta function.

1.8.2 Critical Laplace Transform Relation

$$\bar{f}(p)=\int_0^{+\infty} \mathrm{e}^{-px} f(x)\,\mathrm{d}y \qquad (1.196)$$

$$\Rightarrow f(x)=\frac{1}{2\pi\mathrm{i}}\int_{\gamma-\mathrm{i}\infty}^{\gamma+\mathrm{i}\infty} \mathrm{d}p\,\mathrm{e}^{px}\bar{f}(p) \qquad (1.197)$$

All singularities of $\bar{f}(p)$ lie to the left of $\mathrm{Re}\,p=\gamma$. Substituting (1.196) into (1.197) $\Rightarrow$

$$
\begin{aligned}
f(x) &= \frac{1}{2\pi\mathrm{i}}\int_{\gamma-\mathrm{i}\infty}^{\gamma+\mathrm{i}\infty} \mathrm{d}p\,\mathrm{e}^{px}\int_0^{+\infty} \mathrm{e}^{-p\zeta} f(\zeta)\,\mathrm{d}\zeta \\
&= \frac{1}{2\pi\mathrm{i}}\int_{\gamma-\mathrm{i}\infty}^{\gamma+\mathrm{i}\infty} \mathrm{i}\,\mathrm{d}y\,\mathrm{e}^{(\gamma+\mathrm{i}y)x}\int_0^{\infty} \mathrm{e}^{-\zeta(\gamma+\mathrm{i}y)} f(\zeta)\,\mathrm{d}\zeta \\
&= \frac{1}{2\pi}\int_0^{\infty} \mathrm{d}\zeta\, f(\zeta)\mathrm{e}^{(x-\zeta)\gamma}\int_{-\infty}^{+\infty} \mathrm{d}y\,\mathrm{e}^{\mathrm{i}y(x-\zeta)} \\
&= \frac{1}{2\pi}\int_0^{\infty} \mathrm{d}\zeta\, f(\zeta)\mathrm{e}^{(x-\zeta)\gamma}\,2\pi\delta(x-\zeta) \qquad (1.198)\\
&= \begin{cases} f(x) & \text{if } x>0 \\ 0 & \text{if } x<0 \\ \frac{1}{2}f(0) & \text{if } x=0 \end{cases} \qquad (1.199)
\end{aligned}
$$

2

Semiclassical Phase Integrals

2.1 Approximation

2.1.1 JWKB Approximation

The semiclassical approximation is also known as the JWKB (or WKB) approximation because it was first developed in quantum mechanics by H. Jeffreys [342], G. Wentzel [595], H.A. Kramers [366], and L. Brillouin [87]. Prior to the advent of quantum mechanics, it was also known as the Green–Liouville method [324]. This approximation corresponds to an expansion in powers of $\hbar$. Consider the one-dimensional time-independent Schrödinger equation (TISE)

$$-\frac{\hbar^2}{2\mu}\frac{\mathrm{d}^2u}{\mathrm{d}x^2} + V(x)u = Eu \tag{2.1}$$

$$\Rightarrow \qquad \frac{\mathrm{d}^2u}{\mathrm{d}x^2} + k^2(x)u = 0 \tag{2.2}$$

where

$$k(x) \equiv \frac{1}{\hbar}\left[2\mu\left(E - V(x)\right)\right]^{1/2} \qquad (V(x) < E) \tag{2.3}$$

or

$$\frac{\mathrm{d}^2u}{\mathrm{d}x^2} - k_1^2(x)u = 0 \tag{2.4}$$

where

$$k_1(x) \equiv \frac{1}{\hbar}\left[2\mu\left(V(x) - E\right)\right]^{1/2} \qquad (V(x) > E) \tag{2.5}$$

With S as action and A as amplitude we put

$$u(x) = A\mathrm{e}^{\mathrm{i}S(x)/\hbar} \tag{2.6}$$

Then

$$\frac{\mathrm{d}^2u}{\mathrm{d}x^2} = A\frac{\mathrm{d}}{\mathrm{d}x}\left[\frac{\mathrm{i}}{\hbar}S'\mathrm{e}^{\mathrm{i}S(x)/\hbar}\right]$$
$$= \frac{\mathrm{i}A}{\hbar}\left\{S'' + \frac{\mathrm{i}}{\hbar}(S')^2\right\}\mathrm{e}^{\mathrm{i}S(x)/\hbar} \tag{2.7}$$

Substituting into (2.1) ⇒

$$\mathrm{i}\hbar\frac{\mathrm{d}^2S}{\mathrm{d}x^2} - \left(\frac{\mathrm{d}S}{\mathrm{d}x}\right)^2 + 2\mu[E - V(x)] = 0 \tag{2.8}$$

Expand S in powers of $\hbar$:

$$S = S_0 + \hbar S_1 + \cdots \qquad \text{(Maclaurin expansion in } \hbar \text{ but note } 1/\hbar \text{ in exponential)} \tag{2.9}$$

The terms independent of $\hbar$ give

$$-\left(\frac{\mathrm{d}S_0}{\mathrm{d}x}\right)^2 + 2\mu[E - V(x)] = 0 \tag{2.10}$$

while the terms of first order in $\hbar$ give

$$\mathrm{i}\frac{\mathrm{d}^2S_0}{\mathrm{d}x^2} - 2\frac{\mathrm{d}S_0}{\mathrm{d}x}\cdot\frac{\mathrm{d}S_1}{\mathrm{d}x} = 0 \tag{2.11}$$

Integrating (2.10) gives

$$S_0(x) = \pm\int_{x_0}^{x}\{2\mu(E - V(s))\}^{1/2}\,\mathrm{d}s$$
$$\equiv \pm\hbar\int_{x_0}^{x}k(s)\mathrm{d}s \tag{2.12}$$

and integrating (2.11) ⇒

$$S_1(x) = \frac{1}{2}\mathrm{i}\ln\left(\frac{\mathrm{d}S_0}{\mathrm{d}x}\right)$$
$$= \frac{1}{2}\mathrm{i}\ln k(x) \tag{2.13}$$

including the arbitrary constant of integration in A of (2.6). Neglecting higher-order terms, it follows from (2.6), (2.9) that

$$u(x) \approx A\mathrm{e}^{\mathrm{i}/\hbar(S_0(x)+\hbar S_1(x))}$$
$$= A\mathrm{e}^{\pm\mathrm{i}\int_{x_0}^{x}k(s)\mathrm{d}s - \frac{1}{2}\ln k(x)}$$
$$= A[k(x)]^{-\frac{1}{2}}\mathrm{e}^{\pm\mathrm{i}\int_{x_0}^{x}k(s)\mathrm{d}s} \qquad (V(x) < E) \tag{2.14}$$

Similarly

$$u(x) = B[k_1(x)]^{-\frac{1}{2}}\mathrm{e}^{\pm\int_{x_0}^{x}k_1(s)\mathrm{d}s} \qquad (V(x) > E) \tag{2.15}$$

where $k^2(x_0) = 0 = k_1^2(x_0) \Rightarrow x_0$ is a turning point. We expect these equations to be valid if $\hbar S_1/S_0$ is small. Equation (2.13) $\Rightarrow$

$$\hbar S_1(x) = \frac{\mathrm{i}\hbar}{2} \ln k(x) = \int_c^x \frac{\frac{\mathrm{i}\hbar}{2} \frac{\mathrm{d}k(s)}{\mathrm{d}s}}{k(s)} \mathrm{d}s \tag{2.16}$$

where $k(c) = 1$.

Equations (2.12) and (2.16) $\Rightarrow$

$$\frac{1}{\hbar}|S_0| \gg |S_1|$$

if

$$\left| \frac{\mathrm{d}k(x)/\mathrm{d}x}{2k^2(x)} \right| \ll 1 \tag{2.17}$$

The local de Broglie wavelength λ is $2\pi/k$; thus we may write this condition as

$$\frac{\lambda}{4\pi} \frac{1}{k} \left| \frac{\mathrm{d}k}{\mathrm{d}x} \right| \ll 1 \tag{2.18}$$

Hence the fractional change in k over the distance $\lambda/4\pi$ should be small. This is a small-wavelength or *high-frequency* approximation. In reality this is the inverse of perturbation theory, that is, the basic quantity is large rather than small.

At the turning point(s) of the classical motion where

$$V(x_0) = E \tag{2.19}$$

we see that k (and k_1) vanishes and so condition (2.18) is violated, to the extent that the left-hand side $= +\infty$ ($k'(x_0) \neq 0$). Thus the approximation is valid only several wave-lengths away from the turning point and so is termed an *asymptotic approximation*. Because this approximation is based on the assumption that the higher-order terms in $\hbar$ are negligible, it is a *semiclassical* approximation ($\hbar \to 0$ in classical limit).

We now consider the solution near a linear turning point as indicated in Figure 2.1.

With $V(x_0) = E$,

$$\begin{aligned} V(x) &< E \qquad (x > 0) \\ V(x) &> E \qquad (x < 0) \\ V(x) &= E - Fx \qquad (F > 0) \end{aligned}$$

Define

$$\xi_1(x) = \int_x^0 k_1(s)\,\mathrm{d}s\,, \qquad \xi(x) = \int_0^x k(s)\,\mathrm{d}s \tag{2.20}$$

$$(x < 0) \Rightarrow \mathrm{d}s > 0 \qquad (x > 0) \Rightarrow \mathrm{d}s > 0$$

Region 1 Region 2

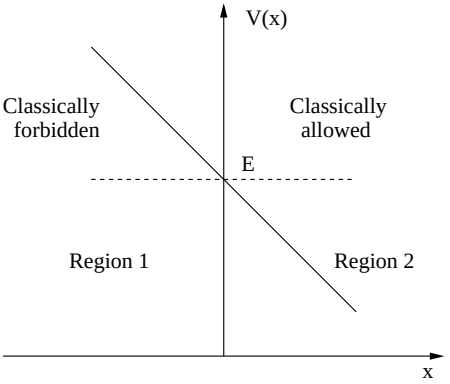

Fig. 2.1. Classical turning point

Both $\xi_1(x)$ and $\xi(x)$ increase as we move away from the turning point. The time independent Schrödinger equations (2.2) and (2.4) can then be solved in each of the two regions, namely

$$u^{\pm}(x) = A_{\pm}\xi^{1/2}(x)k^{-1/2}(x)J_{\pm 1/3}(\xi) \qquad (x > 0) \tag{2.21}$$

$$u_1^{\pm}(x) = B_{\pm}\xi_1^{1/2}(x)k_1^{-1/2}(x)I_{\pm 1/3}(\xi_1) \qquad (x < 0) \tag{2.22}$$

where $J_n(z)$ is a regular Bessel function ([1], Chapter 11) (of the first kind), satisfying

$$\frac{\mathrm{d}^2y}{\mathrm{d}z^2} + \frac{1}{z}\frac{\mathrm{d}y}{\mathrm{d}z} + \left(1 - \frac{n^2}{z^2}\right)y = 0 \tag{2.23}$$

and $I_n(z)$ is a modified Bessel function, given by

$$I_n(z) = \mathrm{i}^{-n}J_n(\mathrm{i}z) \tag{2.24}$$

2.1.2 Gans–Jeffreys Asymptotic Connection Formula

By using the known behaviour of $J_{\pm 1/3}(x)$ and $I_{\pm 1/3}(x)$ as $|x| \to 0$ and as $|x| \to \infty$ ([1], Chapter 10) we may obtain the following connection formulae as follows: consistent with Figure 2.1, with $\gamma = \sqrt{2\mu F}$ we have

$$\frac{\mathrm{d}^2u}{\mathrm{d}x^2} + \gamma^2 xu = 0 \qquad (-\infty < x < +\infty) \tag{2.25}$$

Using a Fourier transform, we deduce that

$$u(+\infty) = (2\pi)^{-1}\gamma^{-2/3}\int_{-\infty}^{+\infty} \mathrm{d}p \exp\left[\mathrm{i}\left(\frac{p^3}{3\gamma^2} - px\right)\right] \tag{2.26}$$

$$\equiv Ai(-\gamma^{2/3}x) \tag{2.27}$$

$$= \begin{cases} \frac{1}{3}\gamma^{1/3}x^{1/2}\left[J_{1/3}\left(\frac{2}{3}\gamma x^{3/2}\right) + J_{-1/3}\left(\frac{2}{3}\gamma x^{3/2}\right)\right] & (x \geq 0) \\ \frac{1}{3}\gamma^{1/3}(-x)^{1/2}\left[I_{-1/3}\left(\frac{2}{3}\gamma(-x)^{3/2}\right) - I_{+1/3}\left(\frac{2}{3}\gamma(-x)^{3/2}\right)\right] & (x \leq 0) \end{cases} \tag{2.28}$$

$$\simeq \begin{cases} \pi^{-1/2}\gamma^{-1/6}x^{-1/4}\sin\left(\frac{2}{3}\gamma x^{3/2} + \frac{\pi}{4}\right) & (x \gg 1) \\ \frac{1}{2}\pi^{-1/2}\gamma^{-1/6}(-x)^{-1/4}\exp\left(-\frac{2\gamma}{3}(-x)^{3/2}\right) & (x \ll -1) \end{cases} \tag{2.29}$$

$$\begin{matrix} \frac{1}{2}k_1^{-1/2}\mathrm{e}^{-\xi_1} \\ (x<0) \end{matrix} \longrightarrow \begin{matrix} k^{-1/2}\sin\left(\xi + \frac{\pi}{4}\right) \\ (x>0) \end{matrix} \tag{2.30}$$

and similarly

$$\begin{matrix} k_1^{-1/2}\mathrm{e}^{\xi_1} \\ (x<0) \end{matrix} \longleftarrow \begin{matrix} k^{-1/2}\sin\left(\xi - \frac{\pi}{4}\right) \\ (x>0) \end{matrix} \tag{2.31}$$

We note in (2.30) that the arrow must point from $x < 0$ to $x > 0$ and *not* from $x > 0$ to $x < 0$, since a small error in the phase of the sine will introduce an e^{ξ_1} component in the solution for $x < 0$, which "blows up," i.e., tends to infinity as $x \to -\infty$. In a similar way in (2.31) the arrow must point in the other direction since a small unobservable component of $\mathrm{e}^{-\xi_1}$, as $x \to -\infty$, will modify the phase of the sine by a significant amount.

One problem with the derivation of (2.26) is that as $x \to +\infty$, $u(x)$ suffers an infinite oscillatory divergence, which is assumed to average out at zero. Also by our choice of Figure 2.1, the quantally allowed region lies to the right and the classically forbidden region to the left. In [324] for instance, the reverse is true. Our choice is more natural because, for the radial coordinate $r \in [0, +\infty]$, the classically forbidden region will always lie to the left for continuum states where two aggregate particles will separate infinitely (r is the positive distance between two particles, by definition of spherical polar coordinates).

A more convincing[1] treatment, tracing the solutions around the complex x-plane, across Stokes lines and avoiding the turning point, is given later. The critical aspect of the Stokes phenomenon is that the coefficient of the exponentially subdominant solution suffers an abrupt change in crossing a Stokes line, that is, in the presence of a nonzero exponentially dominant solution.

2.2 Phase Integrals

2.2.1 Stokes Phenomenon: One Transition Point

From (2.14) and (2.15), we have

[1] After all, it appears, perhaps incorrectly, that the Gans–Jeffreys derivation relates only to the linear potential of Figure 2.1. In fact, as we shall see, the only necessary condition is the existence of a simple transition/turning point.

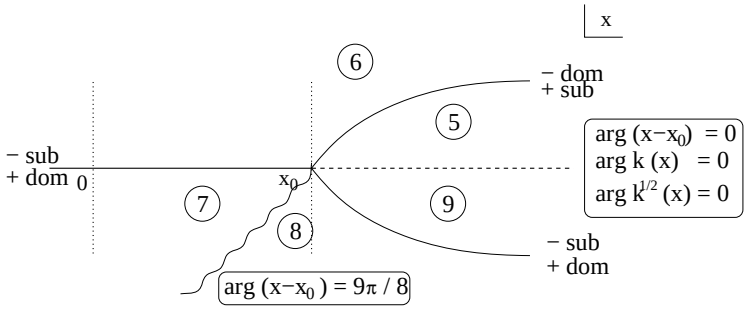

Fig. 2.2. Complex x-plane for the one-transition-point problem

$$u(x) \underset{x \gtrsim x_0}{\simeq} k^{-1/2}(x)\left[A\mathrm{e}^{\mathrm{i}\int_{x_0}^{x} k(s)\,\mathrm{d}s} + B\mathrm{e}^{-\mathrm{i}\int_{x_0}^{x} k(s)\,\mathrm{d}s}\right] \tag{2.32}$$

Similarly

$$u(x) \underset{x \lesssim x_0}{\simeq} k_1^{-1/2}(x)\left[C\mathrm{e}^{\int_{x}^{x_0} k_1(s)\,\mathrm{d}s} + D\mathrm{e}^{-\int_{x}^{x_0} k_1(s)\,\mathrm{d}s}\right] \tag{2.33}$$

These asymptotic formulae have branch-point singularities at x_0 at which u becomes infinite. Of course $x = \infty$ is an essential singularity in all collision problems ($E > 0$).

Expressions on the right-hand side of (2.32) and (2.33) may be termed phase integrals because they are of the form $\exp(\mathrm{i}\theta)$ where θ is expressed as an integral and 'phase' is another word for "angle in radians".

Heavy lines are Stokes lines on which phase integrals are exponentially dominant or subdominant. They emanate from a simple zero at $\pi/3$, π, $-\pi/3\,(= 5\pi/3)$. The Stokes phenomenon may be described as follows. As a Stokes line is crossed, the coefficient of the subdominant solution suffers an abrupt change in order to emerge on the next anti-Stokes line with the appropriate coefficient, required for the next domain in which it is again dominant. The abrupt change is parameterized by the Stokes constant times the coefficient of the dominant term. Thus, we have, with b the unique (by symmetry) positive-direction Stokes constant: in Figure 2.2

$$\text{Region 5}: \quad u \simeq k^{-1/2}\left[A\exp(\mathrm{i}\int_{x_0}^{x} k\,\mathrm{d}s) + B\exp(-\mathrm{i}\int_{x_0}^{x} k\,\mathrm{d}s)\right] \tag{2.34}$$

$$\text{Region 6}: \quad u \simeq k^{-1/2}\left[(A+bB)\exp(\mathrm{i}\int_{x_0}^{x} k\,\mathrm{d}s) + B\exp(-\mathrm{i}\int_{x_0}^{x} k\,\mathrm{d}s)\right] \tag{2.35}$$

$$\text{Region 7}: \quad u \simeq k^{-1/2}\left[(A+bB)\exp(\mathrm{i}\int_{x_0}^{x} k\,\mathrm{d}s) + \{b(A+bB)+B\}\exp(-\mathrm{i}\int_{x_0}^{x} k\,\mathrm{d}s)\right] \tag{2.36}$$

$$\text{Region 8}: \quad u \simeq -\mathrm{i}k^{-1/2}\left[\{b(A+bB)+B\}\exp(\mathrm{i}\int_{x_0}^{x} k\,\mathrm{d}s) + (A+bB)\exp(-\mathrm{i}\int_{x_0}^{x} k\,\mathrm{d}s)\right] \tag{2.37}$$

$$\text{Region 9}: \quad u \simeq -\mathrm{i}k^{-1/2}\left[\{bA+(1+b^2)B\}\exp(\mathrm{i}\int_{x_0}^{x} k\,\mathrm{d}s) + \{A+bB+b\{bA+(1+b^2)B\}\}\exp(-\mathrm{i}\int_{x_0}^{x} k\,\mathrm{d}s)\right] \tag{2.38}$$

Analyticity (which follows from ascending Frobenius series solutions to equation (2.2) in powers of $(x - x_0)$), (2.34) and (2.38) imply

$$b = \mathrm{i} \tag{2.39}$$

A purely subdominant solution on the π Stokes line requires

$$A + bB = 0 \tag{2.40}$$

Setting

$$A = \frac{c}{2}\exp\left(-\frac{\pi\mathrm{i}}{4}\right), \qquad B = \frac{c}{2}\exp\left(\frac{\pi\mathrm{i}}{4}\right) \tag{2.41}$$

gives the Jeffreys' connection formula

$$\frac{c}{2}|\nu|^{-1/2}\exp\left(-\int_{x}^{x_0}|\nu|\,\mathrm{d}s\right) \longrightarrow c\nu^{-1/2}\sin\left[\int_{x_0}^{x}\nu\,\mathrm{d}s + \frac{\pi}{4}\right] \tag{2.42}$$

where we have avoided the no-go area around/near x_0. The ubiquitous $\pi/4$ is thus half the phase of b, the positive Stokes constant.

As stated in [160], it appeared to Budden [100], [101] that Furry [287] was the first author to have treated the idea of the Stokes phenomenon seriously and to have derived the Stokes constants and hence the Jeffreys' connection formula for the one-transition-point problem, by analyticity arguments. However, Stueckelberg [574] not only preceded Furry in this respect by fifteen years but also made an outstanding contribution to the solution of what is essentially a four-transition-point problem. It may be noted that, in particular, Furry's treatment is blurred because he does not specify the location of the branch cut for $k^{1/2}(x)$.

Bohr–Sommerfeld Quantization Rule

Two turning points are given by

$$V(x_1) = E = V(x_2) \tag{2.43}$$

$$\Rightarrow \qquad V(x) > E \qquad (x < x_1 \text{ and } x > x_2) \tag{2.44}$$

$$V(x) < E \qquad (x_1 < x < x_2) \tag{2.45}$$

Concerning the x_1 turning point

$$x > x_1 \Rightarrow (\text{ see (2.35)}) \quad u(x) = Ak^{-1/2} \sin\left(\int_{x_1}^{x} k(s)\,\mathrm{d}s + \frac{\pi}{4}\right) \tag{2.46}$$

where

$$k(s) \equiv \frac{1}{\hbar}\left[2\mu(E - V(s))\right]^{1/2} \tag{2.47}$$

Concerning the x_2 turning point

$$x < x_2 \Rightarrow \quad u(x) = A'k^{-1/2} \sin\left(\int_{x}^{x_2} k(s)\,\mathrm{d}s + \frac{\pi}{4}\right) \tag{2.48}$$

such that as x decreases, the integral term increases. It follows from (2.46), (2.48) that the wave function has the following form:

$$\begin{aligned} u(x) &= -A'k^{-1/2} \sin\left[\int_{x_2}^{x} k(s)\,\mathrm{d}s - \frac{\pi}{4}\right] \\ &= -A'k^{-1/2} \sin\left[\int_{x_1}^{x} k(s)\,\mathrm{d}s - \frac{\pi}{4} - \eta\right] \end{aligned} \tag{2.49}$$

where

$$\eta \equiv \int_{x_1}^{x_2} k(x)\,\mathrm{d}x \tag{2.50}$$

The solutions given by (2.46), (2.49) connect smoothly if $A' = (-1)^{n+1}A$ and $\eta = n\pi + \pi/2$ where $n = 0, 1, 2, \ldots$ Thus we obtain

$$\int_{x_1}^{x_2} k(x)\,\mathrm{d}x = (n + \frac{1}{2})\pi \tag{2.51}$$

which can be written as ($p = \hbar k$)

$$\int_{x_1}^{x_2} \left[2\mu(E - V(x))\right]^{1/2} \mathrm{d}x = (n + \frac{1}{2})\hbar\pi \tag{2.52}$$

($\hbar = h/2\pi = 1$ in atomic units), and determines the energy eigenvalue E_n. Since the linear momentum is given by

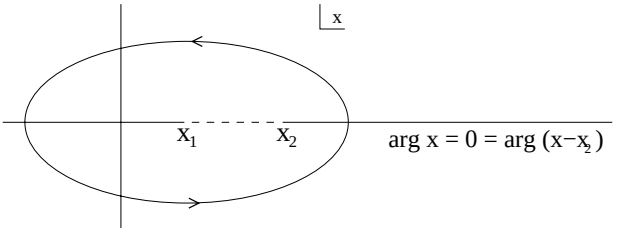

Fig. 2.3. Path of phase integral of (2.54) in complex x-plane

$$p = [2\mu(E - V(x))]^{1/2} \tag{2.53}$$

a classical expression, (2.52) can be written as

$$\frac{1}{2}\oint^{(x_1+,x_2+)} p\,\mathrm{d}x = \frac{1}{2}\left[\int_{x_1}^{x_2} p\,\mathrm{d}x + \int_{x_2}^{x_1} \mathrm{e}^{\mathrm{i}\pi} p\,\mathrm{d}x\right]$$
$$= \int_{x_1}^{x_2} p\,\mathrm{d}x = (n + \frac{1}{2})\hbar\pi \qquad (n = 0, 1, 2, \ldots) \tag{2.54}$$

where the left-hand side is an integral over the complete cycle $x_1 \rightarrow x_2 \rightarrow x_1$. Equation (2.54) is known as the *Bohr–Sommerfeld quantization rule*. Wide-ranging discussions of one-dimensional semiclassical elastic scattering are given by Mott and Massey [443], Brink [88], and Flannery [271].

The cases that arise when (2.41) is not fulfilled are considered by Nakamura [447] and by Coveney et al. [152].

2.2.2 Application of JWKB to Coupled Wave Equations

Introduction

The semiclassical treatment of atom-atom collisions involving electronic transitions is discussed in [40]. As is well known, difficulties occur if the classical trajectories associated with the various states of importance in a collision process differ significantly. A method designed to overcome these is described. It will be referred to as the *forced-common-turning-point method*. The four coupled first-order differential equations that describe the new version of the semiclassical two-state treatment for an atom-atom collision may be reduced to a pair of generalized impact parameter equations.

The first Born approximation to the cross section obtained from the straightforward semiclassical treatment differs from the corresponding cross section obtained from the full quantal treatment mainly in that it contains an anomalous multiplying factor equal to the ratio of the initial to the final velocity of relative motion. This anomaly does not come up with the forced-common-turning-point method.

A model collision process that provides a very searching test is considered. Only two states are included. The initial interaction is zero, the final interaction is Coulombic, and the transition matrix element is exponential. Curve-crossing may occur. The

distorted-wave approximation to the excitation cross section may be found exactly and may also be computed using the forced-common-turning-point method. There is remarkable accord between the results. Thus, in a case where the reduced mass of the colliding systems is 2 on the chemical scale, where the excitation energy is 3.4 eV, and where the incident kinetic energy of relative motion is only 0.85 eV above this, the excitation cross sections obtained differ by as little as 0.01%; moreover, the patterns of the contributions to the cross sections from the separate partial waves are similar.

As was first pointed out by Mott [442] the theory of collisions between atomic systems is greatly simplified by the assumption that the nuclei move like classical particles. This assumption leads immediately to the impact parameter treatment. It was made by Landau [376] and by Zener [611] in their research on the effect of pseudo-crossings of potential energy surfaces. Stueckelberg [574] carried through a much more elaborate analysis in which he described the motion of the nuclei by an expansion in powers of Planck's constant, that is semiclassically (cf. [443] p.351). The semiclassical treatment based on the JWKB or eikonal approximation has received much attention [42], [307], [156], [601], [111]. It is more powerful than the closely related impact parameter treatment.

There remains a general collision problem that has not yet been satisfactorily solved by either treatment: the problem of how to carry out calculations if the classical trajectories in the initial and final states differ markedly.

A possible approach in the distorted-wave approximation is to use semiclassical wave functions in the transition matrix element occurring in the formula for the cross section ([43] [443] p. 354). The behaviour near the classical turning points in the initial and final states, at r_0 and r_1 respectively, causes difficulty. Since the amplitude of a wave function diminishes rapidly as the penetration into the classically forbidden region is increased, it has been suggested that the region within r_m, the greater of r_0 and r_1, contributes little to the transition matrix element and may be neglected. Because of the highly oscillatory nature of the integrand, such neglect is in fact unjustified and, as we have verified by detailed computations, may give rise to serious error. A less crude procedure is needed. Preferably it should not be limited to the distorted-wave approximation but should be widely applicabile.

With this in mind we consider the equations arising in the quantal partial-wave cross section analysis. In order to avoid irrelevant complications, we shall take explicit account of only the initial and final states. Allowance may readily be made for other states, provided the associated classical trajectories are effectively the same as either the initial- or final-state classical trajectories. The restriction is of little practical importance since the classical trajectories do not differ significantly except at very low velocities of relative motion, unless the Coulomb parts of the interaction between the colliding systems for the states concerned differ.

We proceed by modifying the pair of coupled equations so that the classical turning points coincide. Using the one-dimensional JWKB approximation, as Bates and Holt [42] used the three-dimensional JWKB approximation we solve the modified equations accurately both by an elementary method and with the aid of the Green function. As a check we consider a problem that is exactly solvable in the distorted-

wave approximation and demonstrate that in this case the artifice of forcing a common turning point is remarkably successful.

Two-State Approximation in Wave Treatment

For reference purposes we briefly recall the wave treatment (cf. [443] p. 347).

Denoting the reduced mass of the colliding systems by M and the interaction between them by V, write

$$U \equiv 2MV/\hbar^2 \tag{2.55}$$

and represent the matrix elements of this with respect to the electronic wave functions by the same symbol with subscripts affixed to indicate the states. On the two-state approximation the lth partial cross section Q_l^{01} for transitions from the initial state 0 to the final state 1 is determined by the proper solution to the coupled equations

$$\left(\tfrac{\mathrm{d}^2}{\mathrm{d}r^2} + K_{0l}^2(r) + \tfrac{1}{4r^2}\right) G_{0l} = U_{01} G_{1l} \tag{2.56}$$

and

$$\left(\tfrac{\mathrm{d}^2}{\mathrm{d}r^2} + K_{1l}^2(r) + \tfrac{1}{4r^2}\right) G_{1l} = U_{10} G_{0l} \tag{2.57}$$

where $k(r)$ of Section 2.1 is generalized to $K_{jl}(r)$ $(j = 0, 1)$ given by

$$K_{jl}^2(r) = k_j^2(\infty) - U_{jj}(r) - \frac{(l+\frac{1}{2})^2}{r^2} \equiv k_j^2(r) - \frac{(l+\frac{1}{2})^2}{r^2} \qquad (j \equiv 0, 1) \tag{2.58}$$

in which

$$k_j(r) = Mv_j(r)/\hbar \tag{2.59}$$

$v_j(r)$ being the magnitude of the classical speed of relative motion at separation r in state j. The boundary conditions to be satisfied are

$$\left.\begin{aligned} G_{0l}(0) &= G_{1l}(0) = 0 \\ G_{0l}(r) &\underset{r\to\infty}{\simeq} \mathrm{i}^l \sin\{k_0(\infty)r - \tfrac{1}{2}l\pi\} + \alpha_l \exp\{\mathrm{i}k_0(\infty)r\} \\ G_{1l}(r) &\underset{r\to\infty}{\simeq} \beta_l \exp\{\mathrm{i}k_1(\infty)r\} \end{aligned}\right\} \tag{2.60}$$

where α_l and β_l are constants. The partial elastic and inelastic cross sections are related to the values of these constants: in particular

$$Q_l^{01} = \frac{4\pi k_1(\infty)(2l+1)|\beta_l|^2}{k_0^3(\infty)} \tag{2.61}$$

Semiclassical Treatment

Following Langer [378] we replace $l(l+1)$ in (2.56) and (2.57) by $(l+1/2)^2$ to get

$$\left(\frac{\mathrm{d}^2}{\mathrm{d}r^2} + K_{0l}^2(r)\right) G_{0l} = U_{0l} G_{0l} \tag{2.62}$$

$$\left(\frac{\mathrm{d}^2}{\mathrm{d}r^2} + K_{1l}^2(r)\right) G_{1l} = U_{10} G_{0l} \tag{2.63}$$

To force a common turning point we take

$$K_{jl}^2(r) = k_j^2(r)\left\{1 - \frac{(l+\frac{1}{2})^2}{r^2 k_0(r) k_1(r)}\right\} \tag{2.64}$$

except that where the difference, $K_{0l}^2(r) - K_{1l}^2(r)$, occurs we use the exact value, the results being very sensitive to the magnitude of this difference.

We seek solutions to (2.62) and (2.63) in the form

$$G_{jl} = \alpha_{jl}^{+} S_{jl}^{+} + \alpha_{jl}^{-} S_{jl}^{-} \qquad (j = 0, 1) \tag{2.65}$$

where $\alpha_{jl}^{\pm}$ are slowly varying functions of r and where

$$S_{jl}^{\pm} \equiv K_{jl}^{-\frac{1}{2}} \exp \pm \mathrm{i}\left\{\frac{1}{4}\pi + \int_R^r K_{jl}(s)\,\mathrm{d}s\right\} \tag{2.66}$$

are JWKB approximations to the solutions of the equations

$$\left(\frac{\mathrm{d}^2}{\mathrm{d}r^2} + K_{jl}^2(r)\right) F_{jl} = 0 \tag{2.67}$$

which describe the motion in the absence of transitions. The separation R at the turning point is, of course, the greatest positive root of

$$x^2 k_0(x) k_1(x) = (l + \frac{1}{2})^2 \tag{2.68}$$

Substituting (2.65) into (2.62) and (2.63) and ignoring the small terms $\alpha_{jl}^{\pm\prime\prime} S_{jl}^{\pm}$ in which the primes indicate differentiation with respect to r, we obtain

$$2\{\alpha_{0l}^{+\prime} S_{0l}^{+\prime} + \alpha_{0l}^{-\prime} S_{0l}^{-\prime}\} = U_{01}\{\alpha_{1l}^{+} S_{1l}^{+} + \alpha_{1l}^{-} S_{1l}^{-}\} \tag{2.69}$$

and

$$2\{\alpha_{1l}^{+\prime} S_{1l}^{+\prime} + \alpha_{1l}^{-\prime} S_{1l}^{-\prime}\} = U_{10}\{\alpha_{0l}^{+} S_{0l}^{+} + \alpha_{0l}^{-} S_{0l}^{-}\} \tag{2.70}$$

Solutions to these that meet the requirement of being slowly varying functions of r may be derived from

$$2\alpha_{0l}^{\pm\prime} S_{0l}^{\pm\prime} = U_{01}\alpha_{1l}^{+} S_{1l}^{+} + \alpha_{1l}^{\pm} S_{1l}^{\pm} \tag{2.71}$$

and

$$2\alpha_{1l}^{\pm\prime} S_{1l}^{\pm\prime} = U_{10}\alpha_{0l}^{+} S_{0l}^{+} + \alpha_{0l}^{\pm} S_{0l}^{\pm} \tag{2.72}$$

Taking

$$S_{jl}^{\pm\prime} S_{jl}^{\mp} \simeq \pm \mathrm{i} \tag{2.73}$$

we reduce (2.71) and (2.72) to

$$\pm 2\mathrm{i}K_{0l}^{\frac{1}{2}}K_{1l}^{\frac{1}{2}}\alpha_{0l}^{\pm\prime} = U_{01}\alpha_{1l}^{\pm}\exp\{\mp\mathrm{i}\mu_l\} \tag{2.74}$$

and

$$\pm 2\mathrm{i}K_{0l}^{\frac{1}{2}}K_{1l}^{\frac{1}{2}}\alpha_{1l}^{\pm\prime} = U_{10}\alpha_{0l}^{\pm}\exp\{\pm\mathrm{i}\mu_l\} \tag{2.75}$$

where

$$\mu_l = \int_R^r (K_{0l}(s) - K_{1l}(s))\,\mathrm{d}s \tag{2.76}$$

The boundary conditions are

$$\alpha_{0l}^{-}(\infty) = \frac{1}{2}k_0^{\frac{1}{2}}(\infty)\,, \qquad \alpha_{1l}^{-}(\infty) = 0 \tag{2.77}$$

and from the JWKB connection formula

$$\alpha_{jl}^{+}(R) + \alpha_{jl}^{-}(R) = 0 \qquad (j = 0, 1) \tag{2.78}$$

Referring to equation (2.61) we see that the partial cross sections are

$$Q_l^{01} = \frac{4\pi(2l+1)}{k_0^3(\infty)}|\alpha_{1l}^{+}(\infty)|^2 \tag{2.79}$$

The total excitation cross section is

$$Q^{01} = \sum_{l=0}^{\infty} Q_l^{01} \tag{2.80}$$

Great simplification may be effected in (2.74) and (2.75) without further approximation. Changing the independent and dummy variables from r and s to

$$|z| = \int_R^r \left\{1 - \frac{(l+\frac{1}{2})^2}{t^2k_0(t)k_1(t)}\right\}^{-\frac{1}{2}} \mathrm{d}t\,, \quad |\zeta| = \int_R^s \left\{1 - \frac{(l+\frac{1}{2})^2}{t^2k_0(t)k_1(t)}\right\}^{-\frac{1}{2}} \mathrm{d}t \tag{2.81}$$

we obtain

$$\pm 2\mathrm{i}k_0^{\frac{1}{2}}(r)k_1^{\frac{1}{2}}(r)\frac{\mathrm{d}\alpha_{0l}^{\pm}}{\mathrm{d}|z|} = U_{01}\alpha_{1l}^{\pm}\exp\{\mp\mathrm{i}\mu_l\} \tag{2.82}$$

$$\pm 2\mathrm{i}k_0^{\frac{1}{2}}(r)k_1^{\frac{1}{2}}(r)\frac{\mathrm{d}\alpha_{1l}^{\pm}}{\mathrm{d}|z|} = U_{10}\alpha_{0l}^{\pm}\exp\{\pm\mathrm{i}\mu_l\} \tag{2.83}$$

$$\mu_l = \int_0^{|z|} \{k_0(s) - k_1(s)\}\,\mathrm{d}|\zeta| \tag{2.84}$$

Introducing coefficients $c_{jl}(z)$ and functions $\nu_l(z)$ that are defined over the complete range of z by

$$\left.\begin{aligned} c_{jl}(z) &\equiv \alpha_{jl}^{+}(|z|)\,, & \nu_l(z) &\equiv \mu_l(|z|), & (z \geq 0)\\ &\equiv -\alpha_{jl}^{-}(|z|)\,, & &\equiv -\mu_l(|z|), & (z \leq 0) \end{aligned}\right\} \tag{2.85}$$

we reduce the four equations of (2.82) and (2.83) to the two impact-parameter-type equations

$$\mathrm{i}\frac{\mathrm{d}c_{0l}}{\mathrm{d}z} = \frac{U_{01}(r)}{2k_0^{\frac{1}{2}}(r)k_1^{\frac{1}{2}}(r)}c_{1l}\exp(-\mathrm{i}\nu_l(z)) \tag{2.86}$$

and

$$\mathrm{i}\frac{\mathrm{d}c_{1l}}{\mathrm{d}z} = \frac{U_{10}(r)}{2k_0^{\frac{1}{2}}(r)k_1^{\frac{1}{2}}(r)}c_{0l}\exp(\mathrm{i}\nu_l(z)) \tag{2.87}$$

If we take the boundary conditions to be

$$c_{0l}(-\infty) = 1\,, \qquad c_{1l}(-\infty) = 0 \tag{2.88}$$

we see that formula (2.79) for the partial cross section is replaced by

$$Q_l^{01} = \frac{(2l+1)\pi}{k_0^2(\infty)}|c_{1l}(+\infty)|^2 \tag{2.89}$$

It may be noted in parentheses that the variable z has a simple interpretation in the special case where

$$k_0^2(\infty) = k_1^2(\infty) \quad \text{and} \quad U_{00}(r) = U_{11}(r) \tag{2.90}$$

so that the initial and final classical trajectories are identical. Omitting the subscripts as unnecessary and introducing the impact parameter

$$\rho = (l + \frac{1}{2})/k(\infty) \tag{2.91}$$

we see from (2.81) that

$$\mathrm{d}z = \mathrm{d}r \Big/ \left(1 - \frac{\rho^2 k^2(\infty)}{r^2 k^2(r)}\right)^{\frac{1}{2}} \tag{2.92}$$

which is just an element of length along the common trajectory. The difference between equations (2.86) and (2.87) and the corresponding pair of equations for the case of a common rectilinear trajectory (cf. Bates [35]) is therefore as would be expected physically.

Semiclassical Treatment by Green Function Formalism

In general, if

$$U_{jj}(r) \underset{r\to\infty}{\simeq} -2\lambda_j M/r \tag{2.93}$$

then the boundary conditions on the radial wave functions must be generalized to

$$G_{0l}(r) \underset{r\to\infty}{\simeq} \mathrm{i}^l \sin\left[k_0(\infty)r - \frac{l\pi}{2} + \arg\Gamma\left(l+1-\frac{\mathrm{i}\lambda_0}{\nu_0(\infty)}\right) + \frac{\lambda_0}{\nu_0(\infty)}\ln(2k_0(\infty)r)\right] \mathrm{e}^{\mathrm{i}\arg\Gamma(l+1-\mathrm{i}\lambda_0/\nu_0(\infty))} + \alpha_l \exp\left[\mathrm{i}k_0(\infty)r + 2\mathrm{i}\arg\Gamma\left(l+1-\frac{\mathrm{i}\lambda_0}{\nu_0(\infty)}\right) + \frac{\mathrm{i}\lambda_0}{\nu_0(\infty)}\ln(2k_0(\infty)r)\right] \tag{2.94}$$

$$G_{1l}(r) \underset{r\to\infty}{\simeq} \beta_l \exp\left[\mathrm{i}k_0(\infty)r + \mathrm{i}\arg\Gamma\left(l+1-\frac{\mathrm{i}\lambda_1}{\nu_1(\infty)}\right) + \mathrm{i}\arg\Gamma\left(l+1-\frac{\mathrm{i}\lambda_0}{\nu_1(\infty)}\right) + \frac{\mathrm{i}\lambda_1}{\nu_1(\infty)}\ln(2k_1(\infty)r)\right] \tag{2.95}$$

We introduce outgoing Green functions $\mathcal{G}_{jl}$ defined by

$$\mathcal{G}_{jl}(r,r') \equiv \frac{1}{2}\mathrm{i}S^+_{jl}(r_>)[S^+_{jl}(r_<) - S^-_{jl}(r_<)] \tag{2.96}$$

where

$$\left(\frac{\mathrm{d}^2}{\mathrm{d}r^2} + K^2_{jl}(r) + \frac{1}{4r^2}\right) S^\pm_{jl}(r) = 0 \tag{2.97}$$

$$S^\pm_{jl}(r) \underset{r\to\infty}{\simeq} k_j^{-\frac{1}{2}}(\infty)\exp\left[\pm\mathrm{i}\left\{k_j(\infty)r + \eta_{jl} - \frac{1}{2}l\pi + \arg\Gamma\left(l+1-\frac{\mathrm{i}\lambda_j}{\nu_j(\infty)}\right) + \frac{\lambda_j}{\nu_j(\infty)}\ln(2k_j(\infty)r)\right\}\right] \tag{2.98}$$

and

$$r_\lessgtr = \begin{matrix}\min\\ \max\end{matrix}(r,r')$$

It is easy to show that

$$\sin\eta_{jl} = \int_0^\infty \left[U_{jj}(r) + \frac{2\lambda_j}{r}M\right](S^+_{jl} - S^-_{jl})\mathrm{i}\exp(-\mathrm{i}k_j(\infty)r \times \frac{(2k_j(\infty)r)^{l+1})}{k_j^{\frac{1}{2}}(\infty)(2l+1)!}\Gamma\left(l+1+\frac{\mathrm{i}\lambda_j}{\nu_j(\infty)}\right)\exp\left(\frac{\pi\lambda_j}{2\nu_j(\infty)}\right) \times {}_1F_1\left(l+1+\frac{\mathrm{i}\lambda_j}{\nu_j(\infty)}; 2l+2; 2\mathrm{i}k_j(\infty)r\right)\mathrm{d}r \tag{2.99}$$

However, it is not normally necessary to calculate η_{jl} explicitly. It follows that

$$\left(\frac{\mathrm{d}^2}{\mathrm{d}r^2} + K_{jl}^2(r) + \frac{1}{4r^2}\right)\mathcal{G}_{jl}(r,r') = \delta(r-r') \tag{2.100}$$

where δ is the Dirac delta function. Integration by parts of (2.56), (2.57), and (2.100) suitably premultiplied yields the coupled integral equations:

$$G_{0l}(r) = \frac{\mathrm{i}^l k_0^{\frac{1}{2}}(\infty)\exp(\mathrm{i}\eta_{0l})}{2\mathrm{i}}(S_{0l}^+(r) - S_{0l}^-(r)) + \int_0^\infty U_{01}(r')G_{1l}(r')\mathcal{G}_{0l}(r,r')\mathrm{d}r' \tag{2.101}$$

$$G_{1l}(r) = + \int_0^\infty U_{10}(r')G_{0l}(r')\mathcal{G}_{1l}(r,r')\mathrm{d}r' \tag{2.102}$$

Substitution of (2.96) into (2.101) and (2.102), together with definition (2.65), leads without loss of generality to the four coupled integral equations:

$$\begin{aligned}\alpha_{0l}^+(r) = {} & \frac{1}{2}\mathrm{i}^{l-1}k_0^{\frac{1}{2}}(\infty)\exp(\mathrm{i}\eta_{0l}) + \frac{1}{2}\mathrm{i}\int_0^\infty U_{01}(r')G_{1l}(r')S_{0l}^+(r')\,\mathrm{d}r' \\ & - \frac{1}{2}\mathrm{i}\int_0^r U_{01}(r')G_{1l}(r')S_{0l}^-(r')\,\mathrm{d}r'\end{aligned} \tag{2.103}$$

$$-\alpha_{0l}^-(r) = \frac{1}{2}\mathrm{i}^{l-1}k_0^{\frac{1}{2}}(\infty)\exp(\mathrm{i}\eta_{0l}) + \frac{1}{2}\mathrm{i}\int_r^\infty U_{01}(r')G_{1l}(r')S_{0l}^+(r')\,\mathrm{d}r' \tag{2.104}$$

$$\alpha_{1l}^+(r) = \frac{1}{2}\mathrm{i}\int_0^\infty U_{10}(r')G_{0l}(r')S_{1l}^+(r')\,\mathrm{d}r' - \frac{1}{2}\mathrm{i}\int_0^r U_{10}(r')G_{0l}(r')S_{1l}^-(r')\,\mathrm{d}r' \tag{2.105}$$

$$-\alpha_{1l}^-(r) = \frac{1}{2}\mathrm{i}\int_r^\infty U_{10}(r')G_{0l}(r')S_{1l}^+(r')\,\mathrm{d}r' \tag{2.106}$$

Differentiation with respect to r gives four exact first-order coupled differential equations:

$$\alpha_{0l}^{+\prime} = -\frac{1}{2}\mathrm{i}U_{01}S_{0l}^-(\alpha_{1l}^+S_{1l}^+ + \alpha_{1l}^-S_{1l}^-) \tag{2.107}$$

$$\alpha_{0l}^{-\prime} = \frac{1}{2}\mathrm{i}U_{01}S_{0l}^+(\alpha_{1l}^+S_{1l}^+ + \alpha_{1l}^-S_{1l}^-) \tag{2.108}$$

$$\alpha_{1l}^{+\prime} = -\frac{1}{2}\mathrm{i}U_{10}S_{1l}^-(\alpha_{0l}^+S_{0l}^+ + \alpha_{0l}^-S_{0l}^-) \tag{2.109}$$

$$\alpha_{1l}^{-\prime} = \frac{1}{2}\mathrm{i}U_{10}S_{1l}^+(\alpha_{0l}^+S_{0l}^+ + \alpha_{0l}^-S_{0l}^-) \tag{2.110}$$

with

$$\alpha_{0l}^-(\infty) = \frac{1}{2}k_0^{\frac{1}{2}}, \quad \alpha_{1l}^-(\infty) = 0, \quad \alpha_{jl}^+(0) + \alpha_{jl}^-(0) = 0 \quad (j = 0, 1) \tag{2.111}$$

Thus far no approximation has been made and we have reduced two coupled second-order differential equations to four coupled first-order equations by a method that is essentially equivalent to the well-known variation-of-parameters method. We now assume that $\alpha_{jl}^\pm$ are slowly varying functions compared with $S_{jl}^\pm$ and neglect such

terms as $S^-_{jl}S^-_{kl}$ and $S^+_{jl}S^+_{kl}$ in comparison with $S^+_{jl}S^-_{kl}$ on the grounds that oscillatory integrands lead to negligible integrals. This condition will be relaxed in Section 4.5. We thus obtain

$$\alpha^{\pm\prime}_{0l} = \mp\frac{1}{2}\mathrm{i}U_{01}S^{\mp}_{0l}S^{\pm}_{1l}\alpha^{\pm}_{1l} \tag{2.112}$$

$$\alpha^{\pm\prime}_{1l} = \mp\frac{1}{2}\mathrm{i}U_{01}S^{\mp}_{1l}S^{\pm}_{0l}\alpha^{\pm}_{0l} \tag{2.113}$$

where $S^{\pm}_{jl}$ are still the exact functions defined by (2.97) and (2.98). If, however, we now make the semiclassical approximations to $S^{\pm}_{jl}$ given in (2.66) and maintain the exact difference $K^2_{0l}(r)-K^2_{1l}(r)$ as in Section 2.2.2, then we obtain precisely equations (2.74) to (2.78).

Distorted-Wave and Born Approximations

Assuming that the coupling between the initial and final states is weak we may take $c_{0l}(z)$ on the right of (2.87) to be unity. This corresponds to the distorted-wave approximation and leads to

$$\mathrm{i}c_{1l}(+\infty) = \int_{-\infty}^{+\infty} \frac{U_{01}(r)}{2k_0^{\frac{1}{2}}(r)k_1^{\frac{1}{2}}(r)} \exp\{\mathrm{i}\nu_l(z)\}\mathrm{d}z \tag{2.114}$$

$$= \frac{2}{\hbar v_0^{\frac{1}{2}}(\infty)v_1^{\frac{1}{2}}(\infty)} \int_0^{\infty} f(r)V_{10}(r)\cos\{\nu_l(z)\}\mathrm{d}z \tag{2.115}$$

where

$$f(r) = \left[\frac{k_0(\infty)k_1(\infty)}{k_0(r)k_1(r)}\right]^{\frac{1}{2}} \tag{2.116}$$

In the Born approximation $f(r)$ is unity. If ρ_0 and ρ_1 are the impact parameters in the initial and final states then

$$l+\frac{1}{2} = \rho_0 k_0(\infty) = \rho_1 k_1(\infty) \tag{2.117}$$

It is convenient to put

$$\rho_0\rho_1 = \rho^2 \tag{2.118}$$

so that

$$z = \int_{\rho}^{r}\left(1-\frac{\rho^2}{t^2}\right)^{-\frac{1}{2}}\mathrm{d}t = (r^2-\rho^2)^{\frac{1}{2}} \tag{2.119}$$

Formula (2.115) becomes

$$\mathrm{i}c_{1l}(+\infty) = \frac{2}{\hbar v_0^{\frac{1}{2}}(\infty)v_1^{\frac{1}{2}}(\infty)} \int_0^{\infty} V_{10}(r)\cos\left[\frac{2\epsilon_{01}z}{\hbar(v_0(\infty)+v_1(\infty))}\right]\mathrm{d}z \tag{2.120}$$

where ϵ_{01} is the excitation energy. Using (2.89) and replacing the summation over l in (2.80) by an integration we find

$$Q^{01} = \frac{8\pi}{\hbar^2 v_0^2(\infty)} \int_0^\infty \rho \left\{ \int_0^\infty V_{10}(r) \cos\left[\frac{2\epsilon_{01} z}{\hbar(v_0(\infty) + v_1(\infty))} \right] \mathrm{d}z \right\}^2 \mathrm{d}\rho \tag{2.121}$$

This may be rearranged to give

$$Q^{01} = \frac{1}{2\pi\hbar^2 v_0^2(\infty)} \int_{|k_0(\infty)-k_1(\infty)|}^\infty |g(\mathbf{q})|^2 q \, \mathrm{d}q \tag{2.122}$$

where the modulus on the lower limit includes the possibility of deexcitation and where

$$g(\mathbf{q}) = \int \exp(-\mathrm{i}\mathbf{q} \cdot \mathbf{r}) V_{10}(r) \mathrm{d}^3\mathbf{r} \tag{2.123}$$

a summation or average over states differing only in magnetic quantum number being assumed [158]. The corresponding formula obtained from the straightforward semiclassical treatment [42] differs from (2.122) by the factor $v_0(\infty)/v_1(\infty)$, while that obtained from the full quantal treatment differs from (2.122) only in that the upper limit to the integration is $k_0(\infty) + k_1(\infty)$ instead of being infinite. The effect of the latter difference is minute unless extremely close to the threshold. This represents a remarkable success for the forced-common-turning-point version of the semiclassical treatment. Indeed it leads to the possibility that the treatment is useful even for electron–atom collisions [47].

An Exact Distorted-Wave Calculation

It is essential to test the efficacy of (2.86) and (2.87) as a general approximation to equations (2.56) and (2.57) when U_{00} and U_{11} are unequal. From a practical point of view this is most easily achieved by investigating the weak-coupling limit, since its application to (2.86) and (2.87) does not obviate the basic underlying assumption of a forced common turning point. In this same limit, equations (2.56) and (2.57) yield the exact distorted-wave formula:

$$|\beta_l|^2 = \frac{k_0(\infty)}{k_1(\infty)} \left| \frac{1}{2} \int_0^\infty U_{10}(S_{0l}^+ - S_{0l}^-)(S_{1l}^+ - S_{1l}^-) \, \mathrm{d}r \right|^2 \tag{2.124}$$

which is most easily obtained by substituting the first term of (2.101) into (2.102).

To be specific we take

$$U_{00}(r) \equiv 0 \tag{2.125}$$

and

$$U_{11}(r) \equiv -2\lambda M/r \tag{2.126}$$

where all quantities are now in atomic units. Except where otherwise specified we shall use these units throughout the remainder of the section.

We have that η_{0l} and η_{1l} are zero,

$$S_{0l}^{+} - S_{0l}^{-} = \mathcal{F}_0(0) \equiv 2\mathrm{i}k_0^{\frac{1}{2}}(\infty) r\, j_l(k_0(\infty)r) \tag{2.127}$$

and
$$S_{1l}^{+} - S_{1l}^{-} = \mathcal{F}_1(\lambda) \tag{2.128}$$

where

$$\mathcal{F}_j(\mu) \equiv \frac{\mathrm{i}\exp\{-\mathrm{i}k_j(\infty)r\}(2k_j(\infty)r)^{l+1}}{k_j^{\frac{1}{2}}(\infty)(2l+1)!}\left|\Gamma\left(l+1+\frac{\mathrm{i}\mu}{v_j(\infty)}\right)\right|\exp\left\{\frac{\pi\mu}{2v_j(\infty)}\right\}$$
$$\times {}_1F_1\left(l+1+\frac{\mathrm{i}\mu}{v_j(\infty)}; 2l+2; 2\mathrm{i}k_j(\infty)r\right) \tag{2.129}$$

In order to obtain an analytical result in closed form, we must first consider the case

$$U_{10}(r) \equiv (2M/r)\mathrm{e}^{-\alpha r} \tag{2.130}$$

so that

$$\beta_l = \frac{2(4k_0(\infty)k_1(\infty))^{l+1} l!\left|\Gamma\left(l+1+\frac{\mathrm{i}\lambda}{v_1(\infty)}\right)\right|\exp\left\{\frac{\pi\lambda}{2v_1(\infty)}\right\}}{v_1(\infty)[2(2l+1)!]^2}$$
$$\times\int_0^\infty \exp\{-(\alpha+\mathrm{i}k_0(\infty)+\mathrm{i}k_1(\infty))r\}\, r^{2l+1}\,{}_1F_1(l+1;2l+2;2\mathrm{i}k_0(\infty)r)$$
$$\times {}_1F_1\left(l+1+\frac{\mathrm{i}\lambda}{v_1(\infty)}; 2l+2; 2\mathrm{i}k_1(\infty)r\right)\mathrm{d}r \tag{2.131}$$

$$= \frac{2(4k_0(\infty)k_1(\infty))^{l+1} l!\left|\Gamma\left(l+1+\frac{\mathrm{i}\lambda}{v_1(\infty)}\right)\right|\exp\left\{\frac{\pi\lambda}{2v_1(\infty)}\right\}(2l+1)!}{v_1(\infty)[2(2l+1)!]^2[\alpha^2+(k_0(\infty)-k_1(\infty))^2]^{l+1}}$$
$$\times\left[\frac{\alpha+\mathrm{i}k_0(\infty)+\mathrm{i}k_1(\infty)}{\alpha+\mathrm{i}k_0(\infty)-\mathrm{i}k_1(\infty)}\right]^{\mathrm{i}\lambda/v_1(\infty)}$$
$$\times {}_2F_1\left[l+1, l+1+\frac{\mathrm{i}\lambda}{v_1(\infty)}; 2l+2; \frac{-4k_0(\infty)k_1(\infty)}{\alpha^2+(k_0(\infty)-k_1(\infty))^2}\right] \tag{2.132}$$

$$= \frac{l!\exp\{\theta(\frac{1}{2}\pi-\phi)\}\,|\Gamma(l+1+\mathrm{i}\theta)|}{2v_1(\infty)(2l+1)!(-\nu)^{l+1}}\left\{\frac{x+1}{x-1}\right\}^{\pm\frac{1}{2}\mathrm{i}\theta}$$
$$\times {}_2F_1\left(l+1, l+1\pm\mathrm{i}\theta; 2l+1; \frac{1}{\nu}\right) \tag{2.133}$$

$$= \frac{l!\exp\{\theta(\frac{1}{2}\pi-\phi)\}}{v_1(\infty)\,|\Gamma(l+1+\mathrm{i}\theta)|}\left\{\frac{x+1}{x-1}\right\}^{\frac{1}{2}\mathrm{i}\theta} Q_l^{(-\mathrm{i}\theta,+\mathrm{i}\theta)}(x) \tag{2.134}$$

where

$$\nu = \frac{\alpha^2+(k_0(\infty)-k_1(\infty))^2}{-4k_0(\infty)k_1(\infty)} \tag{2.135}$$

$$\theta = \lambda/v_1(\infty) \tag{2.136}$$

$$x = \frac{\alpha^2+k_0^2(\infty)+k_1^2(\infty)}{2k_0(\infty)k_1(\infty)} \tag{2.137}$$

$$\phi = \left\{ \begin{array}{ll} \tan^{-1}\left(\frac{2\alpha k_1(\infty)}{\alpha^2+2M\epsilon_{01}}\right) & \text{if } \alpha^2 + 2M\epsilon_{01} \geq 0 \\ \pi - \tan^{-1}\left(\frac{2\alpha k_1(\infty)}{-\alpha^2-2M\epsilon_{01}}\right) & \text{if } \alpha^2 + 2M\epsilon_{01} \leq 0 \end{array} \right\} \tag{2.138}$$

and where $Q_l^{(\alpha,\beta)}$ is a Jacobi function of the second kind. Recurrence relations for the latter function [32] lead to

$$(l^2+\theta^2)^{\frac{1}{2}}\beta_{l-1} = (2l+1)x\beta_l - \{(l+1)^2+\theta^2\}^{\frac{1}{2}}\beta_{l+1} \tag{2.139}$$

Since x is greater than unity, upward recurrence would rapidly involve numerical instability. Thus downward recurrence is necessary. The method, essentially due to J. C. P. Miller (cf. [14, 429]), requires setting $\beta_{L+1} = 0$ and $\beta_L = 1$ for some sufficiently large L.

However, it is numerically more convenient to consider the case:

$$U_{10}(r) \equiv 2M\mathrm{e}^{-\alpha r} \tag{2.140}$$

The computer program is then amenable to testing in the limit as $\lambda \to 0$, corresponding to the exact first Born case. Use of (2.130) in this limit involves a Cauchy principal value and a transition probability that behaves like $(\ln\rho)^2$ as ρ tends to zero, a circumstance to be expected within the weak-coupling limit. Equations (2.122), (2.123), and (2.140) yield the first Born approximation:

$$Q^{01} = \frac{16\pi\alpha^2}{3v_0^2(\infty)}\{\alpha^2 + (k_0(\infty)-k_1(\infty))^2\}^{-3} \tag{2.141}$$

This provides a simple check on calculations in the zero-distortion limit. The adoption of (2.140) requires that β_l be replaced by

$$\tilde{\beta}_l \equiv \frac{\partial\beta_l}{\partial\alpha} = -\theta\frac{\partial\phi}{\partial\alpha}\beta_l + \frac{\alpha\left(lx\beta_l - \sqrt{(l^2+\theta^2)}\beta_{l-1}\right)}{k_0(\infty)k_1(\infty)(x^2-1)} \tag{2.142}$$

In obtaining this, we have used

$$l(x^2-1)\frac{\partial}{\partial x}Q_l^{(-\mathrm{i}\theta,+\mathrm{i}\theta)}(x) = l(lx+\mathrm{i}\theta)Q_l^{(-\mathrm{i}\theta,+\mathrm{i}\theta)}(x) - (l^2+\theta^2)Q_{l-1}^{(-\mathrm{i}\theta,+\mathrm{i}\theta)}(x) \tag{2.143}$$

Substituting from (2.139) and replacing l by $l-1$ gives $\tilde{\beta}_{l-1}$ in terms of β_l and β_{l-1}:

$$\tilde{\beta}_{l-1} = -\theta\frac{\partial\phi}{\partial\alpha}\beta_{l-1} + \frac{\alpha\left(\sqrt{(l^2+\theta^2)}\beta_l - lx\beta_{l-1}\right)}{k_o(\infty)k_1(\infty)(x^2-1)} \tag{2.144}$$

where, of course,

$$\frac{\partial\phi}{\partial\alpha} = \frac{2k_1(\infty)(2M\epsilon_{01}-\alpha^2)}{(\alpha^2+2M\epsilon_{01})^2 + 4\alpha^2k_1^2(\infty)} \tag{2.145}$$

The β_l were calculated from (2.139) and then the $\tilde{\beta}_l$ were calculated from (2.144). The sequence $\{\tilde{\beta}_l\}$ was normalized by setting

$$\tilde{\beta}_0 = \frac{\exp(-\theta\phi)}{\nu_1(\infty)}\left[\frac{2\pi\theta}{1-\exp(-2\pi\theta)}\right]^{1/2} \times\left[\frac{2k_1(\infty)(2M\epsilon_{10}-\alpha^2)\sin z}{(\alpha^2+2M\epsilon_{01})^2+4k_1^2(\infty)\alpha^2}+\frac{\alpha\cos z}{k_0(\infty)k_1(\infty)(x^2-1)}\right] \tag{2.146}$$

where

$$z=\frac{1}{2}\theta\ln\left(\frac{x+1}{x-1}\right) \tag{2.147}$$

The total cross section was calculated from

$$Q^{01}=\sum_{l=0}^{\infty}\frac{4\pi k_1(\infty)(2l+1)}{k_0^3(\infty)}\left|\tilde{\beta}_l\right|^2 \tag{2.148}$$

Comparison of Results of Exact and Approximate Distorted-Wave Calculations

For potentials (2.125), (2.126), and (2.140) equations (2.89) and (2.115) yield the approximate distorted-wave cross section:

$$Q^{01}=\pi\sum_{l=0}^{\infty}\frac{32(l+\frac{1}{2})}{k_0(\infty)k_1(\infty)v_0^2(\infty)}\left\{\int_0^{\infty}g_l(x)\cos\theta_l(x)\,\mathrm{d}x\right\}^2 \tag{2.149}$$

with

$$g_l(x)=\frac{r\{r^2k_1(r)+\rho^2k_1(\infty)\}^{\frac{1}{2}}\exp(-\alpha r)}{k_1^{\frac{1}{2}}(\infty)\{r^3+(\rho^4/R^3)(r^2+rR+R^2)\}^{\frac{1}{2}}} \tag{2.150}$$

and

$$\theta_l(x)=2\int_0^x\frac{\{k_1(s)-k_0(\infty)\}}{k_1(\infty)}\left\{\frac{s^2k_1(s)[s^2k_1(s)+\rho^2k_1(\infty)]}{s^3+(\rho^4/R^3)(s^2+sR+R^2))}\right\}^{\frac{1}{2}}\mathrm{d}y \tag{2.151}$$

in which $R(\rho)$ is the greatest positive root of

$$t^4+\frac{2\lambda M}{k_1^2(\infty)}t^3-\rho^4=0 \tag{2.152}$$

and in which

$$r=x^2+R \tag{2.153}$$

$$s=y^2+R \tag{2.154}$$

$$k_1^2(r)=k_1^2(\infty)+2\lambda M/r \tag{2.155}$$

At low energies, where distortion becomes important, the summation over l in (2.149) is easier to carry out numerically than an integration over ρ, which is in turn much easier to use at higher energies, where in fact a check was made that (2.149) tends to (2.141). For each l, interpolation in the cosine argument was found to be expedient, except for the higher values of α, which required such fine grids that direct integration for each value of x was probably equally efficient. Newton's

method was used to obtain $R(\rho)$, while the integrations over x and y were effected by splitting the interval and applying a 7-point Curtis–Clenshaw quadrature, checked by a double 5-point Lobatto quadrature. The latter method is due to O'Hara and Smith (private communication) and is closely related to the methods reported in their paper [463]. However, since rapid oscillations in the sign of the r-integrand occur, a local relative error accuracy was employed. One advantage of the particular choice of integration variables in (2.149) and (2.151), namely x and y, is that the integrands are well behaved at $\rho = 0$.

Of major interest are transitions involving one pseudo-crossing point r_c given by the only real positive root of

$$k_0^2(s) = k_1^2(s) \tag{2.156}$$

On the assumption that $v_0(\infty)$ is very much less than unity, $k_0(s) - k_1(s)$ is very large and the method of steepest descent (or stationary phase) may be tentatively applied to (2.115). Integration over ρ, with averaging over the rapidly varying phase, yields

$$Q^{01} = \frac{8\pi^2 r_c^2 V_{10}^2(r_c)}{v_0^2(\infty)\left|k_0'(r_c) - k_1'(r_c)\right|} \tag{2.157}$$

which is just the weak-coupling limit of the Landau-Zener formula and which for the test case reduces to

$$Q^{01} = \frac{8\pi^2 r_c^4 \exp\{-2\alpha r_c\}}{|\lambda| v_0(\infty)} \tag{2.158}$$

where $r_c = \lambda/\epsilon_{01}$ is the crossing point, assuming $\lambda\epsilon_{01} > 0$. In particular, we consider results for $\lambda = +1$ and $\epsilon_{01} = 0.125$ atomic units (a.u.), which correspond to an attractive Coulomb potential in the final state and to excitation, respectively. We take $M = 2 \times 1837$ a.u. and $k_0^2(\infty) = M\epsilon_{01} p$ a.u. with $p = 2.5$, corresponding to an initial relative velocity of 9.223×10^{-3} a.u. and an incident relative kinetic energy of 4.25 eV which is only 0.85 eV above threshold. We confirmed that for $\alpha = 1/2$, the exact formula (2.148) and the forced-common-turning-point formula (2.149) agreed, giving $3747.4(\pi a_0^2)$, while the steepest-descent formula (2.157) gave $3744(\pi a_0^2)$. To obtain a more sensitive test we therefore proceeded to higher values of α, until (2.148) and (2.157) substantially differed, that is, until the individual transition probabilities depended on significant contributions from other than the crossing point. Of course, the evaluation of (2.149) becomes more difficult as α increases. For $\alpha = 2$, we obtained 1635.3, 1635.3, and 1414 (all in units of $10^{-10}\pi a_0^2$) for (2.148), (2.149), and (2.157) respectively, thus showing that the common-turning-point method predicts the wave distortion very accurately for all internuclear separations. Moreover, allowance for deviation from a straight-line trajectory is clearly successful, because although an impact-parameter-type formula, with $\lambda = 0$ except in $k_0(\infty) - k_1(s)$, gives $1677(10^{-10}\pi a_0^2)$, the maximum value of l for which Q_l^{01} contributes to Q^{01} is 200, whereas for (2.148) and (2.149) it is 285. Of course, even the exact Q_l^{01} and the forced-common-turning-point Q_l^{01}, contributing to (2.148) and (2.149) respectively, are somewhat out of phase for all l, but this is not too surprising in view of the very rapid oscillations of Q_l^{01} as a function of l (cf. Table 2.1).

Table 2.1. Oscillation of Q_l^{01} with respect to l

l	Exact Q_l^{01} (πa_0^2)	Approximate Q_l^{01} (πa_0^2)	l	Exact Q_l^{01} (πa_0^2)	Approximate Q_l^{01} (πa_0^2)
100	2.8^{-10}	4.4^{-11}	108	1.2^{-10}	5.2^{-10}
101	4.5^{-10}	4.5^{-10}	109	1.2^{-10}	3.2^{-10}
102	2.8^{-11}	3.4^{-10}	110	5.5^{-10}	7.0^{-14}
103	2.5^{-10}	1.1^{-12}	111	2.3^{-10}	3.4^{-10}
104	4.9^{-10}	3.0^{-10}	112	4.3^{-11}	5.4^{-10}
105	6.0^{-11}	5.0^{-10}	113	5.1^{-10}	1.2^{-10}
106	2.0^{-10}	9.7^{-11}	114	3.7^{-10}	8.3^{-11}
107	5.3^{-10}	1.1^{-10}	115	2.6^{-13}	5.3^{-10}

Note: The exact Q_l^{01} and the approximate (forced-common-turning-point) Q_l^{01} were calculated from (2.148) and (2.149) respectively; the indices give the power of 10 by which the entries must be multiplied.

The evaluation of (2.149) for a low relative velocity is a difficult task due to the severity of the cancellation occurring within each complete cosine wave if α is small or between the different cosine waves if α is large. Some auxiliary computations were carried out to illustrate this cancellation and to demonstrate the extent to which the contribution from the region well away from the crossing is important.

Let the crossing occur at x_c (which of course depends on l and exists only if $l + 1/2 < r_c k_0(\infty)$) and put

$$\theta_l(x_c) \equiv 2n\pi + \delta \tag{2.159}$$

in which n is a positive integer and

$$0 \le \delta < 2\pi \tag{2.160}$$

Consider

$$q_l(m) \equiv \frac{32\pi(l+\frac{1}{2})}{k_0(\infty)k_1(\infty)v_0^2(\infty)} \left\{ \int_{x_m^-}^{x_m^+} g_l(x) \cos\theta_l(x)\, \mathrm{d}x \right\}^2 \tag{2.161}$$

where m is another positive integer and the sequences $x_m^{\pm}$ are such that

$$\theta_l(x_m^{\pm}) = 2(n-m)\pi \tag{2.162}$$

and

$$0 \le x_m^- \le x_c, \qquad x_m^+ \ge x_c \tag{2.163}$$

It may be seen that in going from m to $m+1$ two extra complete cosine waves, one on either side of the crossing, are included in the integral in (2.161); and it may readily be verified that the difference between $q_l(n)$ and the partial cross section Q_l^{01} is insignificant.

The parameters involved in the model were assigned the values used earlier. Computations were carried out for a number of different l's, but it is sufficient to

Table 2.2. Approach of $q_{33}(m)$ to Q_{33}^{01}

m	$q_{33}(m)$ (πa_0^2)	m	$q_{33}(m)$ (πa_0^2)	m	$q_{33}(m)$ (πa_0^2)	m	$q_{33}(m)$ (πa_0^2)
0	8.4^{-9}	7	4.2^{-6}	14	1.5^{-5}	21	1.7^{-6}
1	1.1^{-8}	8	6.4^{-6}	15	1.4^{-5}	22	8.6^{-7}
2	6.1^{-8}	9	8.9^{-6}	16	1.2^{-5}	23	3.9^{-7}
3	2.2^{-7}	10	1.1^{-5}	17	9.2^{-6}	24	1.6^{-7}
4	5.9^{-7}	11	1.3^{-5}	18	6.8^{-6}	25	5.1^{-8}
5	1.3^{-6}	12	1.5^{-5}	19	4.6^{-6}	26	1.1^{-8}
6	2.5^{-6}	13	1.5^{-5}	20	2.9^{-6}	27	5.2^{-11}

Note: $n = 27$, $Q_{33}^{01} = 5.2 \times 10^{-11} \pi a_0^2$; the indices give the power of 10 by which the entries must be multiplied.

give results for the 33rd partial wave as they are quite representative. The values of ρ and n in this case are 1.48 a.u. and 27 respectively. If $\alpha = 0.5$ then

$$q_{33}(0) = 1.3 \times 10^1 , \qquad q_{33}(m) = 2.2 \times 10^1 , \qquad m = 1 \to 27$$

(in units of πa_0^2). The asymptotic value here is reached very close to the crossing because of the cancellation within each complete cosine wave. However, if $\alpha = 2$ the values of $q_{33}(m)$ are as in Table 2.2, from which it is apparent that there is severe cancellation between the different complete cosine waves and that an important contribution to the integral comes even from the complete cosine wave next to the x origin. This emphasizes the severity of the test on the forced-common-turning-point model.

This semiclassical approach has been applied to cold atomic collisions by Bichoutskaia et al. [77] (see Section 4.5).

2.3 Two and Four Transition Points: Crossing and Noncrossing

2.3.1 Introduction

Concerning low-energy heavy-particle collisions embracing excitation and/or charge transfer, much work has been done in the last forty years, not least on the composite Nikitin [453] and generalized Demkov [221] models using both the comparison equation and strong-coupling asymptotics method [167, 193, 467] and the phase-integral method [28]. In principle, a simpler model would appear to be the parabolic model (which has no pole) developed by Crothers [160], using both the phase-integral and comparison equation method, with special reference to strong-coupling asymptotic expansions [161, 476] of parabolic cylinder functions, for both crossing and noncrossing and in the context of the Stokes phenomenon. The asymptotic parameter is the inverse impact velocity (see (2.258)).

We have traced the two solutions of the parabolic differential equation

$$\left(\frac{\mathrm{d}^2}{\mathrm{d}z^2} + p + \frac{1}{2} - \frac{z^2}{4}\right) D_p(z) = 0 \tag{2.164}$$

for the *noncrossing* case, around the T_0 plane, namely $AD_{-\mathrm{i}\gamma}\left(2\mathrm{e}^{\pi\mathrm{i}/4} T_0 \sqrt{\gamma}\right)$ and $BD_{-1+\mathrm{i}\gamma}\left(2\mathrm{e}^{-\pi\mathrm{i}/4} T_0 \sqrt{\gamma}\right)$ in the lower T_0 half-plane clockwise [161] where A and B are arbitrary constants and γ is a reasonably large, positive parameter. The Stokes lines emanate from two transition points $\pm\mathrm{i}$; those in the upper T_0 plane have initial directions $\pi/6$, $-7\pi/6$ and $-\pi/2$. The Stokes lines in the lower T_0 plane are the mirror images of those in the upper plane, reflected in the real T_0-axis, so that we have a double Stokes line running from i to $-\mathrm{i}$ along the imaginary T_0-axis, and our branch cuts are chosen such that they run from $\pm\mathrm{i}$ to $\pm\mathrm{i}\infty$ respectively; since our $D_p(z)$'s, appropriate to collisions, are analytic functions of the positive Stueckelberg variable T_0, we avoid Stueckelberg's choice of nonphysical branch cuts [160, 574]. Thus, there is no simple correspondence between our results and the results of Fröman et al. [284] or Nakamura [447], both of whom use weak-coupling expansions.

We obtain the four parabolic-model Stokes constants (which we name a, b, α, and β), using analyticity and the fact that solutions must connect along the real T_0-axis,

$$a = \beta = -1 + \mathrm{e}^{-2\pi\gamma} \tag{2.165}$$

$$b = \alpha = -1 - \mathrm{e}^{-2\pi\gamma} \tag{2.166}$$

Equations (2.165) and (2.166) agree with Crothers [160], [161] regarding both phase (mod π) and magnitude.

Moreover, in a procedure similar to the one in which Berry [71] shows that the abrupt change in the subdominant solution is continuous across a Stokes line for the one-transition-point problem, we succeed in a similar procedure for our two-transition-point problem using Stirling numbers of the first kind to parameterize our original strong-coupling expansions. We will also consider the crossing case [163], [165] by tracing $D_{-1-\mathrm{i}\gamma}\left(2\mathrm{e}^{-3\pi\mathrm{i}/4} T_0 \sqrt{\gamma}\right)$ anticlockwise in the lower T_0 half-plane.

2.3.2 Exact Resumming of Asymptotic Relations for Parabolic Cylinder Functions of Large Order and Argument

The Weak-Coupling Case

We may take as our definition for the parabolic cylinder function:

$$D_p(z) \equiv \frac{\Gamma(1+p)}{2\pi\mathrm{i}} \mathrm{e}^{-\frac{z^2}{4}} \int_{(-\infty)}^{(0+)} \mathrm{e}^{zs - \frac{s^2}{2}} s^{-1-p}\, \mathrm{d}s \tag{2.167}$$

where p is not an integer. The principal branch of s^{-p} is assumed.

Putting $t = \mathrm{e}^{\pi\mathrm{i}} zs$ and assuming $\arg(z) \in (-\pi/2, +\pi/2)$ we may rewrite (2.167) as

$$D_p(z) = \frac{-\Gamma(1+p)}{2\pi\mathrm{i}} \mathrm{e}^{-\frac{z^2}{4}} z^p \int_{\infty \exp(\mathrm{i}\arg z)}^{(0+)} \mathrm{e}^{-t - \frac{t^2}{2z^2}} \left(t\mathrm{e}^{-\mathrm{i}\pi}\right)^{-1-p}\, \mathrm{d}t \tag{2.168}$$

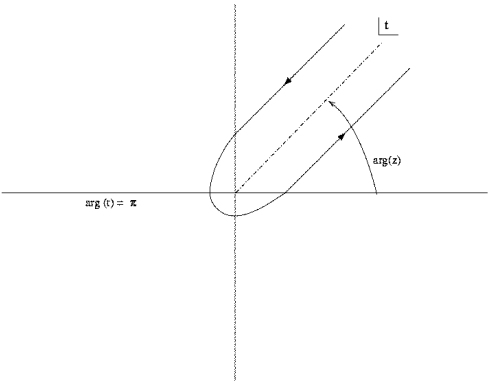

Fig. 2.4. Contour and branch cut for (2.168)

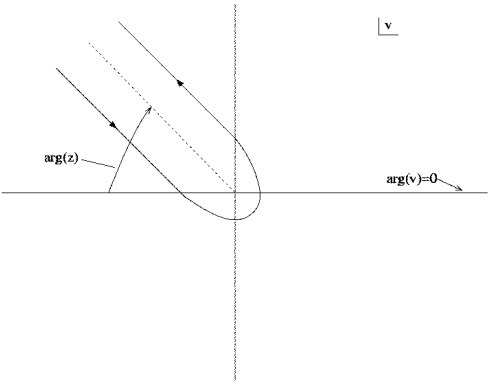

Fig. 2.5. Contour and branch cut for (2.170)

where the contour and branch of t^{-p} are indicated in Figure 2.4. Expanding $e^{(-t-t^2/2z^2)}$ we obtain the usual asymptotic expansion

$$D_p(z) \cong e^{-\frac{z^2}{2}} z^p \, {}_2F_0\left(-\frac{p}{2}, \frac{1-p}{2}; ; -\frac{2}{z^2}\right) \tag{2.169}$$

the first term of which is a good approximation if $|z| \gg \max(1, |p|)$.

The $D_p(z)$ in equation 2.169 is only useful in the weak-coupling case (cf. [506] section 3.2); when $|z|$ is not very much greater than $|p|$, then the expression is poorly determined. Instead we put $\nu = z^{-1}s$ with $\arg(z) \in (-\pi, +\pi)$ so that

$$D_p(z) \equiv \frac{\Gamma(1+p)}{2\pi i} e^{-\frac{z^2}{2}} z \int_{\infty \exp\{i(\pi - \arg z)\}}^{(0+)} \exp\left(z^2\left(\nu - \frac{\nu^2}{2}\right) - (1+p)\ln(z\nu)\right) d\nu \tag{2.170}$$

where the contour and the branch of $\ln(\nu)$ are indicated in Figure 2.5 [161], [476].

The Strong-Coupling Case

We assume that $|z|^2$ and $|p|$ are both large so that the method of steepest descent may be applied. This involves expanding the exponential in the integral about its saddle points. They are calculated by finding the zeros of the differential of the argument of the exponential in question. So, in this case, our argument $f(\nu)$ is

$$f(\nu) = z^2\left(\nu - \frac{\nu^2}{2}\right) - (1+p)\ln(z\nu)$$

and from $f'(\nu_j) = 0$, the two distinct saddle points are given by

$$2z\nu_{\substack{0\\1}} = z \pm \sqrt{z^2 - 4(1+p)} \tag{2.171}$$

provided that $z^2 \neq 4(1+p)$ and the square root branch is chosen so that $\arg(z\nu_j) \in (-\pi, +\pi)$.

Finally we expand about the saddle points (looking only at the integral)

$$I = \int \exp\left(f(\nu_j) + \frac{1}{2}f''(\nu_j)(\nu-\nu_j)^2 + \sum_{n=3}^{\infty}\frac{f^n(\nu_j)}{n!}(\nu-\nu_j)^n\right)\mathrm{d}\nu \tag{2.172}$$

This expression is simplified by making the substitution

$$t^2 = \mathrm{e}^{-\mathrm{i}\pi}\left(\nu-\nu_j\right)^2 f''(\nu_j)$$

which allows us to rewrite I as

$$I = \frac{\mathrm{e}^{(\mathrm{i}\alpha_j + f(\nu_j))}}{\sqrt{|f''(\nu_j)|}}\int_{-\infty}^{\infty}\mathrm{d}t\,\exp\left(-\frac{t^2}{2} + \sum_{n=3}^{\infty}\frac{(-1)^n\mathrm{e}^{\mathrm{i}n\alpha_j}t^n(1+p)}{n\nu_j^n|f''(\nu_j)|^{n/2}}\right) \tag{2.173}$$

and by using the properties of partition functions the result is that

$$\begin{aligned} D_p(z) \cong{}& \frac{\Gamma(1+p)}{\mathrm{i}\sqrt{2\pi}}\mathrm{e}^{-\frac{z^2}{4}}z\sum_{j=0}^{1}\frac{\mathrm{e}^{\mathrm{i}\alpha_j + f(\nu_j)}}{\sqrt{|f''(\nu_j)|}} \\ &\times\left(1 + \sum_{l=2}^{\infty}\frac{(2l-1)!!\mathrm{e}^{2\mathrm{i}l\alpha_j}}{\nu_j^{2l}|f''(\nu_j)|^l}\sum_{\{\lambda_n\}}\prod_{n=3}^{2l}\left(\frac{\left(\frac{1+p}{n}\right)^{\lambda_n}}{\lambda_n!}\right)\right) \end{aligned} \tag{2.174}$$

where

$$f(\nu) \equiv z^2\left(\nu - \frac{\nu^2}{2}\right) - (1+p)\ln(z\nu) \tag{2.175}$$

$$\alpha_j = \frac{\pi}{2} - \frac{1}{2}\arg\left(f''(\nu_j)\right) \tag{2.176}$$

and where the innermost sum is over all distinct partitions of $2l$ given by the non-negative integer solutions $\{\lambda_n\}$ such that

$$\sum_{n=3}^{2l} n\lambda_n = 2l \tag{2.177}$$

The phases α_0 and α_1 that give the directions of the lines of steepest descent are formally ambiguous by an additive factor of π and must be determined absolutely by reference to the prevailing global geometry.

Resumming the Divergent Tail

We again use the method of steepest descent, i.e., we expand the argument of the exponential (in the integral), but we rewrite as follows:

$$I = \int_{-\infty}^{+\infty} \exp\left(-\frac{t^2}{2} + \sum_{k=1}^{\infty} \frac{x_k t^k}{k} - x_1 t - \frac{x_2 t^2}{2}\right) \mathrm{d}t \tag{2.178}$$

where

$$x_k \equiv \left(-\frac{\mathrm{e}^{\mathrm{i}\alpha_j}}{\nu_j \sqrt{|f''(\nu_j)|}}\right)^k (1+p) \equiv (\beta_j)^k (1+p) \tag{2.179}$$

By using a Maclaurin expansion for the power series in the exponential we have

$$I = \int_{-\infty}^{+\infty} \mathrm{d}t \, \exp\left(-x_1 t - \frac{t^2}{2}(1+x_2)\right) \sum_{m=0}^{\infty} \frac{\left(\sum_{k=1}^{\infty} \frac{x_k t^k}{k}\right)^m}{m!} \tag{2.180}$$

Considering the sum only, we see that the innermost sum is the generating function for the multinomial coefficients [1] such that the sum is now

$$1 + \sum_{m=1}^{\infty} \sum_{n=m}^{\infty} \frac{t^n}{n!} \sum (n; \lambda_1, \lambda_2, \ldots, \lambda_n)^* \, x_1^{\lambda_1} x_2^{\lambda_2} \ldots x_n^{\lambda_n} \tag{2.181}$$

where the innermost sum is over $\{\lambda_1, \lambda_2, \ldots, \lambda_n\}$ subject to $\lambda_1 + 2\lambda_2 + \ldots + n\lambda_n = n$ and $\lambda_1 + \lambda_2 + \ldots + \lambda_n = m$. Now,

$$x_1^{\lambda_1} x_2^{\lambda_2} \ldots x_n^{\lambda_n} = (1+p)^m \beta_j^n$$

and

$$\sum (n; \lambda_1, \lambda_2, \ldots, \lambda_n)^* = (-1)^{n-m} S_n^{(m)}$$

where the $S_n^{(m)}$ are the Stirling numbers of the first kind ([1], 24.1.3, page 824).

So, after reversing the order of the summation and replacing x_k by $\beta_j^k(1+p)$ we have

$$\begin{aligned} I = \quad & \int_{-\infty}^{+\infty} \mathrm{d}t \, \mathrm{e}^{-\beta_j(1+p)t - \frac{t^2}{2}(1+\beta_j^2(1+p))} \\ & \times \sum_{n=0}^{\infty} \frac{(-t\beta_j)^n}{n!} \sum_{m=0}^{n} (-1-p)^m S_n^{(m)} \end{aligned} \tag{2.182}$$

which simplifies to

$$\begin{aligned} I = & \int_{-\infty}^{+\infty} \mathrm{d}t \, \mathrm{e}^{-\beta_j(1+p)t - \frac{t^2}{2}(1+\beta_j^2(1+p))} \\ & \times \sum_{n=0}^{\infty} \frac{(t\beta_j)^n}{n!} (1+p)_n \end{aligned} \tag{2.183}$$

Changing the Variable

If we make the substitution

$$T = t + \frac{\beta_j(1+p)}{1+\beta_j^2(1+p)}$$

(which completes the square in the exponential) and use the following integral result

$$\int_{-\infty}^{+\infty} \mathrm{d}T\, \mathrm{e}^{-\mu T^2} T^j = \frac{\Gamma\left(\frac{j+1}{2}\right)}{\mu^{(j+1)/2}}$$

we get

$$I = \sqrt{2\pi}\exp\left[\frac{\beta_j^2(1+p)^2}{2(1+\beta_j^2(1+p))}\right]\sum_{j\,\text{even}}\frac{2^{j/2}\left(\frac{1}{2}\right)_{j/2}}{j!\left(1+\beta_j^2(1+p)\right)^{(j+1)/2}}$$
$$\times\left(\frac{1+\beta_j^2(1+p)}{-\beta_j(1+p)}\right)^j\sum_{n=j}^{\infty}\frac{\left(\frac{-\beta_j^2(1+p)}{1+\beta_j^2(1+p)}\right)^n}{(n-j)!}(1+p)_n \tag{2.184}$$

after reversing the order of summation.

Now using the substitution $n = N + j$ allows us to write the innermost sum as

$$\sum_{N=0}^{\infty}\frac{\left(\frac{-\beta_j^2(1+p)}{1+\beta_j^2(1+p)}\right)^N}{N!}(1+p+j)_N$$

that is the hypergeometric function

$${}_1F_0\left(1+p+j;;-\frac{\beta_j^2(1+p)}{1+\beta_j^2(1+p)}\right)$$

which in turn can be written as

$$\left[1+\frac{\beta_j^2(1+p)}{1+\beta_j^2(1+p)}\right]^{-1-p-j}$$

which means that I can now be written as

$$I = \sqrt{2\pi}\left(\frac{\left(1+\beta_j^2(1+p)\right)^{\left(\frac{1}{2}+p\right)}}{\left(1+2\beta_j^2(1+p)\right)^{(1+p)}}\right)\exp\left[\frac{\beta_j^2(1+p)^2}{2(1+\beta_j^2(1+p))}\right]$$
$$\times{}_2F_0\left(\frac{1+p}{2},1+\frac{p}{2};;\frac{2\beta_j^2\left(1+\beta_j^2(1+p)\right)}{\left(1+2\beta_j^2(1+p)\right)^2}\right) \tag{2.185}$$

But the ${}_2F_0$ can be written [562] in terms of Kummer's confluent hypergeometric function thus ([1], 13.1.10, page 504)

$$ {}_2F_0\left(a, 1+a-b;;-\frac{1}{z}\right) = z^a U(a,b,z) $$

and through this relation ([1], 13.6.36, page 510)

$$ U\left(\frac{\tilde{a}}{2}+\frac{1}{4}, \frac{1}{2}, \frac{z^2}{2}\right) = 2^{\frac{\tilde{a}}{2}+\frac{1}{4}} \mathrm{e}^{\frac{z^2}{4}} D_{-\tilde{a}-1/2}(z) $$

can be connected to the parabolic cylinder function, where $\tilde{a} = 2a - \frac{1}{2}$.

After simplification and summing over both branches of the square root we have

$$ \begin{aligned} D_p(z) = \frac{\Gamma(1+p)}{\sqrt{2\pi}} \exp\left(-\frac{z^2}{4} - \frac{(1+p)}{2}\right) z \sum_{j=0}^{1} \frac{\exp\left(\mathrm{i}\alpha_j + f(\nu_j)\right)}{\sqrt{\left|f''(\nu_j)\right|}} \\ \times \left(\frac{\left(1+\beta_j^2(1+p)\right)^{p/2}}{\beta_j^{1+p}} \exp\left(\frac{\mathrm{i}\pi p}{2} - \frac{1}{4\beta_j^2} - \frac{1+p}{4\left(1+\beta_j^2(1+p)\right)} \right) \right) \\ \times D_{-(1+p)}\left[\frac{\mathrm{i}\left(1+2\beta_j^2(1+p)\right)}{\beta_j \sqrt{1+\beta_j^2(1+p)}} \right] \end{aligned} \tag{2.186} $$

where

$$ \beta_j \equiv -\frac{\mathrm{e}^{\mathrm{i}\alpha_j}}{\nu_j \sqrt{\left|f''(\nu_j)\right|}} $$

so that we have

$$ D_p(z) = \frac{\Gamma(1+p)}{\sqrt{2\pi}} \left[\mathrm{e}^{\mathrm{i}\pi p/2} D_{-1-p}(\mathrm{i}z) + \mathrm{e}^{-\mathrm{i}\pi p/2} D_{-1-p}(-\mathrm{i}z) \right] \tag{2.187} $$

which agrees with the *exact* recurrence relation of Magnus and Oberhettinger [399]. Notice that, from Figure 2.5, strictly $\arg z \in (-\pi/2, +\pi/2)$. However this condition may be relaxed by analytic continuation. Notice also that we have completely resummed the JWKB asymptotic divergent expansions about the saddle points, not just the tails as in Berry [71]. Thus, not surprisingly, the connection formula between (16), (18), and (13)* of Crothers [161] is exact.

The Noncrossing Parabolic Model

Of course, in retrospect, the perhaps surprising result of the previous section should not be too much so, for the following reasons. A solution of the second-order ordinary differential equation

$$\left(\frac{\mathrm{d}^2}{\mathrm{d}z^2} + p + \frac{1}{2} - \frac{z^2}{4}\right)u = 0 \tag{2.188}$$

is given by the parabolic-cylinder function

$$u = D_p(z)$$

where the parabolic potential is given by

$$V(z) = p + \frac{1}{2} - \frac{z^2}{4} \tag{2.189}$$

and the $\mathrm{d}^2/\mathrm{d}z^2$ operator is the scaled (by -2) kinetic energy operator. The complete operator in (2.188) is even in z and invariant under the mappings $p \to -1 - p$ and $z \to \mathrm{i}z$, so that we have four solutions:

$$I(16) \qquad D_p(z) \tag{2.190}$$

$$I(17^*) \qquad D_p(-z) \tag{2.191}$$

$$I(18) \qquad D_{-1-p}(\mathrm{i}z) \tag{2.192}$$

$$I(13^*) \qquad D_{-1-p}(-\mathrm{i}z) \tag{2.193}$$

where * means conjugate (of argument and order, since $D_p(z)$ is a real function of complex variables p and z) and where the left-hand labels refer to Crothers [161], to be referred to hereafter as I. Thus, from ordinary-differential-equation theory, there must be a linear (with respect to z) relationship between any three of the four solutions. These are given by Magnus and Oberhettinger [399] as:

$$I(16) = \frac{\Gamma(1+p)}{\sqrt{2\pi}}\left[\mathrm{e}^{\frac{\mathrm{i}p\pi}{2}} I(18) + \mathrm{e}^{-\frac{\mathrm{i}p\pi}{2}} I(13^*)\right] \tag{2.194}$$

$$= \mathrm{e}^{-p\pi\mathrm{i}} I(17^*) + \frac{\sqrt{2\pi}}{\Gamma(-p)}\mathrm{e}^{-\mathrm{i}(p+1)\frac{\pi}{2}} I(18) \tag{2.195}$$

$$= \mathrm{e}^{p\pi\mathrm{i}} I(17^*) + \frac{\sqrt{2\pi}}{\Gamma(-p)}\mathrm{e}^{\mathrm{i}(p+1)\frac{\pi}{2}} I(13^*) \tag{2.196}$$

By symmetry and rearrangement, any one can be given in terms of any two of the other three. We now set:

$$p = -\mathrm{i}\gamma \tag{2.197}$$

$$z = 2\exp\left(\frac{\pi\mathrm{i}}{4}\right) T_0 \sqrt{\gamma} \tag{2.198}$$

so that, corresponding to (2.190) to (2.193), we have

$$I(16) \qquad D_{-\mathrm{i}\gamma}\left(2\mathrm{e}^{\pi\mathrm{i}/4} T_0 \sqrt{\gamma}\right)$$

$$I(17^*) \qquad D_{-\mathrm{i}\gamma}\left(2\mathrm{e}^{-3\pi\mathrm{i}/4} T_0 \sqrt{\gamma}\right)$$

$$I(18) \qquad D_{-1+\mathrm{i}\gamma}\left(2\mathrm{e}^{3\pi\mathrm{i}/4} T_0 \sqrt{\gamma}\right)$$

$$I(13^*) \qquad D_{-1+\mathrm{i}\gamma}\left(2\mathrm{e}^{-\pi\mathrm{i}/4} T_0 \sqrt{\gamma}\right)$$

We have from $I(14)$ and $I(15)$:

$$\tilde{\theta} = \frac{\gamma}{2} - \frac{\gamma}{2}\ln\gamma + \gamma\ln\left(T_0 + \sqrt{1+T_0^2}\right) + \gamma T_0\sqrt{1+T_0^2} \tag{2.199}$$

$$= \frac{\gamma}{2} - \frac{\gamma}{2}\ln\gamma - \mathrm{i}\frac{\pi\gamma}{2} - 2\gamma\int_{T_0}^{-\mathrm{i}}\left(1+T^2\right)^{\frac{1}{2}}\,\mathrm{d}T \tag{2.200}$$

where the tilde on the theta is to distinguish it from the parameter θ in the $T-\tau$ model of Nikitin, the phase integral is outgoing (flip the limits),

$$g = \tan^{-1}\left\{\sqrt{1+T_0^2} - T_0\right\} \tag{2.201}$$

and we assume for noncrossing (otherwise known as perturbed symmetric resonance [160], [162]) that $T_0 > 0$ and of order unity, and $\gamma \gg 1$. Using the method of the second paragraph of Section 2.3.2, we may write the leading asymptotic expansions as

$$I(16)\quad D_{-\mathrm{i}\gamma}\left(2\mathrm{e}^{\frac{\pi\mathrm{i}}{4}}T_0\sqrt{\gamma}\right) \cong \mathrm{e}^{\frac{\pi\gamma}{4}+\mathrm{i}\gamma-\mathrm{i}\gamma\ln\gamma-\mathrm{i}\tilde{\theta}}\cos g + \mathrm{e}^{-\frac{3\pi\gamma}{4}+\mathrm{i}\tilde{\theta}}\sin g \tag{2.202}$$

$$I(17^*)\quad D_{-\mathrm{i}\gamma}\left(2\mathrm{e}^{\frac{-3\pi\mathrm{i}}{4}}T_0\sqrt{\gamma}\right) \cong \mathrm{e}^{\frac{\pi\gamma}{4}+\mathrm{i}\tilde{\theta}}\sin g + \mathrm{e}^{-\frac{3\pi\gamma}{4}-\mathrm{i}\tilde{\theta}+\mathrm{i}\gamma-\mathrm{i}\gamma\ln\gamma}\cos g \tag{2.203}$$

$$I(18)\quad D_{-1+\mathrm{i}\gamma}\left(2\mathrm{e}^{\frac{3\pi\mathrm{i}}{4}}T_0\sqrt{\gamma}\right) \cong \mathrm{e}^{\frac{\pi\gamma}{4}-\mathrm{i}\tilde{\theta}+\frac{\pi\mathrm{i}}{4}}\frac{\cos g}{\sqrt{\gamma}} - \mathrm{e}^{-\frac{3\pi\gamma}{4}+\mathrm{i}\tilde{\theta}-\mathrm{i}\gamma+\mathrm{i}\gamma\ln\gamma+\frac{\pi\mathrm{i}}{4}}\frac{\sin g}{\sqrt{\gamma}} \tag{2.204}$$

$$I(13^*)\quad D_{-1+\mathrm{i}\gamma}\left(2\mathrm{e}^{\frac{-\pi\mathrm{i}}{4}}T_0\sqrt{\gamma}\right) \cong \mathrm{e}^{\frac{\pi\gamma}{4}-\mathrm{i}\gamma+\mathrm{i}\gamma\ln\gamma+\frac{\pi\mathrm{i}}{4}+\mathrm{i}\tilde{\theta}}\frac{\sin g}{\sqrt{\gamma}} - \mathrm{e}^{\frac{-3\pi\gamma}{4}+\frac{\pi\mathrm{i}}{4}-\mathrm{i}\tilde{\theta}}\frac{\cos g}{\sqrt{\gamma}} \tag{2.205}$$

Letting T_0 in (2.202) be a variable t, we can rewrite (2.188) as

$$\left[\frac{\mathrm{d}^2}{\mathrm{d}t^2} + 4\gamma^2(1+t^2) + 2\mathrm{i}\gamma\right]D_{-\mathrm{i}\gamma}\left(2\sqrt{\gamma}\mathrm{e}^{\frac{\pi\mathrm{i}}{4}}t\right) = 0 \tag{2.206}$$

We may identify t as the Stueckelberg variable [574], [160]. For large γ, using perturbation theory, the transition points are given by $t = \pm\mathrm{i}$, and the JWKB solutions, valid a suitable distance from $t = \pm\mathrm{i}$, are given by

$$\frac{\exp\left(\pm 2\mathrm{i}\gamma\int_{\pm\mathrm{i}}^{t}\left(1+T^2\right)^{\frac{1}{2}}\,\mathrm{d}T\right)}{\left(1+T^2\right)^{\frac{1}{4}}} \tag{2.207}$$

The upper Stokes lines are given by

$$0 = \mathrm{Re}\int_{\mathrm{i}}^{\mathrm{t}}(\mathrm{T}-\mathrm{i})^{1/2}(\mathrm{T}+\mathrm{i})^{1/2}\,\mathrm{dT} \tag{2.208}$$

$$\approx \mathrm{Re}\int_{\mathrm{i}}^{\mathrm{t}}(\mathrm{T}-\mathrm{i})^{1/2}(2\mathrm{i})^{1/2}\,\mathrm{dT} \tag{2.209}$$

$$= \mathrm{Re}\frac{2}{3}(\mathrm{t}-\mathrm{i})^{3/2}(2\mathrm{i})^{1/2} = \mathrm{Re}\frac{2\sqrt{2}}{3}\mathrm{e}^{\frac{\pi\mathrm{i}}{4}+\frac{3\phi\mathrm{i}}{2}} \tag{2.210}$$

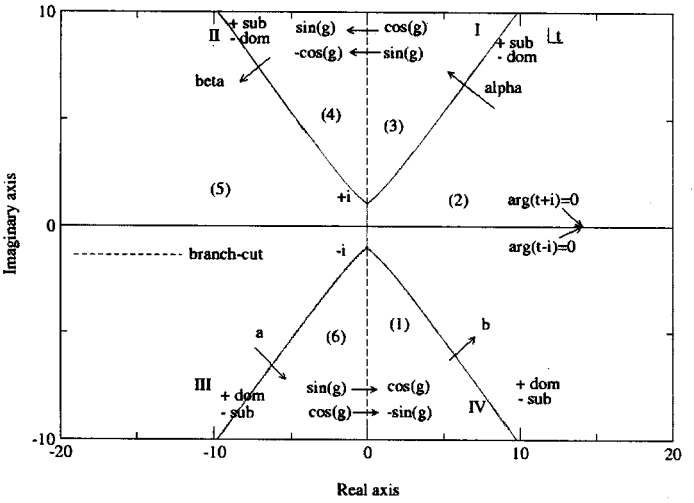

Fig. 2.6. Stokes lines for the two-transition-point problem (with transition points +i and −i)

where

$$\arg(t - \mathrm{i}) = \phi \tag{2.211}$$

so that

$$\cos\left(\frac{3\phi}{2} + \frac{\pi}{4}\right) = 0 \tag{2.212}$$

Then we have that

$$\phi = \frac{\pi}{6}, -\frac{\pi}{2}, -\frac{7\pi}{6} \tag{2.213}$$

give the initial directions of the Stokes lines [160]. The real part of the out/in-going wave is given by

$$\mp \sin\left(\frac{3\phi}{2} + \frac{\pi}{4}\right) \tag{2.214}$$

so that out/in-going waves are subdominant/dominant respectively on both $\phi = \pi/6$ and $\phi = -7\pi/6$ and vice versa on $\phi = -\pi/2$. The reverse is true concerning $\arg(t+\mathrm{i}) = \phi$. These facts are summarised in Figure 2.6.

The Stokes constants crossing I, II, III, and IV, namely $\arg(t - \mathrm{i}) = \pi/6, -7\pi/6$ and $\arg(t + \mathrm{i}) = 7\pi/6, -\pi/6$, respectively, are α, β, a, and b. We note that $\mathrm{e}^{\pm \mathrm{i}\tilde{\theta}}$ are out/in-going respectively and behave as $\mathrm{e}^{\mp \frac{\pi\gamma}{2}}$ (subdominant/dominant) near $t = \mathrm{i}$ and as $\mathrm{e}^{\pm \frac{\pi\gamma}{2}}$ (dominant/subdominant) near $t = -\mathrm{i}$, that is, as viewed on the (positive) γ-axis. It follows that only $I(16)$ and $I(18)$ are truly dominant as functions of both t and γ in the upper half of the t-plane while only $I(17^*)$ and $I(13^*)$ are truly dominant as functions of both t and γ, in the lower half of the t-plane. This explains why we examine the Stokes phenomenon as applied to $I(13^*)$ in the lower-half t-plane and $I(16)$ in the upper-half t-plane. This is consistent with the approach and ideas of

Olver [477] and Dingle [226] who invoke error analysis. Numerically in the upper t-plane and for large γ, $I((17^*)$ and $I(13^*)$ are negligible; in the lower t-plane and for large γ, $I(16)$ and $I(18)$ are negligible.

Compared to Crothers [160] we map $g \to \pi/2 - g$. An important point concerns reversing the direction of application of the Stokes constant as the following argument shows. Suppose we cross the Stokes line and map

$$Au_{\text{dom}} + Bv_{\text{sub}} \to Au_{\text{dom}} + (B + \beta A)v_{\text{sub}} \tag{2.215}$$

Going back across the same Stokes line

$$Au_{\text{dom}} + (B + \beta A)v_{\text{sub}} \to Au_{\text{dom}} + (B + \beta A + \lambda A)v_{\text{sub}} \tag{2.216}$$

It follows that

$$\lambda = -\beta \tag{2.217}$$

not β^* as might be wrongly extrapolated from the one-transition-point problem ($\beta =$ i).

For noncrossing we have, from (2.200),

$$\pm \mathrm{i}\tilde{\theta} = \pm\frac{\mathrm{i}\gamma}{2} \mp \frac{\mathrm{i}\gamma}{2}\ln\gamma \pm \frac{\gamma\pi}{2} \mp 2\mathrm{i}\gamma\int_{T_0}^{-\mathrm{i}} \left(1+T^2\right)^{1/2}\,\mathrm{d}T \tag{2.218}$$

Then tracing clockwise, with B an arbitrary constant,

$$\begin{aligned} BI(13^*) &= BD_{-1+\mathrm{i}\gamma}\left(2\mathrm{e}^{\frac{-\pi\mathrm{i}}{4}}T_0\sqrt{\gamma}\right) \\ &\cong B\mathrm{e}^{\frac{\pi\gamma}{4}-\mathrm{i}\gamma+\mathrm{i}\gamma\ln\gamma+\frac{\pi\mathrm{i}}{4}+\mathrm{i}\tilde{\theta}}\frac{\sin g}{\sqrt{\gamma}} - B\mathrm{e}^{-\frac{3\pi\gamma}{4}+\frac{\pi\mathrm{i}}{4}-\mathrm{i}\tilde{\theta}}\frac{\cos g}{\sqrt{\gamma}} \end{aligned} \tag{2.219}$$

$$\begin{aligned} &= B\mathrm{e}^{\frac{3\pi\gamma}{4}-\frac{\mathrm{i}\gamma}{2}+\frac{\mathrm{i}\gamma}{2}\ln\gamma+\frac{\pi\mathrm{i}}{4}-2\mathrm{i}\gamma\int_{T_0}^{-\mathrm{i}}\left(1+T^2\right)^{1/2}\mathrm{d}T}\frac{\sin g}{\sqrt{\gamma}} \\ &\quad - B\mathrm{e}^{-\frac{5\pi\gamma}{4}-\frac{\mathrm{i}\gamma}{2}+\frac{\mathrm{i}\gamma}{2}\ln\gamma+\frac{\pi\mathrm{i}}{4}+2\mathrm{i}\gamma\int_{T_0}^{-\mathrm{i}}\left(1+T^2\right)^{1/2}\mathrm{d}T}\frac{\cos g}{\sqrt{\gamma}} \end{aligned} \tag{2.220}$$

in sector 2 of Figure 2.6. Crossing Stokes line IV and recalling (2.217), we connect with

$$\begin{aligned} &B\mathrm{e}^{\frac{3\pi\gamma}{4}-\frac{\mathrm{i}\gamma}{2}+\frac{\mathrm{i}\gamma}{2}\ln\gamma+\frac{\pi\mathrm{i}}{4}-2\mathrm{i}\gamma\int_{T_0}^{-\mathrm{i}}\left(1+T^2\right)^{1/2}\mathrm{d}T}\frac{\sin g}{\sqrt{\gamma}} \\ &-B\left(\mathrm{e}^{-\frac{5\pi\gamma}{4}} + b\mathrm{e}^{\frac{3\pi\gamma}{4}}\right)\mathrm{e}^{-\frac{\mathrm{i}\gamma}{2}+\frac{\mathrm{i}\gamma}{2}\ln\gamma+\frac{\pi\mathrm{i}}{4}+2\mathrm{i}\gamma\int_{T_0}^{-\mathrm{i}}\left(1+T^2\right)^{1/2}\mathrm{d}T}\frac{\cos g}{\sqrt{\gamma}} \end{aligned} \tag{2.221}$$

in sector 1 of Figure 2.6. Crossing the branch cut to sector 6, we obtain

$$\begin{aligned} &B\mathrm{e}^{\frac{3\pi\gamma}{4}-\frac{\mathrm{i}\gamma}{2}+\frac{\mathrm{i}\gamma}{2}\ln\gamma+\frac{\pi\mathrm{i}}{4}+2\mathrm{i}\gamma\int_{T_0}^{-\mathrm{i}}\left(1+T^2\right)^{1/2}\mathrm{d}T}\frac{\cos g}{\sqrt{\gamma}} \\ &-B\left(\mathrm{e}^{-\frac{5\pi\gamma}{4}} + b\mathrm{e}^{\frac{3\pi\gamma}{4}}\right)\mathrm{e}^{-\frac{\mathrm{i}\gamma}{2}+\frac{\mathrm{i}\gamma}{2}\ln\gamma+\frac{\pi\mathrm{i}}{4}-2\mathrm{i}\gamma\int_{T_0}^{-\mathrm{i}}\left(1+T^2\right)^{1/2}\mathrm{d}T}\frac{\sin g}{\sqrt{\gamma}} \end{aligned} \tag{2.222}$$

Finally, crossing Stokes line III we connect to

$$- B\frac{\cos g}{\sqrt{\gamma}}\left[\mathrm{e}^{\frac{3\pi\gamma}{4}} - a\left(\mathrm{e}^{\frac{-5\pi\gamma}{4}} + b\mathrm{e}^{\frac{3\pi\gamma}{4}}\right)\right]\mathrm{e}^{-\frac{\mathrm{i}\gamma}{2}+\frac{\mathrm{i}\gamma}{2}\ln\gamma+\frac{\pi\mathrm{i}}{4}+2\mathrm{i}\gamma\int_{T_0}^{-\mathrm{i}}\left(1+T^2\right)^{1/2}\mathrm{d}T}$$
$$- B\left(\mathrm{e}^{\frac{-5\pi\gamma}{4}} + b\mathrm{e}^{\frac{3\pi\gamma}{4}}\right)\mathrm{e}^{-\frac{\mathrm{i}\gamma}{2}+\frac{\mathrm{i}\gamma}{2}\ln\gamma+\frac{\pi\mathrm{i}}{4}-2\mathrm{i}\gamma\int_{T_0}^{-\mathrm{i}}\left(1+T^2\right)^{1/2}\mathrm{d}T}\frac{\sin g}{\sqrt{\gamma}} \tag{2.223}$$

in sector 5 of Figure 2.6. Matching (2.223) and (2.219) on the real t-axis (T_0-axis) and given that $BI(13^*)$ dominates $AI(16)$, for B and A of the same order in γ, we have

$$-\mathrm{e}^{-\frac{5\pi\gamma}{4}} - b\mathrm{e}^{\frac{3\pi\gamma}{4}} = \mathrm{e}^{\frac{3\pi\gamma}{4}} \tag{2.224}$$

and

$$+\mathrm{e}^{-\frac{5\pi\gamma}{4}} = \mathrm{e}^{\frac{3\pi\gamma}{4}} - a\left(\mathrm{e}^{-\frac{5\pi\gamma}{4}} + b\mathrm{e}^{\frac{3\pi\gamma}{4}}\right) \tag{2.225}$$

Solving equations (2.224) and (2.225) gives

$$a = -1 + \exp(-2\pi\gamma) \tag{2.226}$$
$$b = -1 - \exp(-2\pi\gamma) \tag{2.227}$$

which implies

$$\arg a = \pi = \arg b \tag{2.228}$$

Now, also for noncrossing we have

$$\pm\,\mathrm{i}\tilde{\theta} = \pm\frac{\mathrm{i}\gamma}{2} \mp \frac{\mathrm{i}\gamma}{2}\ln\gamma \mp \frac{\pi\gamma}{2} \mp 2\mathrm{i}\gamma\int_{T_0}^{\mathrm{i}}\left(1+T^2\right)^{1/2}\mathrm{d}T \tag{2.229}$$

so that tracing anticlockwise, with A and B arbitrary constants, in sector 2 of Figure 2.6 we have

$$AI(16) + BI(13^*) = AD_{-\mathrm{i}\gamma}\left(2\mathrm{e}^{\frac{\pi\mathrm{i}}{4}}T_0\sqrt{\gamma}\right) + BD_{-1+\mathrm{i}\gamma}\left(2\mathrm{e}^{\frac{-\pi\mathrm{i}}{4}}T_0\sqrt{\gamma}\right) \tag{2.230}$$
$$= A(\text{equation (2.202)}) + \text{B(equation (2.205))} \tag{2.231}$$
$$= A\mathrm{e}^{\frac{\mathrm{i}\gamma}{2}-\frac{\mathrm{i}\gamma}{2}\ln\gamma}\left[\mathrm{e}^{\frac{3\pi\gamma}{4}+2\mathrm{i}\gamma\int_{T_0}^{\mathrm{i}}\left(1+T^2\right)^{1/2}\mathrm{d}T}\cos g\right.$$
$$\left. + \mathrm{e}^{-\frac{5\pi\gamma}{4}-2\mathrm{i}\gamma\int_{T_0}^{\mathrm{i}}\left(1+T^2\right)^{1/2}\mathrm{d}T}\sin g\right]$$
$$+ \frac{B}{\sqrt{\gamma}}\mathrm{e}^{\frac{-\pi\gamma}{4}-\frac{\mathrm{i}\gamma}{2}+\frac{\mathrm{i}\gamma}{2}\ln\gamma+\frac{\pi\mathrm{i}}{4}}\left[\mathrm{e}^{-2\mathrm{i}\gamma\int_{T_0}^{\mathrm{i}}\left(1+T^2\right)^{1/2}\mathrm{d}T}\sin g\right.$$
$$\left. - \mathrm{e}^{2\mathrm{i}\gamma\int_{T_0}^{\mathrm{i}}\left(1+T^2\right)^{1/2}\mathrm{d}T}\cos g\right] \tag{2.232}$$

Crossing Stokes line I from sector 2 to sector 3, we have

$$A\mathrm{e}^{\frac{\mathrm{i}\gamma}{2}-\frac{\mathrm{i}\gamma}{2}\ln\gamma}\left[\mathrm{e}^{\frac{3\pi\gamma}{4}+2\mathrm{i}\gamma\int_{T_0}^{\mathrm{i}}\left(1+T^2\right)^{1/2}\mathrm{d}T}\cos g + \left(\alpha\mathrm{e}^{\frac{3\pi\gamma}{4}} + \mathrm{e}^{\frac{-5\pi\gamma}{4}}\right)\mathrm{e}^{-2\mathrm{i}\gamma\int_{T_0}^{\mathrm{i}}\left(1+T^2\right)^{1/2}\mathrm{d}T}\sin g\right]$$
$$+ \frac{B}{\sqrt{\gamma}}\mathrm{e}^{\frac{-\pi\gamma}{4}-\frac{\mathrm{i}\gamma}{2}+\frac{\mathrm{i}\gamma}{2}\ln\gamma+\frac{\pi\mathrm{i}}{4}}\left[-\mathrm{e}^{2\mathrm{i}\gamma\int_{T_0}^{\mathrm{i}}\left(1+T^2\right)^{1/2}\mathrm{d}T}\cos g + (1-\alpha)\mathrm{e}^{-2\mathrm{i}\gamma\int_{T_0}^{\mathrm{i}}\left(1+T^2\right)^{1/2}\mathrm{d}T}\sin g\right] \tag{2.233}$$

Crossing the upper branch cut from sector 3 to sector 4, we connect to

$$A\mathrm{e}^{\frac{\mathrm{i}\gamma}{2}-\frac{\mathrm{i}\gamma}{2}\ln\gamma}\left[\mathrm{e}^{\frac{3\pi\gamma}{4}-2\mathrm{i}\gamma\int_{T_0}^{\mathrm{i}}\left(1+T^2\right)^{1/2}\mathrm{d}T}\sin g-\left(\alpha\mathrm{e}^{\frac{3\pi\gamma}{4}}+\mathrm{e}^{\frac{-5\pi\gamma}{4}}\right)\mathrm{e}^{2\mathrm{i}\gamma\int_{T_0}^{\mathrm{i}}\left(1+T^2\right)^{1/2}\mathrm{d}T}\cos g\right]$$
$$+\frac{B}{\sqrt{\gamma}}\mathrm{e}^{\frac{-\pi\gamma}{4}-\frac{\mathrm{i}\gamma}{2}+\frac{\mathrm{i}\gamma}{2}\ln\gamma+\frac{\pi\mathrm{i}}{4}}\left[-\mathrm{e}^{-2\mathrm{i}\gamma\int_{T_0}^{\mathrm{i}}\left(1+T^2\right)^{1/2}\mathrm{d}T}\sin g-(1-\alpha)\mathrm{e}^{2\mathrm{i}\gamma\int_{T_0}^{\mathrm{i}}\left(1+T^2\right)^{1/2}\mathrm{d}T}\cos g\right] \quad (2.234)$$

Crossing Stokes line II from sector 4 to sector 5, we obtain

$$A\mathrm{e}^{\frac{\mathrm{i}\gamma}{2}-\frac{\mathrm{i}\gamma}{2}\ln\gamma}\left[\left(\alpha\mathrm{e}^{\frac{3\pi\gamma}{4}}+\mathrm{e}^{\frac{-5\pi\gamma}{4}}\right)\mathrm{e}^{2\mathrm{i}\gamma\int_{T_0}^{\mathrm{i}}\left(1+T^2\right)^{1/2}\mathrm{d}T}\cos g+\left\{-\beta\left(\alpha\mathrm{e}^{\frac{3\pi\gamma}{4}}+\mathrm{e}^{\frac{-5\pi\gamma}{4}}\right)+\mathrm{e}^{\frac{+3\pi\gamma}{4}}\right\}\right.$$
$$\left.\times\,\mathrm{e}^{-2\mathrm{i}\gamma\int_{T_0}^{\mathrm{i}}\left(1+T^2\right)^{1/2}\mathrm{d}T}\sin g\right]+\frac{B}{\sqrt{\gamma}}\mathrm{e}^{\frac{-\pi\gamma}{4}-\frac{\mathrm{i}\gamma}{2}+\frac{\mathrm{i}\gamma}{2}\ln\gamma+\frac{\pi\mathrm{i}}{4}}\left[-(1-\alpha)\mathrm{e}^{2\mathrm{i}\gamma\int_{T_0}^{\mathrm{i}}\left(1+T^2\right)^{1/2}\mathrm{d}T}\cos g\right.$$
$$\left.-\left\{\beta(1-\alpha)+1\right\}\mathrm{e}^{-2\mathrm{i}\gamma\int_{T_0}^{\mathrm{i}}\left(1+T^2\right)^{1/2}\mathrm{d}T}\sin g\right] \quad (2.235)$$

Equating (2.232) and (2.235) along the real $t(=T_0)$ axis, we have with $B=0$,

$$-\mathrm{e}^{\frac{3\pi\gamma}{4}}=\alpha\mathrm{e}^{\frac{3\pi\gamma}{4}}+\mathrm{e}^{\frac{-5\pi\gamma}{4}} \quad (2.236)$$

and

$$-\mathrm{e}^{\frac{-5\pi\gamma}{4}}=\beta\left(\alpha\mathrm{e}^{\frac{3\pi\gamma}{4}}+\mathrm{e}^{\frac{-5\pi\gamma}{4}}\right)-\mathrm{e}^{\frac{3\pi\gamma}{4}} \quad (2.237)$$

Solving equations (2.236) and (2.237) gives

$$\alpha=-1-\mathrm{e}^{-2\pi\gamma} \quad (2.238)$$
$$\beta=-1+\mathrm{e}^{-2\pi\gamma} \quad (2.239)$$

which implies

$$\arg\alpha=\pi=\arg\beta \quad (2.240)$$

Setting $A=0$ gives

$$\alpha=0\,,\qquad \beta=-2 \quad (2.241)$$

which contradicts equations (2.238) and (2.239) and should be discarded, in view of our remarks between equations (2.214) and (2.215).

We have thus derived equations (2.226), (2.227), (2.238), and (2.239) which are expressions for the four Stokes constants, which underscore eqns (34)–(40) of Crothers [164], namely:

$$\alpha_l - \frac{\mathrm{i}}{2} = (-1)^l Q \left(\frac{2}{\gamma k_0(\infty)} \right)^{\frac{1}{2}} \mathrm{e}^{\mathrm{i}(\eta_{0l} - \tilde{\theta} + \frac{\pi}{4}) + \frac{\pi\gamma}{4}} \tag{34}$$

(2.242)

$$\beta_l = -(-\mathrm{i})^l P \left(\frac{2}{k_1(\infty)} \right)^{\frac{1}{2}} \mathrm{e}^{\mathrm{i}(\eta_{1l} + \tilde{\theta}) + \frac{\pi\gamma}{4}} \tag{35}$$

(2.243)

$$-P\gamma D_{-1-\mathrm{i}\gamma}(x_0) + Q D_{\mathrm{i}\gamma}(-\mathrm{i}x_0) - \mathrm{i}\Omega D_{-\mathrm{i}\gamma}(x_0) = 0 \tag{36}$$

(2.244)

$$P D_{-\mathrm{i}\gamma}(x_0) + Q D_{-1+\mathrm{i}\gamma}(-\mathrm{i}x_0) + \Omega D_{-1-\mathrm{i}\gamma}(x_0) = 0 \tag{37}$$

(2.245)

$$x_0 = 2\mathrm{e}^{\frac{\pi\mathrm{i}}{4}} \sqrt{\gamma} T_0) \tag{38}$$

(2.246)

$$P = \frac{-2\Omega \mathrm{e}^{\frac{\pi\mathrm{i}}{4}} \operatorname{Re}\left[\mathrm{e}^{-\frac{\pi\mathrm{i}}{4}} \mathrm{D}_{-1-\mathrm{i}\gamma}(\mathrm{x}_0) \left\{ \mathrm{D}_{-\mathrm{i}\gamma(\mathrm{x}_0)} \right\}^* \right]}{\gamma \left| D_{-1-\mathrm{i}\gamma}(x_0) \right|^2 + \left| D_{-\mathrm{i}\gamma}(x_0) \right|^2} \tag{39}$$

(2.247)

$$Q = -\Omega \frac{\left[\gamma \left\{ D_{-1-\mathrm{i}\gamma}(x_0) \right\}^2 - \mathrm{i} \left\{ D_{-\mathrm{i}\gamma}(x_0) \right\}^2 \right]}{\gamma \left| D_{-1-\mathrm{i}\gamma}(x_0) \right|^2 + \left| D_{-\mathrm{i}\gamma}(x_0) \right|^2} \tag{40}$$

(2.248)

These are parameterized by I (13):

$$D_{-1-\mathrm{i}\gamma}\left(2\mathrm{e}^{\frac{\pi\mathrm{i}}{4}} T_0 \sqrt{\gamma}\right) = \left(\mathrm{e}^{-\frac{7\pi\gamma}{4}} + b\mathrm{e}^{\frac{\pi\gamma}{4}} \right) \mathrm{e}^{\mathrm{i}\gamma - \mathrm{i}\gamma \ln\gamma - \frac{\pi\mathrm{i}}{4} - \mathrm{i}\tilde{\theta}} \frac{\sin g}{\sqrt{\gamma}} - \left[\mathrm{e}^{\frac{5\pi\gamma}{4}} - a\mathrm{e}^{-\frac{3\pi\gamma}{4}} - ab\mathrm{e}^{\frac{5\pi\gamma}{4}} \right] \mathrm{e}^{\mathrm{i}\tilde{\theta} - \frac{\pi\mathrm{i}}{4}} \frac{\cos g}{\sqrt{\gamma}} \tag{2.249}$$

and I (16)

$$D_{-\mathrm{i}\gamma}\left(2\mathrm{e}^{\frac{\pi\mathrm{i}}{4}} T_0 \sqrt{\gamma}\right) = \left(\alpha \mathrm{e}^{\frac{\pi\gamma}{4}} + \mathrm{e}^{-\frac{7\pi\gamma}{4}} \right) \mathrm{e}^{-\mathrm{i}\tilde{\theta} + \mathrm{i}\gamma - \mathrm{i}\gamma \ln\gamma} \cos g + \left(\mathrm{e}^{\frac{5\pi\gamma}{4}} - \beta \mathrm{e}^{-\frac{3\pi\gamma}{4}} - \alpha\beta \mathrm{e}^{\frac{5\pi\gamma}{4}} \right) \mathrm{e}^{\mathrm{i}\tilde{\theta}} \sin g \tag{2.250}$$

Notice that the dependence of (2.249) and (2.250) on the Stokes constants is nonlinear, via ab and $\alpha\beta$, respectively. The resulting S–matrix has the following properties:

$$|S_{01}|^2 = \sin^2 \mathscr{T} \operatorname{sech}^2 \pi\gamma \tag{2.251}$$

$$|S_{00}|^2 = 1 - |S_{01}|^2 = |S_{11}|^2 \tag{2.252}$$

and

$$S_{00} S_{01}^* + S_{01} S_{11}^* = 0 \tag{2.253}$$

Formula (2.251) is exact for perturbed symmetric resonance [162], [519]. The *single* transition probability p_{01} (see Chapter 4, (4.12)) corresponding to (2.251) is $[1 + \exp(2\pi\gamma)]^{-1}$, which is the basis of Miller [427] (2.50). The Massey parameter $\pi\gamma$ is often written as y or δ. The effective frequency $(\nu\mathscr{T}/2\pi)$ is given by

$$\mathscr{T} = 2\tilde{\theta} - \gamma + \gamma \ln \gamma \tag{2.254}$$

$$= 2\gamma T_0 \sqrt{1 + T_0^2} + 2\gamma \ln\left(\sqrt{1 + T_0^2} + T_0\right) \tag{2.255}$$

$$= 4\gamma \int_0^{T_0} \sqrt{1 + T^2}\, \mathrm{d}T \tag{2.256}$$

$$= +2 \int_0^{2\gamma T_0} \sqrt{1 + T^2}\, \mathrm{d}\tau \tag{2.257}$$

$$= \frac{1}{v} \int_0^{Z_0} \sqrt{4H_{12}^2 + (H_{22} - H_{11})^2}\, \mathrm{d}Z \tag{2.258}$$

where $Z = v\tilde{t}$, v is the impact velocity, $Z_0 = v\tilde{t}_0$ and

$$T = \mp \frac{\tau}{2\gamma} + T_0 \qquad (\tau \lessgtr 0) \tag{2.259}$$

so that

$$T(\tau = 0) = T_0 > 0 \tag{2.260}$$

$$\mathrm{d}T = -\frac{\mathrm{d}\tau}{2\gamma} \qquad (\tilde{t} < 0) \tag{2.261}$$

$$\tau = \int_0^{\tilde{t}} H_{12}(\tilde{t})\, \mathrm{d}\tilde{t} \tag{2.262}$$

The Stueckelberg variable T is related to the two-state Hamiltonian matrix elements by

$$T = \frac{H_{22} - H_{11}}{2H_{12}} \tag{2.263}$$

In summary we have used the JWKB /phase-integral analysis, supplemented by the comparison-equation method, to parameterize the two-state noncrossing parabolic model. However, on this occasion, we have explicitly derived simple algebraic expressions for the four Stokes constants: magnitudes and phases. The sign change in (2.259) at $\tau = t = 0$ ($\tau, t > 0 \Rightarrow T = \tau/2\gamma + T_0$) is an important consideration because it is associated with a classical turning point, that is, a simple transition point viewed from the fully quantal radial coordinate, from which the impact-parameter time-dependent problem is deduced.

2.3.3 The Crossing Parabolic Model

Let us now consider the curve-crossing parabolic model. The difference with the noncrossing model is that now T_0 is negative. However, for ease of calculation we map $T_0 \to -T_0$, with the new T_0 positive, and we absorb the minus sign into the arguments of the parabolic cylinder functions and map $g \to \pi/2 - g$. According to [163] the S-matrix is given by

$$S_{00} = \exp\left[2\mathrm{i}\eta_0 - 2\mathrm{i}\tilde{\theta} + \frac{\pi \mathrm{i}}{2}\right]\left(\frac{\gamma\left(D_{-1-\mathrm{i}\gamma}(x_0)\right)^2 - \mathrm{i}\left(D_{-\mathrm{i}\gamma}(x_0)\right)^2}{\gamma|D_{-1-\mathrm{i}\gamma}(x_0)|^2 + |D_{-\mathrm{i}\gamma}(x_0)|^2}\right) \tag{2.264}$$

$$S_{01} = S_{10} = -2\mathrm{i}\sqrt{\gamma}\exp\left[\mathrm{i}(\eta_0+\eta_1)\right]\left(\frac{\mathrm{Re}[\exp(-\frac{\pi\mathrm{i}}{4})\mathrm{D}_{-1-\mathrm{i}\gamma}(\mathrm{x}_0)\left(\mathrm{D}_{-\mathrm{i}\gamma}(\mathrm{x}_0)\right)^*]}{\gamma|D_{-1-\mathrm{i}\gamma}(x_0)|^2+|D_{-\mathrm{i}\gamma}(x_0)|^2}\right) \quad (2.265)$$

$$S_{11} = \exp\left[2\mathrm{i}\eta_1 + 2\mathrm{i}\tilde{\theta} - \frac{\pi\mathrm{i}}{2}\right]\left(\frac{\gamma\left(D_{-1-\mathrm{i}\gamma}(x_0)\right)^{*\ 2} + \mathrm{i}\left(D_{-\mathrm{i}\gamma}(x_0)\right)^{*\ 2}}{\gamma|D_{-1-\mathrm{i}\gamma}(x_0)|^2+|D_{-\mathrm{i}\gamma}(x_0)|^2}\right) \quad (2.266)$$

where

$$x_0 = 2\exp\left(-\frac{3\pi\mathrm{i}}{4}\right)T_0\sqrt{\gamma} \qquad (T_0>0) \quad (2.267)$$

and

$$(4^*)\ \ D_{-\mathrm{i}\gamma}(x_0) \cong \exp\left(-\tfrac{3\pi\gamma}{4}+\mathrm{i}\gamma-\mathrm{i}\gamma\ln(\gamma)-\mathrm{i}\tilde{\theta}\right)\cos g + \frac{\sqrt{2\pi\gamma}}{\Gamma(1+\mathrm{i}\gamma)}\exp\left(-\tfrac{\pi\gamma}{4}-\mathrm{i}\gamma+\mathrm{i}\gamma\ln(\gamma)+\tfrac{\pi\mathrm{i}}{4}+\mathrm{i}\tilde{\theta}\right)\sin g \quad (I17^*)\ (2.268)$$

$$(5^*)\ \ \sqrt{\gamma}D_{-1-\mathrm{i}\gamma}(x_0) \cong -\exp\left(-\tfrac{3\pi\gamma}{4}+\mathrm{i}\gamma-\mathrm{i}\gamma\ln(\gamma)-\tfrac{\pi\mathrm{i}}{4}-\mathrm{i}\tilde{\theta}\right)\sin g + \frac{\sqrt{2\pi\gamma}}{\Gamma(1+\mathrm{i}\gamma)}\exp\left(-\tfrac{\pi\gamma}{4}-\mathrm{i}\gamma+\mathrm{i}\gamma\ln(\gamma)+\mathrm{i}\tilde{\theta}\right)\cos g \quad (I18^*)\ (2.269)$$

where the last two asymptotic expansions correspond to (4^*) and (5^*) of Crothers [163] and

$$\pm\mathrm{i}\tilde{\theta} = \pm\frac{\mathrm{i}\gamma}{2} \mp \frac{\mathrm{i}\gamma}{2}\ln(\gamma) \pm \frac{\pi\gamma}{2} \mp 2\mathrm{i}\gamma\int_{T_0}^{-\mathrm{i}}\sqrt{1+T^2}\mathrm{d}T \quad (2.270)$$

Suffice it to say that (2.269) is derived by rearranging and conjugating (2.194) and expressing I(18)* in exact terms of I(13) and I(16)*. Notice that we make the coefficient of the dominant term more accurate by *not* expanding the $\Gamma(1+\mathrm{i}\gamma)$ for large γ (this is also done by Fröman et al. [284] in their weak-coupling case; see 2.3.6). It follows that

$$\sqrt{\gamma}D_{-1-\mathrm{i}\gamma}(x_0) \cong -\sin g\exp\left(-\frac{5\pi\gamma}{4}+\frac{\mathrm{i}\gamma}{2}-\frac{\mathrm{i}\gamma}{2}\ln(\gamma)-\frac{\pi\mathrm{i}}{4}+2\mathrm{i}\gamma\int_{T_0}^{-\mathrm{i}}\sqrt{1+T^2}\mathrm{d}T\right) + \frac{\sqrt{2\pi\gamma}}{\Gamma(1+\mathrm{i}\gamma)}\cos g\exp\left(\frac{\pi\gamma}{4}-\frac{\mathrm{i}\gamma}{2}+\frac{\mathrm{i}\gamma}{2}\ln(\gamma) - 2\mathrm{i}\gamma\int_{T_0}^{-\mathrm{i}}\sqrt{1+T^2}\mathrm{d}T\right) \quad (2.271)$$

Having mapped $g \to \pi/2 - g$, we see that setting $C_+ = 1$ and $D_+ = 0$ in equation (150) of Crothers [160] leads us to consider, in sector 5 of Figure 2.6:

$$\exp\left(-2\mathrm{i}\gamma\int_{T_0}^{-\mathrm{i}}\sqrt{1+T^2}\mathrm{d}T\right)\cos g \quad (2.272)$$

Tracing anticlockwise and crossing Stokes line III, this connects in sector 6 of Figure 2.6 to

$$\exp\left(-2\mathrm{i}\gamma\int_{T_0}^{-\mathrm{i}}\sqrt{1+T^2}\mathrm{d}T\right)\cos g+\tilde{a}\exp\left(+2\mathrm{i}\gamma\int_{T_0}^{-\mathrm{i}}\sqrt{1+T^2}\mathrm{d}T\right)\sin g \quad (2.273)$$

where the tilde distinguishes the "crossing" Stokes constant from the "noncrossing" Stokes constant of Section 2.3.2. Crossing the lower branch cut in Figure 2.6 we connect in sector 1 of Figure 2.6 to

$$-\exp\left(+2\mathrm{i}\gamma\int_{T_0}^{-\mathrm{i}}\sqrt{1+T^2}\mathrm{d}T\right)\sin g+\tilde{a}\exp\left(-2\mathrm{i}\gamma\int_{T_0}^{-\mathrm{i}}\sqrt{1+T^2}\mathrm{d}T\right)\cos g \quad (2.274)$$

Finally, crossing Stokes line IV we connect in sector 2 of Figure 2.6 with

$$-\left(1+\tilde{a}\tilde{b}\right)\exp\left(2\mathrm{i}\gamma\int_{T_0}^{-\mathrm{i}}\sqrt{1+T^2}\mathrm{d}T\right)\sin g+\tilde{a}\exp\left(-2\mathrm{i}\gamma\int_{T_0}^{-\mathrm{i}}\sqrt{1+T^2}\mathrm{d}T\right)\cos g \quad (2.275)$$

Using

$$\begin{aligned}\Gamma(1+\mathrm{i}\gamma)&=|\Gamma(1+\mathrm{i}\gamma)|\exp\left(\mathrm{i}\arg\Gamma(1+\mathrm{i}\gamma)\right)\\&=\sqrt{\frac{2\pi\gamma}{1-\exp(-2\pi\gamma)}}\exp\left(-\frac{\pi\gamma}{2}+\mathrm{i}\arg\Gamma(1+\mathrm{i}\gamma)\right)\end{aligned} \quad (2.276)$$

we may rewrite (2.271) as

$$\begin{aligned}&\exp\left(-\frac{3\pi\gamma}{4}-\frac{\mathrm{i}\gamma}{2}+\frac{\mathrm{i}\gamma}{2}\ln(\gamma)+\frac{\pi\mathrm{i}}{4}\right)\sqrt{\gamma}D_{-1-\mathrm{i}\gamma}\left(2\exp(-\frac{3\pi\mathrm{i}}{4})T_0\sqrt{\gamma}\right)\\&\cong-\exp\left(-2\pi\gamma+2\mathrm{i}\gamma\int_{T_0}^{-\mathrm{i}}\sqrt{1+T^2}\mathrm{d}T\right)\sin g+\sqrt{1-\exp(-2\pi\gamma)}\\&\times\exp\left(\frac{\pi\mathrm{i}}{4}-\mathrm{i}\gamma+\mathrm{i}\gamma\ln(\gamma)-\mathrm{i}\arg\Gamma(1+\mathrm{i}\gamma)-2\mathrm{i}\gamma\int_{T_0}^{-\mathrm{i}}\sqrt{1+T^2}\mathrm{d}T\right)\cos g\end{aligned} \quad (2.277)$$

Connecting along the real $t(T_0)$ axis, and from (2.275) and (2.277), we have

$$1+\tilde{a}\tilde{b}=+\mathrm{e}^{-2\pi\gamma} \quad (2.278)$$

$$\tilde{a}=\sqrt{1-\mathrm{e}^{-2\pi\gamma}}\exp\left[\mathrm{i}\left(\frac{\pi}{4}-\gamma+\gamma\ln\gamma-\arg\Gamma(1+\mathrm{i}\gamma)\right)\right] \quad (2.279)$$

so that

$$\tilde{a}\tilde{b}=-(1-\mathrm{e}^{-2\pi\gamma}) \quad (2.280)$$

$$\tilde{b}=-\sqrt{1-\mathrm{e}^{-2\pi\gamma}}\exp\left[-\mathrm{i}\left(\frac{\pi}{4}-\gamma+\gamma\ln\gamma-\arg\Gamma(1+\mathrm{i}\gamma)\right)\right] \quad (2.281)$$

Equations (2.279), (2.280), and (2.281) are in accord with equations (175), (83), and (176), respectively, of Crothers [160]. In retrospect we see that the choice of (2.272) is tantamount to taking $\tilde{a}=1=-\tilde{b}$ in the $\gamma\gg1$ limit in the dominant term, near Stokes lines III and IV. Then tracing anticlockwise in the lower half-plane makes for greater accuracy. Also tracing from sector 5 to sector 2, (2.272)

is subdominant crossing the double Stokes line and is therefore continuous (in the absence of a dominant solution). Nor must we forget that the rules for $\sin g$ and $\cos g$ in Figure 2.6 in crossing the branch cuts are subject to the mapping $g \to \pi/2 - g$, so that (2.274) is correct.

In summary we have used the JWKB/phase-integral analysis, supplemented by the comparison-equation method, to parameterize the two-state diabatic curve crossing (avoided adiabatic/pseudo-crossing) parabolic model. However, on this occasion, we have explicitly derived algebraic expansions for the magnitudes and phases of the two Stokes constants associated with the lower half t-plane. Similar considerations apply to the upper half t-plane (see equations (175) and (176) of Crothers [160]).

2.3.4 Connection to Bárány-Crothers Phase-Integral Nikitin-Model Analysis

Let us refer to Bárány and Crothers [28] as II (see 2.4). In the limit as $\theta \to \pi/2$ we have Rosen-Zener-Demkov [519], [221] noncrossing, and equation II (61) gives, using BC as a subscript on the Stokes constants of II:

$$\arg a_{\mathrm{BC}} + \frac{\pi}{2} = \arg c_{\mathrm{BC}} - \frac{\pi}{2} = \arg a - \pi = 0 \tag{2.282}$$

where the latter is (2.228). We have the Nikitin [453] $T - \tau$ model:

$$T = \frac{\lambda}{2(\tau + \tau_\infty)} - \cot\theta = \frac{\lambda}{2\tau_\infty\left(1 + \frac{\tau}{\tau_\infty}\right)} \tag{2.283}$$

$$\cong \frac{-\lambda\tau}{2\tau_\infty^2} + \frac{\lambda}{2\tau_\infty} \qquad (\tau_\infty \gg 1) \tag{2.284}$$

$$\equiv -\frac{\tau}{2\gamma} + T_0 \tag{2.285}$$

As usual, T is the Stueckelberg variable and τ is the reduced time.

Equation II (20) should be corrected to agree with (2.285) for $\tau < 0$. Further connection with the parabolic model requires

$$\gamma = \frac{\tau_\infty^2}{\lambda} > \gtrsim 1 \tag{2.286}$$

$$T_0 = \frac{\lambda}{2\tau_\infty} = \frac{\tau_\infty}{2\gamma} > 0 \tag{2.287}$$

where λ, γ, and τ_∞ are all large but T_0 is of order unity.

Similarly, we have a Landau-Zener-Stueckelberg crossing in the limit as $\lambda \to +\infty$, $\theta \to 0$ so that $\lambda(1 - \cos\theta)$ remains finite and again

$$\arg a_{\mathrm{BC}} + \frac{\pi}{2} = \tilde{\gamma}\left(\frac{\lambda}{2}(1 - \cos\theta)\right) = \arg\tilde{a} \tag{2.288}$$

$$= \frac{\pi}{4} - \gamma + \gamma\ln(\gamma) - \arg\Gamma(1 + \mathrm{i}\gamma) \tag{2.289}$$

where

$$\gamma = \frac{\lambda}{2}(1 - \cos\theta) \tag{2.290}$$

in agreement with II (61) and (2.279) and, of course, with (189) of Crothers [160].

By the same token we have

$$|a_{\mathrm{BC}}| = \sqrt{1 - \exp(-2\pi\gamma)} = |\tilde{a}| \tag{2.291}$$

in agreement with (175) and (176) of Crothers [160]. The case of $\lambda \to +\infty$ and $\theta \to \pi$ so that $\lambda(1 + \cos\theta)$ remains finite and is noncrossing is given by equation (66) of Crothers [167]. As discussed there, this does not fall within the parabolic model, and unsurprisingly the transition probability is nugatory, because $H_{12} \to 0$ and $H_{22} - H_{11}$ is much greater than in (2.288)-(2.291). Analytic continuation of the Nikitin exponential model to nonzero impact parameters is discussed in detail by Nesbitt et al. [450].

2.3.5 Connections to Nakamura and Zhu Phase-Integral Analysis

Using expressions (2.249) and (2.250), we may, for *noncrossing*, write

$$S_{01} = \frac{-2\mathrm{i}\left(b\mathrm{e}^{\frac{\pi\gamma}{4}} + \mathrm{e}^{-\frac{7\pi\gamma}{4}}\right)\left(\mathrm{e}^{\frac{5\pi\gamma}{4}}(1 - ab) - a\mathrm{e}^{-\frac{3\pi\gamma}{4}}\right)\sin\mathscr{T}}{\left(b\mathrm{e}^{\frac{\pi\gamma}{4}} + \mathrm{e}^{-\frac{7\pi\gamma}{4}}\right)^2 + \left(\mathrm{e}^{\frac{5\pi\gamma}{4}}(1 - ab) - a\mathrm{e}^{-\frac{3\pi\gamma}{4}}\right)^2} \tag{2.292}$$

which, in terms of the Stokes constants a and b, represents a cubic divided by a quartic. Notice that $\arg a = \pi$ (2.228) so that S_{01} is analytic in a and b.

Similarly, expression (2.269) and a similar expression, namely,

$$D_{-\mathrm{i}\gamma}\left(\mathrm{e}^{-\frac{3\pi\mathrm{i}}{4}} 2T_0\sqrt{\gamma}\right) \cong (1 + \tilde{a}\tilde{b})\cos g\ \mathrm{e}^{\frac{5\pi\gamma}{4} + \mathrm{i}\gamma - \mathrm{i}\gamma\ln\gamma - \mathrm{i}\tilde{\theta}} + \tilde{a}\sin g\ \mathrm{e}^{\frac{\pi\gamma}{4} + \mathrm{i}\tilde{\theta}} \tag{2.293}$$

may be used, for *crossing*, to write

$$S_{01} = \frac{-2\mathrm{i}\exp(\frac{3\pi\gamma}{2})(1 + \tilde{a}\tilde{b})|\tilde{a}|\sin(\mathscr{T} + \arg\tilde{a})}{(1 + \tilde{a}\tilde{b})^2\exp(\frac{5\pi\gamma}{2}) + |\tilde{a}|^2\exp(\frac{\pi\gamma}{2})} \tag{2.294}$$

which, in terms of the Stokes constants $\tilde{a}$ and $\tilde{b}$, yet again represents a cubic divided by a quartic.

Notice that S_{01} here is a nonanalytic function of $\tilde{a}$ and $\tilde{b}$ because

$$(\pi - \arg\tilde{a}) = +\arg\tilde{b}^* \tag{2.295}$$

are nonzero (see (2.280) and (2.281)). It follows that the function $f(\lambda)$ given by

$$f(\lambda) = \int_0^\infty \mathrm{d}\mathscr{T}\mathrm{e}^{-\lambda\mathscr{T}} S_{01} = -\mathrm{e}^{-\pi\gamma}\left[\frac{\tilde{a}}{\lambda - \mathrm{i}} - \frac{\tilde{a}^*}{\lambda + \mathrm{i}}\right] \tag{2.296}$$

is not a real function of λ and that

$$\arg\tilde{a} = \frac{-\mathrm{i}}{2}\ln\left[\frac{\int^{(\mathrm{i}-)}\mathrm{d}\lambda\int_0^\infty \mathrm{d}\mathscr{T}\,\mathrm{e}^{-\lambda\mathscr{T}}S_{01}}{\int^{(-\mathrm{i}+)}\mathrm{d}\lambda\int_0^\infty \mathrm{d}\mathscr{T}\,\mathrm{e}^{-\lambda\mathscr{T}}S_{01}}\right] \tag{2.297}$$

essentially because, to repeat, S_{01} is not an analytic function.

We may compare equations (5.15)–(5.18) of Nakamura [447] in the crossing case. Adapting his notation to ours, Nakamura obtains for his four-point cluster of transition points,

$$S_{01} = -U_2 \tag{2.298}$$

where

$$U_2 = \frac{2\mathrm{i}\mathrm{Im}\,\mathrm{U}_1}{1+|U_1|^2} \tag{2.299}$$

The single transition probability is given by

$$p_{01} = \frac{1}{1+|U_1|^2} \tag{2.300}$$

For crossing, our corresponding p_{01} is given by

$$p_{01} = \mathrm{e}^{-2\pi\gamma} \tag{2.301}$$

which tends to zero as $\gamma \to +\infty$. This in turn implies that $|U_1|$ tends to $+\infty$ as $\gamma \to +\infty$, that U_2 tends to zero, and that the S–matrix becomes the unit matrix. It may be noted that our crossing Stokes constants $\tilde{a} \to 1$ and $\tilde{b} \to -1$ are finite as $\gamma \to +\infty$. On the other hand, an infinite change in the coefficient of the subdominant solution when crossing a Stokes line with Stokes constant U_1 would appear to be nonphysical, perhaps because it is associated with the momentum plane [447].

Another difference is that equation (4.38) of Nakamura [447] and the last equation of Section A.4 of [324] for the Stokes constant U for the Weber equation are based on weak-coupling asymptotics, that is, in terms of our notation in Section 2.3.2 and (2.188), $|z^2| >\gtrsim (1, |p|)$ rather than our $|z|^2 \sim |p| >\gtrsim 1$. To tie up the three notations (our γ, Heading's a, and Nakamura's β), we have

$$p = -\mathrm{i}\gamma = -\frac{1}{2} - \frac{1}{2}\mathrm{i}a^2 = -\frac{1}{2} - \mathrm{i}\beta \tag{2.302}$$

A symptom of the difference between their weak-coupling and our strong-coupling derivations is the occurrence of $\ln 2$ in their expressions. As observed by Crothers ([161], [175], and Crothers and O'Rourke [193], strong- and weak-coupling asymptotic expansions have different algebraic forms [324]; the advantage of our (2.271) treatment of crossing is that by making the coefficient of the dominant term more accurate, we are able to obtain an expression for the argument/phase of the Stokes constants $\tilde{a}$, $\tilde{b}$, which interpolates uniformly between $\gamma \to +0$ and $\gamma \to +\infty$. Re noncrossing, Nakamura [447] does not appear to have applied (2.295)–(2.297). However, if *we* do, then

$$p_{01} = \frac{1}{1+\mathrm{e}^{2\pi\gamma}} \tag{2.303}$$

so that

$$U_1 = \mathrm{e}^{\pi\gamma + \mathrm{i}(\mathscr{T} + \arg a)} \tag{2.304}$$

$$S_{01} = -\mathrm{i} \sin \mathscr{T} \operatorname{sech} \pi\gamma \tag{2.305}$$

in accord with (2.252). However, once again this implies that $|U_1| \to +\infty$ as $\gamma \to +\infty$ whereas $a \to 1$ and $b \to 1$ as $\gamma \to +\infty$, with similar implications, as in the crossing case.

2.3.6 Connections to the Frömans-Lundborg Phase-Integral Analysis

For the crossing problem, let us consider, for the two-transition point problem, Fröman et al. [284] and their equation (5.6.4d) for the Stokes constant corresponding to our Stokes line III (of Figure 2.6), namely,

$$b_2 = \frac{\mathrm{i}\sqrt{2\pi}}{\Gamma(\frac{1}{2} - \frac{\mathrm{i}\overline{K}}{\lambda})} \exp\left\{ -\frac{\mathrm{i}\overline{K}}{\lambda} \ln\left(\frac{\overline{K}_0}{\lambda}\right) - \frac{\pi\overline{K}}{2\lambda} + \frac{\mathrm{i}\phi^{(1)}}{\lambda} \right\} \tag{2.306}$$

Identifying their equation (5.3.8) with our (2.188), with

$$\mathrm{i}\gamma \to -\frac{\mathrm{i}\overline{K}}{\lambda} - \frac{1}{2} \tag{2.307}$$

and

$$2T_0\sqrt{\gamma} \to \frac{\phi}{\sqrt{\gamma}} \tag{2.308}$$

we may set, identifying $O(\gamma)$ with $O\left(\frac{1}{\lambda}\right)$,

$$\frac{\overline{K}}{\lambda} = -\gamma + \frac{\mathrm{i}}{2} \tag{2.309}$$

$$\frac{\overline{K}_0}{\lambda} = -\gamma = \frac{\phi^{(1)}}{\lambda} \tag{2.310}$$

whereupon we get agreement with our $\tilde{a}$ of (2.279), apart, that is, from the factor of i in (2.306). This is due to the Stueckelberg [574] choice of branch cut [284]. As shown by Crothers [160] the i disappears upon making the choice of branch cut of our Figure 2.6 or Figure 7 of [160]. After all, the $D_p(z)$ are continuous in the finite plane. In any case the definition of the *effective* Stokes constants depends on one's point of view. We rewrite (2.275) as

$$\frac{(\mathrm{i}\sin g)}{\mathrm{i}}(1 + \tilde{A}\tilde{B}) \exp\left(2\mathrm{i}\gamma \int_{T_0}^{-\mathrm{i}} \sqrt{1 + T^2}\,\mathrm{d}T\right)$$
$$+ \tilde{A} \exp\left(-2\mathrm{i}\gamma \int_{T_0}^{-\mathrm{i}} \sqrt{1 + T^2}\,\mathrm{d}T\right) \frac{\cos g}{\mathrm{i}} \tag{2.311}$$

Here the i in the denominator comes from the change in the particular part of $\sin g$ and $\cos g$, namely $(1 + T^2)^{-1/4}$, when crossing the branch cut. The $(-\mathrm{i}\sin g)/\cos g$ may be regarded as part of the in-/out-going fundamental solution, respectively, just as $(-\sin g)$ and $(\cos g)$ were in (2.275). It follows that

$$\tilde{A} = \mathrm{i}\sqrt{1 - \mathrm{e}^{-2\pi\gamma}}\exp\left(\frac{\pi\mathrm{i}}{4} - \mathrm{i}\gamma + \mathrm{i}\gamma\ln\gamma - \mathrm{i}\arg\Gamma(1 + \mathrm{i}\gamma)\right) \tag{2.312}$$

$$\tilde{B} = \mathrm{i}\sqrt{1 - \mathrm{e}^{-2\pi\gamma}}\exp\left(-\frac{\pi\mathrm{i}}{4} + \mathrm{i}\gamma - \mathrm{i}\gamma\ln\gamma + \mathrm{i}\arg\Gamma(1 + \mathrm{i}\gamma)\right) \tag{2.313}$$

now in complete agreement with b_2 and a_1, of Fröman et al. [284]. There is also latitude in the choice of branch cuts in $(1+T^2)^{-1/4}$: $T = \pm\mathrm{i}, \infty$ are three branch points. Each branch point must be connected to another branch point with connecting branch cut. We choose to connect $+\mathrm{i}$ to $+\mathrm{i}\infty$ and $-\mathrm{i}$ to $-\mathrm{i}\infty$. Fröman et al. choose to connect $-\mathrm{i}$ to $+\mathrm{i}$ and to $-\mathrm{i}\infty$. These considerations apply equally well to the noncrossing case of Section 2.3.2. However, close examination of their equations (5.5.1a,b) shows that like Nakamura they (see Section 2.3.5) have used weak-coupling asymptotic expansions [1]. In their equation (5.5.1b), nevertheless they have made the coefficient of their dominant term more accurate using the exact recurrence relation, just as we did in the strong-coupling case in (2.271) and in Crothers [160], [161], [163], [167]; they have, however, continued the expansion of the argument of the exponential in b_2 in inverse powers of γ, which is particularly appropriate to our strong-coupling treatment ($\gamma >\gtrsim 1$).

2.3.7 Conclusions

We effect a JWKB phase-integral analysis for the crossing and noncrossing parabolic-model nonadiabatic transitions using strong-coupling asymptotics based on the Weber comparison (second-order ordinary-differential) equation for parabolic-cylinder functions. We have shown how to calculate the Stokes constants for noncrossing and have given the simple algebraic expressions ((2.226)–(2.228) and (2.239)–(2.241)) and similarly for crossing ((2.279)–(2.281)). In Sections 2.3.3–2.3.6, we have compared, where possible, with our previous phase-integral analysis [28] of the Nikitin model [459] and with the phase-integral analysis of Nakamura and Zhu [447] and Fröman et al. [284].

There are many intricacies of calculation in applying these models, not least concerning the bending of the double Stokes line as the impact parameter (or azimuthal quantum number) increases [27], [29]; for, of course, it is not difficult to generalize one-dimensional problems to nonzero impact parameters, by analytic continuation. There are many other physical problems, for example, predissociation and resonant scattering [152]. We have not discussed the Kummer model [468], [472] nor generalizations to the complex Nikitin model [467].

Moreover, we recall that it was said at the time [160], following Stueckelberg [574], that the pure phase-integral method for the two-transition-point problem could

only predict three of the four Stokes constants, having invoked unitarity and analyticity. However [198], the comparison-equation method and the parabolic model in particular, resolve the otherwise indeterminate fourth Stokes constant.

We also recall writing [160] "A non-adiabatic transition is thus the physical manifestation of the Stokes phenomenon," which was echoed by Eu [256], and we note the conclusions of Nakamura [447]. We *have* developed a unified uniform theory of crossing and noncrossing.

2.3.8 Curve Crossing Reflection Probabilities in One Dimension

Let us summarize the improved Stueckelberg treatment of [160], hereafter referred to as I, as aplied to curve crossings in I (Section 3.2). Electron translation factors and centrifugal potentials are suppressed and we set

$$r = \exp(x) \tag{2.314}$$

so that $(0, \infty)$ maps to $(-\infty, +\infty)$, where r is the internuclear radial coordinate. Neglecting radial coupling between the stationary-state molecular wave functions, the total wave function Φ is given by

$$r\Phi = u_0^{PSS}(r)\chi_0(r) + u_1^{PSS}(r)\chi_1(r) \tag{2.315}$$

where

$$\left(\frac{\mathrm{d}^2}{\mathrm{d}r^2} + \nu_j^2(r)\right) u_j^{PSS}(r) = 0 \qquad (\hbar = 1) \tag{2.316}$$

$$\frac{\nu_j^2(r)}{2m} = E - \epsilon_j(r), \qquad (j = 0, 1) \tag{2.317}$$

Here m is the reduced mass, E is the total energy, and the $\epsilon_j(r)$ are the molecular eigenenergies. Making the JWKB approximation we have

$$u_j^{PSS}(r) = \alpha_j^+ S_j^+(r) + \alpha_j^- S_j^-(r) \qquad (j = 0, 1) \tag{2.318}$$

where $\alpha_j^{\pm}$ are arbitrary constants. The JWKB functions are given by

$$S_j^{\pm}(r) = \nu_j^{-\frac{1}{2}}(r) \exp\left[\pm \mathrm{i}\left(\int_{r_j}^{r} \nu_j(s)\,\mathrm{d}s + \frac{\pi}{4}\right)\right] \tag{2.319}$$

where the superscript $+(-)$ indicates out-going (in-going), r_j is the classical turning/transition point at which $\nu_j^2(r)$ has a zero and the ubiquitous $\pi/4$ is half the phase of the Stokes constant for the one-transition-point problem. We make the linear-combinations-of-atomic-orbitals approximation:

$$\begin{aligned} \chi_0 &= \phi_0 \sin g - \phi_1 \cos g \\ \chi_1 &= \phi_0 \cos g - \phi_1 \sin g \end{aligned} \tag{2.320}$$

where the ϕ_j are r-invariant and

$$\sqrt{2}\left\{\begin{matrix}\sin\\ \cos\end{matrix}\right\} g = \exp\left[\pm\frac{1}{2}\int_0^t \frac{\mathrm{d}\tilde{t}}{(1+\tilde{t}^2)^{1/2}} - \frac{1}{2}\int_0^t \frac{\tilde{t}\,\mathrm{d}\tilde{t}}{1+\tilde{t}^2}\right] \tag{2.321}$$

where t is the Stueckelberg variable given in the LCAO approximation by

$$1 + t^2 = \frac{m^2(\nu_0^2 - \nu_1^2)^2}{H_{12}^2} \tag{2.322}$$

and on the real $t-$ and $r-$ axes

$$\sqrt{2}\left\{\begin{matrix}\sin\\ \cos\end{matrix}\right\} g = \sqrt{1 \pm \frac{t}{\sqrt{1+t^2}}} \tag{2.323}$$

Assuming that $t = \pm\mathrm{i}$ and $r = r_c, r_c^*$ are complex conjugate transition points, we note that as usual $\alpha_j^{\pm}$ suffer discontinuities on crossing the appropriate Stokes lines in accordance with the Stokes phenomenon, the physical manifestation of which is a nonadiabatic transition.

Defining

$$\delta + \mathrm{i}\mathscr{T} = \mathrm{i}\int_{r_0}^{r_c^*} \nu_0\,\mathrm{d}r - \mathrm{i}\int_{r_1}^{r_c^*} \nu_1\,\mathrm{d}r \tag{2.324}$$

where r_c^* is in the lower half-plane, I gives the following connection formulae, where

$$u_0 = u_0^{PSS}\sin g + u_1^{PSS}\cos g \tag{2.325}$$
$$u_1 = -u_0^{PSS}\cos g + u_1^{PSS}\sin g \tag{2.326}$$

namely:

$$u_0\sqrt{2} = (\alpha_0^+ S_0^+ + \alpha_0^- S_0^-)\sin g + (\alpha_1^+ S_1^+ + \alpha_1^- S_1^-)\cos g \tag{2.327}$$
$$u_1\sqrt{2} = -(\alpha_0^+ S_0^+ + \alpha_0^- S_0^-)\cos g + (\alpha_1^+ S_1^+ + \alpha_1^- S_1^-)\sin g \tag{2.328}$$

where $r_{0,1} < r < r_X = \mathrm{Re}\,\mathrm{r_c}$, and

$$u_0\sqrt{2} = (\beta_0^+ S_0^+ + \beta_0^- S_0^-)\sin g + (\beta_1^+ S_1^+ + \beta_1^- S_1^-)\cos g \tag{2.329}$$
$$u_1\sqrt{2} = -(\beta_0^+ S_0^+ + \beta_0^- S_0^-)\cos g + (\beta_1^+ S_1^+ + \beta_1^- S_1^-)\sin g \tag{2.330}$$

where $r > r_X$ and

$$\beta_0^+ = a\alpha_0^+ + \exp(-\delta - \mathrm{i}\mathscr{T})\alpha_1^+ \tag{2.331}$$
$$\beta_0^- = a^*\alpha_0^- + \exp(-\delta + \mathrm{i}\mathscr{T})\alpha_1^- \tag{2.332}$$
$$\beta_1^+ = a^*\alpha_1^+ - \exp(-\delta + \mathrm{i}\mathscr{T})\alpha_0^+ \tag{2.333}$$
$$\beta_1^- = a\alpha_1^- - \exp(-\delta - \mathrm{i}\mathscr{T})\alpha_0^- \tag{2.334}$$

while the Stokes constant a is given by

$$|a| = \sqrt{1 - \mathrm{e}^{-2\delta}} \tag{2.335}$$

$$\arg a = \frac{\pi}{4} + \gamma \ln \gamma - \gamma - \arg \Gamma(1 + \mathrm{i}\gamma) \tag{2.336}$$

$$\gamma = \frac{\delta}{\pi} \tag{2.337}$$

The statement by Jakushina and Linnaeus [340] that I considered only "the model problem with linear potentials and constant coupling." is erroneus, although we will consider such a model problem. In fact, their notation, t of (2.322) is given by

$$t = \frac{[\Phi_1(r) - \Phi_2(r)]}{2\alpha(r)} \tag{2.338}$$

Case A: Similar Slopes

Let us now apply the preceding formulation to the model problem of Child [116], Zhu [612], and Nakamura [447]:

$$\left[\frac{1}{2m}\frac{\mathrm{d}^2}{\mathrm{d}x^2} + E - H_{00}(x)\right] u_0 = H_{01} u_1 \tag{2.339}$$

$$\left[\frac{1}{2m}\frac{\mathrm{d}^2}{\mathrm{d}x^2} + E - H_{11}(x)\right] u_1 = H_{01} u_0 \tag{2.340}$$

and in our notation, where the diabatic potentials are (Figure 2.7)

$$H_{jj}(x) = -F_j x \qquad (j = 0, 1) \tag{2.341}$$

$$H_{01} = A \tag{2.342}$$

and for similar slopes, we have

$$F_0 > F_1 > 0 \tag{2.343}$$

The Stueckelberg variable t is given by:

$$t = \frac{(F_0 - F_1)x}{2A} \tag{2.344}$$

By translation of axes, the curve-crossing and the energy-reference level are located at the origin, without loss of generality. The adiabatic turning points are given by

$$2F_0F_1 x_{\substack{0\\1}} = -E(F_0 + F_1) \mp \sqrt{4A^2F_0F_1 + E^2(F_0 - F_1)^2} \tag{2.345}$$

and the adiabatic energies by

$$\frac{\nu_j^2(x)}{2m} = E - \epsilon_j(x) \tag{2.346}$$

where

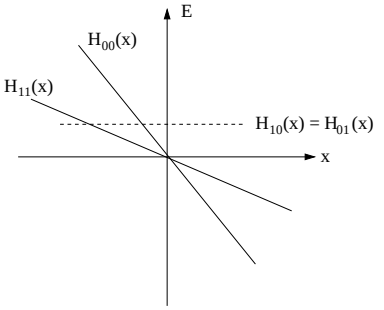

Fig. 2.7. Linear curve crossing: same sign of slopes

$$\epsilon_{\substack{0\\1}}(x) = -(F_0 + F_1)\frac{x}{2} \mp A\sqrt{1+t^2} \tag{2.347}$$

We assume that $E > 0$

From (2.331)–(2.334) and setting (Jeffreys' connection)

$$\alpha_0^+ = -\alpha_0^- = -c \tag{2.348}$$

$$\alpha_1^+ = -\alpha_1^- = -d \tag{2.349}$$

then [324], we have reflection amplitudes ($g = \pi/2$) given by

$$R_0 = -\frac{\beta_0^+}{\beta_0^-} = -\frac{\left(-ac + \mathrm{e}^{-\delta - \mathrm{i}\mathscr{T}} d\right)}{(a^* c - \mathrm{e}^{-\delta + \mathrm{i}\mathscr{T}} d)} \tag{2.350}$$

$$R_1 = -\frac{\beta_1^+}{\beta_0^-} = -\frac{\left(-a^* d + \mathrm{e}^{-\delta + \mathrm{i}\mathscr{T}} c\right)}{(a^* c - \mathrm{e}^{-\delta + \mathrm{i}\mathscr{T}} d)} \tag{2.351}$$

where c/d is given (no in-going incident wave in channel 1)

$$\beta_1^- = 0 \tag{2.352}$$

so that

$$R_0 = \left[\mathrm{e}^{-2\delta - 2\mathrm{i}\mathscr{T}} + \mathrm{e}^{2\mathrm{i}\arg a}(1 - \mathrm{e}^{-2\delta})\right] \tag{2.353}$$

$$R_1 = -2\mathrm{i}\sin(\mathscr{T} + \arg a)\mathrm{e}^{-\delta}\sqrt{1 - \mathrm{e}^{-2\delta}} \tag{2.354}$$

It follows that unitarity is fulfilled

$$|R_0|^2 + |R_1|^2 = 1 \tag{2.355}$$

where

$$|R_1|^2 = 4\mathrm{e}^{-2\delta}(1 - \mathrm{e}^{-2\delta})\sin^2(\mathscr{T} + \arg a) \tag{2.356}$$

Averaging the Stueckelberg oscillations gives

$$P_{01} = 2P(1 - P) \tag{2.357}$$

the familiar Landau-Zener formula where

$$P = \mathrm{e}^{-2\delta} \tag{2.358}$$

and δ is the familiar Massey parameter. Even in this one-dimensional reflection problem, the pseudo-curve-crossing arises on the way in and on the way out:

$$P(1-P) + (1-P)P = 2P(1-P) \tag{2.359}$$

that is, either transition going in and none going out or vice versa. It may be noted that in this derivation, it was not necessary to use the momentum representation that in effect is the impact parameter formulation, unfortunately sometimes also confusingly called the semiclassical treatment.

Case B: Dissimilar Slopes

In Case B we have

$$F_0 > 0 > F_1 \tag{2.360}$$

in contrast with (2.343) in Case A. Further we refer to Figure 2.8 and make the concrete assumption that

$$E > E_b \tag{2.361}$$

Because u_1^{PSS} of (2.318) is now associated with the upper potential-energy curve, the Bohr–Sommerfeld connection requires

$$\alpha_1^+ + \alpha_1^- = 0 \tag{2.362}$$

but

$$\beta_1^+ \mathrm{e}^{\mathrm{i}(\frac{\pi}{2} - \overline{\mathscr{T}})} + \beta_1^- \mathrm{e}^{\mathrm{i}(\overline{\mathscr{T}} - \frac{\pi}{2})} = 0 \tag{2.363}$$

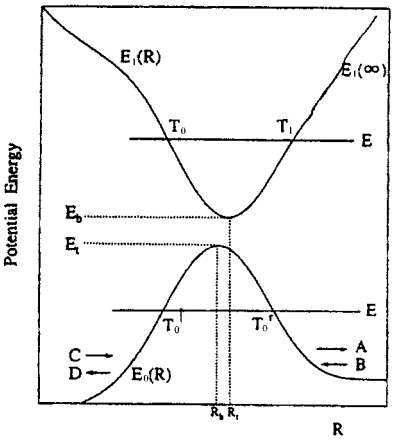

Fig. 2.8. Nonadiabatic tunneling-type curve crossing

where

$$\overline{\mathscr{T}} = -\int_{x_0}^{x_1} \nu_1(x)\,\mathrm{d}x \tag{2.364}$$

There are no incident waves in channel 0 from negative x so that

$$\alpha_0^+ = 0 \tag{2.365}$$

noting that in the x-representation, for negative x, in-going and out-going reverse their meanings and therefore their superscripts. Solving (2.331)–(2.334) gives the reflection amplitude in channel 0 and the transition amplitude in channel 1, respectively, by

$$R_0 = \frac{-\mathrm{i}\mathrm{e}^{-2\delta-2\mathrm{i}\mathscr{T}+\mathrm{i}\overline{\mathscr{T}}}}{2\mathrm{e}^{-\mathrm{i}\arg a}(1-\mathrm{e}^{-2\delta})\cos(\overline{\mathscr{T}}+\arg a)+\mathrm{e}^{-2\delta+\mathrm{i}\overline{\mathscr{T}}}} \tag{2.366}$$

$$T_1 = \frac{2\mathrm{i}\cos(\overline{\mathscr{T}}+\arg a)\sqrt{1-\mathrm{e}^{-2\delta}}}{2\mathrm{e}^{-\mathrm{i}\arg a}(1-\mathrm{e}^{-2\delta})\cos(\overline{\mathscr{T}}+\arg a)+\mathrm{e}^{-2\delta+\mathrm{i}\overline{\mathscr{T}}}} \tag{2.367}$$

As for Case A we have unitarity, but now given by

$$|R_0|^2 + |T_1|^2 = 1 \tag{2.368}$$

where

$$|T_1|^2 = \frac{4(1-\mathrm{e}^{-2\delta})\cos^2(\overline{\mathscr{T}}+\arg a)}{4(1-\mathrm{e}^{-2\delta})\cos^2(\overline{\mathscr{T}}+\arg a)+\mathrm{e}^{-4\delta}} \tag{2.369}$$

The transition amplitude is zero, when

$$\overline{\mathscr{T}} + \arg a = n\pi + \frac{\pi}{2} \tag{2.370}$$

However because $\overline{\mathscr{T}}$ is negative and $\arg a \in (\pi/4, \pi/2)$, including weak and strong coupling, we envisage negative integers n, in which case we have perfect reflection, as remarked by Nakamura [447] and when (2.370) is not satisfied, nonadiabatic tunnelling obtains.

The cases that arise when (2.361) is not fulfilled are considered by Nakamura and by Coveney et al. [152].

2.4 Addition of a Simple Pole

2.4.1 Introduction

A simple but versatile atomic collision model for treating nonadiabatic phenomena associated with curvecrossings and noncrossings is the exponential model of Nikitin. This two-state model leads, within a semiclassical framework, to a collision S-matrix made up of classical trajectory transition probabilities and semiclassical phases. It

can be used to discuss physical processes such as excitation and charge transfer. In applying the model expressions to real situations, phase-integral expressions for the S-matrix elements are needed. Such expressions have been obtained earlier by Crothers through a process of interpretation and abstraction. To shed new light on this interpretation we give a phase-integral derivation of the two-state semiclassical collision S-matrix within a general exponential model [28].

Representing the S–matrix as a product of two halfway house matrices and assuming only one principal transition zone in each half, we may parameterize the elements of S in a semiclassically consistent way. The parameters are computed in terms of certain Stokes constants and complex Coulomb phases arising from the classical trajectory equations describing the evolution of the diabatic linear combination of atomic orbitals electronic states. The Stokes constants and complex Coulomb phases associated with the canonical (pure exponential model) one-pole, two-transition-point problem are parameterized via the comparison equation method, supplemented by strong-coupling asymptotics. The corresponding quantities for a perturbed canonical form (general exponential model) are suitably abstracted in terms of simple known functions and physically significant phase integrals. In this way the complete semiclassical collision S–matrix is derived. A short discussion of its applicability is given.

Many physical processes can be discussed successfully within the framework of simple mathematical models. These models usually select and put forward some special mechanism as being primarily responsible for the observed behaviour of the physical system. Through the simplification of the problem offered by the model, one can get a better understanding of the workings of the mechanism. This can be done by analytical or numerical studies of the model equations, but although numerical investigations may be more straightforward to perform, analytical results are often more useful when it comes to understanding the models and their application to real situations. In this work we present an analytical investigation of a simple but versatile atomic collision model: the exponential model.

In treating low-energy inelastic atomic collision processes (such as excitation, charge transfer, or transfer ionization), one is faced with a complicated quantum mechanical many-body system. Through a series of approximations one may, in many cases, reduce the problem to a manageable semiclassical form, namely, a set of equations describing the quantum mechanical evolution of the electronic states as the nuclei follow classical trajectories (see for example [220]. Using these classical trajectory equations, together with semiclassical phase shifts for the nuclear motion, many collision processes may be explained. Prime examples are the nonadiabatic phenomena, such as curve-crossing transitions and interferences observed as distinct structures in the total and differential collision cross sections [457].

Essential for the understanding of the nonadiabatic collision processes have been two simple two-state models formulated in the semiclassical framework described earlier. One is the Landau–Zener curve-crossing model [376], [611] and the other is the Rosen–Zener noncrossing model [519]. These models represent two extreme situations in which the coupling between adiabatic states is due solely to variation of the diabatic energy difference (Landau–Zener) or to variation of the nondiabatic cou-

pling element (Rosen–Zener). As a generalization of these two extreme situations, the two-state exponential semiclassical model for atomic collisions was introduced by Nikitin [453], [454] and independently by Ellison and Borowitz [242]. In this model both the diabatic energy difference and the nondiabatic coupling element may vary, and through the choice of a certain mixing parameter θ both crossing and noncrossing situations are covered.

To understand the properties of these types of model and to be able to apply them to real situations, general phase-integral expressions for the transition probabilities and phases entering the semiclassical scattering matrix are needed (cf. [175]). The original inventors of the exponential model used confluent hypergeometric functions and weak-coupling asymptotic expansions [161], [167] to derive expressions for the nonadiabatic transition probability and its behaviour under various limiting conditions. A first step towards a more general derivation was taken by Dubrovskiy [232] in tackling the general two-state problem of nonadiabatic transitions. He used both phase-integral [574] and comparison-equation [428] techniques and derived closed-form expressions for the transition probability in the case of an avoided crossing between adiabatic energy levels. His final expressions have been criticized by one of us [160] on the grounds that they vanish for certain types of interaction potentials. Also an attempt by Child [115] to generalize Dubrovskiy's results has been criticized [163]. We will discuss the application of their results to the exponential model in Section 2.4.6. A general discussion on the calculation of transition probabilities was given by Nikitin [455], who stressed the importance of the complex analytic structure of the adiabatic energy difference. An excellent review of the status of the exponential model at the end of the 1960s was written by Nikitin [456]. During the 1970s some major steps towards the understanding of the applicability of the exponential model were taken. First, the validity of the semiclassical treatment (classical trajectories, phase-integral expressions) were investigated in depth. (For classical trajectories, see, for example, [40], [217], [220]. For phase integrals, see the introduction to Bárány and Crothers [27], the review by Crothers [175], and, in a more general context, the review by Berry and Mount [72].) Secondly, the phases of the exponential model were derived [52], [167], [458], [169]. Thirdly, and perhaps most importantly, there were serious applications of the model to real physical collision processes [169], [174], [319].

The applications made by Crothers and Todd [169], [174] rely on a Zwaan–Stueckelberg phase-integral interpretation (abstraction) of the exponential model. Although the results in general were encouraging, there were some difficulties in applying the model to the charge transfer reaction $Mg^{2+} + H \rightarrow Mg^{+} + H^{+}$, because of the existence of two distinct transition regions (of which only one was found to be effective). To pinpoint possible defects of the phase-integral interpretation, it was felt that a phase-integral derivation was needed. That such a derivation might lead to new insights had been shown for the linear model [24], [25], [26].

2.4.2 The Semiclassical Scattering Matrix

The information that is needed for the calculation of differential and total cross sections is conveniently summarized in the partial-wave-scattering matrix. This quantum mechanical scattering matrix can be defined in terms of the solutions to a set of coupled Schrödinger differential equations. Here we shall only consider the semiclassical scattering matrix that can be derived by using semiclassical elastic phase shifts and classical trajectory equations (see, for example, [160]. Even though some of our expressions formally hold true for an arbitrary number of states, we shall immediately specialize to two states only.

The two-state impact-parameter-dependent scattering matrix $\mathbf{S} = \mathbf{S}(E, \rho)$ is unitary and symmetric. This implies that it can be represented as

$$\mathbf{S} = \tilde{\mathbf{S}}_h \mathbf{S}_h \,, \tag{2.371}$$

where $\mathbf{S}_h$ is unitary and $\tilde{\mathbf{S}}_h$ signifies the transposed matrix. In general this representation is purely formal, but for heavy-particle scattering (where semiclassical concepts apply) it is possible to interpret $\mathbf{S}_h$ as a halfway house scattering matrix. The semiclassical structure of $\mathbf{S}_h$ depends on the number of localized transition zones, but for the simplest case of just one zone it is given [52] by

$$\mathbf{S}_h = \mathbf{O} \exp(\mathrm{i}\boldsymbol{\Delta}) \mathbf{T}_h \exp[\mathrm{i}(\boldsymbol{\eta} - \boldsymbol{\Delta})] \tag{2.372}$$

Here $\boldsymbol{\Delta}$ is a diagonal matrix containing the phases that develop between the turning points and the transition zone, $\boldsymbol{\eta}$ is the diagonal semiclassical phase-shift matrix and $\mathbf{T}_h$ is a unitary transition matrix characteristic of the transition zone. This transition matrix is determined by a set of classical trajectory equations and has determinant equal to unity. It is possible to parameterize it as

$$\mathbf{T}_h = \begin{bmatrix} (1 - z^2)^{1/2} \exp(\mathrm{i}\phi) & -z \exp(-\mathrm{i}\chi) \\ z \exp(\mathrm{i}\chi) & (1 - z^2)^{1/2} \exp(-\mathrm{i}\phi) \end{bmatrix} \tag{2.373}$$

where $0 \leq z \leq 1$ and ϕ and χ are real phases.

The matrix $\mathbf{O}$ is a (real orthogonal) rotation matrix that takes into account the fact that the two states forming a basis at infinity may be mixed close to the turning point. It has been found, both analytically and numerically, that for low-energy heavy-particle collisions the matrix $\mathbf{O}$ may be put equal to the unit matrix if the representation is taken to be the adiabatic one, i.e., if $\boldsymbol{\Delta}$ and $\boldsymbol{\eta}$ are adiabatic phases [160], [344], [215]. Then the parameters z, ϕ, and χ are well-behaved functions of E and ρ. This follows from the fact that a correct semiclassical treatment necessarily introduces adiabatic phases, a point already stressed by one of us [160], [164], [167].

Consider then the classical trajectory equations in adiabatic (l.c.a.o.) formulation [216]

$$\mathrm{i} \frac{\mathrm{d}}{\mathrm{d}\tau} a_{1,2} = a_{2,1} \exp\left[\mp 2\mathrm{i} \int_0^\tau T(\tau' \, \mathrm{d}\tau' \right] \tag{2.374}$$

The independent variable τ is defined as

$$\tau = \int_0^t H_{12}\,\mathrm{d}t' \tag{2.375}$$

with the supposition that

$$\tau_\infty = \int_0^{+\infty} H_{12}\,\mathrm{d}t' < +\infty \tag{2.376}$$

and the Stueckelberg variable T by

$$T = (H_{22} - H_{11})/2H_{12} \tag{2.377}$$

where $H_{22} - H_{11} \geq 0$ at infinity. The classical trajectory $R = R(t)$ is assumed to be symmetric, $R(-t) = R(t)$, so that T is an even function of τ and the vector $\mathbf{a}(\tau_\infty)$ is related to $\mathbf{a}(-\tau_\infty)$ by

$$\mathbf{a}(\tau_\infty) = \tilde{\mathbf{G}}^d \mathbf{G}^d \mathbf{a}(-\tau_\infty) \tag{2.378}$$

Here the matrix $\mathbf{G}^d$ propagates $\mathbf{a}$ from $\tau = -\tau_\infty$ to the origin $\tau = 0$. Reverting to the adiabatic representation then gives [218]

$$\mathbf{G}^a = \tilde{\mathbf{R}}\mathbf{G}^d \exp(-\mathrm{i}\frac{1}{2}\boldsymbol{\zeta}) \tag{2.379}$$

where the matrix $\boldsymbol{\zeta}$ is diagonal with elements $\pm\zeta$, given by

$$\zeta = 2\int_{-\tau_\infty}^{0} [(1 + T^2)^{1/2} - T]\mathrm{d}\tau' \tag{2.380}$$

The matrix $\mathbf{R}$ is a (real orthogonal) rotation matrix transforming from the adiabatic to the diabatic representation. From the correspondence

$$\mathbf{G}^a \exp(\mathrm{i}\boldsymbol{\eta}) = \mathbf{S}_h \tag{2.381}$$

we find, using the explicit expression for $\mathbf{S}_h$ with $\mathbf{O} = 1$

$$\mathbf{G}^a = \exp(\mathrm{i}\boldsymbol{\Lambda})\mathbf{T}_h \exp(-\mathrm{i}\boldsymbol{\Lambda}) \tag{2.382}$$

2.4.3 Phase-Integral Treatment

We now set out to determine (within the l.c.a.o. approximation) the matrix $\mathbf{G}^a$, using phase-integral methods. Because of symmetry we need only consider the elements of the first column, G^a_{11} and G^a_{21}. Then we have

$$G^a_{22} = (G^a_{11})^* \,, \qquad G^a_{12} = -(G^a_{21})^* \tag{2.383}$$

Introducing first a new set of dependent variables, c_1, c_2 through

$$c_{1,2} = a_{1,2} \exp\left[\pm\mathrm{i}\int_0^\tau T(\tau')\,\mathrm{d}\tau'\right] \tag{2.384}$$

we find that

$$\mathrm{i}\,\mathrm{d}c_{1,2}/\mathrm{d}\tau = \mp T c_{1,2} + c_{2,1} \tag{2.385}$$

Differentiation and elimination show that c_1 and c_2 satisfy the second-order equations

$$\mathrm{d}^2 c_{1,2}/\mathrm{d}\tau^2 + Q_{1,2}^2(\tau) c_{1,2} = 0 \tag{2.386}$$

where

$$Q_{1,2}^2 = 1 \mp \mathrm{i}\,\mathrm{d}T/\mathrm{d}\tau + T^2 \tag{2.387}$$

We now introduce the following model assumptions: with positive parameters λ and θ subject to $0 < \theta < \pi$ and fulfilling the general inequalities

$$1 \lesssim \lambda \lesssim 2\tau_\infty / \sin\theta \tag{2.388}$$

the function T is given for $\mathrm{Re}\,\tau \leq 0$ by

$$T(\tau) = \lambda/2(\tau + \tau_\infty) - \cot\theta + F(\tau) \tag{2.389}$$

This contrasts [164] with

$$T(\tau) = -\frac{\tau}{2\gamma} + T_0 \tag{2.390}$$

which when substituted into (2.386) yields the so-called parabolic models [163], [164]. In the model relation (2.389) $F(\tau)$ acts as a perturbation in a wide region surrounding the origin ($\tau = 0$) and the pole ($\tau = -\tau_\infty$). For $F = 0$ we retrieve the pure exponential model (with impact parameter zero, rectilinear trajectory, and constant velocity). The canonical form is then a pole plus a constant. The more general case treated here includes generalizations to nonzero impact parameters, curved trajectories, and varying velocity. It also includes certain other potential models, e.g., the Demkov-Kunicke [222] model.

To find out the relation between λ, θ, and the physical potentials, we suppose that

$$\left.\begin{array}{c} \lim_{R\to+\infty}(H_{22} - H_{11}) = \Delta\epsilon > 0 \\ \lim_{R\to+\infty} H_{12} \propto \exp(-\alpha R) \end{array}\right\} \tag{2.391}$$

Calculating the residue of $T(\tau)$ then gives

$$\lambda = \Delta\epsilon/\alpha v \tag{2.392}$$

where $v = \dot{R}(+\infty)$. Again, provided

$$\lambda \ll 2\tau_\infty \cot\theta \tag{2.393}$$

we have

$$-\cot\theta \approx T(0) = [(H_{22} - H_{11})/2H_{12}]|_{R(0)} \tag{2.394}$$

This relation shows, among other things, that, broadly speaking, the potentials H_{11} and H_{22} cross for acute θ, while they are noncrossing for obtuse θ. The angle $\theta =$

$1/2\pi$ corresponds to perturbed symmetric resonance [160], i.e., to potentials that run approximately parallel [221].

We now introduce the Langer-corrected functions

$$q_{1,2}^2(\tau) = Q_{1,2}^2(\tau) - \frac{1}{4(\tau+\tau_\infty)^2}$$
$$= 1 + \cot^2\theta - \lambda\cot\theta/(\tau+\tau_\infty) + (\lambda \pm \mathrm{i})/4(\tau+\tau_\infty)^2 + \ldots \quad (2.395)$$

Writing

$$q_{1,2}(\tau) = [(\tau-\tau_{1,2})(\tau-\tau_{2,1}^*)]^{1/2}/(\tau+\tau_\infty)\sin\theta \quad (2.396)$$

we define the argument of the square root to be zero on the real axis as $\tau \to +\infty$. The branch cuts are inserted from the zeros $\tau_{1,2}$ (upper half-plane) and $\tau_{1,2}^*$ (lower half-plane) according to Figure 2.9. Note that τ_1 and τ_2^* belong to $q_1^2(\tau)$, while τ_2 and τ_1^* belong to $q_2^2(\tau)$.

Concentrating now on the function $c_2(\tau)$, we consider the pattern of Stokes lines emanating from the zeros τ_1^* and τ_2 of q_2^2. These are lines on which

$$\mathrm{Re}\left(\int_{\tau_1^*,\tau_2}^{\tau} \mathrm{q}_2\,\mathrm{d}\tau'\right)$$

is constant, so that

$$\exp\left(\mathrm{i}\int_{\tau_1^*,\tau_2}^{\tau} q_2\,\mathrm{d}\tau'\right)$$

has nonoscillating behaviour. In Figures 2.10a, b, and c these patterns are shown for different values of θ.

We note that two Stokes lines spiral into the pole. An investigation shows that these are logarithmic spirals revolving an infinite number of times around thepole. The choice of branch cuts in Figure 2.9 is, of course, to some extent arbitrary, so that we could, for instance, without loss of generality draw theupper branch cut in Figure 2.10a and the lower branch cut in Figure 2.10c so that they do not cross a Stokes line in the finite plane.

To satisfy the boundary conditions at the pole ($a_1(t=-\infty)=1$, $a_2(t=-\infty)=0$) we write

$$c_{1,2}(\tau) = B_{1,2}q_{1,2}^{-1/2}\exp\left(\mathrm{i}\int_0^{\tau} q_{1,2}\,\mathrm{d}\tau'\right) \quad (2.397)$$

and let τ tend to $-\tau_\infty$. In order that the integrals be well defined we insert a branch cut from $-\tau_\infty$ along the negative real axis in the direction of $-\infty$. Actual oomputations (with use of the first-order equations to connect c_1 and c_2) then give (to within semiclassical accuracy)

$$B_1 = -\frac{1}{2B_2^*} \quad (2.398)$$

$$B_2 = -\frac{1}{\sqrt{2}}[(1+T_0^2)^{1/2} - T_0]^{1/2}\exp(-\nu + \mathrm{i}\Theta + \frac{1}{2}\mathrm{i}\zeta) \quad (2.399)$$

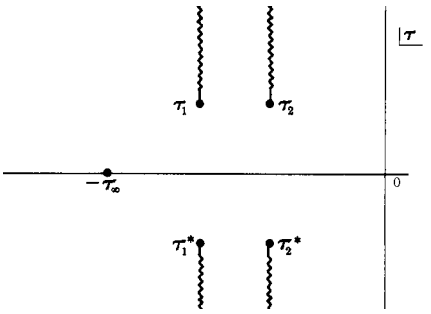

Fig. 2.9. Complex τ-plane showing zeros of $q_{1,2}^2$ and branch cuts (*wiggly lines*). τ_1 and τ_2^* concern c_1 and τ_1^* and τ_2 concern c_2

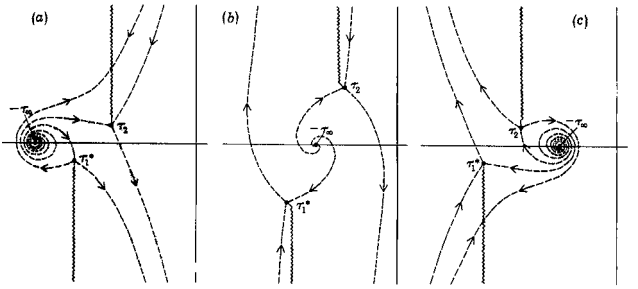

Fig. 2.10. Complex τ-plane showing qualitative behaviour of Stokes lines for c_2 for (**a**) $0 < \theta < 1/2\pi$, (**b**) $\theta = 1/2\pi$, (**c**) $1/2\pi < \theta < \pi$. Arrows show direction of increasing $|\exp[\mathrm{i}\int q_2 \mathrm{d}\tau]|$

where $T_0 = T(\tau = 0)$ and

$$-v + \mathrm{i}\Theta = \mathrm{i}\int_{-\tau_\infty}^{0}\left[q_2 - (1+T^2)^{1/2} - \frac{\mathrm{i}\,\mathrm{d}T/\mathrm{d}\tau}{2(1+T^2)^{1/2}}\right]\mathrm{d}\tau' \tag{2.400}$$

An alternative expression for B_2 is (again to within semiclassical accuracy)

$$B_2 = -\frac{1}{\sqrt{2}}[(1+T_0^2)^{1/2} + T_0]^{1/2}\exp(-u + \mathrm{i}\Theta + \frac{1}{2}\mathrm{i}\zeta)\exp(y_2) \tag{2.401}$$

where y_2 is defined through

$$-\frac{1}{2}x_{1,2} + \frac{1}{2}\mathrm{i}y_{1,2} = \int_0^{\tau_{1,2}} q_{1,2}\,\mathrm{d}\tau' \tag{2.402}$$

and

$$u = \frac{1}{2}(y_1 + y_2) + \mathrm{Im}\int_{-\tau_\infty}^{\tau_1^*}\left[\mathrm{q}_2 - \frac{\mathrm{i}\mathrm{dT}/\mathrm{d}\tau}{2(1+\mathrm{T}^2)^{1/2}}\right]\mathrm{d}\tau' - \mathrm{Im}\int_{\tau_2}^{0}\left[\mathrm{q}_2 - \frac{\mathrm{i}\mathrm{dT}/\mathrm{d}\tau}{2(1+\mathrm{T}^2)^{1/2}}\right]\mathrm{d}\tau' \tag{2.403}$$

Using B_1 and B_2 as determined earlier we have approximate solutions $c_1(\tau)$ and $c_2(\tau)$ that satisfy the boundary conditions at the pole. The solution c_2 may (for acute θ) be traced out into the complex plane on a path leading above the transition region around τ_2. When crossing the Stokes line (see Figure 2.10a) emanating from τ_2 at an angle of $1/3\pi$, the approximate solution experiences the Stokes phenomenon and picks up a multiple of the subdominant solution. On the real axis, close to the origin, the approximate solution becomes

$$c_2(\tau) = \mathrm{i}B_2 q_2^{-1/2}(\tau)\left[\exp\left(-y_2 - \mathrm{i}x_2 - \mathrm{i}\int_0^\tau q_2\,\mathrm{d}\tau'\right) + a_{BC}\exp\left(\mathrm{i}\int_0^\tau q_2\,\mathrm{d}\tau'\right)\right] \quad (2.404)$$

Here a_{BC} is the Stokes constant belonging to the Stokes line considered. Applying the first-order equations to find c_1 close to the origin and then the fact that the Wronskian of c_1^* and c_2 has the same value at the pole as at the origin, we obtain (for $0 < \theta < 1/2\pi$)

$$|a_{BC}|^2 = [1 - \exp(-2u)]/\exp(-2v) \quad (2.405)$$

For obtuse θ we may trace c_2 from the pole to the origin along the real axis. This means that a Stokes line emanating from τ_2 has to be crossed (see Figure 2.10c). Introducing a Stokes constant c_{BC} gives for c_2 close to the origin

$$c_2(\tau) = B_2 q_2^{-1/2}\left[\exp\left(\mathrm{i}\int_0^\tau q_2\,\mathrm{d}\tau'\right) + c_{BC}\exp\left(-y_2 - \mathrm{i}x_2 - \mathrm{i}\int_0^\tau q_2\,\mathrm{d}\tau'\right)\right] \quad (2.406)$$

Use of the first-order equations to find c_1 and the Wronskian of c_1^* and c_2 to connect between the pole and the origin gives (for $1/2\pi < \theta < \pi$)

$$|c_{BC}|^2 = [1 - \exp(-2v)]/\exp(-2u) \quad (2.407)$$

Considering now the approximate solutions c_1 and c_2 at the origin and introducing the notations

$$\cos g_0 = \left[\frac{(1+T_0^2)^{1/2} - T_0}{2(1+T_0^2)^{1/2}}\right]^{1/2}, \qquad \sin g_0 = \left[\frac{(1+T_0^2)^{1/2} + T_0}{2(1+T_0^2)^{1/2}}\right]^{1/2} \quad (2.408)$$

we find (using $a_{1,2}(0) = c_{1,2}(0)$) that

$$\mathbf{a}(0) = \mathbf{R}\begin{bmatrix} G_{11}^a \\ G_{21}^a \end{bmatrix}\exp(\tfrac{1}{2}\mathrm{i}\zeta) \quad (2.409)$$

with

$$\mathbf{R} = \begin{bmatrix} \sin g_0 & \cos g_0 \\ -\cos g_0 & \sin g_0 \end{bmatrix} \quad (2.410)$$

The adiabatic propagated elements are given by

$$G_{11}^a = \begin{cases} \mathrm{i}[1-\exp(-2u)]^{1/2}\exp[\mathrm{i}(\Theta + \arg a_{BC})] & (0 < \theta < \frac{1}{2}\pi) \\ \exp(-v)\exp(\mathrm{i}\Theta) & (\frac{1}{2}\pi < \theta < \pi) \end{cases} \quad (2.411)$$

$$G_{21}^a = \begin{cases} -\mathrm{i}\exp(-u)\exp[\mathrm{i}(\Theta - x_2)] & (0 < \theta < \frac{1}{2}\pi) \\ -[1-\exp(-2v)]^{1/2}\exp[\mathrm{i}(\Theta - x_2 + \arg c_{BC})] & (\frac{1}{2}\pi < \theta < \pi) \end{cases} \quad (2.412)$$

Because the phase-integral derivation is bound to break down when the complex transition points are close to the pole (see Figure 2.10b), we cannot expect the two different expressions given to join up for $\theta = 1/2\pi$ unless there is strong coupling between the states ($y_1, y_2 \gtrsim 1$), in which case we find that provided

$$\arg a_{BC} \to -\frac{1}{2}\pi\,, \qquad \arg c_{BC} \to +\frac{1}{2}\pi \tag{2.413}$$

we do indeed get consistent results. This is because

$$u \approx \frac{1}{2}(y_1 + y_2) = y\,, \qquad v \approx \frac{1}{2}(y_1 - y_2) \approx 0 \tag{2.414}$$

and

$$\begin{aligned}[1 - \exp(-2u)]^{1/2} \approx [1 - \exp(-2y)]^{1/2} &\approx 1\\ \exp(-v) &\approx 1\end{aligned} \tag{2.415}$$

Invoking now the parameterization of $\mathbf{T}_h$ we find

$$\begin{aligned}(1 - z^2)^{1/2}\exp(\mathrm{i}\phi) &= G^a_{11}\\ z\exp(\mathrm{i}\chi)\exp[\mathrm{i}(\Delta_2 - \Delta_1)] &= G^a_{21}\end{aligned} \tag{2.416}$$

Then we have

$$z^2 = \begin{cases} \exp(-2u) & (0 < \theta < \frac{1}{2}\pi)\\ 1 - \exp(-2v) & (\frac{1}{2}\pi < \theta < \pi),\end{cases} \tag{2.417}$$

while

$$\phi = \begin{cases} \Theta + \arg a_{BC} + \frac{1}{2}\pi & (0 < \theta < \frac{1}{2}\pi)\\ \Theta & (\frac{1}{2}\pi < \theta < \pi)\end{cases} \tag{2.418}$$

and

$$\chi = \begin{cases} \Theta & (0 < \theta < \frac{1}{2}\pi)\\ \Theta + \arg c_{BC} - \frac{1}{2}\pi & (\frac{1}{2}\pi < \theta < \pi)\end{cases} \tag{2.419}$$

We have used the abstraction

$$\Delta_1 - \Delta_2 = x_2 + \frac{1}{2}\pi \tag{2.420}$$

to connect between the true adiabatic phases and the model quantity x_2. The factor $1/2\pi$ enters because $x_2 + 1/2\pi \approx x_1 - 1/2\pi$. Note that the phases of the Stokes constants a_{BC} and c_{BC} are undetermined, as is usual in these matters. In the next section we use the comparison-equation technique to derive expressions for $\arg a_{BC}$ and $\arg c_{BC}$.

2.4.4 Comparison Equation

We start by considering the case when the Stueckelberg variable T reduces to the canonical exponential model form (we use a hat to designate canonical quantities)

$$\hat{T}(\tau) = \lambda/2(\tau + \tau_\infty) - \cot\theta \tag{2.421}$$

so that

$$\begin{aligned} T_0 \quad &\equiv \hat{T}(0) = \tfrac{\lambda}{2\tau_\infty} - \cot\theta \\ &\equiv \tfrac{\lambda}{\gamma \sin\theta} - \cot\theta \equiv \tfrac{\left[\frac{A\epsilon}{A} - \cos\theta\right]}{\sin\theta} \end{aligned} \tag{2.422}$$

where $\gamma = A/(\nu\alpha)$ and A is defined by (2.442) or (2.443). This is the case of the exponential model of Nikitin [453], [454], but other models may also reduce to this form when suitable variables are used. It can be shown, by using appropriate recurrence relations, namely equations (2.4.9) and (2.5.1) of [562] that the exact solution is given by

$$\left.\begin{aligned} \hat{c}_1(\tau) &= \exp[-\tfrac{1}{4}\pi\lambda + \tfrac{1}{2}\mathrm{i}(\gamma\cos\theta - \lambda\ln\gamma)][M_{\kappa,-\mu}(\beta)]^* \\ \hat{c}_2(\tau) &= -\tfrac{1}{2}\tfrac{\sin\theta}{1+\mathrm{i}\lambda}\exp[\tfrac{1}{4}\pi\lambda + \tfrac{1}{2}\mathrm{i}(\gamma\cos\theta - \lambda\ln\gamma)]M_{\kappa,\mu}(\beta) \end{aligned}\right\} \tag{2.423}$$

where

$$\kappa = \frac{1}{2}\mathrm{i}\lambda\cos\theta\,, \qquad \mu = \frac{1}{2}(1+\mathrm{i}\lambda)\,, \qquad \beta = (2\mathrm{i}/\sin\theta)(\tau+\tau_\infty) \tag{2.424}$$

and the functions $M_{\kappa,\pm\mu}$ are Whittaker functions (cf. [562]).

Using strong-coupling asymptotic expansions [161], [167] one finds (after some heavy algebra) that

$$\hat{\mathbf{a}}(0) = \hat{\mathbf{R}}\begin{bmatrix} \hat{G}^a_{11} \\ \hat{G}^a_{21} \end{bmatrix}\exp(\frac{1}{2}\mathrm{i}\hat{\boldsymbol{\zeta}}) \tag{2.425}$$

where $\hat{\mathbf{R}}$ and $\hat{\boldsymbol{\zeta}}$ are defined as in the general case, but with the model variable $\hat{T}$ and

$$\begin{aligned} \hat{G}^a_{11} = &\left(\frac{1-\cos\theta}{2}\right)^{\frac{1}{2}}\left|\frac{\Gamma(1+\mathrm{i}\lambda)}{\Gamma(1+\frac{1}{2}\mathrm{i}\lambda(1-\cos\theta))}\right| \\ &\exp[\frac{1}{4}\pi\lambda(1+\cos\theta)]\exp[\mathrm{i}\{\tilde{\gamma}[\frac{1}{2}\lambda(1-\cos\theta)] - \tilde{\gamma}(\lambda)\}] \end{aligned} \tag{2.426}$$

$$\begin{aligned} \hat{G}^a_{21} = &\left(\frac{1+\cos\theta}{2}\right)^{\frac{1}{2}}\left|\frac{\Gamma(1+\mathrm{i}\lambda)}{\Gamma(1+\frac{1}{2}\mathrm{i}\lambda(1+\cos\theta))}\right| \\ &\exp[-\frac{1}{4}\pi\lambda(1-\cos\theta)]\exp[-\mathrm{i}\hat{x} + \mathrm{i}\{\tilde{\gamma}[\frac{1}{2}\lambda(1+\cos\theta)] - \tilde{\gamma}(\lambda)\}] \end{aligned} \tag{2.427}$$

Here

$$\hat{x} = \hat{x}_1 - \frac{1}{2}\pi = \hat{x}_2 + \frac{1}{2}\pi = -2\mathrm{Re}\int_0^{\tau_c}(1+\hat{\mathrm{T}}^2)^{1/2}\,\mathrm{d}\tau' \tag{2.428}$$

where τ_c is the zero of $1+\hat{T}^2$ in the second quadrant and

$$\tilde{\gamma}(\alpha) = \frac{1}{4}\pi + \alpha\ln\alpha - \alpha - \arg\Gamma(1+\mathrm{i}\alpha) \tag{2.429}$$

Introducing the parameterization of the semiclassical scattering matrix and abstracting $\Delta_1 - \Delta_2$ as in Section 2.4.3, we find

$$\left.\begin{array}{ll} \hat{z}^2 = \{\sinh[\frac{1}{2}\pi\lambda(1+\cos\theta)]/\sinh(\pi\lambda)\}\exp[-\frac{1}{2}\pi\lambda(1-\cos\theta)] \\ \hat{\phi} = \hat{\gamma}(\frac{1}{2}\lambda(1-\cos\theta)) - \hat{\gamma}(\lambda) \\ \hat{\chi} = \tilde{\gamma}(\frac{1}{2}\lambda(1+\cos\theta)) - \tilde{\gamma}(\lambda) \end{array}\right\} \tag{2.430}$$

The parameters $\lambda(1 \pm \cos\theta)$ may be abstracted as integrals through

$$\begin{aligned} \hat{y} &= \frac{1}{2}\lambda(1-\cos\theta) = \frac{1}{2}(\hat{y}_1 + \hat{y}_2) = \frac{1}{\pi}\mathrm{Im}\int_{\hat{\tau}_1^*}^{\hat{\tau}_2} \hat{q}_2\, d\tau' \\ \hat{\mu} &= \frac{1}{2}\lambda(1+\cos\theta) = \lambda - \frac{1}{2}(\hat{y}_1 + \hat{y}_2) = -\frac{1}{\pi}\mathrm{Im}\,\bar{\int}_{\hat{\tau}_1}^{\hat{\tau}_2} \hat{q}_2\, d\tau' \end{aligned} \tag{2.431}$$

where the bar on the integral for $\hat{\mu}$, signifies that it should be evaluated on a contour to the left of the pole at $-\tau_\infty$.

We now compare the expressions just derived with those of equations (2.416)–(2.419) of the last section. First, we find expressions for the phases of the Stokes constants, namely

$$\begin{aligned} \arg a_{BC} &= \tilde{\gamma}(y) - \tilde{\gamma}(\mu) - \tfrac{1}{2}\pi \qquad (0 < \theta < \frac{1}{2}\pi) \\ \arg c_{BC} &= \tilde{\gamma}(\mu) - \tilde{\gamma}(y) + \tfrac{1}{2}\pi \qquad (\frac{1}{2}\pi < \theta < \pi) \end{aligned} \tag{2.432}$$

Then the phase-integral expressions become, for $0 < \theta < 1/2\pi$,

$$\begin{aligned} z^2 &= \exp(-2u) \\ \phi &= \Theta + \tilde{\gamma}(y) - \tilde{\gamma}(\mu) \\ \chi &= \Theta \end{aligned} \tag{2.433}$$

For $1/2\pi < \theta < \pi$,

$$\begin{aligned} z^2 &= 1 - \exp(-2v) \\ \phi &= \Theta \\ \chi &= \Theta + \tilde{\gamma}(\mu) - \tilde{\gamma}(y) \end{aligned} \tag{2.434}$$

We note that

$$y = \frac{1}{2}(y_1 + y_2) \tag{2.435}$$

while μ is more complicated and in fact contains contributions from secondary complex transition points in the R-plane [174].

It is of course also possible to take over more of the comparison equation. Thus for $0 < \theta < \pi$, we realize that in the canonical exponential case ($F \equiv 0$ in expression

(2.389)) the imaginary part $\hat{\Theta}$ of the complex Coulomb phase (cf. [283]) of (2.400) is a semiclassical approximation to

$$\tilde{\gamma}(\frac{1}{2}\lambda(1+|\cos\theta|)) - \tilde{\gamma}(\lambda) \tag{2.436}$$

which is interesting in that it has a discontinuous first derivative (with respect to θ) at $\theta = 1/2\pi$.

2.4.5 General Phase-Integral Abstraction

We now propose to parameterize the transition matrix $\mathbf{T}_h$ of (2.373) for $F(\tau) \neq 0$ by calibration with the exact Coulomb case of Section 2.4.4. Thus we propose the following phase-integral abstraction for $0 < \theta < \pi$:

$$\phi \approx \mathrm{Re}\int_{-\tau_\infty}^{0}[\mathrm{q}_2 - \hat{\mathrm{q}}_2 + (1+\hat{\mathrm{T}}^2)^{1/2} - (1+\mathrm{T}^2)^{1/2}]\,\mathrm{d}\tau + \tilde{\gamma}(\mathrm{y}) - \tilde{\gamma}(\lambda) \tag{2.437}$$

$$\chi \approx \mathrm{Re}\int_{-\tau_\infty}^{0}[\mathrm{q}_2 - \hat{\mathrm{q}}_2 + (1+\hat{\mathrm{T}}^2)^{1/2} - (1+\mathrm{T}^2)^{1/2}]\,\mathrm{d}\tau + \tilde{\gamma}(\mu) - \tilde{\gamma}(\lambda) \tag{2.438}$$

while for $0 < \theta < 1/2\pi$ we propose

$$\begin{aligned} z^2 \approx\ & \tfrac{\exp(-2y)[1-\exp(-2\mu)]}{1-\exp[-2(y+\mu)]}\exp\left[-2\mathrm{Im}\int_{-\tau_\infty}^{\tau_1^*}(\mathrm{p}_2-\hat{\mathrm{p}}_2)\,\mathrm{d}\tau\right] \\ & \times\exp\left[-2\mathrm{Im}\int_{\tau_1^*}^{\tau_2}(\mathrm{q}_2-\hat{\mathrm{q}}_2)\,\mathrm{d}\tau + 2\mathrm{Im}\int_{\tau_2}^{0}(\mathrm{p}_2-\hat{\mathrm{p}}_2)\,\mathrm{d}\tau\right] \end{aligned} \tag{2.439}$$

where

$$p_2 \equiv q_2 - \frac{\mathrm{i}}{2}\frac{\mathrm{d}}{\mathrm{d}\tau}\ln[T + (1+T^2)^{1/2}] \tag{2.440}$$

and for $1/2\pi < \theta < \pi$ we propose

$$z^2 \approx 1 - \frac{[1-\exp(-2y)]}{1-\exp[-2(y+\mu)]}\exp\left[-2\mathrm{Im}\int_{-\tau_\infty}^{0}(\mathrm{p}_2-\hat{\mathrm{p}}_2)\,\mathrm{d}\tau\right] \tag{2.441}$$

the different topologies of Figures 2.10a and c being clearly reflected in (2.439) and (2.441).

2.4.6 Discussion

Some interesting mathematical points arising from the preceding treatment appear to be worthy of discussion.

First, the choice of $M_{\kappa,-\mu}(\beta)$ to express $\hat{c}_1^*(\tau)$ in (2.423) is not quite as straightforward [453], [454] as it might appear at first sight, since both $W_{\kappa,\mu}(\beta)$ and $W_{-\kappa,\mu}(\beta)$ are worthy alternative candidates to satisfy the boundary conditions on $\hat{c}_1^*$ at $\tau = -\tau_\infty$. Although physical intuition is suggestive, the correct choice is only dictated by application of the exact first-order coupled equations.

Secondly, there arises the natural question: is $-\tau_\infty$ a transition point, in so far as Stokes lines emanating from the complex transition points pass through $-\tau_\infty$? The

answer is no, except in some technical semantic sense, because, *reductio ad absurdum*, no Stokes phenomenon occurs as we trace the solutions around $-\tau_\infty$ while excluding the other (transition) points. To put it another way, the Stokes constants take zero value. Another indicator is that both arrows in Figures 2.10a–c are outward on the Stokes lines emanating from $-\tau_\infty$. Finally, we note that in the limit as $\lambda \to i$, for acute θ the lower transition point τ_1^* coalesces with the double pole to yield a simple pole that is a transition point [282]. No contradiction arises. (For obtuse θ, the upper transition point τ_2 coalesces with $-\tau_\infty$.) It will also be observed in Figures 2.10a–c that we have adopted "physical" branch cuts [160]. This choice is essential for the comparison-equation method of Section 2.4.4, if we are to avoid discontinuities in both amplitude and wave function [163].

Next, in deriving expressions (2.404) and (2.406) for θ acute and obtuse respectively, we have of course assumed that there exists a "good path" in the sense of Fröman and Fröman [282]. This is not unreasonable bearing in mind that $\hat{c}_2$ is necessarily subdominant near $-\tau_\infty$. Perhaps on less firm ground, one may for instance trace $\hat{c}_1^*$, from $-\tau_\infty$ to 0, circumventing τ_1^*, in the lower half-plane of Figure 2.10a (acute θ). To the right of the branch cut there are two Stokes lines to be crossed, each with its own Stokes constant. There is thus in effect a double Stokes phenomenon [167], and it may be shown that the effective compound Stokes constant is related to c_{BC}, the Stokes constant occurring in equation (2.406).

Perhaps we should say a few words about other related work. One of the principal advantages of the JWKB or Liouville–Green approximation, which we have adopted here, is that it is a *uniform* approximation as emphasized by Olver [478]. However, it should be noted that the latter is primarily concerned with isolated transition points, thus excluding the case of a uniform pair of transition points considered here. As mentioned in the Introduction, an earlier JWKB attempt to describe uniformly two transition points and a pole [232], later applied by Child [115], was not satisfactory in that a transformation of the dependent variable (the amplitude a_2 in our notation), involving the square root of the interaction potential, resulted in a second-order differential equation rather more complicated than our equation (2.386). Indeed, one of the advantages of our choice of dependent and independent variables is that the model represents a holomorphic mapping in that just as [167]

$$\begin{aligned} H_{22} - H_{11} &\equiv \Delta\epsilon - A\cos\theta\exp(-\alpha R) \\ H_{12} &\equiv \tfrac{1}{2}A\sin\theta\exp(-\alpha R) \end{aligned} \tag{2.442}$$

yield the pure exponential model, so do

$$\begin{aligned} H_{22} - H_{11} &\equiv \Delta\epsilon(1+\tanh(\alpha R)) - A\cos\theta\,\mathrm{sech}^2(\alpha \mathrm{R}) \\ H_{12} &\equiv \tfrac{1}{2}A\sin\theta\,\mathrm{sech}^2(\alpha \mathrm{R}) \end{aligned} \tag{2.443}$$

Notice that neither $H_{22} - H_{11}$ nor H_{12} is constant (cf. [340]). Another defect in the treatment of Dubrovskiy [232] is his use of weak-coupling asymptotics [163] in the resolution of his comparison equations. This results in an erroneous factor in his transition probability and arises from an incorrect handling of $\hat{\mathbf{R}}$ in equation (2.425).

2.5 Other Generalizations

2.5.1 Four Close Curve-Crossing Transition Points

A discussion of the semiclassical two-channel close curve-crossing *S*–matrix is given, with special reference to Stueckelberg phases as calculated within the nonadiabatic parabolic model [166]. It is shown that the phase Γ_1, normally associated with elastic adiabatic evolution through the curve crossing, is considerably in error when calculated within the Landau–Zener approximation - but shows favourable agreement with earlier numerical evaluations from coupled equations, provided the full Zwaan–Stueckelberg phase-integral interpretation is effected.

Previously we reviewed the status of Stueckelberg curve-crossing phases within the parabolic model [163], and in Crothers [165], we refined the nonadiabatic theory of the semiclassical two-channel *S*–matrix by fully developing the two-state exponential model to describe both crossing and noncrossing. Happily the Zwaan–Stueckelberg phase-integral method [160] provides a consistent interpretation of both models, and it is our purpose to report that such an interpretation effectively applies to the close-curve-crossing problem, in which the impact parameter increases until the classical turning point approaches and eventually reaches the diabatic crossing point.

The close curve-crossing problem was originally formulated by Bykovskii et al. [105] and later analysed by Delos and Thorson [216], [217], and by Child [116]. In summary, with reference to [216], the diabatic two-state impact-parameter equations for the state amplitudes c_1 and c_2 may be reduced to

$$\mathrm{i}\frac{\mathrm{d}c_1}{\mathrm{d}s} = c_2 \exp\left(-2\mathrm{i}\int_0^s T(s')\,\mathrm{d}s'\right) \tag{2.444}$$

$$\mathrm{i}\frac{\mathrm{d}c_2}{\mathrm{d}s} = c_1 \exp\left(+2\mathrm{i}\int_0^s T(s')\,\mathrm{d}s'\right) \tag{2.445}$$

where the Stueckelberg variable T is given in terms of the diabatic interaction matrix V by

$$T = (V_{22} - V_{11})/(2V_{12}) \tag{2.446}$$

where

$$s(\tilde{t}) = \int_0^{\tilde{t}} V_{12}\,\mathrm{d}t' \tag{2.447}$$

in which the time is given by $\tilde{t}$. The essence of the close curve-crossing model is to assume that T may be expanded thus

$$T(s) = -\epsilon + 4s^2/\beta^2 \tag{2.448}$$

in which β and ϵ are two independent constant parameters. Equations (2.444) and (2.445) are solved subject to

$$c_1(s(-\infty)) = 1 \tag{2.449}$$

$$c_2(s(-\infty)) = 0 \tag{2.450}$$

in which case the S matrix is given by

$$S_{21} = S_{12} = c_2(s(+\infty)) = -2\mathrm{i}z(1-z^2)^{1/2}\sin(\Gamma_1+\Gamma_2) \tag{2.451}$$

$$S_{22}^{*} = S_{11} = \mathrm{e}^{-\mathrm{i}\zeta}c_1(s(+\infty)) = (1-z^2)\mathrm{e}^{2\mathrm{i}\Gamma_1} + z^2\mathrm{e}^{-2\mathrm{i}\Gamma_2} \tag{2.452}$$

The extra adiabatic phase ζ is fully explained in [167] and need not be elaborated here. Delos and Thorson [217] calculated z, Γ_1, and $\Gamma_1+\Gamma_2-\pi$ in particular for large β, as recorded in their figures 8, 10, and 9, respectively. Although Stueckelberg estimates of z and $\Gamma_2-\pi$ were given, none was given for Γ_1. Numerical values of z have also been compared with Stueckelberg estimates by Child [116] for $\beta = 5$. It is therefore of interest to obtain a Stueckelberg estimate of Γ_1. Within the Zwaan–Stueckelberg interpretation of the parabolic model [160], [167], the parameters of the S–matrix are given by

$$\Gamma_1 = \frac{\pi}{4} + \frac{y}{\pi}\ln\left(\frac{y}{\pi}\right) - \frac{y}{\pi} - \arg\Gamma\left(1+\mathrm{i}\frac{y}{\pi}\right) \tag{2.453}$$

$$\Gamma_2 = x \tag{2.454}$$

$$z = \exp(-y) \tag{2.455}$$

where

$$x+\mathrm{i}y = 2\int_0^{\frac{1}{2}\beta(\mathrm{i}+\epsilon)^{1/2}} (1+T^2)^{1/2}\mathrm{d}s = \frac{\beta}{2}\int_{-\epsilon}^{\mathrm{i}}\left(\frac{1+T^2}{\epsilon+T}\right)^{1/2}\mathrm{d}T \tag{2.456}$$

We note that these formulae differ in two respects from those of Delos and Thorson [219] and therefore of Delos [215]. Firstly, there is a formal difference of π in the definition of Γ_2. This is due to our adoption of an external minus in expression (2.451), in accordance with a positive potential V_{12} [167]. Secondly, and of some fundamental importance, the y in (2.453) is given by (2.456) and not by $\pi T_0/2$, the Landau–Zener value adopted by Delos (cf. also expression (72) of [160]) in which T_0 is the value of the Stueckelberg variable T at the diabatic curve crossing.

Expression (2.456) may be evaluated as follows. Setting

$$2s/\beta = (T+\epsilon)^{1/2} = \sin\theta(\mathrm{i}+\epsilon)^{1/2} \tag{2.457}$$

we obtain

$$\begin{aligned} x+\mathrm{i}y &= \beta\exp\left(\frac{1}{4}\pi\mathrm{i}\right)(1-\mathrm{i}\epsilon)(1+\mathrm{i}\epsilon)^{1/2} \\ &\quad\times\int_0^{\pi/2}\mathrm{d}\theta\,\cos^2\theta\left(1+\frac{(1-\mathrm{i}\epsilon)}{(1+\mathrm{i}\epsilon)}\sin^2\theta\right)^{1/2} \qquad (2.458) \\ &= \beta\exp\left(\frac{1}{4}\pi\mathrm{i}\right)(1-\mathrm{i}\epsilon)(1+\mathrm{i}\epsilon)^{1/2}\frac{1}{4}\pi\,{}_2F_1\left(-\frac{1}{2},\frac{1}{2};2;-\frac{(1-\mathrm{i}\epsilon)}{(1+\mathrm{i}\epsilon)}\right) \qquad (2.459) \\ &= \frac{\beta\exp\left(\frac{1}{4}\pi\mathrm{i}\right)(1+\epsilon^2)\pi^{3/2}}{4\sqrt{2}}\left[\left(\frac{{}_2F_1(\frac{1}{4},\frac{5}{4};\frac{1}{2};-\epsilon^2)}{\Gamma(\frac{3}{4})\Gamma(\frac{7}{4})}\right)\right. \\ &\quad\left.-2\mathrm{i}\epsilon\left(\frac{{}_2F_1(\frac{3}{4},\frac{7}{4};\frac{3}{2};-\epsilon^2)}{\Gamma(\frac{5}{4})\Gamma(\frac{1}{4})}\right)\right] \qquad (2.460) \end{aligned}$$

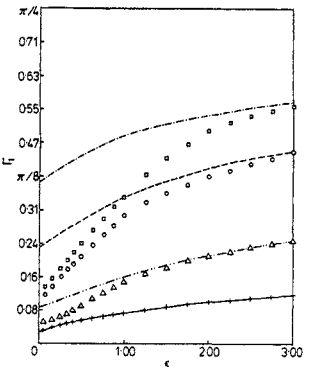

Fig. 2.11. The phase $\Gamma_1(\beta, \epsilon)$ as given by (2.453). This work: —·— $\beta = 1$; – – – $\beta = 2$; —··— $\beta = 5$; — $\beta = 10$. [217] *square* $\beta = 1$; *circle* $\beta = 2$; *triangle* $\beta = 5$; *cross* $\beta = 10$

where we have applied the binomial series in (2.458) and used identities (5.4.14) and (8.1.4) of [1] to obtain (2.460) from (2.459). Expression (2.460) may of course be continued analytically for larger values of ϵ^2. For $\epsilon = 0$, the curve-crossing point coincides with the point of closest approach, that is, the classical turning point, so that T_0 is zero and the Γ_1 of [219] is $1/4\pi$, whereas (2.460) gives

$$x + \mathrm{i}y = \frac{\beta \exp\left(\frac{1}{4}\pi \mathrm{i}\right) \pi^{3/2}}{4\sqrt{2}\,\Gamma(\frac{3}{4})\Gamma(\frac{7}{4})} \approx 0.618(1 + \mathrm{i})\beta \tag{2.461}$$

For larger positive values of ϵ, it was found more expedient to put $T = i\tau$ to evaluate y as

$$y = \frac{1}{2}\beta \int_0^1 (1 - \tau^2)^{1/2}(\epsilon^2 + \tau^2)^{-1/4} \cos[\frac{1}{2} \tan^{-1}(\tau/\epsilon)]\mathrm{d}\tau \tag{2.462}$$

To evaluate expression (2.453) for Γ_1 we used

$$\arg \Gamma(1 + \mathrm{i}y) = -\gamma c + \sum_{n=0}^{\infty} \left[\frac{\gamma}{n+1} - \tan^{-1}\left(\frac{\gamma}{n+1}\right)\right] \tag{2.463}$$

$$= \gamma \ln \gamma - \gamma + \frac{1}{4}\pi - \sum_{n=1}^{\infty} \frac{(-1)^{n-1} B_{2n}}{(2n-1)(2n)\gamma^{2n-1}} \qquad (\gamma \gg 1) \tag{2.464}$$

where c is Euler's constant and B_{2n} is a Bernoulli number. The results for Γ_1 are presented in Figure 2.11. As β increases, the accuracy of our Γ_1 improves rapidly over an ever-increasing range of ϵ. Even for the worst case shown, namely $\beta = 1$ and $\epsilon = 0$, which corresponds to a very close crossing at high speed, the antithesis of nonadiabatic conditions, the error is only of the order of 15°. We therefore conclude that for the Stokes constant Γ_1 the Stueckelberg strong-coupling limit, namely zero, is a better approximation than the Landau–Zener weak-coupling limit, namely $1/4\pi$ at ($\epsilon = 0$), the more so the higher is β.

We have not attempted comparison between the Φ_A of figure 9 of [217] and our $\Gamma_1 + \Gamma_2$ since we note considerable difference between their adiabatic-perturbation estimate and our $x - \pi$ at $\epsilon = 0$, particularly for $\beta = 10$. However, we do note that addition of our Γ_1 to their adiabatic-perturbation estimates improves agreement with their coupled-equation values, at the higher ϵ-values and lower β-values of their figure 9.

In conclusion, we observe that the acceleration effects at the close crossing, represented by the occurrence of T in the denominator of (2.456), may largely be simulated by the correct Zwaan–Stueckelberg interpretation of the parabolic model. Semiclassical deflection fuctions [25] and semiclassical probabilities [26] are presented for close curve-crossing.

2.5.2 Circuit-Dependent Adiabatic Phase Factors from Phase Integral Theory

We show that circuit-dependent adiabatic phase factors occur naturally in the phase-integral theory of atomic collisions, being a physical manifestation of the Stokes phenomenon familiar in asymptotic analysis. This implies a generalisation of Berry's work on geometric phase factors for situations involving adiabatic parallel transport around closed circuits in *the complex plane* [153].

There has been considerable interest in "geometric" phase factors arising from adiabatic transitions [69] in many areas of physics, including optics [114], [582], [70], and quantum theory [561], [374], [375], [397], [4], [80], [540]. When a system is adiabatically transported around a closed circuit, the system returns to its original state apart from a phase factor. This factor contains, in addition to the usual dynamical phase e^{-iEt}, a circuit-dependent component [69].

These latter adiabatic phases arise naturally in the phase-integral theory [324], [477] of heavy-atom collision processes, due originally to Zwaan [614] and Stueckelberg [574]. The nature of the adiabatic phase then depends on particular properties of the adiabatic potentials governing the motion, which must be analytically continued into the complex plane.

Indeed, such phases occur generally in the theory of differential equations, whether associated with classical or quantal phenomena [324]; their origin is rooted within the Liouville–Green (more commonly known as the JWKB) phase-integral method of solution. The Zwaan–Stueckelberg technique is based on continuing analytically the asymptotic JWKB phase integrals into the complex R-plane (R being, for example, the internuclear distance in typical atomic problems) at sufficient distance from any points where such solutions break down (turning points, etc.) [160]. An alternative yet related method based on convergent series expansions, but still involving analytical continuation, is that due to Fröman and Fröman [282]. The point we wish to draw attention to here is the key role played by the *Stokes phenomenon* in obtaining the correct phase-integral solutions [160], [28], [152].

For the description of nonadiabatic transitions accompanying atomic collisions, a consistent phase-integral analysis can only be made within the adiabatic representation [160], [152]. The adiabatic phase that arises may then be due to a branch point of the quantal wave function at a regular singular point, where a JWKB solution is

uniformly valid. Equally, it may result from the presence of a (complex) adiabatic degeneracy, which is an isolated transition point at which JWKB solutions break down [175], [28], [152].

For integral transition points in the context of coupled channels, the adiabatic phase is typically an elastic Stueckelberg phase, which in turn is related to the phase of a Stokes constant associated with a particular Stokes line [160], [28], [152].

More generally, when both types of point occur [28], the adiabatic phase derives from a Stokes constant and/or a complex Coulomb phase. For the purposes of illustration, consider a time-dependent treatment in which the wave function is written

$$\Psi = c_1(\tilde{t})\psi_1(\mathbf{R}, \mathbf{r}) + c_2(\tilde{t})\psi_2(\mathbf{R}, \mathbf{r}) \tag{2.465}$$

with $\tilde{t}$ being the time, R the internuclear separation of two heavy nuclei, and r denoting the internal electronic degrees of freedom; ψ_1 and ψ_2 are assumed to be orthogonal and to have adiabatic eigenenergies E_1 and E_2. Then in the one-pole, two-transition-point theory [28], the time-dependent coefficients c_1 and c_2 are given by

$-\infty \le \tilde{t} \ll -t_x$:

$$c_1(\tilde{t}) = \exp\left(-\mathrm{i}\int_{-\infty}^{\tilde{t}} E_1 \,\mathrm{d}t'\right) \qquad c_2(\tilde{t}) = 0$$

$-t_x \ll \tilde{t} \ll t_x$:

$$c_1(\tilde{t}) = (1-P)^{1/2} \exp\left(\mathrm{i}\phi - \mathrm{i}\int_{-\infty}^{\tilde{t}} E_1 \,\mathrm{d}t'\right)$$

$$c_2(\tilde{t}) = P^{1/2} \exp\left(\mathrm{i}\chi - \mathrm{i}\int_{-\infty}^{-t_x} E_1 \,\mathrm{d}t' - \mathrm{i}\int_{-t_x}^{\tilde{t}} E_2 \,\mathrm{d}t'\right)$$

$t_x \ll \tilde{t} \le +\infty$:

$$c_1(\tilde{t}) = (1-P)\exp\left(2\mathrm{i}\phi - \mathrm{i}\int_{-\infty}^{\tilde{t}} E_1 \,\mathrm{d}t'\right)$$
$$+P\exp\left(2\mathrm{i}\chi - \mathrm{i}\int_{-\infty}^{-t_x} E_1 \,\mathrm{d}t' - \mathrm{i}\int_{-t_x}^{t_x} E_2 \,\mathrm{d}t' - \mathrm{i}\int_{t_x}^{\tilde{t}} E_1 \,\mathrm{d}t'\right)$$

$$c_2(\tilde{t}) = -P^{1/2}(1-P)^{1/2}\exp\left(\mathrm{i}\phi - \mathrm{i}\chi - \mathrm{i}\int_{-\infty}^{t_x} E_1 \,\mathrm{d}t' - \mathrm{i}\int_{t_x}^{\tilde{t}} E_2 \,\mathrm{d}t'\right)$$
$$+P^{1/2}(1-P)^{1/2}\exp\left(\mathrm{i}\chi - \mathrm{i}\phi - \mathrm{i}\int_{-\infty}^{-t_x} E_1 \,\mathrm{d}t' - \mathrm{i}\int_{-t_x}^{\tilde{t}} E_2 \,\mathrm{d}t'\right)$$

from which the independent elements of the scattering matrix are obtained as

$$S_{11} = [P\exp(-2\mathrm{i}\sigma + 2\mathrm{i}\chi) + (1-P)\exp(2\mathrm{i}\phi)]\exp(2\mathrm{i}\eta_1) \tag{2.466a}$$
$$S_{12} = -2\mathrm{i}P^{1/2}(1-P)^{1/2}\sin(\sigma + \phi - \chi)\exp[\mathrm{i}(\eta_1 + \eta_2)] \tag{2.466b}$$

In these equations, P is the single transition probability

$$P = \exp(-\delta)\sinh\mu/\sinh(\mu + \delta)$$

the elastic scattering phase shifts are

$$\eta_j = -\frac{1}{2}\int_{-\infty}^{+\infty} E_j \,\mathrm{d}t' \qquad j = 1, 2$$

and the real nonadiabatic parameters σ and δ are defined in terms of the phase integral

$$\sigma + \mathrm{i}\delta = \int_0^{t_c} (E_2 - E_1)\,\mathrm{d}t'$$

In the last equation, t_c is a zero of the integrand (point of complex adiabatic degeneracy); t_x is the point at which the double Stokes line connecting t_c, with t_c^* intersects the real axis. The important additional phases ϕ and χ can be expressed as

$$\phi = \Delta(\delta) - \Delta(\lambda)$$
$$\chi = \Delta(\mu) - \Delta(\lambda)$$

where μ and λ are defined phase integrals [28], and

$$\Delta(x) = \frac{1}{2}\pi + x\ln x - x - \arg\Gamma(1 + \mathrm{i}x)$$

where Γ is the gamma function.

Now the adiabatic limit corresponds to that in which both λ and μ tend to $+\infty$: P, ϕ, and χ then all tend to zero. However, P tends to zero much faster than Δ and therefore χ and ϕ (see, e.g., [459]); indeed ϕ must remain finite for any collision process. It follows that the additional adiabatic phase γ, which is the difference between twice the dynamical adiabatic phase η_1 and the phase of the exact S_{11} matrix element in (2.466a), is given by

$$\gamma(\tilde{t}) = \phi[H(\tilde{t} + t_x) + H(\tilde{t} - t_x)]$$

where $H(x)$ is the Heaviside step function. Hence

$$\dot{\gamma}(\tilde{t}) = \phi[\delta(\tilde{t} + t_x) + \delta(\tilde{t} - t_x)]$$

with $\delta(x)$ the one-dimensional Dirac delta function. γ is thus a discontinuous constant that arises from the fact that JWKB phase integrals must be traced away from the points t_x, t_c, and t_c^*.

Defining the vector of coefficients $\left[\, c_1(t)\ c_2(t) \,\right]^{\mathrm{T}}$ from (2.465), then what we have done amounts to adiabatic parallel transport of $\left[\, c_1\ c_2 \,\right]^{\mathrm{T}}$ around the perimeter of an infinite semicircle in the complex plane whose base is the real t-axis, as a result of which an adiabatic phase factor $\exp(\mathrm{i}\gamma)$ is acquired.

Other two-transition-point (parabolic) problems are all special limits of this case [28]. Moreover, the phase integral analysis can easily be adapted to handle fractional transition points [426], [183].

An example of the application of phase-integral methods to experimental atomic collision phenomena concerns the two-electron capture process:

$$\mathrm{C}^{4+} + \mathrm{He} \rightarrow \mathrm{C}^{2+} + \mathrm{He}^{2+}$$

at energies from 300 eV to 1.5 keV. Oscillations in the experimental energy gain, and differential cross sections for this reaction are interpreted as being due to Stueckelberg interferences arising from a phase-integral analysis; agreement between theory and experiment is very good [29].

We conclude that, from the standpoint of phase-integral theory, both nonadiabatic transitions [160] and the adiabatic phase γ are physical manifestations of the Stokes phenomenon. There is a certain similarity between γ and Berry's geometric phase: both are associated with cyclic evolution in the adiabatic limit of a gauge-invariant theory [4]. However, whereas the latter arises as a real-surface anholonomic phase, in our situation the closed circuit lies in the complex plane and the resulting phase is associated with a different geometric structure. Simon [561] points out that Berry's phase can only arise in connection with phenomena involving magnetic fields or some other condition producing a nonreal Hamiltonian. By contrast, the phase-integral approach deals with real Hamiltonians, which are continued analytically into the complex plane in order to derive consistent solutions on the real axis.

3

Semiclassical Method for Hyperspherical Coordinate Systems

3.1 Wannier's Classical Treatment of Electron Correlation

In Chapter 2 we considered the one-dimensional semiclassical JWKB approximation, the price paid being that the wave function was singular at the transition/turning point in the first-order quantal correction to the classical zero-order wave function. As in so many branches of mathematics and physics, in order to generalize to reality we must generalize to higher dimensions. This requirement was reinforced by the renaissance in classical mechanics, following Thomas [580] and Wannier [593] and continued by Gryziński [314] and Bates [38], given the computational intensity required to solve fully quantal coupled partial differential equations.

In particular, Wannier considered negative hydrogen-ion-like continua comprising one nucleus and two highly correlated electrons. Generalized hyperspherical coordinates are well suited to describing such continua. Once again the two-dimensional singularity, a caustic, results in complete breakdown of the wave function just where the two electrons emerge diametrically opposed. Unsurprisingly classical (Wannier [593]) and raw semiclassical (Peterkop [486], Rau [505]) mechanics were only able to reveal relative threshold scaling laws of the type E^{α} where E is the excess-of-threshold energy and α is an irrational constant. The absolute scale of such cross section laws remained indeterminate until the uniform treatment of Crothers [186]: see section 52.2 of [200]. Here we present a simplified derivation of Wannier's law.

In hyperspherical coordinates the Schrödinger wave equation for the two-electron wave function pertinent to ionization:

$$e^- + A^{(Z-1)+}(1s) \rightarrow 2e^- + A^{Z+} \tag{3.1}$$

where A is an atomic ion of nuclear charge Z, may be written as

$$\left[\frac{1}{\rho^5}\frac{\partial}{\partial\rho}\left(\rho^5\frac{\partial}{\partial\rho}\right) + \frac{1}{\rho^2\sin^2\alpha\cos^2\alpha}\frac{\partial}{\partial\alpha}\left(\sin^2\alpha\cos^2\alpha\frac{\partial}{\partial\alpha}\right)\right.$$
$$\left. + \frac{4}{\rho^2\sin^2 2\alpha}\frac{1}{\sin\theta_{12}}\frac{\partial}{\partial\theta_{12}}\sin\theta_{12}\frac{\partial}{\partial\theta_{12}} + \frac{1}{\hbar^2}\left(2E + \frac{2Z}{\rho}\zeta(\alpha,\theta_{12})\right)\right]\Psi_f^{-*} = 0 \tag{3.2}$$

where E is the excess-of-threshold energy, Ψ_f^{-*} is the conjugated incoming final-state wave function, and the hyperspherical coordinates are $(\rho, \alpha, \theta_{12})$ where

$$r_1 = \rho \cos\alpha, \qquad r_2 = \rho \sin\alpha, \qquad \theta_{12} = \cos^{-1}(\hat{\mathbf{r_1}} \cdot \hat{\mathbf{r_2}}) \tag{3.3}$$

We assume $L = 0$ and $0 \le \alpha \le \pi/2$, $0 \le \rho \le +\infty$[1], and $0 \le \theta_{12} \le \pi$. We assume an infinite stationary nucleus A^{Z+} relative to which electrons 1 and 2 have position coordinates $\mathbf{r}_1$ and $\mathbf{r}_2$, respectively. In the preceding,

$$\zeta(\alpha, \theta_{12}) = \sec\alpha + \csc\alpha - \frac{1}{Z(1 - \sin 2\alpha \cos\theta_{12})^{1/2}} \tag{3.4}$$

It should be stressed that (3.2) is nonseparable. Setting

$$\Psi_f^{-*} = \frac{\Theta}{\rho^{5/2} \sin\alpha \cos\alpha} \tag{3.5}$$

and employing the Langer correction ($\rho = \mathrm{e}^x$), we obtain

$$\left(\frac{\partial^2}{\partial\rho^2} + \frac{1}{\rho^2}\frac{\partial^2}{\partial\alpha^2} + \frac{4}{\rho^2 \sin^2 2\alpha \sin\theta_{12}}\frac{\partial}{\partial\theta_{12}}\sin\theta_{12}\frac{\partial}{\partial\theta_{12}} + \frac{1}{\hbar^2}\left(2E + \frac{2Z\zeta}{\rho}\right)\right)\Theta = 0 \tag{3.6}$$

Setting

$$\Theta = P^{1/2}\mathrm{e}^{\frac{\mathrm{i}}{\hbar}S} \tag{3.7}$$

we have to order $1/\hbar^2$

$$\left(\frac{\partial S}{\partial\rho}\right)^2 + \frac{1}{\rho^2}\left(\frac{\partial S}{\partial\alpha}\right)^2 + \frac{4}{\rho^2 \sin^2 2\alpha}\left(\frac{\partial S}{\partial\theta_{12}}\right)^2 = 2E + \frac{2Z\zeta}{\rho} \tag{3.8}$$

and to order $1/\hbar$

$$D_0\left(P\frac{\partial S}{\partial\rho}\right) + \frac{1}{\rho^2}\left\{D_1\left(P\frac{\partial S}{\partial\alpha}\right) + D_2\left(P\frac{\partial S}{\partial\theta_{12}}\right)\right\} = 0 \tag{3.9}$$

where

$$\begin{aligned} D_0(\cdot) &= \frac{1}{\rho^5}\frac{\partial}{\partial\rho}\left(\rho^5(\cdot)\right) \\ D_1(\cdot) &= \frac{1}{\sin^2 2\alpha}\frac{\partial}{\partial\alpha}\left((\cdot)\sin^2 2\alpha\right) \\ D_2(\cdot) &= \frac{4}{\sin^2 2\alpha \sin\theta_{12}}\frac{\partial}{\partial\theta_{12}}\left((\cdot)\sin\theta_{12}\right) \end{aligned} \tag{3.10}$$

Setting

[1] The hyperspherical radius should not be confused with ρ, the impact parameter of Chapters 2 and 4.

$$S \approx S_0(\rho) + \frac{1}{2}S_1(\rho)(\Delta\alpha)^2 + \frac{1}{8}S_2(\rho)(\Delta\theta_{12})^2 \tag{3.11}$$

$$\frac{\mathrm{d}S_0}{\mathrm{d}\rho} = w \equiv \sqrt{2E + \frac{2Z_0}{\rho}} \tag{3.12}$$

and

$$w\frac{\mathrm{d}S_i}{\mathrm{d}\rho} + \frac{S_i^2}{\rho^2} = \frac{Z_i}{\rho} \qquad (i = 1, 2) \tag{3.13}$$

which is a Ricatti nonlinear equation [492] in view of the S_i^2-term. We write

$$S_i = \rho^2 w \frac{\mathrm{d}}{\mathrm{d}\rho} \ln u_i \tag{3.14}$$

Then we have, setting $2E = X^2$,

$$\left(\rho^2X^2 + 2Z_0\rho\right)\frac{\mathrm{d}^2u_i}{\mathrm{d}\rho^2} + \left(2\rho X^2 + 3Z_0\right)\frac{\mathrm{d}u_i}{\mathrm{d}\rho} - \frac{Z_iu_i}{\rho} = 0 \tag{3.15}$$

ζ is stationary at $\alpha = \pi/4$, $\theta_{12} = \pi$, and we have

$$Z\zeta \approx Z_0 + \frac{1}{2}Z_1(\Delta\alpha)^2 + \frac{1}{8}Z_2(\Delta\theta_{12})^2 \tag{3.16}$$

where

$$\begin{aligned} Z_0 &= \tfrac{(4Z-1)}{\sqrt{2}}\,, \qquad Z_1 = \frac{(12Z-1)}{\sqrt{2}}\,, \qquad Z_2 = \frac{-1}{\sqrt{2}} \\ \Delta\alpha &= \alpha - \tfrac{\pi}{4}\,, \qquad \Delta\theta_{12} = \pi - \theta_{12}\,. \end{aligned} \tag{3.17}$$

Setting

$$\mu_i = \rho^{m_i}F\left(-\frac{E\rho}{Z_i}\right) \tag{3.18}$$

and

$$2Z_0m_i^2 + Z_0m_i - Z_i = 0 \tag{3.19}$$

$$u_1 = \rho^{m_{12}}{}_2F_1\left(m_{12}, 1 + m_{12}; 2m_{12} + \frac{3}{2}; -\frac{-E\rho}{Z_0}\right) \tag{3.20}$$

$$u_2 = \rho^{m_{21}}{}_2F_1\left(m_{21}, 1 + m_{21}; 2m_{21} + \frac{3}{2}; -\frac{-E\rho}{Z_0}\right) \tag{3.21}$$

where the Gauss hypergeometrics may be expressed as Legendre functions [593]. In particular we may write

$$u_1 = \rho^{-1/4}P_{\frac{1}{2}}^{-2m_{12}-\frac{1}{2}}\left(\sqrt{1 + \frac{E\rho}{Z_0}}\right) \tag{3.22}$$

$$u_2 = \rho^{-1/4} P_{\frac{1}{2}}^{-2m_{21}-\frac{1}{2}}\left(\sqrt{1+\frac{E\rho}{Z_0}}\right) \tag{3.23}$$

Because of the logarithmic derivative, the u_i may be scaled arbitrarily by a nonzero constant. Consistent with Peterkop [486], we have

$$m_{\substack{12\\11}} = \tfrac{1}{4}\left[\pm\sqrt{\tfrac{100Z-9}{4Z-1}}-1\right] \tag{3.24}$$

$$m_{\substack{21\\22}} = -\tfrac{1}{4}\left[\pm \mathrm{i}\sqrt{\tfrac{9-4Z}{4Z-1}}+1\right] \tag{3.25}$$

provided $(9/100 <) 1/4 < Z < 9/4$ and where upper or lower indices and signs are taken. In our choice of u_1 and u_2 we reject m_{22} (outgoing waves) and m_{11} (singular at $\rho = 0$). The case of $Z = 1/4$ is considered in Section 3.4.3. For $Z = 1$, $m_{12} \approx 1.127$, and for $Z = 2$, $m_{12} \approx 1.056$.

The classical limit of this section is now obtained by letting $\hbar \to 0$, in which case [533] we have

$$\frac{\partial W}{\partial t} + H = 0\,, \qquad \mathbf{p}_i = \boldsymbol{\nabla}_i W \tag{3.26}$$

where H is the Hamiltonian, $\mathbf{p}_i$ the momentum of electron i, and W the principal function given by

$$W = S - Et \tag{3.27}$$

where S is the action of (3.7).

It follows that

$$\frac{\mathrm{d}\alpha}{\mathrm{d}t} = \frac{1}{\rho^2}\frac{\partial S}{\partial \alpha} = -\frac{1}{\rho^2} S_1(\rho)(\Delta\alpha) \tag{3.28}$$

Thus

$$\frac{\mathrm{d}}{\mathrm{d}t}(\Delta\alpha) = w\Delta\alpha\frac{\mathrm{d}}{\mathrm{d}\rho}\ln u_1 \underset{\rho\to\infty}{\simeq} X\Delta\alpha\frac{\mathrm{d}}{\mathrm{d}\rho}\ln u_1 \tag{3.29}$$

But

$$\frac{\mathrm{d}P}{\mathrm{d}t} = \frac{\partial S}{\partial \rho} \cong X \qquad \Rightarrow \tag{3.30}$$

$$\frac{\mathrm{d}(\Delta\alpha)}{\Delta\alpha} \simeq \frac{\mathrm{d}u_1}{u_1} \qquad \Rightarrow \qquad \Delta\alpha = c_1 u_1 \tag{3.31}$$

Similarly we have

$$\Delta\theta_{12} = c_2 u_2 \tag{3.32}$$

where c_1 and c_2 are arbitrary constants.

Following Peterkop [486] equation (45), we solve (3.9) to zero order to obtain the probability of ionization occurring as

$$P_0 \propto \frac{1}{\rho^5 w \Delta\alpha \Delta\theta_{12}^2} = \frac{1}{\rho^5 w u_1 u_2^2} \tag{3.33}$$

However, u_1 is given asymptotically, for large ρ, by

$$\left(\frac{Z_0}{E}\right)^{m_{12}} \frac{\Gamma(2m_{12}+\frac{3}{2})}{\Gamma(m_{12}+\frac{3}{2})m_{12}!} \tag{3.34}$$

and

$$|u_2| \simeq E^{-1/4} \quad \text{while} \quad \frac{1}{w} \simeq E^{-1/2} \tag{3.35}$$

It follows that the total cross section (sum of all such events) is given by

$$\int_0^E \left|P_0(\tilde{E})\right| \mathrm{d}\tilde{E} \;\propto\; E^{m_{12}} \tag{3.36}$$

which is the highly original result of Wannier [593], but using a judicious contribution of classical, semiclassical, and semiquantal mechanics. However, we iterate that the constant of proportionality is unobtainable because the wave function is singular just where the two detectors would be placed to record the two electrons in coincidence.

Since, classically, we have

$$E = E_1 + E_2 \tag{3.37}$$

it is clear that Wannier's criterion of ergodicity is fulfilled, that is, all couples (c_1, c_2) and (E_1, E_2) are equiprobable.

In conclusion we note that we have avoided the rather tedious classical mechanics of Wannier, namely his equations (8–12, 16–18) upon identifying his $(r, \psi, \gamma, \beta, \epsilon)$ with our $(\rho, 2\alpha, \theta_{12}, \zeta, E)$. In verifying his equations (17–18), the following are required:

$$\left[\frac{\mathrm{d}}{\mathrm{d}q}(\ln\rho)\right]^2 = 1 \tag{3.38}$$

$$\left(\theta'_{12}\frac{\partial}{\partial\theta'_{12}} + \alpha'\frac{\partial}{\partial\alpha}\right)\ln\zeta = 0 \tag{3.39}$$

where $'$ means $\mathrm{d}/\mathrm{d}q$ $\quad(q = \ln(\rho/b))$ and, conservative force,

$$H = T + V = E \tag{3.40}$$

where T is the sum of kinetic energies.

The fact is that (3.31) and (3.34) show that only in the limit as $E \to 0+$, is it true that $\alpha = \pi/4$. For $E \neq 0$ there is necessarily a fuzziness or spread about $\alpha = \pi/4$ and about $\theta_{12} = \pi$, consistent with (3.11) and (3.16).

Finally we note that in the limit of $Z \to +\infty$ (in reality $Z \gtrsim 3$), (3.24) and (3.36) give the E^1 law of Wigner [600], noting $(Z \gtrsim 9/4)$ that $(m_{21}, m_{22}) \equiv (0, -1/2)$ are not physically appropriate.

3.2 Differential and Integrated Wannier Cross Sections

The phrase *Wannier cross sections* on Google achieves more than 2300 hits. Thus we need to be selective. We shall present our a priori *ab initio* calculated absolute $(e, 2e)$, $(\gamma, 2e)$, and (e^+, e^+e^-) differential cross sections in comparison with experiment, where possible. Of course, other authors prefer to curve fit, for instance, semiempirical total $(e, 2e)$ cross sections (cf. Rost and Pattard [524], Pattard and Rost [482]), from threshold to high-impact nonrelativistic energies.

A more accurate variant [202] of the semiclassical quantum-mechanical treatment of [186] is used to reinvestigate the ionization cross sections of He by electron impact at an excess energy of 2 eV above the threshold. All partial wave contributions for singlets and triplets are accounted for up to $L = 6$. It is found that within the coplanar geometry, both the symmetric and asymmetric triple differential cross sections, peaking at and near theWannier ridge, are greatly improved when compared to the measurements of Rösel et al. [518]. Far away from the Wannier ridge the triple differential cross sections tend to show qualitative differences from their measurements. The essential features in the observed TDCS show a certain variance with the existing theoretical calculations. The semiclassical quantal treatment of [186] was the first attempt to calculate the TDCS for He in its singlet states of s, p, d, and f waves at an excess energy of 1 and 2 eV. The final state wave function for the two outgoing electrons was derived with uniform asymptotic behaviour. The results, however, were obtained after introducing some approximations such as (i) taking the limit $E\rho \to 0$ (here E is the excess energy over the threshold and ρ the hyperspherical radial coordinate) and (ii) treating the classical action variables S_0, S_1, and S_2 approximately. Even so, the qualitative features of the TDCS were confirmed by the subsequent experiments of Rösel et al. [518] and Selles et al. [541] for most angles. In this section we refine our method to calculate the TDCS for electron-impact ionization of He at an excess energy of 2 eV(26.6 eV incident electron energy) for equal energy sharing of the two outgoing electrons. The nature of the improved accuracy incorporated is as follows: (a) both the singlet and the triplet states of the He atom are considered, (b) all partial-wave contributions up to $L = 6$ are taken into account for better convergence, (c) the limit $E\rho \to 0$ in the calculation of [186] is removed, and (d) all the classical action variables in the final state wave function are treated without any approximation. To assess the overall improvement over the earlier results, we have, however, used the same ground state wave function of the He atom as used by Crothers [186]. Some correlation effects in this wave function are accounted for by an effective nuclear charge. A more accurate correlated wave function due to Pluvinage [493] was used by Copeland and Crothers [148] but no significant improvements were noticed, which indicates that the precise correlation effects in the ground state He wave function may not be of such crucial importance. However in their 1995 paper [149] they did find significant improvement when the preceding improvement (c) was adopted.

Our uniform semiclassical wave function was analytically continued below the threshold for the doubly excited states of He^-, and impressive resonance energy positions were obtained (see 3.3). Here we extend our investigation for the above

threshold ionization of He by retaining the term $2L(L+1)/\rho^2$ (point (b)) in the hyperspherical equation

$$\left[\frac{1}{\rho^5}\frac{\partial}{\partial\rho}\rho^5\frac{\partial}{\partial\rho}+\frac{1}{\rho^2\sin^2 2\alpha}\frac{\partial}{\partial\alpha}\sin^2 2\alpha\frac{\partial}{\partial\alpha}+\frac{4}{\rho^2\sin\theta_{12}}\frac{\partial}{\partial\theta_{12}}\sin\theta_{12}\frac{\partial}{\partial\theta_{12}}+2E+\frac{2\zeta(\alpha,\theta_{12})}{\rho}-\frac{2L(L+1)}{\rho^2}\right]\Psi=0 \tag{3.41}$$

Following the procedure of section 2 in [186], one obtains

$$\Psi_f^{-*}=\frac{c^{1/2}E^{m_{12}/2}u_1^{1/2}}{\tilde{\omega}^{1/2}\rho^{5/2}\sin\alpha\cos\alpha}\delta(\hat{\mathbf{k}}_1-\hat{\mathbf{r}}_1)\delta(\hat{\mathbf{k}}_2-\hat{\mathbf{r}}_2)\exp\left(\frac{4\mathrm{i}}{(8Z_0\rho)^{1/2}}(\Delta\theta_{12})^{-1/2}\right)\times\exp\left[-\mathrm{i}\left(S_0+\frac{1}{2}S_1(\Delta\alpha)^2+\frac{1}{8}S_2(\Delta\theta_{12})^2+\frac{\pi}{4}\right)-\text{ conjugate}\right] \tag{3.42}$$

Notice that here in (3.42) the ubiquitous $\pi/4$ is half of the phase of the Stokes constant (cf. Chapter 2). Here the classical action variables are given by

$$S_0=\int_0^{\rho}\mathrm{d}\tilde{\rho}\tilde{\omega} \tag{3.43}$$

$$S_i=\rho^2\omega(lnu_i)'\,,\qquad i=1,2 \tag{3.44}$$

with

$$\tilde{\omega}=(\omega^2-\omega\{\ln u_2-\mathrm{i}\ln u_1\}')^{1/2} \tag{3.45}$$

$$\omega^2=2E+2Z_0/\rho-2L(L+1)/\rho^2 \tag{3.46}$$

The primes in (3.44) and (3.45) denote derivatives with respect to ρ and $\tilde{\rho}$ respectively. The inclusion of this angular-momentum term moves the classical turning point from the origin to ρ_+ where

$$\rho_+=\frac{-Z_0+\sqrt{Z_0^2+4EL(L+1)}}{2E} \tag{3.47}$$

As a result, the lower limit of ρ integration will be replaced by ρ_+. In Section 3.1 we assumed $L=0$. Using the final state wave function in (3.42) we calculate first the direct ionization amplitude. The exchange ionization amplitudes for the two indistinguishable atomic electrons were then obtained by interchanging the angles θ_1 and θ_2 in the direct amplitude.

Here we present results of TDCS for some symmetric and asymmetric cases in the coplanar geometry at an excess energy of 2 eV to make a direct comparison with the absolute measurement of Rösel et al. [518]. In the coplanar symmetric geometry ($\phi_2=180^\circ$; $\theta_1=\theta_2$) there is only singlet scattering. In Figure 3.1 we present our results for this case along with the measurement and theory [186]. Significant improvement over the earlier results is noticed around the cross-section peak. Several

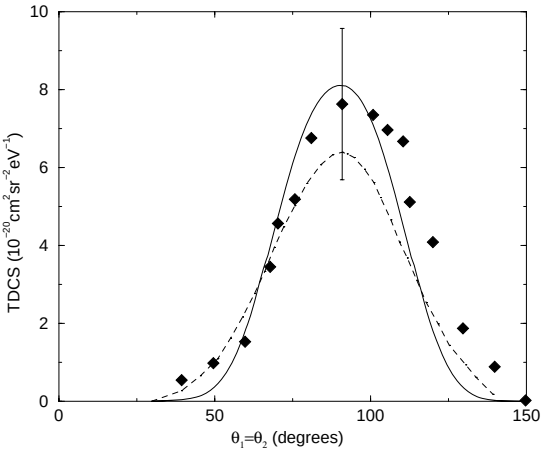

Fig. 3.1. Triple differential cross sections (TDCS) for the coplanar symmetric geometry ($\theta_1 = \theta_2$) at $E = 2$ eV over the threshold. *Filled diamonds*, measurement of Rösel et al. [518]; *dashed curve*, Crothers [186]; *solid curve*, Deb and Crothers [202]

factors contribute to this improvement, mostly due to the exact treatment of the classical action and partly due to the inclusion of three more partial waves ($L = 4 - 6$) compared to the earlier calculation where contributions up to only $L = 3$ were included. The last three partial-wave contributions, although small compared to those of the first four, turn out to be significant in the present investigation. We also check the contributions beyond $L = 6$; convergence is obtained. It is interesting to note that for θ_2 below 60° and above 120° the present results came out to be slightly smaller than those of the calculation of [186]. The breaking of symmetry around 90° discussed by Rösel et al. [518], although noticeable in both calculations, is not as prominent as in the measurement.

We now consider coplanar asymmetric geometry ($\phi_1 = 0°$, $\phi_2 = 180°$; θ_1 fixed and θ_2 varying). In Figure 3.2 we compare present results for $\theta_1 = 90°$ with the same measurement and the earlier calculation. The present results show excellent agreement, especially for $\theta_2 \geq 50°$. In this case there is a general increase of scattering throughout the entire angular range compared to the results of [186]. Interestingly, the increase in cross section around the peak is maximal just where the triplet contribution tends to zero. This demonstrates that the three improvements (b), (c), and (d) described in the first paragraph are contributing significantly. From our numerical values, we see that away from the cross-section peak the triplet contribution is small but not insignificant. The peak position is still at 90° in contrast with 100° for the measurement. Theoretically, the peak is expected to be at the Wannier ridge ($\theta_1 = 90° = \theta_2$) near threshold, but as the energy increases, the TDCS are expected to be strongly peaked in the forward direction rather than in the backward direction, in conformity with the high-energy results. In the present case we are, however, only at 2 eV above threshold.

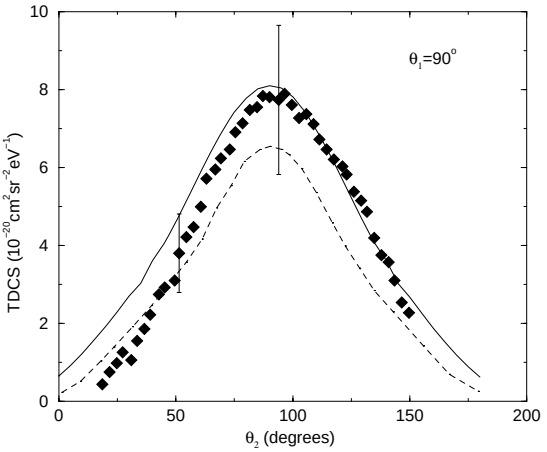

Fig. 3.2. TDCS for the coplanar asymmetric geometry for $\theta_1 = 90°$ (θ_2 varying) at 2 eV over the threshold. *Filled diamonds*, measurement of Rösel et al. [518]; *dashed curve*, Crothers [186]; *solid curve*, Deb and Crothers [202]

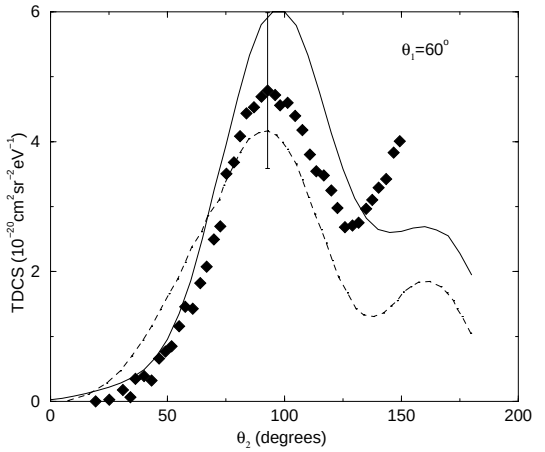

Fig. 3.3. As for Figure 3.2 but for $\theta_1 = 60°$ and *dotted curve*; Jones et al. [345]

Next we present TDCS at the same energy for $\theta_1 = 60°$ (Figure 3.3) and $\theta_1 = 120°$ (Figure 3.4). In Figure 3.3 the present result is strongly peaked around $\theta_2 = 95°$. The height of this peak has been increased dramatically compared to the earlier calculation but still lies within the experimental error bar. The contributions from the triplets are largely responsible for this dramatic increase around $\theta_2 = 95°$. The peak position in Figure 3.4 appears to be at a slightly larger angle compared to the measurement and the previous calculation. The second peak around $\theta_2 = 160°$ has also increased significantly due to the triplet contributions. The measurement shows a much stronger peak at this angle. Rösel et al. [518] also report the results

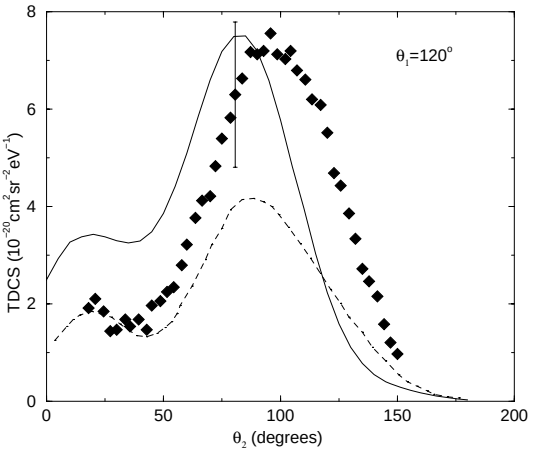

Fig. 3.4. As for Figure 3.2 but for $\theta_1 = 120°$ and *dotted curve* as in Figure 3.3

of Jones et al. [345]. This model is an improvement over their distorted-wave Born approximation (DWBA) calculation in that they include exchange distortion of continuum and target electrons. While the importance of exchange distortion was also confirmed by Pan and Starace [480], the predicted results (dashed curves in Figures 3.3 and 3.4) in the [345] model were not very good either in peak position or in peak height. For all the angles, the position of the primary peak in the [345] model is shifted to either the forward or the backward direction relative to the measurement and our calculation. However, the position of the secondary peak for $\theta_1 = 60°$ (Figure 3.3) and $\theta_1 = 120°$ (Figure 3.4) seems to agree with the measurement and the present calculation. From Figure 3.4 we note that the height of the primary peak in the present calculation agrees very well with that of the measurement but the peak position is shifted by a few degrees to the left.

In conclusion, the semiclassical–quantal treatment of [186] has been applied in a more precise manner to calculate the TDCS for electron-impact ionization of He. Good results are obtained at and around the Wannier ridge in the coplanar symmetric and asymmetric geometry. However, away from the Wannier ridge only qualitative agreement was found. Further theoretical calculations and accurate measurements are needed for this near-threshold region. In Figures 3.5 ($\theta_1 = 90°$) and 3.6 ($\theta_1 = 60°$) we present our singlet and triplet contributions to the full TDCS along with the measurements [518] and earlier singlet TDCS of Crothers [186]. As expected, the singlet contributions dominate the TDCS at both angles. The triplet contributions in general enhance the TDCS by a few percent away from the primary peak at $\theta_1 = \theta_2 = 90°$ in Figure 3.5. For the case of $\theta_1 = 60°$ (Figure 3.6) our full (singlet + triplet) TDCS show the primary peak around $\theta_2 = 100°$ and another peak far away (around 165°), which we refer to as the secondary peak. Theoretically, the triplet contributions are coming from $0.75|f - g|^2$ and will be zero at equal angles, which can be seen from Figures 3.5 and 3.6. However, the triplets contribute to the peaks

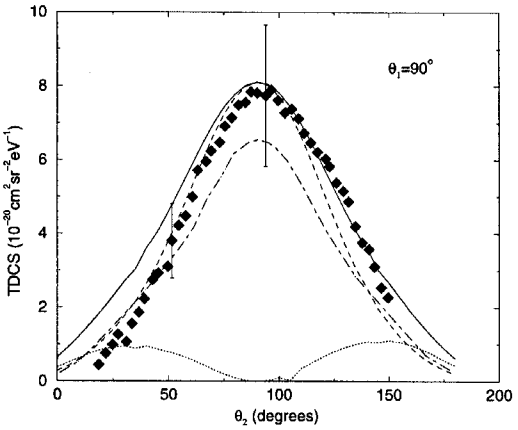

Fig. 3.5. TDCS in the coplanar asymmetric geometry for $\theta_1 = 90°$ at $E = 2$ eV above threshold. *Filled diamond*; measurement [518]; *dashed-dotted* line; Crothers [186]; *dotted line*; present triplet; *dashed line*; present singlet; and *solid line*; present full (singlet plus triplet) calculation

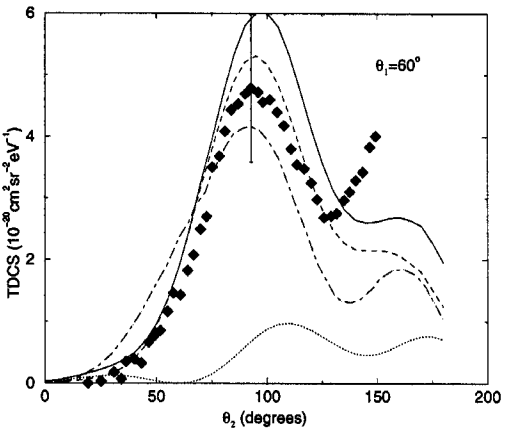

Fig. 3.6. Same as Figure 3.5 but for $\theta_1 = 60°$

of the full TDCS significantly at unequal angles. This property was also noted in the theoretical calculation reported by Rösel et al. [518]. A careful observation of Figure 3.6 suggests that the triplet contribution not only enhanced the primary peak but also moved this peak position slightly to higher angles.

It is puzzling that for $\theta_1 = 90°$ (Figure 3.5) the TDCS peak occurs theoretically at $\theta_2 = 90°$ but experimentally [518] at $\theta_2 = 100°$, whereas for $\theta_1 = 60°$ (Figure 3.6) the situation is exactly reversed, i.e., the theoretical primary peak occurs at $\theta_2 = 100°$ when the experimental primary peak seems to occur at $\theta_2 = 90°$. In the

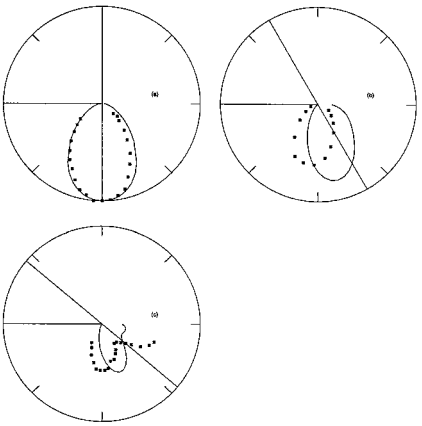

Fig. 3.7. Polar plots of the TDCS for (**a**) $\theta_1 = 90°$, (**b**) $\theta_1 = 60°$, and (**c**) $\theta_1 = 140°$ at $E = 1$ eV above threshold. *Square*; measurement [541] and *solid line*; present full (singlet plus triplet) calculation. The radius of the circle represents the maximum TDCS at $\theta_1 = \theta_2 = 90°$, which is 1.24×10^{-19} cm^2 sr^{-2} eV^{-1}

coplanar asymmetric geometry, the present TDCS maximum for the electron-impact ionization of He has occurred at $\theta_1 = 90° = \theta_2$ where the two outgoing electrons are on opposite sides and on the Wannier saddle. The relative measurement of Selles et al. [541] at $E = 1$ eV also supports (Figure 3.7(a)) this behaviour. Here it is noteworthy that for $\theta_1 = 120°$ we found [203] that the theoretical primary peak position shifted by about 10° towards the smaller angle compared to the corresponding experimental peak. It therefore appears that for $\theta_1 \geq 90°$ the present theoretical TDCS primary peaks are shifted by about 10° towards the smaller angles compared to the measurement whereas for $\theta_1 < 90°$ it moves by the same angular domain towards higher angles. To resolve these discrepancies of the peak positions, more accurate measurements and calculations need to be encouraged.

In Figure 3.7 we present the polar plots of the TDCS at an excess energy of 1 eV above the threshold. In this figure we compare our results with the relative measurements of Selles et al. [541] at several angles. The radius of all the circles are normalized to unity, which corresponds to 1.23×10^{-19} cm^2 sr^{-2} eV^{-1}, the present maximum TDCS value at $\theta_1 = \theta_2 = 90°$. The corresponding singlet result recorded earlier [186] was 0.89×10^{-19} cm^2 sr^{-2} eV^{-1}. Considering the fact that at this angle ($\theta_1 = \theta_2 = 90°$) the triplet contribution is exactly zero, there is about 38% enhancement in the absolute value of the singlet TDCS. We observe that this enhancement is mostly a result of treating the classical action variables exactly and partly due to the inclusion of a few more partial waves in the present calculation. Going back to Figure 3.5 we note that the corresponding enhancement at 2 eV is about 20%. Therefore, as the excess energy $E \to 0$ the classical action variable is becoming increasingly important. Since the absolute experimental value [541] at $E = 1$ eV is not known it is difficult to assess the accuracy of the present results. Nevertheless, Figure

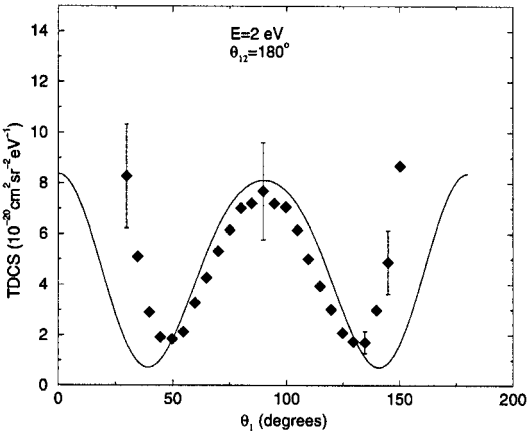

Fig. 3.8. TDCS at coplanar constant geometry for $\theta_{12} = 180°$ at $E = 2$ eV. *Diamond*; measurement [518]; and *solid line*; present full (singlet plus triplet) calculation

3.7(a) shows good qualitative agreement between the present results and those of the relative measurement of Selles et al. [541]. Figures 3.7(b) and 3.7(c) show similar comparison of the present calculation and the measurement [541] for $\theta_1 = 120°$ and $\theta_1 = 140°$ respectively. These two figures show that the present TDCS maxima at these angles are shifted towards the smaller θ_2 compared to the measurement – a behaviour already noted for the $\theta_1 = 120°$ case at 2 eV excess energy [203]. Unlike the case where $E = 2$ eV, here ($E = 1$ eV) both the measurement [541] and the present calculation show a single peak structure for $\theta_1 = 120°$ (Figure 3.7(b)) although the intensity of the theoretical peak is slightly higher than that of the measurement. Figure 3.7(c) ($\theta_1 = 140°$), however, shows a double-peak structure in both the measurement and the present calculation. In this case the intensity of the primary peak shows agreement between the two sets of results but large discrepancies are noted for the secondary peak intensity.

In the coplanar constant geometry (i.e., θ_{12} = constant, θ_1 and hence θ_2 both varying) we have also calculated the TDCS at $E = 2$ eV and compared our results with those of Rösel et al. [518] in Figure 3.8. Here we have considered the case $\theta_{12} = 180°$. Although the general behaviour of the TDCS peak around the Wannier ridge ($\theta_1 = \theta_2 = 90°$) agrees well with the measurement, the cross sections differ considerably for $\theta_1 < 40°$ or $\theta_1 > 140°$. The measurements tend to show very large cross sections at extreme forward or backward angles at an energy close to the threshold. It is to be noted here that in the present case $\Delta\theta_{12}$ is exactly zero and the improvement made in the present investigation through the classical action variable S_2 is no longer accountable. In addition the present numerical technique being based on the method of steepest descent may not provide a good description of the dynamical behaviour of the ionization process far away from the ridge.

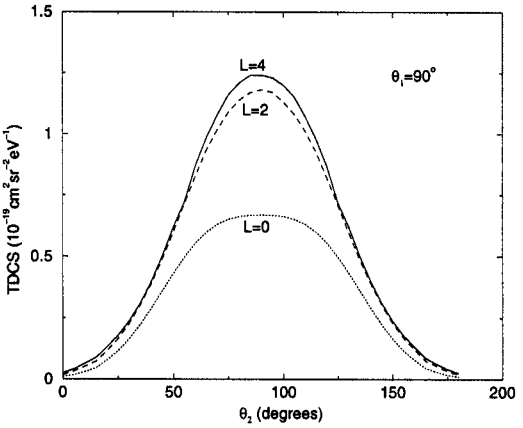

Fig. 3.9. Contributions of various partial waves (up to and including the respective L-values) to the TDCS for $\theta_1 = 90^\circ$ at $E = 1$ eV above threshold

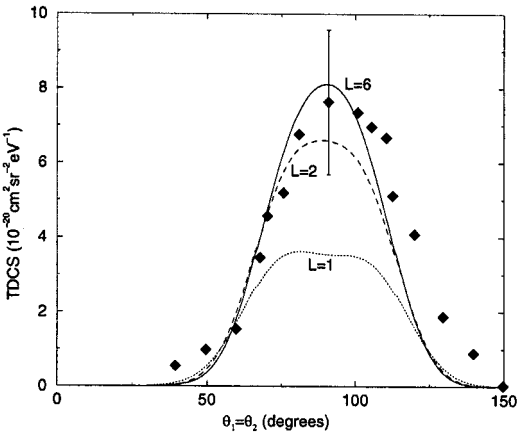

Fig. 3.10. Contributions of various partial waves (up to and including the respective L-values) to the TDCS for coplanar symmetric geometry for $\theta_1 = \theta_2$ at $E = 2$ eV above threshold

To check the convergence of our calculations as a function of partial-wave contributions we present in Figure 3.9 the coplanar symmetric TDCS at $E = 1$ eV up to three different partial waves ($L = 0, 2$, and 4). We found that the ${}^1S^e$ contribution is about 54% of the full TDCS maximum (0.669×10^{-19} cm^2 sr^{-2} eV^{-1} out of 1.23×10^{-19} cm^2 sr^{-2} eV^{-1}). In our formulation it is very difficult to isolate the contributions of individual nonzero partial waves to the full TDCS. However, with a closer look at the TDCS after adding each nonzero partial wave we surmise that the next important contributions came from the ${}^{1,3}D^e$, and ${}^3F^o$ levels. Nonnegligible contributions totalling up to a few percent are coming from ${}^{1,3}P^o$, ${}^1F^o$ and ${}^{1,3}G^e$

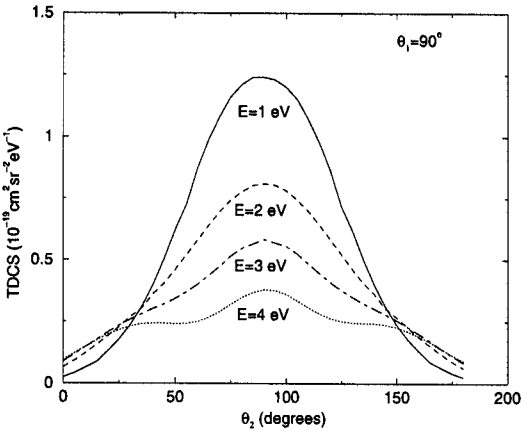

Fig. 3.11. TDCS for $\theta_1 = 90^\circ$ at $E = 1, 2, 3$, and 4 eV

levels. No other partial waves at this energy are necessary to achieve a four-figure accuracy maintained in the present calculation. Similar results are found at 2 eV in the same geometry with an exception that $^1S^e$ this time contributes about 44% (0.357×10^{-19} cm^2 sr^{-2} eV^{-1} out of 0.810×10^{-19} cm^2 sr^{-2} eV^{-1}). This implies that the relative importance of the $^{1,3}D^e$ and $^3F^o$ increases with the excess energy. At this energy, however, we needed $L = 6$ to achieve the similar accuracy with $^{1,3}H^o$ giving almost zero contributions. The importance of $L = 3$ contributions, especially from $^3F^o$ levels, agrees with the finding of the JM calculation [345] reported by Rösel et al. [518]. We next considered the TDCS at 2 eV in the coplanar symmetric geometry where the triplets are exactly zero and the results are shown in Figure 3.10. Here we have noticed that the contributions up to $L = 4$ are about 1% smaller than the corresponding values up to $L = 6$. We decided, therefore, to keep values up to $L = 6$. The contributions from $L = 0, 2$, and 3 again turn out to be very important. It is interesting to note that the higher L contributions not only increased the height of the TDCS peaks but also improved the flat low-L peaks to sharper peaks. We also found that the contributions from odd $L > 3$ are practically zero. Even values of higher partial waves ($L > 6$) are contributing only within a small angular range close to the beam direction i.e $\theta_1, \theta_2 \rightarrow 0^\circ$, or 180°. Finally, in Figure 3.11 we present the behaviour of our TDCS as a function of the excess energy over the threshold, at the Wannier ridge ($\theta_1 = \theta_2 = 90^\circ$). As expected the TDCS peaks become sharper with excess energy $E \rightarrow 0$. Here we have also noted that as E increases more partial waves are needed to achieve convergent results. As an example, $L = 4$ was sufficient for $E = 1$ eV whereas $L = 8$ was needed for the case of $E = 4$ eV. Various theoretical models predicted various energy ranges as the valid threshold region. Selles et al. [541] predicted this range of validity to be 2 eV above the threshold. In the present calculation we are able to go without any difficulty up to 4 eV above the threshold.

We have presented a systematic study of the near-threshold ionization of He by using a more accurate version of the quantal-semiclassical treatment of Crothers [186]. Various aspects of the triple differential cross sections are studied, such as contributions from singlets and triplets, effects of the higher partial waves in various coplanar geometries, and energy dependence. It is found that the improvements made in the present investigation, by including the classical action variables exactly, produce better overall agreement with the available measurements, especially around the Wannier ridge. However, far away from the ridge only qualitative agreement is achieved. More rigorous theory and accurate measurements in this area are needed to resolve the existing discrepancies. Singlet contributions are dominating at all angles, and triplet contributions are responsible for the enhancement of the secondary peaks by a few percent, mostly at unequal scattering angles. In terms of partial waves, $L = 0$, 2, and 3 contribute most (at all angles) whereas the higher partial waves give small contributions at angles close to the beam direction.

The uniform semiclassical approximation is employed to calculate absolute Wannier cross sections for two-electron photo detachment from He^- ($1s2s2p\,^4P^o_{5/2}$) near threshold. This is the first absolute theory in which the initial state involved nonzero total angular momentum: $^3P^o_1$ in the initial state and $^3P^e_1$ in the final state. It also permits the first absolute comparison between theoretical and experimental cross sections. Our theory predicts a cross section of 1.89×10^{-20} cm^2 at an excess photon energy of $E = 0.41$ eV. This compares favourably with the experimental estimate 2×10^{-20} cm^2 of Bae et al. [17]. Our cross section, as a function of excess energy E in a.u., is given by $2.14\,E^{1.127} \times 10^{-18}$ cm^2.

The theory of Crothers [186] was adapted to calculate the first absolute Wannier threshold cross section for single-photon two-electron detachment (McCann and Crothers [410], hereafter referred to as II). This original application was to H^-, an ion of zero total angular momentum. The theory predicted a cross section parameterized by E, the excess energy above the double ionisation threshold in eV, and given by

$$\sigma(\gamma, 2e) = (3.14 \times 10^{-20}) E^{1.127} \text{ cm}^2 \tag{3.48}$$

which clearly demonstrates the law of Wannier [593]. Unfortunately we were unaware of any experimental measurement of such a cross section. To remedy this deficiency we subsequently [107] used the continuum distorted-wave function of Dulieu and Le Sech [233] to extend our theory to K^- for which we found $\sigma(\gamma, 2e) = (66.7 \times 10^{-20}) E^{m_{12}}$ cm^2 a factor of four larger than the experiment of Bae and Peterson [18] who found $\sigma(\gamma, 2e) = (17.7 \times 10^{-20}) E^{m_{12}}$ cm^2. We also applied [190] our uniform semiclassical approximation to calculate absolute Wannier threshold cross sections for single-photon two-electron detachment from He^- ($1s2s2p\,^4P^o_{5/2}$), for which cross sections have been measured by Bae et al. [17]. A direct comparison of absolute cross sections between theory and experiment thus became possible for the first time, despite the obvious caveat that the experimental cross sections were subject to nontrivial error bars, mainly due to competing second-order processes such as two-photon two-step ionization. On the other hand this He^- ion provided a good test of the theory. First it is genuinely metastable, autoionisation being prohibited

by selection rules [330], and second it involves a $(1s2s)\,^3S$ core and a total angular momentum of one atomic unit.

In the past, Roth [525] had considered a ψ_{100} final-state wave function that, in the notation of Morse and Feshbach [440], is given by

$$\psi_{100} = \sin\Psi \sin\Theta f_{100} \tag{3.49}$$

where the first subscript on ψ gives the value of total angular momentum, the second its z component, and the last its symmetry properties. In (3.49) Θ may be interpreted as θ_1, the polar angle for electron 1, while Ψ is defined as the angle between the (r_1, r_2)-plane and the (r_1, z)-plane. In fact ψ_{100} is an even-parity state with $L = 1$ and $M_L = 0$ and in principle is accessible from a He^- p_o odd-parity state through the odd-parity dipole operator. However, as remarked by Roth "the amplitude of the wave function will be small in the far zone due to the node along the Wannier line". In short, application of our variation perturbation principle (see II) leads precisely to zero transition amplitude, because the following integral is zero:

$$\begin{aligned}\int_0^{2\pi} \mathrm{d}\Psi(\sin\Psi\sin\theta_1)\,[\cos\theta_1(1-\cos\gamma)+\sin\theta_1\sin\gamma\cos\Psi] \\ \times[\cos\theta_1(1+\cos\gamma)-\sin\theta_1\sin\gamma\cos\Psi]\end{aligned} \tag{3.50}$$

where γ is given by

$$\gamma = \pi - \cos^{-1}(\hat{\mathbf{r}}_1 \cdot \hat{\mathbf{r}}_2) \tag{3.51}$$

The three brackets of expression (3.50) represent the angular behaviour of, in order, a final-state $^3P_0^e$, the $^1P_0^o$ dipole interaction, and the $^3P_0^o$ initial state. We have thus established the selection rule for $^3P_0$ states, namely

$$M_L = 0 \tag{3.52}$$

leads to a nugatory Wannier cross section. On the other hand we do find that the $^3P_{\pm1}$ states are accessible with nonzero cross sections. These states correspond to the $\psi_{1,10}$ and $\psi_{1,-10} = \psi^*_{1,10}$ of Morse and Feshbach. Their angular behaviour is given by

$$(\mathrm{e}^{\pm\mathrm{i}\Phi}\sin\theta/\sqrt{2})(\cos\Psi \mp \mathrm{i}\cos\Theta\sin\Psi) \equiv \frac{(\mathrm{e}^{\pm\mathrm{i}\phi_2}\sin\theta_2\cos\theta_1 - \mathrm{e}^{\pm\mathrm{i}\phi_1}\sin\theta_1\cos\theta_2)}{\gamma\sqrt{2}} \tag{3.53}$$

where Φ is φ_1 and that corresponds to the $(y/\gamma)^1P^o$ state in the H^- problem. Of course, magnetic selection rules require the p electron to occupy a $P_{\pm1}$ state. The initial wave function must therefore correspond, in the notation of Morse and Feshbach, to ϕ_{-11a} or $\phi_{-1,-1a}$, whose unnormalised angular behaviour is given by

$$\begin{aligned}&\frac{(\mathrm{e}^{\pm\mathrm{i}\phi_1}\sin\theta_1 - \mathrm{e}^{\pm\mathrm{i}\phi_2}\sin\theta_2)}{\sqrt{2}} \\ &= \frac{\mathrm{e}^{\pm\mathrm{i}\Phi}}{\sqrt{2}}\,[\sin\Theta(1+\cos\gamma) \mp \mathrm{i}\sin\gamma\sin\Psi + \sin\gamma\cos\Theta\cos\Psi]\end{aligned} \tag{3.54}$$

Taking the upper signs in (3.53) and (3.54), that is, taking $M_L = +1$, the crucial angular integration in the transition amplitude is

$$\begin{aligned}\tfrac{1}{2}\int_0^{2\pi} \mathrm{d}\Psi \int_0^{2\pi} \mathrm{d}\varphi_1 \int_0^{\infty} \gamma\, \mathrm{d}\gamma \int_0^{\pi} \sin\theta_1\, \mathrm{d}\theta_1\, (\cos\Psi + \mathrm{i}\cos\theta_1 \sin\Psi)\mathrm{e}^{-\eta_f^2\gamma^2} \\ \times(\cos\theta_1(1-\cos\gamma) + \sin\theta_1 \sin\gamma\cos\Psi) \\ \times(\sin\theta_1(1+\cos\gamma) + \cos\theta_1 \sin\gamma\cos\Psi - \mathrm{i}\sin\gamma\sin\Psi) \qquad (3.55)\\ \simeq \frac{\pi^{5/2}}{4\eta_f^5} + \frac{2\pi^{5/2}}{3\eta_f^3} \qquad (3.56)\end{aligned}$$

where the brackets are final-state ${}^3P_1^e$, dipole ${}^1P_0^o$ and initial-state ${}^3P_1^o$, and where

$$\eta_f^2 = -\frac{1}{8}\sqrt{2z_0\rho}\,\mathrm{Im}\,\mathrm{m}_{21} \qquad (3.57)$$

in the standard notation of II. As it happens, expression (3.56) also agrees in value with the corresponding angular integral of II, namely

$$\int \frac{y}{\gamma}(\cos\theta_1 + \cos\theta_2)\mathrm{e}^{-\eta_f^2\gamma^2}\, \mathrm{d}\hat{\mathbf{r}}_1\, \mathrm{d}\hat{\mathbf{r}}_2 \qquad (3.58)$$

It follows that the cross section is given by

$$\sigma(\gamma, 2e) = \frac{2}{3}\frac{3}{8\pi}\frac{(2\pi)^5}{9} E_0 \alpha a_0^2 |\tilde{t}|^2 \qquad (3.59)$$

where the transition amplitude $\tilde{t}$ is given by

$$\tilde{t} = \frac{Z^{3/2}M}{z_0 m_{12}^{1/2}(\mathrm{Im}\,\mathrm{m}_{12})}\int_0^{\infty} \mathrm{d}\rho\, \rho^{3+m_{12}/2} \sin\left(\sqrt{8z_0\rho} - \frac{2\pi}{\sqrt{3}} + \frac{\pi}{2}\right)\phi(r_1, r_2) \qquad (3.60)$$

where we have averaged over the initial states and summed over the final states, that is, assuming circular polarisation of the photon beam, so that the cross section is $2/3$ of that for $M_L = +1$ or -1. In (3.59) $E_0 = 4.845/27.21$ is the double ionization threshold energy in a.u., α is the fine structure constant in au and a_0 is the Bohr radius. In (3.60) the parameters M, z_0, m_{12}, m_{21}, and ρ are exactly as in II. The extra phase of $2\pi/\sqrt{3}$ in (3.60) comes from Roth's analysis of the ${}^3P$ state. The factor of $3/8\pi$ in (3.59) is just the normalisation of the $\mathrm{e}^{\mathrm{i}\varphi}\sin\theta$ initial angular state. Clearly the distance of the electron $n(=1,2)$ from the nucleus is given by $r_n = \rho/\sqrt{2}$ while $r_{12} = \rho\sqrt{2}$, since we are on the Wannier ridge. For the radial part of the He^- bound-state wave function represented by $\phi(r_1, r_2)$ in (3.60), we take that of Bunge and Bunge [102]. We assume that the inner $1s$ electron is essentially a spectator that we may ignore and employ their first term in a Slater orbital expansion, namely

$$\phi(r_1, r_2) \equiv \frac{1}{\sqrt{4\pi}}\sqrt{\frac{3}{8\pi}}\frac{(2\alpha)^{5/2}}{\sqrt{24}} r_1\, \mathrm{e}^{-\alpha r_1}\frac{(2\beta)^{5/2}}{\sqrt{24}} r_2\, \mathrm{e}^{-\beta r_2} \qquad (3.61)$$

where

$$\begin{aligned} \alpha &= 0.72 \\ \beta &= 0.53 \end{aligned} \tag{3.62}$$

and where electron 1 is the $2s$ electron and electron 2 is the $2p$ electron. A simple numerical calculation gives

$$\sigma(\gamma, 2e) = 1.89 \times 10^{-20}\ \text{cm}^2 \tag{3.63}$$

for $E = 0.41$ eV. This compares very favourably with the cross section of Bae et al. [17], which can probably be given as $(2 \pm 0.4) \times 10^{-20}$ cm^2, the large error bars being due to the already mentioned competing two-stage processes. Our more general result can be written as a function of E as

$$\sigma(\gamma, 2e) = (2.14 \times 10^{-18}) E^{1.127}\ \text{cm}^2 \tag{3.64}$$

where E is in au. We also used a more cumbersome and older four-term wave function of Holøien and Midtdal [330] not as good a physical representation as that of Bunge and Bunge [102], in contrast with the assertion of Haritos et al. [323]. It gave a cross section of 1.1×10^{-20} cm^2 for $E = 0.41$ eV and definitely lies outside the error bars of Bae et al. [17]. We conclude that the more recent and physically more plausible wave function gives very good consistency with the experimental estimates. In turn, we may state that the current theory (in contrast with the K^- case) affords the first successful *absolute* test of the Wannier threshold law in photo-double detachment and that the test has proved reasonably successful. Undoubtedly further theoretical and experimental determinations are desirable.

Finally, in this section we turn to an accurate, absolute theoretical calculation of positron impact ionization of He for energies 0.5 – 10 eV above threshold [205]. Our quantal-semiclassical calculation shows excellent agreement for the total ionization cross section with the absolute measurement of Ashley et al. [16] who measured total cross sections Q_i^+ in the range $(0.0 - 0.6) \times 10^{-21}$ m^2, for the impact energy range 24.58 – 34.00 eV, that is, an excess energy E' (= $E - E_i$) above threshold E_i in the range 0.0-9.42 eV. Extending the classical treatment of Wannier [593] from e^- to e^+ impact, Klar [357] determined $Q_i^+ \propto (E')^{2.651}$ while Rost and Heller [523] semiclassically determined $(E')^{2.67}$. However, Ashley et al. [16] obtained $Q_i^+ \propto (E')^{1.99 \pm 0.19}$ over $1 < E' < 3$ eV and $(E')^{2.27 \pm 0.08}$ over $3 < E' < 9$ eV. As stated by Ashley et al. [16], the process of positron impact near-threshold ionization of helium is also interesting because of the absence of an exchange interaction and the possibility of the formation of an electron–positron bound state, positronium (Ps), with a threshold energy 6.8 eV below the threshold E_i for direct ionization. They also reported that by measuring e^+–ion coincidences, ions resulting from Ps formation (the dominant ionization process near E_i) were largely undetected. However, random coincidences between ions and uncorrelated positrons result in a background that can be measured by preventing the positrons that have produced an ion (and have hence lost E_i which is 24.58 eV for He) from reaching the detector.

It is well known [593], [357], [486], [487], [505] that purely classical mechanics cannot obtain the absolute constant of proportionality in the $Q_i^{\pm}/E'$ power relations

for positron/electron impact. To rephrase, the constant of proportionality, however restricted the E' domain, is a purely quantal effect. In 1986 Crothers [186] published the first account of absolute electron-impact single, double and triple differential and total integrated cross sections, using quantum mechanics and a semiclassical asymptotically correct final-state wave function Ψ_f^-. Good agreement with experimental absolute and relative cross sections was obtained. Over concentration on the immediate threshold region had led to a perturbative expansion of the zero-order complex action in Ψ_f^- and the omission of triplets which were known to be small experimentally.

In 1997–8 Loughan and Crothers [386], [387] analytically continued the Ψ_f^- of Crothers [186] below threshold ($E' < 0$), and immediately realized that a perturbation expansion of the zero-order complex action would be incorrect and that both transition points (real or complex, depending on the value of L, the total angular momentum azimuthal quantum number) had to be determined exactly to be able to invoke a complex Bohr–Sommerfeld quantization rule. Excellent results for the doubly highly excited states of He^- ($L = 0$ [386] and $L = 1, 2$ [387]) and of He [195] were obtained for resonance positions, lifetimes, intensities, and scaling rules, in comparison with experiment. In the case of $L = 1$, an irrational quantum number was derived and attosecond lifetimes were obtained (see Section 3.3). This persuaded us to analytically continue back above threshold, retaining the complex zero-order action in Ψ_f^- without perturbative expansion, retaining triplets, and extending $L_{\max}$ [202], [203], [204]. Here we apply, without approximation, our full quantal matrix element with semiclassical Ψ_f^-, to determine Q_i^+ for absolute comparison with Ashley et al. [16].

We now give a brief résumé of our mathematical expressions, taking the position vectors of e^+ and e^- relative to the He^+ core ($Z = 1$) as $\mathbf{r}_1$ and $\mathbf{r}_2$, respectively, with $r_{12} = |\mathbf{r}_1 - \mathbf{r}_2|$. The interaction potential is given by

$$\frac{1}{r_1} - \frac{1}{r_2} - \frac{1}{r_{12}} = \frac{\zeta(\alpha, \theta_{12})}{\rho} \tag{3.65}$$

where the effective charge ρ is given by

$$\zeta(\alpha, \theta_{12}) = \sec\alpha - \csc\alpha - (1 - \cos\theta_{12} \sin 2\alpha)^{-1/2} \tag{3.66}$$

with ρ, α, and θ_{12} the usual hyperspherical coordinates associated with $\mathbf{r}_1$ and $\mathbf{r}_2$ [186], respectively, hyperspherical radius and angle and mutual polar angle. The Wannier saddle is given by making ζ stationary as a function of α and θ_{12}, namely $\theta_{12} = 0$ and $\alpha = \alpha_0 \approx 24.9060°$. This implies that $r_1/r_2 = 2.15372$ and that the negatively charged electron nestles roughly halfway between the positively charged He^+ and e^+. Near the saddle, we have

$$\zeta \approx Z_0 + Z_1(\alpha - \alpha_0)^2 + Z_2\theta_{12}^2 \tag{3.67}$$

where

$$\begin{aligned} Z_0 &\approx 3.33019 \\ Z_1 &\approx 55.6414 \\ Z_2 &\approx -13.3207 \end{aligned} \tag{3.68}$$

and the Wannier–Peterkop indices are given by

$$\begin{aligned} m_{12} &= \left[\left(1+\tfrac{8Z_1}{Z_0}\right)^{1/2}-1\right]/4 \approx 2.65 \\ m_{21} &= \left[-\mathrm{i}\left(-1-\tfrac{8Z_2}{Z_0}\right)^{1/2}-1\right]/4 \end{aligned} \tag{3.69}$$

The scattering amplitude is f, given by

$$\begin{aligned} f(\hat{\mathbf{k}}_1,\hat{\mathbf{k}}_2) \approx{}& \frac{2\mathrm{i}}{\pi[2(1+S)]^{1/2}}\int \mathrm{d}\mathbf{r}_1\,\mathrm{d}\mathbf{r}_2\,\mathrm{d}\mathbf{r}_3\;\Psi_f^{-*}(\mathbf{r}_1,\mathbf{r}_2)\varphi(r_3,2)\mathrm{e}^{\mathrm{i}\mathbf{k}_0\cdot\mathbf{r}_1} \\ &\times\left[\left(\frac{z_0}{r_1}-\frac{1}{r_{12}}\right)\varphi(r_2,z_0)\varphi(r_3,\beta)+\left(\frac{z_0}{r_1}-\frac{1}{r_{13}}\right)\varphi(r_3,z_0)\varphi(r_2,\beta)\right] \end{aligned} \tag{3.70}$$

where $\mathbf{k}_0$ is the momentum of the incident positron and we allow for exchange between the two bound-state electrons $\mathbf{r}_2, \mathbf{r}_3$ using an open-shell independent-electron model in which the outer electron sees a charge z_0 and the inner electron sees a charge β (φ, S, z_0, and β are defined in equations (69)–(73) in [186]). Notice that the ground-state helium wave function contains electron correlation implicitly through the parameter z_0 in $\varphi(r, z_0)$ and goes beyond the Hartree–Fock description. An explicitly correlated wave function was used by Copeland and Crothers [148] for the electron impact ionization of helium resulting in very little change in the cross sections. By the same token, it makes little difference to the present wave function and calculations. Moreover this initial-state description in no way contradicts the Wannier description of the final state in which both the incident positron and the ejected electron are far away from the residual He^+ core that is $l_1, l_2 \gg 1$ so that the total angular momentum quantum number $L \in [|l_1 - l_2|, l_1 + l_2]$ and $\in [0, L_{\max}]$. The final state is given by

$$\begin{aligned} \Psi_f^{-*} = {}& \frac{c^{1/2}(E')^{m_{12}/2}u_1^{1/2}}{\tilde{\omega}^{1/2}\rho^{5/2}\sin\alpha\cos\alpha}\delta(\hat{\mathbf{k}}_1-\hat{\mathbf{r}}_1)\delta(\hat{\mathbf{k}}_2-\hat{\mathbf{r}}_1)\exp\left(\frac{4\mathrm{i}}{(8Z_0\rho)^{1/2}}\theta_{12}^{-2}\right) \\ &\times\left\{\exp\left[-\mathrm{i}\left(S_0+\frac{1}{2}S_1(\Delta\alpha)^2+\frac{1}{8}S_2\theta_{12}^2+\frac{\pi}{4}\right)\right]-\text{ conjugate}\right\} \end{aligned} \tag{3.71}$$

where c is given by equation (42) of [186], $\mathbf{k}_1$ and $\mathbf{k}_2$ are the momenta of the positron and ejected electron, respectively, and $\Delta\alpha = \alpha - \alpha_0$. The actions are given by

$$S_0 = \int_{\rho_+}^{\rho}\mathrm{d}\tilde{\rho}\,\tilde{\omega}(\tilde{\rho}) \tag{3.72}$$

$$S_j = \rho^2\omega\frac{\mathrm{d}}{\mathrm{d}\rho}(\ln u_j) \qquad (j=1,\,2) \tag{3.73}$$

$$\omega^2(\rho) = 2E' + \frac{2Z_0}{\rho} - \frac{L(L+1)\sec^2\alpha_0}{\rho^2} \tag{3.74}$$

$$\tilde{\omega}^2(\rho) = \omega^2 - \omega\frac{\mathrm{d}}{\mathrm{d}\rho}(\ln u_2 - \mathrm{i}\ln u_1) \tag{3.75}$$

$$u(m) = \rho^m\,{}_2F_1\left(m, m+1; 2m+3/2; \frac{-E'\rho}{Z_0}\right) \tag{3.76}$$

$$u_1 = u(m_{12}), \qquad u_2 = u(m_{21}) \tag{3.77}$$

and where ${}_2F_1$ is the Gauss hypergeometric function and ρ_+ is given by

$$\rho_+ = \frac{\left[Z_0^2 + 2E'L(L+1)\sec^2\alpha_0\right]^{1/2} - Z_0}{2E'} \tag{3.78}$$

We note that the effective azimuthal quantum number $\mathcal{L}$ (where $\mathcal{L} = \{[1 + 4L(L + 1)\sec^2\alpha_0]^{1/2} - 1\}/2$) is now irrational for all positive L, in contrast (e.g., $L = 2$) to the electron case [387].

It is no accident that $\tilde{\omega}$ is a complex effective wave number (both i and u_2): this represents loss of flux to other channels. The integration over $\mathbf{r}_3$ is trivial and analytical, that over α is effected using the method of stationary phase and the rest are effected numerically with some changes of dummy variables to avoid removable singularities. Given that $E' > 0$, the nonnegative ρ_+ is the outer classical turning point, while the other root ρ_- (of (3.74)) is always classically inaccessible, so that the Jeffreys connection formula in (3.71) guarantees rapid exponential decay for $0 \leq \rho \leq \rho_+$. Expanding the plane wave and the first two-dimensional Dirac delta function as a sum over L simplifies the calculation.

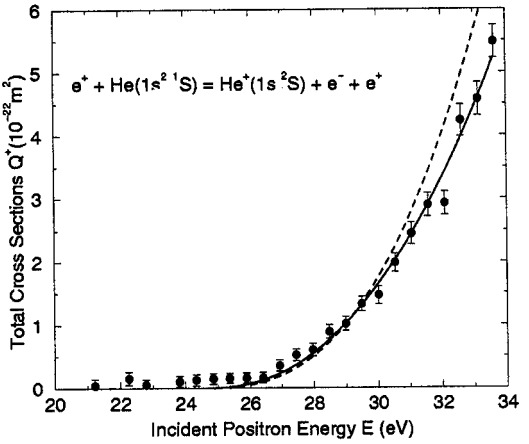

Fig. 3.12. Total cross sections in units of 10^{-22} m^2 plotted against the incident positron energy E (in eV). *Full circles*; measurement [16]; *full curve*; present theory with $L_{\mathrm{MAX}} = 11$; *broken curve*; present result fitted to a pure Wannier threshold law

In Figure 3.12 we compare our results with the experimental results [16], taking $L_{\max} = 11$. With the possible exception of the experimental results at 28.5 and 32 eV, agreement is very encouraging. Given that both scales are linear and both sets of results are absolute, this is a remarkable vindication of both the experiment and our new extended semiclassical, quantal Wannier theory, notably in the range $E \in [26, 34]$ eV. Our success is undoubtedly due to our nonperturbative, exact treatment of S_0 (3.72), to our treatment of the centrifugal potential (3.74), and to our

sum over $L \in [0, 11]$. The complex action variables ((3.72) and (3.73)) imply that continuum coupling with the Ps formation channel is included in the present calculation. The importance of the contributions to the integrated cross sections from $L > 0$ partial waves has already been demonstrated for the electron impact case [203]. In the present positron impact case we observe a similar trend in the need for higher partial waves as the excess energy increases. For example $L_{\max} = 5$ for $E' = 2$ eV and $L_{\max} = 7$ for $E = 4$ eV were sufficient for convergence.

The experimental results [16] contradict previous tentative experimental conclusions [361], [575] that the electron and positron impact ionization cross sections may exhibit a similar energy dependence close to the threshold and yet qualitatively agree with Wannier-type theories that, as we see from our introduction, predict a larger exponent for the case of e^+. The non-Wannier-type theory such as the Coulomb dipole approximation of Temkin applied to both electron [578] and positron [579] impact ionization predicted a modulated threshold law proportional to $E/(\ln E)^2$, which could be described as "quasilinear". Ihra et al. [336] applied hidden-crossing theory to the calculation of Q_i^+. They included anharmonic corrections (roughly equivalent to extending our Taylor expansion in (3.67)). As their log–log figure 1 illustrates, they concluded that experiment [16] and their theory [336] indicated a "less extended energy range in which the Wannier law is valid", that is, in contrasting the positron case with the electron case. This is in direct contradiction with our conclusion, based on the theory presented earlier. In a semiclassical Feynman path integral formalism Rost [520] obtained a similar extended energy range for the validity of the Wannier law but for positron impact ionization of hydrogen. In any case, as did Rost and Heller [523] before them, Ihra et al. [336] took $L_{\max}$ to be $L_{\min} = 0$.

Finally if we try to fit our results to a threshold law of the form

$$Q_i^+ = C(E - E_i)^{m_{12}} \tag{3.79}$$

with $m_{12} = 2.65$ from (3.69) we find $C \approx 0.02$ in units of 10^{-22} $m^2/(eV)^{m_{12}}$ and the resulting fit produces the broken curve in Figure 3.12. This shows that our results might give a threshold law for the excess energy $E' < 5$ eV with the exponent similar to those already predicted [357], [523]. However, this fit deviates significantly from our actual results and the experiment [16], above 5 eV excess energy.

In conclusion, we have applied a significantly revised, more sophisticated semiclassical quantal theory, in contrast with our original paper [186], to describe single-ionization positron-impact collisions on helium in the 0.5-10 eV excess of threshold energy. Our results show excellent agreement with Ashley et al. [16]. The curve-fit (3.79), a pure Wannier threshold law, is in agreement with both our theory and experiment [16] for excess of threshold energy up to 5 eV, but not in the domain 5 – 10 eV.

3.2.1 Conclusions

Semiclassical theory is quantitative in a wide range of quantum physics problems ($1/\hbar \gg 1$). S_0, S_1, and S_2 actions are necessary as is the Stokes phenomenon. Our

treatment is three-dimensional with $1/|\Delta\alpha|$, $1/|\Delta\theta_{12}| \gg 1$, which implies anomalous Wannier threshold phenomena in $(e^{\pm}/\gamma)$ behaviour. We have obtained the first absolute ab initio Wannier cross sections due to the 1986 semiclassical treatment and its extensions, not just to electron impact single ionization (cf. Sadeghpour et al. [527]) but also to photo-double-detachment and to doubly excited states (3.3).

Our semiclassical/quantal description of Wannier highly correlated states is robust, providing absolute parameters (cross sections above and resonances below threshold) that agree well with experiment.

3.3 Doubly Excited States and Their Lifetimes

The analytic continuation of Crothers' uniform semiclassical wave function to below threshold is extended to include resonant states for $L = 1$ and $L = 2$, where L is the total angular momentum azimuthal quantum number of the two excited electrons. Using the Bohr–Sommerfeld complex quantisation rule with two complex transition points the complex eigenvalues for doubly excited states of He^- are calculated. The resonance energy positions, which are parameterized in terms of an irrational azimuthal quantum number $\mathcal{L}$ for $L = 1$ $\left(\mathcal{L} = \left(\sqrt{17} - 1\right)/2\right)$ and an integer $\mathcal{L}$ for $L = 2$ $(\mathcal{L} = 3)$, are in good agreement with the experimental results of Buckman et al. [98].

The structure and dynamics of doubly excited states, where one approaches the limit of two electron break-up, are dominated by the correlated motion of the two excited electrons. The subject of electron correlations in general is of considerable interest and has resulted in an intensive theoretical and experimental investigation into the spectroscopy of He^- and the mechanisms responsible for the formation of negative-ion states.

In a high-resolution experiment Buckman et al. [98] measured the electron impact excitation for metastable (2^3S and 2^1S) helium atoms and revealed a Rydberg-like series of resonances converging on the He^+ threshold. They argued that some of these features, particularly the lowest member of each multiple, involved the excitation of two electrons in a highly correlated state. Following the suggestion of Fano [263], that the form of the two electron potential ridge might give rise to a series of quasi-standing waves with reflection at the classical turning points of the system, they concluded that for doubly excited states of helium the highly correlated two electron excitations manifest themselves as "Wannier ridge" resonances. The most notable effect of electron correlated motion is the $E^{1.127}$ Wannier threshold law [593], which has been confirmed semiclassically [486] and quantum mechanically [505]. The absolute magnitude of the scattering amplitude remained unknown until 1986 when Crothers [186] published the first absolute theoretical singlet triple-differential and integrated cross sections for the threshold electron impact single ionisation of helium using a uniform semiclassical approximation to evaluate the final-state wave function.

Both above and below the double-continuum threshold semiclassical theory holds but unlike the free $2 - e^-$ states, where classical dynamics applies in many

situations, as in Wannier [593], semiclassical analysis of the negative energy states remains indispensable [313]. For instance, the above threshold semiclassical treatment of [186] for the unstable motion of a pair of electrons along the potential ridge has been extended to the near-threshold capture excitation process

$$e^- + He \rightarrow (He^-)^*$$

([386] and [194]). This involved the analytic continuation of the semiclassical wave function of [186] to below the energy threshold in order to calculate the complex eigenvalues E_N of doubly excited states of He^- where

$$E_N = E_R^N - \frac{i}{2}\Gamma_N \tag{3.80}$$

These inaugural investigations were restricted to $L = 0$ states only (see Tables 3.1, 3.2, and 3.3). The resonance energy positions, given by E_R^N were found to be in good agreement with the experimental results of Buckman and Newman [99] for the $(ns)^2\,^2S$ intrashell series and Buckman [98] for the $\overline{s}\,^2S$ (that is, $(ns, (n+1)s)\,^2S$) intershell series for values of n up to $n = 9$ and $n = 7$, respectively. Hereafter, we adopt the notation of Buckman et al. [98], where n is the lower of the two principal quantum numbers n_1, n_2 of the two excited electrons.

We extend this work to include resonance states for $L \neq 0$, in particular for $L = 1$ and $L = 2$ since Buckman et al. [98] have published experimentally determined values of the resonance energies for these quantum numbers.

Table 3.1. Resonance position energies for $(He^-)^*$ for $L = 0$, $n_1 = n$, $n_2 = n_1 \Rightarrow N = n_1 + n_2 - 1 = 2n - 1$ and $L = 0'$, $n_1 = n$, $n_2 = n_1 + 1 \Rightarrow N = n_1 + n_2 - 1 = 2n$ since $N = n_1 + n_2 - |l_1 - l_2| - 1$ where L=$|l_1 - l_2|$. The experimental values are from (a) Buckman et al. [98] and (b) Buckman and Newman [99]. The number in brackets indicates the error in the second and third decimal places

Present Results Resonance Position Energies (eV)					b	a
n	N	$L = 0$	N	$L = 0'$	$L = 0$	$L = 0'$
2	3	19.492			19.367(5)	
3	5	22.330	6	22.963	22.451(10)	22.881(05)
4	7	23.368	8	23.641	23.435(10)	23.667(05)
5	9	23.833	10	23.973	23.850(10)	23.983(10)
6	11	24.077	12	24.158	24.080(10)	24.176(10)
7	13	24.220	14	24.271	24.217(10)	24.288(10)
8	15	24.311			24.307(15)	
9	17	24.372			24.387(15)	

As outlined in [186], a uniform semiclassical approximation is adopted to evaluate a final-state wave function for the electron impact single ionisation of helium near threshold.

Table 3.2. Resonance position energies for $(He^-)^*$ for $L = 0$. The experimental values (the number in brackets indicates the error in the second and third decimal places) are from Buckman et al. [98] and Buckman and Newman [99]; theory: z current results; (a) Rau [505]; (b) Lin and Watanabe [382]; (c) Komninos et al. [364]; (d) Rost and Briggs [521]; (e) Fon et al. [272]

			Theory					
n	N	Experiment	z	a	b	c	d	e
3	5	22.451(10)	22.330	–	–	22.432	22.774	22.439
4	7	23.435(10)	23.368	–	–	23.408	23.578	23.434
5	9	23.850(10)	23.833	23.857	23.865	23.843	23.879	–
6	11	24.080(10)	24.077	24.087	24.095	24.077	24.090	–
7	13	24.217(10)	24.220	24.223	24.230	24.213	24.219	–
8	15	24.307(15)	24.311	24.310	24.316	24.301	24.304	–
9	17	24.387(15)	24.372	24.369		24.361	24.362	–

Table 3.3. Relative intensity values for $L = 0$ resonances in$(He^-)^*$. The experimental values (the number in brackets indicates the error in the last and second to last decimal places) are from Buckman and Newman [99]

	Relative Intensity		
N	Experiment [99]	$1/2\Gamma_N * \lvert E_R^N - i/2\Gamma_N \rvert$	Ratio
5	0.53(1)	0.0050	0.0094
7	0.048(1)	0.00099	0.021
9	0.0105(2)	0.00029	0.028
11	0.0021(3)	0.00011	0.052
13	0.0011(1)	0.000049	0.045
15	0.00054(12)	0.000024	0.044
17	0.00030(12)	0.000013	0.043

In hyperspherical coordinates, the Schrödinger equation can be written as

$$\left[\frac{1}{\rho^5}\frac{\partial}{\partial\rho}\left(\rho^5\frac{\partial}{\partial\rho}\right) + \frac{1}{\rho^2\sin^2\alpha\cos^2\alpha}\frac{\partial}{\partial\alpha}\left(\sin^2\alpha\cos^2\alpha\frac{\partial}{\partial\alpha}\right)\right. \tag{3.81}$$

$$\left. -\frac{L^2(\hat{\mathbf{r}}_1)}{\rho^2\cos^2\alpha} - \frac{L^2(\hat{\mathbf{r}}_2)}{\rho^2\sin^2\alpha} + X^2 + \frac{2Z(\alpha,\theta_{12})}{\rho}\right]\Psi = 0 \tag{3.82}$$

where, as usual,

$$\rho^2 = r_1^2 + r_2^2 \qquad 0 \le \rho \le +\infty \tag{3.83}$$

$$\alpha = \tan^{-1}\left(\frac{r_2}{r_1}\right) \qquad 0 \le \alpha \le \pi/2 \tag{3.84}$$

$$\theta_{12} = \cos^{-1}(\hat{\mathbf{r}}_1.\hat{\mathbf{r}}_2) \qquad 0 \le \theta_{12} \le \pi \tag{3.85}$$

and where $\mathbf{r}_1$ and $\mathbf{r}_2$ are the position vectors of the two electrons with respect to an infinitely massive proton. The total wave number X is given by $X = (2E)^{1/2} =$

$\left(k_1^2 + k_2^2\right)^{1/2}$, where E is the excess of threshold energy and $\mathbf{k}_1$, $\mathbf{k}_2$ are the momenta of the final-state electrons 1 and 2, while the charge Z is given by

$$Z(\alpha, \theta_{12}) = \frac{1}{\cos\alpha} + \frac{1}{\sin\alpha} - \frac{1}{(1 - \cos\theta_{12}\sin 2\alpha)^{1/2}} \tag{3.86}$$

Relative to a space-fixed frame of reference with incident wave vector $\mathbf{k}_0$ as polar axis and the collision plane as the azimuthal plane, $\mathbf{r}_i$ has spherical polar angles (θ_i, ϕ_i), with $\hat{\mathbf{r}}_1 . \hat{\mathbf{r}}_2 = \cos\theta_{12}$, and $\mathbf{k}_i$ has spherical polar angles (Θ_i, Φ_i) with $\hat{\mathbf{k}}_1 \cdot \hat{\mathbf{k}}_2 = \cos\Theta_{12}$.

Considering the simplest case of motion when $L = 0$, equation (3.82) can be written

$$\left[\frac{1}{\rho^5}\frac{\partial}{\partial\rho}\left(\rho^5\frac{\partial}{\partial\rho}\right) + \frac{1}{\rho^2\sin^2\alpha\cos^2\alpha}\frac{\partial}{\partial\alpha}\left(\sin^2\alpha\cos^2\alpha\frac{\partial}{\partial\alpha}\right) + \frac{1}{\rho^2\sin^2\alpha\cos^2\alpha}\frac{1}{\sin\theta_{12}}\frac{\partial}{\partial\theta_{12}}\sin\theta_{12}\frac{\partial}{\partial\theta_{12}} + X^2 + \frac{2Z(\alpha,\theta_{12})}{\rho}\right]\Psi = 0 \tag{3.87}$$

On adopting a transformation of the dependent variable

$$\Psi = \frac{x|\sin(\alpha - \pi/4)|^{1/2}}{\rho^{5/2}\sin\alpha\cos\alpha(\sin\theta_{12})^{1/2}} \tag{3.88}$$

two pseudo-potentials appear that are large near the saddle point of the potential, making it appropriate to apply the Jeffreys, Wentzel, Kramers, Brillouin (JWKB) ansatz

$$x = P^{\frac{1}{2}}\exp\left(-\frac{\mathrm{i}S}{\hbar}\right) \tag{3.89}$$

where S is given by the Hamilton–Jacobi equation, (22) of [186], and P is given by the continuity equation, (23) of [186]. On setting $\Delta\alpha = \alpha - \pi/4$ and $\Delta\theta_{12} = \pi - \theta_{12}$ and assuming they are small, we may expand P and S about the most important region for the threshold escape of two electrons, i.e., at $\alpha = \pi/4$, $\theta_{12} = \pi$, corresponding to the Wannier line $\mathbf{r}_1 = -\mathbf{r}_2$. In [186] the charge Z is expanded correct to second order

$$Z(\alpha, \theta_{12}) \approx Z_0 + \frac{1}{2}Z_1(\Delta\alpha)^2 + \frac{1}{8}Z_2(\Delta\theta_{12})^2 \tag{3.90}$$

and the expansion of S is generalised to

$$S = s_o\ln|\Delta\alpha| + s_1\ln(\Delta\theta_{12}) + S_0(\rho) + \frac{1}{2}S_1(\rho)(\Delta\alpha)^2 + \frac{1}{8}S_2(\rho)(\Delta\theta_{12})^2 \tag{3.91}$$

Equations (3.90) and (3.91) are substituted into the Hamilton-Jacobi equation and powers of $\Delta\alpha$ and $\Delta\theta_{12}$ are equated. The resulting equations are solved perturbatively so that with $s_o = -\mathrm{i}/2$ and $s_1 = 1/2$, S_0 is given exactly by

$$S_0 = \int_0^\rho \mathrm{d}\tilde{\rho}\,\overline{w}(\tilde{\rho}) \tag{3.92}$$

where with $w^2 = 2E + 2Z_0/\rho$

$$\overline{w}^2 \simeq w^2 - w\frac{\mathrm{d}}{\mathrm{d}\rho}(\ln u_2) + iw\frac{\mathrm{d}}{\mathrm{d}\rho}(\ln u_1) \tag{3.93}$$

($\sim$ indicates dummy variable of integration). The subsequent Ricatti equation

$$w\frac{\mathrm{d}S_i}{\mathrm{d}\rho} + \frac{S_i^2}{\rho^2} = \frac{Z_i}{\rho} \qquad (i = 1, 2) \tag{3.94}$$

is solved in direct analogy with Peterkop [486] such that

$$S_i = \rho^2 w\frac{1}{u_i}\frac{\mathrm{d}u_i}{\mathrm{d}\rho} \qquad (i = 1, 2) \tag{3.95}$$

The Wannier–Peterkop functions u_1 and u_2 are, as usual, given by

$$u_1 = \rho^{m_{12}}\,{}_2F_1\left(m_{12}, m_{12}+1; 2m_{12}+3/2; \frac{-E\rho}{Z_0}\right) \tag{3.96a}$$

$$u_2 = \rho^{m_{22}}\,{}_2F_1\left(m_{22}, m_{22}+1; 2m_{22}+3/2; \frac{-E\rho}{Z_0}\right) \tag{3.96b}$$

noting that $m_{22} = m_{21}*$. These Wannier functions are related to the radial and angular correlated motion of the two electrons. This can be seen by considering the set of orbits described by S, which yields $u_1(\rho) = \Delta\alpha$ and $u_2(\rho) = \Delta\theta_{12}$.

The final-state JWKB ingoing wave function takes the form

$$\Psi_f{}^{-*} = \frac{C^{1/2}\exp\left\{-\frac{1}{2}\mathrm{i}\ln\Delta\theta_{12} - \mathrm{i}\left[S_0 + \frac{1}{2}S_1(\Delta\alpha)^2 + \frac{1}{8}S_2(\Delta\theta_{12})^2\right]\right\}}{\overline{w}^{1/2}\rho^{5/2}\sin\alpha\cos\alpha} \tag{3.97}$$

In [186], a factor

$$\delta\left(\hat{\mathbf{k}}_1 - \hat{\mathbf{r}}_1\right)\delta\left(\hat{\mathbf{k}}_2 - \hat{\mathbf{r}}_2\right) \tag{3.98}$$

is included in $\Psi_f{}^{-*}$ to represent the fact that the two electrons have specific asymptotic directions and to project out the required outgoing scattering amplitude. Since each delta function may be expanded as

$$\frac{1}{4\pi}\sum_{l_i=0}^{\infty}\sum_{m_i=-l_i}^{+l_i} Y_{l_i}^{m_i}(\hat{\mathbf{r}}_i)\,Y_{l_i}^{m_i}\left(\hat{\mathbf{k}}_i\right) \qquad (i = 1, 2) \tag{3.99}$$

then the inclusion of these factors means, in effect, including arbitrary angular momentum states for each of the two electrons. In [186] it is assumed that for low L values, the approximation, given by the product of expressions (3.97) and (3.98), is valid.

We now consider the analytic continuation of this above threshold theory to below threshold for $L = 1$ and $L = 2$ states. We consider the electron capture by helium, for energies below the first ionisation potential of helium but above the first

ionisation potential of He^-. The $(He^-)^{**}$ is perceived as consisting of a positively charged core ($Z = 1$) with two excited electrons in a high Rydberg state where the core electron has position $\mathbf{r}_3$ while the doubly excited electrons have positions $\mathbf{r}_1$ and $\mathbf{r}_2$. In addition we avoid for $L \neq 0$, the approximation given by expressions (3.97) and (3.98).

The Schrödinger equation in hyperspherical coordinates is given by (3.82), where [440]

$$L^2(\hat{\mathbf{r}}_i) = -\left[\frac{1}{\sin\theta_i}\frac{\partial}{\partial\theta_i}\left(\sin\theta_i\frac{\partial}{\partial\theta_i}\right) + \frac{1}{\sin^2\theta_i}\frac{\partial^2}{\partial\phi_i^2}\right] \tag{3.100}$$

For states with $L \neq 0$ and $M = 0$ we proceed with the following ansatz [541]

$$\Psi = f(\rho, \alpha, \theta_{12})\, P_L(\cos\theta_1) \tag{3.101}$$

where P_L is the Legendre polynomial. Strictly this should be symmetrised so that

$$\Psi = f(\rho, \alpha, \theta_{12})\, P_L(\cos\theta_1) \pm \tilde{f}(\rho, \alpha, \theta_{12})\, P_L(\cos\theta_2) \tag{3.102}$$

where the interchanged function $\tilde{f}(\mathbf{r}_1, \mathbf{r}_2) = f(\mathbf{r}_2, \mathbf{r}_1)$ and where particle exchange implies $\Delta\theta_{12} \to \Delta\theta_{12}$ and $\Delta\alpha \to -\Delta\alpha$. Applying the Hamiltonian of (3.82) and using (3.100) the following equation for f is obtained

$$\left[\frac{1}{\rho^5}\frac{\partial}{\partial\rho}\rho^5\frac{\partial}{\partial\rho} + \frac{1}{\rho^2\sin^2 2\alpha}\frac{\partial}{\partial\alpha}\sin^2 2\alpha\frac{\partial}{\partial\alpha} + \frac{4}{\rho^2\sin\theta_{12}}\frac{\partial}{\partial\theta_{12}}\sin\theta_{12}\frac{\partial}{\partial\theta_{12}} + 2E + \frac{2Z}{\rho} - \frac{2L(L+1)}{\rho^2}\right] f = 0 \tag{3.103}$$

We have neglected the cross term

$$\frac{4\sin\theta_1(-\sin\theta_1\cos\theta_2 + \cos\theta_1\sin\theta_2\cos(\phi_1 - \phi_2))}{\rho^2\sin\theta_{12}}\frac{P_L'(\cos\theta_1)}{P_L(\cos\theta_1)}\frac{\partial f}{\partial\theta_{12}} \tag{3.104}$$

(where $'$ indicates $\mathrm{d}/\mathrm{d}(\cos\theta_1)$) which involves Euler angles and can be shown, in common with the equivalent term in (3) of Roth [525], trivially to vanish on the Wannier line ($\alpha = \pi/4, \theta_{12} = \pi$). The apparent singularity due to $\sin\theta_{12}$ in the denominator requires the use of L'Hospital's rule with the numerator expressed in terms of the following identity

$$\cos\theta_{12} = \cos\theta_1\cos\theta_2 + \sin\theta_1\sin\theta_2\cos(\phi_1 - \phi_2) \tag{3.105}$$

It follows that $f = \tilde{f}$.

We now proceed as in [186], except that the w-term becomes L-dependent

$$w^2 = 2E_N + \frac{2Z_0}{\rho} - \frac{2L(L+1)}{\rho^2} \tag{3.106}$$

noting that the factor of 2 in the last term comes from $\sec^2\alpha$ evaluated at $\alpha = \pi/4$ which is the fundamental cause of the irrational azimuthal quantum number

($L \neq 0, 2$). Thus the Ricatti equation given in (3.94), which is reduced to a linear second-order equation by removing the nonlinear S_i^2 term with the substitution given by (3.95), becomes

$$\rho^2 w^2 \frac{\mathrm{d}^2 u_i}{\mathrm{d}\rho^2} + \left(2\rho w^2 - Z_0 + \frac{2L\,(L+1)}{\rho}\right) \frac{\mathrm{d}u_i}{\mathrm{d}\rho} = \frac{Z_i u_i}{\rho} \qquad (i = 1, 2) \tag{3.107}$$

Following [186] we set

$$u_i = \rho^{m_i} F_i\,(\rho) \qquad (i = 1, 2) \tag{3.108}$$

so that with $m_i = -1/4 \pm 1/4\,(1 + 8Z_i/Z_0)^{1/2}$ the equation for F becomes

$$\begin{aligned} &\left[2E_N\rho^2 + 2Z_0\rho - 2L\,(L+1)\right] F_i'' \\ &+ \left[4\,(m_i+1)\,E_N\rho + (4m_i+3)\,Z_0 - \tfrac{2(2m_i+1)L(L+1)}{\rho}\right] F_i' \\ &+ \left[2m_i\,(m_i+1)\,E_N - \tfrac{2m_i^2 L(L+1)}{\rho^2}\right] F_i = 0 \end{aligned} \tag{3.109}$$

This is clearly a linear differential equation of the Heun type [509], which has four regular singular points at $\rho = 0, \infty$, and $\rho_\pm$ which are the solutions of $w^2 = 0$ where

$$\rho_\pm = \frac{-Z_0 \pm \sqrt{Z_0^2 + 4E_N L\,(L+1)}}{2E_N} \tag{3.110}$$

However, detailed knowledge of the Heun equations is limited. Since we may assume that ρ is of the order of $1/|E_N|$, then all the nonazimuthal terms in the coefficients of equation (3.109) are of the order of $1/|E_N|$. Therefore neglecting the L terms, by setting $L = 0$, is a good approximation. For $L = 0$ with $F = F\,(-E\rho/Z0)$ a three-regular-singular-point differential equation obtains and takes the form of the Gauss-hypergeometric differential equation resulting in the Wannier–Peterkop functions given in equations (3.96a) and (3.96b) [593]. The solution of (3.107) then has the general form

$$u_i = A\rho^{m_{12}} F\,(m_{12}) + B\rho^{m_{22}} F\,(m_{22}) \tag{3.111}$$

where F is given by (3.96a) and (3.96b). Using equations (3.97), (3.93), and (3.99) the asymptotic form of the final-state wave function that corresponds to the electron capture by helium, for energies below the first ionisation potential of He but above the first ionisation potential of He^-, is given by

$$\begin{aligned} \Psi_f^{-*} = {} & \frac{C_N^{1/2} Y_{LM}\,(\hat{\mathbf{r}}_1, \hat{\mathbf{r}}_2)\, 2^{\frac{3}{2}} \exp\left(-2r_3 - \frac{\mathrm{i}}{2} \ln \Delta\theta_{12}\right) / \sqrt{\pi}}{\rho^{5/2} \sin\alpha \cos\alpha} \\ & \times \frac{\sin\left[\int_{\rho_+}^{\rho} \mathrm{d}\tilde{\rho} \left(w^2 - w\,\{\ln u_2 - \mathrm{i} \ln u_1\}'\right)^{\frac{1}{2}}\right.}{\left. + \frac{\rho^2}{2}\omega\,(\ln u_1)'\,(\Delta\alpha)^2 + \frac{\rho^2}{8}\omega\,(\ln u_2)'\,(\Delta\theta_{12})^2 + \frac{\pi}{4}\right]} \\ & \frac{}{\left[\omega^2 - \omega\,\{\ln u_2 - \mathrm{i} \ln u_1\}'\right]^{\frac{1}{4}}} \end{aligned} \tag{3.112}$$

where $'$ indicates $\mathrm{d}/\mathrm{d}\tilde{\rho}$ or $\mathrm{d}/\mathrm{d}\rho$ and where in the JWKB treatment the Gans–Jeffreys [289], [342] connection formula (2.1) has been applied with $\rho = \rho_+$ as the classical turning point. This is a product of the analytic continuation of the final-state wave function of [186] to negative energy, including both ingoing and outgoing waves, representing the two excited electrons, and the wave function of the core electron given by the ground-state He^+ wave function.

The $-1/4\rho^2$ Langer modification term [378] has also been considered where it has been found to be cancelled by two terms, namely $-15/4\rho^2$ and $4/\rho^2$, resulting from the substitution of (3.88) into (3.87). In the region beyond the two turning points the solution is required to be the decreasing JWKB solution, in order to satisfy the boundary conditions at 0 and ∞. The two JWKB solutions must join smoothly in the region between the two transition points $\rho_\pm$, which are both complex. This requires that

$$\int_{\rho+}^{\rho-} \mathrm{d}\rho \sqrt{w^2 - w\left(\frac{\mathrm{d}}{\mathrm{d}\rho}\ln u_2 - i\frac{\mathrm{d}}{\mathrm{d}\rho}\ln u_1\right)} = N\pi + \frac{\pi}{2} \tag{3.113}$$

where w is given by (3.106), which is clearly of the form of a complex Bohr–Sommerfeld quantisation rule. Therefore the wave function has N nodes between the two transition points where N is a hyperspherical radial quantum number of the two excited electrons. Equation (3.112) must be amended by symmetrising the spherical harmonic, for $^3P^0$ and for $^1D^e$. On changing the dummy variable according to

$$\rho = \frac{-(Z_0 + Zx)}{2E_N} \tag{3.114}$$

where $Z = \sqrt{Z_0^2 - 2c^2L(L+1)}$ and $c = \sqrt{-2E_N}$ (3.113) becomes

$$Z\int_{-1}^{1} \mathrm{d}x \sqrt{\varpi^2 - \frac{c}{Z}\varpi\left(\frac{\mathrm{d}}{\mathrm{d}x}\ln\frac{u_2}{u_1^i}\right)} = c\left(N + \frac{1}{2}\right)\pi \tag{3.115}$$

where

$$\varpi^2 = -1 + \frac{2Z_0}{Z_0 + Zx} - \frac{2c^2L(L+1)}{(Z_0 + Zx)^2} \tag{3.116}$$

Equation (3.115) has been solved, numerically, for c by the complex Newton–Raphson method. Note that neither $|E_N|$ nor $|E_N|^2$ is analytic (see Chapter 1)

3.3.1 Results

The results obtained from this calculation for the $L = 1$ and $L = 2$ resonant energy positions are given in Tables 3.4 and 3.5, respectively. They have been compared with the experimental results of Buckman et al. [98], who measured the yield of metastable atoms resulting from electron impact excitation of helium in the energy region just below threshold. Most relevant to this work are the ^2P and ^2D resonances, which were traced from $n = 3$ to $n = 5$ and $n = 3$ to $n = 7$, respectively. These states

have been classified as intrashell states [10], [449], [96], i.e., $n_1 = n_2$ giving $n = n_1$. This equal sharing of energy, where the electrons are approximately equidistant from the nucleus, minimising their mutual screening, produces the most stable configuration. Any partitioning of the total energy is possible, resulting in strong mixing of such configurations.

As such, we seek the central (narrowest) resonance peak, since it gives the highest peak corresponding to the complex eigenenergy E_N closest to the real axis. It has been found that the calculated eigenvalues for both $L = 1$ and $L = 2$ resonant states correspond to those of experiment for

$$N = 2n - \mathcal{L} - 1 \tag{3.117}$$

where for $L = 1, \mathcal{L} = \left(-1 + \sqrt{17}\right)/2$ and for $L = 2$, $\mathcal{L} = 3$ and where $2n = n_1 + n_2$ in line with the intrashell classification. Thus for $L = 0$ and $L = 2$ we have an integer hyperspherical azimuthal quantum number, but for $L = 1$ the mapping of $2L(L + 1)$ to $\mathcal{L}(\mathcal{L} + 1)$ in the Bohr–Sommerfeld quantisation rule results in an irrational hyperspherical azimuthal or total angular momentum quantum number.

Agreement with experiment is increasingly good for higher values of N. In particular, for $L = 1$ and $n = 4$ or 5 and for $L = 2$ and $n = 6$ or 7, experiment and theory agree within the experimental error. This is to be expected due to the semiclassical nature of the calculation and our perturbative solution of the Heun differential equation.

Table 3.4. Resonance position energies for $(He^-)^*$ $(1s\,^2S(n_1sn_2p\,^3P^o))\ ^2P$, $L = 1$, $M = 0$, $n_1 = n$, $n_2 = n_1 \Rightarrow N = 2n - \mathcal{L} - 1$ where $\mathcal{L}$ is the irrational azimuthal quantum number and has the value $(\sqrt{17} - 1)/2$. The experimental values are from Buckman et al. [98]. The number in brackets indicates the error in the second and third decimal places

	Resonance Energies (eV)	
n	Present Results	Experiment
3	22.639	22.600(10)
4	23.518	23.518(10)
5	23.915	23.907(10)

Table 3.5. Resonance position energies for doubly excited $(He^-)^*$ $\left(1s^2S\left(n_1sn_2d\ ^1D^e\right)\right)\ ^2D$, $L = 2$, $M = 0$, $n_1 = n$, $n_2 = n_1 \rightarrow N = 2n - 4$. The experimental values are from Buckman et al. [98]. The number in brackets indicates the error in the second and third decimal places

	Resonance Energies (eV)	
n	Present Results	Experiment
3	22.715	22.660(10)
4	23.544	23.579(10)
5	23.927	23.952(10)
6	24.133	24.144(15)
7	24.256	24.261(15)

Table 3.6. Average widths and associated energy positions for $\left(1s^2S\left(n_1sn_2d\ {}^1D^e\right)\right)\ {}^2D, L = 2, M = 0, n_1 = n,\ n_2 = n_1 \Rightarrow N = 2n - 4$. Units are eV

n	Γ^a (au)	E_{Γ^a} (eV)	Experiment (eV)	Half-life time τ_a (attosec)
4	0.3401	23.578	23.579	35.56
5	0.2313	23.952	23.952	52.29
6	0.1252	24.144	24.144	96.60
7	0.0680	24.261	24.261	177.84

Heretofore we have neglected the issue of the width and intensity of these resonances allowing Γ_N to tend to zero in order to determine the E_R^N closest to the real axis. In doing so a convergence limit was reached, yielding the energy positions tabulated in Tables 3.4 and 3.5. The problem with these closely spaced P and D resonances is that they overlap so that the width for a given E_R^N is smeared by the neighbouring resonance (Andrick [10]). As such we have taken a sum over the unobserved final states (Feagin and Macek [264]) in order to obtain an average half-width half-maximum Γ^a. Our intensity is taken as being proportional to $1/2\,\Gamma_N|E_N|$ (Loughan and Crothers [386]), therefore

$$\Gamma^a = \frac{\frac{1}{n}\sum_{i=1}^{n}\Gamma_N^i|E_N^i|}{\frac{1}{n}\sum_{i=1}^{n}|E_N^i|} \tag{3.118}$$

In Table 3.6 we present the Γ^a-values for the ${}^2D$ case. The lower limit of the sum is determined by the convergence limit for a given n while the upper limit is determined by the position of the neighbouring observed resonance. Admittedly the choice of the upper limit is somewhat arbitrary in that the extent of the overlapping is not definite. Nevertheless with an appropriate choice of upper limit the energy positions E_{Γ^a} corresponding to width Γ^a show excellent agreement with experiment. Convergence difficulties have restricted the application of (3.118) to higher n-values of the ${}^2D$ case only. Moreover the half-life times τ_a presented in Table 3.6 suggest attotechnology (where atto is nano-squared).

3.3.2 Doubly Excited States of He

Now we apply the below-threshold theory for $L = 0$ developed earlier to the doubly excited states of atomic helium. In direct analogy with the He^- case we consider the electron capture by the "parent" $He^+(1s)$ to form the DES of atomic He with the grandparent core He^{++}. The energy of the incident electron lies below the first ionisation potential of He but above the first ionisation potential of He^+. For He^{**} the Coulomb potential experienced by the excited electrons is such that it can support an infinite Rydberg series with electron correlations dominating the motion close to the resonance region. We consider the two excited electrons in terms of our semiclassical Wannier wave function. The continuum between the first and second ionization thresholds of the helium atom has been investigated theoretically in a number of

diverse studies [285], [313], [327], [328], [445], [479], [521]. This work was initiated by Madden and Codling [396] who, in a photo-absorption experiment, were the first to observe doubly excited autoionising states of atomic helium. Subsequent photo absorption experiments (Domke et al. [228], Zubek et al. [613]) have yielded further information about states of ^1P symmetry with electron impact experiments (Brotton et al. [92], Hicks et al. [325]), revealing the full spectrum of the S, P, D, F, and G states. An infinite number of Rydberg series of auto-ionising states exist within the continuum. However, these studies have predominantly concentrated on the lower Rydberg series, which converge to the He^+ n=2-6 thresholds with the diabatic molecular approach of Rost and Briggs [522] producing intrashell S resonance positions for $n \leq 15$. Here we present intrashell and intershell S resonance energy positions for the higher quantum numbers $5 \leq n \leq 15$, with the semiclassical limitations of our theory producing poor results for lower n-values. Clearly the core charge in this case is $Z = 2$, which reflects the increasing Coulomb attraction of the He^{++} core over the $Z = 1$ He^+ core. This gives the three-body charge as

$$\zeta(\alpha, \theta_{12}) = \frac{2}{\cos\alpha} + \frac{2}{\sin\alpha} - \frac{1}{(1 - \cos\theta_{12}\sin 2\alpha)^{\frac{1}{2}}} \tag{3.119}$$

which is expanded according to (3.67) where

$$Z_0 = \frac{7}{\sqrt{2}}, \quad Z_1 = \frac{23}{\sqrt{2}}, \quad Z_2 = -\frac{1}{\sqrt{2}} \tag{3.120}$$

Retaining Z in the semiclassical analysis gives the Wannier indices

$$m_{i1} = -\frac{1}{4} - \frac{1}{2}\mu_i \qquad m_{i2} = -\frac{1}{4} + \frac{1}{2}\mu_i \tag{3.121}$$

where

$$\mu_1 = \frac{1}{2}\sqrt{\frac{100Z - 9}{4Z - 1}} \qquad \mu_2 = \frac{1}{2}\sqrt{\frac{4Z - 9}{4Z - 1}} \tag{3.122}$$

The method used to determine the complex eigenenergies E_N is completely analogous to the procedure followed in Section 3.2 with the Wannier indices and charges calculated for $Z = 2$.

The results from the present calculation, given in Tables 3.7 and 3.8, show poor agreement with the available experimental and theoretical results for values of n up to $n = 7$, for both the intrashell ($n_1 = n_2$) and intershell ($n_1 \neq n_2$) states. Other theories, such as the complex-coordinate rotation theory [327], [328], close-coupling method [479], and hyperspherical approach [285], have produced accurate energy positions for lower n but require greater numerical effort for higher values of principal quantum number. Rost and Briggs [521] have produced intrashell energy positions for $n \leq 15$ using an adiabatic molecular potential. For $n \leq 7$ these results are in excellent agreement with the highly accurate results of Ho [327], [328]. We have compared our resonance energy positions for He^{**} $^1S^e$ intrashell states for $7 \leq n \leq 15$

with those of Rost and Briggs [521]. We find the results for $7 \leq n \leq 10$ to be in agreement within 10% and for $n \geq 11$ within 4%. Thus, as might be expected for a semiclassical method, agreement with other theory is seen to improve for increasing n. Rost and Briggs have employed a simple hydrogenic wave function, of the form $e^{-\alpha(r_1+r_2)}$, which is clearly symmetric in r_1 and r_2. Thus their approach does not allow for the determination of resonance positions where the energy of the two electrons is not evenly distributed, i.e., only energy positions for intrashell states could be calculated. In summary, we have analytically continued the above-threshold Wannier quantal ionisation theory of [186] to below threshold for Wannier quantal doubly excited states. We have presented results for ^2S and $\overline{s}\ ^2S$ doubly excited states of He^-, where for the principal series, $n_1 = n_2 = n$ and $N = 2n - 1$, $L = 0$, while for the subsidiary series, $n_2 = n_1 + 1 = n + 1$ and $N = 2n$, L = 0′, in the notation of Buckman et al. [98]. We have extended this theory to $L = 1$ and $L = 2$ $^2P^o$ and ^2D states where, with the inclusion of angular momentum terms evaluated on the Wannier ridge, an irrational principal quantum number was obtained for $L = 1$, namely $N = 2n - (17^{1/2} - 1/2) - 1$ while for $L = 2$ $N = 2n - 4$. The calculated resonance positions were found to be in good agreement with experiment, the agreement increasing for higher n. This is to be expected due to the semiclassical nature of the calculation, and certainly much can be done to improve our description of the initial state. The width and intensity of these states were also considered using the imaginary parts of the calculated complex eigenenergies, which give directly the lifetime of these Wannier doubly excited Rydberg states. This is unique in that other theories address the problem of resonance position only. We also applied the below-threshold analysis for $L = 0$ to the DES of He, where a simple change in the magnitude of the core charge produced reasonable results for the high values of n. As far as we know, the intershell energies are the first to be presented for these higher quantum numbers; other theories are restricted by computational demands at the higher end of the spectrum.

Table 3.7. Resonance position energies (RPEs) for He $L = 0, n_1 = n, n_2 = n_1 \Rightarrow N = 2n - 1$; other theory (a); Rost & Briggs [521], [522]

			RPEs (au)	
ns^2	$(K,T)^A$	N	Present results	a
$7s^2$	$(6,0)^+$	13	0.073667	0.066716
$8s^2$	$(7,0)^+$	15	0.055528	0.051207
$9s^2$	$(8,0)^+$	17	0.043310	0.040538
$10s^2$	$(9,0)^+$	19	0.034702	0.032887
$11s^2$	$(10,0)^+$	21	0.028415	0.027365
$12s^2$	$(11,0)^+$	23	0.023688	0.023205
$13s^2$	$(12,0)^+$	25	0.020044	0.01964
$14s^2$	$(13,0)^+$	27	0.017179	0.01695
$15s^2$	$(14,0)^+$	29	0.014885	0.01478

Table 3.8. Resonance position energies (RPEs) for He $L = 0, n_1 = n$, $n_2 = n_1 + 1 \Rightarrow N = 2n$; other theory (a); Fukuda et al. [285] (b) Ho [327]

			RPEs (au)	
$n_1 s n_2 s$	$(K,T)^A$	N	Present results	Other theories
$5s6s$	$(4,0)^+$	10	0.122978	0.10964[b]
$6s7s$	$(5,0)^+$	12	0.086212	0.07865[a]
$7s8s$	$(6,0)^+$	14	0.063650	0.0599[a]
$8s9s$	$(7,0)^+$	16	0.048856	
$9s10s$	$(8,0)^+$	18	0.038652	
$10s11s$	$(9,0)^+$	20	0.031325	
$11s12s$	$(10,0)^+$	22	0.025891	
$12s13s$	$(11,0)^+$	24	0.021753	
$13s14s$	$(12,0)^+$	26	0.018529	
$14s15s$	$(13,0)^+$	28	0.015970	
$15s16s$	$(14,0)^+$	30	0.013906	

There is no doubt that this below-threshold theory is an exciting development in the Wannier description of DES and reinforces the above-threshold theory as a fully fledged quantal treatment of ionisation. Most significant for future work is the advances made for $L \neq 0$ states. Throughout the years the difficulties encountered manifested themselves as triplet triple differential cross sections for threshold ionisation, which were much too large, but recent progress has produced improved results [186], [108]. We are now confident that the additional angular momentum term in ω, namely $2L(L+1)/\rho^2$, is the required amendment to our above-threshold theory where preliminary investigations are more than promising [387]. It is worth noting that the cross term (see (3.104)) should not be completely dismissed due to its disappearance on the Wannier ridge. Closer inspection, with symmeterisation for P and D states, shows that it vanishes specifically for ${}^3P$ and ${}^1D$ states. There is, of course, room for many further improvements such as the inclusion of exchange to improve results for the lower quantum numbers.

3.4 Divergent Exponents

We consider [146] a nonstandard application of Wannier's theory [593]. A physical example is the single ionization of a hydrogenic beryllium ion with a fully stripped beryllium ion, where the ratio of the charge of the third particle to the charges of the escaping particles is $1/4$; we investigate the single ionization by an electron of an atom comprising an electron and a nucleus of charge $1/4$ [337], [225], [117]. An infinite exponent is obtained, suggesting that this process is not tractable within the Wannier model.

A modified version of Crothers' uniform semiclassical wave function [186] for the outgoing particles has been adopted, since the Wannier exponents m_{12} and m_{21} are infinite. As $Z_0 = 0$ we are able to use Bessel functions to describe u_1 and u_2

and to derive a new turning point ρ_+. As u_1 is well-behaved at infinity, there exists only the singularity in u_2 at infinity; thus we employ a one- (rather than two-) dimensional change of dependent variable, ensuring a uniform solution is obtained that avoids semiclassical breakdown on the Wannier ridge. The regularised final-state asymptotic wave function is employed, along with a continuum-distorted-wave approximation for the initial-state wave function to obtain total cross sections on an absolute scale.

The applicability of Wannier's theory is somewhat limited in the range over which a value of the exponent can be calculated. In this section we examine a non-standard application of this theory, namely the single ionization by an electron of an atom comprising an electron and a nucleus of charge $1/4$. Clearly the ratio of the charge of the third particle to the charges of the escaping particles is $1/4$. As an infinite exponent is obtained, this process appears not to be tractable within the Wannier model, although, as will become evident, the relation between quantum and classical mechanics is simply a little more subtle than previously encountered.

Some theoretical analysis of a similar process, in which $Z = 1/4$ also, i.e., a collision of a hydrogenic beryllium ion with a fully stripped beryllium ion

$$Be^{4+} + Be^{3+} \rightarrow Be^{4+} + e^- + Be^{4+} \tag{3.123}$$

has been carried out by Ihra et al. [337], [117] and Dimitrijevic et al. [225]. Ihra et al. [337], found that the threshold behaviour changed from a power law to an exponential law

$$\sigma \propto E^{-1/6} \exp\left(-\frac{\kappa}{E^{1/6}}\right) \tag{3.124}$$

where E is the excess of threshold energy in atomic units. In contrast to the original Wannier model, the classical and quantum results obtained were different, although their work did show that Wannier's picture of propagation on the ridge remained valid. The same authors in 1998 [117] when using semiclassical methods, found that the power law deduced by Wannier was replaced by an exponential law of the form

$$\sigma \propto \exp\left(-\frac{\lambda}{\sqrt{E}}\right) \tag{3.125}$$

showing exponential suppression of the ionization probability at threshold. Dimitrijevic et al. [225] used a classical trajectory method to derive an exponential law of the form 3.125, although their value for the proportionality constant was somewhat larger than that in [117]. All of these results were valid only over a limited energy range and none produced cross sections on an absolute scale.

In Section 3.4.1 a brief summary of the Wannier theory is outlined, followed by a description of the semiclassical JWKB approximation in Section 3.4.2, which forms the basis of Section 3.4. In Section 3.4.3 we extend the theory to the case where the exponent diverges, and the results obtained are outlined in Section 3.4.4.

3.4.1 Wannier's Theory

Wannier's original paper [593] treated the subject of the double escape of an electron pair at asymptotically large distances from an ionic core, in the framework of a purely

classical analysis of the three-body Hamiltonian. The reactants were found to be close together and interacting strongly within the "reaction zone", in which the finer details of the reaction occur.

For simplicity, Wannier restricted his discussion to the case of zero total angular momentum (L) and spin (S) of the escaping electrons in the three-body continuum final state. Wannier also assumed that the residual ion was infinitely heavy in comparison with the interacting electrons, effectively allowing him to describe the ion as being at rest and situated at the origin of a laboratory fixed frame of reference, O_{xyz}. Hyperspherical coordinates, which effectively describe the correlated electron motion, were used

$$\rho = \sqrt{r_1^2 + r_2^2}, \quad \alpha = \tan^{-1}\left(\frac{r_2}{r_1}\right), \quad \theta_{12} = \cos^{-1}(\hat{\mathbf{r}}_1 \cdot \hat{\mathbf{r}}_2) \tag{3.126}$$

where $\mathbf{r}_1$ and $\mathbf{r}_2$ are the electron position vectors relative to the stationary nucleus. The potential of the two escaping electrons is $-\zeta/\rho$, where the effective charge ζ is given by

$$\zeta(\alpha, \theta_{12}) = \frac{Z}{\cos\alpha} + \frac{Z}{\sin\alpha} - \frac{1}{\sqrt{1 - \cos\theta_{12}\sin 2\alpha}} \tag{3.127}$$

and double escape ensues for those orbits that approach the "point"

$$\alpha = \frac{\pi}{4}, \qquad \theta_{12} = \pi \tag{3.128}$$

Asymptotically this "point" is referred to as the "Wannier ridge". Wannier's threshold law [$Z = 1$] , which describes the functional behaviour of the cross section for the single ionization by electron impact of a neutral atom, was described by

$$\sigma \propto E^{m_{12}} \qquad m_{12} \approx 1.127 \tag{3.129}$$

3.4.2 The Semiclassical JWKB Approximation

The semiclassical approach lies at the intersection of quantum and classical mechanics; the method was first adopted by Peterkop [486] and then later extended by Crothers [186]. Unlike Peterkop, Crothers identified a uniform semiclassical wave function that for the first time allowed absolute total, partial, and differential cross sections to be calculated, through the avoidance of a singular wave function, classical differential cross sections, and matching procedures.

In solving the Schrödinger equation, Crothers introduced a change of dependent variable

$$\Psi_f^{-*} = \frac{x \mid \sin(\alpha - \pi/4) \mid^{1/2}}{\rho^{5/2} \sin\alpha \cos\alpha (\sin\theta_{12})^{1/2}} \tag{3.130}$$

to avoid semiclassical breakdown on the Wannier ridge. A JWKB ansatz was employed

$$x = P^{1/2} \exp\left(\frac{\mathrm{i}S}{\hbar}\right) \tag{3.131}$$

where the action S and the density P are solved by series expansion about the Wannier point. Crothers [186] then

- normalised the wave function,
- included the angular symmetry of the final state,
- used Jeffreys' 1-dimensional ρ-connection formula [342], and
- applied the Kohn 6-dimensional variational principle [363].

The resultant total singlet cross section was then calculated, including the dominant angular momentum states, and confirmed the absolute Wannier law according to

$$\sigma = 2.37E^{m_{12}}a_0^2 \tag{3.132}$$

where the Wannier exponents are defined as

$$m_{12} = \frac{1}{4}\left[\sqrt{\frac{100Z-9}{4Z-1}} - 1\right] \tag{3.133}$$

$$m_{21} = -\frac{1}{4}\left[i\sqrt{\frac{9-4Z}{4Z-1}} + 1\right] \tag{3.134}$$

Expressions (3.133) and (3.134) take the approximate values 1.127 and $-0.25 - i0.323$, for $Z = 1$. Evidently, process (3.123) is not tractable, in this model, when the exponent becomes infinite as

$$\begin{aligned} E^{\infty} &= \infty \quad \text{for} \quad \mathrm{E} > 1 \\ E^{\infty} &= 1 \quad \text{for} \quad \mathrm{E} = 1 \\ E^{\infty} &= 0 \quad \text{for} \quad \mathrm{E} < 1 \end{aligned} \tag{3.135}$$

3.4.3 Semiclassical Theory when the Exponent Diverges

The wave function must remain valid for the physical limits most pertinent to threshold ionization, ensuring that a uniform solution is obtained that avoids semiclassical breakdown on the Wannier ridge. As the Wannier exponents (3.133) and (3.134) are infinite at $Z = 1/4$, it becomes clear that a change of dependent variable must be applied, namely

$$\Psi_f^{-*} = \frac{x}{\rho^{5/2}\sin\alpha\cos\alpha(\sin\theta_{12})^{1/2}} \tag{3.136}$$

where x differs from that in (3.130) and now satisfies the equation

$$\left[\frac{\partial^2}{\partial\rho^2} + \frac{1}{\rho^2\sin|\Delta\alpha|}\frac{\partial}{\partial\alpha}\left(\sin|\Delta\alpha|\frac{\partial}{\partial\alpha}\right) + \frac{1}{\rho^2\sin^2\alpha\cos^2\alpha}\frac{\partial^2}{\partial\theta_{12}^2} + X^2 + \frac{2\zeta}{\rho} + \frac{\frac{1}{4} + \csc^2(\Delta\theta_{12})/4}{\rho^2\sin^2\alpha\cos^2\alpha}\right]x = 0 \tag{3.137}$$

and where $\Delta\theta_{12} = \pi - \theta_{12}$ and $\Delta\alpha = \alpha - \pi/4$. A regular JWKB solution of the final state is obtained because, after and only after, the change of dependent variable ($\Psi_f^{-*} \to x$), is the effective potential large on and near the Wannier ridge ($\Delta\theta_{12} = 0$).

In contrast with (3.130), in (3.136) the factor $|\sin\Delta\alpha|^{1/2}$ is omitted, accordingly only the θ_{12} centripetal pseudopotential arises in (3.137), and near the saddle point this pseudopotential is large. This is possible because $u_1(+\infty) = 1$ (3.167). Notice that no centrifugal/centripetal pseudopotential arises in (3.130) of [186]. In direct analogy with Peterkop and Crothers a JWKB ansatz is employed

$$x = P^{1/2}\exp\left(\frac{\mathrm{i}S}{\hbar}\right) \tag{3.138}$$

allowing the Hamilton–Jacobi equation for the phase function S to be given as

$$\left(\frac{\partial S}{\partial\rho}\right)^2 + \frac{1}{\rho^2}\left(\frac{\partial S}{\partial\alpha}\right)^2 + \frac{4}{\rho^2\sin^2 2\alpha}\left(\frac{\partial S}{\partial\theta_{12}}\right)^2 = 2E + \frac{2\zeta(\alpha,\theta_{12})}{\rho} + \frac{\csc^2\theta_{12}}{4\rho^2\sin^2\alpha\cos^2\alpha} \tag{3.139}$$

and the continuity equation for the amplitude P as

$$D_0\left[P\frac{\partial S}{\partial\rho}\right] + \frac{1}{\rho^2}\left[D_1(P\frac{\partial S}{\partial\alpha}) + D_2(P\frac{\partial S}{\partial\theta_{12}})\right] = 0 \tag{3.140}$$

where we define

$$\begin{aligned} D_0 &= \frac{\partial}{\partial\rho} \\ D_1 &= \frac{1}{\sin(\Delta\alpha)}\frac{\partial}{\partial\alpha}\sin(\Delta\alpha) \\ D_2 &= \frac{4}{\sin^2 2\alpha}\frac{\partial}{\partial\theta_{12}} \end{aligned} \tag{3.141}$$

In this case the perturbative expression for the action S must now be generalized to

$$S = s_1\ln(\Delta\theta_{12}) + S_0(\rho) + \frac{1}{2}S_1(\rho)(\Delta\alpha)^2 + \frac{1}{8}S_2(\rho)(\Delta\theta_{12})^2 \tag{3.142}$$

thus identifying the direction of motion of the particles and where the logarithmic term takes into account the long-range nature of the centripetal potential. The centrifugal potential does not arise as u_1 is well behaved even at infinity.

Rewriting the Hamilton–Jacobi equation

$$\left[S_0' + \frac{1}{2}S_1'(\Delta\alpha)^2 + \frac{1}{8}S_2'(\Delta\theta_{12})^2\right]^2 + \frac{1}{\rho^2}S_1(\Delta\alpha)^2 + \frac{4}{\rho^2}\left(\frac{s_1}{\Delta\theta_{12}} + \frac{1}{4}S_2(\Delta\theta_{12})\right)^2 = \omega^2(\rho) + \frac{Z_1}{\rho}(\Delta\alpha)^2 + \frac{Z_2}{4\rho}(\Delta\theta_{12})^2 + \frac{1}{\rho^2(\Delta\theta_{12})^2} \tag{3.143}$$

and equating coefficients of powers of $\Delta\alpha$ and $\Delta\theta_{12}$, we obtain

$$\omega^2(\rho) = (S_0')^2 + \frac{2s_1S_2}{\rho^2} - \frac{2L(L+1)}{\rho^2} \tag{3.144}$$

$$\frac{Z_i}{\rho} = S_0'S_i' + \frac{S_i^2}{\rho^2} \tag{3.145}$$

$$s_1^2 = \frac{1}{4} \tag{3.146}$$

We are able to rewrite (3.145) in the form of a Ricatti equation and obtain a linear second-order equation by the removal of the nonlinear S_i^2-term, with the substitution

$$S_i = \rho^2\omega\frac{1}{u_i}\frac{\mathrm{d}u_i}{\mathrm{d}\rho} \qquad i = 1, 2 \tag{3.147}$$

If we now define

$$\omega^2 = X^2 + \frac{2Z_0}{\rho} \tag{3.148}$$

where $X^2 = 2E$, then the equation transforms to

$$\rho^2\omega^2\frac{\mathrm{d}^2u_i}{\mathrm{d}\rho^2} + \left(2\rho\omega^2 - Z_0 + \frac{2L(L+1)}{\rho^2}\right)\frac{\mathrm{d}u_i}{\mathrm{d}\rho} = \frac{Z_iu_i}{\rho} \qquad i = 1, 2 \tag{3.149}$$

Upon consideration of the two-dimensional Maclaurin expansion of $\zeta(\alpha, \theta_{12})$, i.e.,

$$\zeta(\alpha, \theta_{12}) = Z_0 + \frac{1}{2}Z_1(\Delta\alpha)^2 + \frac{1}{8}Z_2(\Delta\theta_{12})^2 + \cdots \tag{3.150}$$

we can now define for this singular process

$$Z_0 = 0, \qquad Z_1 = \sqrt{2}, \qquad Z_2 = -\frac{1}{\sqrt{2}} \tag{3.151}$$

allowing for the reduction of (3.149) to

$$\rho^2\frac{\mathrm{d}^2u_i}{\mathrm{d}\rho^2} + 2\rho\frac{\mathrm{d}u_i}{\mathrm{d}\rho} - \frac{Z_iu_i}{X^2\rho} = 0 \tag{3.152}$$

after making the $L = 0$ approximation [385].

A comparison of this equation with that of (9.1.53) of Abramowitz and Stegun [1] allows for Bessel functions to be introduced as the method of solving for u_i. After some slight manipulation (3.152) is solved as

$$u_i = \frac{1}{\sqrt{\rho}}C_{\pm1}\left(\frac{2i}{X}\frac{\sqrt{Z_i}}{\sqrt{\rho}}\right), \qquad i = 1, 2 \tag{3.153}$$

where C is the general cylinder function, and which after applying the boundary conditions, at $\rho = 0$ and $+\infty$, and with arbitrary normalization of logarithmic derivatives yields the values

$$u_1 = \frac{2^{3/4}}{\sqrt{E\rho}} K_1\left(\frac{2^{3/4}}{\sqrt{E\rho}}\right) \qquad u_2 = \frac{2^{3/4}\sqrt{E}}{\sqrt{\rho}} J_1\left(\frac{2^{1/4}}{\sqrt{E\rho}}\right), \tag{3.154}$$

thus describing the radial and angular correlated motion of the two electrons (see (3.142) and (3.147)).

After careful consideration of the form of the wave function, paying particular attention to its outgoing property, we select $s_1 = 1/2$ in (24), allowing for (3.144) to be rewritten as

$$(S_0')^2 = \tilde{\omega}^2 = X^2 + \frac{2Z_0}{\rho} - \frac{S_2}{\rho^2} + \frac{2L(L+1)}{\rho^2} \tag{3.155}$$

with (3.145) left unchanged. By adopting the same method as used by Crothers [186], we set $S_2 = 0$ and $L = 0$ in (22) in order to obtain S_0, after which we solve (3.145) for $i = 1, 2$. These solutions are then iterated back into (3.148) to give

$$\tilde{\omega}^2 = \omega^2 - \omega \frac{\mathrm{d}}{\mathrm{d}\rho}(\ln u_2) + \frac{2L(L+1)}{\rho^2} \tag{3.156}$$

It is now possible to define the terms contained in (3.142) as

$$S_0 = \int_{\rho_+}^{\rho} \mathrm{d}\tilde{\rho}\ \tilde{\omega}(\tilde{\rho}) \tag{3.157}$$

with ρ_+ describing the classical turning point, and similar to Peterkop's method we have from (3.147)

$$S_i = \rho^2 \omega \frac{\mathrm{d}}{\mathrm{d}\rho} \ln u_i \tag{3.158}$$

Now, with ω^2 as defined by (3.148) and (3.151), the substitution of (3.156) into (3.157) allows us to rewrite (3.157) as

$$S_0(\tilde{\rho}) = \int_{\rho_+(L)}^{\rho} \mathrm{d}\tilde{\rho} \left(2E + \frac{J_0(y)}{2^{1/4}\tilde{\rho}^{3/2} J_1(y)} + \frac{2L(L+1)}{\tilde{\rho}^2}\right)^{1/2} \tag{3.159}$$

where we define the term $y = 2^{1/4}/\sqrt{E\tilde{\rho}}$.

Careful attention must be given to the turning point ρ_+. In [186] this was assumed to be zero, for $L = 0$. Subsequent work, in which these restrictions were not pertinent, most notably Loughan's [387], in which $L = 1$, 2 doubly excited He^- states were considered, a zero value did not suffice and a new relation was derived,

$$\rho_+ = \frac{-Z_0 + \sqrt{Z_0^2 + 4EL(L+1)}}{2E} \tag{3.160}$$

In the problem under investigation we initially restricted the angular momentum to $L = 0$, and having already ascertained that $Z_0 = 0$, we once more obtained $\rho_+ = 0$ from (3.160). This is not a feasible value, as the integrand (3.159) at this point equals infinity, thus a new turning point must be derived. If we take the numerator of the square of the integrand in (3.159):

$$T(\rho) = 2E\rho^{3/2}J_1(y) + 2^{-1/4}J_0(y) + 2L(L+1)\rho^{-1/2}J_1(y) \tag{3.161}$$

then differentiating we obtain

$$T'(\rho) = \left[4E\rho^{3/2} + \frac{1}{2E^{1/2}\rho^{3/2}} - \frac{L(L+1)}{\rho^{3/2}} - 2^{3/4}E^{1/2}(L+1/2)^2\right]J_1(y) + \left[\frac{2L(L+1)}{\rho^{1/2}} - 2^{1/4}E^{1/2}\right]J_0(y) \tag{3.162}$$

It is now possible to obtain the value of the new turning point, through the employment of the Newton–Raphson method. We record specimen values of $\rho_+(E)$ in Table 3.9.

After substitution and some slight manipulation we are also able to obtain

$$S_1(\rho) = \frac{2^{1/4}\rho^{1/2}K_0(y\sqrt{2})}{K_1(y\sqrt{2})}, \qquad S_2(\rho) = -\frac{\rho^{1/2}J_0(y)}{2^{1/4}J_1(y)} \tag{3.163}$$

so that all the values in the action $S(\rho)$ are now defined in terms of Bessel functions.

We now turn our attention to the density function; the continuity equation is solved using the method adopted by Peterkop, where the generalised action described by (3.140) gives the density to leading order as

$$P_0^{1/2} = \frac{C^{1/2}u_2^{1/2}}{\tilde{\omega}^{1/2}u_1} \tag{3.164}$$

Normalization of the wave function (not to be confused with u_i) is necessary. Similar to [186], the current probability density (CPD) is matched to

$$\lim_{\rho\to\infty}\int \frac{C\exp(2\mathrm{Im}S)}{u_1^2\tilde{\omega}}\frac{\partial}{\partial\rho}(\mathrm{Re}S)\mathrm{d}\alpha\,\mathrm{d}\hat{\mathbf{r}}_1\,\mathrm{d}\hat{\mathbf{r}}_2 = 4\pi^2 \tag{3.165}$$

Now, since

$$u_1 \sim_{\rho\to\infty} 1 \tag{3.166}$$

we are able to deduce nontrivially,

Table 3.9. Specimen values for $\rho_+(E)$, E, and ρ_+ in atomic units

Energy (E)	$\rho_+(E)[L=0]$	$\rho_+(E)[L=4]$
0.10	1.7266	13.0913
0.30	0.6328	7.6618
0.50	0.3947	5.9189
0.80	0.2547	4.6035
1.00	0.2067	3.7128
1.30	0.1615	2.9468
1.50	0.1411	2.4217

$$\lim_{\rho\to\infty}\int C\,\mathrm{d}\alpha\,\mathrm{d}\hat{\mathbf{r}}_1\,\mathrm{d}\hat{\mathbf{r}}_2 = 4\pi^2 \tag{3.167}$$

allowing for the constant of normalization to be given as $C = 1$. Subsequently the unsymmetrised final-state asymptotic two-electron wave function is defined as

$$\begin{aligned}\Psi_f^{-*} = {} & \frac{1}{X^{1/2}\rho^{5/2}\sin\alpha\cos\alpha\,u_1^{1/2}}\delta(\hat{\mathbf{k}}_1-\hat{\mathbf{r}}_1)\delta(\hat{\mathbf{k}}_2-\hat{\mathbf{r}}_2)\\ & \exp\left(-\mathrm{i}S_0(\rho)-\frac{\mathrm{i}}{2}S_1(\rho)(\Delta\alpha)^2-\frac{\mathrm{i}}{8}S_2(\rho)(\Delta\theta_{12})^2\right)\end{aligned} \tag{3.168}$$

where $\delta(\hat{\mathbf{k}}_1-\hat{\mathbf{r}}_1)\delta(\hat{\mathbf{k}}_2-\hat{\mathbf{r}}_2)$ is included to specify the asymptotic directions of the electrons, and to project out the required scattering amplitude, though in practice this reduces to $P_L\cos(\theta_1)$.

We must now turn our attention to the initial-state wave function; we employ a continuum-distorted-wave approximation, the necessity for which becomes apparent when attempting the integration with respect to $\Delta\theta_{12}$ using the method adopted in [186]. A singularity occurred and a new approach was necessary, subsequently using the method of Crothers and Dubé [192], the revised initial-state wave function can be written as

$$\begin{aligned}\Psi_i^{+} = {} & \psi_i(\mathbf{r}_2)\exp(\mathrm{i}\mathbf{k}_0\cdot\mathbf{r}_2)\Gamma\left(1-\frac{\mathrm{i}}{4k_0}\right)\exp\left(\frac{\pi}{8k_0}\right)M\left(\frac{\mathrm{i}}{4k_0},1,\mathrm{i}k_0r_2+\mathrm{i}\mathbf{k}_0\cdot\mathbf{r}_2\right)\\ & \Gamma\left(1+\frac{\mathrm{i}}{2k_0}\right)\exp\left(-\frac{\pi}{4k_0}\right)M\left(-\frac{\mathrm{i}}{2k_0},1,\mathrm{i}k_0r_{12}+\mathrm{i}\mathbf{k}_0\cdot\mathbf{r}_{12}\right)\end{aligned} \tag{3.169}$$

where we have $2E = X^2 = k_0^2 = v^2$, with $\mathbf{v} = \mathbf{k}_0$ defined as the impact velocity, M defined as the regular Kummer function, and the target function defined as

$$\psi_i(\mathbf{r}_2) = \frac{(1/4)^{3/2}}{\sqrt{\pi}}\exp\left(-\frac{\rho\cos\alpha}{4}\right) \tag{3.170}$$

With the Hamiltonian for this system being defined as

$$\begin{aligned}H = {} & -\frac{1}{2}\nabla_{\mathbf{r}_1}^2-\frac{1}{2}\nabla_{\mathbf{r}_2}^2-\nabla_{\mathbf{r}_{12}}^2-\nabla_{\mathbf{r}_1}\cdot\nabla_{\mathbf{r}_{12}}+\nabla_{\mathbf{r}_2}\cdot\nabla_{\mathbf{r}_{12}}\\ & +\frac{1}{r_{12}}-\frac{1}{4r_1}-\frac{1}{4r_2}\end{aligned} \tag{3.171}$$

and with both the final- and initial-state wave functions now fully defined, we proceed, as [186], by replacing the 2-electron Schrödinger equation by the Kohn variational principle, i.e.,

$$\begin{aligned}f(\hat{\mathbf{k}}_1,\hat{\mathbf{k}}_2) \approx {} & -\int\int\Psi_f^{-*}(H-E)\Psi_i^{+}\mathrm{d}\mathbf{r}_1\,\mathrm{d}\mathbf{r}_2\\ = {} & -\int\int\Psi_f^{-*}(\nabla_{\mathbf{r}_1}\cdot\nabla_{\mathbf{r}_{12}}-\nabla_{\mathbf{r}_2}\cdot\nabla_{\mathbf{r}_{12}})\Psi_i^{+}\mathrm{d}\mathbf{r}_1\,\mathrm{d}\mathbf{r}_2\end{aligned} \tag{3.172}$$

which is the prior-interaction formulation. If we now use the substitution

$$\mathrm{d}\mathbf{r}_1\,\mathrm{d}\mathbf{r}_2 = \rho^2\,\mathrm{d}\rho\,\sin^2\alpha\cos^2\alpha\,\mathrm{d}\alpha\mathrm{d}\hat{\mathbf{r}}_1\mathrm{d}\hat{\mathbf{r}}_2 \tag{3.173}$$

and apply the method of steepest descent to integrate over α, where the saddle point $\alpha = \pi/4$ is consistently taken as the point of stationary phase, then the scattering amplitude is given as

$$\begin{aligned} f \approx \frac{N\mathrm{i}}{\pi^{1/2}} \sum_{L=0}^{L_{\mathrm{MAX}}} \int_{\rho_+}^{\infty} \mathrm{d}\rho \frac{\rho^{5/2}\Gamma\left(1-\frac{\mathrm{i}}{4k_0}\right)\Gamma\left(1+\frac{\mathrm{i}}{2k_0}\right)}{\tilde{\omega}^{1/2}u_1^{1/2}S_1^{1/2}} P_L(\cos\Theta_1) \\ \exp\left(-\frac{\lambda\rho}{2^{1/2}}\right)\exp\left(-\frac{\pi}{8k_0}\right)\exp\left(-\mathrm{i}\left(S_0+\frac{1}{8}S_2(\Delta\Theta_{12})^2\right)-\frac{\pi\mathrm{i}}{4}\right) \\ \left[\frac{\lambda}{2}(1-\cos\Theta_{12}-2^{1/2}\cos\Theta_1)\exp\left(\frac{\mathrm{i}}{2^{1/2}}k_0\rho\cos\Theta_2\right)\right. \\ M\left(1-\frac{\mathrm{i}}{2k_0},2,\frac{\mathrm{i}k_0\rho}{2^{1/2}}(2^{1/2}-\cos\Theta_1+\cos\Theta_2)\right)M\left(\frac{1}{4k_0},1,\frac{\mathrm{i}k_0\rho}{2^{1/2}}(1+\cos\Theta_{12})\right) \\ +B(\cos\Theta_{12}-\cos\Theta_1+(2^{1/2}-1)\cos\Theta_2)\exp\left(\frac{\mathrm{i}}{2^{1/2}}k_0\rho\cos\Theta_{12}\right) \\ \left.M\left(2+\frac{\mathrm{i}}{2k_0},2,\frac{\mathrm{i}k_0\rho}{2^{1/2}}(2^{1/2}-\cos\Theta_1+\cos\Theta_2)\right)M\left(1+\frac{1}{4k_0},1,\frac{\mathrm{i}k_0\rho}{2^{1/2}}(1+\cos\Theta_2)\right)\right] \end{aligned} \tag{3.174}$$

where we define $N = 1/8\pi^{1/2}$, $\lambda = 1/4$, $B = (\mathrm{i}k_0 - 1/2)/4$, and where the delta functions as written in (3.168) has resulted in the angles θ_1, θ_2, and θ_{12}, corresponding to $\hat{\mathbf{r}}_i$, being converted to Θ_1, Θ_2, and Θ_{12}, corresponding to $\hat{\mathbf{k}}_i$, respectively.

The total cross section can now be derived using spin averaging

$$\sigma = \int \mathrm{d}\hat{\mathbf{k}}_1\,\mathrm{d}\hat{\mathbf{k}}_2\left(\frac{1}{4}\mid f+g\mid^2+\frac{3}{4}\mid f-g\mid^2\right) \tag{3.175}$$

where

$$\int \mathrm{d}\hat{\mathbf{k}}_1\,\mathrm{d}\hat{\mathbf{k}}_2 = 2\pi\int_0^{2\pi}\mathrm{d}\Phi\int_0^{\pi}\mathrm{d}\Theta_2\sin\Theta_2\int_0^{\pi}\mathrm{d}\Theta_1\sin\Theta_1 \tag{3.176}$$

and where g is defined as the exchange amplitude and is obtained by interchanging Θ_1 and Θ_2 in (3.174). This four-fold integral now allows for total cross sections to be calculated on an absolute scale.

3.4.4 Results, Discussion, and Conclusions

We are now able to present the first theoretical estimate for absolute cross sections, for the case when $Z = 1/4$. This has been made possible due to our derived initial- and final-state wave functions which are both regular and nonsingular.

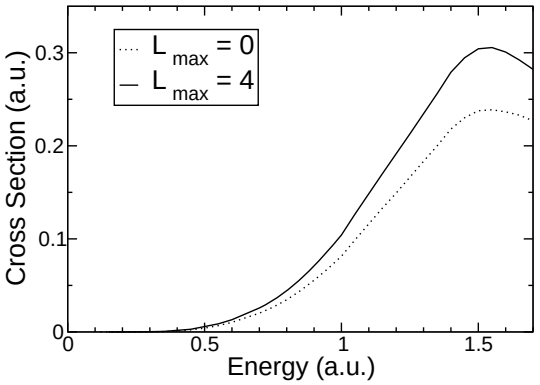

Fig. 3.13. Total ionization cross section for $Z = 1/4$ as a function of impact energy

As is clearly evident from Figure 3.13, it is the $L = 0$ contribution that is most dominant when calculating the cross section. The total cross section does converge when the value for L_{MAX} increases, with an increase from $L_{\mathrm{MAX}} = 3$ to $L_{\mathrm{MAX}} = 4$,resulting only in an increase of the cross section in the fourth significant figure. As we would expect, the cross section increases almost exponentially, as found in [337], [225], [117], before reaching a peak and then decreasing. The shape of the graph is quite similar to that produced in [117], although a comparison of the magnitude of the cross section is not possible as the results in [117] are not absolute; we can see that the magnitude of the energy that gives the highest cross section has increased dramatically. If we look again at (3.174), it is the $\rho^{5/2} \exp(-\lambda\rho/\sqrt{2})$ factor that has the greatest effect on the magnitude of the cross section, in particular the $\lambda = 1/4$ term in the exponential that arises due to the weak nuclear charge.

In figure 2 of [146] we see graphs relating to the cross sections derived in [337], [225], [117], the equations (3.124) and (3.125) are used with our numerically derived cross sections and plotted in logarithmic graphs. The lower energy range is to the left of the first two graphs and to the right of the final graph. As is clearly evident, linear dependence is limited to a comparatively narrow low-energy domain, so that laws (3.124) and (3.125) have limited relevance.

It should be noted that the process we have studied is probably not accessible experimentally, and the only theoretical results that have been published related to an interaction similar to ours [337], [225], [117] do not provide cross sections on an absolute scale and are confined to a limited energy range. However, we can now model process (3.123) with confidence.

4

Ion–Atom Collisions

4.1 The Semiclassical Impact Parameter Treatment

A third meaning of semiclassical (cf. Chapters 2 and 3) concerns an ion–atom collision in which the relative motion of the two nuclei is treated classically while the motion of one or more electrons is treated fully quantally [442]. In fact the impact parameter ρ was already encountered in Section 2.2.2 (2.91) and (2.92). Physically it corresponds to the distance of closest approach, assuming that the classical relative motion of the nuclei follows a straight-line trajectory. This is justified formally if it is assumed that on an atomic electron scale, the nuclear masses are taken to be infinite: an excellent assumption. We have that the electron has position $\mathbf{r}_T$, $\mathbf{r_P}$ relative to the target T and projectile P, and the internuclear vector $\overrightarrow{TP}$ is given by

$$\mathbf{R} = \boldsymbol{\rho} + \mathbf{v}t \tag{4.1}$$

where $\mathbf{v}$ is the laboratory impact velocity and

$$\mathbf{R} = \mathbf{r}_P - \mathbf{r}_T \tag{4.2}$$

$$\mathbf{r} = \frac{1}{2}(\mathbf{r}_P + \mathbf{r}_T) \tag{4.3}$$

where the electron is $\mathbf{r}$ from the midpoint of P and T (an arbitrary centre of mass, since $M_P = M_T \equiv +\infty$). It follows that

$$\frac{\mathrm{d}\mathbf{R}}{\mathrm{d}t} = \mathbf{v}\,, \qquad \boldsymbol{\rho} \cdot \mathbf{v} = 0 \tag{4.4}$$

and $|Z| = v|t|$ is the distance of P from the point of closest approach and $t \in [-\infty\,, +\infty]$ along the classical straight-line trajectory with the time origin at the instant of nearest approach. For one-electron processes, there are four types of collision: perfectly elastic, excitation, ionization, and charge transfer. For multi-electron processes, additional channels are transfer-excitation, transfer-ionization, double capture, double excitation, double ionization (Section 4.3.6), etc. For clarity we follow the trickier

case of one-electron charge transfer, and in anticipation of Section 4.3, we follow the notation of Crothers and Dubé [192]. The Lagrangian is given by

$$\begin{aligned} H - \mathrm{i}\frac{\mathrm{d}}{\mathrm{d}t_{\mathbf{r}}} &= T + V - \mathrm{i}\frac{\partial}{\partial t_{\mathbf{r}}} \\ &= -\frac{1}{2}\boldsymbol{\nabla}_{\mathbf{r}}^2 + V_T(r_T) + V_P(r_P) + V_{PT}(R) - \mathrm{i}\frac{\partial}{\partial t_{\mathbf{r}}} \end{aligned} \tag{4.5}$$

where H is the Hamiltonian, the potentials are given by

$$\begin{aligned} V_C(r_C) &= -\frac{Z_C e}{r_C} \qquad (C = P,\ T) \\ V_{PT} &= +\frac{Z_P Z_T e^2}{R} \end{aligned} \tag{4.6}$$

and it is assumed that the independent variables are $(\mathbf{r}, t)$ and that a subscript indicates which variable is kept constant. Following [423] the total wave function Ψ_i^+ satisfies the time-dependent Schrödinger equation

$$\left(H - \mathrm{i}\frac{\partial}{\partial t_{\mathbf{r}}}\right)\Psi_i^+ = 0 \tag{4.7}$$

subject to the initial and final boundary conditions:

$$\begin{aligned} &\lim_{t\to-\infty} \Psi_i^+ = \xi_i^+ \\ \text{and} \quad &\lim_{t\to\infty} \Psi_i^+ = \xi_i^+ + A_{fi}^+ \xi_f^- \end{aligned} \tag{4.8}$$

Similarly the total wave function Ψ_f^- satisfies the equation

$$\left(H - \mathrm{i}\frac{\mathrm{d}}{\mathrm{d}t}\right)\Psi_f^- = 0 \tag{4.9}$$

subject to

$$\begin{aligned} \lim_{t\to+\infty} \Psi_f^- &= \xi_f^- \\ \lim_{t\to-\infty} \Psi_f^- &= \xi_f^- + A_{fi}^- \xi_i^+ \end{aligned} \tag{4.10}$$

The total cross section is given by

$$\sigma^{\pm}(i|f) = \int \mathrm{d}\boldsymbol{\rho} \left|A_{fi}^{\pm}(f)\right|^2 \tag{4.11}$$

Now, wrongly as it will turn out in 4.3, we assume that V_P may be neglected in the initial channel so that

$$\xi_i^+ = \phi_i^T(\mathbf{r}_T)\, \mathrm{e}^{-\frac{\mathrm{i}}{8}v^2 t - \mathrm{i}\epsilon_i^T t - \frac{1}{2}\mathrm{i}\mathbf{v}\cdot\mathbf{r}} \tag{4.12}$$

and V_T may be neglected in the final channel so that

$$\xi_f^- = \phi_f^P(\mathbf{r}_P)\,\mathrm{e}^{-\frac{1}{8}v^2 t - \mathrm{i}\epsilon_f^P t + \frac{1}{2}\mathrm{i}\mathbf{v}\cdot\mathbf{r}} \tag{4.13}$$

This is the basis of traveling atomic orbitals (Section 4.2); the electron translation factors (ETFs), originally obtained by Bates and McCarroll [44] using Fourier transforms arise typically as follows from the chain rule:

$$\frac{\partial}{\partial t_{\mathbf{r}}} = \frac{\partial \mathbf{R}}{\partial t_{\mathbf{r}}}\cdot(\boldsymbol{\nabla}_{\mathbf{R}})_{\mathbf{r}_T} + \frac{\partial \mathbf{r}_T}{\partial t_{\mathbf{r}}}\cdot(\boldsymbol{\nabla}_{\mathbf{r}_T})_{\mathbf{R}} = \left(\frac{\partial}{\partial t}\right)_{\mathbf{r}_T} + \frac{1}{2}\mathbf{v}\cdot\boldsymbol{\nabla}_{\mathbf{r}_T} \tag{4.14}$$

since

$$\mathbf{r}_T = \mathbf{r} + \frac{1}{2}\mathbf{R} \tag{4.15}$$

and since we are changing from independent variables $(\mathbf{r}, t)$ to $(\mathbf{r}_T, t)$. The preceding notation involves the initial target bound state ϕ_i^T with eigenvalue ϵ_i^T and the final projectile bound state ϕ_f^P with eigenvalue ϵ_f^P. The impressed electron kinetic energies $1/2\,(v/2)^2$ arise automatically. For the time being the superscripts $\pm$ on ξ are redundant due to our neglect of the other Coulomb potential. The amplitudes are given by

$$A_{fi}^+ = -\mathrm{i}\int_{-\infty}^{+\infty}\mathrm{d}t\,\left\langle \xi_f^- \left| \left(H - \mathrm{i}\frac{\mathrm{d}}{\mathrm{d}t}\right)^\dagger \right| \Psi_i^+ \right\rangle \tag{4.16}$$

$$\approx -\mathrm{i}\int_{-\infty}^{+\infty}\mathrm{d}t\,\left\langle \xi_f^- \left| \left(H - \mathrm{i}\frac{\mathrm{d}}{\mathrm{d}t}\right)^\dagger \right| \xi_i^+ \right\rangle \tag{4.17}$$

and by

$$A_{fi}^- = -\mathrm{i}\int_{-\infty}^{+\infty}\mathrm{d}t\,\left\langle \Psi_f^- \left| H - \mathrm{i}\frac{\mathrm{d}}{\mathrm{d}t} \right| \xi_i^+ \right\rangle \tag{4.18}$$

$$\approx -\mathrm{i}\int_{-\infty}^{+\infty}\mathrm{d}t\,\left\langle \xi_f^- \left| H - \mathrm{i}\frac{\mathrm{d}}{\mathrm{d}t} \right| \xi_i^+ \right\rangle \tag{4.19}$$

where (4.17) and (4.19) are the impact parameter versions of the Oppenheimer–Brinkman–Kramers (OBK) approximation [89], [466] and where we use the Dirac bracket notation to indicate integration over $\mathbf{r}$ for fixed t. Galilean invariance is guaranteed due to the ETFs [44]. However, gauge invariance is not: the cross sections depend on whether or not V_{PT} is included, and indeed there is a post-prior discrepancy, that is, (4.17) and (4.19) give different results.

Some of these defects may be removed in a two or more traveling atomic-orbital expansion:

$$\Psi = c_i(t)\xi_i^+ + c_f(t)\xi_f^- \tag{4.20}$$

with the second-order Jacobi variational principle

$$\delta L = \delta\int_{-\infty}^{+\infty}\mathrm{d}t\,\langle\Psi|\,H - \mathrm{i}\frac{\mathrm{d}}{\mathrm{d}t}\,|\Psi\rangle = 0 \tag{4.21}$$

giving

$$\mathrm{i}\left(1-\left|N_{if}^{+-}\right|^2\right)\dot{c}_i = \left(H_{ii}^{++} - N_{if}^{+-}H_{fi}^{-+}\right)c_i + \left(H_{if}^{+-} - N_{if}^{+-}H_{ff}^{--}\right)c_f \tag{4.22}$$

$$\mathrm{i}\left(1-\left|N_{if}^{-+}\right|^2\right)\dot{c}_f = \left(H_{fi}^{-+} - N_{fi}^{-+}H_{ii}^{++}\right)c_i + \left(H_{ff}^{--} - N_{fi}^{-+}H_{if}^{+-}\right)c_f \tag{4.23}$$

where

$$N_{if}^{+-} = \left\langle \xi_i^+ | \xi_f^- \right\rangle \tag{4.24}$$

$$H_{if}^{+-} = \left\langle \xi_i^+ \left| H - \mathrm{i}\frac{\mathrm{d}}{\mathrm{d}t} \right| \xi_f^- \right\rangle \tag{4.25}$$

Notice N_{fi}^{-+}, H_{ii}^{++}, and H_{ff}^{--} are included in these definitions. Setting

$$c_i = C_i \exp\left[-\mathrm{i}\int_{-\infty}^{t} x_i(t')\mathrm{d}t'\right] \tag{4.26}$$

$$b_f = B_f \exp\left[-\mathrm{i}\int_{-\infty}^{t} y_f(t')\mathrm{d}t'\right] \tag{4.27}$$

where

$$x_i = \frac{H_{ii}^{++} - N_{if}^{+-}H_{fi}^{-+}}{1-\left|N_{if}^{+-}\right|^2} \tag{4.28}$$

$$y_f = \frac{H_{ff}^{--} - N_{fi}^{-+}H_{if}^{+-}}{1-\left|N_{if}^{-+}\right|^2} \tag{4.29}$$

we use the integrating-factor method to obtain two coupled first-order equations

$$\mathrm{i}\dot{A}_i = B_f\left[\frac{H_{if}^{+-} - N_{if}^{+-}H_{ff}^{--}}{1-\left|N_{if}^{+-}\right|^2}\right]\mathrm{e}^{\mathrm{i}\gamma_{if}} \tag{4.30}$$

$$\mathrm{i}\dot{B}_f = A_i\left[\frac{H_{fi}^{-+} - N_{fi}^{-+}H_{ii}^{++}}{1-\left|N_{if}^{+-}\right|^2}\right]\mathrm{e}^{-\mathrm{i}\gamma_{if}} \tag{4.31}$$

where

$$\gamma_{if} = \int_{-\infty}^{t}\left(x_i(t') - y_f(t')\right)\mathrm{d}t' \tag{4.32}$$

$$A_i(-\infty) = 1\,, \quad B_f(-\infty) = 0 \tag{4.33}$$

The advantage of what Bates [34] called the refined orthogonal treatment with γ_{if} the distortion is that (4.30) and (4.31) are gauge-invariant. They do not depend on V_{PT}, which appears physically sensible since M_P and M_T are infinite masses, by assumption, immovable in their relative trajectory. Of course (4.20) is generalized in Section 4.2 by including many more states. Moreover, unitarity and detailed balance are also guaranteed. Notice that the perturbative solution of (4.30) and (4.31), subject to (4.33), is also gauge-invariant:

$$B_f(+\infty) \approx -\mathrm{i}\int_{-\infty}^{+\infty} \mathrm{d}t\, \frac{\left(H_{fi}^{-+} - N_{fi}^{-+}H_{ii}^{++}\right)}{1-\left|N_{if}^{+-}\right|^2}\mathrm{e}^{-\mathrm{i}\gamma_{if}(t)} \tag{4.34}$$

The Born distortion approximation cross sections for both excitation and ionization in the impact parameter treatment may be deduced from (4.34) making the N-matrix into the unit matrix.

Ignoring distortion ($\gamma_{if} = 0$), the total cross section is given by

$$\sigma(i/f) = \int \mathrm{d}\boldsymbol{\rho}\left|\int_{-\infty}^{+\infty}\mathrm{d}t\, H_{fi}(t)\right|^2 \qquad (f \neq i) \tag{4.35}$$

which, using two-dimensional transforms, may be written in the equivalent wave treatment [45], [85] as

$$\sigma(i/f) = \frac{1}{2\pi v^2}\int_{(\epsilon_f-\epsilon_i)/v}^{\infty} q\mathrm{d}q\left|\int \mathrm{e}^{\mathrm{i}\mathbf{q}\cdot\mathbf{R}}H_{fi}(\mathbf{R})\mathrm{d}\mathbf{R}\right|^2 \tag{4.36}$$

provided we sum over the final-state and average over the initial-state degeneracies [158]. In (4.36) $\mathbf{R}$ remains the internuclear vector, given by (4.2) but not by (4.1).

We shall return to this theme in Section 4.5, since the proper Born wave treatment gives (4.36) but with upper limit $k_i + k_f$ and lower limit $|k_i - k_f|$ where k_j is the wave number associated with the relative momentum of the heavy particles in state j. In quantal treatments of heavy-particle collisions

$$\mathrm{e}^{\mathrm{i}\mathbf{q}\cdot\mathbf{R}} = \mathrm{e}^{\mathrm{i}\mathbf{k}_i\cdot\mathbf{R}}\cdot\mathrm{e}^{-\mathrm{i}\mathbf{k}_f\cdot\mathbf{R}} \tag{4.37}$$

being the product of the initial-state plane wave and the conjugated final-state plane wave. Moreover the semiclassical interpretation of a plane wave at the point of closest approach, even at large impact parameter, requires some subtlety in considering generalized-function contributions asymptotically [444].

Given our treatment of degeneracies, we may assume that the t-integral in (4.35) is independent of the azimuthal angle of $\boldsymbol{\rho}$ so that the total differential cross section is given, to a very good approximation, by:

$$\frac{\mathrm{d}\sigma}{|\mathrm{d}(\cos\Theta)|} = 2\pi k_i^2\left|\int_0^{\infty}\rho\mathrm{d}\rho\, J_0\left(2k_i\rho\sin\frac{\Theta}{2}\right)\int_{-\infty}^{+\infty}\mathrm{d}t\, H_{fi}(t)\right|^2 \tag{4.38}$$

which to a very good small-angle approximation, reduces to

$$\frac{\mathrm{d}\sigma}{|\mathrm{d}(\cos\Theta)|} = 2\pi k_i^2 \left| \int_0^\infty \rho \mathrm{d}\rho \, J_0\left(k_i \rho \Theta\right) \int_{-\infty}^{+\infty} \mathrm{d}t \, H_{fi}(t) \right|^2 \tag{4.39}$$

In (4.38), (4.39) the dependence of H_{fi} on ρ is suppressed in the notation.

We have used

$$\begin{aligned} q^2 &= k_i^2 + k_f^2 - 2k_i k_f \cos\Theta \\ &= K_\perp^2 + \left(k_i - k_f\right)^2 \end{aligned} \tag{4.40}$$

so that

$$q\mathrm{d}q = K_\perp \, \mathrm{d}K_\perp = k_i^2 \sin\Theta \, \mathrm{d}\Theta \tag{4.41}$$

since $k_f \approx k_i$ apart from $\left(k_i - k_f\right)$ and where $K_\perp$ is the transverse component of the change in relative linear momentum of the heavy particles [192]. Often $K_\perp$ is written as η (cf. Crothers and McCann [182]).

The remarkable aspect of (4.38) and (4.39) is that we have expressions for the differential cross sections (functions of Θ) even though the straight-line impact parameter semiclassical method assumes à priori that $\Theta = 0$ [415]. As remarked by McCarroll in five special lectures in Queen's University Belfast in May 1991 this impact parameter semiclassical approach to differential cross sections is often called the*e*ikonal method. Perhaps as he remarked on that occasion this may account for the sparse account of the impact parameter treatment, by Mott and Massey [443]. Equally it can be said that when Bates returned to Queen's University Belfast in 1951, Massey and he had agreed that UCL would concentrate on electron-atom collisions and Queen's University Belfast on heavy-particle collisions. Notice also that the impact parameter is not an experimental observable since a given Θ angle of scattering, or deflection, often corresponds to two or more impact parameters.

One last word in this section on the impact parameter treatment: of course it lends itself to perturbation theory, for instance, the second-order iterative treatment of (4.30) and (4.31), when v is large (fast collision): see Bates [35]. On the other hand, as will be seen in Section 4.3, the first-order wave treatment permits the separation of a six-fold integral into the product of two three-fold dipole integrals. Nevertheless the generalizations of (4.20) into large atomic-and/or molecular-orbital expansions will be discussed and illustrated in Section 4.2, albeit using the semiclassical impact parameter treatment of this section, on the assumption that the impact energy exceeds c 1 eVu^{-1} [40] or at any rate, 100 eVu^{-1} (see Figure 4.2).

Of course, another meaning of semiclassical concerns highly excited atoms in Rydberg states. For a discussion of classical and quantal chaos in low-dimensional systems including scarring and random fluctuations see [214].

4.2 Traveling Atomic and Molecular Orbitals

As we have already seen in Section 4.1 (4.12) and (4.13), in ion–atom collisions we must attach electron translation factors (ETFs) to ion and atom wave functions to

represent the physical fact that the electrons, attached to the projectile, are traveling at $+1/2\,\mathbf{v}$, and those to the target at $-1/2\,\mathbf{v}$, relative to the heavy particle centre of mass (equivalently the midpoint of TP, since each nucleus has infinite mass, relative to the electrons).

In electron–atom collisions, the standard R-matrix method [103] permits, for each partial wave l, a large linear expansion in L^2, that is, finitely normalizable, wave functions inside a large sphere, possibly with pseudostates, followed by logarithmic-derivative matching on its surface with appropriate JWKB asymptotic functions. No ETFs arise. Moreover, because $1/2\,v^2$, the kinetic energy of the electron, must exceed the ionization potential of the target, v is bounded below; in heavy-particle collisions, the large reduced mass μ permits v to be very much less than 1, so that $1/v$ may be a comparatively large parameter. Further, since we have

$$\rho k = l + \frac{1}{2} \tag{4.42}$$

where ρ is the impact parameter, l the partial wavenumber, and k the wavenumber given by

$$k = \mu v \tag{4.43}$$

then for every N partial waves in electron–atom collisions, there are μN in ion–atom collisions.

Thus, although the R-matrix method has been applied to ion–atom collisions at impact thermal energies, it generally becomes impracticable for higher energies. Fortunately we may consider ρ to be a continuous variable, and instead of summing over l, we make the semiclassical approximation and integrate over ρ.

Nevertheless there arises the question of how to generalize (4.20). As reviewed by Bransden [86] and Fritsch and Lin [279], the provisional answer is to generalize (4.20) by including many traveling atomic orbitals (AO) on both centres, T and P, including pseudostates (AO+) to simulate the continuum of either T or P. Of course there immediately arises the problem of double counting since the two continua overlap. Also there is the problem that apparent convergence to a probability or a cross section may be a false convergence due to the limited representation of the continuum. The possible solutions are traveling molecular orbitals (MO) [37] expansions, or the triple-centre method [610], or the unified treatment [352] in which AO and MO expansions are matched at a strategic internuclear separation.

Since exact stationary molecular orbitals are available for H_2^+ [497], we start with a discussion of $H^+ + H(1s)$ collisions at low-impact energies, concerning capture and excitation.

4.2.1 Traveling Molecular H_2^+ Orbitals

The method of Löwdin is adopted to orthogonalize optimized traveling molecular orbitals symmetrically. Second-order terms in velocity are consistently retained, and it is shown that these terms have a significant influence on H($2p$) and H($2s$) charge exchange and direct cross sections in the 1–10 keV proton impact energy range.

The original choice of ETF by Bates and McCarroll [44] is adequate for some purposes and certainly avoids long-range spurious couplings. However, this ETF causes problems in the united-atoms limit where the incomplete nature of the basis set [251] results in nonphysical phases in large-angle capture probabilities [168], [177]. Recent trends in the approach to translation factors may be discerned and reviewed in terms of either parameterized switching functions (f_j) or common translation factors [251], [252], [394], [395], which by their very name are state-independent and lead to simplicity in the algebra and analysis. By comparison, the switching functions are more complicated and are usually state-dependent. Three trends are apparent here. First, there is the ad hoc variety (cf. Shimakura et al. [552] and references therein) based on some intuitively appealing criteria. Second, there is the strategy of Thorson [581], [353], [354], [355], based on the physically sound proposition of pragmatically minimizing coupling between discrete states and the continuum. Third, there is the Euler–Lagrange variational choice which has been pursued independently by both Green et al. [511], [305], [306], [308], [309], [557] and Crothers et al. [168], [171], [172], [173], [176], [177]. There are, of course, other differences in the trends. For instance, Thorson, in common with most authors, chooses the switching function to vary with the electronic coordinate and curve-fits to intelligently chosen analytic formulae. By contrast, Green and Crothers choose the switching function to vary only with the internuclear coordinate, thus averaging over the electronic coordinate, and are content to work with purely numerical values. Minor variations in their treatments concerning ρ dependence and direction of electronic momentum appear to be in general of comparatively little importance.

Of the various approaches that are not ad hoc, only Crothers and Hughes (CH) [173] and Kimura and Thorson (KT) [353] have been applied to the basic proton–hydrogen problem.

It has been asserted [353] that the non-Hermitian character of the coupling matrices should not be destroyed by taking Hermitian averages and that a defect in the calculations of CH is their neglect of the non-Hermitian character in the couplings between ETF corrected molecular basis sets.

While it is true that non-Hermitian equations are sufficient (cf. Green [304], Pfeifer and Garcia [489]), it is also the case that Hermitian equations are sufficient, though of course not necessary. Actually the two are equivalent if, in the matrix elements, the functional dependence on velocity is retained exactly to all orders. However, if one wishes to retain a precise order of terms, then it is essential to have Hermitian equations for such a perturbation theory. The difficulty with non-Hermitian equations has been well illustrated by Riera and Salin [510] and Burns and Crothers [104].

The exact equivalence, assuming that matrix elements are calculated exactly to all orders, is shown by enforcing symmetric orthogonalization in the manner of Löwdin [388], [389] (see also [335], [569], [534]), namely by defining "real" orthonormal traveling orbitals by

$$\boldsymbol{\phi} = \boldsymbol{\chi}\,(\boldsymbol{\chi}^{+}\boldsymbol{\chi})^{-1/2} \tag{4.44}$$

where $\boldsymbol{\chi}$ is a row matrix of the linearly independent nonorthogonal traveling molecular orbital kets given by

$$\boldsymbol{\chi} = (|\chi_1\rangle|\chi_2\rangle \cdots |\chi_n\rangle) \tag{4.45}$$

Thus the standard Gram–Schmidt system of orthonormalization is sufficient but not necessary and not symmetrical. Care is required in selecting the correct matrix square root to avoid coupling at infinity and the equivalence of the non-Hermitian $\boldsymbol{\chi}$ equations (see (4.46)) and the Hermitian $\boldsymbol{\phi}$ equations are simply demonstrated using the Sil variational principle and the adjoint of (4.44). Thus, writing

$$\begin{aligned} |\boldsymbol{\Psi}\rangle &= \boldsymbol{\phi}\tilde{\mathbf{c}} \\ &= \boldsymbol{\chi}\,(\boldsymbol{\chi}^{+}\boldsymbol{\chi})^{-1/2}\,\tilde{\mathbf{c}} \\ &= \boldsymbol{\chi}\tilde{\mathbf{d}} \end{aligned} \tag{4.46}$$

where $\tilde{\mathbf{c}}$ and $\tilde{\mathbf{d}}$ are column vectors, the Sil variational principle gives

$$\langle \chi_m \left| H - \mathrm{i}\frac{\mathrm{d}}{\mathrm{d}t} \right| \Psi\rangle = 0 \qquad m \in [\mathrm{i}, n] \tag{4.47a}$$

$$\langle \phi_m \left| H - \mathrm{i}\frac{\mathrm{d}}{\mathrm{d}t} \right| \Psi\rangle = 0 \qquad m \in [\mathrm{i}, n] \tag{4.47b}$$

The adjoint of (4.44), namely,

$$\boldsymbol{\phi}^{+} = (\boldsymbol{\chi}^{+}\boldsymbol{\chi})^{-1/2}\boldsymbol{\chi}^{+} \tag{4.48}$$

ensures that (4.47a) imply (4.47b), while the inverse of (4.48)

$$\boldsymbol{\chi}^{+} = (\boldsymbol{\chi}^{+}\boldsymbol{\chi})^{1/2}\,\boldsymbol{\phi}^{+} \tag{4.49}$$

ensures that (4.47b) imply (4.47a). We have of course assumed that $\boldsymbol{\chi}$ reduces to a row matrix of orthonormal traveling atomic orbitals at infinity.

In effect, the independent approach of Crothers et al. [168], [171], [172], [173], [176], [177], [170] to the question of symmetric orthogonality is just a perturbative variant of Löwdin's equation (4.44). To be precise, Crothers and Todd [176] expand their time-dependent (t), impact-parameter-dependent wave function as a linear combination of traveling molecular orbitals thus

$$\Psi(\mathbf{r}, t) = \sum_j c_j(t)\Phi_j(\mathbf{r}, t) \tag{4.50}$$

where $\mathbf{r}$ is the electronic position coordinate and

$$\Phi_j(\mathbf{r}, t) = \chi_j(\mathbf{r}, R)T_j(\mathbf{R}, \mathbf{r})E_j(t) \tag{4.51}$$

$$T_j(\mathbf{R}, \mathbf{r}) = \exp\left\{\mathrm{i}\, f_j(\mathbf{R})\mathbf{v}\cdot\mathbf{r}\right\} \tag{4.52}$$

$$E_j(t) = \exp\left\{-\mathrm{i}\int_0^t \langle \chi_j T_j \left| H_e - \mathrm{i}\frac{\mathrm{d}}{\mathrm{d}\tilde{t}} \right| \chi_j T_j\rangle \mathrm{d}\tilde{t}\right\} \tag{4.53}$$

in which $\mathbf{R}$ is the internuclear coordinate and the χ_j are the stationary molecular orbitals of the electronic Hamiltonian H_e with corresponding eigenvalue $\epsilon_j(R)$, and $\mathbf{v}$ is the impact velocity. It may be noted that

$$\int \chi_f^*(\mathbf{r},\mathbf{R})\frac{1}{v}\frac{\partial}{\partial t_{\mathbf{r}}}\psi_k(\mathbf{r},\mathbf{R})\mathrm{d}\mathbf{r} = \frac{vt}{R}\int \chi_j^*\frac{\mathrm{d}}{\mathrm{d}R_{\mathbf{r}}}\chi_k\mathrm{d}\mathbf{r} + \frac{\rho\mathrm{i}}{R^2}\int \chi_j^* L_y\chi_k\mathrm{d}\mathbf{r} \tag{4.54}$$

comprising, respectively, the radial and rotational coupling (at $v = 0$) where L_y is the component of the electronic orbital angular momentum perpendicular to the collision plane. Although the χ_j form an orthonormal set, the Φ_j do not because of the traveling state-dependent factor T_j. However, they found that correct to second order in v, the following traveling molecular orbitals do form an orthonormal set, namely ϕ_j where

$$\phi_j = \Phi_j - \frac{1}{2}\sum_{l\neq j}\Phi_l S_{lj} + \frac{3}{8}\sum_{l\neq j}\sum_{k\neq l}\Phi_k S_{kl}S_{lj} \tag{4.55}$$

where the overlap matrix is defined by

$$S_{lj} = \int \Phi_l^*\Phi_j\mathrm{d}\mathbf{r} \tag{4.56}$$

The coefficients $-1/2$ and $3/8$ in (4.54) agree with the corresponding coefficients of Löwdin [389]. It should be noted that Löwdin would refer to the ϕ_j given by (4.55) as representing the "real" orbitals as against the Φ_j. Also it may be noted that the third term in (4.55) was not required by CH due to the special gerade and ungerade partitioning in the symmetric case. It is, of course, necessary to use the well-known relation

$$\mathrm{i}\frac{\mathrm{d}}{\mathrm{d}t}\left(\chi_k\middle|\chi_j\right) = \left(\chi_j\middle|H - \mathrm{i}\frac{\mathrm{d}}{\mathrm{d}t}\middle|\chi_k\right)^* - \left(\chi_k\middle|H - \mathrm{i}\frac{\mathrm{d}}{\mathrm{d}t}\middle|\chi_j\right) \tag{4.57}$$

in order to complete the justification of Hermitian averaging using the perturbative variant of Löwdin's symmetric orthonormalization scheme.

Of course it is possible to avoid the non-Hermitian problem ab initio by adopting a common translation factor [251], [252], [394], [395], [413]. Such an approach may well have an important role to play in calculating, say, total inelastic cross sections. However, since switching functions depend critically on strong coupling between state j and any energetically close-lying state at any given internuclear separation [176], and since the phase of large-angle capture probabilities in turn depends critically on f_j [168], [177], it seems likely that an accurate description of differential cross sections requires the more detailed approach provided by state-dependent switching functions. In general, such an approach is potentially rather time-consuming. Nevertheless, provided the velocity is not too high, great simplification ensues if terms of order v^2 are retained, thus optimizing between the requirement of accuracy and the requirement to minimize computer time. Terms of order v^2 can only be retained consistently if the non-Hermitian problem is resolved in the

manner of Löwdin, as described earlier. Accordingly we continue to disagree with KT and therefore with Fritch and Lin [279]; moreover we disagree with Thorson et al. [581] regarding their imputation that CH "criticize the idea of a switching function as somehow implying a violation of the uncertainty principle." CH merely invoked the uncertainty principle to justify averaging the switching function over the electron coordinate, a strategy also adopted by Green [511], [305], [306], [308], [309], [557].

Total cross sections for the four reactions

$$\left.\begin{aligned} H^+ + H(1s) &\rightarrow H(2s, 2p) + H^+ \\ H^+ + H(1s) &\rightarrow H^+ + H(2s, 2p) \end{aligned}\right\} \tag{4.58}$$

have been the subject of considerable experimental and theoretical investigation. For a detailed historical account up to 1978, the reader is referred to CH. In order to resolve the discrepancies between KT and CH, we repeated the calculations of CH on a powerful computer.

In Table 4.1 we present results for direct and exchange $2s$ cross sections using 10 states ($1s\sigma_g$, $2p\sigma_u$, $3d\pi_g$, $2p\pi_u$, $2s\sigma_g$, $3p\sigma_u$, $3d\sigma_g$, $4f\sigma_u$, $4d\pi_g$, $3p\pi_u$) (Bates and Reid [46]). Turning points still appear but are less pronounced when terms of order v^2 are retained. Thus there is a minimum in the $2s$ exchange cross section at 2.25 keV and a maximum and a minimum in the $2s$ direct cross section at 1.5 and 3 keV, respectively. It is apparent from Table 4.1 that the major source of discrepancy between KT and CH is the *consistent* retention by CH, unlike KT, of all terms of order v^2. This is not surprising in that the v^2 terms have a significant influence on the diagonal matrix elements and therefore the phases, which are in turn crucial when combining typically four transition amplitudes. Thus the disagreement between CH and KT is primarily not due to either the different choice of ETFs *nor* to inaccuracies in the numerical calculations as has been suggested [274], [276], [279] but rather to the neglect of some second-order terms by KT.

Table 4.1. Ten state calculations: Cross sections $Q^C(2s)$ and $Q^D(2s)$ in 10^{-17} cm^2 as a function of proton impact energy E (keV) and using the ten-state approximation, respectively, for $H^+ + H(1s) \rightarrow H(2s) + H^+$, $H^+ + H(1s) \rightarrow H^+ + H(2s)$. Boxes indicate turning points

Order v	Order v^2		Order v^2	Order v
$Q^C(2s)$	$Q^C(2s)$	E	$Q^D(2s)$	$Q^D(2s)$
0.085	0.118	1	0.117	0.088
0.133	0.162	1.5	0.191 max	0.151
0.199	0.182	2	0.186	0.207
0.236	0.179 min	2.55	0.179	0.232
0.274	0.187	2.5	0.179	0.254
0.342	0.197	3	0.176 min	0.301
0.577	0.228	4	0.229	0.380

Table 4.2. Eight state calculations (as for Table 4.1, but using the eight-state approximation and including the polarization Π and the cross sections $Q^C(2p)$ and $Q^D(2p)$, respectively, for $H^+ + H(1s) \rightarrow H(2p) + H^+$, $H^+ + H(1s) \rightarrow H^+ + H(2p)$)

Order v^2					
E	$Q^D(2p)$	$Q^C(2p)$	$Q^D(2s)$	$Q^C(2s)$	Π
1.0	2.784	2.844	0.055	0.056	-0.258
2.0	3.021	2.904	0.162	0.159	-0.243
3.0	3.029	2.998	0.283	0.258	-0.225
4.0	2.967	2.949	0.406	0.309	-0.204
5.0	3.012	2.906	0.523	0.341	-0.186
7.0	3.246	3.352	0.689	0.554	-0.166
10.0	4.094	5.743	1.086	1.606	-0.139
Order v					
E	$Q^D(2p)$	$Q^C(2p)$	$Q^D(2s)$	$Q^C(2s)$	Π
1.0	2.959	2.608	0.068	0.069	-0.255
2.0	3.592	3.549	0.264	0.248	-0.234
3.0	4.339	4.254	0.509	0.444	-0.213
4.0	5.048	5.097	0.747	0.640	-0.199
5.0	5.773	6.084	0.952	0.897	-0.191
7.0	7.330	7.932	1.313	1.555	-0.183
10.0	9.496	10.082	1.691	2.787	-0.183

Nevertheless the critical evaluation by KT, of the effect of the switching function f_0 of CH on the $4f\sigma_u$ populations at the higher energies, is valid. This may be gauged implicitly in two ways. First the switching function f_0 of CH was only optimized for the comparatively compact $1s\sigma_g$ and $2p\sigma_u$ orbitals, since they were primarily motivated by the proton–hydrogen large-angle capture probability problem [168]. Since then, of course, it has become widely recognized [176], [177], [305], [306] that state-by-state optimization is required, that is, different switching functions for different molecular states. Thus it is clear that in physical terms for a diffuse orbital like $4f\sigma_u$, the switching function should on average be much closer to the united atoms value of zero than to the CH f_0 choice. Second, and related to this latter point, it may be noted that the $2p\sigma_u$–$4f\sigma_u$ dipole matrix element, which multiples f_0 in the zero-order radial-coupling matrix element, is particularly large.

To gauge the explicit effect, we present in Table 4.2 and Figures[1] 4.1 and 4.2 both direct (D) and capture (C) $2s$ and $2p$ cross sections using eight states ($1s\sigma_g$, $2p\sigma_u$, $3d\pi_g$, $2p\pi_u$, $2s\sigma_g$, $3p\sigma_u$, $4d\pi_g$, $3p\pi_u$). Table 4.2 also includes the polarization. Although the turning points in the direct $2s$ cross section $Q^D(2s)$ have disappeared, the capture $2s$ cross section $Q^C(2s)$ still exhibits a point of inflexion. Moreover, the inclusion of terms of order v^2 in the eight-state calculation clearly improves agreement with the experimental results of Morgan et al. [435] for $Q^C(2p)$ and $Q^D(2p)$ and with Morgan et al. [436] for $Q^D(2s)$. So far as $Q^C(2s)$ is concerned, the effect of

[1] In our original paper [181] these two figures were published incorrectly.

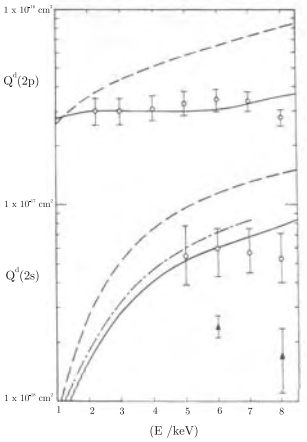

Fig. 4.1. Exchange: Cross sections $Q^C(2s, 2p)$ in square centimeters as a function of proton impact energy E (keV) for the processes $H^+ + H(1s) \rightarrow H(2s, 2p) + H^+$. Theories – · – Kimura and Thorson [353]; – – this work, to order v using eight states; —- this work, to order v^2 using eight states. Experiment: ▲Bayfield [50]; ■ Hill et al. [326]; ○Morgan et al. [435], [436] $Q^C(2p)$, $Q^C(2s)$, respectively

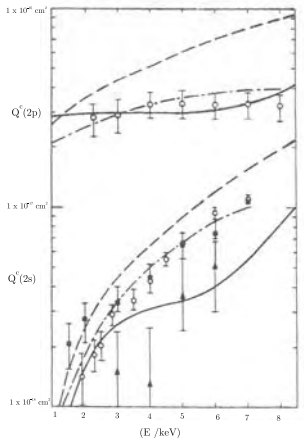

Fig. 4.2. Excitation: Cross sections for $Q^D(2s, 2p)$ in square centimeters as a function of proton impact energy E (keV) for the processes $H^+ + H(1s) \rightarrow H^+ + H(2s, 2p)$. Theories and experiments as for Figure 4.1, but $C \rightarrow D$

including terms of $O(v^2)$ in the KT calculation can only be surmised. However, it is notable that in Figure 4.1 our $Q^C(2s)$, omitting such terms, lies typically 30% to 40% above the analogous KT values, which is precisely the experience of KT. Between 2 and 3 keV our second-order $Q^C(2s)$ favors the experimental values of Morgan et al. [436], but between 5 and 6 keV it continues to favor the experimental values of Bayfield [50] rather than either Morgan et al. or Hill et al. [326]. We have not plotted the apparently only other experimental values of $Q^C(2s)$ given by Chong and Fite [118] since at their lowest energy of measurement $6\,keV$, their value lies above even our first-order results. Above 6 keV there is a reasonable consensus between the 1977 [118], 1979 [326], and 1980 [436] experiments. So far as other theoretical results for $Q^C(2s)$ are concerned, we note that the independent calculations of Lüdde and Dreizler [390], [391], [392] based on molecular pseudostate two-centre spheroidal wave functions of the Hylleraas type, show excellent accord with the differential cross sections of CH. The agreement between Lüdde and Dreizler [392], CH, and KT on differential cross sections and capture probabilities is not surprising, since all three use essentially molecular approaches and large-angle scattering is dominated by the united-atom value of the switching function, namely zero [168]. Interestingly enough, on total cross sections there is also quite good agreement between Lüdde and Dreizler [391] and our eight-state second-order results at 2 and 4 keV. Thus they obtain 0.13 and 0.34 (10^{-17} cm^2) while we obtain (Table 4.2) 0.16 and 0.31, respectively. However, since ETF effects increase at 6 and 8 keV (compare the relative divergence between our first- and second-order results), it is not surprising that their results lie somewhat higher than ours at these higher energies since of course they make no explicit provision for ETFs. The pseudomolecular calculations of Winter and Lin [610] use a 28–36 three-centre expansion comprising orbitals centered on the target and the projectile, each with a classical Bates–McCarroll choice of ETF ($f_0 = 1$) and the midpoint ($f_0 = 0$). Naturally we would not consider this latter choice of ETF to be optimal; nevertheless their result at 2 keV agrees with Lüdde and Dreizler and our present result. At 3 and 6 keV they are much closer to KT and indeed find weak points of inflexion.

Returning to $Q^C(2p)$ in Figure 4.1, we have already noted good agreement between the plotted experimental values of Morgan et al. [435] and our second-order results. Not plotted are the experimental values of Kondow et al. [365], which, above 2 keV, lie somewhat below these other two sets of values. However, below 2 keV we note that our rather flat second-order curve at about 3×10^{-17} cm^2 is in excellent accord with Kondow et al. unlike the curve of KT, which dips rather rapidly to 2×10^{-17} cm^2. We also note a nuance of a dip between 4 and 6 keV, a feature more definitely present in the theoretical result of Lüdde and Dreizler [391] and Winter and Lin [610] described earlier.

On the question of direct excitation (Figure 4.2), the good agreement between our second-order $Q^D(2p)$ and Morgan et al. [435] and between our second-order $Q^D(2s)$ and Morgan et al. [436] must be tempered by the knowledge that both Lüdde and Dreizler [391] and Winter and Lin [610] find rather deep minima in both $Q^D(2p)$ and $Q^D(2s)$ in the region of 8 to 10 keV. Unfortunately, this range is just beyond the reach of our second-order theory, and we must keep an open mind until a calculation

with matrix elements correct to all orders in velocity has been carried out. Nevertheless regarding the polarization Π of Lyman-α emission, associated with direct excitation, our eight state values listed in Table 4.2, with and without second-order contributions, are in fair accord with the first-order values of KT, namely −0.247, −0.212, −0.166, and −0.140 at 1, 3, 5, and 7 keV, respectively. As implied by KT, the discrepancy between our eight state values and the ten state values of CH at the higher energies is entirely due to the latter's inclusion of the diffuse $4f\sigma_u$ orbital with a nonoptimal nondiffuse switching function, as explained earlier. Clearly Π is relatively insensitive to the inclusion of second-order terms.

For completeness, we include as Table 4.3, Table 1 of Crothers and Hughes [168] which gives the turning points in the capture probability at 3° scattering in $H^+ + H(1s)$ collisions in the range 0.7 to 20 keV impact energy. Their results (column 2) agree remarkably well with experiment (Lockwood and Everhart [384]). We also include Figure 3 (Crothers and Hughes [172]) which gives the H(2p) excitation probability in the same $H^+ + H(1s)$ collisions but in the range 125 to 500 eV and plotted as a function of impact parameter. Curve A based on a Coulomb trajectory shows a double-peak structure at 500 eV, in common with Knudson and Thorson [362] and reflecting rotational coupling and symmetric resonance.

We conclude that the calculation of proton–hydrogen excitation and capture cross sections in the low-energy range requires, in the perturbed stationary state (PSS) method, the use of traveling molecular orbitals whose effect must be carried through

Table 4.3. Values of the energy E_T/keV at the turning points of $P_C(E)$ at 3° scattering angle in $H^+ + H(1s)$ collisions

Expt	Theoretical					Type of turning point
(1)	(2)	(3)	(4)	(5)	(6)	
0.78	0.81	0.77	0.81	-	0.80	max
1.11	1.11	1.05	1.09	-	1.10	min
1.57	1.59	1.45	1.55	1.51	1.55	max
2.39	2.40	2.40	2.32	1.96	2.30	min
3.92	3.92	3.15	3.71	2.70	3.70	max
7.69	7.40	5.10	6.65	4.06	-	min
20.1	19.8	9.0	15.0	6.95	-	max

(1) Experiment of Lockwood and Everhart [384]
(2) This work: three-state calculation with momentum translation factors; $f(Z)$ given by (35) of [168]
(3) As in (2) but with $f(Z)$ equal to unity
(4) As in (2) but neglecting momentum translation factors
(5) Ferguson [265]: two-state calculation with the momentum translation factors of Bates and McCarroll [44] using approximate wave functions (π phase change inserted)
(6) Bates and Williams [39]: three-state calculation neglecting momentum translation effects
Note this table may be compared with table 1 of Bransden [86]

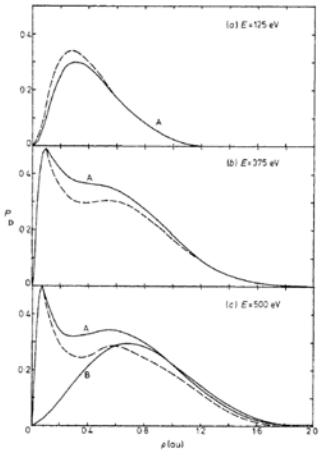

Fig. 4.3. H(2p) excitation probability $P_D(\rho)$ plotted against impact parameter ρ at (a) $E = 125$ eV, (b) $E = 375$ eV, and (c) $E = 500$ eV. Full curve: this work (A, Coulomb trajectory; B, straight line trajectory). Broken curve: Knudson and Thorson [362]

consistently to at least second order in the velocity. We also conclude that Löwdin's method of symmetric orthonormalization of the traveling molecular orbitals is indispensable in this regard. Nevertheless, given the power of modern computers, the ideal algorithm comprises optimization of the switching function for each state and the retention [308], [309], [557] of all functional dependence on v, the velocity, in which case the distinction between Hermitian and non-Hermitian equations becomes academic. We note that unlike pseudostate methods including the AO+ and three-centre atomic orbital (AO) models [274], [275] [276], [610], [381], [277], our approach to low-energy collisions is variational at all steps: the choice of molecular orbitals, the choice of ETF, and the derivation of coupled equations; the only limitation is the inevitable variation–perturbation selection of ETF, which nevertheless is justified by the Löwdin method. We also note that Winter and Lin [610] in their three-centre AO model find the $Q^C(2p)$ results in Figure 4.1 agree more closely (within about 18%) with theirs than to KT and the $Q^D(2p)$ results in Figure 4.1 agree very closely (within 9%) with theirs, except at about 8 keV where our result is 40% higher. Their expansion set included up to 36 hydrogen–like states: on projectile, target, and midpoint $1s$–$3l_{|m|}$ orbitals plus $4p_{|m|}$ and $4f_{|m|}$ on the midpoint.

Capture in H^+, He^{++} collisions with excited H(2s, 2p) is described by Esry et al. [255], with particular reference to formation of capture states H(nl) ($n = 2, 3$) and He^+(nl) ($n = 3, 4$).

Traveling AO are applied by Fritsch [280] to the more complicated symmetric process: He^{2+} + He collisions that involve two electrons. Traveling MO are applied by McCarroll and Piacentini [414] to He^+ + He collisions involving three electrons.

4.2.2 Traveling Molecular HeH^{2+} Orbitals

Introduction

A traveling molecular orbital approach is applied to the $He^{2+} + H \rightarrow He^{+} + H^{+}$ charge transfer process, where translation factors are determined variationally, and where all orders of impact velocity v are preserved. Comparison with experiment and other theories for this low-energy regime are included for total capture and capture into the $He^{+}(2s)$ excited state.

Since the pioneering work of Bates et al. [43] and Ferguson and McCarroll [266], *molecular orbital* (MO) expansions have been employed in close-coupling processes, when the impact velocity v is regarded as small relative to the orbital velocity of the active electron, v_e, but great enough for the semiclassical time-dependent formulation to be valid. These MO wave functions are the exact solutions of the Hamiltonian, when the motion of the nuclei is neglected. Hence, this relative motion of the nuclei is the perturbation causing the transition between *adiabatic* (or *stationary*) states.

Massey and Smith [405] were the first to use the wave version of *perturbed stationary states* (PSS), for exact resonance, while Mott (1931) [442] developed a semiclassical impact parameter version, in which he chose as basis functions

$$\xi_j(\mathbf{r},\, \mathbf{R}) \exp\{-\mathrm{i}\epsilon_j(R)t\} \tag{4.59}$$

where $\xi_j(\mathbf{r}, \mathbf{R})$ is the adiabatic wave function corresponding to the eigenenergy $\epsilon_j(R)$ and $\mathbf{R}$ is the internuclear vector, t is the time, and $\mathbf{r}$ is the electronic coordinate referred to, say, the internuclear midpoint O. Each such adiabatic (or stationary) state will, in principle, have a *separated-atom* limit, centred on either the projectile nucleus B or the target nucleus A, corresponding to a Stark-effected linear combination of atomic states:

$$\begin{aligned} \lim_{R\to\infty} \xi_j = \phi_j^A(\mathbf{r}_A) \qquad & \lim_{R\to\infty} \epsilon_j = \epsilon_j^A(\infty) \\ \text{or} & \\ \lim_{R\to\infty} \xi_j = \phi_j^B(\mathbf{r}_B) \qquad & \lim_{R\to\infty} \epsilon_j = \epsilon_j^B(\infty) \end{aligned} \tag{4.60}$$

where $\mathbf{r}_A$ and $\mathbf{r}_B$ are the position vectors of the electron relative to the target nucleus and projectile nucleus, respectively. Both excitation and charge transfer may be considered as resulting from transitions between adiabatic states.

Bates et al. [43] later reviewed this formulation, and certain theoretical and physical defects were discovered. First, they realized that the eigenenergy should be integrated with respect to time, not merely multiplied.

$$\epsilon_j(R)t \longrightarrow \int_0^t \epsilon_j(\tilde{R})\, \mathrm{d}\tilde{t} \tag{4.61}$$

Second, they discovered that charge transfer transition probabilities depended on the origin of $\mathbf{r}$, violating Galilean invariance. In Mott's theory, the choice of origin for

r, as *A*, *B*, or *O* leads to three different results. In particular, it was possible to have states still coupled at infinity, a situation not only impracticable but also unphysical. To ensure that such couplings are avoided, Bates [34] showed that it was necessary to expand the total wave function as

$$\Psi(\mathbf{r},t) = \sum_j a_j(t)\Psi_j(\mathbf{r},t) \tag{4.62}$$

where

$$\lim_{R\to\infty} \Phi_j = \Psi_j^{A,B} \exp\{\mp\frac{1}{2}\mathrm{i}\mathbf{v}\cdot\mathbf{r} - \mathrm{i}\epsilon_j^{A,B}(\infty)t - \frac{1}{8}\mathrm{i}v^2 t\} \tag{4.63}$$

according to whether the dissociation limit was *A* or *B* (− for *A*, + for *B*) and where Ψ_j is an atomic-state function. For concreteness, the origin was chosen to be at the midpoint of the internuclear axis.

In order that these boundary conditions are matched trivially, Bates and McCarroll [44], [45] chose as their basis functions

$$\Psi_j = \chi_j^{A,B} \exp\left(\mp\mathrm{i}\frac{1}{2}\mathbf{v}\cdot\mathbf{r}\right) \exp\left\{\mathrm{i}\int_0^t \left(\epsilon_j + \frac{1}{8}v^2\right) \mathrm{d}\tilde{t}\right\} \tag{4.64}$$

However, this makes the basis functions nonorthogonal, and while (4.63) is acceptable at large internuclear separations, where the electron is well localized around one or another centre, its motion has more of a molecular nature at short internuclear separations. Of course, at large distances, the choice (4.64) is perfectly reasonable, as the stationary (adiabatic) states can be approximated by an appropriate linear combination of atomic states. To overcome this general criticism, the following basis functions may be chosen [536]:

$$\Phi_j = \chi_j \exp\left(\frac{1}{2}\mathrm{i}f(\mathbf{r},\mathbf{R})\mathbf{v}\cdot\mathbf{r}\right) \exp\left\{-\mathrm{i}\int_0^t \left[\epsilon_j + \frac{1}{8}\int |\chi_j|^2 (\nabla_{\mathbf{r}}\mathbf{v}\cdot\mathbf{r}\, f)^2 \mathrm{d}^3\mathbf{r}\right] \mathrm{d}\tilde{t}\right\} \tag{4.65}$$

where the function f is known as the *switching function* and obeys the following conditions:

$$\lim_{R\to\infty} f(\mathbf{r},\mathbf{R}) = \pm 1 \qquad \text{as} \qquad \mathbf{r} \to \pm\frac{1}{2}\mathbf{R} \tag{4.66}$$

as well as

$$\lim_{R\to\infty} f(\mathbf{r},\mathbf{R}) = o \tag{4.67}$$

Vaaben and Taulbjerg [589], in studying the $He^{2+}H$ charge-transfer process, employed a switching function of the form

$$f(\mathbf{r},\mathbf{R}) = \frac{1}{2}\frac{r_A^3 Z_A - r_B^3 Z_B}{r_A^3 Z_A + r_B^3 Z_B} + \frac{1}{2}\frac{Z_A - Z_B}{Z_A + Z_B} \tag{4.68}$$

where the origin is chosen at the centre of charge. This choice of translation factor reduced discrete–discrete couplings. Their work also highlighted the crucial importance of the choice of the electron translation factor (ETF) at small internuclear separations, since spurious short-range couplings may exist whenever the radial coupling

element is nonvanishing in this limit, i.e., the adiabatic condition is violated. They also concluded that since ETFs form an inherent part of the basis states for the MO expansion, used in seeking a solution to the collision problem, they cannot be solely determined from a unique set of *objective* criteria, and hence that the ad hoc choice of common translation factors is, accordingly, likely to remain a matter of dispute.

Winter [602] also studied He^{2+} – H collisions, where a coupled-state approach was taken using large triple-centre bases centred on the two nuclei and a third centre was chosen to be the equiforce point (saddle point of the potential) between the nuclei. The following linear combination of traveling atomic orbitals on three centres was used:

$$\Psi(\mathbf{r},t) = \sum_{k,\alpha} a_{k\alpha}(\rho,t)\psi_{k\alpha}(\mathbf{r}_\alpha(\mathbf{r},t)) \exp(-\mathrm{i}E_{k\alpha}t + \mathrm{i}q_\alpha \mathbf{v}\cdot\mathbf{r} - \frac{1}{2}\mathrm{i}q_\alpha^2 v^2 t^2) \tag{4.69}$$

where α denotes the centre A (= H^+), B (= He^{2+}) or C and the translation factor q_α is given by

$$q_\alpha \begin{cases} -\frac{1}{2}\,, & \alpha = A \\ +\frac{1}{2}\,, & \alpha = B \\ p - \frac{1}{2}\,, & \alpha = C \end{cases} \tag{4.70}$$

where

$$p = \frac{\sqrt{Z_A}}{\sqrt{Z_A} + \sqrt{Z_B}} \tag{4.71}$$

Errea and co-workers in a series of papers [245], [246], [253] used common translation factors (CTF) and the second of these applied the so-called *norm method* to He^{2+} – H collisions. The method is based on the minimization of a measure of all dynamical couplings between the states included in, and omitted from, the molecular expansion. Using the Euclidean norm:

$$N^2[U_n] = \sum_{m=1}^{\aleph} \left\| Q\left[\mathrm{i}\left.\frac{\partial}{\partial t}\right|_{\mathbf{r}} - H_{el}\right] P\phi_m \exp\left[\mathrm{i}\left(U_m - \int_0^t E_m \,\mathrm{d}\tilde{t}\right)\right]\right\|^2 \tag{4.72}$$

where P is the projector operator over the manifold spanned by the set of functions $\phi_n e^{\mathrm{i}U_n}$; $n = 1,\ldots,\aleph$; and $Q = 1 - P$ and where overlap effects are taken into account. Thus, $N[U_n]$ is minimized for each nuclear trajectory, within a trial space for U_n and for a group manifold $\phi_n; 1,\ldots,\aleph$. The translation factors are thus viewed as providing the smallest set of couplings from P to Q space.

In their application to He^{2+} + H(1*s*) collisions, they chose a common translation factor with two adjustable parameters:

$$f(\mathbf{r},\mathbf{R}) = \frac{R}{R^2+\beta^2}\left[\mathbf{r}\cdot\hat{\mathbf{R}} + (p-p_0)R\right] - (p-p_0) \tag{4.73}$$

where the origin of electronic coordinates is situated a distance pR from the helium nucleus. The trial space for the CTF is defined by two parameters β and p_0, which have the physical interpretation that β defines the extent of a cutoff factor in f , and

$(p - p_0)R$ is the distance between the arbitrary origin of electronic coordinates in their system and a fixed point on the internuclear axis, situated a distance p_0R from the helium nucleus.

Haansen et al. [317] employed a common translation factor in calculating electron-capture cross sections in ion collisions, C^{4+}, N^{5+}, O^{6+} with atomic hydrogen. For a tour de force on CTFs, see Elizaga et al. [241]. While results compared with experiment were favourable at low impact velocities ($v_0 \leq 1$ au), the calculated cross sections fail to show the steep decline indicated by the experimental data. Newby [452] reinforced this conclusion by showing that the calculated cross sections for the $He^{2+} + H \rightarrow He^{+}(n = 2) + H^{+}$ reaction also failed to fall off rapidly, and at higher velocities the differences between results became very sensitive to the choice of translation factor. It is clear that if a uniform model capable of producing accurate cross sections is required at both low and high impact velocities, more elaborate translation factors must be employed. This is reinforced by the work of Errea et al. [250], [248], [249], [254], [247], of Harel et al. [321], [320], and of McCarroll and Crothers [413]. Our work is not intended to compete, at energies above that at which the maximum total cross section occurs, with the continuum-distorted-wave method, which in itself is a dynamic molecular model. Moreover, at chemical, thermal, and very low energies, Eckart, reaction, or hyperspherical coordinates are useful alternatives (McCarroll and Crothers [413]. For a discussion of ion–molecule reactions, see Lindinger et al. [383].

Theory

The first to consider a fully variational approach were Riley and Green [511]. They considered a number of alternative proposals, each of which resulted in impracticable complexity, where the switching functions in principle were to be obtained simultaneously with the transition amplitudes, satisfying a system of coupled nonlinear equations. This scheme was not implemented for a semiclassical impact parameter treatment.

We consider

$$He^{2+} + H(1s) \longrightarrow He^{+} + H^{+} \tag{4.74}$$

not only because it is a benchmark process for differing theoretical approaches to atomic collisions, but also because it is important in the study of thermonuclear fusion and in astrophysical processes. It has been studied experimentally by Fite et al. [270], Keever and Everhart [350], Bayfield and Khayrallah [51], Shah and Gilbody [544], and Nutt et al. [462]. It had been studied theoretically, using PSS formulations, by Piacentini and Salin [490], [491], Hatton et al. [322], Winter and Lane [609], Vaaben and Taulbjerg [589], Winter and Hatton [608], Newby [452], Errea et al. [246], and Winter [602].

In considering the process (4.74) switching functions are derived by averaging over the electronic coordinate, endorsing the argument put forward by Crothers and Hughes [168], [173], [172], [171], that the purpose of the translation factor is to represent the translation of the electron, due purely to motion of the nuclei. The

electron's orbital motion will be described, as in the standard PSS and Bates and McCarroll formulation, by the adiabatic or molecular wave functions.

Considering the general collision system, within the semiclassical impact parameter treatment, the total wave function may be expressed as a linear combination of basis functions

$$\Psi(\mathbf{r}, t) = \sum_j c_j(t)\Phi_j(\mathbf{r}, t) \tag{4.75}$$

where the basis functions are given by

$$\Phi_j(\mathbf{r}, t) = \chi_j(\mathbf{r}, \mathbf{R})T_j(\mathbf{R}, \mathbf{r})E_j(t) \tag{4.76}$$

where $\chi_j(\mathbf{r}, \mathbf{R})$ is the exact adiabatic wave function satisfying

$$\left(-\frac{1}{2}\nabla^2_{\mathbf{r}} - \frac{Z_A}{r_A} - \frac{Z_B}{r_B}\right)\chi_j = \epsilon_j\chi_j \tag{4.77}$$

where $E_j(t)$ is an energy phase factor, and where $T_j(\mathbf{R}, \mathbf{r})$ is an electronic translation factor given by

$$T_j = \exp(\mathrm{i} f_j \mathbf{v} \cdot \mathbf{r}) \tag{4.78}$$

where f_j is the *switching function* for each independent state j. Crothers and Todd [176] noted, on the grounds that any two states normally only couple at specific nonadiabatic separations (unlike the symmetric resonance case, where the electron resonates to and fro continually between the two principal states), each state should have its own associated switching function, similar to the work of Riley and Green [511] and Ponce [495]. Crothers and Todd allowed for a greater flexibility by allowing the switching function to be a function of the *internuclear vector* $\mathbf{R}$ and not the *internuclear distance R*. Nevertheless, in this argument, $f_j\mathbf{v}$ continues to represent the effective velocity of the electron for any particular orientation $\hat{\mathbf{R}}$ of the molecule, the orbital velocity implicitly being described by the adiabatic wave function χ_j.

Derivation of Coupled Equations and VTFs

We can now apply the variational principle to obtain, first, the coupled equations and second, the switching functions. With the wave function defined by (4.76), satisfying the Schrödinger equation, we have (see Section 1.3)

$$\delta I = 0 \tag{4.79}$$

where

$$I = \int_{-\infty}^{\infty} \mathrm{d}t \left\langle \Phi \left| H_e - \mathrm{i}\frac{\mathrm{d}}{\mathrm{d}t} \right| \Phi \right\rangle = 0 \tag{4.80}$$

By considering arbitrary variations in c_j^*, we have the condition, consistent with (4.80), that

$$\left\langle \frac{\partial \Phi}{\partial c_j} \left| H_{el} - \mathrm{i}\frac{\mathrm{d}}{\mathrm{d}t_{\mathbf{r}}} \right| \Phi \right\rangle = 0 \tag{4.81}$$

By varying c_j, we obtain the standard coupled equations in matrix form

$$\mathrm{i}\mathbf{S}\dot{c} = \mathbf{H}\mathbf{c} \tag{4.82}$$

where

$$S_{lj} = \left\langle \Phi_l | \Phi_j \right\rangle \tag{4.83}$$

and

$$H_{lj} = \left\langle \Phi_l \left| H_{el} - \mathrm{i}\frac{\mathrm{d}}{\mathrm{d}t_{\mathbf{r}}} \right| \Phi_j \right\rangle \tag{4.84}$$

We note that $S_{jj} = 1$ and that if $H_{jj} = 0$, then the c_j will be well behaved.

Now we wish to include all orders of velocity and to derive an expression for the matrix elements used in the coupled equations. We use expression (4.76) for the basis functions, where

$$E_j(t) = \exp\left(-\mathrm{i}\int_0^t \left(\epsilon_j + \frac{1}{2}v^2 f_j^2 + v^2 \frac{\mathrm{d}f_j}{\mathrm{d}Z_{\mathbf{r}}}\langle \chi_j | z | \chi_j \rangle\right) \mathrm{d}\tilde{t}\right) \tag{4.85}$$

is the energy phase factor and

$$T_j(\mathbf{r}, \mathbf{R}) = \exp(\mathrm{i} f_j(\mathbf{R})\mathbf{v} \cdot \mathbf{r}) \tag{4.86}$$

is the electron translation factor, and $\chi_j(\mathbf{r}, \mathbf{R})$ satisfies (4.77). Substituting (4.77) into (4.84), we have

$$H_{lj} = \langle \chi_l(\mathbf{r}, \mathbf{R}) T_l(\mathbf{r}, \mathbf{R}) E_l(t) | H_{el} - \mathrm{i}\frac{\mathrm{d}}{\mathrm{d}t_{\mathbf{r}}} | \chi_j(\mathbf{r}, \mathbf{R}) T_j(\mathbf{r}, \mathbf{R}) E_j(t) \rangle \tag{4.87}$$

If we consider (4.87), the second term simplifies to

$$-\mathrm{i}\frac{\mathrm{d}}{\mathrm{d}t_{\mathbf{r}}} | \chi_j(\mathbf{r}, \mathbf{R}) T_j(\mathbf{r}, \mathbf{R}) E_j(t) \rangle = -\left(\epsilon_j + \frac{1}{2}v^2 f_j^2(\mathbf{R}) + v^2 \frac{\mathrm{d}f_j}{\mathrm{d}Z_{\mathbf{r}}}\langle \chi_j | z | \chi_j \rangle\right) \tag{4.88}$$

$$\times E_j T_j \chi_j - \mathrm{i}v E_j T_j \left[\frac{\mathrm{d}\chi_j}{\mathrm{d}Z_{\mathbf{r}}} + \mathrm{i}v z \chi_j \frac{\mathrm{d}f_j}{\mathrm{d}Z_{\mathbf{r}}}\right] \tag{4.89}$$

Similarly, the first term of (4.87) can be simplified to

$$E_j(t) T_j(\mathbf{r}, \mathbf{R}) \left[\epsilon_j \chi_j(\mathbf{r}, \mathbf{R}) - \mathrm{i} f_j(R) v \frac{\partial \chi_j}{\partial z} + \frac{1}{2} f_j^2(R) v^2 \chi_j(\mathbf{r}, \mathbf{R})\right] \tag{4.90}$$

Therefore, using equations (4.89) and (4.90), we have

$$\left(H_{el} - \mathrm{i}\frac{\mathrm{d}}{\mathrm{d}t_{\mathbf{r}}}\right) | \Phi_j \rangle = E_j(t) T_j(\mathbf{r}, \mathbf{R}) \left[-\mathrm{i}v \frac{\mathrm{d}\chi_j}{\mathrm{d}Z_{\mathbf{r}}} + v^2 z \chi_j(\mathbf{r}, \mathbf{R}) - \mathrm{i} f_j(\mathbf{R}) v \frac{\partial \chi_j}{\partial z}\right. \tag{4.91}$$

$$\left. - v^2 \frac{\mathrm{d}f_j}{\mathrm{d}Z_{\mathbf{r}}} \langle \chi_j | z | \chi_j \rangle \chi_j \right]. \tag{4.92}$$

Now using equation (4.92), we have

$$H_{lj} = \langle \Phi_l | H_{el} - \mathrm{i}\frac{\mathrm{d}}{\mathrm{d}t_{\mathbf{r}}} | \Phi_j \rangle = -\mathrm{i}v\langle \chi_l(\mathbf{r},\mathbf{R}) | T_{lj}\left(\frac{\mathrm{d}}{\mathrm{d}Z_{\mathbf{r}}} + f_j\frac{\partial}{\partial z}\right)|\chi_j(\mathbf{r},\mathbf{R})\rangle E_j E_l^*$$
$$+v^2\langle \chi_l(\mathbf{r},\mathbf{R}) | T_{lj}(z - \langle \chi_j | z | \chi_j \rangle)\frac{\mathrm{d}f_j}{\mathrm{d}Z_{\mathbf{r}}}|\chi_j(\mathbf{r},\mathbf{R})\rangle E_j E_l^* \tag{4.93}$$

where

$$T_{lj} = T_l^* T_j = \exp(\mathrm{i}f_{lj}(\mathbf{R})\mathbf{v}\cdot\mathbf{r}) \tag{4.94}$$

and

$$f_{lj} = f_l - f_j \tag{4.95}$$

Note that if we approximate to order v, we obtain

$$H_{lj} = -\mathrm{i}v\langle \chi_l(\mathbf{r},\mathbf{R})|\frac{\partial}{\partial Z_{\mathbf{r}}} + f_j\frac{\partial}{\partial z}|\chi_j(\mathbf{r},\mathbf{R})\rangle E_j E_l^* \tag{4.96}$$

in agreement with Crothers and Todd [176].

If, in the separated-atom limit, the electron is attached to the same nucleus for both states l and j, then

$$f_l - f_j \sim 0 \qquad (t \to \pm\infty) \tag{4.97}$$

otherwise

$$f_l - f_j \sim \pm 1 \qquad (t \to \pm\infty) \tag{4.98}$$

positive if l is on the target and j is the projectile, and negative if vice versa.

Derivation of Switching Functions

We employ the same derivation and argument as Crothers and Todd [176], where each state has its own independent switching function f_j regarded as a function of the internuclear vector $\mathbf{R}$. By employing the standard Euler–Lagrange variational technique for arbitrary variations δf_j, the following expression for f_j is obtained:

$$f_j = \frac{\langle \chi_j | z\frac{\mathrm{d}}{\mathrm{d}Z_{\mathbf{r}}}|\chi_j\rangle - \sum_k \langle \chi_j | z | \chi_k\rangle\langle \chi_k | \frac{\mathrm{d}}{\mathrm{d}Z_{\mathbf{r}}}|\chi_j\rangle}{-\langle \chi_j | z\frac{\mathrm{d}}{\mathrm{d}z}|\chi_j\rangle - \sum_k \langle \chi_j | z | \chi_k\rangle\langle \chi_k | \frac{\mathrm{d}}{\mathrm{d}z}|\chi_j\rangle} + O(v) \tag{4.99}$$

Expression (4.99) is in terms of stationary-frame matrix elements, and these can be transformed into terms involving the moving molecular-frame matrix elements. In particular,

$$f_j(Z,\rho) = \frac{Z^2 R_1 + \rho^2 T_1}{Z^2 R_2 + \rho^2 T_2} \tag{4.100}$$

where

$$R_1 = \langle \chi_j | z' \frac{\partial}{\partial R_{\mathbf{r}}} | \chi_j \rangle - \sum_k \langle \chi_j | z' | \chi_k \rangle \langle \chi_k | \frac{\partial}{\partial R_{\mathbf{r}}} | \chi_j \rangle \tag{4.101}$$

$$R_2 = -\langle \chi_j | z' \frac{\partial}{\partial z'} | \chi_j \rangle + \sum_k \langle \chi_j | z' | \chi_k \rangle \langle \chi_k | \frac{\partial}{\partial z'} | \chi_j \rangle \tag{4.102}$$

$$T_1 = \langle \chi_j | x' \left(-\frac{\mathrm{i}}{R} L_{y'} \right) | \chi_j \rangle - \sum_{k'} \langle \chi_j | x' | \chi_{k'} \rangle \langle \chi_{k'} | - \frac{\mathrm{i}}{R} L_{y'} | \chi_j \rangle \tag{4.103}$$

$$T_2 = -\langle \chi_j | x' \frac{\partial}{\partial x'} | \chi_j \rangle + \sum_{k'} \langle \chi_j | x' | \chi_{k'} \rangle \langle \chi_{k'} | \frac{\partial}{\partial x'} | \chi_j \rangle \tag{4.104}$$

Here $\mathbf{r}'$ is referred to the rotating frame of reference ($y = y'$) so that all matrix elements involved in equations (4.101)–(4.104) may be evaluated as triple integrals over the prolate spheroidal coordinates, λ, μ and ϕ, that is, $(r_A \pm r_B)/R$ and the azimuthal angle relative to the collision plane.

In practice, since we wish only to perform a five-state close-coupling calculation, $j \in \{2s\sigma, 2p\sigma, 2p\pi, 3d\sigma, 3d\pi\}$, the dummy indices k' and k are allowed to run over all appropriate states in the first four united-atom principal shells. In practice, the ϕ integrals can be evaluated analytically, and they provide selection rules that mean k' and k differ for any given j, and in general states that couple radially, do not couple rotationally, and vice versa. The partitioning of the coupled states facilitates the investigation of two intermediary functions, namely,

$$R_j = \frac{R_1}{R_2} = f_j(R, 0) \tag{4.105}$$

which is obtained by setting $\rho = 0$ in equation (4.100); setting $Z = 0$ in (4.100), we obtain the second intermediary function

$$T_j = \frac{T_1}{T_2} = f_j(0, R) \tag{4.106}$$

Calculation Details

The first step is to calculate the normalized wave functions and their derivatives. The wave function can be expanded in terms of prolate spheroidal coordinates, and, by making use of a program by Power [497], the wave functions may be calculated. Full details of the expansions and calculation can be found in the thesis of McCaig [407]. Having calculated the normalized wave functions, we may then proceed to calculate the switching functions, given by (4.101)–(4.104). These expressions are given in terms of the coordinates of the moving molecular frame. They must be transformed into expressions involving prolate spheroidal coordinates, λ, μ, and ϕ, so that we can easily calculate expressions (4.101)–(4.106). We can simplify some of the expressions by noting that the first terms of equations (4.102) and (4.104) consist of the matrix elements

$$\langle \chi_j | z' \frac{\partial}{\partial z'} | \chi_j \rangle = -\frac{1}{2} \tag{4.107}$$

Table 4.4. Radially coupled states

States j	Coupled states k
$2s\sigma$	$1s\sigma$, $2p\sigma$, $3s\sigma$, $3p\sigma$, $3d\sigma$, $4s\sigma$, $4p\sigma$, $4d\sigma$, $4f\sigma$
$2p\sigma$	$1s\sigma$, $2s\sigma$, $3s\sigma$, $3p\sigma$, $3d\sigma$, $4s\sigma$, $4p\sigma$, $4d\sigma$, $4f\sigma$
$2p\pi$	$3p\pi$, $3d\pi$, $4p\pi$, $4d\pi$, $4f\pi$
$3d\sigma$	$1s\sigma$, $2s\sigma$, $2p\sigma$, $3s\sigma$, $3p\sigma$, $4s\sigma$, $4p\sigma$, $4d\sigma$, $4f\sigma$
$3d\pi$	$2p\pi$, $3p\pi$, $4p\pi$, $4d\pi$, $4f\pi$

Table 4.5. Rotationally coupled states

States j	Coupled states k'
$2s\sigma$	$2p\pi$, $3p\pi$, $3d\pi$, $4p\pi$, $4d\pi$, $4f\pi$
$2p\sigma$	$2p\pi$, $3p\pi$, $3d\pi$
$2p\pi$	$2s\sigma$, $2p\sigma$, $3s\sigma$, $3p\sigma$, $3d\sigma$
$3d\sigma$	$2p\pi$, $3p\pi$, $3d\pi$, $4p\pi$, $4d\pi$, $4f\pi$
$3d\pi$	$3d\delta$, $4d\delta$, $4f\delta$

and

$$\langle \chi_j | x' \frac{\partial}{\partial x'} | \chi_j \rangle = -\frac{1}{2} \tag{4.108}$$

Also, the matrix element

$$\langle \chi_k | \frac{\partial}{\partial R_{\mathbf{r}}} | \chi_j \rangle \tag{4.109}$$

may be simplified by using the commutator relationships of Ponomarev and Puzynina [496]. However, the awkward numerical differentiation involved in the first term of (4.101) must be performed, as detailed in the previous section. By using the transformations of appendix B of McCaig [407], the matrix elements of equations (4.104)–(4.108) may be performed as triple integrals over λ, μ, and ϕ. The ϕ integration in practice is performed analytically and provides "selection rules." This reduces the computation required in the summations, as k and k' differ from j, and the expressions for R_1 and R_2 effectively only allow $\sigma \to \sigma$ and $\pi \to \pi$ radial couplings, while expressions for T_1 and T_2 only allow for $\sigma \to \pi$ and $\pi \to \delta$ rotational couplings. This may be summed up in Tables 4.4 and 4.5, which show which states are coupled to each of our five principal states in the calculation.

With the expressions for R_1, R_2, T_1, and T_2 we may calculate the intermediary functions given by (4.105) and (4.106). Figure 1 of [408] shows R_j as a function of internuclear distance R, while figure 2 of [408] similarly shows T_j.

The first observation is that the boundary conditions inherent in the derivation are satisfied, namely

$$\lim_{R \to \infty} R_j = \pm \frac{1}{2} \tag{4.110}$$

$$\lim_{R \to \infty} T_j = \pm \frac{1}{2} \tag{4.111}$$

and so

$$\lim_{|R|\to\infty} f_j(\mathbf{R}) = \pm\frac{1}{2} \tag{4.112}$$

The second observation is that all the switching functions have the same united-atom limit, namely

$$\lim_{R\to 0} R_j = -\frac{1}{6} \qquad \forall j \tag{4.113}$$

$$\lim_{R\to 0} T_j = -\frac{1}{6} \qquad \forall j \tag{4.114}$$

which imply that

$$\lim_{R\to 0} f_j(\mathbf{R}) = -\frac{1}{6} \qquad \forall j \tag{4.115}$$

The limit expressed in (4.115) is in accordance with our interpretation of the purpose of translation factors, as in the united-atom limit the electron classically orbits the centre of charge and so will have an effective translation equivalent to that of the centre of charge relative to the origin. This argument gives a value of $-1/6$, when the origin is situated at the internuclear midpoint.

We can also see from figures 1 and 2 of [408] that as the principal quantum number of the united atom increases the further out will the switching functions represent the behaviour of the centre of charge. We note that classically, for $3d\pi$, the molecule is formed for $R < 21.728$ (au) so it is perhaps surprising that the behaviour of $3d\pi$ as close in as 12 au shows that the effective translation of the electron is still associated with the He^{2+} nucleus.

The seemingly unphysical behaviour of the $2s\sigma$, $2p\sigma$, and $2p\pi$ switching functions at zero impact parameter can be seen to quickly disappear when the impact parameter increases (figures 3–5 of [408]). By using the more general form given in equation (4.100), we may calculate the switching functions for various values of impact parameter. Figures 3–7 of [408] show the switching functions for our five principal states, for a variety of impact parameters. These are included for completeness, to show precisely the exact variation with respect to internuclear R of each of our five state-dependent switching functions f_j, used in the calculation of S_{lj} and H_{lj} matrix elements.

It is worth noting that for $2p\sigma$ and $3d\sigma$ (figures 4 and 6 of [408]), it was particularly important to include $1s\sigma$ and $4f\sigma$, respectively, as these exhibit the special non-crossings of one-electron molecules.

Calculation of S_{lj} and H_{lj} Matrix Elements

The interaction matrix elements H_{lj} are given by the expression

$$H_{lj} = \langle \Phi_l | H_{el} - \mathrm{i}\frac{\mathrm{d}}{\mathrm{d}t_{\mathbf{r}}} | \Phi_j \rangle \tag{4.116}$$

To evaluate these matrix elements, we must transform them into expressions in prolate spheroidal coordinates. First we obtain the first term of H_{lj} to be

$$H_{lj} = -\mathrm{i}v\langle\chi_l|\exp(-\mathrm{i}f_{lj}vB)\left\{\frac{Z}{R}\frac{\partial}{\partial R_{\lambda,\mu}} + P\frac{\partial}{\partial\lambda} + Q\frac{\partial}{\partial\mu} + R\frac{\partial}{\partial\phi}\right\}|\chi_j\rangle E_l^* E_j \tag{4.117}$$

where the coefficients P, Q, and R are given by

$$P = \frac{Z}{R^2}\frac{(\lambda^2-1)}{\lambda^2-\mu^2}\{-\lambda + 2\mu f_j\} + \frac{\rho}{R^2}\frac{\sqrt{(\lambda^2-1)(1-\mu^2)}}{\lambda^2-\mu^2}\cos\phi\{-\mu + 2\lambda f_j\} \tag{4.118}$$

$$Q = \frac{Z}{R^2}\frac{(1-\mu^2)}{\lambda^2-\mu^2}\{-\mu + 2\lambda f_j\} + \frac{\rho}{R^2}\frac{\sqrt{(\lambda^2-1)(1-\mu^2)}}{\lambda^2-\mu^2}\cos\phi\{\lambda - 2\mu f_j\} \tag{4.119}$$

$$R = \frac{\rho}{R^2}\frac{\sin\phi}{\sqrt{(\lambda^2-1)(1-\mu^2)}}\{\lambda\mu - 2f_j\} \tag{4.120}$$

and where B is given by

$$B = \frac{Z}{2}\lambda\mu + \frac{\rho}{2}\sqrt{(\lambda^2-1)(1-\mu^2)}\cos\phi \tag{4.121}$$

Now we look at the second term of (4.116). Using the appropriate transformations, we find that this term can be written as

$$v^2\langle\chi_l|\exp(-\mathrm{i}f_{lj}vB)\{B - \langle\chi_j|B|\chi_j\rangle\}\left(\frac{Z}{R}\frac{\partial f_j}{\partial R_r} + \frac{\rho}{R^2}(-\mathrm{i}L_{y'})f_j\right)|\chi_j\rangle E_l^* E_j \tag{4.122}$$

where B is given by (4.121). Now, since we also have

$$\frac{\partial f_j}{\partial\lambda} = \frac{\partial f_j}{\partial\mu} = \frac{\partial f_j}{\partial\phi} = 0 \tag{4.123}$$

(4.122) simplifies to

$$v^2\langle\chi_l|\exp(-\mathrm{i}f_{lj}vB)\{B - \langle\chi_j|B|\chi_j\rangle\}\frac{Z}{R}\frac{\mathrm{d}f_j}{\mathrm{d}R}|\chi_j\rangle E_l^* E_j \tag{4.124}$$

Adding (4.117) and (4.124) gives the complete expression for evaluating the interaction matrix elements in terms of prolate spheroidal coordinates. We write the matrix elements in the following form:

$$H_{lj} = \tilde{H}_{lj}E_l^* E_j \tag{4.125}$$

where $\tilde{H}_{lj}$ become the integrals from equations (4.117) and (4.124). To evaluate these integrals, we take one term at a time. The terms of equation (4.117) involving $\partial/\partial\lambda$ give

$$-\mathrm{i}v\int_1^\infty\int_{-1}^1\int_0^{2\pi}\Lambda_l M_l\Phi_l\exp(-\mathrm{i}f_{lj}vB)\left\{\frac{ZR}{8}(\lambda^2-1)(-\lambda+2\mu f_j)\right.$$
$$\left.+\frac{\rho R}{8}\sqrt{(\lambda^2-1)(1-\mu^2)}\cos\phi[-\mu+2\lambda f_j]\right\}\frac{\mathrm{d}\Lambda_j}{\mathrm{d}\lambda}M_j\Phi_j\mathrm{d}\lambda\mathrm{d}\mu\mathrm{d}\phi \tag{4.126}$$

The terms involving $\partial/\partial\mu$ give

$$-\mathrm{i}v\int_1^\infty\int_{-1}^1\int_0^{2\pi}\Lambda_l M_l\Phi_l\exp(-\mathrm{i}f_{lj}vB)\left\{\frac{ZR}{8}(1-\mu^2)(-\mu+2\lambda f_j)\right.$$
$$\left.+\frac{\rho R}{8}\sqrt{(\lambda^2-1)(1-\mu^2)}\cos\phi[\lambda+2\mu f_j]\right\}\Lambda_j\frac{\mathrm{d}M_j}{\mathrm{d}\mu}\Phi_j\mathrm{d}\lambda\mathrm{d}\mu\mathrm{d}\phi \tag{4.127}$$

The terms involving $\partial/\partial\phi$ give

$$-\mathrm{i}v\frac{\rho}{8}\int_1^\infty\int_{-1}^1\int_0^{2\pi}\Lambda_l M_l\Phi_l\exp(-\mathrm{i}f_{lj}vB)\left\{\frac{(\lambda^2-\mu^2)(\lambda\mu-2f_j)}{\sqrt{(\lambda^2-1)(1-\mu^2)}}\sin\phi\right\}$$
$$\times\Lambda_l M_l\frac{\mathrm{d}\Phi_j}{\mathrm{d}\phi}\mathrm{d}\lambda\mathrm{d}\mu\mathrm{d}\phi \tag{4.128}$$

The terms involving $\partial/\partial R_{\lambda\mu}$ give

$$-\mathrm{i}v\frac{ZR^2}{8}\int_1^\infty\int_{-1}^1\int_0^{2\pi}\Lambda_l M_l\Phi_l\exp(-\mathrm{i}f_{lj}vB)[\lambda^2-\mu^2]\Phi_j$$
$$\times\left\{M_j\frac{\partial\Lambda_j}{\partial R_{\lambda\mu}}+\Lambda_j\frac{\partial M_j}{\partial R_{\lambda\mu}}\right\}\mathrm{d}\lambda\mathrm{d}\mu\mathrm{d}\phi \tag{4.129}$$

The integral involved in equation (4.124) is written as

$$v^2\frac{ZR^2}{8}\int_1^\infty\int_{-1}^1\int_0^{2\pi}\Lambda_l M_l\Phi_l\exp(-\mathrm{i}f_{lj}vB)\{B-\langle\chi_j|B|\chi_j\rangle\}$$
$$\times(\lambda^2-\mu^2)\frac{\mathrm{d}f_j}{\mathrm{d}R}\Lambda_j M_j\Phi_j\mathrm{d}\lambda\mathrm{d}\mu\mathrm{d}\phi \tag{4.130}$$

Equations (4.126)–(4.130) give the integrals involved in calculating the interaction matrix elements. Since we differ from low-order velocity approximations by essentially retaining all orders of velocity inherent in the $\exp(-\mathrm{i}f_{lj}\mathbf{v}\cdot\mathbf{r})$ term, we can see the increased computational difficulty in expressions (4.126)–(4.130). The integrals were performed by using a nested-loop Legendre quadrature technique, where the range of the integrals must be transformed to $\{-1,1\}$. By using an appropriate number of subinterval divisions for each variable in the integrand, an accuracy of at least 1.0×10^{-4} was maintained.

Now consider the overlap matrix elements given by

$$S_{lj}=\langle\Phi_l|\Phi_j\rangle \tag{4.131}$$

By using the expression for Φ_j given by (4.76), we find that if $l=j$ so that $f_l=f_j$ we have that

$$S_{jj}=\langle\chi_j|\chi_j\rangle E_j^*E_j=1 \tag{4.132}$$

as before. The overlap matrix elements can be written in prolate spheroidal coordinates as

$$S_{lj} = \langle \chi_j | \exp(-\mathrm{i} f_{lj} v B) | \chi_j \rangle E_l^* E_j \tag{4.133}$$

where B and f_{lj} are given as before, and by writing

$$S_{lj} = \tilde{S}_{lj} E_l^* E_j \tag{4.134}$$

we may evaluate S_{lj} by calculating the integral

$$\tilde{S}_{lj} = \frac{R^3}{8} \int_1^\infty \int_{-1}^1 \int_0^{2\pi} \Lambda_l M_l \Phi_l \exp\{-\mathrm{i} f_{lj} v B\} (\lambda^2 - \mu^2) \Lambda_j M_j \Phi_j \mathrm{d}\lambda \mathrm{d}\mu \mathrm{d}\phi \tag{4.135}$$

Application, Results, and Conclusions

Having shown how to calculate the wave function, state-dependent switching functions, and the interaction and overlap matrix elements, we solve the coupled equations

$$\mathrm{i}\mathbf{S}\dot{\mathbf{c}} = \mathbf{H}\mathbf{c} \tag{4.136}$$

By retaining the $\exp(\mathrm{i} f_j(\mathbf{R})\mathbf{v} \cdot \mathbf{r})$ term in the wave function, we have a nonorthogonal basis set and a non-Hermitian $\mathbf{H}$ matrix. Effectively we cannot analytically rearrange the coupled equations. We can integrate the coupled equations numerically using a computer program developed by Shampine and Gordon [551], which can solve problems of the type

$$\dot{\mathbf{c}} = \mathbf{A}\mathbf{c} \tag{4.137}$$

Therefore we may write

$$\mathbf{A} = -\mathrm{i}\mathbf{S}^{-1}\mathbf{H} \tag{4.138}$$

It must be stressed that in practice the $\mathbf{S}$-matrix is inverted at every time step in the integration. The coupled equations can be integrated with the following initial conditions:

$$\begin{aligned} c_1(-\infty) &= 1 \\ c_j(-\infty) &= 0 \qquad \forall j (\neq = 1) \end{aligned} \tag{4.139}$$

where

$$\begin{aligned} j &= 1 \equiv \mathrm{H}(1\mathrm{s}) \\ j &= 2 \equiv \mathrm{He}^+(2\mathrm{p}_1) \\ j &= 3 \equiv \mathrm{He}^+(2\mathrm{s}) \\ j &= 4 \equiv \mathrm{He}^+(3\mathrm{p}_1, 3\mathrm{d}_1) \\ j &= 5 \equiv \mathrm{He}^+(2\mathrm{p}_0) \end{aligned} \tag{4.140}$$

For the actual numerical procedure of solving the coupled equations (4.137), it is necessary to choose Z_c (+ve) such that $\mathrm{d}|c_j|^2/\mathrm{d}Z$ is negligible for $Z > Z_c$. We can then integrate from $Z = -Z_c$ to $Z = Z_c$ (usually in the range 50-100 au).

The **H**-matrix depends on both v and ρ, which gives us transition amplitudes also dependent on v and ρ. The matrix elements were calculated at a mesh of 0.25 a.u., in the velocity range 3-31 keV and for impact parameters in the range 0-10 a.u. (with a finer mesh for small impact parameters, which are important at lower energies). Obviously the boundary conditions become

$$\begin{aligned} c_1(-Z_c) &= 1 \\ c_j(-Z_c) &= 0 \qquad \forall j \end{aligned} \tag{4.141}$$

We calculate cross sections by evaluating

$$Q = 2\pi \int_0^{\rho_{max}} P_j(\rho)\rho \mathrm{d}\rho \tag{4.142}$$

where

$$P_j(\rho) = |c_j(Z_c)|^2 \tag{4.143}$$

is the probability for a transition to a state on nucleus A or B to which j tends in the separated-atom limit for a given impact parameter ρ (these limits are shown in figure 8 of [408]) and where $\rho_{\max}$ was chosen to be 10 a.u. and was in practice sufficient; because the matrix elements were relatively difficult to calculate, it was impractical to allow ρ to vary too arbitrarily, and so ρ-values were chosen at certain intervals in the range $0 \leq \rho \leq \rho_{\max}$. Hence the integration was performed using Simpson's rule.

Total Capture

The total capture cross-section results of this five-state calculation, retaining all orders of velocity, are shown in figure 9 of [408]. The experimental data are the results of Bayfield and Khayrallah [51] and Shah and Gilbody [544]. The energy range of the calculation shown is $3-31$ keV. We can see that there is excellent agreement with the experimental data of Shah and Gilbody [544] (which have been normalized for $^4He^{2+}$ energy), even in a range beyond the typical domain of low-energy collisions.

Table 4.6. Total capture cross section data. Winter and Hatton [608] – ten-molecular-state calculation with plane-wave translation factor. Winter [602] – 15-state triple-centre basis set. Kimura and Thorson [353] – ten-state close-coupling calculation with Bates–McCarroll translation factors. Errea et al. [246] – four-state calculation with common translation factor, using simplified norm method. Shah and Gilbody [544] – experimental data ($^3He^{2+}$ renormalized for $^4He^{2+}$ energy). 20 keV has been interpolated from given data

Total Capture						
Energy (keV)	Winter (1980)	Winter (1988)	KT (1981)	Errea (1987)	This calculation	Shah and Gilbody (1978)
3	1.49		1.43		1.51	
8	6.01	5.9	6.15		6.09	6.0
20	10.8	11.1	11.23	11.48	11.01	11.09

Table 4.7. $He^+(2s)$ production cross section data. Winter and Hatton [608] – ten-molecular-state calculation with plane-wave translation factor. Winter [602] – 15-state triple-centre basis set. Kimura and Thorson [353] – ten-state close-coupling calculation with Bates–McCarroll translation factors. Errea et al. [246] – four-state calculation with common translation factor, using simplified norm method. Shah and Gilbody [544] – experimental data ($^3He^{2+}$ renormalized for $^4He^{2+}$ energy). 20 keV has been interpolated from given data

$He^+(2s)$ Production						
Energy (keV)	Winter (1980)	Winter (1988)	KT (1981)	Errea (1987)	This calculation	Shah and Gilbody (1978)
3	0.397				0.51	
8	1.27	1.32	1.21		1.29	0.96
20	2.37	2.17	2.18	2.51	2.05	1.44

At these higher energies we should expect terms of order v^2 and above to have more of an effect. Table 4.6 shows some comparison with other theories for some common low energies.

At 3 keV we can see that there is general agreement among the three values shown, while at 8 keV there is close agreement with Winter and Hatton [608] and Kimura and Thorson [353], while the absolute difference between experiment and the result of Winter [602] is also comparable with differences between experiment and other theories. Using a 24-state basis, Winter obtains a value of 6.33×10^{-16} cm^2, which appears to have a greater error than the 15-state basis set.

At the common energy of 20 keV, there are a number of theoretical predictions with which to make comparisons. We see that there is excellent agreement between this work and the calculations of Winter [602] and the experimental results of Shah and Gilbody [544], while the Bates–McCarroll translation factor formulation of Kimura and Thorson [353] differs by only a few percent. If we look at the results of Kimura and Thorson [353] and Errea et al. [246], we see that translation factors become more important and that a variational approach, while hardly sacrosanct, provides a better framework than more common types of translation factor. However, we may note close agreement with the 66-state CTF results of Harel et al. [320].

$He^+(2s)$ *Production*

In Figure 4.4b results for $He^+(2s)$ are shown, and we can see that agreement with the experimental data points is not so good. In fact, like the theories of Winter and Hatton [608], Kimura and Thorson [353], Errea et al. [246], Winter [602], and Harel et al. [320], results lie well above experiment. In Table 4.7 our five-molecular-state $He^+(2s)$ production cross sections and other theories are presented at the impact energies of 3.8 and 20 keV. At 3 keV there is some discrepancy between the current result and that of Winter and Hatton, but at 8 keV agreement in the results of Winter and Hatton [608], Kimura and Thorson [353], Winter [602], and the present results is

very good. However, there is still some discrepancy (around 26%) with experiment. At 20 keV there is a discrepancy of almost 30%, though our results, while in general agreement with Winter [602] and Kimura and Thorson [353] (around 6%), do not overestimate as much as other theories. Winter and Hatton [608] have suggested that it is more difficult to extract this excited-state cross section if plane wave factors are neglected. It is therefore possible that variational translation factors may result in a better estimation, and perhaps for energies above 15 keV, and as we approach 25 keV (1 au), that terms in v of order higher than two are required. Also it may be that the use of an atomic basis set is inappropriate in this energy range, since both total capture and $He^+(2s)$ production are overestimated. Since there is long-range coupling among the three states $2s$, $2p_{0,1}$, this requires that the coupled equations are integrated to a large chosen value of Z_c, where, of course, $Z = vt$.

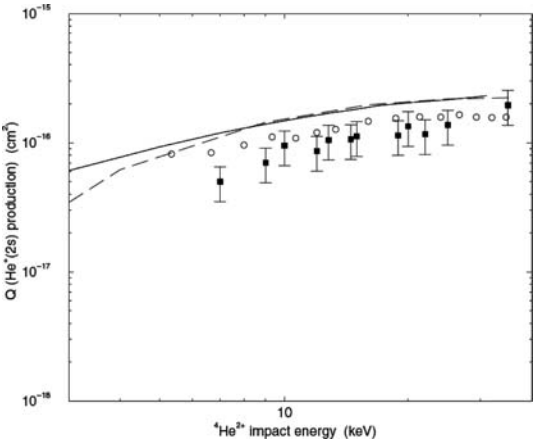

Fig. 4.4a. Total capture cross sections for the He^{2+} + H collision energy; this calculation(—), Bayfield and Khayrallah [51] (○), Shah and Gilbody [544] (■), Harel et al. [320](– – –)

Conclusions

We have applied variational translation factors to full order in v, to the He^{2+}-H charge transfer process. Agreement in the total capture was excellent, and the five-state molecular approach is comparable to the ten-state Bates–McCarroll plane wave translation factor formulation of Winter and Hatton [608], the triple-centre 15-state atomic basis approach of Winter [602] and the 66-state CTF treatment of Harel et al. [320]. Also this seems to provide a much more favourable approach than the four-molecular-state approach using the simplified norm method with common translation factor of Errea et al. [246]. Moreover, the employment of traveling MOs seems to provide better agreement for $He^+(2s)$ production than other atomic orbital formulations. This is not to say that further experimentation would be redundant. The variational switching functions provide a better alternative than other ad hoc approaches,

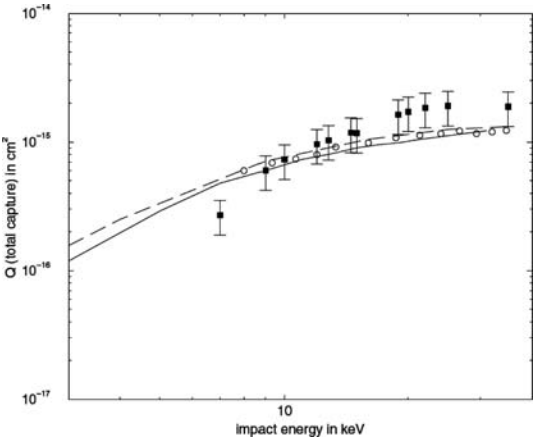

Fig. 4.4b. Cross section for He^{2+} production, for $^4He^{2+}$ collision energy: this calculation (—), Bayfield and Khayrallah [51] (○), Shah and Gilbody [544] (■), Harel et al. [320](– – –)

while retaining matrix elements to full order in v yields better agreement with experiment than theories that have "averaged" to order v [589] or v^2 [176], [177], at energies beyond 15 keV where terms of order higher than v^2 are expected to become more important.

However, calculation of the variational switching functions and the accompanying matrix elements becomes somewhat unwieldy and requires much greater computational effort than simply "averaging" over order v or v^2. The nature of this computation could make application to much higher energies and to other ion–atom collision systems such as (C^{6+}-H) problematic. For order v calculations on capture in O^{6+}-He collisions, see Shimakura et al. [553], where the two-electron system requires use of the pseudopotential method.

4.2.3 Traveling Atomic Orbitals

As we have seen in our discussion, molecular H_2^+ and HeH^{2+} orbitals are well suited to low-collisional-impact energies. Excellent reviews of the measurement of slow - and fast (nonrelativistic) energy ion–atom collisions are given by Gilbody [295], [296], [446]; capture and ionization in slow H^+, He^{2+}+He collisions [550], excitation in He^{2+} + H collisions at intermediate energies [332], and charge transfer and single and double ionization in fast He^{2+} + He collisions are all measured.

For intermediate to high-energy (nonrelativistic) collisions we can expect the interactions to be comparatively fleeting and so accordingly we can expect traveling-atomic-orbital semiclassical impact-parameter treatments to be valid, with the use of close coupling and pseudostates.

This is a vast subject so we shall be content to mention the review of McGuire [419] and the work of the influential groups of Bransden, of Lin and of Winter, in particular Slim et al. [564], [565], [566], Shingal and Lin [555], [556], Jain and Winter

[339] and Winter [603], [604], [605], [606], [607]. Proceses include single and double capture, excitation, ionization, transfer excitation, and ionization and excitation-ionization depending on whether we have one or two active electrons. Cross sections and (Shingal and Lin [556]) density matrices are calculated. Fritsch and Lin [279] report that Winter uses Sturmian pseudostates.

4.3 Continuum Distorted Waves and Their Generalizations

4.3.1 Introduction

In Section 4.1 we considered traveling molecular orbitals that reduce at large times, impact velocities, and impact parameters, to traveling atomic orbitals. However, another dynamic molecular theory is the continuum-distorted-wave (CDW) theory [112], [62], [63], [192], which describes a three-body collision involving charge transfer, excitation, and/or ionization. It is molecular because all three Coulomb interactions are treated nonperturbatively, in either the wave or the semiclassical impact parameter treatment. Of course the three-body problem cannot in general be solved exactly. The perturbation is the nonorthogonal kinetic energy comprising a negative dipole-dipole differential operator. Thus each dipole includes radial and rotational coupling in its own frame. Accordingly no singularities arise and there is no elastic divergence [191] since the dipole-dipole operator connects all three particles ensuring a connected kernel in the integral equations. Both short- and long-range boundary conditions are satisfied and, with the inclusion of ETFs, Galilean and gauge invariance are guaranteed. This generalizes to Lorentz invariance, in Section 4.4. The CDW wave functions themselves are on-(energy) shell [192]. The CDW Neumann–Born series encapsulates [187] all of this, where it is understood that the initial and final states in the wave treatment include the appropriate plane waves for the relative internuclear motion.

By using generalized nonorthogonal coordinates the use of logarithmic potentials is transparently avoided. One of the advantageous aspects of the early use of CDWs in the wave treatment was that the core six-dimensional integral separated into two three-dimensional integrals. Early doubts about CDW were dispelled when Crothers [184], [185] showed that second-order CDW fully describes Thomas resonance double scattering. However, it had also been shown [178] that the fundamental defect of bare CDW theory was that, apart from the final state in ionization, the CDW functions were unnormalized. However even this defect it transpired could be circumvented by a full semiclassical variational Jacobi–Sil treatment leading to coupled equations with detailed balance, unitarity (flux conservation) and lack of post-prior discrepancy while avoiding spurious nonlocal potentials [93], [94]. Other advantages of CDW are that strong and intermediate-continuum coupling is automatically included, and in the case of the final ionized state, the description is uniformly two-centred while much of so-called post-collision interaction is included [179], [110]. This is of particular importance to saddle electrons and to electron capture to the continuum (of the projectile). Generalizations of CDW to include electron correlation are: the use of Hartree–Fock–Roothan–Roeti independent electron orbitals

[260], [471], the independent-event model [189], generalized CDW [197], complete four-body formulation [484], and the CDW formulation (sometimes referred to as BBK) of light-particle collisions [178]. A good introduction to CDW methods is given in [84].

4.3.2 Charge Transfer

Simple electron capture processes are studied using an orthonormal two-state continuum-distorted-wave (CDW) basis. The suitability of the basis set is tested by comparing predictions for total and differential cross sections with available experimental data. Overall good agreement is obtained, and it is concluded that a relatively small CDW basis set may be suitable to model a wide variety of low-energy collisions if the members of this extended set are astutely chosen.

Charge-transfer processes are of fundamental interest to physicists studying a wide range of phenomena in astrophysics, where the displacement of electrons effects the behavior of all interstellar gases [154], and to plasma physics where edge effects, in part due to electron transfer, have detrimental consequences on the process of thermonuclear fusion [398]. Concurrent improvement in the accuracy of detection methods, like photon emission spectroscopy (PES) and translational energy spectroscopy (TES), has allowed charge transfer to be studied at the lowest impact energies leading to a wealth of experimental data being available. Unfortunately the development of theoretical models has not advanced at the same pace, and while models exist that can produce reliable cross sections for charge transfer at moderate and high energies there is little consensus at impact energies below 1 keV amu^{-1} [586].

The purpose of this discussion is to assess the suitability of a continuum-distorted-wave based model to study charge transfer. As already discussed, the advantages of this treatment are many-fold. A fully orthogonal and normalized CDW basis set is used when deriving the appropriate coupled equations. This feature ensures that probability is conserved throughout the collision and that estimates for cross sections remain sensible regardless of the impact velocity.

First we consider resonant collisions where the entrance and exit channels of the active electron are both 1s states and the transfer of the electron leaves the binding energy of the electron unchanged. This transfer process should be dominant during the collision, and the coupling between the entrance and exit channels will be much stronger than in any other reaction path. Hence a two-state approximation should be valid and any error in the results can be attributed to the use of a CDW basis set rather than to the truncation of the total wave function to two terms.

In the semiclassical straight-line impact parameter representation the initial-(i) and final-(f) state wave functions:

$$\psi_i(\boldsymbol{r},t) = N(\nu_P)\varphi_i(\boldsymbol{r_T})\exp(-\mathrm{i}\varepsilon_i t - \frac{\mathrm{i}\boldsymbol{v}\cdot\boldsymbol{r}}{2} - \frac{\mathrm{i}v^2 t}{8}) \times {}_1F_1(\mathrm{i}\nu_P;1;\mathrm{i}(vr_P + \boldsymbol{v}\cdot\mathbf{r_P}))(vR - v^2 t)^{\frac{\mathrm{i}Z_T Z_P}{v}} \tag{4.144}$$

$$\psi_f(\boldsymbol{r},t) = N^*(\nu_T)\varphi_f(\boldsymbol{r_P})\exp(-\mathrm{i}\varepsilon_f t + \frac{\mathrm{i}\boldsymbol{v}\cdot\boldsymbol{r}}{2} - \frac{\mathrm{i}v^2 t}{8}) \times {}_1F_1(-\mathrm{i}\nu_T;1;-\mathrm{i}(vr_T + \boldsymbol{v}\cdot\boldsymbol{r_T}))(vR + v^2 t)^{\frac{-\mathrm{i}Z_T Z_P}{v}} \tag{4.145}$$

are used to construct a fully orthogonal basis set to describe the collision:

$$P^{Z_P+} + T^{(Z_T-1)+}(1s) \rightarrow P^{(Z_P-1)+}(nl) + T^{Z_T+} \tag{4.146}$$

where φ_i and φ_f are representations of the motion of the single electron present in the appropriate undisturbed state and the remaining variables are defined in Crothers [178]. In a two-state approximation the total wave function for this collision can be written as:

$$\Psi(\boldsymbol{r},t) = c_i(\boldsymbol{\rho},t)\hat{\psi}_i + c_f(\boldsymbol{\rho},t)\hat{\psi}_f \tag{4.147}$$

where:

$$\hat{\psi}_i = \frac{\psi_i}{\sqrt{\langle\psi_i|\psi_i\rangle}} \tag{4.148}$$

$$\hat{\psi}_f = a(\boldsymbol{\rho},t)\psi_i + b(\boldsymbol{\rho},t)\psi_f \tag{4.149}$$

$$a(\boldsymbol{\rho},t) = \frac{-s_{if}}{\sqrt{s_{ii}}\sqrt{s_{ii}s_{ff} - s_{if}s_{fi}}} \tag{4.150}$$

$$b(\boldsymbol{\rho},t) = \sqrt{\frac{s_{ii}}{s_{ii}s_{ff} - s_{if}s_{fi}}} \tag{4.151}$$

$$s_{jk}(\boldsymbol{\rho},t) = \langle\psi_j|\psi_k\rangle \tag{4.152}$$

$$s_{kj}(\boldsymbol{\rho},t) = s_{jk}(\boldsymbol{\rho},t)^* \tag{4.153}$$

$$\langle\hat{\psi}_j|\hat{\psi}_k\rangle = \delta_{jk} \tag{4.154}$$

Defining

$$H = -\frac{1}{2}\nabla_{\boldsymbol{r}}^2 - \frac{Z_T}{r_T} - \frac{Z_P}{r_P} + \frac{Z_P Z_T}{R}\ , \tag{4.155}$$

and applying the variational principle of Sil [560],

$$\delta\int_{-\infty}^{+\infty} dt\langle\Psi(\boldsymbol{r},t)|H - \mathrm{i}\frac{d}{dt}|\Psi(\boldsymbol{r},t)\rangle = 0 \tag{4.156}$$

to the coefficients $c_i(\boldsymbol{\rho},t)$ and $c_f(\boldsymbol{\rho},t)$, it can be deduced that the coupled equations governing the system are:

$$\mathrm{i}\frac{d}{dt}c_i(\boldsymbol{\rho},t) = c_i(\boldsymbol{\rho},t)\langle\hat{\psi}_i\big|(H-\mathrm{i}\frac{d}{dt})\big|\hat{\psi}_i\rangle + c_f(\boldsymbol{\rho},t)\langle\hat{\psi}_i\big|(H-\mathrm{i}\frac{d}{dt})\big|\hat{\psi}_f\rangle \tag{4.157}$$

$$\mathrm{i}\frac{d}{dt}c_f(\boldsymbol{\rho},t) = c_i(\boldsymbol{\rho},t)\langle\hat{\psi}_f\big|(H-\mathrm{i}\frac{d}{dt})\big|\hat{\psi}_i\rangle + c_f(\boldsymbol{\rho},t)\langle\hat{\psi}_f\big|(H-\mathrm{i}\frac{d}{dt})\big|\hat{\psi}_f\rangle \tag{4.158}$$

which is a result identical to one obtained by a second-order Euler–Lagrange method.

In order to solve the coupled equations it is necessary to evaluate the matrix elements:

$$s_{jk}(\boldsymbol{\rho},t) = \langle\psi_j|\psi_k\rangle \tag{4.159}$$

and

$$h_{jk}(\boldsymbol{\rho},t) = \langle\psi_j|(H-i\frac{d}{dt})|\psi_k\rangle \tag{4.160}$$

This is done by treating $\mathbf{r_P}$, $\mathbf{r_T}$, and t as generalized nonorthogonal coordinates in a manner similar to the method used in Crothers [178]. As the entrance and exit channels in this discussion are both 1*s* states, the matrix element $h_{fi}^{1s-1s}(\boldsymbol{\rho},t)$ is evaluated here explicitly with the evaluation of the elements $S_{if}^{1s-1s}(\boldsymbol{\rho},t)$ and $h_{if}^{1s-1s}(\boldsymbol{\rho},t)$ being achieved using the standard Nordsieck integral [461]. If $\mathbf{q}$ is expressed in terms of cylindrical polar coordinates the angular dependence is contained entirely in the exponential term and thus one integration can be performed analytically and the resulting function is *independent* of the orientation of the vector $\boldsymbol{\rho}$. Unfortunately the matrix elements $s_{jj}^{1s-1s}(\rho,t)$ and $h_{kk}^{1s-1s}(\rho,t)$ do not lend themselves to calculation via a Fourier transform and are most efficiently evaluated as they stand, using a parabolic coordinate system with the origin chosen so that the number of evaluations of the Kummer function is minimized. These integrals could be reduced to a lower dimension but the method is tedious and does not give any significant advantage numerically. The remaining quantities required can be deduced using Hermiticity.

The probability amplitude associated with electron capture to the state ψ_f at impact parameter $\boldsymbol{\rho}$ is defined as $c_f(\boldsymbol{\rho}, t=+\infty)$. The capture probability $|c_f(\boldsymbol{\rho}, t=+\infty)|^2$ will be independent of the orientation of the collision plane with respect to any fixed plane including the incident polar axis and the cross section σ, for capture to this state is simply defined as:

$$\sigma = 2\pi\int_0^\infty \rho|c_f(\rho, t=+\infty)|^2 d\rho \tag{4.161}$$

It should be noted that the total cross section for capture is independent of the term $Z_P Z_{T/R}$, which could have been removed from equation (4.155) by means of a simple transformation. Consequently the phase factors $(vR-v^2t)^{iZ_TZ_P/v}$ and $(vR+v^2t)^{-iZ_TZ_P/v}$ could have been omitted from $\psi_i\mathbf{r},t)$ and $\psi_f(\mathbf{r},t)$.

In ion–atom collisions many important quantities need to be measured in order to accurately compare experimental data and theoretical predictions. The more quantities that can be measured the more stringent a test may be placed upon the theoretical predictions and thus assess their suitability at describing a particular physical situation. Otherwise the unmeasured quantities must be integrated over all possible values and possibly mask important insights and hinder understanding of the associated problem. For this reason, predictions of differential cross sections are much more useful than that of total cross sections. The differential cross section $\mathrm{d}\sigma/\mathrm{d}\Omega$ in the straight-line impact parameter formulation is calculated from McCarroll and Salin [415] and is defined by (4.38).

The preceding theory, now called CDW2S, is applied to two of the most basic resonant charge-transfer processes: first to electron capture between atomic hydrogen and a proton and second to a collision between a singly charged helium ion and a helium atom. In the first collision the total cross section, σ_T, has been estimated using the n^{-3} scaling law [466]:

$$\sigma_T \approx 1.202\sigma_{1s\to 1s} \tag{4.162}$$

The second collision, involving the helium nuclei, presents the dilemma of how to model the motion of the electrons present. As CDW2S is not yet sufficiently versatile to account for the motion of two electrons simultaneously the helium atom (ion) is approximated using a hydrogen-like atom (ion) with an appropriately chosen charge. This charge is chosen using a variational principle so that the energy levels of the electron in the replacement system and that in the helium atom coincide. In both cases a multiplying factor is used to account for the fact that two electrons are available for capture.

The differential cross sections as a function of laboratory scattering angle are shown in Figures 4.5a and 4.5b at impact energies of 25 and 60 keV, respectively, along with the appropriate estimates of Martin et al. [402].

Generally, accord with experimental values for σ_T is good with the CDW2S theory differing by no more than 10% over the energy range considered, and it is noted that the use of an orthonormal basis set has resulted in the estimates remaining realistic regardless of impact energy in contrast to previous CDW-based models where lack of unitarity results in severely excessive cross sections as the impact velocity decreases.

A more rigorous test of the theory is provided by comparing estimates for differential cross sections with experimental values. In this respect agreement is excellent at energies of 25 and 60 keV, especially at the smaller scattering angles, and though the level of accuracy does decrease as θ increases, the CDW2S estimates do fall off at a rate comparable to experiment. Thus in relation to this collision it is concluded that most of the physics of the problem has been included in the theory.

The CDW2S method described here is a definite improvement over many of the other existing models for studying charge transfer [585] at lower collision energies where results are in excellent agreement with experiment. The implementation of the model is relatively easy, providing reliable cross sections in relation to experiment over a wide range of collision energies. As the original CDW states become

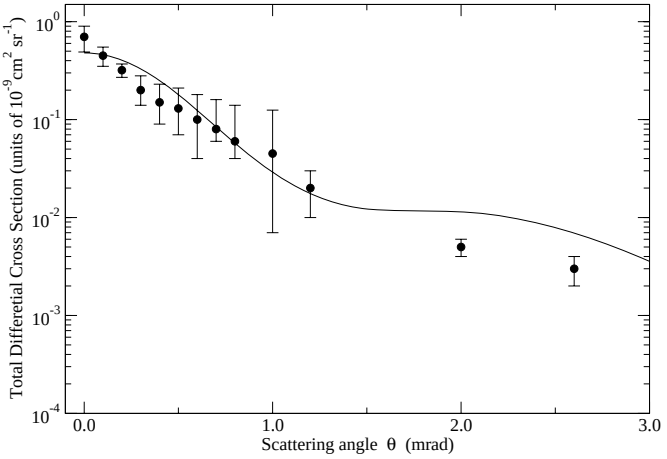

Fig. 4.5a. Differential cross sections $d\sigma_T/d\Omega$ measured in the center of mass frame, at an impact energy of 25keV for electron capture by H^+ from $H(1s)$. Theory; *solid line*: **CDW2S** (this work)

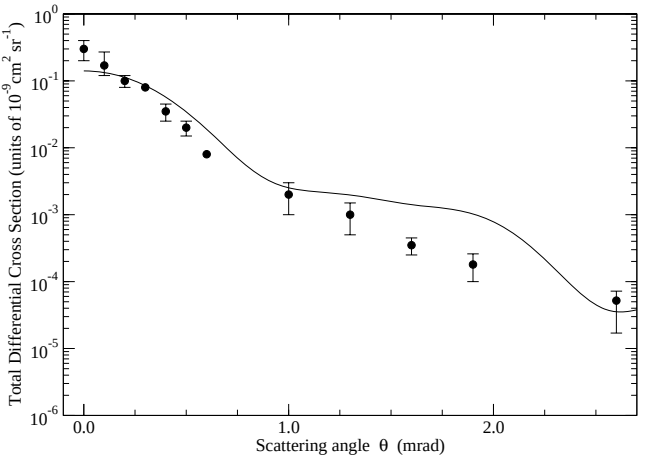

Fig. 4.5b. Total differential cross sections $d\sigma_/d\Omega$ measured in the center of mass frame, at an impact energy of 60keV for electron capture by H^+ from $H(1s)$. Theory; *solid line*: **CDW2S** (this work). Experiment; *circles*: Martin et al. [402]

orthonormal as $v \rightarrow \infty$ the quantity $\dot{s}_{if}$ becomes negligible at high impact energies. Unsurprisingly then the CDW2S approximation concurs with the unnormalized CDW theory of Cheshire [112] and the previously proven symmetrized variational CDW theory of Brown and Crothers [93] at collision energies above 70 keV. At very low energies there is good accord with the Firsov approximation [268], [150].

Overall, the following inferences are drawn from the study. First a CDW-based model will provide accurate cross sections only if all the dominant exit channels are explicitly included in the calculation. Thus to successfully model electron transfer between multiply charged ions it may be necessary to extend the basis set to include all the states whose energy levels lie in close proximity to that of the entrance channel. Without this refinement the model will fail regardless of the type of basis set used. The most notable feature of the model presented is that it adheres to the law of probability conservation at all times. Previous CDW-based models have ignored the fact that in general the appropriate CDW functions are neither orthogonal nor normalized. While it may be valid to disregard this fact at moderate- to high-impact energies the effect of this assumption becomes more pronounced as the energy decreases. This may lead to excessively large cross sections, like those in Crothers and Dunseath [188], and to unexpected features in the differential cross sections [64]. Thus the use of a fully orthonormal basis set is an essential component in any low-energy CDW approximation.

In conclusion, CDW2S [82] represents a sound platform on which to base future research. CDW (2S) is a dynamic molecular theory [346], [347] in which the equivalent of PSS radial and rotational coupling is the proverbial dipole–dipole coupling.

However, for the system

$$H^+ + H(1s) \rightarrow H(1s,2s,2p) + H^+ \tag{4.163}$$

a basis set (CDW4S) of dimension 4, consisting of the ground states of both heavy particles as well as the $2s$ and $2p$ states of the projectile, is used [83]. An adaptive Runge–Kutta fifth order method is employed to solve the appropriate coupled equations with the stability of the method tested by comparing results when the relevant tolerances are increased by one order of magnitude. To illustrate the fact that the $n = 2$ capture channels have relatively little influence on the overall capture cross section the capture profiles for this calculation and from an identical method using only the ground states of both charge centres, at 16keV, is shown in Figure (4.6a). Clearly the introduction of the extra states has had little effect, and this demonstrates the fact that the coupling between the two ground states is the dominant process throughout this collision.

Figure (4.6b) shows the total capture cross section predicted by this theory for the collision given by equation (4.163) compared with the experimental values from Janev and Smith [341] and the theoretical results from a unitarized traveling atomic orbital (UTAO) expansion due to McCarroll [412]. Unsurprisingly the accord is excellent with this theory and experiment, differing by no more than 15% over the energy range considered. Although not shown, the resonant capture cross sections from this theory trivially converge to other CDW, possibly unnormalized, models e.g., Belkić [61] at impact energies above 100 keV amu^{-1}, due to the fact that the

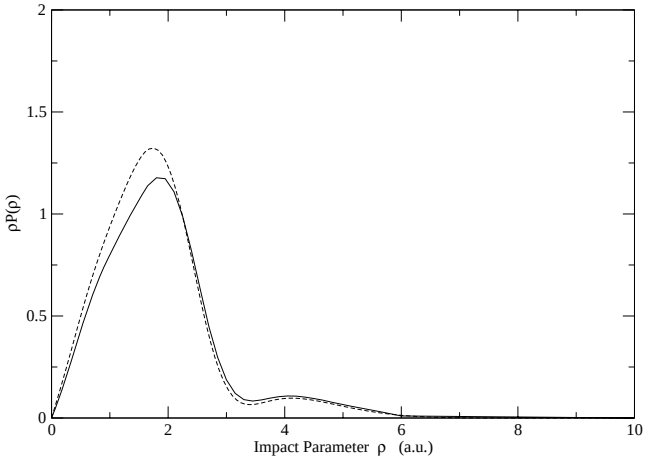

Fig. 4.6a. Weighted probability of electron capture, $\rho P(\rho)$, against impact parameter, ρ at 16 keV for re [illegible] oxi-mation (th

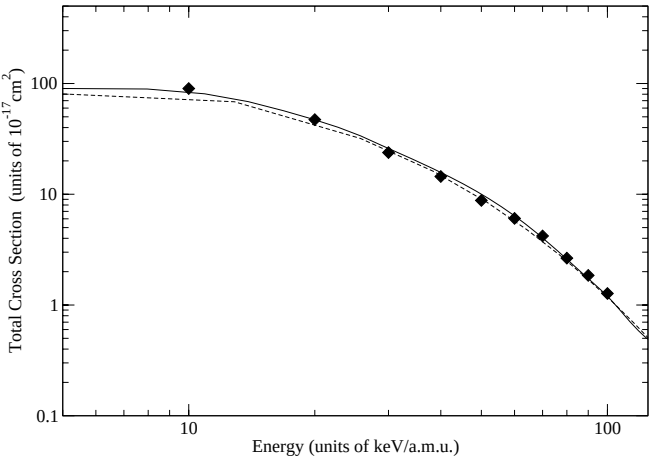

Fig. 4.6b. Total cross section for electron capture from the ground state of the target during $p - H$ collisions. *solid line*: CDW4S approximation (this work); *diamonds*: UTAO expansion from McCarroll [412]; *dashed line*: experiment (Janev and Smith [341])

wave descriptions are inherently orthogonal as $v \to \infty$, a region in which the quantity $\mathrm{d}/\mathrm{d}t \langle \psi_j | \psi_k \rangle$ becomes negligible. At high energies the agreement of this and other CDW models with experimental total cross sections is not found in most of the AO expansions (e.g., [412]). These methods consistently overestimate total capture cross sections as the velocity of the projectile increases, due to charge transfer essentially only occurring at small impact parameters and the single-centre nature of the basis set used.

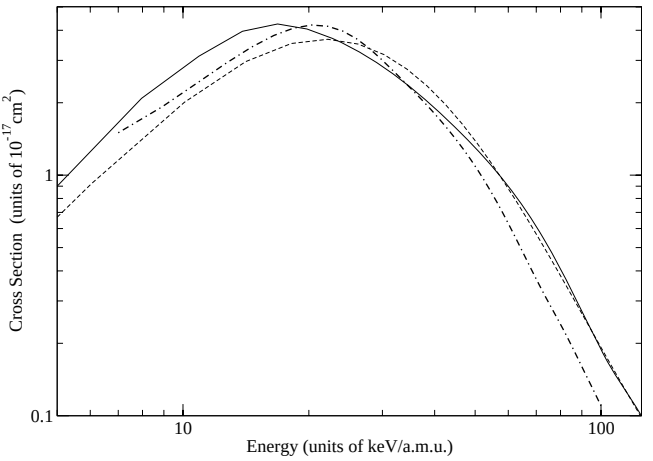

Fig. 4.7a. Cross section for electron capture to the 2*s* state of the projectile from the ground state of the target during $p - H$ collisions. *Solid line*: **CDW4S** approximation (this work); *dot-dashed line*: **SVCDW** of Brown and Crothers [94]; *dashed line*: experiment (Janev and Smith [341])

In Figures (4.7a) and (4.7b) the partial cross sections for electron capture to the 2*s* and 2*p* states respectively are shown. Reliable prediction of these quantities is a much more intricate task due to the fact that these processes are overshadowed by the resonant $1s^{\mathrm{T}} \leftrightarrow 1s^{\mathrm{P}}$ transition channel. However, the approximation performs adequately at the lower energies, while falling off in accordance with the experimental values of Janev and Smith [341] as the impact energy becomes large. At first glance it can be seen that the results of Brown and Crothers [94] do not compare as favourably to the experimental results of Janev and Smith [341] at impact energies above 50 keV amu^{-1} as those from the CDW4S ansatz presented here, even though Brown and Crothers [94] have included twice as many channels in their calculation. Had this approximation been able to utilize a similarly sized basis set it would have been expected that the corresponding results would move closer to experiment, especially at lower impact energies. It is surprising that agreement between the two CDW capture theories is not better at intermediate- and high-impact energies when considering nonresonant electron capture, but this may be how the discontinuity in the wave functions at the point of closest approach manifests itself in the SVCDW calculation. Unfortunately these $n = 2$ cross sections are generally too large, especially at lower impact velocities. This cannot be attributed to the use of a straight-line path for the trajectory of the incoming projectile as previous experiments by Hill et al. [326] have shown that the use of equivelocity hydrogen isotopes has little effect on capture cross sections at the energies considered. A more plausible explanation may be the fact that the possibility of electron excitation from the ground state of the target has been excluded. The electron is confined to the $n = 1$ state of the target, increasing the possibility of charge transfer when in physical reality excitation may be a distinct possibility. This is reinforced by the fact that a detailed study of

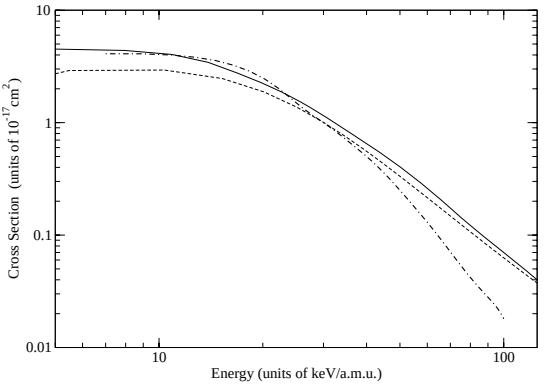

Fig. 4.7b. Cross section for electron capture to the $2p$ state of the projectile from the ground state of the target during $p - H$ collisions. *Solid line*: **CDW4S** approximation (this work); *dot-dashed line*: **SVCDW** of Brown and Crothers [94]; *dashed line*: experiment (Janev and Smith [341])

the collision at an individual impact parameter *suggests* that the electron does not arrive at the $n = 2$ states of the projectile directly but that the nonresonant states are populated predominantly by excitation from the ground state of the projectile. The architecture of the basis set has allowed the electron freedom to move between all bound states included and indeed certain virtual ionized states. In agreement with Brown and Crothers [94] it is observed that, at the velocities considered, the $n = 2$ states contribute more than 12% of the total cross section for the capture process. To highlight how the basis set has affected the calculation it is noted that the intrinsic orthonormality has resulted in the quantity $\sum_{\text{states}} |c_i(\boldsymbol{\rho}, t)|^2$ deviating by no more than 1×10^{-4} from unity at all times and impact parameters. Hence the difficulties associated with the fact that certain matrix elements, e.g., $s_{1s1s}(\boldsymbol{\rho}, t)$, may diverge as $t \to +\infty$ and $v \to 0$ are overcome.

In conclusion, before highlighting the reasons for the present theory's success it is prudent to point out the aspects of the approximation that the authors find unsatisfactory. The most obvious deficiency is the lack of target-centred excited states used in the basis set. The homonuclear collision studied is highly symmetric, and it would have been advantageous to use a trial wave function that reflected this fact. Second the degeneracy associated with incoming and outgoing distorted waves was largely ignored in this calculation. In both cases the result has been a basis set that is not as complete as might have been desired. Unfortunately both assumptions were necessary to enable a calculation to be performed in a reasonable time and with the available resources.

On the positive side the theory has successfully modeled the underlying features of a quantum mechanical system accurately without having to numerically integrate large-scale coupled equations. Rather than including a large number of atomic orbitals and pseudostates, this approximation has used CDWs to construct a basis set

that includes the desirable features of orthonormality, gauge invariance, and Galilean invariance. Furthermore the set is not biased toward either of the Coulomb potentials generated by the heavy bodies present, but rather treats both in unison. Hence the basis set is connected and the associated perturbation on the system, namely $-\nabla_{\mathbf{r}_T}.\nabla_{\mathbf{r}_P}$, simultaneously depends on the position of the electron with respect to both the target and projectile.

Thus while the basis still has its deficiencies, the dynamic nature of its elements has ensured a trial wave function sufficiently versatile to model the atomic behaviour of the collision at high energies and to adapt to the ever–increasing molecular character of the process as the impact velocity decreases. As a result, the theory could be viewed as a hybrid of atomic and molecular theories incorporating the advantages of both formulations into a more complete quantum approximation and the authors surmise that the essential criterion for a basis set should be the ability of the elements to adapt in a manner so that at any particular instance the coupled equations reflect the environment in which the electron is predominantly situated. This is contrary to the underlying principle of other expansions where the suitability of a basis set is assessed according to its ability to span the model space of the electron; the manner in which our basis has been constructed has much in common with the basis generator method suggested previously by Kroneisen et al. [370]. Furthermore our theory does, to a certain extent, include the effect of ionization as the distorted waves describe an electron bound to one nucleus while also moving in the continuum of the other one. To conclude, the multistate approximation considered is still a work in progress but it has demonstrated the fact that it may be possible to model a variety of ion–atom collisions accurately with a relatively small CDW basis set. The theory could be extended in a variety of directions; a simple adaptation would allow electron excitation to be studied. However, future work is mainly concerned with its application to charge transfer during heteronuclear collisions and may offer advantages over the methods of Section 4.2.

4.3.3 Ionization

Total cross sections are calculated for the ionization of a hydrogen atom by multicharged fully stripped ions in the 20-1000 keV amu^{-1} impact-energy range. Distortion is accounted for in the entrance channel (via the eikonal approximation) and in the exit channel (via the continuum-distorted-wave approximation). The transition amplitude is calculated in the post form so that the electronic nonorthogonal kinetic energy is treated as the perturbation. It is concluded that of the currently available models this theory is the most successful and versatile over a considerable range of energies and charges. Specifically for ionization of a hydrogen atom by 50 keV protons we present doubly differential cross sections for electrons ejected in the forward direction and singly differential cross sections as a function of emission energy. The question of cusps and peaks in the differential cross sections is considered, as is the question of charge scaling of the total cross section.

Over the years there has been intensive study, both experimental and theoretical, of the processes resulting from the impact of multicharged ions with hydrogenic

target atoms, a primary motivation being the wide-ranging applications within the fusion energy program. It is important to assess which reactions are significant and to calculate their effects upon the plasma. Of particular interest is the problem of ionization of neutral hydrogen atoms by highly charged ions, namely

$$B^{Z+} + H(1s) \rightarrow B^{Z+} + H^{+} + e^{-} \tag{4.164}$$

Such reactions occur in the supplementary heating of the plasma when the highly stripped impurities present interact with the injected neutral beam of hydrogen. The relevant energy range of these collisions is 10-200 keV amu^{-1}. To predict the cross section accurately in this energy regime we must improve upon the simple first-order weak-perturbation theories. For an adequate description we must include second-order effects. The need for such a refinement is evidenced in recent reviews of theory [417], [526] and experiment [547].

The evidence indicates that although there is a consensus at high energies, where all the results conform to the first Born (B1) approximation [41], there is marked disagreement below 200 keV u^{-1}. Of the various theories presented, the most consistently successful over a wide range of values, for both impact energy and ion charge, has been the Glauber approximation [302], [303] and to a lesser extent the classical trajectory Monte Carlo (CTMC) method [474]. We propose a theoretical model of the process

$$B^{Z_3+} + A^{(Z_1-1)+} \rightarrow B^{Z_3+} + A^{Z_1+} + e^{-} \tag{4.165}$$

which includes second-order refinements, and we describe its relation to the other theories. In this respect the model can be viewed as a hybrid of the eikonal approximation and the continuum-distorted-wave approximation.

In previous work [62] the CDW theory has been derived using the distorted-wave formalism [227], [292] and the equivalent impact-parameter model [112]. In this presentation we adopt the semiclassical impact parameter ($\boldsymbol{\rho}$) time(t)-dependent treatment and develop the theory using the formalism of Crothers [178].

We make the two-state approximation and assume that direct coupling to excitation and transfer channels is negligible along with all explicit bound-state and continuum intermediate coupling. The initial and final states $\Psi_{i,f}$ are asymptotically ($t \rightarrow \pm\infty$) correct distorted-wave solutions of the Schrödinger equation:

$$\left(H_e - \mathrm{i}\frac{\partial}{\partial t_r}\right)\Psi = 0 \tag{4.166}$$

Numbering the particles, target (1), electron (2), and projectile (3) we define

$$\begin{aligned} \mathbf{x} &= \mathbf{r}_2 - \mathbf{r}_1 \qquad & \mathbf{s} &= \mathbf{r}_2 - \mathbf{r}_3 \\ \mathbf{R} &= \mathbf{r}_3 - \mathbf{r}_1 = \boldsymbol{\rho} - \mathbf{v}t \qquad & \mathbf{r} &= \frac{1}{2}(\mathbf{x} + \mathbf{s}) \end{aligned} \tag{4.167}$$

Then the electronic Hamiltonian is given by

$$H_e = -\frac{1}{2}\boldsymbol{\nabla}_{\mathbf{r}}^2 - \frac{Z_3}{s} - \frac{Z_1}{x} + \frac{Z_1 Z_3}{R} \tag{4.168}$$

Furthermore if we neglect back-coupling, nonorthogonality, and distortion of the distorted waves [179], the transition amplitude in the post form is

$$a_{if}(\boldsymbol{\rho}) = -\mathrm{i}\int_{-\infty}^{+\infty} \mathrm{d}t\, \langle \Psi_i^{(+)} \left| H_e - \mathrm{i}\frac{\partial}{\partial t_r} \right| \Psi_f^{(-)} \rangle \tag{4.169}$$

In the B1 and Glauber approximations the chosen final state [404] is not an asymptotically correct solution of (4.166) but is given by

$$^{\mathrm{B1}}\Psi_f^{(-)} = (2\pi)^{-3/2} \exp\left(\mathrm{i}\mathbf{K}\cdot\mathbf{x} - \frac{1}{2}\mathrm{i}\mathbf{v}\cdot\mathbf{r} - \frac{1}{8}\mathrm{i}v^2 t - \mathrm{i}E_K t\right) \tag{4.170}$$

$$\times N^*(Z_1/K)\,{}_1F_1(-\mathrm{i}Z_1/K; -\mathrm{i}Kx - \mathrm{i}\mathbf{K}\cdot\mathbf{x}) \tag{4.171}$$

where

$$E_K = \frac{1}{2}K^2 \qquad N(\eta) = \exp(\frac{1}{2}\pi\eta)\Gamma(1-\mathrm{i}\eta) \tag{4.172}$$

This represents, asymptotically, a Coulomb distorted plane wave with wave vector **K**, plus a distorted ingoing spherical wave. In this approximation the scattered projectile is regarded as a perturbing influence as may be seen from the relation

$$\left(H_e - \mathrm{i}\frac{\partial}{\partial t_r}\right)^{\mathrm{B1}}\Psi_f^{(-)} = \left(-\frac{Z_3}{s}\right)^{\mathrm{B1}}\Psi_f^{(-)} \tag{4.173}$$

The treatment of Z_3/s as a perturbation is clearly unacceptable if either s is small or Z_3 is large or both. Therefore B1 is not a satisfactory physical representation when the charge of the projectile is large and/or the ejected electron is scattered in the forward direction close to the projectile, i.e., $\mathbf{K} \simeq \mathbf{v}$. Consequently B1 theory fails to predict accurate differential cross sections. This region of the electron spectrum gives important contributions to the total cross section at intermediate energies. Attempts to correct this fault by centering the continuum states on the projectile are self-defeating and inevitably fail to reproduce the correct high-energy B1 total cross section [526].

Our chosen final state, unlike the B1 choice, satisfies the correct boundary condition

$$\Psi_f^{(-)} \underset{\substack{t\to+\infty \\ x\to\infty \\ s\to\infty}}{\sim} (2\pi)^{-3/2} \exp\left(\mathrm{i}\mathbf{K}\cdot\mathbf{x} - \frac{1}{2}\mathrm{i}\mathbf{v}\cdot\mathbf{r} - \frac{1}{8}\mathrm{i}v^2 t - \mathrm{i}E_K t\right)$$
$$\times \exp\left(\frac{\mathrm{i}Z_1}{K}\ln(Kx + \mathbf{K}\cdot\mathbf{x}) + \frac{\mathrm{i}Z_3}{p}\ln(ps + \mathbf{p}\cdot\mathbf{s}) - \frac{\mathrm{i}Z_1 Z_3}{v}\ln(vR + \mathbf{v}\cdot\mathbf{R})\right) \tag{4.174}$$

where $\boldsymbol{\rho} = \mathbf{K} - \mathbf{v}$ is the momentum of the electron relative to the projectile. We introduce the distorted wave function

$$\Psi_f^{(-)} = {}^{\mathrm{B1}}\Psi_f^{(-)}\mathcal{F}_f \tag{4.175}$$

and transform the operator of equation (4.166) using the generalized nonorthogonal coordinate system $(\mathbf{x}, \mathbf{s}, t)$ [178] to obtain

$$H_e - \mathrm{i}\frac{\partial}{\partial t_r} = -\frac{1}{2}\boldsymbol{\nabla}_{\mathbf{x}}^2 - \boldsymbol{\nabla}_{\mathbf{x}} \cdot \boldsymbol{\nabla}_{\mathbf{s}} - \frac{1}{2}\boldsymbol{\nabla}_{\mathbf{s}}^2 - \frac{Z_1}{x} - \frac{Z_3}{s} + \frac{Z_1 Z_3}{R} - \mathrm{i}\left(\frac{\partial}{\partial t}\right)_{\mathbf{x},\mathbf{s}} - \frac{1}{2}\mathrm{i}\mathbf{v} \cdot \boldsymbol{\nabla}_{\mathbf{x}} + \frac{1}{2}\mathrm{i}\mathbf{v} \cdot \boldsymbol{\nabla}_{\mathbf{s}} \tag{4.176}$$

Since we have

$$\left(-\frac{1}{2}\boldsymbol{\nabla}_{\mathbf{x}}^2 - \frac{Z_1}{x} - \mathrm{i}\frac{\partial}{\partial t_x} - \frac{1}{2}\mathrm{i}\mathbf{v} \cdot \boldsymbol{\nabla}_{\mathbf{x}}\right)^{\mathrm{B1}}\Psi_f^{(-)} = 0 \tag{4.177}$$

it follows that

$$\begin{aligned} &{}^{\mathrm{B1}}\Psi_f^{(-)}\left(-\frac{1}{2}\boldsymbol{\nabla}_{\mathbf{s}}^2 - \frac{Z_3}{s} + \frac{Z_1 Z_3}{R} - \mathrm{i}\frac{\partial}{\partial t_s} - \mathrm{i}\mathbf{p} \cdot \boldsymbol{\nabla}_{\mathbf{s}}\right)\mathcal{F}_f \\ &= {}^{\mathrm{B1}}\Psi_f^{(-)}\left[\boldsymbol{\nabla}_{\mathbf{x}} \ln {}_1F_1(-\mathrm{i}Z_1/K; 1; -\mathrm{i}Kx - \mathrm{i}\mathbf{K} \cdot \mathbf{x})\boldsymbol{\nabla}_{\mathbf{s}}\mathcal{F}_f\right] \end{aligned} \tag{4.178}$$

Neglecting the nonorthogonal kinetic energy on the right-hand side we get an approximation to $\mathcal{F}_f$, denoted by χ_f, which satisfies

$$\left(-\frac{1}{2}\boldsymbol{\nabla}_{\mathbf{s}}^2 - \frac{Z_3}{s} + \frac{Z_1 Z_3}{R} - \mathrm{i}\frac{\partial}{\partial t_s} - \mathrm{i}\mathbf{p} \cdot \boldsymbol{\nabla}_{\mathbf{s}}\right)\chi_f = 0 \tag{4.179}$$

and has the solution, consistent with the restriction (4.174),

$$\chi_f = \exp\left(-\mathrm{i}\frac{Z_1 Z_3}{v}\ln(vR + \mathbf{v} \cdot \mathbf{R})\right)N^*\left(\frac{Z_3}{p}\right){}_1F_1\left(-\mathrm{i}\frac{Z_3}{p}; 1; -\mathrm{i}ps - \mathrm{i}\mathbf{p} \cdot \mathbf{s}\right) \tag{4.180}$$

It follows that since the CDW theory treats the nonorthogonal kinetic energy as the perturbation, the CDW final state is given [62] by

$${}^{\mathrm{CDW}}\Psi_f^{(-)} = {}^{\mathrm{B1}}\Psi_f^{(-)}\chi_f \tag{4.181}$$

with the property

$$\begin{aligned} \left(H_e - \mathrm{i}\frac{\partial}{\partial t_r}\right){}^{\mathrm{CDW}}\Psi_f^{(-)} &= -\boldsymbol{\nabla}_{\mathbf{s}} \ln {}_1F_1(-\mathrm{i}\zeta; 1; -\mathrm{i}ps - \mathrm{i}\mathbf{p} \cdot \mathbf{s}) \\ &\quad \cdot \boldsymbol{\nabla}_{\mathbf{x}} \ln {}_1F_1(-\mathrm{i}\xi; 1; -\mathrm{i}Kx - \mathrm{i}\mathbf{K} \cdot \mathbf{x})^{\mathrm{CDW}}\Psi_f^{(-)} \end{aligned} \tag{4.182}$$

where we define

$$\zeta = Z_3/p \qquad \xi = Z_1/K \tag{4.183}$$

Furthermore we have that

$$\mathrm{i}\mathbf{K} \cdot \mathbf{x} - \frac{1}{2}\mathrm{i}\mathbf{v} \cdot \mathbf{r} - \frac{1}{2}\mathrm{i}K^2 t - \frac{1}{8}\mathrm{i}v^2 t = \mathrm{i}\mathbf{p} \cdot \mathbf{s} + \frac{1}{2}\mathrm{i}\mathbf{v} \cdot \mathbf{r} - \frac{1}{2}\mathrm{i}p^2 t - \frac{1}{8}\mathrm{i}v^2 t + \mathrm{i}\boldsymbol{\rho} \cdot \mathbf{K} \tag{4.184}$$

The final term on the right hand side contributes a $\boldsymbol{\rho}$-dependent phase to the state function, which does not affect the cross-section differential with respect to the electron parameters and thus may be ignored. On inspection of the form of ${}^{\mathrm{CDW}}\Psi_f^{(-)}$, it

is apparent that the chosen final state does not discriminate between the nuclei, A and B, nor between which contributes the "pure continuum wave" and which the "distorted wave." Thus the centres A and B are treated on an equal footing in this theory. Furthermore it completely accounts for the "capture to continuum states" and "direct ionization" processes and establishes that there are not in reality two distinct processes and that they should not be treated as such.

The initial state has beeen represented in several different ways, the plane-wave Born approximation [41], the distorted-wave Born approximation [526], the Glauber approximation [301], and the continuum-distorted-wave approximation [112], [62]. Of these models, the best convergence with experimental data had up to then been obtained using the Glauber approximation. In view of the excellent physical picture given by CDW for the final state, it is perhaps surprising that previous CDW calculations [62] give results that are in worse agreement with experiment than the simple B1 theory. The reason for this failure is simply that the original CDW initial-state ansatz is not properly normalized [178]. Calculations assessing the effect of the renormalization in the intermediate energy range have been made [179] in connection with charge-transfer studies. The corrections substantially improve the agreement with experimental work. For the B1 approximation we have

$$ {}^{\mathrm{B1}}\Psi_i^{(+)} = \varphi_i(\mathbf{x}) \exp\left(-\frac{1}{2}\mathrm{i}\mathbf{v}\cdot\mathbf{r} - \frac{1}{8}\mathrm{i}v^2 t - \mathrm{i}\epsilon_i t\right) \tag{4.185} $$

as a solution to the equation

$$ \left(-\frac{1}{2}\boldsymbol{\nabla}_{\mathbf{r}}^2 - \frac{Z_1}{x} - \mathrm{i}\frac{\partial}{\partial t_r}\right) {}^{\mathrm{B1}}\Psi_i^{(+)} = 0 \tag{4.186} $$

where $\varphi_i(\mathbf{x})$ is the normalised initial bound-state wave function with eigenenergy

$$ \epsilon_i = -\frac{1}{2}Z_1^2 \tag{4.187} $$

The inclusion of a distortion factor $\mathcal{F}_i(\mathbf{s}, t)$ gives, from (4.176) and (4.186),

$$ {}^{\mathrm{B1}}\Psi_i^{(+)}\left(-\frac{1}{2}\boldsymbol{\nabla}_{\mathbf{s}}^2 - \frac{Z_3}{s} + \frac{Z_1 Z_3}{R} - \mathrm{i}\frac{\partial}{\partial t_s} + \mathrm{i}\mathbf{v}\cdot\boldsymbol{\nabla}_{\mathbf{s}}\right)\mathcal{F}_i = {}^{\mathrm{B1}}\Psi_i^{(+)}\left(\boldsymbol{\nabla}_{\mathbf{x}} \ln\varphi_i(\mathbf{x})\cdot\boldsymbol{\nabla}_{\mathbf{s}}\mathcal{F}_i\right) \tag{4.188} $$

Imposing the correct Coulombic boundary condition

$$ \Psi_i \underset{t\to-\infty}{\sim} {}^{\mathrm{B1}}\Psi_i^{(+)} \exp\left(\mathrm{i}\frac{Z_1 Z_3}{v}\ln(vR - \mathbf{v}\cdot\mathbf{R}) - \mathrm{i}\frac{Z_3}{v}\ln(vs + \mathbf{v}\cdot\mathbf{s})\right) \tag{4.189} $$

and neglecting the right hand side of (4.188), we obtain a zero-order solution to $\mathcal{F}_i$, namely

$$ \mathcal{F}_i \simeq \chi_i \equiv \exp\left(\mathrm{i}\frac{Z_1 Z_3}{v}\ln(vR - \mathbf{v}\cdot\mathbf{R})\right) N(\nu)\,{}_1F_1(\mathrm{i}\nu; 1; \mathrm{i}vs + \mathrm{i}\mathbf{v}\cdot\mathbf{s}) \tag{4.190} $$

where we have

$$\nu = Z_3/v \tag{4.191}$$

This is the CDW approximation [112]. Then the appropriate initial state [178] is

$${}^{\mathrm{CDWN}}\Psi_i^{(+)} = (S_{ii}^{++})^{-1/2}\,{}^{\mathrm{CDW}}\Psi_i^{(+)} \tag{4.192}$$

where we have

$${}^{\mathrm{CDW}}\Psi_i^{(+)} = {}^{\mathrm{B1}}\Psi_i^{(+)}\chi_i \tag{4.193}$$

and

$$S_{ii}^{++} = \langle {}^{\mathrm{CDW}}\Psi_i^{(+)} \big| {}^{\mathrm{CDW}}\Psi_i^{(+)} \rangle \tag{4.194}$$

This ideal ansatz includes contributions from projectile-electron continuum intermediate states. Unfortunately calculations that retain the dependence of S_{ii}^{++}on $\boldsymbol{\rho}$ and t are computationally expensive. However, a comparatively simple approximation to the initial state results from the adoption of the asymptotic development of ${}^{\mathrm{CDWN}}\Psi_i^{(+)}$, namely (4.189), which is valid for $|vs + \mathbf{v}\cdot\mathbf{s}| \gg 1$. This approximates (4.192) for sufficiently large v and ρ. The associated initial state is equivalent to that obtained by means of the eikonal approximation used in previous calculations [417]. It follows directly from (4.188) if, in addition to the right hand side, the term $-1/2\,\boldsymbol{\nabla}_{\mathbf{s}}^2\mathcal{F}_i$ is neglected, which is reasonable under certain restrictions. Firstly the translational kinetic energy of the electron $(1/2\,v^2)$ must greatly exceed the interaction $(Z_1Z_3/R - Z_3/s)$. Second the diffractive components of the term must be negligible within the transition region. In particular we note that the equation obtained,

$$\left(\frac{Z_1Z_3}{R} - \frac{Z_3}{s} - \mathrm{i}\frac{\partial}{\partial t_{\mathbf{s}}} + \mathrm{i}\mathbf{v}\cdot\boldsymbol{\nabla}_{\mathbf{s}}\right){}^{\mathrm{E}}\chi_i = 0 \tag{4.195}$$

integrates exactly to give

$${}^{E}\chi_i = \exp\left(\mathrm{i}\frac{Z_1Z_3}{v}\ln(vR - \mathbf{v}\cdot\mathbf{R}) - \mathrm{i}\frac{Z_3}{v}\ln(vs + \mathbf{v}\cdot\mathbf{s})\right) \tag{4.196}$$

We have thus obtained the eikonal initial-state (EIS) approximation

$${}^{\mathrm{EIS}}\Psi_i^{(+)} = {}^{\mathrm{B1}}\Psi_i^{(+)\mathrm{E}}\chi_i \tag{4.197}$$

where the component factors are given by (4.185) and (4.196).

A loose validity criterion, for target hydrogen atoms ($Z_1 = 1$), may be derived as $v^2 \gg Z_3$. At high energies this reduces to the usual B1 condition. In the calculation of transition probabilities using (4.169), if ${}^{\mathrm{B1}}\Psi_i^{(+)}$ is chosen as the initial state and ${}^{\mathrm{CDW}}\Psi_f^{(-)}$ as the final state then we arrive at the "distorted-wave Born" (DWB) approximation of Belkić [62]. This is also termed the modified Vainshtein–Presnyakov–Sobelman (MVPS) approximation [291] and may be considered as an extension of the continuum intermediate states (CIS) model of charge exchange [61]. An alternative choice of states, namely ${}^{\mathrm{EIS}}\Psi_i^{(+)}$ and ${}^{\mathrm{B1}}\Psi_f^{(-)}$, gives the eikonal (unrestricted Glauber) approximation. In the following calculation we have selected the states ${}^{\mathrm{EIS}}\Psi_i^{(+)}$ and ${}^{\mathrm{CDW}}\Psi_f^{(-)}$ so that distortion is accounted for in both entrance and

exit channels. Moreover, the initial state ${}^{\mathrm{EIS}}\Psi_i^{(+)}$ is normalized at all times and all impact parameters, and although we do not explicitly include any continuum intermediate states we do include multiple scattering terms. On the other hand ${}^{\mathrm{CDW}}\Psi_f^{(-)}$ is only approximately normalized at finite ρ and t, and indeed the CDW states of different $\mathbf{K}$ are only quasiorthogonal because they are not exact eigenfunctions of the total electronic Hamiltonian. Nevertheless as a good approximation we assume that the final states are orthonormal and uncoupled, an exact approximation at infinite internuclear separation. Actually a continuum state such as ${}^{\mathrm{CDW}}\Psi_f^{(-)}$ can only be normalized when both x and s tend to $+\infty$. Nonorthogonality of the initial and final states is in principle more troublesome [179] but in fact is less of a problem for ionization than for charge transfer.

Denoting the total ionization cross section by Q, the triply differential cross section, $\sigma(\mathbf{K})$, is given by integration over all projectile impact parameters as

$$\frac{\mathrm{d}Q}{\mathrm{d}\tau_{\mathbf{K}}} = \sigma(\mathbf{K}) = \int \mathrm{d}\boldsymbol{\rho}\left|a_{if}(\boldsymbol{\rho})\right|^2 \tag{4.198}$$

Defining

$$a_{if}(\boldsymbol{\rho}) = \mathrm{i}(\rho v)^{2\mathrm{i}Z_1Z_3/v}\tilde{a}_{if}(\boldsymbol{\rho}) \tag{4.199}$$

and introducing the two-dimensional Fourier transform

$$R(\boldsymbol{\eta}) = \frac{1}{2\pi}\int \mathrm{d}\boldsymbol{\eta}\exp(\mathrm{i}\boldsymbol{\eta}\cdot\boldsymbol{\rho})\tilde{a}_{if}(\boldsymbol{\rho}) \tag{4.200}$$

where

$$\boldsymbol{\eta}\cdot\hat{\mathbf{v}} = 0 \tag{4.201}$$

then we have, by Parseval's theorem,

$$\sigma(\mathbf{K}) = \int \mathrm{d}\boldsymbol{\eta}|\mathbf{R}(\boldsymbol{\eta})|^2 \tag{4.202}$$

From equations (4.169), (4.182), and (4.197), it follows that

$$\begin{aligned}\tilde{a}_{if}^*(\boldsymbol{\rho}) = \frac{N(\zeta)N(\xi)}{(2\pi)^{3/2}}\int_{-\infty}^{+\infty}\mathrm{d}t\int \mathrm{d}\mathbf{r}\,\exp\left((\mathrm{i}\Delta\epsilon)t - \mathrm{i}\mathbf{K}\cdot\mathbf{x}\right)\varphi_i(\mathbf{x})\\ \times\boldsymbol{\nabla}_{\mathbf{x}}\,{}_1F_1(\mathrm{i}\xi;1;\mathrm{i}Kx + \mathrm{i}\mathbf{K}\cdot\mathbf{x})\\ \times\exp(-\mathrm{i}\nu\ln(vs + \mathbf{v}\cdot\mathbf{s}))\cdot\boldsymbol{\nabla}_{\mathbf{s}}\,{}_1F_1(\mathrm{i}\zeta;1;\mathrm{i}ps + \mathrm{i}\mathbf{p}\cdot\mathbf{s})\end{aligned} \tag{4.203}$$

where we have

$$\Delta\epsilon = \frac{1}{2}(K^2 + Z_1^2) \tag{4.204}$$

So, from equations (4.200) and (4.202), we get

$$\begin{aligned}\sigma(\mathbf{K}) = a_0^2\,|N(\zeta)N(\nu)|^2\int_{\Delta\epsilon/v}^{\infty}2\pi q\,\mathrm{d}q\,A\,|{}_2F_1(\mathrm{i}\nu,\mathrm{i}\zeta;1;z) - \mathrm{i}\nu\Omega\\ \times\,{}_2F_1(\mathrm{i}\nu+1,\mathrm{i}\zeta+1;2;z)|^2\left|{}^{\mathrm{B1}}\mathbf{R}(\boldsymbol{\eta})\right|^2\end{aligned} \tag{4.205}$$

The symbols are defined as follows

$$\mathbf{q} = -\boldsymbol{\eta} - \frac{\Delta\epsilon}{v}\hat{\mathbf{v}} \tag{4.206}$$

$$A = \exp(-2\pi\nu) \tag{4.207}$$

$$\alpha = \frac{1}{2}q^2 \qquad \beta = -\Delta\epsilon \tag{4.208}$$

$$\gamma = \frac{1}{2}\left[Z_1^2 + (\mathbf{q}+\mathbf{K})^2\right] \qquad \delta = \mathbf{p}\cdot\mathbf{v} - p\nu - \Delta\epsilon \tag{4.209}$$

$$z = 1 - (\alpha\delta/\beta\gamma) \tag{4.210}$$

$$B = \mathbf{q}\cdot[\mathbf{q} + \mathbf{K}(1+\mathrm{i}\xi)] \tag{4.211}$$

$$C = (\nu/p)\left[\mathbf{K}\cdot\mathbf{q} + K^2(1+\mathrm{i}\xi)\right] + (1+\nu/p)\left[\Delta\epsilon - \mathbf{v}\cdot\mathbf{K}(1+\mathrm{i}\xi)\right] \tag{4.212}$$

$$\Omega = \alpha(B\delta + \gamma C)/(\gamma\beta B) \tag{4.213}$$

and

$$\left|{}^{\mathrm{B1}}\mathbf{R}(\boldsymbol{\eta})\right|^2 = \left(\frac{2^7 Z_1^5 Z_3^2}{\pi^2 v^2 q^4}\right)|N(\xi)|^2 \exp\left[-2\xi\tan^{-1}\left(\frac{2Z_1K}{q^2+Z_1^2-K^2}\right)\right] \times \frac{\left[(\mathbf{q}^2+\mathbf{q}\cdot\mathbf{K})^2 + (\mathbf{q}\cdot\mathbf{K})^2\xi^2\right]}{\left[Z_1^2+(q+K)^2\right]\left[Z_1^2+(q-K)^2\right]\left[Z_1^2+(\mathbf{q}+\mathbf{K})^2\right]^4} \tag{4.214}$$

As in the pure CDW theory of Belkić [62], $a_0^2\left|{}^{\mathrm{B1}}\mathbf{R}(\boldsymbol{\eta})\right|^2 \mathrm{d}\boldsymbol{\eta}$ denotes the result of the B1 approximation, the remaining factors being the effect of distortion. As $v \to \infty$ their influence is negligible and the asymptotic high energy limit of the theory is the B1 approximation. Ionization is a predominantly single-scattering process at high energy in contrast to charge transfer for which the double-scattering term is more effective [231].

We take the opportunity to correct some misprints in published expressions for C and $\left|{}^{\mathrm{B1}}\mathbf{R}(\boldsymbol{\eta})\right|^2$ but note that other quantities such as A and z take a different algebraic form in the CDW-EIS theory as against the pure CDW theory. Calculations were performed for total cross sections and for singly and doubly differential cross sections. Specifically, for the prototypical reaction,

$$\mathrm{H}^+ + \mathrm{H}(1\mathrm{s}) \rightarrow \mathrm{H}^+ + \mathrm{H}^+ + \mathrm{e}^- \tag{4.215}$$

some differential cross sections are displayed as an illustration of the model predictions. Results for B1, DWB, and CDW were calculated in addition to the CDW-EIS values. Finally we compare the various theoretical and experimental results for total hydrogen atom ionization cross sections for H^+, He^{2+}, Li^{3+}, Be^{4+}, and C^{6+} projectiles.

The doubly differential cross section (DDCS) is given by the formula

$$\frac{\mathrm{d}^2Q}{\mathrm{d}E_K\mathrm{d}(\cos\theta)} = K\int_0^{2\pi}\mathrm{d}\phi\sigma(\mathbf{K}) \tag{4.216}$$

where θ and ϕ are, respectively, the polar and azimuthal angles of the wave vector $\mathbf{K}$ with respect to the polar axis $\hat{\mathbf{v}}$ and the collision plane. From the DDCS we can get a clear physical picture of the process in terms of the angular and energy distributions of the ejected electrons. The linear scaling procedure

$$\sigma^H(\mathbf{K}) = \frac{1}{2}\sigma^{H_2}(\mathbf{K}) \tag{4.217}$$

is seriously in doubt, so comparison with experiment is given later. Details of such work have been published by various authors (Belkić [62], Rødbro and Andersen [514], Ryufuku [526]). The forward-scattering ($\theta = 0$) cross section is presented in Figure 4.8a for 50 keV proton impact. The now familiar cusp occurring at $\mathbf{K} = \mathbf{v}$ features prominently and results from the singular behaviour of the factor $|N(\zeta)|^2$. To be precise, for vanishingly small p, the hypergeometric functions of the integrand tend to the confluent form and so the curve is singular like p^{-1}, in agreement with the DWB and second Born (B2) results [223]. However, the curve is not symmetrical about the singularity, showing a much steeper decay for $K > v$ than for $K < v$. The asymmetry arises in the fourth argument of the hypergeometrics and is superimposed on the B1 background contribution. Such features of the DDCS have been confirmed by experiment, and measurements of the width and asymmetry of the cusp have been made [514]. The DWB shows a similar behaviour to the CDW-EIS but predicts much larger values. The cusp is of course absent from the B1 curve since the projectile–electron interaction in the exit channel is ignored. Also shown is our pure CDW calculation, the result of which differs from that of Belkić [62]. For example we do not get the peak he observed at $E_K = 6.2$ eV. It is not clear what the source of disagreement is, but presumably it arises from the treatment of the analytical continuations of the hypergeometric functions.

The singly differential cross section (SDCS), differential with respect to the electron emission energy, is by definition

$$\frac{\mathrm{d}Q}{\mathrm{d}E_K} = \int_{-1}^{+1} \mathrm{d}(\cos\theta)\, K \int_0^{2\pi} \mathrm{d}\phi\, \sigma(\mathbf{K}) \tag{4.218}$$

Similarly the SDCS, differential with respect to the polar angle of emission, is defined by

$$\frac{\mathrm{d}Q}{\mathrm{d}(\cos\theta)} = \int_0^{\infty} \mathrm{d}E_K\, K \int_0^{2\pi} \mathrm{d}\phi\, \sigma(\mathbf{K}) \tag{4.219}$$

The chosen observation energy for $\mathrm{d}Q/\mathrm{d}E_K$ is 50 keV as before. Thus we may readily compare Figure 4.8b with the CDW results given by Belkić [62]. Again we note the absence of the low-energy peak in our calculations for the CDW approximation, otherwise the curves agree closely at higher emission energies. Furthermore the CDW-EIS results lie well below the CDW and B1 values for smaller emission energies. It is clear that it is the low-energy range of the spectrum that contributes most to the total cross section. Thus we expect total cross sections much smaller than both CDW and B1. In comparison with the Glauber theory [481], it is evident that there is a significant enhancement of the SDCS in the region $E_K \simeq 1/2\, v^2$. This is due to the

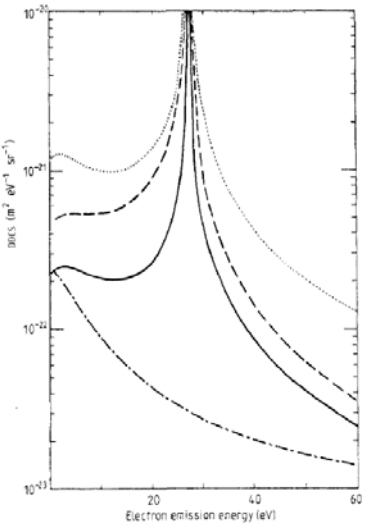

Fig. 4.8a. Doubly differential cross sections for $H^+ + H \rightarrow H^+ + H^+ + e^-$, with electrons ejected in the forward direction ($\theta = 0$) and for a collision energy of 50 keV. – · – · –, B1; · · ·, DWB [62]; - - - - -, CDW [180]; —, CDW-EIS [180]

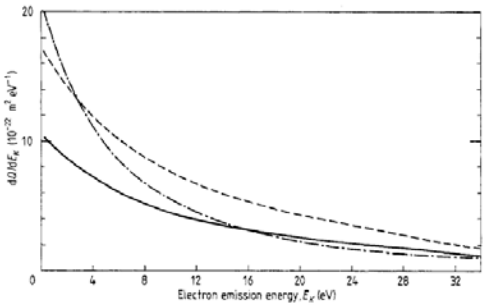

Fig. 4.8b. Singly differential cross sections with respect to electron emission energy for 50 keV incident protons upon H(1s). – · – · –, B1; - - - - -, CDW [180]; —, CDW-EIS [180]

effect of the final channel distortion and gives cross sections somewhat larger than the Glauber theory, which takes no account of this effect. McGuire [417] (cf. Park et al. [481]) correctly attributes the defect of the Glauber theory to the omission of this distortion. At higher incident proton energies this region of the electronic spectrum is shifted to correspondingly higher energies and thus contributes little to the integral cross section. So it is indeed a valid approximation to neglect such contributions for fast collisions. However, this is not so when working in the intermediate- and/or low-energy regimes. Experimental work coinciding with the parameters of Figure 4.8b has been carried out by Park et al. [481] using energy-loss spectroscopy. The results obtained confirm the role of distortion in guiding electrons ejected with

velocity close to that of the projectile. The phenomenon is most clearly seen when the results of Figure 4.8b are converted to a Platzmann plot [481]. Both our CDW and CDW-EIS show the same qualitative behaviour as the experiment although the absolute values apparently fit the CDW curve more closely. These measurements seem to have overestimated the SDCS as indicated by the derived total cross section. However, on renormalization of these results by reference to the work of Shah and Gilbody [545], we obtain excellent quantitative agreement with the CDW-EIS curve.

Finally, integrating over the ejected-electron energy spectrum we obtain the total cross section Q. The series of multiple integrations outlined earlier presents some technical difficulties and is computationally expensive compared with the Born or Glauber approximations. Even so, we were able to evaluate the cross sections to one percent accuracy. Our CDW-EIS results are shown in Figure 4.9 in a format introduced by Shah and Gilbody [547] and adopted by McGuire [417] who give a comprehensive theoretical review. Of the many theories available for comparison, three have been chosen: first the B1 theory (which is valid at high energies), second the CTMC method (which roughly accords with experiment in the intermediate energy range), and third the Glauber approximation. The experimental data are normalized by reference to the B1 theoretical curve for H^+ impact in the energy range 1000-1500 keV amu^{-1}. The values for He^{2+} and Li^{3+} impact are then determined by

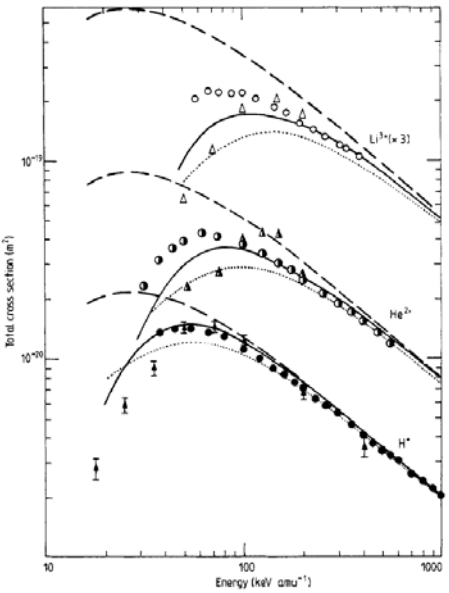

Fig. 4.9. Total ionization cross sections for a hydrogen-atom target in collision with fully stripped ions. Theory: – – ––, B1 [41]; · · · · ·, Glauber approximation [417]; —, CDW-EIS [180]; △, *half-filled triangle*, CTMC [474]; ▲, CTMC [23]. Experiment ○, *half-filled circle*, ●, [545], [547]

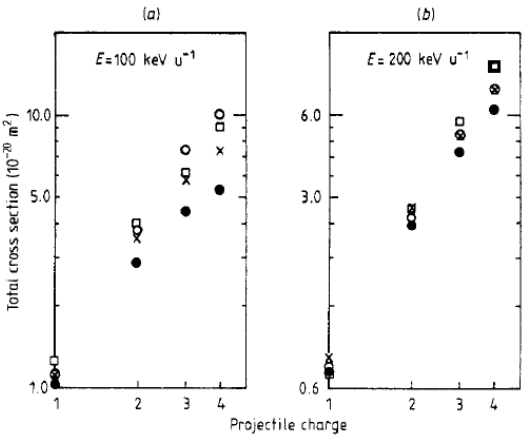

Fig. 4.10. (**a**) and (**b**) Total ionization cross sections as a function of projectile charge. •, Glauber approximation [417]; □, CTMC [474]; × CDW-EIS [180]; ○, experiment [545], [546], [547]

reference to this standard [545]. The accuracy of these measurements is remarkably good, typically better than 10% (this includes the uncertainties associated with the normalization procedure). The quantum mechanical theories all tend at high energy to the B1, which decays in the well-known manner $E^{-1} \ln E$, whereas the theories based on classical mechanics fall off as E^{-1}. The pure CDW results, without the renormalization correction, lie above the B1 curve at all energies. The pure CDW in its present form must therefore be considered unreliable for the reasons previously stated and so results are not presented. Incidentally these unnormalized calculations are only slightly below those of Belkić [62] since the peak he obtained in the SDCS contributes comparatively little. As noted previously [417] in its region of validity, the Glauber approximation is rather successful in predicting the experimental results. The new CDW-EIS calculations show equal success at the high energies but also interpret experiment rather well at intermediate energies. Further calculations on more highly charged projectiles, namely C^{6+}, show excellent agreement with experiment. For example, at 400 keV amu^{-1}, $Q = 10.4 \times 10^{-16}$ cm^2 (CDW-EIS) compares favourably with $(10.7 \pm 0.6) \times 10^{-16}$ cm^2 [548], as does $Q = 9.1 \times 10^{-16}$cm^2 for Glauber [417], whereas B1 gives $Q = 15.6 \times 10^{-16}$cm^2. However, controversy between experiment and theory continues; near 50 keV, Sidky and Lin [559] find a maximal cross section, 22% higher than that of Shah and Gilbody [542], using a two-center momentum-space discretization method.

The discrepancies that occur between CDW-EIS and experiment at lower energy show the important contributions to the ionization cross section, of transitions via intermediate bound states of the target and projectile. The importance of coupling to these discrete states is graphically depicted by the experimental results for capture [546]. It is particularly significant for highly charged ions, $Z_3 \gg 1$, as indicated by the Z_3^3 scaling law for total capture cross sections [174]. However, taking into

account the limitations of this CDW-EIS model, even at these comparatively low energies the agreement is still satisfactory, especially in light of the extension of *p*-H measurements down to 9.4 keV [542] and the He^{++}–H measurements down to 18.6 keV [543]. Sahoo et al. [528] improve agreement with the *p*-H measurements, below 25 keV by including 1*s* capture as an important intermediate step before ionization. Above 100 keV their strategy breaks down. This is understandable since ionization dominates capture at the higher energies and vice versa at lower energies.

In a more general investigation of the problem it is natural to look for a scaling law from which it may be possible to predict cross sections for ions of arbitrary charge and energy. This question is particularly relevant to fusion research where a wide variety of ionic species exist in the plasma. For a fully stripped projectile of charge Z, traveling with incident velocity v relative to a hydrogen atom target, it is an exact law in the B1 approximation that

$$^{B1}Q(Z, v) = Z^2\ {}^{B1}Q(1, v) \tag{4.220}$$

Several authors have addressed themselves to the validity of a more general rule [526], [297], [298], [67], [68], for example, a simple scaling law of the type

$$Q(Z, v) = Z^{\alpha} Q(1, v) \tag{4.221}$$

where α is velocity-dependent and tends to the value 2 at asymptotically high energies. Two energies were chosen to test for such a rule, 100 keV u^{-1} and 200 keV u^{-1}, and charge states 1^+-4^+. There is no experimental data available for Be^{4+}; however we include for the sake of completeness measurements obtained for C^{4+} ions [546]. From Figure 4.10a it is clear that there is little consensus between theory and experiment, although the trends are similar. If the C^{4+} point is omitted we get an experimental scaling law, $\alpha_{ex} \simeq 1.7$. At 200 keV u^{-1} (Figure 4.10b) the agreement is much better, particularly between CDW-EIS and experiment. The value $\alpha_{ex} \simeq 1.83$ illustrates the tendency towards the Z^2 scaling law. At still higher energies there is only a small deviation from this law. Indeed most estimates of α [68] have been carried out at much higher energies, e.g., 1100 keV u^{-1}, albeit with large charges, (11^+ – 22^+). Satisfactory agreement was obtained with CTMC calculations ($\alpha_{ex} = 1.43$). The significance of this value for α is doubtful since this data were subsequently well fitted by a value of 1.82 for α [526]. A more elaborate scaling law has been proposed within the context of the Bethe–Born approximation [297], [298], which apparently fits the data fairly well.

On the evidence presented we may claim that the CDW-EIS model appears to be the most successful and versatile theory devised within a two-state perturbation theory. Of course the CDW-EIS perturbation is the nonorthogonal kinetic energy of the electron, which arises from the fact that its kinetic energy is not simply associated exclusively with one or other of the nuclei. In contrast, other quantum mechanical theories adopt one or more of the Coulomb interactions as perturbations. A more rigorous test of theory is the measurement of the differential cross sections for an atomic hydrogen target. The failing of the EIS approximation is that the distortion correction to the bound state breaks down for small impact-parameter collisions. This

is not a severe drawback, however, in view of the important contributions from a wide range of impact parameters at intermediate and high energies and the CDWN theory would, in principle, improve this aspect of the initial state. Preliminary calculations using CDWN are promising. However it appears that a more important correction would be the inclusion of intermediate projectile and target-bound states.

Equation (4.216) for DDCS and (4.218) and (4.219) for various SDCS concern important diagnostic tools.

Here we consider the process of electron emission as a result of electron capture to the continuum (ECC) and in the origin of saddle point electrons. Saddle point electrons are those electrons that find themselves on the moving saddle point of the Coulomb potential between the projectile ion and the target; feeling no force they are promoted into the continuum. This occurs at $k \sim v/2$. ECC electrons are emitted at angles ~ 0 degrees with respect to the projectile direction and have velocities close to the incident projectile, i.e., $k \sim v$.

These are good examples of two-centre effects. The emission of these electrons at zero degrees have been studied for H^+ collisions with He and H_2 at the incident energies of 40 and 100 keV. Experiments were carried out by McGrath and Shah. The DDCS of (4.216) are illustrated by, for instance, figure 2 (40 keV), figure 10 (80 keV) of Nesbitt et al. [451], and figure 11 (100 keV) of McGrath et al. [416] for collisions of protons and these impact energies with H_2 molecules. The 40 and 100 keV results are for forward scattering of the electron. The 80 keV results comprise surface plots that clearly show the $k = v$ ECC and the $k = v/2$ saddle electrons. Figure 19 of McSherry et al. [420] presents DDCS for 1.5 MeV protons on Ar for various angles (15-125°) of the electron emission.

We also consider longitudinal momentum distributions. From momentum and conservation laws it is required that

$$p_{R\|} = p_{P\|} - p_{e\|} = \frac{E_K - \epsilon_i}{v} - k\cos\theta_k \tag{4.222}$$

where $p_{R\|}$ is the longitudinal recoil–ion momentum, $p_{P\|}$ is the longitudinal momentum transfer, and $p_{e\|}$ is the longitudinal momentum of the ejected electron. E_K is the electron energy in the final continuum state, and $\mathbf{k}$ is the momentum of the ejected electron with respect to a reference frame fixed on the target nucleus. v is the impact velocity, and ϵ_i is the binding energy of the neutral target atom. This equation is valid if

- the mass of the projectile ion is much heavier than the electron,
- the initial collision energy is much larger than $E_K - \epsilon_i$, and
- the projectile scattering angle is small.

The longitudinal electron momentum distribution may be found from

$$\frac{\mathrm{d}Q}{\mathrm{d}p_{e\|}} = \int_{p_{e\|}^2/2}^{\infty} \frac{1}{k} \frac{\mathrm{d}^2Q}{\mathrm{d}E_K \mathrm{d}\Omega_K} \mathrm{d}E_K \tag{4.223}$$

where Q is the total cross section and $\mathrm{d}^2Q/\mathrm{d}E_k\mathrm{d}\Omega_k$ is the standard DDCS (equation (4.216)/2π). Similarly for the longitudinal recoil momentum distribution,

$$\frac{\mathrm{d}Q}{\mathrm{d}p_{R\|}} = \int_{E_K^-}^{E_K^+} \frac{1}{k} \frac{\mathrm{d}^2 Q}{\mathrm{d}E_K \mathrm{d}\Omega_k} \mathrm{d}E_k \tag{4.224}$$

where the integration limits are $E_K^{\pm} = 1/2(k^{\pm})^2$ with

$$k^{\pm} = v\cos\theta \pm \sqrt{v^2\cos^2\theta_k + 2(p_{R\|}v - |\epsilon_i|)} \tag{4.225}$$

Finally the longitudinal momentum projectile transfer is obtained from

$$\frac{\mathrm{d}Q}{\mathrm{d}p_{P\|}} = v\frac{\mathrm{d}Q}{\mathrm{d}E_k} \tag{4.226}$$

Equations (4.223) and (4.224) are illustrated for CDWEIS by figures 2 and 3 of O'Rourke and Crothers [469] for 3.6 MeV u^{-1} Ni^{24+} ions on He. Equation (4.224) is illustrated likewise, but for Se^{28+} in figures 5 and 6 of O'Rourke et al. [470] (without and with experimental convolution).

We also consider further the double differential cross sections as a function of the longitudinal electron velocity $v_{e\|}$ for various transverse velocity $v_{e\perp}$ cuts. This can be derived remembering

$$E_k = \frac{1}{2}k^2 = \frac{1}{2}\left(p_{e\|}^2 + p_{e\perp}^2\right) \tag{4.227}$$

where $p_{e\perp}$ is the transverse momentum of the ejected electron. Hence

$$\frac{1}{2\pi v_{e\perp}} \frac{\mathrm{d}^2 Q}{\mathrm{d}v_{e\|}\mathrm{d}v_{e\perp}} = \frac{1}{2\pi}\int_0^{2\pi} \sigma(\mathbf{k})\mathrm{d}\phi_{\mathbf{k}} \tag{4.228}$$

Equation (4.228) is illustrated for 3.6 MeV u^{-1} Au^{53+} on He by figure 1 of Schmitt et al. [535]. Developments in efficient electron spectrometers combined with recoil-ion momentum spectroscopy (RIMS) allow for targets heavier than helium to be considered.

In binary projectile-electron scattering the singly differential cross section as a function of Ω_P may be derived from the transverse projectile momentum transfer given by

$$\frac{\mathrm{d}Q}{\mathrm{d}p_{P\perp}} = 2\pi p_{P\perp}\int \left|R_{if}(\boldsymbol{\eta})\right|^2 \mathrm{d}\mathbf{k} \tag{4.229}$$

provided θ_P is small so that the relation

$$\eta \equiv p_{P\perp} = \mu v\theta_P \tag{4.230}$$

is a good approximation, where $p_{P\perp}$ is the transverse component of the change in relative momentum of the heavy particles. Typical results are given in figure 2 of Schulz et al. [537] by the full open circles (classical trajectory Monte Carlo) and by the full closed circles [369] (experiment).

4.3.4 Fully differential cross sections for ionization

Experimental data for fully differential cross sections have been compared to various continuum-distorted-wave eikonal-initial-state models without much success, despite good agreement with double-differential cross sections. A four-body model is formulated here, and results are presented both when the internuclear potential is omitted and when it is included. They are compared with recent experimental data for fully differential cross sections for 3.6 MeV u^{-1} Au^{Z_P+}+He collisions, $Z_P = 24, 53$.

The subject of single ionization of neutral target atoms by charged particle impact has been the focus of intense interest for decades by both theoretical and experimental physicists due to its practical applications in various fields such as fusion research and astrophysics. In recent years advances in experimental techniques have made it possible to make measurements of a large variety of processes, in different energy regimes, for different targets and projectile charge states. For example, ejected electron spectroscopy has been very successful at reproducing measurements of double-differential cross sections as a function of ionized electron energy and angle [573]. More recently the advent of reaction microscopy enables measurements to be made simultaneously of the momenta of the emitted electrons and the recoiling residual target ion, which gives direct evidence of the momentum transferred in the collision. For fast heavy ions Moshammer et al. [441] measured the momentum vectors of the ejected electron and recoil-ion and obtained the scattered projectile momentum from the momentum conservation law. However, in the analysis of this and subsequent experiments Schmitt et al., [535] focused on differential and recoil-ion momentum distributions. More recently, Schulz et al. and Fischer et al. [538], [269] have used reaction microscopy to examine triply and fully differential cross sections, respectively, for fast ion–atom collisions at large perturbations.

From a theoretical standpoint, the main difficulty is that it is not possible to solve the Schrödinger equation in closed analytical form, even for three mutually interacting particles. A comprehensive formulation of the complete collision involving interaction between the projectile, electron, and residual ion thus necessitates a numerical approach.

A number of different computer simulations have been used to model ion–atom collisions: classical trajectory Monte Carlo [2], [3], first Born approximation [41], coupled-state [583], [371], [607], and continuum-distorted-wave eikonal-initial-state [62], [180] calculations to name a few. In particular, the single ionization of helium has been widely studied [538], [269], [119], [267], [475], [356], [516].

The simplest model for the ionization process involves a three-particle system interacting through long-range Coulomb potentials. From a theoretical perspective the main problem is the representation of the final electronic state, where the ionized electron travels under the influence of the Coulomb potentials due to both the projectile and target nuclei. Due to the long-range behaviour of the Coulomb interaction this cannot be represented by a plane wave. Although an exact analytical solution of the three-body problem is not possible, its asymptotic form may be found [180], [260], [316], [471], [470]. One useful perturbative method that accounts for long-range Coulomb potentials at intermediate and high energies is continuum-distorted-

wave theory. It was originally introduced by Cheshire [112] to model the process of charge transfer during the collision of an atom or ion with an ion and later applied to single ionization for ion–atom collisions by Belkić [62]. However, one major defect of the CDW ionization theory developed by Belkić [62], was that it led to unphysical results due to the fact that the initial state was not normalized at low impact energies [178]. This flaw was corrected by the continuum-distorted-wave theory first introduced by Crothers and McCann [180]. The original model itself was developed to accommodate multielectron targets [471], [469], [470], [262], [421]. CDW-EIS takes into account most of the post-collision interaction (PCI) that occurs [179], due to the final-state CDW two-centre wave function being projectile and target based. The model approximates the ionized electron-residual target interaction by a Coulombic potential with the ejected electron ionized from an orbital of Roothan-Hartree-Fock (RHF) type and moves in the residual potential. Continuum states are described by hydrogenic wave functions with an effective charge chosen from the energy of the initial bound state.

Theoretical results presented for fully differential cross sections in [269], [538], [273] have shown that, at large perturbations, Z_p/v_p, where Z_p and v_p are the charge and velocity of the projectile, respectively, the discrepancy between CDW-EIS and experimental results is very apparent. In particular, what was initially thought to be the recoil peak, see [269], [273], which occurs in the forward-scattering direction, is not reproduced. One of the advantages of CDW-EIS is that most of the PCI is included [179]. It was initially thought [538] that this discrepancy was due to the lack of orthogonality between the EIS- and the CDW-state wave functions. However, Bubelev and Madison [97] reported that orthogonality was not required as the interaction potential was already included in the wave functions. Therefore, it was concluded that the missing projectile-target internuclear potential might account for the lack of the recoil peak.

We will discuss the formulation and results of a new four-body model to study the fully differential cross section (FDCS) for the single ionization of a neutral helium target by 3.6 MeV amu^{-1} Au$^{Z_P+}$, $Z_P = 24, 53$, where the ion is treated as if it were fully stripped since the electrons are so tightly bound.

The case of ionization of the projectile may be neglected due to its large charge, which as we have indicated means that the electrons will be tightly bound and therefore very unlikely to be ionized.

Atomic units are used throughout and will be explicitly stated later.

The FDCS is given by

$$\frac{\mathrm{d}^5 Q}{\mathrm{d}E_k \mathrm{d}\Omega_k \mathrm{d}\Omega_f} = \frac{\mu^2 k}{4\pi^2}\left|T_{if}\right|^2 \tag{4.231}$$

where T_{if}, the transition matrix in the wave treatment, is given by

$$\mathrm{T}^+(\boldsymbol{k}_T;\eta) = \langle \chi_f^-|W_f^+|\chi_i^+\rangle \tag{4.232}$$

μ is the reduced mass of the heavy particles, and Ω_k and Ω_f are the solid angles about the direction of the ejected electron momentum $\boldsymbol{k}$ and final wave vector $\boldsymbol{k}_f$, respectively.

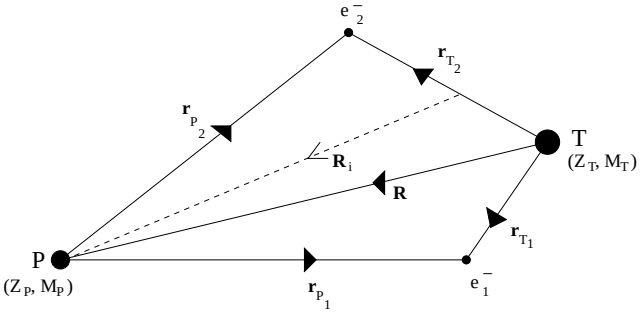

Fig. 4.11. The four-body diagram

It is important to note that in some work what is referred to here as the quintuple differential cross section is also called the triple differential cross section [273], [269]. This is because the $d\Omega$ may be counted as a single or double differential, where in the latter it is recognised that differentiation of the θ and ϕ variables is required.

In this new formulation the neutral helium target is considered in detail and its two electrons are treated as indistinguishable and explicitly correlated. This system with the projectile traveling with impact velocity $\boldsymbol{v}$ is shown in Figure 4.11. $\boldsymbol{R}_i$ is the position vector of the projectile with respect to the centre of mass of the target system and $\boldsymbol{K}_i$ is the relative momentum of the projectile with respect to the target system. Also

$$\begin{aligned} \boldsymbol{r}_{12} &= \boldsymbol{r}_{T_1} - \boldsymbol{r}_{T_2} \\ &= \boldsymbol{r}_{P_1} - \boldsymbol{r}_{P_2} \end{aligned} \tag{4.233}$$

and the momentum of the ejected electron relative to the projectile nucleus is $\boldsymbol{p} = \boldsymbol{k} - \boldsymbol{v}$.

The initial-state wave function (with eigenvalue ϵ_{pluv}) is taken from Pluvinage [493], [494], [189], where the electron-translation factors have been included for completeness [192], even though they cancel at a later stage. The initial-state wave function is taken to be

$$\begin{aligned} \chi_i^+ = N(k')\frac{2^3}{\pi} &\exp(-2(r_{T_1} + r_{T_2}) - \mathrm{i}k' r_{12} + i\mu \boldsymbol{v_i}.\boldsymbol{R_i}) \\ &\exp\left(-\frac{\mathrm{i}}{2}\boldsymbol{v}.\boldsymbol{r}_{T_1} - \frac{\mathrm{i}}{2}\boldsymbol{v}.\boldsymbol{r}_{T_2}\right) M\left(1 + \frac{1}{2\mathrm{i}k'}; 2; 2\mathrm{i}k' r_{12}\right) \\ &\exp\left(\frac{-\mathrm{i}Z_P}{v} \ln[(v r_{P_1} + \boldsymbol{v}.\boldsymbol{r}_{P_1})(v r_{P_2} + \boldsymbol{v}.\boldsymbol{r}_{P_2})]\right). \end{aligned} \tag{4.234}$$

The regular Kummer function, $M(a, b, z)$, represents correlation between the two electrons bound to the target. It may be thought of as representing a continuum-distorted-wave treatment of bound-state electrons, each of which lies in the continuum of the other. The last exponential relates to the two electrons being in the

continuum of the projectile. It is clear in the initial wave function that if the two target electrons are swapped, there is no difference to the initial-state wave function.

The final-state wave function is a continuum-distorted-wave final state, given by

$$\begin{aligned}\chi_f^- = {} & \frac{1}{\sqrt{2}}[1 + \boldsymbol{P}_{12}](2\pi)^{-3/2}\sqrt{\frac{2^3}{\pi}}2k\exp\left(\frac{-\pi}{4k}+\frac{\pi}{k}\right)\\ & \sqrt{\sinh\left(\frac{\pi}{2k}\right)}\sqrt{\sinh\left(\frac{2\pi}{k}\right)}\exp\left(-\frac{\mathrm{i}}{2}\boldsymbol{v}.\boldsymbol{r}_{T_1}-\frac{\mathrm{i}}{2}\boldsymbol{v}.\boldsymbol{r}_{T_2}\right)\\ & \exp\left(-2r_{T_1}+\mathrm{i}\boldsymbol{k}.\boldsymbol{r}_{T_2}+\mathrm{i}\mu\boldsymbol{v}_f.\boldsymbol{R}_i-\mathrm{i}kr_{12}\right)\\ & M\left(1+\frac{1}{2\mathrm{i}k};2;2\mathrm{i}kr_{12}\right)M\left(\frac{-2\mathrm{i}}{k};1;-\mathrm{i}kr_{T_2}-\mathrm{i}\boldsymbol{k}.\boldsymbol{r}_{T_2}\right)\\ & D_P^-(\boldsymbol{p},\boldsymbol{r}_{P_2})\exp\left(\frac{-\mathrm{i}Z_P}{v}\ln(vr_{P_1}+\boldsymbol{v}.\boldsymbol{r}_{P_1})\right)\end{aligned} \tag{4.235}$$

given that $\boldsymbol{P}_{12}$ is the permutation operator, which interchanges electrons 1 and 2, and

$$k' = 0.41 \quad N(k') = 1.5365 \quad \epsilon_{\text{pluv}} = -2.878 \tag{4.236}$$

and

$$D_P^-(\boldsymbol{p},\boldsymbol{r}_{P_2}) = N^-\left(\frac{Z_P}{p}\right)M\left(-\mathrm{i}\frac{Z_P}{p}1,-\mathrm{i}pr_{P_2}-\mathrm{i}\boldsymbol{p}.\boldsymbol{r}_{P_2}\right), \tag{4.237}$$

as in [192].

Notice that in (4.235) the electron-translation factors have again been included to give the full final-state wave function.

The final-state is very similar to a CDW approximation except that we have included a new Kummer function, $M(1 + (1/2\mathrm{i}k); 2; 2\mathrm{i}kr_{12})$, and an extra term in the exponential involving r_{12}. It was chosen by analogy with the initial-state continuum correlation. Electron 1 is in the projectile continuum and bound to the target; electron 2 is ionized.

The analysis of this new model was carried out in generalized nonorthogonal coordinates $(\boldsymbol{r}_{T_1}, \boldsymbol{r}_{T_2}, \boldsymbol{r}_{P_1}, \boldsymbol{r}_{P_2}, \boldsymbol{r}_{12}, \boldsymbol{R})$ and from consideration of the Schrödinger equation, 12 nonorthogonal kinetic energy terms were found. These were

$$\begin{aligned}&-\nabla_{\boldsymbol{r}_{T_1}}.\nabla_{\boldsymbol{r}_{T_2}} \; -\nabla_{\boldsymbol{r}_{T_1}}.\nabla_{\boldsymbol{r}_{12}} \; +\nabla_{\boldsymbol{r}_{T_2}}.\nabla_{\boldsymbol{r}_{12}}\\ &-\nabla_{\boldsymbol{r}_{P_1}}.\nabla_{\boldsymbol{r}_{12}} \; +\nabla_{\boldsymbol{r}_{P_2}}.\nabla_{\boldsymbol{r}_{12}} \; -\nabla_{\boldsymbol{r}_{P_1}}.\nabla_{\boldsymbol{r}_{P_2}}\\ &-\nabla_{\boldsymbol{r}_{T_2}}.\nabla_{\boldsymbol{r}_{P_1}} \; -\frac{1}{M}\nabla_{\boldsymbol{r}_{T_1}}.\nabla_{\boldsymbol{R}} \; +\frac{1}{M}\nabla_{\boldsymbol{r}_{P_1}}.\nabla_{\boldsymbol{R}}\\ &-\frac{1}{M}\nabla_{\boldsymbol{r}_{T_2}}.\nabla_{\boldsymbol{R}} \; -\frac{1}{M}\nabla_{\boldsymbol{r}_{P_2}}.\nabla_{\boldsymbol{R}} \; -\nabla_{\boldsymbol{r}_{T_2}}.\nabla_{\boldsymbol{r}_{P_2}}\end{aligned}$$

The final term for the nonorthogonal kinetic energies is taken to be the perturbation, as in standard perturbation methods. It was found that all other terms canceled when operating on the final state, therefore the residual interaction, in post form, is:

$$
\begin{aligned}
W_f\chi_f^- = {} & \frac{1}{\sqrt{2}}[1 + \boldsymbol{P}_{12}](2\pi)^{-3/2}\sqrt{\frac{2^3}{\pi}}2k\exp\left(\frac{-\pi}{4k} + \frac{\pi}{k}\right) \\
& \sqrt{\sinh\left(\frac{\pi}{2k}\right)}\sqrt{\sinh\left(\frac{2\pi}{k}\right)}\exp\left(-\frac{\mathrm{i}}{2}\boldsymbol{v}.(\boldsymbol{r}_{T_1} + \boldsymbol{r}_{T_2})\right) \\
& \exp\left(-2r_{T_1} + \mathrm{i}\boldsymbol{k}.\boldsymbol{r}_{T_2} + \mathrm{i}M\boldsymbol{v}_f.\boldsymbol{R}_i - \mathrm{i}kr_{12}\right) \\
& \boldsymbol{\nabla}_{\boldsymbol{r}_{T_2}}\left(M\left(1 + \frac{1}{2\mathrm{i}k}; 2; 2\mathrm{i}kr_{12}\right)\right. \\
& \left. M\left(\frac{-2\mathrm{i}}{k}; 1; -\mathrm{i}kr_{T_2} - \mathrm{i}\boldsymbol{k}.\boldsymbol{r}_{T_2}\right)\right) \\
& .\boldsymbol{\nabla}_{\boldsymbol{r}_{P_2}}(D_P^-(\boldsymbol{p}, \boldsymbol{r}_{P_2}))\exp\left(\frac{-\mathrm{i}Z_P}{v}\ln(vr_{P_1} + \boldsymbol{v}.\boldsymbol{r}_{P_1})\right)
\end{aligned}
\tag{4.238}
$$

In (4.238) the very last eikonal factor represents the interaction of the projectile with the bound electron. When the coordinates of the electrons are interchanged, so that electron 2 becomes the bound electron, using the permutation operator, the transition amplitude is identical to that when electron 1 is the bound electron. Hence, the permutation operator gives:

$$
\frac{1}{\sqrt{2}}[1 + \boldsymbol{P}_{12}] = \sqrt{2} \tag{4.239}
$$

The position vector of the projectile with respect to the centre of mass of the target system, $\boldsymbol{R}_i$, may be rewritten in terms of $\boldsymbol{r}_{T_2}$ and $\boldsymbol{r}_{P_2}$ as

$$
\begin{aligned}
\boldsymbol{R}_i &= \boldsymbol{R} - \frac{m}{M_T + 2m}(\boldsymbol{r}_{T_1} + \boldsymbol{r}_{T_2}) \\
&= \boldsymbol{r}_{T_2} - \boldsymbol{r}_{P_2} - \frac{m}{M_T + 2m}(\boldsymbol{r}_{T_1} + \boldsymbol{r}_{T_2}) \\
&\approx \boldsymbol{r}_{T_2} - \boldsymbol{r}_{P_2} + O\left(\frac{1}{M_T}\right)
\end{aligned}
$$

and the fact that r_{12} can be written as $r_{12} = |\boldsymbol{r}_{P_1} - \boldsymbol{r}_{P_2}|$, which implies that r_{12} can be regarded as independent of $\boldsymbol{r}_{T_2}$, such that the Kummer function involving r_{12} may be taken outside the influence of the $\boldsymbol{\nabla}_{\boldsymbol{r}_{T_2}}$, simplifies the calculation of the transition amplitude.

The transition amplitude can then be found from (4.232). After manipulation of the terms involving r_{12} and $\boldsymbol{r}_{T_1}$ by Fourier and inverse Fourier transforms the transition amplitude may be separated into a three-fold integral.

$$
\begin{aligned}
\mathrm{T}^{+}(\boldsymbol{k}_T;\eta) = {} & N(k')\frac{2^3}{\pi}(2\pi)^{-3/2}\times 16(2\pi\mathrm{i})^{-1}2k\sqrt{\frac{2^4}{\pi}} \\
& \times\exp\left(\frac{-\pi}{4k}+\frac{\pi}{k}\right)\sqrt{\sinh\left(\frac{\pi}{2k}\right)}\sqrt{\sinh\left(\frac{2\pi}{k}\right)} \\
& \times\int\frac{\mathrm{d}\boldsymbol{P}}{P}(F(-P)-F(P))\frac{1}{(16+P^2)^2} \\
& \times\int\mathrm{d}\boldsymbol{r}_{T_2}\exp(-\mathrm{i}\boldsymbol{P}.\boldsymbol{r}_{T_2}-2r_{T_2}+\mathrm{i}\boldsymbol{q}.\boldsymbol{r}_{T_2}-\mathrm{i}\boldsymbol{k}.\boldsymbol{r}_{T_2})\boldsymbol{\nabla}_{\boldsymbol{r}_{T_2}} \\
& \times\left[M\left(\frac{2\mathrm{i}}{k};1;\mathrm{i}kr_{T_2}+\mathrm{i}\boldsymbol{k}.\boldsymbol{r}_{T_2}\right)\right] \\
& \times\int\mathrm{d}\boldsymbol{r}_{P_2}\exp\left(-\mathrm{i}\boldsymbol{q}.\boldsymbol{r}_{P_2}-\frac{\mathrm{i}Z_P}{v}\ln[(vr_{P_2}+\boldsymbol{v}.\boldsymbol{r}_{P_2})]\right) \\
& \times\boldsymbol{\nabla}_{\boldsymbol{r}_{P_2}}(D_P^{-*}(\boldsymbol{k}_P,\boldsymbol{r}_{P_2}))
\end{aligned}
\tag{4.240}
$$

Each of the two integrations involving $\boldsymbol{r}$ is solvable (see Section 1.4) by using the Nordsieck integral [461], or a generalized form of the Nordsieck integral [157] to give the final form of the FDCS to be

$$
\begin{aligned}
\frac{\mathrm{d}^5Q}{\mathrm{d}E_k\,\mathrm{d}\Omega_k\,\mathrm{d}\Omega_f} = {} & \frac{\mu^2k}{4\pi^2}\left|T_{if}\right|^2 \\
= {} & \frac{\mu^2k}{4\pi^2}|C|^2\left|\int\frac{\mathrm{d}\boldsymbol{P}}{P}(\,F(-P)-F(P))\frac{1}{(16+P^2)^2}\frac{1}{\alpha_2(\alpha_2+\beta_2)}\right. \\
& \times\left(\frac{\alpha_2}{\alpha_2+\beta_2}\right)^{\mathrm{i}\epsilon}\left[(\boldsymbol{q}-\boldsymbol{P}-\boldsymbol{k})-2\mathrm{i}\hat{\boldsymbol{k}}\right]\frac{1}{\alpha_1\gamma_1}\left(\frac{\alpha_1}{\beta_1}\right)^{\mathrm{i}\nu}\left(\frac{\alpha_1}{\gamma_1}\right)^{\mathrm{i}\zeta} \\
& \left[-\boldsymbol{q}\,{}_2F_1(\mathrm{i}\nu,\mathrm{i}\zeta;1;z)-\mathrm{i}\left(\frac{\alpha_1}{\gamma_1\beta_1}\right)\nu\,(\gamma_1(\hat{\boldsymbol{p}}v-\boldsymbol{v})-\delta_1\boldsymbol{q})\right. \\
& \left.\left.\times{}_2F_1(1+\mathrm{i}\nu,1+\mathrm{i}\zeta;2;z)\right]\right|^2
\end{aligned}
\tag{4.241}
$$

The terms in (4.241) are defined as follows:

$$F(P) = \frac{(\Lambda - iP)^{\frac{i}{2k} - \frac{i}{2k'}}}{(\Lambda - iP + 2ik)^{1+\frac{i}{2k}}(\Lambda - iP - 2ik')^{1-\frac{i}{2k'}}}$$
$${}_2F_1\left(1 - \frac{i}{2k'}, 1 + \frac{i}{2k}; 2; \frac{4kk'}{(\Lambda - iP + 2ik)(\Lambda - iP - 2ik')}\right) \tag{4.242}$$

$$\alpha_1 = \frac{1}{2}\boldsymbol{q}^2 \tag{4.243}$$

$$\beta_1 = -\boldsymbol{v}.\boldsymbol{q} \tag{4.244}$$

$$\delta_1 = \boldsymbol{p}.\boldsymbol{v} - pv + \beta_1 \tag{4.245}$$

$$\gamma_1 = -\boldsymbol{p}.\boldsymbol{q} + \alpha_1 \tag{4.246}$$

$$z = \frac{\beta_1\gamma_1 - \alpha_1\delta_1}{\beta_1\gamma_1} \tag{4.247}$$

$$\alpha_2 = \frac{1}{2}((\boldsymbol{q} - \boldsymbol{P} - \boldsymbol{k})^2 + 4) \tag{4.248}$$

$$\beta_2 = \boldsymbol{k}.(\boldsymbol{q} - \boldsymbol{P} - \boldsymbol{k}) - 2\mathrm{i}k \tag{4.249}$$

$$\epsilon = \frac{2.0}{k} \tag{4.250}$$

$$\nu = \frac{Z_P}{v} \tag{4.251}$$

$$\zeta = \frac{Z_P}{p} \tag{4.252}$$

$$\Lambda = \mathrm{i}k' - \mathrm{i}k \tag{4.253}$$

$$C = N(k')N^*(\zeta)N(\nu)\,k\,Z_P\,\mathrm{i}\,2^{21/2}\pi^{-2}\exp\left(\frac{3\pi}{4k}\right) *$$
$$\sqrt{\sinh\left(\frac{\pi}{2k}\right)}\sqrt{\sinh\left(\frac{2\pi}{k}\right)} \tag{4.254}$$

The results of this theory are presented later. They are compared to the absolute experimental data of [538], as in [269], and all the theoretical results are absolute.

The results are [483], [484] of FDCSs for 3.6MeV amu^{-1} Au$^{Z_P+}$+He collisions, $Z_P = 24, 53$, and they all have a period of 2π. The units are given in atomic units. Therefore, the calculations for the FDCS in (4.231) have units of

$$a_0^2 u^{-2} ster^{-2} / \left(\frac{e^2}{a_0}\right) = a_0^3 u^{-2} ster^{-2} e^{-2} \tag{4.255}$$

These units may be deduced by looking at the left-hand side of (4.231).

Figures 4.12a and b show the FDCS for 3.6 MeV amu^{-1} Au^{24+}+He collisions for momentum transfers of $q = 0.45$ a.u. and 0.65 a.u., respectively, and ejected electron energy of 4 eV. The results for the new formulation are the solid line, while the experimental data (dots) are from Fischer et al. [269].

By examining Figures 4.12a and b it is seen that the theoretical results predict a structure or a "bulge" in the forward direction; it may not be to a similar extent as

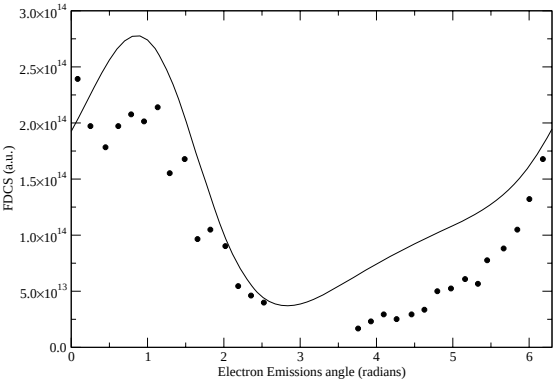

Fig. 4.12a. FDCS for electrons emitted into the scattering plane for a fixed electron energy, $E_k = 4\ eV$, and fixed magnitude of the momentum transfer $q = 0.45$ a.u., as a function of the polar electron emission angle for 3.6 MeV amu^{-1} Au^{24+}+ He collisions. • experimental data [269] — theoretical results

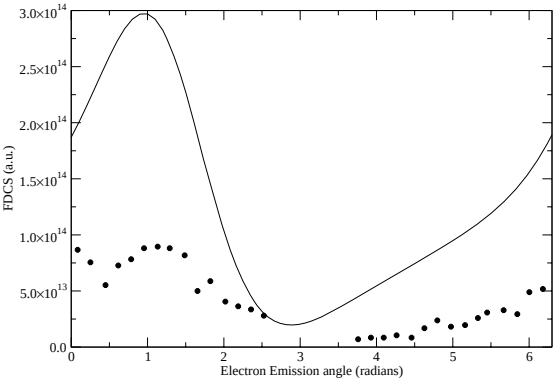

Fig. 4.12b. As in Figure 4.12a except with $q = 0.65$ a.u.

the experimental results, but it is present for these particular values of momentum transfer and ejected electron energy, unlike previous CDW-EIS results [269], [538], [273]. This may be attributed to the fact that the current model is a four-body model whereas the previous models are only three-body models. A peak in the direction of $\boldsymbol{q}$ is not present in the experimental data but it is present in some existing CDW-EIS calculations, [269, 538, 273]; the current results agree with the experimental data in that they do not exhibit a peak in the direction of $\boldsymbol{q}$. In Figures 4.12a and b the peak referred to as the binary peak in Foster et al. [273] is observed in about the same position as the experimental binary peak.

The agreement, in terms of magnitude, between experiment and the theoretical calculations is mixed. In Figure 4.12a the theoretical calculation for $q = 0.45$ a.u. is in much better agreement with experiment than the CDW-EIS results from [273], figure 2, top graph. The new theoretical calculation is slightly larger than experiment

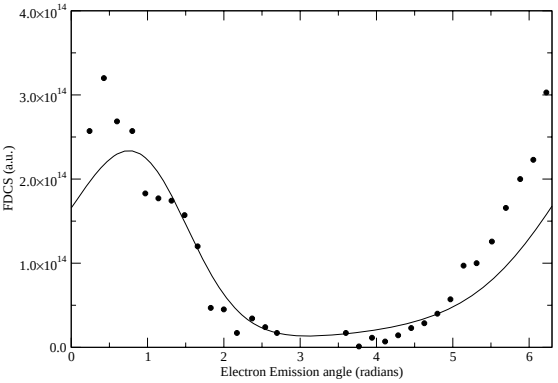

Fig. 4.13a. As in Figure 4.12a except for FDCS for Au^{53+}+ and with $q = 0.65$ a.u.

and by comparison with the top graph of figure 2 from [273] it is seen that the three-distorted-wave eikonal-initial-state, (3DW-EIS) results from Foster et al. are closer, in magnitude to the absolute experimental results for the region 3.7 radians to 4.7 radians. In Figure 4.12b the theoretical calculation is much larger than the theoretical 3DW-EIS and CDW-EIS results from [273], figure 2, bottom graph.

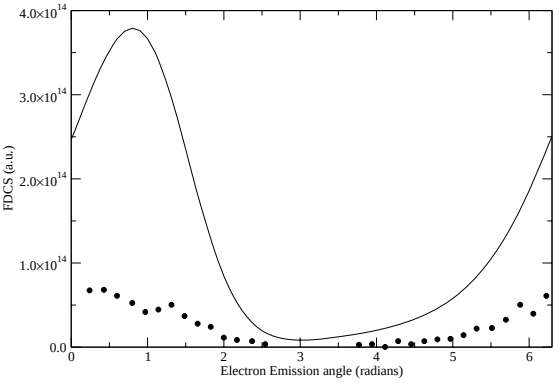

Fig. 4.13b. As in Figure 4.13a except with $q = 1.0$ a.u.

Figures 4.13a and b show the FDCS for 3.6 MeV amu^{-1} Au^{53+}+He collisions for momentum transfers of $q = 0.65$ a.u. and 1.0 a.u., respectively, and ejected electron energy of 4 eV. The results for the new formulation are the solid line, while the experimental data (dots) are from Fischer et al. [269].

By examination of Figures 4.13a and b one can see that once again, this current formulation produces a forward-scattering structure. However, in Figure 4.13b the magnitude of the forward structure is larger than experiment, but in 4.13a the forward structure predicted by theoretical results is just below the experimental data.

In Figure 4.13a the experimental data show that there is one large peak at about $30^\circ = 0.5$ radians. The theoretical results, despite predicting only one peak, at about 1.0 radian, are in good agreement with the absolute experimental results.

In Figure 4.13b theoretical calculations reproduce the forward structure, but it is dominated by a binary peak, which is not prominent in the experimental data. There is a peak about 1.4 radians in the experimental data but it is not very large, certainly not to the extent of the theoretical data. Also, the angle of the binary peak for the theoretical data appears too early, about 1.0 radian. In both Figures 4.13a and b the magnitude of these current results is in much better agreement than 3DW-EIS and CDW-EIS [273], as their theoretical results have been scaled up by a factor of 20.

In this new four-body model we have shown that there is mixed agreement with experimental data. The shape agrees well but the agreement of the magnitude is varied. However, there is one piece of information missing from this model. It is the internuclear potential. Previously [269], the inclusion of it made a significant difference to results, so its inclusion in this current model is imperative. The internuclear potential is included by the following equation:

$$T_{if}(\boldsymbol{\eta}) = \int_0^\infty \mathrm{d}\rho \mathrm{J}_0(\eta\rho)(\rho)^{1+\frac{2\mathrm{i}Z_T Z_P}{v}} \int_0^\infty T'_{if}(\boldsymbol{\eta}')\mathrm{J}_0(\eta'\rho)\eta'\mathrm{d}\eta' \tag{4.256}$$

using two semiclassical transformations. The phase involving only the velocity has been omitted as when the square of the modulus of the transition amplitude is taken it contributes a factor of 1.

Including (4.256) into the analysis means that two extra integrations have to be added to the computer program. This itself is of no consequence but the integration over ρ contains the term $\rho^{1+(2\mathrm{i}Z_T Z_P/v}$, which is oscillatory, and when integrating it adds considerable computing time. To overcome this, the order of integration is changed. This means that:

$$T_{if}(\boldsymbol{\eta}) = \int_0^\infty \eta'\mathrm{d}\eta' T'_{if}(\eta')F(\eta,\eta') \tag{4.257}$$

where

$$F(\eta,\eta') = \int_0^\infty (\rho)^{1+\frac{2\mathrm{i}Z_T Z_P}{v}} \mathrm{J}_0(\eta'\rho)\mathrm{J}_0(\eta\rho)\mathrm{d}\rho \tag{4.258}$$

This is the same as [515] but with $m = 0$. The difference in the following work from [515] is the way (4.258) is solved. The inner integral from (4.257), $F(\eta,\eta')$, is of Weber-Schafheitlin type and may be solved using equations 11.4.33 and 11.4.34 from [1]. They have the basic solution:

$$\int_0^\infty \mathrm{J}_0(at)\mathrm{J}_0(bt)t^{-\lambda}\mathrm{d}t = \frac{\Gamma\left(\frac{1-\lambda}{2}\right)}{2^\lambda b^{1-\lambda}\Gamma\left(\frac{1+\lambda}{2}\right)} {}_2F_1\left(\frac{1-\lambda}{2},\frac{1-\lambda}{2};1;\frac{a^2}{b^2}\right) \tag{4.259}$$

One condition on (4.259) is $0 < a < b$. If $0 < b < a$, then a and b are simply interchanged in (4.259).

Letting a be the minimum of $(\eta,\ \eta')$ while b is the maximum of $(\eta,\ \eta')$ and

$$\lambda = -1 - \frac{2iZ_TZ_P}{v}$$

(4.258) is solved. We assume that $\Re(\lambda) = -1 + \varepsilon$ $(\varepsilon > 0)$. After simplification of the gamma functions and the hypergeometric function, it is seen that (4.258) gives

$$F(\eta,\eta') = \frac{2Z_TZ_P}{v} b^{-2\left(1+\frac{iZ_TZ_P}{v}\right)} \mathrm{J}_0\left(\frac{2Z_TZ_Pa}{vb}\right) \tag{4.260}$$

When (4.260) is substituted back into (4.257) the internuclear potential is found through one extra numerical integration;

$$I(\eta) = \frac{2Z_TZ_P}{v} \int_0^\infty \eta' \mathrm{d}\eta' T'_{if}(\eta') b^{-2\left(1+\frac{iZ_TZ_P}{v}\right)} \mathrm{J}_0\left(\frac{2Z_TZ_Pa}{vb}\right) \tag{4.261}$$

This equation is much easier to calculate given, that it is not as oscillatory as (4.256) and the fact that only one extra numerical integration is required compared to the previous two.

In (4.261) it is assumed that b is the maximum of (η, η'); this means that b changes during the integration in (4.261). To overcome this difficulty the integration in (4.261) is split into two: one where η is the larger and the other where η' is the larger. This gives:

$$I(\eta) = \frac{2Z_TZ_P}{v} \left[\int_0^\eta \eta' \mathrm{d}\eta' T'_{if}(\eta') \eta^{-2\left(1+\frac{iZ_TZ_P}{v}\right)} \mathrm{J}_0\left(\frac{2Z_TZ_P\eta'}{v\eta}\right) + \int_\eta^\infty \eta' \mathrm{d}\eta' T'_{if}(\eta') \eta'^{-2\left(1+\frac{iZ_TZ_P}{v}\right)} \mathrm{J}_0\left(\frac{2Z_TZ_P\eta}{v\eta'}\right) \right] \tag{4.262}$$

Figures 4.14a to b show the FDCS for 3.6 MeV amu^{-1} Au^{24+}+He collisions for momentum transfers of $q = 0.45$ a.u. and 0.65 a.u. and ejected electron energy of 4 eV, while Figures 4.15a to b show the FDCS for 3.6MeV amu^{-1} Au^{53+}+He collisions for momentum transfers of $q = 0.65$ a.u. and 1.0 a.u., respectively, and ejected electron energy of 4 eV.

Each figure includes the absolute experimental data from [269], *dots* $(\cdot)$; the theoretical results from section III, *solid line* (—, without nn); and the theoretical results including the internuclear potential, *dot dash line* ($\cdot\cdot$ —, with nn). The factor of any required scaling is displayed on the individual graphs.

In Figures 4.14a and b it is clear to see that the predicted position of the binary peak has shifted to the left upon inclusion of the internuclear potential. This means that the theoretical structure changes slightly, but for Figure 4.14a it is in better agreement with the first half of the experimental data. In comparison, the inclusion of the

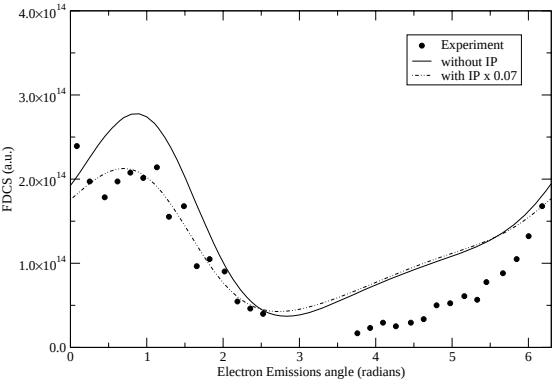

Fig. 4.14a. FDCS for electrons emitted into the scattering plane for a fixed electron energy, $E_k = 4$ eV, and fixed magnitude of the momentum transfer $q = 0.45$ a.u., as a function of the polar electron emission angle for 3.6 MeV amu^{-1} Au^{24+}+ He collisions. • experimental data [269] — theoretical results, – · ·– theoretical results including internuclear potential [484]

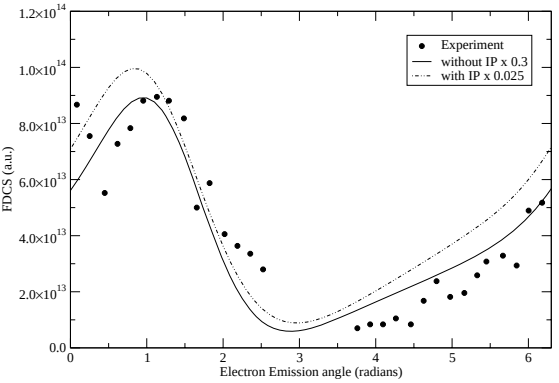

Fig. 4.14b. FDCS for 3.6 MeV amu^{-1} Au^{24+}+ He collisions. $E_k = 4$ eV and $q = 0.65$ a.u.

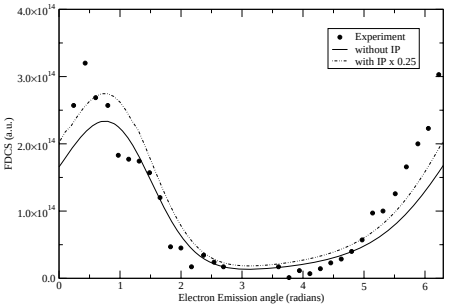

Fig. 4.15a. FDCS for 3.6 MeV amu^{-1} Au^{53+}+ He collisions. $E_k = 4$ eV and $q = 0.65$ a.u.

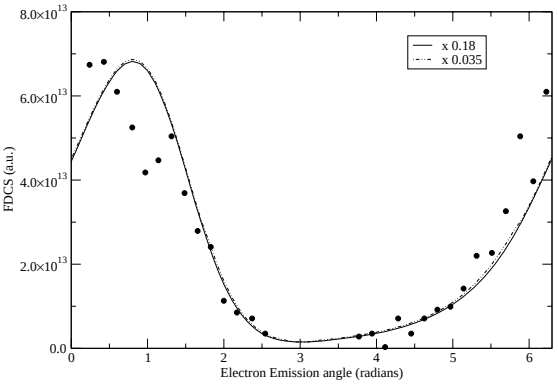

Fig. 4.15b. FDCS for 3.6 MeV amu^{-1} Au^{53+}+ He collisions. $E_k = 4$ eV and $q = 1.0$ a.u.

internuclear potential in Figures 4.15a and b has very little effect on the structure of the theoretical results and only seems to effect the magnitude. The inclusion of the internuclear potential has increased the magnitude of the theoretical results, which in Figures 4.14a–4.15b leaves the theoretical results without the internuclear potential, in better agreement with experimental data. However, it is important to note that in Figures 4.15a and b the internuclear potential results have been scaled down by factors of 4 and 5.5 and are therefore still closer to the experimental data than the results in [273], which have been scaled up by a factor of 20; see figure 4 of [273].

It is hard to compare the theoretical results obtained in this paper for the collisions mentioned due to the lack of absolute experimental and theoretical data. Another problem when comparing with other theoretical results is the units; these are not always consistent and quite often the FDCS in one paper have different units from those in another.

Despite these problems, what has been presented here is a four-body formulation that in some cases is in good agreement with experiment. When a higher momentum transfer is considered for 3.6 MeV amu^{-1} Au^{24+}+He collisions, as in Figures 4.12b and 4.14b, the theoretical calculations overestimate the experimental data and for a higher momentum transfer of 1.0 a.u. for 3.6 MeV amu^{-1} Au^{53+}+He collisions, this formulation also overestimates the experimental data.

We have presented new theoretical results from a four-body treatment for FDCSs of 3.6 MeV amu^{-1} Au^{Z_P+}+He collisions, $Z_P = 24, 53$, with ejected electron energy of 4 eV. It gives theoretical results for the inclusion and omission of the internuclear potential. Results are an improvement on current CDW-EIS calculations for these collisions, especially in the Au^{53+} case. The experimental forward-scattering peak is visible in the form of a "bulge" in the theoretical results.

The inclusion of the internuclear potential has shifted all the Au^{24+} results to the left, resulting in improved agreement in Figure 4.14a with the shape of the experimental data.

In the case of Au^{53+} it is seen that the inclusion of the internuclear potential has had very little effect on the shape of the theoretical data. However, due to lack of

other absolute theoretical data it is difficult to compare these results. Nevertheless, the shapes of all sets of data are in good accord.

The discrepancies between theory and experiment might be resolved if and when the magnetic quantum numbers are taken into consideration using generalized CDW-EIS (GCDW-EIS) [197]. Figure 5 in [197] shows very good agreement with experimental results.

4.3.5 Generalized Continuum Distorted Waves

A new derivation of continuum-distorted-wave theory is presented. It is generalized to magnetically quantized continuum-distorted waves. The context is analytic continuation of hydrogenic-state wave functions from below to above threshold, using parabolic coordinates and quantum numbers including m the magnetic quantum number. This continuation applies to excitation, charge transfer, ionization, and double and hybrid events for both light- and heavy-particle collisions. It is applied to the calculation of double-differential cross sections for the single ionization of the hydrogen atom and for a hydrogen molecule by a proton for electrons ejected in the forward direction at a collision impact energy of 50 and 100 keV, respectively.

A continuum-distorted-wave [113] theory for charge transfer in ion–atom collisions was first presented by Cheshire [112]. It proved to be a remarkably successful, flexible, and pragmatic theory [63]. Many improvements have since been made. Crothers [178] showed that CDW bound states are in general unnormalized (and proposed CDW for light-particle collisions). The use of a gauge transformation in the impact parameter (ρ) time-dependent treatment leads to a ρ-dependent phase factor [415] with the internuclear potential eliminated. A necessarily on-shell derivation of CDW is more physically understandable and avoids artificial logarithmic potentials and spurious nonlocal operators [192]. The net perturbation is the nonorthogonal kinetic energy $-\partial_{\mathbf{r_T}}.\partial_{\mathbf{r_P}}$, where the electron has position vectors $\mathbf{r_P}$, $\mathbf{r_T}$ with respect to the projectile (P) and target (T) nucleus. Elastic divergence-free CDW Neumann-Born series may be derived [187] with connected kernel.

Thomas double scattering is a second-order event leading to electron capture [184], [185]. Fortunately CDW2 resolves the matter, with only one Thomas resonance, and including all strong and intermediate coupling. Moreover consideration of CDW3 [471] shows that the Thomas CDW series has converged. In the case of capture/excitation, variational coupled equations may be formulated and applied [94], [95].

For ionization, following the CDW final state of Belkič [62], Crothers and McCann [180] introduced CDW-EIS. Some of the major advantages are that both the initial and final states are normalized, all long-range Coulomb boundary conditions are satisfied, and the full two-centre final state is a product of two CDWs, one T- and one P-based, so that most of the post-collision interaction is included. A dynamic molecular theory CDW-EIS has been generalized to electron impact [346], [347] and to R (relativistic) CDW-EIS [196].

O'Rourke et al. [473] have described the application of CDW-EIS to doubly differential cross sections (DDCS) including complete longitudinal momentum distri-

butions (electron, recoil, and projectile ion). They also considered DDCS 2D plots against k/v at forward scattering and 3D plots against k/v and θ_k (where $\mathbf{v}$ is the impact velocity, $\mathbf{k}$ is the ejected electron velocity, and θ_k is the polar angle of the ejected electron).

However, no evidence was found, by our experimental and theoretical group [451], for saddle points for collisions of 40 keV protons with either He or H_2. Moreover, for 100 keV proton collisions with H_2, CDW-EIS calculations predict saddle points in contradiction with our experimental group [416]. This was puzzling, since saddle point electrons are normally associated with lower impact energies. We were therefore moved to reconsider the very basis of CDW-EIS. Accordingly a new derivation of continuum-distorted-wave theory is presented. It is generalized to magnetically quantized continuum distorted waves. The context is an analytic continuation of hydrogenic-state wave functions from below to above threshold, using parabolic coordinates and quantum numbers, including m the magnetic quantum number.

In the time-independent distorted-wave formalism, the exact transition amplitude is given in the post-interaction formulation [424] by

$$T_{fi} = \langle \psi_f^- | (H - E)^\dagger | \Psi_i^+ \rangle + \langle \psi_f^- | H - H^\dagger | \psi_i^+ \rangle \tag{4.263}$$

Here Ψ_i^+ is the exact total scattering wave function satisfying $(H-E)\Psi_i^+ = 0$ and outgoing-wave boundary conditions. The total Hamiltonian is H, the total energy is E, and dagger means complex conjugate and operating to the left. The distorted initial- and final-state CDW wave functions are ψ_i^+ and ψ_f^-, given by

$$\begin{aligned} \psi_i^+ &= \phi_i(\mathbf{r_T}) \exp(-\frac{1}{2} \mathrm{i}\mathbf{v} \cdot \mathbf{r} + \mathrm{i}\mathbf{K_i} \cdot \mathbf{R}) \\ &\quad {}^{m_i} D_{-\mathbf{v}}^+(\mathbf{r_P}, Z_P) \exp(\frac{\mathrm{i} Z_P Z_T}{v} \ln(vR - \mathbf{v} \cdot \mathbf{R})) \end{aligned} \tag{4.264}$$

$$\begin{aligned} \psi_f^- &= (2\pi)^{-\frac{3}{2}} \exp(-\frac{1}{2} \mathrm{i}\mathbf{v} \cdot \mathbf{r} + \mathrm{i}\mathbf{K_f} \cdot \mathbf{R} + \mathrm{i}\mathbf{k} \cdot \mathbf{r_T}) \\ &\quad {}^{m_T} D_{\mathbf{k}}^-(\mathbf{r_T}, Z_T)\, {}^{m_P} D_{\mathbf{k}-\mathbf{v}}^-(\mathbf{r_P}, Z_P) \\ &\quad \exp(-\frac{\mathrm{i} Z_P Z_T}{v} \ln(vR + \mathbf{v} \cdot \mathbf{R})) \end{aligned} \tag{4.265}$$

having included the internuclear eikonal phases [415]. The plane waves of the nuclear motion are parameterized by the initial ($\mathbf{K_i}$) and final ($\mathbf{K_f}$) relative momentum of the nuclei, with $\mathbf{R}$ the position vector of P with respect to T. The electron translation factor is $\exp(-1/2\, \mathrm{i}\mathbf{v} \cdot \mathbf{r})$, where $\mathbf{r}$ is the electron position vector relative to the midpoint of the nuclei. Z_T and Z_P are the target and projectile charges and $\phi_i(\mathbf{r_T})$ the initial stationary bound state. m_T, m_P, and m_i are the magnetic quantum numbers of the target, projectile, and initial state, respectively, and without any loss of generality we can set $m_i = 0$.

Here we define the CDW given by

$$
\begin{aligned}
{}^{m}D^{+}_{\mathbf{v}}(\mathbf{r};Z) &= \exp(\mathrm{i}m\phi + \frac{\pi\nu}{2}) \\
&\times \ (vr - \mathbf{v}\cdot\mathbf{r})^{\frac{|m|}{2}}(vr + \mathbf{v}\cdot\mathbf{r})^{\frac{|m|}{2}} \\
&\times \ \frac{\Gamma(1+\frac{1}{2}|m| - \mathrm{i}\nu)\Gamma(1+\frac{1}{2}|m|)}{\Gamma^2(1+|m|)} \\
&\times \ M(\mathrm{i}\nu + \frac{1}{2}|m|, 1+|m|, \mathrm{i}vr - \mathrm{i}\mathbf{v}\cdot\mathbf{r}) \\
&\times \ M(\frac{1}{2}|m|, 1+|m|, -\mathrm{i}vr - \mathrm{i}\mathbf{v}\cdot\mathbf{r}) \\
&\underset{r\to\infty}{\simeq} \exp(\mathrm{i}m\phi)(vr - \mathbf{v}\cdot\mathbf{r})^{-\mathrm{i}\nu}
\end{aligned}
\tag{4.266}
$$

where $\nu = Z/v = \mu Z/k$, μ is the reduced mass, M is the regular Kummer function, and

$$
{}^{m}D^{-}_{\mathbf{v}}(\mathbf{r};Z) = [{}^{m}D^{+}_{-\mathbf{v}}(\mathbf{r};Z)]^{*} \tag{4.267}
$$

where distorted waves satisfy the correct asymptotic boundary conditions. The results (4.266), (4.267) indicate that the three two-body phases accumulating asymptotically in equation (4.265) are correct [508]. The exact Ψ_i^+ is approximated by ψ_i^+ with the CDW taken in its eikonal form (equation (4.266)): hence G/CDW-EIS.

We note $\mathbf{p}$ is the momentum of the ejected electron relative to the projectile. ϕ_T is the angle between the planes $(\mathbf{r_T}, \mathbf{k})$ and $(\mathbf{v}, \mathbf{k})$ and ϕ_P is the angle between the planes $(\mathbf{r_P}, \mathbf{p})$ and $(\mathbf{v}, \mathbf{p})$. We note also that, although $\mathbf{p} = \mathbf{k} - \mathbf{v}$, $\mathbf{p}$ and $\mathbf{k}$ are skew vectors.

Equations (4.264) to (4.267) represent a generalization of previous CDWs [192], [179], following the introduction of three magnetic quantum numbers. They afford the inclusion of a rapidly convergent complete set of CDWs, which permits (especially target) continuum rotational coupling, an important physical mechanism. We shall present details elsewhere, while only mentioning here that, in Schiff [533] (equations 16.36, 16.37) we interchange η and ξ for convenience and set

$$
\begin{aligned}
\lambda_1 &= \frac{1}{2} - \mathrm{i}\nu \quad \text{and} \quad n_1 = -\frac{1}{2}|m| - \mathrm{i}\nu \qquad (\nu = \frac{Z}{v}) \\
\lambda_2 &= \frac{1}{2} \quad \text{and} \quad n_2 = -\frac{1}{2}|m|
\end{aligned}
\tag{4.268}
$$

where λ_1 and λ_2 are separation constants and n_1 and n_2 are the standard parabolic quantum numbers.

The uniform two-centre nature of ψ_f^- may be confirmed by noting that

$$
\exp(\mathrm{i}\mathbf{k}\cdot\mathbf{r_T})E_{\mathbf{k},-\frac{1}{2}\mathbf{v}}(\mathbf{r},t) = \exp(\mathrm{i}\mathbf{p}\cdot\mathbf{r_P} + \mathrm{i}\boldsymbol{\rho}\cdot\mathbf{k})E_{\mathbf{p},\frac{1}{2}\mathbf{v}}(\mathbf{r},t) \tag{4.269}
$$

where in the semiclassical impact parameter treatment

$$
E_{\mathbf{k},\mathbf{u}}(\mathbf{r},t) = \exp(i\mathbf{u}\cdot\mathbf{r} - \mathrm{i}\frac{u^2 t}{2} - i\frac{k^2 t}{2}) \tag{4.270}
$$

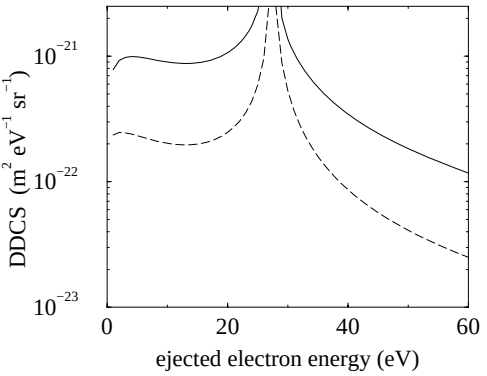

Fig. 4.16. The DDCS for the collision of 50keV proton with a hydrogen atom at an electron emission angle of 0 degrees. *Dashed line* - GCDW-EIS with $m_P = m_T = 0$ (= CDW-EIS); *solid line* - GCDW-EIS with double summation over m_P and m_T from -1 to +1

It may also be noted that in ${}^mD^+_{\mathbf{v}}(\mathbf{r};Z)$, the first M function is outgoing, whereas the second is ingoing and vice versa for ${}^mD^-_{\mathbf{v}}(\mathbf{r};Z)$.

Since $H^\dagger\psi_f^{-*}$ and $H\psi_i^+$ both contain the nonorthogonal kinetic energy $-\partial\mathbf{r_T}\cdot\partial\mathbf{r_P}$, the second term in equation (4.263) may be neglected, and the generalized (G)CDW in equation (4.264) may assume its asymptotic eikonal form, for all but the smallest partial-wave azimuthal angular momentum quantum numbers. Thus we have derived GCDW-EIS.

In Figure 4.16 we present DDCS for proton hydrogen-atom 50 keV collisions for forward scattering. We plot
$D^2\sigma/\mathrm{d}\Omega_k dE_k$ versus E_k, the ejected electron energy, where Ω_k is the solid angle $\sin\theta_k \mathrm{d}\theta_k \mathrm{d}\phi_k$. The dashed line corresponds to $m_P = 0 = m_T$ [179]. The solid line corresponds to the inclusion of $m_P = -1, 0, +1$ and $m_T = -1, 0, +1$, making nine contributions, in our new G (generalized) CDW-EIS theory for DDCS. There is a shallow minimum implying a saddle point. In Figure 4.17, we show that for $m_T = 0$, $m_P = 0$ dominates $m_P = \pm 1$, which dominates $m_P = \pm 2$.

In Figure 4.18, we show that for $m_P = 0$, $m_T = \pm 1$ dominates $m_T = \pm 2$, except very close to the cusp. However, to the left down to 10 eV, $m_T = \pm 1$ dominates $m_T = 0$. Results not shown for $m_P = \pm 2$, with $m_T = 0, \pm 1, \pm 2$, for $m_P = \pm 3$, with $m_T = 0, \pm 1, \pm 2, \pm 3$ and for $m_P = \pm 4$, with $m_T = 0, \pm 1, \pm 2, \pm 3, \pm 4$, all show DDCS orders of magnitude less and with strong anticusps.

In Figures 4.19 and 4.20, we illustrate proton hydrogen-molecule 100 keV forward-scattering DDCS, namely $k\mathrm{d}^2\sigma/\mathrm{d}E_k \mathrm{d}\cos\theta_k$ plotted against k/v. In Figure 4.19, we include only $m_P = 0 = m_T$ in the lower curve [179], whereas in the upper curve we sum the DDCS over m_P and m_T, each from minus 2 through 0 to +2. The minimum at $k/v = 0.5$ is so shallow as to be almost indistinguishable from a horizontal point of inflexion. This implies a shelf rather than a saddle.

In Figure 4.20, the DDCS of the upper curve in Figure 4.19 (summed over m_P and m_T each from minus 2 to +2) are plotted against our relative experimental re-

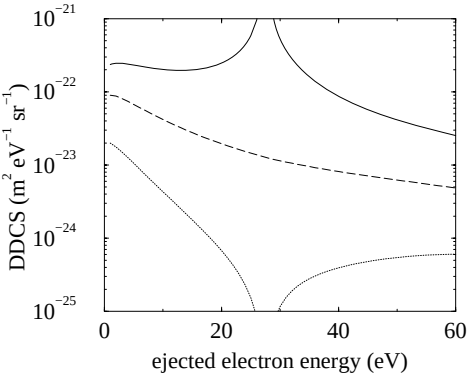

Fig. 4.17. The DDCS for the collision of 50 keV proton with a hydrogen atom at an electron emission angle of 0 degrees. *Solid line* - GCDW-EIS with $m_P = m_T = 0$ (= CDW-EIS); *dashed line* - GCDW-EIS with $m_T = 0$ and $m_P = \pm 1$; *dotted line* - GCDW-EIS with $m_T = 0$ and $m_P = \pm 2$

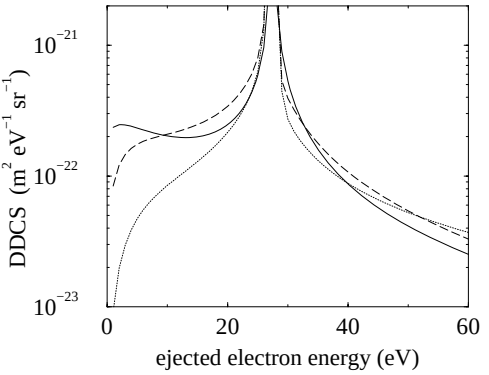

Fig. 4.18. The DDCS for the collision of 50 keV proton with a hydrogen atom at an electron emission angle of 0 degrees. *Solid line* - GCDW-EIS with $m_P = m_T = 0$ (= CDW-EIS); *dashed line* - GCDW-EIS with $m_P = 0$ and $m_T = \pm 1$; *dotted line* - GCDW-EIS with $m_P = 0$ and $m_T = \pm 2$

sults [416] suitably scaled. The agreement is much improved compared to our basic $m_P = 0 = m_T$ theory [416]. From Figure 4.19, we note that for $k < v$, the DDCS are increased and the cusp is broadened, compared to the original $m_P = 0 = m_T$ theory. This makes physical sense because slower electrons will have more time to experience rotational coupling out of their azimuthal plane. For $k > v$, the cusp is not broadened per se but for the highest values of k, the DDCS are increased. In conclusion [197], CDW, CDW-EIS, and GCDW-EIS theories have been shown to be remarkably robust in rising to the experimental challenges, both theory and experiment being generated within our own group.

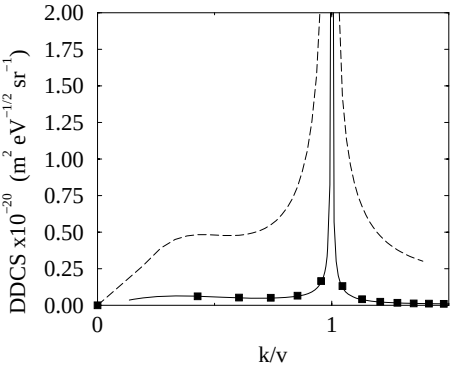

Fig. 4.19. The DDCS for the collision of 100 keV proton with H_2 at an electron emission angle of 0 degrees. *Solid line* - CDW-EIS; squares - GCDW-EIS with $m_P = m_T = 0$ showing it reduces down to original CDW-EIS theory; *dashed line* - GCDW-EIS with double summation over m_P and m_T from −2 to +2

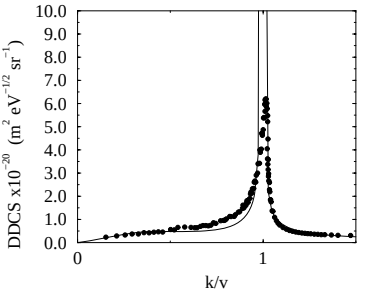

Fig. 4.20. The DDCS for the collision of 100keV proton with H_2 at an electron emission angle of 0 degrees. *Solid line* - GCDW-EIS with double summation over m_P and m_T from -2 to +2. *Circles* - experimental results of [20]

4.3.6 Double Ionization

As an example of a two-electron process we present cross sections for double ionization of helium by alpha-particle impact within the independent-event model [201]. Within this model the probability of ionizing the first electron (P_1) from neutral helium is calculated in the continuum-distorted-wave approximation using an explicitly correlated wave function of Pluvinage, whereas the probability of ionizing the second electron (P_2) from the He^+ ion is calculated in the CDW approximation with an eikonal initial state. The total probability for double ionization is then P_1P_2 rather than P_1^2, which is usually assumed in the independent-electron model. The calculated cross sections in the present model show excellent agreement with the measurement of Shah and Gilbody [549], at all energies above 200 keV u^{-1}. Two-electron transfer from a helium atom by fully stripped ions has received much attention, one of the motivations being to understand the role of electron–electron correlation in a variety

of collision processes. Double ionization is one of these processes where electron–electron correlation may be expected to contribute to the total cross section in the lower and intermediate energy regions. Indeed, Fritsch and Lin [278] found that electron–electron correlation also plays an important role in other processes, such as double excitation, for projectiles of smaller charges. Because of the complexity of a correlated two-electron wave function, most of the previous theoretical investigations are based on the independent-electron model. In this model the target wave function is described either by a one-electron hydrogenic wave function or by an uncorrelated Hartree–Fock type of wave function. Having calculated the single ionization probability by using these wave functions, one then squares this probablity, weights it by the impact parameter (ρ), and finally integrates it over the impact parameter to get the double-ionization cross sections. In other words, and in particular if an uncorrelated Hartree–Fock type of two-electron wave function is considered for the target atom, the independent-electron model does not account for correlation, as it squares the single-ionization probability to get the corresponding double-ionization probability. Shingal and Lin [555] reported a coupled-channel calculation with a large number of basis sets on each centre for one- and two-electron transfer processes within the independent-electron model. For very fast projectiles the effect of electron–electron correlation may not be significant. In this case the independent-electron model might be a reasonable description for double ionization (cf. Salin [529]).

After the first ionization event occurs, the Hamiltonian, energy, and target charge all change. The interacting system is now He^{++} on He^{+} with the other electron removed to the continuum. This is a purely Coulombic system and may be handled by an appropriately simple theoretical model. Besides, the probability of ionizing the second electron (P_2) from He^{+} by an alpha particle is expected to be smaller (cf. Basbas et al. [31]) than the probability of ionizing the first electron (P_2) from neutral helium. It is therefore advisable to calculate the two probabilities separately using suitable theoretical models and multiply them to get the double-ionization probability, especially when one does not account for the continuum electron–electron correlation explicitly through the wave function. Here we address these points in the independent-event model originally proposed by Crothers and McCarroll [189]. In our interpretation and extension of this model the two probabilities are calculated by applying two variants of the continuum-distorted-wave approximation. To calculate P_1 we use the conventional CDW theory, where we represent the target helium atom by the explicitly correlated two-electron Pluvinage [493] wave function given by

$$\Psi_{\text{Pluv}}(r_1, r_2, r_{12}) = c(k)(Z_T^3/\pi)\exp(-Z_T r_1 - Z_T r_2 - \mathrm{i}kr_{12})\,{}_1F_1\left(1 + \frac{1}{2\mathrm{i}k}; 2; 2\mathrm{i}kr_{12}\right) \tag{4.271}$$

where $r_{12} = |\mathbf{r}_1 - \mathbf{r}_2|$, $c(k)$ is the normalization constant, and the variational parameter k is determined by the usual energy minimization process. In (4.271) electron j has position coordinate $\mathbf{r}_j$ relative to the nucleus of the target with charge Z_T.

It is important to note that the Pluvinage wave function is in various ways a better approximation to the exactly correlated helium wave function than the Hartree–Fock or any other independent-electron model wave function. First, it accounts for

the static angular correlation [418]. Second, it gives a more accurate estimation of the ground-state energy than the Hartree–Fock wave function. Third, it accounts for nearly 50% of the total correlation energy. The second ionization probability P_2 has been calculated by using the hybrid form of CDW and eikonal approximations introduced by Crothers and McCann [180]. Total double-ionization cross sections are then calculated in the semiclassical impact parameter method by

$$\sigma_{DI} = 2\pi a_0^2 \int_0^\infty \rho P_1(\rho) P_2(\rho)\, \mathrm{d}\rho \tag{4.272}$$

where

$$P_j(\rho) = \int \mathrm{d}\boldsymbol{\kappa}_T\, |a_j(\rho, \boldsymbol{\kappa}_T)|^2 \qquad j = 1, 2 \tag{4.273}$$

and

$$a_j(\rho, \boldsymbol{\kappa}_T) = \frac{1}{2\pi\nu} \int_0^\infty \eta J_0(\eta\rho) T_j(\eta, \boldsymbol{\kappa}_T)\, \mathrm{d}\eta \tag{4.274}$$

where $\boldsymbol{\kappa}_T$ is the momentum of the ionized electron and η is the transverse component of the change in momentum of the relative motion of the heavy particles. The combinatorics inherent in (4.272) demonstrates the power of the semiclassical method.

The transition amplitude for the first ionization event is given by

$$T_1(\eta, \boldsymbol{\kappa}_T) = \langle \chi_f^{(-)} | W_f^\dagger | \chi_i^{(+)} \rangle \tag{4.275}$$

where

$$\chi_i^{(+)} = \frac{1}{2}(1 + \mathcal{P}_{12}) \Psi_{\mathrm{Pluv}}(r_{T1}, r_{T2}, r_{T12}) \exp(\mathrm{i}\mathbf{K}_i \cdot \mathbf{R}_i) D_P^{(+)}(\boldsymbol{\kappa}_P, \mathbf{r}_{P1}) \tag{4.276}$$

$$\begin{aligned} W_f \chi_f^{(-)} = &-\frac{1}{\sqrt{2}}(1 + \mathcal{P}_{12})(2\pi)^{-3/2} \phi(r_{T2}) \exp(\mathrm{i}\boldsymbol{\kappa}_T \cdot \mathbf{r}_{T1} + \mathrm{i}\mathbf{K}_{Tf} \cdot \mathbf{R}_i) \\ &\times \nabla_{r_{T1}} D_T^{(-)}(\boldsymbol{\kappa}_T, \mathbf{r}_{T1}) \cdot \nabla_{r_{P1}} D_P^{(-)}(\boldsymbol{\kappa}_P, \mathbf{r}_{P1}) \end{aligned} \tag{4.277}$$

$$D_i^{(\pm)}(\boldsymbol{\kappa}_i, \mathbf{r}_i) = N^{(\pm)}(Z_i/\kappa_i)\, {}_1F_1(\pm\mathrm{i}Z_i/\kappa_i; \pm\mathrm{i}\kappa_i r_i - \mathrm{i}\boldsymbol{\kappa}_i \cdot \mathbf{r}_i) \tag{4.278}$$

$$N^{(\pm)}(\nu) = \exp(\pi\nu/2)\Gamma(1 \mp \mathrm{i}\nu) \tag{4.279}$$

Here the subscript i refers to the corresponding quantities associated with either the target (T) or the projectile (P) nucleus. Accordingly, $\mathbf{r}_{T1}, \mathbf{r}_{P1} \ldots$ are the position vectors of the electron 1 with respect to the target and projectile nucleus, respectively, and $r_{T12} = |\mathbf{r}_{T1} - \mathbf{r}_{T2}|$. $\mathbf{K}_i$ is the initial relative momentum and $\mathbf{K}_{Tf}$ is the final relative momentum of the aggregate heavy particles and $\boldsymbol{\kappa}_P = \boldsymbol{\kappa}_T - \mathbf{v}$, where $\mathbf{v}$ is the impact velocity. The permutation operator $\mathcal{P}_{12}$ in (4.276) and (4.277) stands for interchanging coordinates of two indistinguishable electrons 1 and 2.

From (4.277) note that in the final channel we considered a ground-state hydrogenic orbital $\phi(r_{T2})$ for the second electron remaining bound to the target nucleus, and we describe the ionized electron 1 by a hydrogenic target continuum orbital

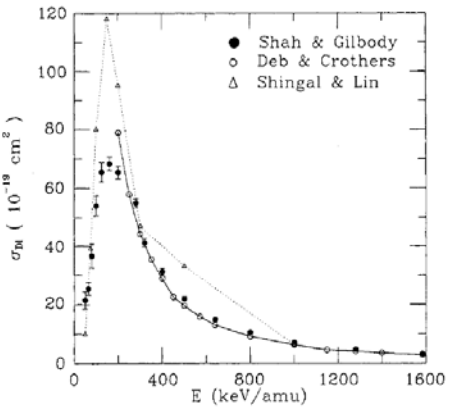

Fig. 4.21. Total cross sections for double ionization of He by He^{++} impact as a function of incident energy E (keV/amu). *Full circles*: measurement of Shah and Gilbody [549]; *open circles*: present calculation; *open triangles*: Shingal and Lin [555]. Full and dotted curves are drawn through the theoretical results to guide the eye

simultaneously distorted by the projectile in the usual CDW manner [409]. However, we do not account for the so-called scattering correlation [418], i.e., the explicit correlation of these two electrons through the Coulomb repulsion ($1/r_{12}$) in the scattering operator. The integrals in (4.275) are then separable into one-centre integrals: a three-dimensional integral with respect to the projectile nucleus and a six-dimensional integral with respect to the target nucleus. The first one is evaluated analytically while, following closely the appendix of Crothers and McCarroll [189], the second integral has been reduced to a two-dimensional integral [234], [235]. Ionization of the second electron from the residual He^+ ion by an alpha particle is considered to be an isolated second event with the first electron removed to the continuum and the transition amplitude for this system is calculated using the CDW-EIS model of Crothers and McCann [180]. This, after all, follows the prescription of the first event, in the absence of electron 1, but with a normalized eikonal initial state. This approximation has had considerable success in describing single ionization in a one-active-electron situation [409], [259], [260], [261]. Measurements of Andersen et al. [9] also provided strong evidence of the suitability of the CDW-EIS approximation for single ionization.

In Figure 4.21 we present total cross sections for double ionization of He by alpha-particle impact together with the measurements of Shah and Gilbody [549] and the multistate coupled-channel calculation of Shingal and Lin [555]. The impact energy is denoted by E (keV u^{-1}). Above 200 keV u^{-1} our results give excellent agreement with the measurement at all the energies at which the measurements are reported. However, below 200 keV u^{-1} our results start to overestimate the data and fail to peak at lower energies. This is due in part to the usual CDW normalization problem at the lower energies. It is interesting to note that the coupled-channel cal-

culation of Shingal and Lin [555] involves as many as 79 atomic states (pure and pseudo) based on each of the alpha particle nuclei. Their results, however, do not appear to be as accurate. Further modifications have been made [554] to this coupled-channel calculation, by employing a two-step mechanism to account to some extent for correlation; the preliminary results show some improvement over the results of Shingal and Lin [555]. The excellent agreement of our results with the measurements indicates the importance of the role of correlation in two-electron processes like double ionization. The essence of the present calculation is not only that we account for correlation through the initial target wave function, but also that we include dynamic correlation by our very formulation of the independent-event model in which first one electron is ionized and then the second one; that is, we invoke the concept of correlation of events, as against particles. For completeness we also present our numerical cross sections for double ionization in Table 4.8 together with measurements of Shah and Gilbody at several energies.

Ionization of highly excited Rydberg states would appear to be best described classically [400].

4.4 Relativistic CDW

A good introduction is in Crothers et al., Section 5.1 [200]. The Dirac equation (for fermions) is:

$$\left[-\mathrm{i}c\boldsymbol{\alpha}\cdot\boldsymbol{\nabla}_{\mathbf{r}_T}+\gamma_4 c^2+V^T(\mathbf{r}_T)+S^2V^{P'}(\mathbf{r}_{P'})-\mathrm{i}\frac{\partial}{\partial t_{\mathbf{r}_T}}\right]\Psi(\mathbf{r}_T,t)=0 \tag{4.280}$$

Then making the Darwin approximation, correct to (αZ_T), (αZ_P), we have ($\alpha = 1/137$) the relativistic continuum-distorted-wave (RCDW) approximation, to describe ionization. The initial semirelativistic wave function:

$$\Psi_i=\Psi_{0i}+\Psi_{1i} \tag{4.281}$$

$$\Psi_{0i}=Z_T^{3/2}\pi^{-1/2}\mathrm{e}^{-Z_T r_T-\mathrm{i}c^2t-\mathrm{i}E_{si}t} \tag{4.282}$$

$$\Psi_{1i}=Z_T^{3/2}\pi^{-1/2}\left[-\frac{\mathrm{i}}{2c}\boldsymbol{\alpha}\cdot\boldsymbol{\nabla}_{\mathbf{r}_T}\mathrm{e}^{Z_T r_T}\right]\mathrm{e}^{-\mathrm{i}c^2t-\mathrm{i}E_{si}t}\boldsymbol{\omega}_i \tag{4.283}$$

Table 4.8. Total double ionization cross sections in units of 10^{-19} cm^2 for alpha particle impact on helium atoms. DC: present calculation; SG: measurement of Shah and Gilbody [549]

E keV u^{-1}	DC (10^{-19} cm^2)	SG (10^{-19} cm^2)
400.0	28.83	31.1 ± 1.1
500.0	19.52	21.9 ± 0.7
640.0	13.03	14.8 ± 0.5
800.0	9.15	10.53 ± 0.47
1000.0	6.29	7.07 ± 0.5

where $\boldsymbol{\alpha}$ is a $4 \times 4 \times 1$ tensor:

$$\left(\alpha\right) = \begin{pmatrix} \mathbf{0} & \boldsymbol{\sigma} \\ \boldsymbol{\sigma} & \mathbf{0} \end{pmatrix} \qquad \left(\gamma_4\right) = \begin{pmatrix} \mathbf{1} & \mathbf{0} \\ \mathbf{0} & -\mathbf{1} \end{pmatrix} \tag{4.284}$$

where $\boldsymbol{\gamma}_4$ is sometimes written as β and the Cartesian coordinates of $\boldsymbol{\alpha}$ are the 2×2 Pauli matrices:

$$\boldsymbol{\sigma}_1 = \begin{pmatrix} 0 & 1 \\ 1 & 0 \end{pmatrix} \qquad \boldsymbol{\sigma}_2 = \begin{pmatrix} 0 & -\mathrm{i} \\ \mathrm{i} & 0 \end{pmatrix} \qquad \boldsymbol{\sigma}_3 = \begin{pmatrix} 1 & 0 \\ 0 & -1 \end{pmatrix} \tag{4.285}$$

and the following are 4×1 column vectors

$$\boldsymbol{\omega}_i = \begin{pmatrix} 1 \\ 0 \\ 0 \\ 0 \end{pmatrix} \qquad \boldsymbol{\omega}_f = \begin{pmatrix} 1 \\ 0 \\ 0 \\ 0 \end{pmatrix} \text{ spin up} \tag{4.286a}$$

$$\text{or} \quad \boldsymbol{\omega}_f = \begin{pmatrix} 0 \\ 1 \\ 0 \\ 0 \end{pmatrix} \text{ spin down} \tag{4.286b}$$

The RCDW initial *distortion* is

$$\text{scalar:} \qquad L'_{0i} = N(\nu_P) M(\mathrm{i}\nu_P, 1, \mathrm{i}\gamma(vr'_P + \mathbf{v} \cdot \mathbf{r}'_P))\mathbf{I} \tag{4.287}$$

$$\text{vector:} \quad L'_{1i} = N(\nu_P)\mathbf{S}^{-1}\left[-\tfrac{\mathrm{i}}{2\gamma c}\boldsymbol{\alpha} \cdot \boldsymbol{\nabla}_{\mathbf{r}'_P} M(\mathrm{i}\nu_P, 1, \mathrm{i}\gamma(vr'_P + \mathbf{v} \cdot \mathbf{r}'_P))\right]\mathbf{S} \tag{4.288}$$

where the Sommerfeld parameter is $\nu_P = Z_P/v_e$ and $N(\nu_P) = \Gamma(1 - \mathrm{i}\nu_P)\mathrm{e}^{\pi\nu P/2}$. Here c is the speed of light and $\gamma = 1/\sqrt{1-\beta^2}$ where $\beta = v/c$. Equations (4.1) and (4.2) generalize to

$$\mathbf{r}'_P = \mathbf{r}_T - \mathbf{b} + (\gamma - 1)(\mathbf{r}_T \cdot \hat{\mathbf{v}})\hat{\mathbf{v}} - \gamma \mathbf{v} t \tag{4.289}$$

where the impact parameter is now written as $\mathbf{b}$ rather than ρ. A Lorentz boost from the T to the P frame is given by

$$\mathbf{S} = \left(\frac{1+\gamma}{2}\right)^{1/2}\left(\mathbf{I} - \frac{\beta\gamma}{\gamma+1}\boldsymbol{\alpha} \cdot \hat{\mathbf{v}}\right) \tag{4.290}$$

The initial- and final-state wave functions are

$$\psi_i = L'_{0i}\Psi_{0i} + L'_{1i}\Psi_{0i} + L'_{0i}\Psi_{1i} \tag{4.291}$$

$$\psi_f = L'_{0f}\Psi_{0f} + L'_{1f}\Psi_{0f} + L'_{0f}\Psi_{1f} \tag{4.292}$$

The RCDW wave function is given by

$$\Psi_f = \Psi_{0f} + \Psi_{1f} \tag{4.293}$$

The component wave functions are

$$\Psi_{0f} = (2\pi)^{-3/2} N^*(\omega_T) M(-\mathrm{i}\omega_T, 1, -\mathrm{i}\gamma_e(v_e r_t + \mathbf{v}_e \cdot \mathbf{r}_T)) \\ \mathrm{e}^{-\mathrm{i}\gamma_e c^2 t + \mathrm{i}\gamma_e \mathbf{v}_e \cdot \mathbf{r}_T} \mathbf{S}_{\mathbf{v}_e}^{-1} \boldsymbol{\omega}_f \tag{4.294}$$

which is scalar and

$$\Psi_{1f} = (2\pi)^{-3/2} N^*(\omega_T) \left[-\tfrac{\mathrm{i}}{2\gamma_e c} \boldsymbol{\alpha} \cdot \boldsymbol{\nabla}_{\mathbf{r}_T} M(-\mathrm{i}\omega_T, 1, -\mathrm{i}\gamma_e(v_e r_T + \mathbf{v}_e \cdot \mathbf{r}_T)) \right] \\ \mathrm{e}^{-\mathrm{i}\gamma_e c^2 t + \mathrm{i}\gamma_e \mathbf{v}_e \cdot \mathbf{r}_T} \mathbf{S}_{\mathbf{v}_e}^{-1} \boldsymbol{\omega}_f \tag{4.295}$$

which is a Furry vector function. Here we have

$$\mathbf{S}_{\mathbf{v}_e} \;\Rightarrow\; \mathbf{v} \to \mathbf{v}_e \text{ in } \mathbf{S} \tag{4.296}$$

and the Sommerfeld parameter

$$\omega_T = \frac{Z_T}{v_e} \qquad \omega'_P = \frac{Z_P}{v'_e} \tag{4.297}$$

$$L'_{0f} = N^*(\omega'_P) M(-\mathrm{i}\omega'_P, 1, -\mathrm{i}\gamma'_e(v'_e r'_P + \mathbf{v}'_e \cdot \mathbf{r}'_P))\mathbf{I} \tag{4.298}$$

$$L'_{1f} = N^*(\omega'_P)\mathbf{S}^{-1} \left[-\frac{\mathrm{i}}{2\gamma_e c} \boldsymbol{\alpha} \cdot \boldsymbol{\nabla}_{\mathbf{r}_{P'}} M(-\mathrm{i}\omega_{P'}, 1, -\mathrm{i}\gamma_e(v'_e r'_P + \mathbf{v}'_e \cdot \mathbf{r}_{P'})) \right] \mathbf{S} \tag{4.299}$$

$\mathbf{v}_e$ is the velocity of e^- relative to T, in frame T, and $\mathbf{v}'_e$ is the velocity of e^- relative to P, in frame P, so that

$$\mathbf{v}'_e = \left(1 - \frac{v v_e}{c^2} \cos\theta\right)^{-1} \gamma^{-1} (v_e \sin\theta, 0, v_e \cos\theta - v) \tag{4.300}$$

noting that as $c \to \infty$, $\gamma \to 1$, which implies

$$\mathbf{v}'_e = \mathbf{v}_e - \mathbf{v} \tag{4.301}$$

as in classical relativity. The transition amplitude is given by

$$A(\mathbf{b}) = -\mathrm{i} \int_{-\infty}^{+\infty} \mathrm{d}t \, \langle \chi_f | \left(H - \mathrm{i}\frac{\partial}{\partial t} \right)^{\dagger} | \chi_i \rangle \tag{4.302}$$

$$= -\mathrm{i} \int_{-\infty}^{+\infty} \mathrm{d}t \, \langle \mathbf{W}_f \chi_f | \chi_i \rangle \tag{4.303}$$

$$= -\frac{\mathrm{i}}{(2\pi)^2 \gamma v} \int \mathrm{d}^2\boldsymbol{\eta} \, T(\boldsymbol{\eta}) \mathrm{e}^{\mathrm{i}\boldsymbol{\eta}\cdot\mathbf{b}} \tag{4.304}$$

The TDCS are given by

$$\sigma(\mathbf{v}_e) = \int \mathrm{d}^2\mathbf{b} \, |A(\mathbf{b})|^2 \tag{4.305}$$

$$= \frac{1}{(2\pi\gamma v)^2} \int \mathrm{d}^2\boldsymbol{\eta} \, |T(\boldsymbol{\eta})|^2 \tag{4.306}$$

where the two-dimensional Fourier transform is

$$T(\boldsymbol{\eta}) = \gamma v \int \mathrm{d}^2\mathbf{b}\, \mathrm{e}^{-\mathrm{i}\boldsymbol{\eta}\cdot\mathbf{b}} A(\mathbf{b}) \tag{4.307}$$

The residual interaction $\mathbf{W}_{f\chi_f}$ is derived as follows

$$\begin{aligned}\mathbf{W}_{f\chi_f} = &\left(-\mathrm{i}c\boldsymbol{\alpha}\cdot\boldsymbol{\nabla}_{\mathbf{r}_T} + \gamma_4 c^2 + \mathbf{S}^2 V'_P(\mathbf{r}'_P) + V_T(\mathbf{r}_T) - \mathrm{i}\frac{\partial}{\partial t}\right)\\ &\left(\mathbf{L}'_{0f}\phi_{0f} + \mathbf{L}'_{1f}\phi_{0f} + \mathbf{L}'_{0f}\phi_{1f}\right)\mathrm{e}^{-\mathrm{i}c^2 t_e}\mathbf{S}^{-1}_{\mathbf{v}_e}\boldsymbol{\omega}_f\end{aligned} \tag{4.308}$$

where t_e is the time referred to the electron's rest frame, and it is understood that ϕ_f is just the final-state wave function defined earlier with the t_e-dependent factor removed. This perturbation can be rearranged in the following manner:

$$= \left[\left(-\mathrm{i}c\boldsymbol{\alpha}\cdot\boldsymbol{\nabla} - \mathrm{i}\frac{\partial}{\partial t} + \mathbf{S}^2 V'_P\right)\mathbf{L}'_{0f}\right](\phi_{0f} + \phi_{1f})\mathrm{e}^{-\mathrm{i}c^2 t_e}\mathbf{S}^{-1}_{\mathbf{v}_e}\boldsymbol{\omega}_f \tag{4.309a}$$

$$+\mathbf{L}'_{0f}\left(-\mathrm{i}c\boldsymbol{\alpha}\cdot\boldsymbol{\nabla} - \mathrm{i}\frac{\partial}{\partial t} + \gamma_4 c^2 + V_T\right)\left[(\phi_{0f} + \phi_{1f})\mathrm{e}^{-\mathrm{i}c^2 t_e}\right]\mathbf{S}^{-1}_{\mathbf{v}_e}\boldsymbol{\omega}_f \tag{4.309b}$$

$$+\left(-\mathrm{i}c\boldsymbol{\alpha}\cdot\boldsymbol{\nabla} - \mathrm{i}\frac{\partial}{\partial t} + \gamma_4 c^2 + \mathbf{S}^2 V'_P\right)\left[(\mathbf{L}'_{0f} + \mathbf{L}'_{1f})\mathrm{e}^{-\mathrm{i}c^2 t_e}\right]\phi_{0f}\mathbf{S}^{-1}_{\mathbf{v}_e}\boldsymbol{\omega}_f \tag{4.309c}$$

$$+\left[(-\mathrm{i}c\boldsymbol{\alpha}\cdot\boldsymbol{\nabla} + V_T)\,\phi_{0f}\right](\mathbf{L}'_{0f} + \mathbf{L}'_{1f})\mathrm{e}^{-\mathrm{i}c^2 t_e}\mathbf{S}^{-1}_{\mathbf{v}_e}\boldsymbol{\omega}_f \tag{4.309d}$$

$$-\left[\left(-\mathrm{i}c\boldsymbol{\alpha}\cdot\boldsymbol{\nabla} - \mathrm{i}\frac{\partial}{\partial t} + \mathbf{S}^2 V'_P\right)\mathbf{L}'_{0f}\right]\phi_{0f}\mathrm{e}^{-\mathrm{i}c^2 t_e}\mathbf{S}^{-1}_{\mathbf{v}_e}\boldsymbol{\omega}_f \tag{4.309e}$$

$$-\mathbf{L}'_{0f}\phi_{0f}\left[\left(-\mathrm{i}c\boldsymbol{\alpha}\cdot\boldsymbol{\nabla} - \mathrm{i}\frac{\partial}{\partial t} + \gamma_4 c^2\right)\mathrm{e}^{-\mathrm{i}c^2 t_e}\right]\mathbf{S}^{-1}_{\mathbf{v}_e}\boldsymbol{\omega}_f \tag{4.309f}$$

$$-\left[(-\mathrm{i}c\boldsymbol{\alpha}\cdot\boldsymbol{\nabla} + V_T)\,\phi_{0f}\right]\mathbf{L}'_{0f}\mathrm{e}^{-\mathrm{i}c^2 t_e}\mathbf{S}^{-1}_{\mathbf{v}_e}\boldsymbol{\omega}_f \tag{4.309g}$$

It is clear that (4.309f) is equal to zero because when it is transformed to the electron's rest frame it becomes

$$-\mathbf{L}'_{0f}\phi_{0f}\left[\left(-\mathrm{i}\frac{\partial}{\partial t_e} + \gamma_4 c^2\right)\mathrm{e}^{-\mathrm{i}c^2 t_e}\right]\omega_f = -\mathbf{L}'_{0f}\phi_{0f}(\gamma_4 - 1)c^2\mathrm{e}^{-\mathrm{i}c^2 t_e}\boldsymbol{\omega}_f \tag{4.310}$$

and noting that $\gamma_4\omega_f = \omega_f$ the result is apparent.

Combining terms (4.309a) and (4.309e) yields

$$\left[\mathbf{S}(-\mathrm{i}c\boldsymbol{\alpha}\cdot\boldsymbol{\nabla}'\mathbf{L}'_{0f})\mathbf{S} + \mathbf{S}^2 V'_P\mathbf{L}'_{0f}\right]\phi_{1f}\mathrm{e}^{-\mathrm{i}c^2 t_e}\mathbf{S}^{-1}_{\mathbf{v}_e}\boldsymbol{\omega}_f \tag{4.311}$$

while (4.309d) and (4.309g) together give

$$\left[(-\mathrm{i}c\boldsymbol{\alpha}\cdot\boldsymbol{\nabla}\phi_{0f}) + V_T\phi_{0f}\right]\mathbf{L}'_{1f}\mathrm{e}^{-\mathrm{i}c^2 t_e}\mathbf{S}^{-1}_{\mathbf{v}_e}\boldsymbol{\omega}_f \tag{4.312}$$

Parts (4.309b) and (4.309c) reduce to give

$$\mathbf{L}'_{0f}V_T\phi_{1f}\mathrm{e}^{-\mathrm{i}c^2 t_e}\mathbf{S}^{-1}_{\mathbf{v}_e}\boldsymbol{\omega}_f \tag{4.313}$$

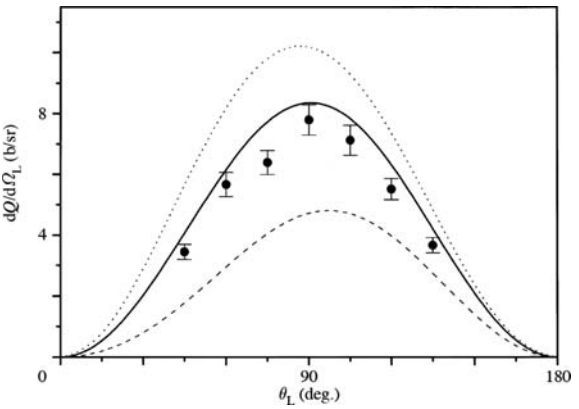

Fig. 4.22. Differential cross section, as a function of laboratory angle θ_L, for *nonflip* RSE and peaked DWIA approximations for Xe^{54+} incident on Be at 197 MeV u^{-1}. Theory: *solid line*, Darwin DWIA; *dashed line*, Dirac DWIA; *dotted line*, Darwin RSE. Experiment data (*filled circle*) is from Anholt et al. [11]

and

$$\mathbf{S}^2 V_P' \mathbf{L}_{1f}' \phi_{0f} \mathrm{e}^{-\mathrm{i}c^2 t_e} \mathbf{S}_{\mathbf{v}_e}^{-1} \omega_f \tag{4.314}$$

respectively. These are the Darwin correction terms, which arise as a direct consequence of using approximate wave functions. The residual interaction can therefore be written as

$$\begin{aligned} \mathbf{W}_f \chi_f = \Big[\left(-\mathrm{i}c\boldsymbol{\alpha} \cdot \boldsymbol{\nabla} \phi_{of}\right) \mathbf{L}_{1f}' + \mathbf{S}(-\mathrm{i}c\boldsymbol{\alpha} \cdot \boldsymbol{\nabla}' \mathbf{L}_{0f}') \mathbf{S} \phi_{1f} \\ + (V_T + \mathbf{S}^2 V_P')(\mathbf{L}_{0f}' \phi_{1f} + \mathbf{L}_{1f}' \phi_{0f}) \Big] \mathrm{e}^{-\mathrm{i}c^2 t_e} \mathbf{S}_{\mathbf{v}_e}^{-1} \omega_f \end{aligned} \tag{4.315}$$

We have seen in the analysis for the prior interaction codes that the time-dependent exponents are accounted for in the Fourier transform method and so should be omitted from the following analysis.

Figure 4.22 shows the singly differential cross section for the peaked distorted-wave impulse approximation (RCDW) for nonflip. We find excellent agreement with experiment [11] for the RCDW model in which Darwin final states were used; the Dirac model overestimated the cross section by 20–30%.

The good agreement of RCDW with experiment (Figure 4.23a) for small and medium Z-values is indicative of the importance of including the strong multiple scattering intermediate states, which are approximated by the Coulomb distortions. Second-order relativistic Oppenheimer-Brinkman-Kramers (ROBK2) using a plane wave propagator only includes explicitly the two-step process. There is considerable uncertainty in the literature on the effectiveness of this model. Early work [333], [334], which relied on various peaking approximations, specifically designed for small charges and large velocities, only managed a small improvement on the ROBK1 results. These had been shown to be at least one order of magnitude bigger than experiment [430]. Later an "averaging approximation" was introduced that brought ROBK2 into good agreement with experiment [432], [433]. More recently,

however, Decker [207] has shown that an exact numerical calculation of the ROBK2 amplitude leads to corrections to ROBK2 that actually worsen the accord with experiment. This has led to a stimulating debate on how best to treat simultaneous expansions in the fine structure constant and the Born series itself [434], [208]. It is our opinion that although ROBK2 is an excellent guide in collisions involving very low charges, it is inherently a poor perturbative series for capture in the highly charged systems that have been studied experimentally to date. In Figure 4.23b, the scalar and spinor theories are compared with the experimental data presented by Anholt [12]. Although relativistic capture is dominated by inner-shell transitions [237], capture to and from the L-shell sometimes has a significant contribution at these energies. Our calculations include only results for capture from and to the K-shell. These results can be scaled (multiplied by a factor 1.202) to take account of the contributions arising from capture to excited projectile states. The inclusion of capture from the target L-shell required a more detailed calculation. However, these contributions are quite significant for highly charged targets and low collision energies [12]. The results for scalar TCDW are very similar (at most ~ 10% larger) to those of the spinor TCDW for these collisions; the curve has been omitted for the sake of clarity. In our calculation, we have used experimental binding energies and K-shell Slater screening for the target charges. These experimental data are not particularly well suited to emphasizing the differences between spinor and scalar theories due to the dominance of nonflip capture. However, the tendency for spinor TEIK to be markedly lower than scalar TEIK is clear, especially for high-projectile energies. As TCDW nonflip is reasonably insensitive to the high-momentum part of the distortion, both versions give similar results. As mentioned earlier, the rather large discrepancies between theory and experiment are mainly due to capture from the target L-shell [12]. Conversely, theories based on projectile distortion and using Z_T as a small parameter can be used. These models, which can be termed PEIK and PCDW, give results for these collisions that lie well above experiment for large target charges. For lower Z_P

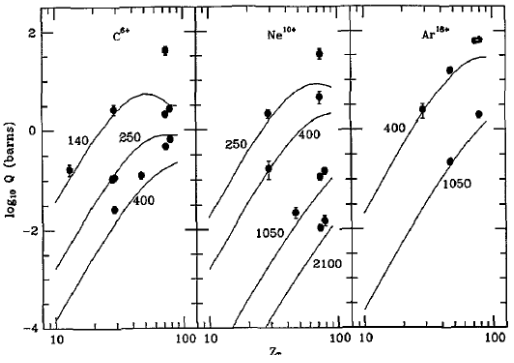

Fig. 4.23a. Total cross sections Q for electron capture as a function of target charge Z_T for bare carbon, neon, and argon nuclei impact. Projectile energies indicated in figures are in MeV u^{-1}. RCDW theoretical results: *solid line*; experimental data: *filled circles*, Crawford [155]

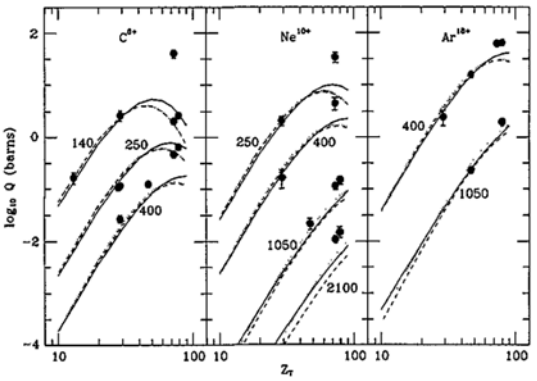

Fig. 4.23b. Total cross sections Q for electron capture as a function of target charge Z_T for bare carbon, neon, and argon nuclei impact. Projectile energies indicated in figures are in MeV u^{-1}. Theoretical results (capture from K-shell to K-shell): *solid line*, spinor TCDW; *dashed line*, spinor TEIK; *dotted line*, scalar TEIK. Experimental data (including capture from all states): *filled circles*, [155]

and Z_T, the results converge slowly towards the corresponding target distortion theories. Neither PCDW nor TCDW can be considered very satisfactory whenever Z_P and Z_T are comparable, both in practical terms and on theoretical grounds.

Results are presented for simulations of electron-positron pair production in relativistic heavy-ion collisions leading to electron capture and positron ejection. We apply a two-centre relativistic continuum-distorted-wave model to represent the electron/positron dynamics during the collision process. The results are compared with experimental cross-section data for La^{57+} and Au^{79+} impact on gold, silver, and copper targets. The theory is in good agreement with experiment for La^{57+} impact, verifying the result that the process increases in importance with both collision energy and target atomic number and improves upon previous simulations of this process.

Early theoretical work on the production of an e^-–e^+ pair through heavy-ion collisions considered only the creation of the electron and positron in the continuum. However *capture by pair production* (CPP), in which the electron is formed in a bound state of one or another ion, becomes a significant process at highly relativistic energies. Remarkably, this process was sufficiently important to enable the synthesis of atomic antihydrogen using the low-energy antiproton ring at CERN. A beam of fast antiprotons impacting on a xenon gas target [49] led to pair production with positron capture. Theory predicted [73], [19] that cross sections for CPP would increase with energy, and indeed this has been verified experimentally [56], [57], [368]. In fact, this process eventually becomes the dominant mechanism for charge exchange in highly relativistic atomic collisions [368], [196]. As well as being an interesting area of study in its own right, this process has important applications in the physics of heavy-ion colliders, such as the large-hadron collider (LHC) and the relativistic heavy-ion collider (RHIC) [60]. The process of CPP will lead to depletion of the charge state of the beam and hence a loss in luminosity of the collider.

For typical operating conditions of such facilities, these losses might amount to 50% [60] or more.

Although the process is strongly coupled at high energy, simulations based on relativistic coupled-channel calculations [20], [21] have indicated that leading-order perturbation theory is adequate for total cross-section estimates for energies (E) up to 150 GeV/u [368]. Nonetheless in the energy range $E \sim 1$ GeV/u, where reliable experimental data exist, theory and experiment have been in least agreement. It is this region we address here.

It is now some 20 years since Becker and co-workers [54], [55], [13] obtained the first estimates of cross sections for pair creation with simultaneous capture of the electron into the K-shell of one of the colliding ions. However, with the exception of Deco and Rivarola, who gave a two-centre description of the continuum positron [210], two somewhat artificial modes of reaction have been distinguished and treated separately when modeling this process: excitation from the negative energy continuum of an ion to one of its bound states [73], [55], [209] or transfer to a bound state of the other ion [238], [338]. Such approaches, while suited to circumstances in which one ion is much more highly charged than the other, lack symmetry and make a distinction between two separate modes of CPP. They lead to different formulae within first-order perturbation theory [238] and hence different projectile charge (Z_P), target charge (Z_T), and E dependencies. As a result, theoretical estimates of the asymptotic ($E \to \infty$) energy dependence of the total cross sections are not in agreement with estimates of [73], [19] $\sigma_{\mathrm{CPP}} \sim \ln(E)$, and later [238] $\sigma_{\mathrm{CPP}} \sim E^2$. The former is based on the positron-electron pair being created around the same ion, the latter assuming that the pair is divided between the two ions. Of course both pathways will interfere and contribute to the process, thus pointing to the necessity of a two-centre treatment for the positron and electron. Moreover it has been shown [210] that the two-centre description is essential in obtaining the correct positron emission spectrum and accurate total cross section for CPP. However, leading-order perturbation theory (the first Born approximation) does give reasonably good estimates for the cross section in the high-energy region ($E \sim 150$ GeV/u) [368] for collisions of heavy ions and has been a reliable model for fast collisions of light ions with low Z targets in the process of antihydrogen formation involving CPP by antiprotons [49], [74].

Experimental results for highly relativistic heavy ions on a variety of targets [60] support the simple scaling law derived from the virtual-photon method (Born approximation) which included multiple scattering from the projectile ion [73] alone, $\sigma_{\mathrm{CPP}} \sim Z_T^2$, for a given energy. At lower energies, this is not the case [57], [58], [59]; the Z_T dependence is more complex, showing an enhancement in excess of the Z_T^2-scaling. Here we propose a refinement of the Born approximation to take into account higher-order scattering processes. In particular, we tackle the question of the two-centre nature of the continuum positron and the polarization of the captured electron. We find both these effects are vital and lead to theoretical results that are in accord with experiment. We discuss the physical explanation for scaled cross-section enhancement and provide numerical estimates that agree well with experiment in qualitative and quantitative terms.

Through crossing symmetries, the leading-order matrix element for the pair-production process, in which the electron is captured by the projectile P,

$$P + T \rightarrow (P, e^-) + T + e^+ \tag{4.316}$$

is the same as that for the related reaction, $e^- + P + T \rightarrow (P, e^-) + T$, which is mathematically equivalent to the time-reversed ionization process

$$(P, e^-) + T \rightarrow e^- + P + T \tag{4.317}$$

In each crossing symmetry the equivalence relies on the electron-positron interaction being much weaker than their interactions with the highly charged ions, a reasonable assumption. Let $\boldsymbol{r}_P, t$, and $\boldsymbol{r}'_T, t'$ be the space and time coordinates of the electron in the projectile and target frames, respectively. The nuclei follow straight-line paths with relative velocity $\boldsymbol{v}$. The Hamiltonian, in the projectile frame of reference and in atomic units, is given by:

$$H = -\mathrm{i}c\boldsymbol{\alpha} \cdot \boldsymbol{\nabla}_{\boldsymbol{r}_P} + \beta c^2 + V_P(\boldsymbol{r}_P) + S^2 V'_T(\boldsymbol{r}'_T) \tag{4.318}$$

where $\boldsymbol{\alpha}$ and β are Dirac matrices and S is the operator that transforms the wave function from the projectile frame to the target frame, namely

$$S = (\tfrac{1}{2} + \tfrac{1}{2}\gamma)^{\frac{1}{2}}(\mathbf{1} - x\boldsymbol{\alpha} \cdot \widehat{\boldsymbol{v}}) \tag{4.319}$$

where $x = v\gamma c^{-1}(\gamma + 1)^{-1}, \gamma = (1 - v^2/c^2)^{-1/2}$, and $\mathbf{1}$ represents the unit matrix. For a given impact parameter $\boldsymbol{b}$, the transition amplitude can be written in the form [180]

$$A(\boldsymbol{b}) = -\mathrm{i}\int_{-\infty}^{\infty} \mathrm{d}t \int \mathrm{d}\boldsymbol{r}_P \ \chi_f^\dagger (H - \mathrm{i}\partial_t)\chi_i \tag{4.320}$$

where χ_i and χ_f are the initial and final states.

The undistorted bound state is approximated by a semirelativistic ($Z_T \ll c$) wave function :

$$\Phi_i = \Phi_{0i} + \Phi_{1i} \tag{4.321}$$

where

$$\Phi_{0i} = Z_P^{\frac{3}{2}} \pi^{-\frac{1}{2}} e^{-Z_P r_P - \mathrm{i}c^2 t - \mathrm{i}E_{si} t} \boldsymbol{\omega}_i \tag{4.322}$$

and

$$\Phi_{1i} = (2ic)^{-1} \boldsymbol{\alpha}.\boldsymbol{\nabla}_{\mathbf{r}_P} \Phi_{0i} \tag{4.323}$$

with E_{si} the nonrelativistic eigenenergy, and the electron spin along the beam axis defined as "up" by $\boldsymbol{\omega}_i^T = (1\ 0\ 0\ 0)$ and "down" by $\boldsymbol{\omega}_i^T = (0\ 1\ 0\ 0)$.

The continuum function is given by

$$\Phi_f = \Phi_{0f} + \Phi_{1f} \tag{4.324}$$

where

$$\Phi_{0f} = (2\pi)^{-\frac{3}{2}} N^*(\omega_P)\, {}_1F_1(-\mathrm{i}\omega_P; 1; -\mathrm{i}\gamma_e(v_e r_P + \boldsymbol{v}_e \cdot \boldsymbol{r}_P)) \times e^{-\mathrm{i}\gamma_e c^2 t + \mathrm{i}\gamma_e \boldsymbol{v}_e \cdot \boldsymbol{r}_P} S^{-1}_{\boldsymbol{v}_e} \boldsymbol{\omega}_f \tag{4.325}$$

The spinor correction term is given by

$$\Phi_{1f} = (2\pi)^{-\frac{3}{2}} (2\mathrm{i}\gamma_e c)^{-1} N^*(\omega_P) \times \boldsymbol{\alpha}.\boldsymbol{\nabla}_{r_P} {}_1F_1(-\mathrm{i}\omega_P; 1; -\mathrm{i}\gamma_e(v_e r_P + \boldsymbol{v}_e \cdot \mathbf{r}_P)) \times e^{-\mathrm{i}\gamma_e c^2 t + \mathrm{i}\gamma_e \boldsymbol{v}_e \cdot \mathbf{r}_P} S^{-1}_{\boldsymbol{v}_e} \boldsymbol{\omega}_f \tag{4.326}$$

with $\omega_P = Z_P/v_e$, where $\boldsymbol{v}_e$ is the electron velocity. $N(\zeta) = \exp(\pi\zeta/2)\,\Gamma(1 - i\zeta)$ and

$$S_{\boldsymbol{v}_e} = (\tfrac{1}{2} + \tfrac{1}{2}\gamma_e)^{\frac{1}{2}} (\mathbf{1} - x_e \boldsymbol{\alpha}.\widehat{\boldsymbol{v}_e}) \tag{4.327}$$

where $x_e = v_e\gamma_e c^{-1}(\gamma_e+1)^{-1}$ and $\gamma_e = (1-v_e^2/c^2)^{-1/2}$. These functions are appropriate when $Z_{P,T} \ll c$.

The initial distortion factor $\boldsymbol{L}'_i$ is a matrix given by:

$$\boldsymbol{L}'_i = \boldsymbol{L}'_{0i} + \boldsymbol{L}'_{1i} \tag{4.328}$$

where the asymptotic ${}_1F_1$, or eikonal, initial state is

$$\boldsymbol{L}'_{0i} = \exp(-\mathrm{i}\nu_T \ln[\gamma v r'_T + \gamma \boldsymbol{v} \cdot \boldsymbol{r}'_T])\mathbf{1} \tag{4.329}$$

and

$$\boldsymbol{L}'_{1i} = S^{-1}(2\mathrm{i}\gamma c)^{-1} \boldsymbol{\alpha} \cdot \boldsymbol{\nabla}_{r'_T} \boldsymbol{L}_{0i} S \tag{4.330}$$

with $\nu_T = Z_T/v$.

Similarly the distortion factor on the final state [210] is given by:

$$\boldsymbol{L}'_f = \boldsymbol{L}'_{0f} + \boldsymbol{L}'_{1f} \tag{4.331}$$

where

$$\boldsymbol{L}'_{0f} = N^*(\omega'_T)\, {}_1F_1(-\mathrm{i}\omega'_T; 1; -\mathrm{i}\gamma'_e(v'_e r'_T + \boldsymbol{v}'_e \cdot \boldsymbol{r}'_T))\mathbf{1} \tag{4.332}$$

and

$$\boldsymbol{L}'_{1f} = S^{-1}(2\mathrm{i}\gamma'_e c)^{-1} \boldsymbol{\alpha} \cdot \boldsymbol{\nabla}_{r'_T} \boldsymbol{L}'_{0f} S \tag{4.333}$$

Retaining terms of first order in Z/c, we have relativistic continuum-distorted-wave eikonal-initial-state wave functions [180], [209]:

$$\chi_i = \boldsymbol{L}'_{0i}\Phi_{0i} + \boldsymbol{L}'_{1i}\Phi_{0i} + \boldsymbol{L}'_{0i}\Phi_{1i} \tag{4.334}$$

$$\chi_f = \boldsymbol{L}'_{0f}\Phi_{0f} + \boldsymbol{L}'_{1f}\Phi_{0f} + \boldsymbol{L}'_{0f}\Phi_{1f} \tag{4.335}$$

We first compare our results for the relativistic distorted wave Born (RDWB) approximation [210], where the two-centre positron wave function is used but the initial-state distortion is omitted, and the relativistic first Born (R1B), projectile centred, approximation, in which the initial- and final-state distortions are neglected. The Born approximation, which assumes that the positron is in the continuum of

only one of the ions, is ambiguous. The Born approximation of Bertulani and Baur [73] takes the positron wave function as projectile centered, while the Born approximation of Eichler [238] takes the scattering center at the target nucleus. As the Born approximation of Eichler is analagous to the OBK theory of electron capture, we henceforth refer to it as OBK. These two models (R1B and OBK) can be viewed as approximations to the wavefunction (4.335) in which $\omega_T' = 0$ and $\omega_P = 0$, respectively. By retaining both scattering centre contributions, the interference effects are taken into account. In comparing RDWB and R1B, it is known that these two-centre interference effects reduce the cross section for CPP in the relativistic domain [210]. This suppression of CPP is the converse of the two-centre enhancement (capture to the continuum) that arises in ion–atom ionization [180] and is analogous to the effect of the Fermi function for $\beta^{\pm}$ decay [243].

The triply differential cross section, with respect to the electron momentum ($\boldsymbol{p}_e$), is defined as

$$\sigma(\boldsymbol{p}_e) = (\mathrm{d}\sigma_{\mathrm{CPP}}/\mathrm{d}\boldsymbol{p}_e) = \int \mathrm{d}\boldsymbol{b}\, |A(\boldsymbol{b})|^2 \tag{4.336}$$

Using the Fourier transform method [180], we define

$$T(\boldsymbol{\eta}) = \gamma v \int \mathrm{d}\boldsymbol{b}\ \exp(-\mathrm{i}\boldsymbol{\eta}\cdot\boldsymbol{b}) A(\boldsymbol{b}) \tag{4.337}$$

where $T(\boldsymbol{\eta})$ is a product of single-centre integrals. The total cross section is obtained from the integral over the ejectile momentum (or velocity) and takes the form

$$\sigma_{\mathrm{CPP}} = \sum_{\mathrm{spins}} \frac{1}{2\pi(\gamma v)^2} \int_0^c \mathrm{d}v_e\, \gamma_e^5 v_e^2 \int_0^{\pi} \mathrm{d}\theta \sin\theta \int \mathrm{d}\boldsymbol{\eta} |T(\boldsymbol{\eta})|^2 \tag{4.338}$$

where we sum over all the spin states of the electron and positron pair.

In order to compute CPP cross sections (4.316), we note that a positron with energy ϵ_+ and momentum $\mathbf{p}_+$ traveling forward in time in the final state is equivalent to an electron with energy $-\epsilon_+$ and momentum $-\mathbf{p}_+$ in the initial state. Thus we must take

$$\begin{aligned} v_e &\to -v_+ \qquad v_e' \to -v_+' \\ \epsilon_f &\to -\epsilon_+ \qquad \epsilon_f' \to -\epsilon_+' \end{aligned} \tag{4.339}$$

The experiments of Belkacem et al. [57], [58], [59] were for fully stripped lanthanum ions (La^{57+}) striking thin foils of copper ($Z_T = 29$), silver ($Z_T = 47$), and gold ($Z_T = 79$). The collision energies were $E = 0.405,\ 0.956,$ and 1.300 GeV/u. The two graphs presented compare the scaled total cross sections ($\sigma_{\mathrm{CPP}}/Z_T^2$) given by theory and experiment. Consider figure 1 of [380], which compares R1B and RDWB with the measured values. Of course, the scaled R1B curve is independent of Z_T, and it clearly shows the increase in importance of CPP with increasing collision energy. Considering the RDWB model, however, we see a progressive reduction in the scaled cross section as Z_T increases. This is in agreement with the findings of Deco and Rivarola [210], who reported a decrease in the size of the singly differential cross

sections by an order of magnitude. Their model is similar to our RDWB approximation, but using only the scalar part of the final-state distortion factor (4.332). While this model shows Z_T dependence for the scaled cross section, the trends and absolute values are incorrect. It predicts a suppression of the scaled cross section rather than an enhancement as Z_T increases. Thus the RDWB theory data for gold gives the lowest scaled cross section, while experiment shows that it should be the highest. This same incorrect trend is obtained in the target-centred Born approximation (OBK) [238], as can be seen in figure 2 of [380]. These results were also calculated using the semirelativistic wave functions (4.321) and (4.324).

In Figure 4.24 the equivalent results for RCDWEIS show the observed enhancement with increasing Z_T. However, the theoretical data lie below the experiment for the more energetic collisions. In comparing with experiment we have only presented simulations for the dominant channel, that is, capture to the 1*s* ground state. At very high energies capture to excited states is thought to contribute $\sim 30\%$ to the total capture cross section [368], [22]. This would partly explain the differences between our results and the experimental data. Nonetheless, given the approximate nature of the semirelativistic wave functions used, the theoretical results are very encouraging in that, for the first time, the correct ordering of the total cross sections with respect to nuclear charge, is obtained. It is expected that the implementation of full Coulomb-Dirac wave functions within the overall context of this model will lead to a similar increase in total cross sections as that observed by Ionescu and Eichler [338] in their fuller calculations using Dirac wave functions within the OBK approximation. Thus the present underestimation of the cross sections at higher energy and charge [55], [238] may well be revised in a treatment employing fully relativistic wave functions (see Figure 4.24).

Other experimental results are available for the impact of faster and more highly charged beams: 10.8 GeV/u Au^{79+} [60] and 0.956 GeV/u U^{92+} [56] for the same targets. The gold beam results (Table 4.9) indicate that the Z_T^2 dependence is es-

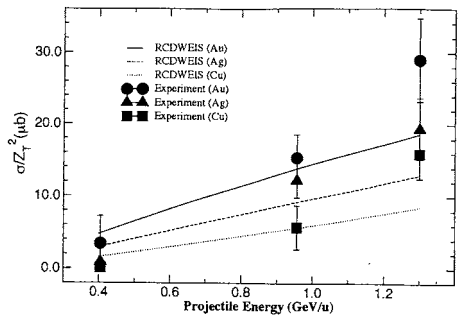

Fig. 4.24. Scaled cross sections, $\sigma_{\mathrm{CPP}}/Z_T^2$ in microbarns, for pair production with electron capture by fully stripped lanthanum ions (La^{57+}) striking thin foils of copper ($Z_T = 29$), silver ($Z_T = 47$), and gold ($Z_T = 79$). Comparison with RCDWEIS theory for capture to the 1*s*-state

tablished at the higher energies, as predicted by the simple projectile-centred Born approximation [54]. Even at this higher energy our theoretical results (Table 4.9) show an enhancement in excess of Z_T^2. The experiment is in much better accord with the flat scaled cross-section data given by the Born approximation [54]. For U^{92+} the high value of Z/c means that the semirelativistic approximations used for the wave functions are not valid.

Table 4.9. Total cross sections, σ_{CPP} in barns, for electron capture from pair production for 10.8 GeV/nucleon Au^{79+} impact on gold, silver, and copper foils.

Z_T	Experiment [60]	CDWEIS theory	Becker et al. [54]
79	8.8 ± 1.5	15.85	10.1
47	4.4 ± 0.73	3.44	3.6
29	1.77 ± 0.31	0.74	1.36

The validity of the semirelativistic continuum-distorted wave approach has been questioned [584] on the grounds that the approximate wave functions might produce unphysical transitions [211]. However, Glass et al. [299], [300] considered symmetric-eikonal wave functions with the prior interaction and showed that the spurious spin-flip contribution to the amplitude vanishes when full cognisance is taken of the two-centre spinor nature of the noncommuting operators. This is the procedure used here, which thus avoids unphysical effects.

In summary, we have proposed and tested a new distorted-wave model that improves on approximations used previously to describe CPP. We confirm that, as has previously been shown [210], the inclusion of distortions from both ions on the positron continuum state leads to a reduction in the cross sections. However, including distortion of the bound electron leads to an increase in the total cross sections and a more accurate fit to the experimental data for fully stripped relativistic lanthanum ions. This demonstrates once more the necessity of a two-centre treatment for an accurate theoretical description of this reaction. However, our cross-section predictions for faster and more highly charged gold ions do not accord with the experimental data, which show a Z_T^2 dependence. While the refinements introduced in our model are significant theoretical improvements, clearly there still exist several unresolved important differences between theory and experiment.

4.4.1 Antihydrogen Production

Many aspects of relativistic atomic-scattering theory are still at an early stage of development (indeed even the asymptotic form of the nonradiative capture cross section is still under active consideration [208], [411], [431]). The production of nine antihydrogen atoms in an experiment at CERN (PS210) ten years ago created much excitement inside and outside the scientific world [49]. In the CERN experiment a fast antiproton made a close encounter with a highly charged nucleus in the form of a xenon ($Z = 54$) gas target:

$$\mathrm{Xe} + \bar{\mathrm{p}} \rightarrow \mathrm{Xe} + \overline{\mathrm{H}}^{0} + \mathrm{e}^{-} \tag{4.340}$$

The antiproton was energetic enough to create an electron-positron pair. The positron was then captured by the antiproton, and an atom of antihydrogen was created. Viewed from Dirac sea theory, the antiproton had a filled set of negative energy bound and continuum states. Given enough energy, the $1s^2$ states could escape to the positive continuum leaving a hole (positron) behind and an electron emerged. Present theoretical calculations to describe this reaction are at the level of the relativistic first Born approximation. Agreement with experiment is satisfactory, but large errors remain.

So for the theoretician this is a rich field of study. In particular, many of the physical processes peculiar to the relativistic domain are amenable to the application of RCDW theory which, by virtue of being able to describe two-centred effects, is well suited to those problems [311].

Further results were expected from the CERN antiproton decelerator [15], [310] and its large hadron collider [257].

Since the production of antihydrogen at both CERN and Fermilab at relativistic speeds, there has been considerable interest in cooling the antihydrogen to study its properties in low-energy collisions, both experimentally [109] and theoretically [15], [310]. The advantage of AD is that violations of the CPT theorem may be tested [236]. The advantage of RCDW over traveling molecular orbitals, other than for super-heavy atoms, is that the prior interaction forms a suitable perturbation, whereas there are extra problems with traveling molecular orbitals concerning the electron translational motion. In RCDW, the electron translation factors are automatically included and the RCDW description of the post interaction automatically allows for strong coupling between the charged particles, the perturbation being the non-orthogonal kinetic energy.

In the CERN PS210 experiment, the impact kinetic energy is 1.217 GeV/u so the Lorentz factor is not much greater than 2. Our models should therefore describe the process adequately. Baur [48] predicted, with good accuracy, the cross section for this process using the virtual photon method. He suggested that the cross section would be around $2 \times Z^2$ *pb* where Z is the nuclear charge of the gaseous target. Thus, during the 15-hour run of the CERN experiment they reckoned that $30\overline{\mathrm{H}}^{0}$ atoms would be produced. Since their detector efficiency was determined to be 0.3, they expected to observe nine antihydrogens, which is within the error of the reported experimental results. Baur et al. [49] noted that the model of Eichler [238] produced a negligible cross section for the process as did the other model of Baur [48], based on a bound-free pair production of Bremsstrahlung. In Figure 4.25 we show the doubly differential cross section in the forward direction for the given mechanism and see that the inclusion of the distortions results in a huge increase over the undistorted R1B model. Thus, we would expect to get a much improved total cross section.

Baur's formula suggests that the cross section should be around 6 nb while the R1B approximation gives a value of 0.095 nb. The RCDWEIS approximation is an improvement on this but at 0.39 nb it is still an order of magnitude too low. Further

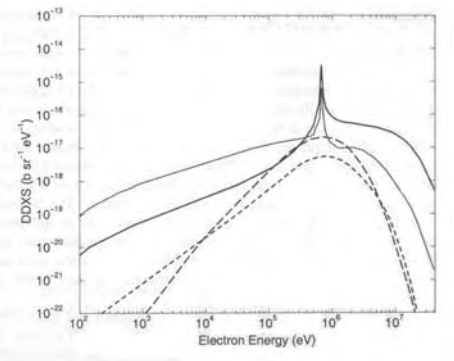

Fig. 4.25. Comparison of the R1B and RCDWEIS doubly differential cross-section profiles (lower and upper lines respectively) for the antihydrogen production process where the electron is ejected in the forward direction. The *solid lines* represent opposite spins while the *dashed lines* denote aligned spins of the lepton pair

work on the integration techniques may be called for, as Figure 4.25 suggests that the increase of more than a factor of 4 over R1B is to be expected.

For future development it will be necessary, as for ionization, to reformulate the expressions using the continuity relation if highly relativistic energies are to be considered. It also seems essential that the contribution of the neglected term be investigated fully. Initially it could be included to observe the effect on the double differential cross sections as this would not require a dramatic increase in computation. If it must be included then the computational approach must be altered if total cross sections are to be obtained. It may be possible to efficiently calculate the problematic ${}_2F_1$ on a multidimensional grid and then to use the stored data to approximate the values at the quadrature points using extrapolation. In this way the total cross sections would be attainable using reasonable computational resources.

To describe this process better, two-centred wave functions, which can describe the distortion of the Dirac sea before and after the collision, are required. The RCDW wave functions have the necessary properties, and their application to this process will prove illuminating. New experiments are planned over the next few years at Fermilab to further investigate antihydrogen production, and the availability of an improved theoretical model is timely. Indeed the experiment (E862) [81] at Fermilab has produced 57 antihydrogen atoms by passing an antiproton beam in the 3.5 to 8.9 GeV/c range through a hydrogen gas jet as in the CERN experiment. The method of production comprises pair-production capture of a positron by an anti-proton, in collision with a proton that survives, together with the ejected-partner electron. The measured cross section [81] is, within error bars, close to the plane wave Born calculation of Bertulani and Baur [74] and Meier et al. [422].

Blanford et al. [81] claim that the result of Bertulani and Baur [74] is, however, not consistent with the CERN experimental result of Baur et al. [49] since their signal of 11 events, with an estimated background of two, corresponds to a cross section

of at least 6000 pb, in contrast to 671 pb for reaction (4.340) with 1.94 GeV/c $\overline{p}$ momentum, according to Bertulani and Baur. Perhaps a future RCDW calculation will clarify these discrepancies.

4.5 Semiclassical Acausality

4.5.1 Introduction

Coupled second-order quantal wave equations are considered for a noncrossing atomic collision [78]. They are reduced to *exactly* equivalent first-order equations. The semiclassical approximation transforms these equations into generalized projectile–target time-dependent interaction impact-parameter equations. We show that in the suggested approach acausal, cybernetic effects are observed when terms propagate in the acausal (negative to positive time) direction. We summarize the results obtained and illustrate these effects in the quantal first Born approximation.

In the quantum mechanics of atomic collisions, the time-dependent Schrödinger equation (TDSE) is causal with respect to the time behaviour. This includes the impact-parameter treatment of ion–atom collisions. This latter treatment assumes that the relative motion of the nuclei is described a priori by a classical trajectory, for instance, a straight line or a Coulomb curved line. Nevertheless, the behaviour of the electrons is described by quantum mechanics.

However, there is a major difference, depending on whether we consider the general causal TDSE or the impact-parameter treatment. In the fully quantal TDSE describing three particles (an electron colliding with a one-electron atom, or a proton or other heavy-particle colliding with a similar atom), the time dependence may be removed immediately by a gauge transformation: factoring out $\exp(-\mathrm{i}E_t/\hbar)$, where E is the total energy. This is because we may assume that, in these three-body collisions, all three two-body interactions are time-independent and may be described using the time-independent (or stationary) Schrödinger equation. Note that we are excluding time-dependent external fields in these statements. To continue with the major difference, consider further the impact-parameter treatment. The classical treatment of the relative motion of the collidants means that a gauge transformation $\exp\left(-\mathrm{i}/\hbar \int_0^t (z_P z_T)/(R')\mathrm{d}t'\right)$ removes the internuclear interaction (here the charge of the bare projectile is z_P and of the target nucleus is z_T, and the internuclear distance is R, which may be taken as $\sqrt{\rho^2 + v^2t^2}$ in the straight-line case, with impact parameter ρ, time t, and impact velocity v). However, the price one pays is that the TDSE must be used since the two other two-body interactions are time-dependent. Nevertheless, a major advantage is that the variational principle (second-order in space, first-order in time Jacobi–Euler–Lagrange–Sil) leads to coupled first-order ordinary differential equations in the impact-parameter treatment [560]. In contrast, in the time-independent Schrödinger equation quantal wave treatment the variational principle (second-order in space Jacobi-Euler-Lagrange-Kohn) leads to coupled second-order ordinary differential equations, by separating the variables and following a partial-wave analysis [443].

Equally well, it is known that these wave- and impact-parameter treatments of an ion–atom collision are effectively equivalent in the first Born perturbation approximation, under rather minimal assumptions, notably a large reduced mass of the projectile and the nuclear target [158]. Thus it should come as no surprise that the so-called time-independent treatment actually does involve an underlying time dependence that is equivalent to the impact-parameter time. As we shall demonstrate in what follows, this underlying time involves acausal effects, as viewed from the impact-parameter treatment. This will be interpreted as a generalized impact-parameter treatment.

When we use the word semiclassical we shall be referring to the Jeffreys–Wentzel–Kramers–Brillouin approximation, rather than the impact-parameter method for which the relative motion of the heavy particles is described classically and the electrons quantally. In some countries, the impact-parameter method is described as semiclassical!

In Bichoutskaia et al. [77] we introduce in the notation of Mott and Massey ([443] chapter XIII, equations (10), (11)) the atomic-collision problem in the two-state approximation described in terms of two coupled radial Schrödinger equations:

$$\begin{aligned}\frac{\mathrm{d}^2 G_{0l}}{\mathrm{d}r^2} + \left(k_0^2 - \frac{l(l+1)}{r^2} - U_{00}(r)\right) G_{0l} &= U_{01} G_{1l} \\ \frac{\mathrm{d}^2 G_{1l}}{\mathrm{d}r^2} + \left(k_1^2 - \frac{l(l+1)}{r^2} - U_{11}(r)\right) G_{1l} &= U_{10} G_{0l}\end{aligned} \tag{4.341}$$

for each value of the total angular-momentum quantum number l. These may be derived from a two-state ansatz using second-order Euler–Lagrange variational theory (for the latest development in variational principles for second-order differential equations; see Grifone and Muzsnay [312]). In (4.341), $U_{10} = U_{01} \equiv 2MV_{01}/\hbar^2$ is the coupling matrix element, where V_{01} is the off-diagonal interaction matrix element for the colliding systems and the wavenumbers $k_j = k_j(\infty)$, $j = 0, 1$, are related to the relative velocity $v_j(\infty)$ of separated atoms in the state j as

$$k_j = \frac{M v_j(\infty)}{\hbar} \tag{4.342}$$

where M is the reduced mass; r is the projectile–target separation. The distortion of state i (0 or 1) due to interaction with the state $j\,(j \neq i)$ is given by the diagonal matrix element $U_{ii}(r)$. The channel wave functions G_{jl} are regular at the origin,

$$G_{0l}(0) = G_{1l}(0) = 0 \tag{4.343}$$

and satisfy, as $r \to \infty$, the boundary conditions

$$\begin{aligned}G_{0l}(r \to \infty) &= \mathrm{i}^l \sin(k_0(\infty) r - l\pi/2) + \alpha_l \exp(\mathrm{i} k_0(\infty) r) \\ G_{1l}(r \to \infty) &= \beta_l \exp(\mathrm{i} k_1(\infty) r)\end{aligned} \tag{4.344}$$

if the colliding entities are prepared in the state 0, where α_l and β_l are constants (independent of r). The constant β_l is the inelastic amplitude related to the S-matrix element S_{01}^l by

$$S_{01}^{l} = 2\mathrm{i}\sqrt{\frac{k_1(\infty)}{k_0(\infty)}}\beta_l$$

and the (partial) transition probability P_l is given traditionally by

$$P_l = \frac{4k_1^2(\infty)}{k_0^2(\infty)}|\beta_l|^2 = \frac{k_1(\infty)}{k_0(\infty)}|S_{01}^{l}|^2 \tag{4.345}$$

4.5.2 Generalized Impact-Parameter Treatment

The two coupled channel equations (4.341) can be transformed into four first-order ones ([40], to be referred to as (I)) by introducing the uncoupled channel wave functions $S_{jl}^{\pm}$ (solutions of (4.341) without the right-hand side) containing at $r \to \infty$ only the outgoing and incoming waves, respectively:

$$S_{jl}^{\pm}(r) \simeq k_j^{-1/2}\exp\left(\pm\mathrm{i}\left(k_j r - \frac{l\pi}{2}\right)\right) \tag{4.346}$$

Expanding the solutions $G_{jl}(r)$ in the form

$$G_{jl}(r) = \alpha_{jl}^{+}(r)S_{jl}^{+}(r) + \alpha_{jl}^{-}(r)S_{jl}^{-}(r) \tag{4.347}$$

leads (I) to the following exact equations for the coefficient functions $\alpha_{jl}^{\pm}$:

$$\begin{aligned}
\alpha_{0l}^{+\prime} &= -\frac{1}{2}\mathrm{i}U_{01}S_{0l}^{-}\left(\alpha_{1l}^{+}S_{1l}^{+} + \alpha_{1l}^{-}S_{1l}^{-}\right)\\
\alpha_{0l}^{-\prime} &= +\frac{1}{2}\mathrm{i}U_{01}S_{0l}^{+}\left(\alpha_{1l}^{+}S_{1l}^{+} + \alpha_{1l}^{-}S_{1l}^{-}\right)\\
\alpha_{1l}^{+\prime} &= -\frac{1}{2}\mathrm{i}U_{10}S_{1l}^{-}\left(\alpha_{0l}^{+}S_{0l}^{+} + \alpha_{0l}^{-}S_{0l}^{-}\right)\\
\alpha_{1l}^{-\prime} &= +\frac{1}{2}\mathrm{i}U_{10}S_{1l}^{+}\left(\alpha_{0l}^{+}S_{0l}^{+} + \alpha_{0l}^{-}S_{0l}^{-}\right)
\end{aligned} \tag{4.348}$$

In terms of $\alpha_{jl}^{\pm}$, the boundary conditions (4.343) and (4.344) may now be written as

$$\begin{aligned}
\alpha_{0l}^{-}(\infty) &= \frac{1}{2}k_0^{1/2}(\infty)\,, \qquad \alpha_{1l}^{-}(\infty) = 0\\
\alpha_{jl}^{+}(0) + \alpha_{jl}^{-}(0) &= 0 \qquad (j = 0, 1)
\end{aligned} \tag{4.349}$$

The advantage of representation (4.348) is that the properties of the uncoupled system enter the equations through $S_{jl}^{\pm}(r)$. This makes (4.348) a convenient basis for semiclassical treatment, as one only needs to replace the $S_{jl}^{\pm}(r)$ by their semiclassical asymptotes.

Thus far no approximation has been made and we have reduced two coupled second-order differential equations to four coupled first-order equations by a method that is essentially equivalent to the well-known variation-of-parameters method.

For simplicity we consider the noncrossing model in which 0 and 1 are the separated-atom eigenenergies:

$$U_{00} = U_{11} = 0 \tag{4.350}$$

and define

$$W(r) \equiv \frac{V_{01}(r)}{v} \tag{4.351}$$

In the noncrossing case $k_0^2 - U_{00}(r) \neq k_1^2 - U_{11}(r)$ for all r, whereas for pseudo or avoided crossings there exists at least one r for which the inequality becomes an equality. Following (I) we introduce the diabatic JWKB semiclassical approximation (with Langer correction)

$$S_{jl}^{\pm}(r) = k_j^{-1/2} \exp\left(\pm \mathrm{i}\left(\frac{\pi}{4} + k_j\left(r - \frac{\pi}{2}\rho_j\right)\right)\right) \tag{4.352}$$

which holds asymptotically and which includes an extra $\pm \mathrm{i}\pi/4$, compared to (4.346) (and with an eye on the connection formula at the classical turning point), and where we have impact parameters given by

$$\rho_0 k_0 = l + \frac{1}{2} = \rho_1 k_1 \tag{4.353}$$

and

$$\rho^2 = \rho_0 \rho_1 \tag{4.354}$$

In contrast to the adiabatic model of slowly varying behaviour for which we could diagonalize the matrix $\mathbf{V}$ ($V_{01} = 0$), in the diabatic treatment we neglect $\mathbf{W}$ (i.e., V_{01}, U_{01}, U_{10}) and solve the remaining homogeneous equations (4.341) to obtain $S_{jl}^{\pm}(r)$ of (4.352). We define, with $c_0(-\infty) = 1$ and $c_1(-\infty) = 0$, and suppressing l

$$c_j(z) = \begin{cases} +\alpha_{jl}^{+}(|z|) & (z \geq 0) \\ -\alpha_{jl}^{-}(|z|) & (z \leq 0) \end{cases} \tag{4.355}$$

where the path length z satisfies

$$|z| = v|t| = \sqrt{r^2 - \rho^2} \tag{4.356}$$

The remnant distortion [35] is given by

$$\left.\begin{matrix} \mu \\ \gamma \end{matrix}\right\} = \left[k_0|z| - \left(l + \frac{1}{2}\right)\frac{\pi}{2} + \frac{\pi}{4}\right] \mp \left[k_1|z| - \left(l + \frac{1}{2}\right)\frac{\pi}{2} + \frac{\pi}{4}\right] \tag{4.357}$$

(upper sign for μ being $+-$ or $-+$ distortion, lower sign for γ being $++$ or $--$ distortion), so that

$$\mu = (k_0 - k_1)|z| \tag{4.358}$$

$$\gamma = (k_0 + k_1)|z| - l\pi \tag{4.359}$$

Treating W as slowly varying and invoking the Gans–Jeffreys connection formula based on (4.349), and by the substitution of (4.352) and (4.355), (4.348) may now be rewritten in the classically allowed region (cf. "forbidden" region in Coveney et al. [152]) as the generalized impact-parameter equations

$$\frac{\mathrm{i}\mathrm{d}c_0(z)}{\mathrm{d}z} = W[c_1(z)\mathrm{e}^{\mp\mathrm{i}\mu} - c_1(-z)\mathrm{e}^{\mp\mathrm{i}\gamma}] \tag{4.360}$$

$$\frac{\mathrm{i}\mathrm{d}c_1(z)}{\mathrm{d}z} = W[c_0(z)\mathrm{e}^{\pm\mathrm{i}\mu} - c_0(-z)\mathrm{e}^{\mp\mathrm{i}\gamma}] \tag{4.361}$$

upper or lower sign according to $z > 0$ or $z < 0$. The second terms in the right-habd side square brackets in (4.360) and (4.361) may be regarded as acausal because for negative z they have not yet been reached by the classical trajectory. These acausal terms come from the $S^-_{0l}S^-_{1l}$ and $S^+_{0l}S^+_{1l}$ terms in (4.348). The difference between (4.360) and (4.361) and the standard impact-parameter treatment [35] lies entirely in the $c_j(-z)$ terms. The normal argument in ion–atom collisions is that $\mathrm{e}^{\pm\mathrm{i}\gamma}$ averages out at zero for large γ. Mathematically, we have $c_j(-z)$ as against $c_j(z)$ and the terms that run backwards in time do occur. We call them acausal terms in contrast with causal processes of movement forward in time. It follows that the exact relations hold, namely

$$\frac{\mathrm{d}c_0(-z)}{\mathrm{d}z} = \exp\left(\pm\mathrm{i}(\mu+\gamma)\right)\frac{\mathrm{d}c_0(z)}{\mathrm{d}z} \tag{4.362}$$

$$\frac{\mathrm{d}c_1(-z)}{\mathrm{d}z} = \exp\left(\pm\mathrm{i}(\gamma-\mu)\right)\frac{\mathrm{d}c_1(z)}{\mathrm{d}z} \tag{4.363}$$

By inspection, these relations embrace cybernetic (or feedback) effects. To wit, if $z > 0$, then earlier amplitudes (or rather, their rates of change) are given in terms of the later amplitudes. Viewed from the impact-parameter trajectory, the absence of acausal terms in (4.360) and (4.361) would negate relations (4.362) and (4.363).

4.5.3 Perturbation Theory

We now apply double-perturbation theory (Born approximation), which invokes $W \ll 1$, which implies $c_1(+\infty) \simeq 0$ and neglecting the oscillatory acausal term in (4.361), we obtain

$$\frac{\mathrm{i}\mathrm{d}c_1(z)}{\mathrm{d}z} \simeq W\mathrm{e}^{\pm\mathrm{i}\mu} \tag{4.364}$$

$$\Rightarrow \quad \mathrm{i}c_1(+\infty) \cong 2\int_0^\infty \mathrm{d}z\, W\cos\mu \tag{4.365}$$

and

$$\frac{\mathrm{i}\mathrm{d}c_1(-z)}{\mathrm{d}z} \simeq W\mathrm{e}^{\pm\mathrm{i}\gamma} \tag{4.366}$$

$$\Rightarrow \quad \mathrm{i}c_1(-\infty) \cong 2\int_0^\infty \mathrm{d}z\, W\cos\gamma \tag{4.367}$$

This implies that the net inelastic transition probability is

$$P_{01} = \left|2\int_0^\infty \mathrm{d}z\, W\cos\mu\right|^2 - \left|2\int_0^\infty \mathrm{d}z\, W\cos\gamma\right|^2 \tag{4.368}$$

Using Fourier transforms and the Faltung theorem [158], it follows that the total cross section is

$$Q_{01}/a_0^2 = 2\pi\int_0^\infty \rho\,\mathrm{d}\rho\, P_{01}(\rho) \tag{4.369}$$

$$Q_{01}/a_0^2 = \frac{1}{(2\pi v)^2}\int_{|k_0-k_1|}^{k_0+k_1} q\,\mathrm{d}q\int_0^{2\pi}\mathrm{d}\phi\left|\mathrm{d}\mathbf{r}\,\mathrm{e}^{\mathrm{i}\mathbf{q}\mathbf{r}}V_{01}(r)\right|^2 \geq 0 \tag{4.370}$$

where the change in relative momentum of the atomic particles is

$$\mathbf{q} = \mathbf{k}_0 - \mathbf{k}_1 \tag{4.371}$$

so that

$$q^2 = k_0^2 + k_1^2 - 2k_0k_1\cos\theta \tag{4.372}$$

where

$$\cos\theta = \hat{\mathbf{k}}_0\cdot\hat{\mathbf{k}}_1 \tag{4.373}$$

Despite inequality (4.370), $P_{01}(\rho)$ of (4.368) could, in principle, lie outside the physical range $[0,1]$ [36], in which case, strictly speaking, the perturbation treatment is invalid for the particular ρ-domain. To rephrase, the step leading to (4.364) becomes invalid. Nevertheless, since $k_0 + k_1 > |k_0 - k_1|$, the second integral in (4.368) has the higher frequency leading to greater cancellation. This is illustrated as follows: for $V_{01}(r) \equiv \exp(-\alpha r)$, P_{01} of (4.368) is given by

$$P_{01} = \frac{4\alpha^2\rho^2}{v^2}\left[K_1^2\left(\rho\sqrt{\alpha^2+(k_0-k_1)^2}\right) - K_1^2\left(\rho\sqrt{\alpha^2+(k_0+k_1)^2}\right)\right] \tag{4.374}$$

However, we have

$$K_1(\zeta) \underset{\zeta\gg 1}{\simeq} \sqrt{\frac{\pi}{2\zeta}}\exp(-\zeta) \tag{4.375}$$

and

$$K_1(\zeta) \underset{\zeta\sim 0}{\simeq} \frac{1}{\zeta} \tag{4.376}$$

Thus, if we take, say, $\alpha = 1$, $k_0 = 2$, and $k_1 = 1$ (in atomic units), which are light-particle parameters, we see that the causal term is very much larger than the acausal term, so that the double-perturbation treatment is justified and consistent; moreover, the link with the first Born wave treatment (4.370) is justified.

4.5.4 Discussion and Conclusions

The quantity Q_{01} (equation (4.370)) is the quantal first Born cross section in which the lower limit corresponds to $\theta = 0$ and is causal, whereas the upper limit corresponds to $\theta = \pi$ and is acausal. The classical purely impact-parameter first Born approximation comprises $k_0 - k_1 \to (\epsilon_1 - \epsilon_0)/v$ and $k_0 + k_1 \to +\infty$. We may interpret (4.360) and (4.361) as generalized impact-parameter equations with the first terms on the right-hand side causal and the second terms acausal, at least as viewed from the derived time-dependent treatment that arises when the acausal terms are neglected. Thus not only does semiclassical mechanics here interpolate between quantal and classical mechanics, but it explicitly demonstrates cybernetic effects by which the propagation of waves $-\infty$ to $+\infty$ in time simultaneously invokes propagation of waves $+\infty$ to$-\infty$ in time in a consistently dovetailed unitary manner, the essence of quantum mechanics (here we are not referring to perturbation theory). Clearly our technique, based on the Green function method of (I), generalizes to $U_{00} \neq 0$ and $U_{11} \neq 0$. Moreover, although the semiclassical treatment of Stueckelberg [574], considered in paragraph 3 of chapter XIII of Mott and Massey [443], concerns ion–atom collisions, our treatment given here need not be so limited. Our treatment clearly generalizes to any number of coupled states [42]. A simple consideration of the leading terms in both versions (with and without the cybernetic acausal terms) of the first Born approximation shows that the impact-parameter treatment erroneously produces a finite cross section at threshold [158], whereas the wave treatment (in the form of generalized impact-parameter equations (sic)) at least gives a zero cross section [600].

As presented here, the semiclassical treatment of the four exact first-order equations (4.348) leads to generalized projectile-target time-dependent interaction impact-parameter equations (4.360), (4.361). These equations contain acausal behaviour embedded entirely in the $c_j(-z)$-terms, which are absent in the standard impact-parameter treatment (see, for example, equation (2.13) of Bichoutskaia et al. [77]). The relevance of the approach described, to ultracold collisions, lies in the consideration of equations (4.360) and (4.361) in the closely coupled perturbed symmetric resonance model [162] in which both k_0 and k_1 are sufficiently small, that neither causal nor acausal terms can be ignored, relative to each other, $\epsilon_1 - \epsilon_0$ is small and $k_0 - k_1 \neq (\epsilon_1 - \epsilon_0)/v$. The consequence is that a typical very low-energy fine-structure ion–atom collision [224] will yield to a generalized impact-parameter treatment description of its experimental realization.

In conclusion, in the standard impact-parameter treatment, we may have a straight-line trajectory at impact parameter ρ or, indeed, a curved trajectory (e.g., Coulomb), each of which has a point of closest approach, dividing the trajectory into two. On the inward half, this corresponds to radially incoming waves; on the outward half, to radially outgoing waves.

In standard one-dimensional scattering, there are ingoing waves (incident beam) and outgoing waves (transmitted and reflected beams); there are no ingoing waves in the negative direction by assumption.

However, in a three-dimensional spherical interior, a priori they may simultaneously be both radially ingoing and outgoing waves in all directions. A counterexample is given by the well-known plane-wave asymptotic expansion

$$\mathrm{e}^{\mathrm{i}\mathbf{k}\cdot\mathbf{r}} \underset{kr\gg 1}{\simeq} \frac{2\pi}{\mathrm{i}kr}\left[\mathrm{e}^{\mathrm{i}kr}\delta(\hat{\mathbf{k}}-\hat{\mathbf{r}}) - \mathrm{e}^{-\mathrm{i}kr}\delta(\hat{\mathbf{k}}+\hat{\mathbf{r}})\right] \tag{4.377}$$

with ingoing waves $\mathrm{e}^{-\mathrm{i}kr}$ (direction $\hat{\mathbf{r}} = -\hat{\mathbf{k}}$, momentum $\sim -\hbar k\hat{\mathbf{r}}$) and outgoing waves $\mathrm{e}^{\mathrm{i}kr}$ (direction $\hat{\mathbf{r}} = \hat{\mathbf{k}}$, momentum $\sim +\hbar k\hat{\mathbf{r}}$). Here, the delta functions are two-dimensional, and admittedly there is a problem at $\hat{\mathbf{k}}\cdot\hat{\mathbf{r}} = 0$ [444]. The picture here is of a wave lying in a plane that sweeps through the spherical interior in the $\mathbf{k}$ direction, in, say, the $\phi = 0$ plane, ϕ being the cylindrical polar azimuthal angle. The complication, compared to one-dimensional scattering, is that the coordinate $r \in [0, +\infty]$, because the distance between two objects must always be nonnegative. The plane wave can represent, in principle, an electron, a photon, an ion, etc, impinging on some fixed centre that does not perturb the projectile.

Nevertheless, as semiclassical analysis shows, this comprises a rather classical picture in which the impact parameter is given by $(l+1/2)/k$ where l is the azimuthal quantum number of the partial wave (see also (4.353)).

When an interaction occurs, however, (4.360)–(4.363) show that, in quantum mechanics, there are ingoing waves, simultaneously in both halves of the spherical interior, and outgoing waves also in both halves of the interior, in this case $\phi = 0$ and $z \in [-\infty, +\infty]$. From the stationary Schrödinger equation point of view, this is all prescribed instantaneously. From the generalized impact-parameter-treatment point of view, this comprises acausal cybernetic effects. Of course, this would appear to be implausible at impact energies that are in any way appreciable, but then the generalized treatment does yield the impact-parameter treatment in such a limit.

5

Diffusion in Liquids and Solids

5.1 Single-Domain Ferromagnetic Particles

Chapters 3 and 4 concerned atomic and molecular physics of particles in the gaseous phase under single-collision conditions. Here in Chapter 5 we are concerned with the condensed-matter physics in the liquid and solid phases. In Section 5.3 we will discuss dielectric relaxation but first we discuss single-domain ferromagnetic particles.

There are at least three types of magnetism: (a) diamagnetism–the phenomenon exhibited by substances that have a relative permeability less than unity and a negative susceptibility. It is caused by the orbital motion of electrons in the atoms of the material and is unaffected by temperature; (b) paramagnetism–the phenomenon exhibited by substances that have a relative permeability slightly greater than unity and a positive susceptibility (the effect is due to alignment of unpaired spins of electrons in atoms of the material); and (c) ferromagnetism, the topic of this section–the phenomenon exhibited by substances, such as iron, that have relative permeabilities much greater than unity and magnetization increasing with applied magnetizing field. Certain of these substances retain their magnetization in the absence of the applied field: permanent after effect. The effect is caused by the alignment of electron spin in regions called *domains*. A key role for (c) is found in electric generators, transformers, and relays, in data storage and processing, in the recording industry, in miniaturization, and in energy conservation. More generally, magnetic fields have the important role of confining hot, dense plasma to the inside of a tokamak. Other phenomena include giant magnetoresistance and magnetic circular dichroism. Ferromagnetism is caused by atoms with incomplete electron shells, behaving like tiny bar magnets, that is, like magnetic dipoles. The strength of an atomic dipole comprises two components; magnetic spin and magnetic orbital angular momentum, which are coupled by spin-orbit interaction. Occasionally the magnetic moments of the individual atoms also couple together, in which case they all point in the same direction. This occurs due to the quantum mechanics of exchange interaction. Materials of this type are ferromagnets (first observed in iron, the Latin for which is *ferrum*.) The vector sum of the atomic magnetic moments gives rise to the magnetization.

Note that on an atomic scale, it is the orbital angular momentum and the deliberately perturbed material structure that are responsible for hard magnetic properties. All the better permanent magnets are made of compounds of the ferromagnetic elements Fe or Co with the lighter rare earths, such as Nd, Pr, or Sm, which have a very high magnetic orbital angular momentum that is about 60 times greater than that of iron. By incorporating lighter elements we can make the structure more anisotropic and thus magnetically harder, that is, reversing the magnetization of the domains requires a large amount of energy or a stronger external field.

In a crystal or other condensed matter the magnetic moment orients to minimise the electron energy. In soft iron, the spins can easily align with an external field. In hard magnetic material, as in a bar magnet, the magnetization can only be influenced by strong external magnetic fields.

Ferromagnetism is associated with magnetic domains of dimension 10^{-6}–10^{-3} mm and 10^{23} electrons. For this reason, classical statistical mechanics is appropriate, rather than quantum mechanics.

Accordingly we now apply the semiclassical theory of Brownian motion to the asymptotic dependence of the relaxation time of the magnetization of a ferromagnetic particle on its anisotropy, semiclassical in the sense that the anisotropy energy, divided by both the absolute temperature and Boltzmann's constant, is reasonably greater than unity and is the barrier height parameter. This is consistent with the assumption that the lowest eigenvalue is small, the temperature is small, the volume of the single ferromagnetic domain is large, and Boltzmann's constant is small. Appropriately we now consider the stated problem in detail.

It is known that the direction of the magnetization vector of very fine single-domain ferromagnetic particles fluctuates under the influence of thermal agitation. Perturbation theory is applied rigorously to a singular integral equation to derive an asymptotic formula for the relaxation time of the magnetization, for the case of uniaxial anisotropy and an applied magnetic field. The result agrees with that of Brown [91] as described succinctly by Aharoni [6]. It should be emphasised that both Gilbert's equation and the earlier Landau–Lifshitz equation are merely phenomenological equations, which are used to explain the time decay of the average magnetization. Brown suggested that the Gilbert equation should be augmented by a white noise driving term in order to explain the effect of thermal fluctuations of the surroundings on the magnetization.

We consider a single-domain ferromagnetic particle with uniaxial anisotropy [53]. The internal magnetic potential of such a particle has two stable stationary points π^c apart with a potential barrier between. If the particle is sufficiently small and under the influence of thermal agitation, the direction of magnetization may undergo a Brownian-type rotation, overcoming the barrier as first pointed out by Néel [448]. Here we find an expression for the relaxation time of $\mathbf{M}$, the magnetization vector.

We assume that there is a magnetic field H applied parallel to the easy axis of the anisotropy. The potential energy of the particle may then be written

$$V = -HM_s \cos\theta - K\cos^2\theta \tag{5.1}$$

where H and M_s are the magnitudes of $\mathbf{H}$ and $\mathbf{M}$, respectively, K is the anisotropy energy per unit volume, and θ is the angle between $\mathbf{M}$ and the easy axis of the anisotropy.

Brown [91] used Brownian-motion theory to write a Fokker–Planck-type equation to describe the motion of $\mathbf{M}$. For the case when V is a function of the polar angle θ only, this is

$$2\tau_D \sin\theta \frac{\partial W}{\partial t} = \frac{\partial}{\partial \theta}\left[\sin\theta\left[\frac{v}{kT}\frac{\mathrm{d}V}{\mathrm{d}\theta}W + \frac{\partial W}{\partial \theta}\right]\right] \tag{5.2}$$

where $W(\theta, t)$ the probability distribution function is the probability that $\mathbf{M}$ has orientation θ at time t, v is the volume of the particle, k is Boltzmann's constant, and T is the absolute temperature. The characteristic time τ_D is defined as

$$\tau_D = \frac{v}{kT}\left[\frac{(1/\gamma^2) + \eta^2 M_s^2}{2\eta}\right]$$

where γ is the gyromagnetic ratio and η is the damping constant from Gilbert's equation [294]

$$\frac{\mathrm{d}\mathbf{M}}{\mathrm{d}t} = \gamma \mathbf{M} \times \left[\mathbf{H} - \eta \frac{\mathrm{d}\mathbf{M}}{\mathrm{d}t}\right]$$

on which Brown's equation is based.

It should be emphasized that both Gilbert's equation and the earlier Landau–Lifshitz equation are merely phenomenological equations used to explain the time decay of the average magnetization. Brown [91] suggested that the Gilbert equation should be augmented by a white noise driving term to explain the effect of thermal fluctuations of the surroundings on the magnetization.

If we let

$$x = \cos\theta \tag{5.3}$$

then using the separation ansatz proposed by Risken [507] and following Brown [91] we write

$$W(x, t) = \sum_{n=0}^{\infty} a_n(t) F_n(x)$$

with

$$a_n(t) = a_n(0)\mathrm{e}^{-p_n t}$$

where the p_n are the eigenvalues and F_n the corresponding eigenfunctions of the Fokker–Planck operator, determined by the boundary conditions that F must be finite at $x = \pm 1$. Equation (5.2) then becomes

$$\frac{\mathrm{d}}{\mathrm{d}x}\left[(1 - x^2)\mathrm{e}^{-\beta V}\frac{\mathrm{d}}{\mathrm{d}x}\left[\mathrm{e}^{\beta V} F_n(x)\right]\right] + \lambda_n F_n(x) = 0 \tag{5.4}$$

where

$$\lambda_n = 2\tau_D p_n$$

and

$$\beta = v/kT$$

By writing

$$\varphi_n(x) = \mathrm{e}^{\beta V} F_n(x)$$

equation (5.4) becomes

$$\frac{\mathrm{d}}{\mathrm{d}x}\left[(1-x^2)\mathrm{e}^{-\beta V}\frac{\mathrm{d}\varphi}{\mathrm{d}x}\right] + \lambda \mathrm{e}^{-\beta V}\varphi = 0 \tag{5.5}$$

subject to $\varphi(\pm 1)$ being finite. By writing

$$h = \frac{HM_s}{2K}$$

and

$$\alpha = \beta K$$

also sometimes called σ, in accordance with Aharoni [6], (5.5) is

$$\frac{\mathrm{d}}{\mathrm{d}x}\left[(1-x^2)\mathrm{e}^{\alpha(x^2+2hx)}\frac{\mathrm{d}\varphi}{\mathrm{d}x}\right] + \lambda \mathrm{e}^{\alpha(x^2+2hx)}\varphi = 0 \tag{5.6}$$

where $0 \le h < 1$. The value $h = 0$ corresponds to zero applied field [5], and at $h = 1$ the two-minima structure of V disappears. Multiplying across by $\mathrm{e}^{\alpha h^2}$ to complete the square and integrating once, we have

$$(1-x^2)\mathrm{e}^{\alpha(x+h)^2}\frac{\mathrm{d}\varphi}{\mathrm{d}x} = -\lambda \int_{\pm 1}^{x} \mathrm{e}^{\alpha(t+h)^2}\varphi(t)\mathrm{d}t \tag{5.7}$$

from which it follows immediately that

$$\int_{-1}^{1} \mathrm{e}^{\alpha(t+h)^2}\varphi(t)\mathrm{d}t = 0 \tag{5.8}$$

which is Brown's [91] equation (4.15). Integrating (5.7) , we have the singular integral equations

$$\varphi(x) - \varphi(d) = -\lambda \int_{d}^{x} \frac{\mathrm{d}y}{(1-y^2)}\mathrm{e}^{-\alpha(y+h)^2}\int_{c}^{y} \mathrm{e}^{\alpha(t+h)^2}\varphi(t)\mathrm{d}t \tag{5.9}$$

where c and d are both $+1$ or -1. For $c = d = -1$, assuming real transition points θ_1 and θ_2, where, following Brown [91], $0 < \theta_1 < \theta_2 < \pi$, we may assume that

$$\varphi(x) = \varphi(-1)\mathrm{e}^{-\alpha(x+1)^2} \tag{5.10}$$

The t integral in (5.9) has no point of stationary phase and may be integrated to give the semiclassical result ($\alpha \gtrsim 1$)

$$\frac{\varphi(-1)}{2\alpha(h-1)}\left(\mathrm{e}^{\alpha[(y+h)^2-(y+1)^2]} - \mathrm{e}^{\alpha(h-1)^2}\right)$$

Substitution of this into (5.9) gives convergence at $y = -1$. Application of the method of steepest descents at the saddle point $y = -h$ gives the semiclassical result ($\alpha \gtrsim 1$)

$$\varphi(x) = \begin{cases} \varphi(-1) + \dfrac{\lambda\varphi(-1)}{2\alpha(h-1)} \dfrac{\sqrt{\pi}}{\sqrt{\alpha}} \dfrac{\mathrm{e}^{\alpha(h-1)^2}}{1-h^2} & \text{for } x > -h \qquad (5.11a) \\ \varphi(-1) + \dfrac{\lambda\varphi(-1)}{2\alpha(h-1)} \dfrac{\sqrt{\pi}}{2\sqrt{\alpha}} \dfrac{\mathrm{e}^{\alpha(h-1)^2}}{1-h^2} & \text{for } x = -h \qquad (5.11b) \end{cases}$$

where in (5.11b) the extra factor of 2 arises, since the saddle point is then an endpoint in the domain of integration.

We may repeat the process taking $c = d = +1$. We assume that

$$\varphi(x) = \varphi(1)\mathrm{e}^{-\alpha(x-1)^2} \qquad (5.12)$$

and we obtain

$$\varphi(x) = \begin{cases} \varphi(1) - \dfrac{\lambda\varphi(1)}{2\alpha(h+1)} \dfrac{\sqrt{\pi}}{\sqrt{\alpha}} \dfrac{\mathrm{e}^{\alpha(1+h)^2}}{1-h^2} & \text{for } x < -h \qquad (5.13a) \\ \varphi(1) - \dfrac{\lambda\varphi(1)}{2\alpha(h-1)} \dfrac{\sqrt{\pi}}{2\sqrt{\alpha}} \dfrac{\mathrm{e}^{\alpha(1+h)^2}}{1-h^2} & \text{for } x = -h \qquad (5.13b) \end{cases}$$

Matching $\varphi(-h)$ via (5.11b) and (5.13b) gives

$$\varphi(1)\left(1 - \frac{\lambda \mathrm{e}^{\alpha(1+h)^2}\sqrt{\pi}}{4\alpha^{3/2}(h+1)(1-h^2)}\right) = \varphi(-1)\left(1 - \frac{\lambda \mathrm{e}^{\alpha(1-h)^2}\sqrt{\pi}}{4\alpha^{3/2}(1-h)(1-h^2)}\right) \qquad (5.14)$$

Using (5.8), (5.10), and (5.12), we may show that

$$\begin{aligned} 0 = &\int_{\cos\theta_1}^{1} \mathrm{d}x\, \varphi(1)\mathrm{e}^{\alpha(x+h)^2 - \alpha(x-1)^2} \\ &+ \int_{\cos\theta_2}^{\cos\theta_1} \mathrm{d}x\, \varphi(-h)\left(1 + \frac{\lambda}{2\alpha(1-h^2)}\left(\mathrm{e}^{\alpha(x+h)^2} - 1\right)\right) \\ &+ \int_{-1}^{\cos\theta_2} \mathrm{d}x\, \varphi(-1)\mathrm{e}^{\alpha(x+h)^2 - \alpha(x+1)^2} \qquad (5.15) \\ \approx &\frac{\varphi(1)\mathrm{e}^{\alpha(h+1)^2}}{2\alpha(h+1)} - \frac{\varphi(-1)\mathrm{e}^{\alpha(h-1)^2}}{2\alpha(h-1)}, \quad \alpha \gtrsim 1 \qquad (5.16) \end{aligned}$$

In (5.15) we have integrated the first and third integrals by parts to order $1/\alpha$ and have neglected the middle integral as being of higher order, anticipating that λ is exponentially decreasing with α and where we obtained its integrand by taking $c = d = -h$ in (5.9) and correctly assuming $\varphi(-h) = 0$. Equations (5.14) and (5.16) give the result

$$\lambda \approx 2\alpha^{3/2}(1-h^2)\pi^{-1/2}\left[(1+h)\mathrm{e}^{-\alpha(1+h)^2} + (1-h)\mathrm{e}^{-\alpha(1-h)^2}\right] \quad \text{for } \alpha \gtrsim 1 \qquad (5.17)$$

which for $h = 0$ is

$$\lambda \approx 4\alpha^{3/2}\pi^{-1/2}\mathrm{e}^{-\alpha} \quad \text{for } \alpha \gtrsim 1 \tag{5.18}$$

These formulae agree with the formulae given by Aharoni [6] and Brown [91], respectively. Equation (5.18) holds well down to $\alpha = 1.5$. For values of α less than approximately 1.5, the formula based on Dawson's integral implied by (29) of Raĭkher and Shliomis [500] is an exceedingly good approximation to the exact numerical result [120].

We now note that the relaxation time τ is equal [90] to $1/p$, that is,

$$\tau = 2\tau_D/\lambda \approx \frac{\tau_D}{\alpha^{3/2}(1-h^2)\pi^{-1/2}\left[(1+h)\mathrm{e}^{-\alpha(1+h)^2} + (1-h)\mathrm{e}^{-\alpha(1-h)^2}\right]} \tag{5.19}$$

Rearranging the denominator and letting

$$\xi = 2\alpha h \tag{5.20}$$

we obtain the result

$$\tau = \frac{1}{2}\tau_D\pi^{1/2}\alpha^{-3/2}\mathrm{e}^{\alpha}\left[\frac{\mathrm{e}^{\xi^2/4\alpha}}{(1-\xi^2/4\alpha^2)[\cosh\xi - (\xi/2\alpha)\sinh\xi]}\right] \tag{5.21}$$

We have obtained the results of Brown [91] and Aharoni [6] by applying perturbation theory to solve the singular integral equation, thus avoiding some of the approximations previously made and presenting a more rigorous treatment of the problem. We have adopted the notation of Aharoni in preference to Brown's, since it lends itself to a higher degree of transparency. The method appears to be promising for application to a wider range of potentials and dimensions.

We now generalise Scully et al. [539] to consider integral representation of exact solutions for the correlation times of rotators in periodic potentials and the derivation of asymptotic expansions.

The derivation of asymptotic expansions from the exact solution of the three-term recurrence relations arising in the study of the Brownian movement in a periodic potential is discussed. The discussion is illustrated by showing how the exact formulae for the longitudinal and transverse correlation times of a single-axis rotator with two equivalent sites, which have been previously given as a series of products of modified Bessel functions, may be rendered in integral form using Watson's integral formula for the product of two modified Bessel functions. The method of steepest descents is applied to these solutions to obtain rigorous semiclassical asymptotic formulae for the correlation times in the high potential barrier limit. The analogous results for rotation in three dimensions in the Maier–Saupe potential are treated also.

The study of the Brownian motion of a rotator in a potential containing a single periodic term invariably reduces to the problem of solving a three-term matrix recurrence relation in the frequency domain. Further, if the inertia of the rotator is ignored the recurrence relation becomes a scalar one, the exact solution of which may be expressed as a series of products of infinite continued fractions [128]. This technique has recently been applied to a number of problems, including dielectric relaxation

of polar molecules [128], Néel [91] relaxation of single-domain ferromagnetic particles, quantum noise in ring laser gyroscopes [127], etc.

The quantity of greatest interest in dielectric and Néel relaxation is generally the correlation time of the electric or magnetic polarisation. This characterises the time of reversal of the polarisation in the presence of a potential barrier arising from the crystalline anisotropy. Up to the present, this has usually been calculated [91] only in the high potential barrier limit by making use of approximate methods based on the Kramer transition-state theory.

It has recently been demonstrated, by proceeding to the zero frequency limit of the exact solution of the appropriate three-term recurrence relation, how exact expressions for the dielectric and magnetic correlation times may be written in series form. In particular, the longitudinal $T_{\|}$ and transverse $T_{\perp}$ correlation times for rotation in two dimensions for the simplest uniaxial potential of the crystalline anisotropy may be written as an infinite series of products of modified Bessel functions of integer and half-integer order. Furthermore, $T_{\|}$ for rotation in three dimensions may [125] be written as a series of products of confluent hypergeometric functions. In all cases the terms *longitudinal* and *transverse* pertain to the directions parallel and perpendicular to the axis of symmetry of the potential. Similar considerations apply to the Brownian motion in a single-well cosine potential. This problem arises when we study the effect of a DC bias field on the Debye relaxation process.

An important question that arises in the course of this discussion is whether it is possible to rigorously derive asymptotic expansions from the series form of the exact solution.

It is the purpose of this section to demonstrate how the series solution may also yield an exact expression for the correlation time in integral form, allowing one to rigorously construct an asymptotic expansion in the high potential barrier limit. We shall illustrate our method by referring to the most elementary problem for which exact solutions for $T_{\|}$ and $T_{\perp}$ exist, namely the Brownian motion of a two-dimensional rotator in the simplest uniaxial potential of the crystalline anisotropy [379].

The derivation of asymptotic expansions for large barrier heights from these exact solutions [128] is not a straightforward procedure as the exact solution depends on two variables–the barrier height, which is the argument of the modified Bessel functions, and their order, giving rise to nonuniform convergence. Thus the order-dependence must first be eliminated. This is accomplished by replacing the order dependent sum in the exact solution by an integral using Watson's [594] integral representation of a product of Bessel functions. This renders the exact solution in integral form. The method of steepest descents is then used to calculate the asymptotic values of these integrals in the high barrier limit. The leading term in the asymptotic formula for $T_{\|}$ so derived is in agreement with the result of the Kramers barrier-crossing theory as discussed in [128]. Furthermore, the effective eigenvalue method provides a good description for $T_{\perp}$.

We consider the Smoluchowski equation for a single-axis rotator with two equivalent sites separated by a potential barrier of height U. We have seen that this has recently been solved [128] to yield exact expressions for the longitudinal and transverse electric polarisabilities and the corresponding relaxation times. In this problem,

a typical dipole of the assembly is constrained to rotate about a fixed axis under the influence of a potential

$$V = U \sin^2 \phi \tag{5.22}$$

determined by the crystalline field. ϕ is the angle describing the orientation of the dipole about its axis of rotation. The initial line $\phi = 0$ is taken for convenience as the direction that an applied DC field $\mathbf{E}$ had, that field having been switched off at an initial time $t = 0$.

The procedure carried out in [128] to obtain an exact solution for the complex polarisabilities, and thus the relaxation times, is to expand the solution of the Smoluchowski equation

$$\frac{\partial W}{\partial t} = \frac{\partial}{\partial \phi}\left(\frac{W}{\zeta}\frac{\partial V}{\partial \phi}\right) + \frac{1}{\tau}\frac{\partial^2 W}{\partial \phi^2} \tag{5.23}$$

as a Fourier series in the angle ϕ. $W(\phi, t)$ is the probability density of orientations of a dipole on the unit circle. ζ is the viscous drag coefficient of a dipole, k is the Boltzmann constant, and T is the absolute temperature:

$$\tau = \frac{\zeta}{kT} \tag{5.24}$$

the Debye [206] relaxation time. The dipole rotates about the ~~ex~~is before the field has been switched off under the influence of the potential

$$V(\phi) = U \sin^2 \phi - \boldsymbol{\mu}\dot{\mathbf{E}} \tag{5.25}$$

where $\boldsymbol{\mu}$ is the dipole moment of the rotator. In order to study the relaxation, it is supposed that $\boldsymbol{E}$ is switched off at time $t = 0$ and that

$$\xi = \frac{\mu E}{kT} \ll 1 \tag{5.26}$$

so that we confine ourselves to the linear response to the applied field:

$$\sigma = \frac{U}{2kT} \tag{5.27}$$

so that 2σ is the barrier height parameter. Let us now suppose that

$$W(\phi, t) = \sum_{p=-\infty}^{\infty} a_p(t) \mathrm{e}^{ip\phi} \tag{5.28}$$

Whence [128]

$$\langle \cos(2p+1)\phi \rangle = f_{2p+1}(t) = \frac{a_{2p+1}(t) + a_{-(2p+1)}(t)}{2a_0} \tag{5.29}$$

satisfies the set of differential-difference equations

$$\dot{f}_{2p+1}(t) + \frac{(2p+1)^2}{\tau} f_{2p+1}(t) = \frac{\sigma(2p+1)}{\tau}\left[f_{2p-1}(t) - f_{2p+3}(t)\right] \tag{5.30}$$

with

$$f_{-p}(t) = f_p(t)\,, \qquad f_0(t) = 1\,, \qquad t > 0 \tag{5.31}$$

and [128] is, in the linear approximation in ξ,

$$f_{2p+1}(0) = \frac{\xi}{2}\left(\frac{I_{p+1}(\sigma) + I_p(\sigma)}{I_0(\sigma)}\right) \tag{5.32}$$

The $I_p(\sigma)$ are the modified Bessel functions of the first kind of order p. By taking the Laplace transform of (5.30) and using the methods described in [128] we have for the Laplace transform $\tilde{f}_1(s)$ of the decay function $f_1(t)$ of the dielectric polarisation

$$\tilde{f}_1(s) = \frac{\tau}{s\tau + (1-\sigma) + \sigma\tilde{S}_3(s)}\left(f_1(0) + \sum_{p=1}^{\infty}\frac{(-1)^p}{2p+1} f_{2p+1}(0)\prod_{k=1}^{p}\tilde{S}_{2k+1}(s)\right) \tag{5.33}$$

where

$$\tilde{S}_p(s) = \frac{\sigma p}{s\tau + p^2 + \sigma p\tilde{S}_{p+2}(s)} \tag{5.34}$$

which is an infinite continued fraction. On noting that

$$T_{\parallel} = \lim_{s\to 0}\int_0^{\infty} C_1^{\parallel}(t)\mathrm{e}^{-st}\mathrm{d}t = \lim_{s\to 0}\tilde{C}_1^{\parallel}(s) = \tilde{C}_1^{\parallel}(0) \tag{5.35}$$

and that for the linear response the autocorrelation function is

$$C_1^{\parallel}(t) = \frac{f_1(t)}{f_1(0)} \tag{5.36}$$

We have, with the aid of (5.35) and (5.36),

$$\begin{aligned} T_{\parallel} &= \frac{\tilde{f}_1(0)}{f_1(0)} \\ &= \frac{\tau}{(1-\sigma) + \sigma\tilde{S}_3(0)}\left(1 + \sum_{p=1}^{\infty}\frac{(-1)^p}{2p+1}\frac{f_{2p+1}(0)}{f_1(0)}\prod_{k=1}^{p}\tilde{S}_{2k+1}(0)\right) \end{aligned} \tag{5.37}$$

By inspection of (5.34) at $s = 0$

$$\tilde{S}_{2k+1}(0) = \frac{I_{k+1/2}(\sigma)}{I_{k-1/2}(\sigma)} \tag{5.38}$$

and so (5.37) becomes

$$\frac{T_{\parallel}}{\tau} = \frac{1}{1-\sigma+\sigma\left[I_{3/2}(\sigma)/I_{1/2}(\sigma)\right]}\left(1 + \sum_{p=1}^{\infty}\frac{(-1)^p}{2p+1}\frac{\left[I_p(\sigma) + I_{p+1}(\sigma)\right]I_{p+1/2}(\sigma)}{\left[I_0(\sigma) + I_1(\sigma)\right]I_{1/2}(\sigma)}\right) \tag{5.39}$$

The functions $I_{p+1/2}(\sigma)$ may be represented in terms of elementary functions as described in [128], so that the prefactor

$$\frac{1}{1-\sigma+\sigma\left[I_{3/2}(\sigma)/I_{1/2}(\sigma)\right]}=\frac{1}{\sigma(\coth\sigma-1)}=\frac{\mathrm{e}^{2\sigma}-1}{2\sigma} \tag{5.40}$$

Equation (5.39) is the exact solution for $T_{\|}$ rendered in series form.

The difficulty in constructing an asymptotic series from the exact solution when it is in the form of (5.39) is that it is, in effect, a function of two variables–the order p of the Bessel functions and their argument σ. It is therefore necessary, when proceeding to the high σ limit, to have some means of eliminating the p-dependence; otherwise we would have to treat nonuniform asymptotic expansions [1]. This difficulty may be removed by first writing the exact solution in integral form using the integral formula for the product of two modified Bessel functions of the first kind given by Watson [594] (page 441, 13.72, eq. (2)),

$$I_\mu(z)I_\nu(z)=\frac{2}{\pi}\int_0^{\pi/2}I_{\mu+\nu}(2z\cos\theta)\cos\left[(\mu-\nu)\theta\right]\mathrm{d}\theta \tag{5.41}$$

Thus we have, applying this to the products in (5.39),

$$\begin{aligned}I_{p+1/2}(\sigma)I_p(\sigma)&=I_{p+1/2}(\sigma)I_{-p}(\sigma)\\&=\frac{2}{\pi}\int_0^{\pi/2}I_{1/2}(2\sigma\cos\theta)\cos\left[(2p+\frac{1}{2})\theta\right]\mathrm{d}\theta\end{aligned} \tag{5.42}$$

and

$$\begin{aligned}I_{p+1/2}(\sigma)I_{p+1}(\sigma)&=I_{p+1/2}(\sigma)I_{-1-p}(\sigma)\\&=\frac{2}{\pi}\int_0^{\pi/2}I_{-1/2}(2\sigma\cos\theta)\cos\left[(2p+\frac{3}{2})\theta\right]\mathrm{d}\theta\end{aligned} \tag{5.43}$$

where we have used the fact that

$$I_p(z)=I_{-p}(z) \tag{5.44}$$

for integer p. Thus, using (5.42) and (5.43), (5.39) becomes

$$\begin{aligned}\frac{T_{\|}}{\tau}=\frac{1}{1-\sigma+\sigma\left[I_{3/2}(\sigma)/I_{1/2}(\sigma)\right]}&\left[1+\sum_{p=1}^{\infty}\frac{(-1)^p}{2p+1}\frac{2}{\pi}\frac{1}{\left[I_0(\sigma)+I_1(\sigma)\right]I_{1/2}(\sigma)}\right.\\&\times\left(\int_0^{\pi/2}I_{1/2}(2\sigma\cos\theta)\cos\left[(2p+\frac{1}{2})\theta\right]\mathrm{d}\theta\right.\\&\left.\left.+\int_0^{\pi/2}I_{-1/2}(2\sigma\cos\theta)\cos\left[(2p+\frac{3}{2})\theta\right]\mathrm{d}\theta\right)\right]\end{aligned} \tag{5.45}$$

Only the cosine part of the integral in (5.45) is now p-dependent. This dependence may in turn be eliminated as follows. On reversing the order of summation and integration in that equation, we have

$$\sum_{p=1}^{\infty} \frac{(-1)^p}{2p+1} \cos\left[(2p+\frac{1}{2})\theta\right] = \mathrm{Re}\left(\mathrm{e}^{\mathrm{i}\theta/2} \sum_{\mathrm{p}=1}^{\infty} \frac{(\frac{1}{2})_{\mathrm{p}} (\mathrm{ie}^{\mathrm{i}\theta})^{2\mathrm{p}}}{\mathrm{p}+\frac{1}{2}}\right) \tag{5.46}$$

$$= \mathrm{Re}\left(\mathrm{e}^{\mathrm{i}\theta/2} \sum_{\mathrm{p}=1}^{\infty} \frac{(\frac{1}{2})_{\mathrm{p}} \mathrm{p}! \left[(\mathrm{ie}^{\mathrm{i}\theta})^2\right]^{\mathrm{p}}}{(\frac{3}{2})_{\mathrm{p}} \mathrm{p}!}\right) \tag{5.47}$$

Such a series may be expressed in terms of a Gauss hypergeometric function [1] as

$$\mathrm{Re}\left\{\mathrm{e}^{\mathrm{i}\theta/2}\left[{}_2\mathrm{F}_1(1, \frac{1}{2}; \frac{3}{2}; (\mathrm{ie}^{\mathrm{i}\theta})^2) - 1\right]\right\} \tag{5.48}$$

This in turn may be expressed in terms of the elementary functions, using (15.1.4) of [1], as

$$\mathrm{Re}\left\{\mathrm{e}^{\mathrm{i}\theta/2}\left[\frac{1}{2\mathrm{ie}^{\mathrm{i}\theta}} \ln\left(\frac{1+\mathrm{ie}^{\mathrm{i}\theta}}{1-\mathrm{ie}^{\mathrm{i}\theta}}\right) - 1\right]\right\} \tag{5.49}$$

Or, on simplification,

$$\left(\frac{1}{4}\pi - 1\right)\cos\frac{1}{2}\theta - \frac{1}{2}\sin\frac{1}{2}\theta \ln\tan\left(\frac{1}{4}\pi - \frac{1}{2}\theta\right) \tag{5.50}$$

which has a weak singularity at $\theta = 1/2\pi$. Likewise, for the second integrand in (5.45) we have

$$\sum_{p=1}^{\infty} \frac{(-1)^p}{2p+1} \cos\left[(2p+\frac{3}{2})\theta\right] = \frac{1}{4}\pi\cos\frac{1}{2}\theta - \cos\frac{3}{2}\theta + \frac{1}{2}\sin\frac{1}{2}\theta \ln\tan\left(\frac{1}{4}\pi - \frac{1}{2}\theta\right) \tag{5.51}$$

This also has a weak singularity at $\theta = 1/2\pi$. The foregoing steps are the crucial ones that allow us to remove the p-dependent summation in (5.45). The next step in the simplification of (5.45) is to recall that the Bessel functions of half-integer order, that is, the spherical Bessel functions, may always be expressed in terms of the elementary functions [594]. In particular,

$$I_{1/2}(z) = \sqrt{\frac{2}{\pi z}} \sinh z \tag{5.52}$$

$$I_{-1/2}(z) = \sqrt{\frac{2}{\pi z}} \cosh z \tag{5.53}$$

Thus, on using this definition in conjunction with (5.50) and (5.51) in (5.45), we have

$$\frac{T_{\parallel}}{\tau} = \left(\frac{e^{2\sigma}-1}{2\sigma}\right)\Bigg\{1 + \frac{\sqrt{2}}{\pi\,[I_0(\sigma)+I_1(\sigma)]\sin\sigma}\int_0^{\pi/2}\frac{d\theta}{\sqrt{\cos\theta}}$$
$$\times\left[\frac{1}{4}\pi e^{2\sigma\cos\theta}\cos\frac{1}{2}\theta + \frac{1}{2}e^{-2\sigma\cos\theta}\sin\frac{1}{2}\theta\ln\tan\left(\frac{1}{4}\pi-\frac{1}{2}\theta\right)\right.$$
$$\left.-\cos\frac{1}{2}\theta\sinh(2\sigma\cos\theta) - \cos\frac{3}{2}\theta\cosh(2\sigma\cos\theta)\right]\Bigg\} \tag{5.54}$$

This is the exact formula, (5.39), for the longitudinal correlation time rendered in integral form. The integrand of (5.54) has a weak singularity at $\theta = \pi/2$. This may be removed by integration by parts, having divided the range of integration into the intervals $0 < \theta < \pi/4$ and $\pi/4 < \theta < \pi/2$. The same procedure may be used to write the transverse correlation time in integral form. The transverse correlation time is (for the details see [128])

$$\frac{T_{\perp}}{\tau} = \frac{1-e^{-2\sigma}}{2\sigma}\left(1 + \sum_{p=1}^{\infty}\frac{(-1)^p}{2p+1}\frac{\left[I_p(\sigma)-I_{p+1}(\sigma)\right]I_{p+1/2}(\sigma)}{[I_0(\sigma)-I_1(\sigma)]\,I_{1/2}(\sigma)}\right) \tag{5.55}$$

On applying (5.41) to this equation we find that, on reversing the order of integration and summation as before, and proceeding as in (5.46) to (5.50)

$$\frac{T_{\perp}}{\tau} = \frac{1-e^{-2\sigma}}{2\sigma}\Bigg(1 + \frac{\sqrt{2}}{\pi}\frac{1}{[I_0(\sigma)-I_1(\sigma)]\sinh\sigma}\int_0^{\pi/2}\frac{d\theta}{\sqrt{\cos\theta}}$$
$$\times\Bigg\{\sinh(2\sigma\cos\theta)\left[\left(\frac{1}{4}\pi-1\right)\cos\frac{1}{2}\theta\right.$$
$$\left.-\frac{1}{2}\sin\frac{1}{2}\theta\ln\tan\left(\frac{1}{4}\pi-\frac{1}{2}\theta\right)\right] - \cosh(2\sigma\cos\theta)\left[\frac{1}{4}\pi\cos\frac{1}{2}\theta\right.$$
$$\left.\left.-\cos\frac{3}{2}\theta + \frac{1}{2}\sin\frac{1}{2}\theta\ln\tan\left(\frac{1}{4}\pi-\frac{1}{2}\theta\right)\right]\Bigg\}\Bigg) \tag{5.56}$$

This is the exact formula (5.55) for the transverse correlation time rendered in integral form. It also has a removable weak singularity at $\theta = \pi/2$. The method of steepest descents [343],[401] may now be used to find the asymptotic value of (5.54) and (5.56), as we shall describe. In order to derive an asymptotic formula for $T_{\parallel}$ in the high σ approximation, we recall that (5.54) is computable as a simple finite quadrature, provided we take out the removable weak singularity arising from the

$$\ln\tan\left(\frac{1}{4}\pi-\frac{1}{2}\theta\right) \tag{5.57}$$

term. The method of steepest descents [343], [401] may then be applied. In order to accomplish this we first note that, for large σ [568],

$$I_p(\sigma) \simeq \frac{\mathrm{e}^{\sigma}}{\sqrt{2\pi\sigma}} \sum_{k=0}^{\infty} \frac{(-1)^k}{(2\sigma)^k} \frac{\Gamma(p+k+1/2)}{k!\Gamma(p-k+1/2)} + \frac{\mathrm{e}^{-\sigma \pm [((p+1/2))\mathrm{i}\pi]}}{\sqrt{2\pi\sigma}} \sum_{k=0}^{\infty} \frac{(-1)^k}{(2\sigma)^k} \frac{\Gamma(p+k+1/2)}{k!\Gamma(p-k+1/2)} \tag{5.58}$$

For large σ, only the first term is of significance. On noting that

$$I_p(\sigma) \simeq \frac{\mathrm{e}^{\sigma}}{\sqrt{2\pi\sigma}} \left(1 - \frac{4p^2-1}{(8\sigma)} + \frac{(4p^2-1)(4p^2-9)}{2!(8\sigma)^2} - \frac{(4p^2-1)(4p^2-9)(4p^2-25)}{3!(8\sigma)^3} + \cdots\right) \tag{5.59}$$

we have

$$I_0(\sigma) \simeq \frac{\mathrm{e}^{\sigma}}{\sqrt{2\pi\sigma}} \left(1 + \frac{1}{8\sigma} + \cdots\right) \tag{5.60}$$

and

$$I_1(\sigma) \simeq \frac{\mathrm{e}^{\sigma}}{\sqrt{2\pi\sigma}} \left(1 - \frac{3}{8\sigma} - \cdots\right) \tag{5.61}$$

On utilising the asymptotic formulae (5.60) and (5.61) in (5.54) and discarding the terms prefixed by $\exp[-2\sigma\cos\theta]$, we have

$$\frac{T_{\|}}{\tau} \simeq \frac{\mathrm{e}^{2\sigma}}{2\sigma} \left(1 + \frac{\sqrt{2}\int_0^{\pi/2} G(\theta)\mathrm{e}^{2\sigma\cos\theta}\mathrm{d}\theta}{\frac{1}{2}\pi\mathrm{e}^{\sigma(\mathrm{e}^{\sigma}/2\pi\sigma)}(2+1/8\sigma-3/8\sigma)}\right), \qquad \sigma \gtrsim 1 \tag{5.62}$$

where

$$G(\theta) = \frac{\frac{1}{4}\pi\cos\frac{1}{2}\theta - \frac{1}{2}\cos\frac{1}{2}\theta - \frac{1}{2}\cos\frac{3}{2}\theta}{\sqrt{cos\theta}} \tag{5.63}$$

Consider

$$\int_0^{\pi/2} \mathrm{e}^{F(\theta)} G(\theta) \equiv \mathcal{J} \tag{5.64}$$

where

$$F(\theta) = 2\sigma\cos\theta \tag{5.65}$$

This integral has a saddle point at $\theta = 0$, which is an endpoint in the domain of integration as in [539]. We now apply the method of steepest descents [343] so that

$$\mathcal{J} = \int_0^{\pi/2} \mathrm{d}\theta \left[G(0) + \theta G'(0) + \frac{1}{2}\theta^2 G''(0) + \cdots\right] \times \exp\left[F(0) + \theta F'(0) + \frac{1}{2}\theta^2 F''(0) + \frac{1}{6}\theta^3 F'''(0) + \frac{1}{24}\theta^4 F^{\mathrm{IV}}(0) + \cdots\right] \tag{5.66}$$

where

$$F(0) = 2\sigma\,, \quad F'(0) = 0\,, \quad F''(0) = -2\sigma\,, \quad F'''(0) = 0\,, \quad F^{\mathrm{IV}}(0) = 2\sigma \tag{5.67}$$

$$G(0) = \frac{1}{4}\pi - 1\,, \quad G'(0) = 0\,, \quad G''(0) = \frac{1}{16}\pi + \frac{3}{4} \tag{5.68}$$

Thus in accordance with the method of steepest descents,

$$\mathcal{J} \simeq \frac{\mathrm{e}^{2\sigma\left[\frac{1}{4}\pi - 1\right]}\sqrt{\pi}}{2\sqrt{\sigma}}\left(1 + \frac{1}{16\sigma} + \frac{(\frac{1}{16}\pi + \frac{3}{4})}{4\sigma(\frac{1}{4}\pi - 1)}\right) \tag{5.69}$$

so that (5.62) becomes

$$\frac{T_{\|}}{\tau} \simeq \frac{\mathrm{e}^{2\sigma}}{2\sigma}\left[1 + (\frac{1}{4}\pi - 1)\left(1 + \frac{1}{16\sigma} + \frac{(\frac{1}{16}\pi + \frac{3}{4})}{4\sigma(\frac{1}{4}\pi - 1)}\right)\left(1 + \frac{1}{8\sigma}\right)\right] \tag{5.70}$$

$$= \left(\frac{\pi}{8\sigma}\mathrm{e}^{2\sigma}\right)\left(1 + \frac{1}{4\sigma}\right) \tag{5.71}$$

The leading term in (5.71) may be written, as in [128], by substituting the high σ limit of the modified Bessel functions directly into the series representation of the exact solution, (5.39), and then summing the resulting series using the properties of the Riemann-Zeta function [1]. However, such a method is open to criticism since the next-to-leading term $1/4\sigma$ in (5.71) may not be obtained by such a method. *To be precise, the coefficient of the* $1/\sigma$ *term is found to include a divergent series, namely,*

$$\sum_{p=1}^{\infty}(-1)^p(2p+1) \tag{5.72}$$

Higher-order terms are even more divergent. The reason is that in trying to use (5.39) one is faced with two competing limits, $p \to +\infty$ *and* $\sigma \to +\infty$ *associated with which there is a lack of uniform convergence*. This is why summing over the infinite series in p so as to obtain (5.54), which is a *finite* integral representation of the exact solution, is so important. It avoids the problem of the competing infinite limits and permits precise evaluation of higher-order asymptotic correction terms via the method of steepest descents. The inclusion of such terms is important because it is obvious that (5.71) provides a closer approximation to the exact solution for large σ than the leading term

$$\frac{T_{\|}}{\tau} = \left(\frac{\pi}{8\sigma}\mathrm{e}^{2\sigma}\right) \tag{5.73}$$

on its own, as shown in Figure 5.1. In Figure 5.1, the bold line is (5.39), the small dashing step is (5.71), and the large dashing is (5.73). To obtain convergence for values up to $\sigma = 60$, the first 20 terms of the infinite sum in (5.39) were used. It is apparent from Figure 5.1 that (5.71) provides a very close approximation to the exact solution for $\sigma \geq 1.5$ $(U \geq 3kT)$. This is particularly important in the case of magnetic relaxation [91]. We remark that (5.71) is similar in form to an equation originally derived by Visscher [591], his (14), which calculated the rate of escape of a Brownian particle from a one-dimensional potential well using an improved version

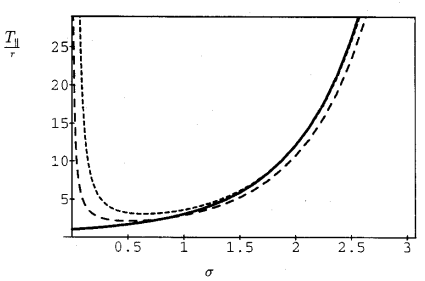

Fig. 5.1. Plot of $T_\parallel$ as a function of σ

of the barrier crossing theory of Kramers [318]. In applying Visscher's method to the present problem, the modifications for a periodic potential to the escape rate from a single-well potential, described in [498] and [151], must be incorporated in his result. The transverse relaxation time (5.56) may be treated in a similar manner. For large σ,

$$\frac{T_\perp}{\tau} = \frac{1}{2\sigma}\Bigg[1 + \frac{2}{\pi}\frac{1}{(\mathrm{e}^\sigma/\sqrt{\pi\sigma}\,[(1+1/8\sigma)-(1-3/8\sigma)]\sinh\sigma}\int_0^{\pi/2}\frac{\mathrm{d}\theta}{\sqrt{\cos\theta}} \times\Bigg\{\sinh(2\sigma\cos\theta)\left[(\frac{1}{4}\pi-1)\cos\frac{1}{2}\theta-\frac{1}{2}\sin\frac{1}{2}\theta\ln\tan(\frac{1}{4}\pi-\frac{1}{2}\theta)\right] -\cosh((2\sigma\cos\theta)\left[\frac{1}{4}\pi\cos\frac{1}{2}\theta-\cos\frac{3}{2}\theta+\frac{1}{2}\sin\frac{1}{2}\theta\ln\tan(\frac{1}{4}\pi-\frac{1}{2}\theta)\right]\Bigg\}\Bigg] \tag{5.74}$$

so that

$$\frac{T_\perp}{\tau} \simeq \frac{1}{2\sigma}\Bigg(1+\frac{2}{\sqrt{\pi}}\frac{1}{(\mathrm{e}^{2\sigma}/\sqrt{\sigma})(1/2\sigma)}\int_0^{\pi/2}\frac{\mathrm{e}^{2\sigma\cos\theta}}{\sqrt{\cos\theta}} \times\left[-\cos\frac{1}{2}\theta+\cos\frac{3}{2}\theta-\sin\frac{1}{2}\theta\ln\tan\left(\frac{1}{4}\pi-\frac{1}{2}\theta\right)\right]\mathrm{d}\theta\Bigg) \tag{5.75}$$

In order to apply the method of steepest descents we again write

$$\mathcal{J} \equiv \int_0^{\pi/2}\mathrm{e}^{F(\theta)}H(\theta)\mathrm{d}\theta \tag{5.76}$$

where

$$F(\theta) = 2\sigma\cos\theta \tag{5.77}$$

as before. This time

$$H(\theta) = \frac{\cos\frac{3}{2}\theta - \cos\frac{1}{2}\theta - \sin\frac{1}{2}\theta \ln\tan(\frac{1}{4}\pi - \frac{1}{2}\theta)}{\sqrt{\cos\theta}} \tag{5.78}$$

and so

$$\mathcal{J} = \mathrm{e}^{F(0)}\left[\frac{H''(0)}{2}\int_0^{\pi/2} \mathrm{d}\theta\, \theta^2 \mathrm{e}^{-\sigma\theta^2}\right] \tag{5.79}$$

In accordance with the method of steepest descents,

$$\mathcal{J} = \frac{\mathrm{e}^{2\sigma}(-\frac{1}{2})\sqrt{\pi}}{4\sigma^{3/2}} \tag{5.80}$$

equation (5.75) becomes

$$\frac{T_{\parallel}}{\tau} = \frac{1}{4\sigma} \tag{5.81}$$

Thus, the transverse relaxation does not proceed by means of a barrier crossing process.

We remark that in order to obtain (5.81) it is necessary to proceed from the integral representation of the exact solution. If one attempts the naive procedure of simply substituting the leading term in the asymptotic values of the $I_p(\sigma)$ and $I_{p+1/2}(\sigma)$ in the series representation of the exact solution (5.55) one is led to an *alternating* series for $T_{\perp}$. This is once again a direct consequence of the lack of uniform convergence that results if one adopts such a limiting procedure. We also remark that (5.81) may be obtained in a very simple manner using the effective eigenvalue technique described in [530] and [129]. This procedure is carried out in [128].

If the method of steepest descents is carried a stage further, to include terms of order $1/\sigma^2$, and further terms are included in the expansion of $I_0(\sigma)$ and $I_1(\sigma)$, (5.81) becomes

$$\frac{T_{\parallel}}{\tau} = \frac{1}{4\sigma}\left(1 + \frac{1}{2\sigma}\right) \tag{5.82}$$

In order to obtain (5.82) we proceed as follows. We first note that in (5.56) we must retain the third term in the asymptotic expansion of $I_0(\sigma) - I_1(\sigma)$ so that

$$I_0(\sigma) - I_1(\sigma) \simeq \mathrm{e}^{\sigma}/\sqrt{2\pi\sigma}\left[\left(1 + \frac{1}{8\sigma} + \frac{9}{128\sigma^2}\right) - \left(1 - \frac{3}{8\sigma} - \frac{15}{128\sigma^2}\right)\right] \tag{5.83}$$

which simplifies to

$$\left(\mathrm{e}^{\sigma}/\sqrt{2\pi\sigma}\right)\frac{1}{2\sigma}\left(1 + \frac{3}{8\sigma}\right) \tag{5.84}$$

Thus, (5.75) becomes

$$\frac{T_{\perp}}{\tau} \simeq \frac{1}{2\sigma}\left(1 + \frac{2}{\sqrt{\pi}}\frac{1}{(\mathrm{e}^{2\sigma}/\sqrt{\sigma})(1/2\sigma)(1 + 3/8\sigma)}\mathcal{J}\right) \tag{5.85}$$

In addition, we must proceed as far as terms in $H^{\mathrm{IV}}(0)$ in applying the method of steepest descents. Thus $\mathcal{J}$ becomes

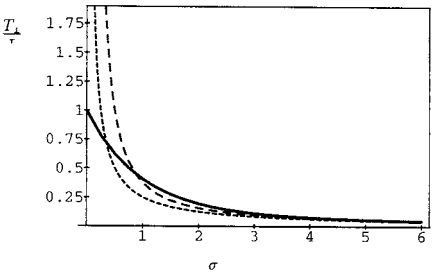

Fig. 5.2. Plot of $T_\perp$ as a function of σ. The *bold line* is the exact solution, (5.55), the *large dashed line* is the asymptotic formula (5.82), and the *small dashed line* is the asymptotic formula (5.81), which ignores terms $O(\sigma^{-2})$

$$\mathcal{J} = \int_0^{\pi/2} \mathrm{d}\theta \left[-\frac{1}{2}\theta^2 + \frac{1}{24} H^{\mathrm{IV}}(0)\theta^4 \right] \mathrm{e}^{2\sigma - \sigma\theta^2 2 + \sigma\theta^4/12} \tag{5.86}$$

$$\simeq \mathrm{e}^{2\sigma} \int_0^{\pi/2} \mathrm{d}\theta \left[-\frac{1}{2}\theta^2 + \frac{1}{24} H^{\mathrm{IV}}(0)\theta^4 \right] \mathrm{e}^{-2\sigma\theta^2} \left(1 + \frac{1}{12}\sigma\theta^4 \right) \tag{5.87}$$

Thus, by parametric differentiation,

$$\mathcal{J} = -\frac{1}{2} \left[\mathrm{e}^{2\sigma} \frac{\sqrt{\pi}}{4\sigma^{3/2}} \left(1 - \frac{1}{8\sigma} \right) \right] \tag{5.88}$$

We have

$$\frac{T_\perp}{\tau} = \frac{1}{4\sigma} \left(1 + \frac{1}{2\sigma} \right) \tag{5.89}$$

The values for $T_\perp$ yielded by this approximate formula and the exact formula (5.55) are compared in Figure 5.2. It is apparent that the asymptotic formula (5.82) provides an acceptable description of the transverse relaxation for $\sigma \geq 2$ that is $U \geq 4kT$. It is again apparent that the $1/2\sigma$ correction term provides a more accurate description of the asymptotic behaviour. We note that the correction $1/2\sigma$ is also yielded by the effective eigenvalue method. The effective relaxation time from this method [530], [129] is

$$\tau_{\mathrm{ef}}^{\perp} = \tau \frac{I_0(\sigma) - I_1(\sigma)}{I_0(\sigma) + I_1(\sigma)} \tag{5.90}$$

which, on insertion of the asymptotic expansions of the $I_p(\sigma)$, yields

$$\tau_{\mathrm{ef}}^{\perp} = \tau \frac{1}{4\sigma} \left(1 + \frac{1}{2\sigma} \right) \tag{5.91}$$

in agreement with (5.82). This simple procedure is very useful in the case of $T_\perp$ as it avoids the steepest-descent calculations. However, it is not useful for the calculation

of the longitudinal relaxation time as the effective eigenvalue method, by definition, cannot furnish an accurate description of the relaxation behaviour when an activation process is involved. The merit of (5.90) in the present context is that it provides a simple formula for $T_\perp$, which is valid for all σ-values; see Table 4 of [128].

The original problem considered by Brown [91] is rotation in three dimensions in the context of Néel relaxation of single-domain ferromagnetic particles. The appropriate Fokker–Planck equation is, where τ denotes the Néel relaxation time,

$$2\tau \sin\vartheta \frac{\partial W}{\partial t} = \frac{\partial}{\partial \vartheta}\left[\sin\vartheta\left(\frac{\partial}{\partial\vartheta} + \frac{v}{kT}\frac{\partial}{\partial\vartheta}W\right)\right] \tag{5.92}$$

where

$$\frac{vV}{kT} = \sigma \sin^2\vartheta - \xi\cos\vartheta \tag{5.93}$$

and this time the barrier height parameter $\sigma = Kv/kT$. $W(\vartheta, t)$ is the probability density of orientations of the magnetisation vector $\mathbf{M}$ on a sphere of radius M_s and the orientation of $\mathbf{M}$ is specified by the spherical polar coordinates ϑ and φ. v is the volume of the particle, M_s is the saturation magnetisation, K is the anisotropy constant, and $\xi = M_s vH/kT$. A similar model was discussed by Martin et al. [403] in the context of dielectric relaxation. We assume that the after-effect solution of (5.92) is of the form

$$W(\vartheta, t) = \sum_{n=0}^{\infty} a_n(t) P_n(\cos\vartheta)$$

$$\text{with} \quad \langle P_n(\cos\vartheta)\rangle = \frac{1}{2n+1}\frac{a_n(t)}{a_0} = f_n(t) \tag{5.94}$$

where P_n is the Legendre polynomial of order n, which on using the orthogonality properties of the P_n leads to (having switched off a steady magnetic field $\mathbf{H}$ at time $t = 0$)

$$\begin{aligned}\dot{f}_{2n+1}(t) = {} & \frac{(2n+1)(n+1)}{\tau}\left(\frac{2\sigma}{(4n+1)(4n+5)} - 1\right) f_{2n+1}(t) \\ & + \frac{4\sigma n(2n+1)(n+1)}{(4n+3)\tau(4n+1)} f_{2n-1}(t) \\ & - \frac{2\sigma(2n+1)(2n+3)(n+1)}{(4n+3)(4n+5)\tau} f_{2n+3}(t)\end{aligned} \tag{5.95}$$

with $f_0(t) = 1$ where the initial conditions are

$$f_{2n+1}(0) = \xi \frac{\int_{-1}^{+1} \mathrm{e}^{\sigma x^2} x P_{2n+1}(x)\,\mathrm{d}x}{\int_{-1}^{+1} \mathrm{e}^{\sigma x^2}\,\mathrm{d}x} \tag{5.96}$$

Thus

$$\begin{aligned}\tilde{f}_1(s) = {} & \frac{\tau}{\tau s + 1 - \frac{2}{5}\sigma + \frac{2}{5}\sigma\tilde{S}_3(s)} \\ & \times\left(f_1(0) + \frac{4}{3}\sum_{n=1}^{\infty}(-1)^n \frac{f_{2n+1}(0)}{f_1(0)} \frac{(n+\frac{3}{4})(\frac{1}{2})_n}{\Gamma(n+2)} \prod_{k=1}^{n} \tilde{S}_{2k+1}(s)\right)\end{aligned}$$

where

$$\left(\frac{1}{2}\right)_n = \frac{\Gamma(n+\frac{1}{2})}{\Gamma(\frac{1}{2})} \tag{5.97}$$

and the continued fraction

$$\tilde{S}_n(s) = \frac{\frac{2\sigma(n-1)}{4n^2-1}}{1+\frac{2\tau s}{n(n+1)}-\frac{2\sigma}{(2n-1)(2n+3)}+\frac{2\sigma(n+2)}{(2n+1)(2n+3)}\tilde{S}_{n+2}(s)} \tag{5.98}$$

Γ denotes the gamma function and the initial conditions satisfy on expanding x^{2r+1} as a series of the $P_{2n+1}(x)$,

$$f_{2n+1}(0) = \frac{\xi\sigma^n\Gamma(n+\frac{3}{2})M(n+\frac{3}{2},2n+\frac{5}{2},\sigma)}{2\Gamma(2n+\frac{5}{2})M(\frac{1}{2},\frac{3}{2},\sigma)} \tag{5.99}$$

where $M(a,b,z)$ is Kummer's function (the confluent hypergeometric function) [1]. The exact formula (5.97) allows one to calculate the longitudinal susceptibility since [531] ($s = \mathrm{i}\omega$)

$$\frac{\chi_\parallel(\omega)}{\chi'_\parallel(0)} = 1 - \mathrm{i}\omega\int_0^\infty \mathrm{e}^{-\mathrm{i}\omega t}C_1(t)\mathrm{d}t = 1 - \mathrm{i}\omega\frac{\tilde{f}_1(\mathrm{i}\omega)}{f_1(0)} \tag{5.100}$$

Thus

$$\begin{aligned}\frac{\chi_\parallel(\omega)}{\chi'_\parallel(0)} = {} & \frac{1}{\mathrm{i}\omega\tau+1-\frac{2}{5}\sigma+\frac{2}{5}\sigma\tilde{S}_3(\mathrm{i}\omega)} \\ & \left(1-\frac{2}{5}\sigma+\frac{2}{5}\sigma\tilde{S}_3(\mathrm{i}\omega)-\mathrm{i}\omega\tau\right. \\ & \left.\times\frac{4}{3}\sum_{n=1}^{\infty}(-1)^n\frac{f_{2n+1}(0)}{f_1(0)}\frac{(n+\frac{3}{4})(\frac{1}{2})_n}{\Gamma(n+2)}\prod_{k=1}^{n}\tilde{S}_{2k+1}(\mathrm{i}\omega)\right)\end{aligned} \tag{5.101}$$

Equation (5.97) with $s = 0$ yields

$$\begin{aligned}T_\parallel = {} & \frac{\tilde{f}_1(0)}{f_1(0)} \\ = {} & \frac{\tau}{1-\frac{2}{5}\sigma+\frac{2}{5}\sigma\tilde{S}_3(0)}\left(1+\frac{4}{3}\sum_{n=1}^{\infty}(-1)^n\frac{f_{2n+1}(0)}{f_1(0)}\right. \\ & \left.\times\frac{(n+\frac{3}{4})(\frac{1}{2})_n}{\Gamma(n+2)}\prod_{k=1}^{n}\tilde{S}_{2k+1}(0)\right)\end{aligned} \tag{5.102}$$

Equation (5.102) is an exact analytical formula that allows $T_\parallel$ to be calculated to any desired degree of accuracy by computing successive convergents of the continued fraction $\tilde{S}_{2k+1}(0)$. The $\tilde{S}_{2k+1}(0)$ are in terms of Kummer's functions

$$\tilde{S}_{2k+1}(0) = \frac{4k\sigma}{(4k+1)(4k+3)} \frac{M(k+1, 2k+\frac{5}{2}, \sigma)}{M(k, 2k+\frac{1}{2}, \sigma)} \tag{5.103}$$

so that (5.102) with (5.103) becomes (for a detailed treatment see [130])

$$\frac{T_{\|}}{\tau} = M(1, \frac{5}{2}, \sigma) + \frac{\frac{3}{2}}{M(\frac{3}{2}, \frac{5}{2}, \sigma)} \sum_{n=1}^{\infty} \frac{(-\sigma^2)^n (n+\frac{3}{4})\Gamma(n+\frac{3}{2})\Gamma(n+\frac{1}{2})}{(n+1)\left[\Gamma(2n+\frac{5}{2})\right]^2}$$
$$\times M(n+\frac{3}{2}, 2n+\frac{5}{2}, \sigma) M(n+1, 2n+\frac{5}{2}, \sigma) \tag{5.104}$$

where we note that $M(1, 5/2, \sigma)$ has a representation in terms of the error function as [499]

$$\frac{3}{2\sigma}\left(\frac{1}{2}\sqrt{\frac{\pi}{\sigma}} e^{\sigma} erf(\sqrt{\sigma}) - 1\right) \tag{5.105}$$

Equation (5.102) is the exact solution in terms of known functions for the longitudinal relaxation time for the $Kv \sin^2 \vartheta$ potential. In order to write our series solution for $T_{\|}/\tau$ (5.104) in integral form we note the formula from Bateman [33] (vol 1: 6.15.3, eq. (18)),

$$M(a,b,z)M(a,b,-z) = \frac{[\Gamma(b)]^2 z^{1-b}}{\Gamma(a)\Gamma(b-a)} \int_{-\infty}^{\infty} \mathrm{sech\,t}\ \mathrm{I}_{b-1}(z\,\mathrm{sech\,t}) e^{(b-2a)t} dt$$
$$\mathrm{Re}\{a\} > 0\,, \qquad \mathrm{Re}\{b-a\} > 0 \tag{5.106}$$

where I_{b-1} is the modified Bessel function of the first kind of order $b-1$. Thus the product of two Kummer functions may be expressed as an integral. In order to apply the formula to (5.104) we note the Kummer transformation (eq. (13.1.27) of [1]])

$$M(a,b,z) = e^z M(b-a, b, -z) \tag{5.107}$$

so that (5.104), taking

$$a = n + \frac{3}{2}\,,\ b = 2n + \frac{5}{2} \tag{5.108}$$

becomes

$$M(n+\frac{3}{2}, 2n+\frac{5}{2}, \sigma) M(n+1, 2n+\frac{5}{2}, \sigma)$$
$$= e^{\sigma} M(n+\frac{3}{2}, 2n+\frac{5}{2}, \sigma) M(n+\frac{3}{2}, 2n+\frac{5}{2}, -\sigma) \tag{5.109}$$

so casting (5.104) into a form suitable for conversion to an integral. Thus that equation becomes

$$\frac{T_{\|}}{\tau} = M(1,\frac{5}{2},\sigma) + \frac{3/2}{M(\frac{3}{2},\frac{5}{2},\sigma)}\sum_{n=1}^{\infty}\frac{(-\sigma^2)^n(n+\frac{3}{4})\Gamma(n+\frac{3}{2})\Gamma(n+\frac{1}{2})}{(n+1)[\Gamma(2n+\frac{5}{2})]^2}$$
$$\times\frac{e^{\sigma}\sigma^{-3/2-2n}[\Gamma(2n+\frac{5}{2})]^2}{\Gamma(n+1)\Gamma(n+\frac{3}{2})}\int_{-\infty}^{\infty} e^{-t/2}\operatorname{sech} t\, I_{2n+3/2}(\sigma\operatorname{sech} t)dt$$
$$= M(1,\frac{5}{2},\sigma) + \frac{3/2}{M(\frac{3}{2},\frac{5}{2},\sigma)}e^{\sigma}\sigma^{-3/2}\sum_{n=1}^{\infty}\frac{(-1)^n(n+\frac{3}{4})\Gamma(n+\frac{1}{2})}{\Gamma(n+2)}.2$$
$$\times\int_0^{\infty} I_{2n+3/2}(\sigma\operatorname{sech} t)\frac{\cosh(\frac{1}{2}t)}{\cosh t}dt \tag{5.110}$$

which, using the change of variable

$$\operatorname{sech} t = \sin\theta \tag{5.111}$$

so that

$$\operatorname{sech}^2\left(\frac{1}{2}t\right) = \frac{2\sin\theta}{1+\sin\theta} \tag{5.112}$$

and choosing the positive square root reduces to

$$\frac{T_{\|}}{\tau} = M\left(1,\frac{5}{2},\sigma\right) + \frac{3}{M(\frac{3}{2},\frac{5}{2},\sigma)}e^{\sigma}\sigma^{-3/2}\sum_{n=1}^{\infty}\frac{(-1)^n(n+\frac{3}{4})\Gamma(n+\frac{1}{2})}{\Gamma(n+2)}$$
$$\times\int_0^{\pi/2} d\theta\, I_{2n+3/2}(\sigma\sin\theta)\sqrt{\frac{1+\sin\theta}{2\sin\theta}}$$
$$= M(1,\frac{5}{2},\sigma) + \frac{3e^{\sigma}\sigma^{-3/2}}{M(\frac{3}{2},\frac{5}{2},\sigma)}\int_0^{\pi/2} d\theta\,\sqrt{\frac{1+\sin\theta}{2\sin\theta}}F(\theta) \tag{5.113}$$

where

$$F(\theta) = \sum_{n=1}^{\infty}\frac{(-1)^n(n+\frac{3}{4})\Gamma(n+\frac{1}{2})}{\Gamma(n+2)}I_{2n+3/2}(\sigma\sin\theta) \tag{5.114}$$

It may be shown [130] that the series (5.114) may be expressed in the integral form

$$F(\theta) = -\frac{1}{2}\frac{\Gamma(\frac{3}{2})}{\Gamma(2)\sqrt{\sigma\sin\theta}}\int_0^{\sigma\sin\theta} t^{1/2}I_{5/2}(t)\,dt \tag{5.115}$$

Thus

$$\frac{T_{\|}}{\tau} = M(1,\frac{5}{2},\sigma) - \frac{3e^{\sigma}\sigma^{-3/2}\sqrt{\pi}}{4M(\frac{3}{2},\frac{5}{2},\sigma)\sqrt{2\sigma}}\int_0^{\pi/2} d\theta\,\frac{\sqrt{1+\sin\theta}}{\sin\theta}\int_0^{\sigma\sin\theta} t^{1/2}I_{5/2}(t)\,dt \tag{5.116}$$

so removing the order dependence n from (5.104). Equation (5.116) may be further simplified by noting the representation of the $I_{5/2}(t)$ in terms of the elementary functions so that

$$\int_0^x t^{1/2} I_{5/2}(t)\,\mathrm{d}t = \sqrt{2/\pi}\left(\cosh x - 3\frac{\sinh x}{x} + 2\right) \tag{5.117}$$

Thus (5.116) may be rendered by the single integral

$$\begin{aligned}\frac{T_\parallel}{\tau} =& M(1,\frac{5}{2},\sigma) - \frac{3\mathrm{e}^{\sigma}\sigma^{-2}}{4M(\frac{3}{2},\frac{5}{2},\sigma)} \\ &\times \int_0^{\pi/2} \mathrm{d}\theta\,\frac{\sqrt{1+\sin\theta}}{\sin\theta}\left(\cosh(\sigma\sin\theta) - \frac{3\sinh(\sigma\sin\theta)}{\sigma\sin\theta} + 2\right)\end{aligned} \tag{5.118}$$

which for the purpose of applying the method of steepest descents may be expressed as

$$\begin{aligned}\frac{T_\parallel}{\tau} =& M(1,\frac{5}{2},\sigma) - \frac{3\mathrm{e}^{\sigma}\sigma^{-2}}{4M(\frac{3}{2},\frac{5}{2},\sigma)}\int_0^{\pi/2}\mathrm{d}\theta\frac{\sqrt{1+\sin\theta}}{\sin\theta} \\ &\times\left[\frac{1}{2}(\mathrm{e}^{\sigma\sin\theta}+\mathrm{e}^{-\sigma\sin\theta}) - \frac{3}{2}\left(\frac{\mathrm{e}^{\sigma\sin\theta}-\mathrm{e}^{-\sigma\sin\theta}}{\sigma\sin\theta}\right)+2\right]\end{aligned} \tag{5.119}$$

which is the exact solution in integral form. In order to apply the method of steepest descents to obtain the asymptotic expansion of the exact solution we note that the exact solution (5.119) has no singularity at $\theta = 0$ and has a saddle point at $\theta = 1/2\pi$. Since the saddle point is at $\theta = 1/2\pi$ it will be convenient to replace θ by $1/2\pi - \theta$ in (5.119) so that $\theta = 0$ is now the saddle. Thus

$$\begin{aligned}\frac{T_\parallel}{\tau} =& M(1,\frac{5}{2},\sigma) - \frac{3\mathrm{e}^{\sigma}\sigma^{-2}}{4M(\frac{3}{2},\frac{5}{2},\sigma)}\int_0^{\pi/2}\mathrm{d}\theta\frac{\sqrt{1+\cos\theta}}{\cos\theta} \\ &\times\left[\frac{1}{2}(\mathrm{e}^{\sigma\cos\theta}+\mathrm{e}^{-\sigma\cos\theta}) - \frac{3}{2}\left(\frac{\mathrm{e}^{\sigma\cos\theta}-\mathrm{e}^{-\sigma\cos\theta}}{\sigma\cos\theta}\right)+2\right]\end{aligned} \tag{5.120}$$

Let us now write

$$\int_0^{\pi/2} \mathrm{e}^{\sigma\cos\theta} G(\theta)\mathrm{d}\theta \equiv \mathcal{J} \tag{5.121}$$

where

$$G(\theta) = \frac{\sqrt{1+\cos\theta}}{2\cos\theta}\left(1 - \frac{3}{\sigma\cos\theta}\right) \tag{5.122}$$

This, in accordance with the method of steepest descents, is

$$\begin{aligned}&\int_0^{\pi/2}\mathrm{d}\theta\left[G(0)+\theta G'(0)+\frac{1}{2}\theta^2 G''(0)+\cdots\right] \\ &\quad\times\exp\left[F(0)+\theta F'(0)+\frac{1}{2}\theta^2F''(0)+\frac{1}{6}\theta^3F'''(0)+\frac{1}{24}\theta^4F^{IV}(0)+\cdots\right]\end{aligned} \tag{5.123}$$

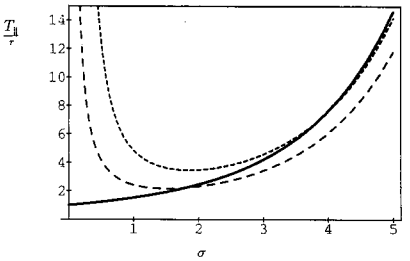

Fig. 5.3. Plot of $T_\parallel$ as a function of σ

Thus, proceeding exactly as in the two-dimensional case, on noting the asymptotic form of $M(a, b, z)$ as $|z| \leftarrow \infty$, namely [1]

$$M(a,b,z) = \frac{\Gamma(b)}{\Gamma(a)} e^z z^{a-b} \left[1 + O(|z|^{-1})\right] , \qquad \mathrm{Re}(z) > 0 \tag{5.124}$$

we have with (5.120)

$$\frac{T_\parallel}{\tau} \simeq \frac{1}{2} \sqrt{\pi} e^\sigma \sigma^{-3/2} \left(1 + \frac{1}{\sigma}\right) \tag{5.125}$$

in agreement with Storonkin [572], [571] when his result is truncated at the term of order $1/\sigma$ in the parentheses. Equation (5.125) is compared with the exact solution and Brown's asymptotic formula

$$\frac{T_\parallel}{\tau} \simeq \frac{1}{2} \sqrt{\pi} e^\sigma \sigma^{-3/2} \tag{5.126}$$

In Figure 5.3, the bold line is (5.104), the large dashing is (5.126), and the small dashing is (5.125). It is apparent that (5.125) reproduces the asymptote far more accurately than Brown's asymptotic formula for $\sigma \geq 2.5$. Brown's formula gives a closer approximation to the exact solution for σ in the range 1.5–2.5. If the $1/\sigma^2$ term is included in the asymptotic expansion, using the method of steepest descents one finds, after a tedious calculation, that

$$\frac{T_\parallel}{\tau} \simeq \frac{1}{2} \sqrt{\pi} e^\sigma \sigma^{-3/2} \left(1 + \frac{1}{\sigma} + \frac{7}{4\sigma^2}\right) \tag{5.127}$$

Equation (5.127) provides an even closer approximation to the asymptotic behaviour for large σ. Its first term agrees with Brown [91], Aharoni [6], and Scully et al. [539]. The other terms require summation over p and the method of steepest descent to fourth order in the slow part and to sixth order in the fast part.

We have shown how Watson's integral formula for the product of two Bessel functions may be used to render the exact solutions for the correlation times $T_\parallel$ and $T_\perp$ for the two-dimensional rotator in integral form. This facilitates the use of the method of steepest descents in order to obtain semiclassical asymptotic formulae for $T_\parallel$ and $T_\perp$ in the high σ approximation. The asymptotic results for $T_\parallel$ are in

agreement with those obtained by the method proposed by Visscher [591] when due account is taken of the periodic nature of the potential. In the case of $T_\perp$, the effective eigenvalue method yields asymptotic behaviour that is identical to that yielded by the exact solution cf (5.82) and (5.89). Similar considerations hold for $T_\parallel$ for rotation in three dimensions, the only essential difference being that Watson's integral formula for the product of two modified Bessel functions is replaced by the formula for the product of two Kummer functions given by Bateman [33] (vol: 6.15.3), which amounts to a generalisation of Watson's integral formula (5.41). We remark that if an electric field is applied to a nematic liquid crystal in the transverse direction then one may also write the exact solution $T_\perp$ for the extended Debye theory of dielectric relaxation in a form similar to (5.102) [132]. This is trickier than it seems. The principal reason for this is the loss of axial symmetry arising from the transverse application of the field. Fortunately, the effective eigenvalue also provides an accurate description in this instance showing the characteristic $1/\sigma$ dependence of $T_\perp$ for large σ. The difficulty mentioned earlier does not arise for rotation in two dimensions as the underlying continued fraction $\tilde{S}_p(s)$ is the same for both orientations of the applied field.

We remark that we have been able to obtain exact solutions of the problems described by virtue of the fact that the Laplace transform of the solution of the differential-difference equations underlying the Smoluchowski equation takes the form of a three-term recurrence relation. This in turn allows one to convert the series form of the solution to an integral using what are essentially properties of hypergeometric functions.

We further remark that a number of investigators have obtained approximate integral solutions for correlation times using adaptations of the mean first passage time method [485], [439]. The procedure is discussed in some detail by Hänggi et al. [318] and by Risken [507], who describes how the technique may be used to calculate an approximate expression for the inverse of the lowest eigenvalue for a metastable potential.

We believe that an attractive feature of the present method is its ability to demonstrate clearly the connection between the continued fraction and integral forms of the exact solution. The integral form has the merit that it allows one to rigorously derive asymptotic expansions from the exact solution in the high barrier limit with no approximations other than those inherent in the method of steepest descents.

These considerations are of particular importance in view of the comments of Klik and Gunther [358] concerning the $T^{-1/2}$ behaviour of the relaxation rate prefactor $\sigma^{3/2}\tau^{-1}$ in Brown's equation (5.126). They argue that this behaviour arises from the lack of a saddle point in the Hamiltonian for the $K\nu\sin^2\vartheta$ potential. This argument is refuted by Bessais et al. [75] in heuristic fashion. They conjecture that the $T^{-1/2}$ behaviour arises from the asymptotic behaviour of the solution of (5.104). Our analysis reinforces this argument, as it clearly demonstrates that the $T^{-1/2}$ behaviour arises from the asymptotic behaviour of the hypergeometric function $M(1, 5/2, \sigma)$, which is the dominant term in the exact solution for large σ.

5.2 The Fokker–Planck and Langevin Equations

The Fokker–Planck equation [126] is an equation for the evolution of the distribution function (which is defined on the phase space for the problem) of fluctuating macroscopic variables [286]. It is essentially a specialised form of the Boltzmann integral equation [592], [512] with the *stosszahlansatz* of Brownian motion. The diffusion equation [142](1.4.11) for the distribution function of an assembly of free Brownian particles is a simple example of such an equation. The main use of the Fokker–Planck equation is as an approximate description for any Markov process $\xi(t)$ in whick the individual jumps are small [590]. We shall derive the Fokker–Planck equation following the exposition of Coffey et al. [126], [142].

Consider a stochastic process $\xi(t)$ in which we take a set of instants $t_1 < t_2 < t_3$ where for the present we assume that y_1 and t_1 are fixed. We define the conditional probability $P_2(y_2, t_2|y_1, t_1)\mathrm{d}y_2$ as the probability that $\xi(t_2)$ lies in the interval $(y_2, y_2 + \mathrm{d}y_2)$ given that $\xi(t_1)$ had a value y_1 at time t_1 and $P_3(y_3, t_3|y_2, t_2; y_1, t_1)\mathrm{d}y_3$ the probability that $\xi(t_3)$ lies in the interval $(y_3, y_3 + \mathrm{d}y_3)$ given that $\xi(t_2)$ had a value y_2 at time t_2 and $\xi(t_1)$ had a value y_1 at time t_1. If we multiply P_2 by P_3 and integrate with respect to y_2, the resulting probability density function will only depend on y_1 and t_1, i.e.,

$$P_3(y_3, t_3|y_1, t_1)\mathrm{d}y_3 = \int_{-\infty}^{\infty} P_2(y_2, t_2|y_1, t_1)P_3(y_3, t_3|y_2, t_2; y_1, t_1)\,\mathrm{d}y_2\,\mathrm{d}y_3 \tag{5.128}$$

or

$$P_3(y_3, t_3|y_1, t_1) = \int_{-\infty}^{\infty} P_2(y_2, t_2|y_1, t_1)P_3(y_3, t_3|y_2, t_2; y_1, t_1)\,\mathrm{d}y_2 \tag{5.129}$$

which is called the *Chapman-Kolmogorov equation*. If we restrict ourselves to a *Markov process*, we will then have

$$P_3(y_3, t_3|y_2, t_2; y_1, t_1) = P_2(y_3, t_3|y_2, t_2) \tag{5.130}$$

or

$$P_2(y_3, t_3|y_1, t_1) = \int_{-\infty}^{\infty} P_2(y_2, t_2|y_1, t_1)P_2(y_3, t_3|y_2, t_2)\mathrm{d}y_2 \tag{5.131}$$

which is the Chapman-Kolmogorov equation for a Markov process also known as the *Smoluchowski integral equation*, essentially due to Einstein [240]. In (5.131) let us write

$$P_2 = W\,, \quad y_3 = y\,, \quad y_2 = z\,, \quad y_1 = x\,, \quad t_2 = t\,, \quad t_3 = t + \Delta t$$

and suppress the t_1 dependence so that (compare [142] (1.4.1))

$$W(y, t + \Delta t|x) = \int_{-\infty}^{\infty} W(y, t + \Delta t|z, t)W(z, t|x)\,\mathrm{d}z \tag{5.132}$$

In (5.132), we write for economy of notation

$$W(y, t + \Delta t|z, t) = W(y, \Delta t|z) \tag{5.133}$$

so that

$$W(y, \Delta t|x) = \int_{-\infty}^{\infty} W(z, t|x) W(y, \Delta t|z)\, \mathrm{d}z \tag{5.134}$$

We wish to derive a partial differential equation for the *transition probability* $W(y, t|x)$ from this integral equation under certain limiting conditions. We have to consider

$$\int_{-\infty}^{\infty} R(y) \frac{\partial W(y, t|x)}{\partial t} \mathrm{d}y \tag{5.135}$$

where $R(y)$ is an arbitrary function satisfying

$$\lim_{y \to \pm\infty} R(y) = 0\,, \quad \text{and} \quad R^{(n)}(y) \quad \text{exists at} \quad y = \pm\infty \tag{5.136}$$

In (5.136), $R^{(n)}(y)$ is the nth derivative of $R(y)$ with respect to y. Using the definition of the partial derivative, we have

$$\int_{-\infty}^{\infty} R(y) \frac{\partial W}{\partial t} \mathrm{d}y = \int_{-\infty}^{\infty} R(y) \lim_{\Delta t \to 0} \left[\frac{W(y, t + \Delta t|x) - W(y, t|x)}{\Delta t} \right] \mathrm{d}y \tag{5.137}$$

If we assume that we can interchange the order of the limit and integration, then (5.137) reads

$$\int_{-\infty}^{\infty} R(y) \frac{\partial W}{\partial t} \mathrm{d}y = \lim_{\Delta t \to 0} \int_{-\infty}^{\infty} R(y) \left[\frac{W(y, t + \Delta t|x) - W(y, t|x)}{\Delta t} \right] \mathrm{d}y \tag{5.138}$$

We now substitute for $W(y, t + \Delta t|x)$ in (5.138) using

$$\int_{-\infty}^{\infty} R(y) W(y, t|x)\, \mathrm{d}y = \int_{-\infty}^{\infty} R(z) W(z, t|x)\, \mathrm{d}z \tag{5.139}$$

to obtain

$$\begin{aligned} \int_{-\infty}^{\infty} R(y) \frac{\partial W}{\partial t} \mathrm{d}y = \lim_{\Delta t \to 0} \frac{1}{\Delta t} \Bigg[& \int_{-\infty}^{\infty} W(z, t|x) \int_{-\infty}^{\infty} R(y) W(y, \Delta t|z) \mathrm{d}y \mathrm{d}z \\ & - \int_{-\infty}^{\infty} R(z) W(z, t|x) \mathrm{d}z \Bigg] \end{aligned} \tag{5.140}$$

Let us expand $R(y)$ in a Taylor series about the point $y = z$ so that

$$R(y) = R(z) + (y - z) R'(z) + \frac{(y - z)^2}{2!} R''(z) + \cdots \tag{5.141}$$

Therefore

$$\begin{aligned} \int_{-\infty}^{\infty} R(y) \frac{\partial W}{\partial t} \mathrm{d}y = \lim_{\Delta t \to 0} \frac{1}{\Delta t} \Bigg[& \int_{-\infty}^{\infty} W(z, t|x) \int_{-\infty}^{\infty} \{ R(z) + (y - z) R'(z) \\ & + \frac{(y - z)^2}{2!} R''(z) + \cdots \} W(y, \Delta t|z) \mathrm{d}y \mathrm{d}z - \int_{-\infty}^{\infty} R(z) W(z, t|x) \mathrm{d}z \Bigg] \end{aligned} \tag{5.142}$$

In (5.142) we have

$$\int_{-\infty}^{\infty} W(y, \Delta t|z)\,\mathrm{d}y = 1 \tag{5.143}$$

since $W(y, \Delta t|z)$ is a probability density function. Therefore

$$\begin{aligned}\int_{-\infty}^{\infty} R(y)\frac{\partial W}{\partial t}\mathrm{d}y = \lim_{\Delta t\to 0}\frac{1}{\Delta t}\Bigg[\int_{-\infty}^{\infty} W(z,t|x)\int_{-\infty}^{\infty}\{(y-z)R'(z)\\ +\frac{(y-z)^2}{2!}R''(z)+\cdots\}W(y,\Delta t|z)\mathrm{d}y\mathrm{d}z\Bigg]\end{aligned} \tag{5.144}$$

Let us write

$$a_n(z, \Delta t) = \int_{-\infty}^{\infty}(y-z)^n W(y, \Delta t|z)\mathrm{d}y \tag{5.145}$$

Then

$$\begin{aligned}\int_{-\infty}^{\infty} R(y)\frac{\partial W}{\partial t}\mathrm{d}y = \lim_{\Delta t\to 0}\frac{1}{\Delta t}\int_{-\infty}^{\infty} W(z,t|x)\\ \times\left\{a_1(z,\Delta t)R'(z)+\frac{a_2(z,\Delta t)}{2!}R''(z)+\cdots\right\}\mathrm{d}z\end{aligned} \tag{5.146}$$

Interchanging limits with integration again, (5.146) reads

$$\begin{aligned}\int_{-\infty}^{\infty} R(y)\frac{\partial W}{\partial t}\mathrm{d}y = \int_{-\infty}^{\infty} W(z,t|x)\Bigg[\lim_{\Delta t\to 0}\frac{a_1(z,\Delta t)}{\Delta t}R'(z)\\ +\lim_{\Delta t\to 0}\frac{a_2(z,\Delta t)}{2!\Delta t}R''(z)+\cdots\Bigg]\mathrm{d}z\end{aligned} \tag{5.147}$$

We now suppose that [cf. (5.162) and (5.163)]

$$\lim_{\Delta t\to 0}\frac{a_n(z,\Delta t)}{\Delta t} = 0\,, \quad \text{for } n > 2 \tag{5.148}$$

Thus

$$\int_{-\infty}^{\infty} R(y)\frac{\partial W}{\partial t}\mathrm{d}y = \int_{-\infty}^{\infty} W(z,t|x)\left[D^{(1)}(z,t)R'(z)+D^{(2)}(z,t)R''(z)\right]\mathrm{d}z \tag{5.149}$$

where

$$D^{(1)}(z,t) = \lim_{\Delta t\to 0}\frac{a_1(z,\Delta t)}{\Delta t} \tag{5.150}$$

$$D^{(2)}(z,t) = \lim_{\Delta t\to 0}\frac{a_2(z,\Delta t)}{2\Delta t} \tag{5.151}$$

We need to factor $R(z)$ out of the right-hand side of (5.149). To do this, we use integration by parts. Thus, we have

$$\int_{-\infty}^{\infty} W(z,t|x)D^{(1)}(z,t)R'(z)\mathrm{d}z = \int_{-\infty}^{\infty} u\mathrm{d}v = uv\Big|_{-\infty}^{\infty} - \int_{-\infty}^{\infty} v\mathrm{d}u \tag{5.152}$$

where

$$u = W(z,t|x)D^{(1)}(z,t) \quad \text{and} \quad \mathrm{d}v = R'(z)\mathrm{d}z \tag{5.153}$$

so that

$$du = \frac{\partial}{\partial z}\left[W(z,t|x)D^{(1)}(z,t)\right]\mathrm{d}z \quad \text{and} \quad v = R(z) \tag{5.154}$$

Hence

$$\int_{-\infty}^{\infty} W(z,t|x)D^{(1)}(z,t)R'(z)\,\mathrm{d}z = -\int_{-\infty}^{\infty} R(z)\frac{\partial}{\partial z}\left[D^{(1)}(z,t)W(z,t|x)\right]\mathrm{d}z \tag{5.155}$$

by (5.136). Similarly applying integration by parts twice to the last term of (5.149), we have

$$\int_{-\infty}^{\infty} W(z,t|x)D^{(2)}(z,t)R''(z)\mathrm{d}z = \int_{-\infty}^{\infty} R(z)\frac{\partial^2}{\partial z^2}\left[D^{(2)}(z,t)W(z,t|x)\right]\mathrm{d}z \tag{5.156}$$

Substituting (5.155) and (5.156) into (5.149), we have

$$\int_{-\infty}^{\infty} R(y)\left(\frac{\partial W}{\partial t} + \frac{\partial}{\partial y}\left[D^{(1)}W\right] - \frac{\partial^2}{\partial y^2}\left[D^{(2)}W\right]\right)\mathrm{d}y = 0 \tag{5.157}$$

(since z is a dummy variable). Thus suppressing the initial value x,

$$\frac{\partial W(y,t)}{\partial t} = -\frac{\partial}{\partial y}\left[D^{(1)}(y,t)W(y,t)\right] + \frac{\partial^2}{\partial y^2}\left[D^{(2)}(y,t)W(y,t)\right] \tag{5.158}$$

Equation (5.158) is the *Fokker–Planck equation* for $W(y,t)$ the probability distribution function of a particle leaving "position" y at time t for a one-dimensional Markov process governed by the random variable $\xi(t)$. $D^{(1)}$ is called the *drift coefficient* (sometimes "vector") and $D^{(2)}$ the *diffusion coefficient* (sometimes "tensor") which are to be calculated from the Langevin equation. The condition that the Taylor series may be truncated at $n = 2$ will be justified if the driving stimulus is white noise in the underlying stochastic differential equation (Langevin equation). This is apparent from the properties of white noise, i.e.,

$$\overline{F(t_1)F(t_2)} = 2D\delta(t_1 - t_2) \tag{5.159}$$

and Isserlis' theorem, namely

$$\overline{F(t_1)F(t_2)\ldots F(t_{2n})} = \sum \prod_{i_r > i_s} \overline{F(i_r)F(i_s)}\,, \quad \overline{F(t_1)F(t_2)\ldots F(t_{2n+1})} = 0 \tag{5.160}$$

For $n = 2$, for example,

$$\begin{aligned}\overline{F(t_1)F(t_2)F(t_3)F(t_4)} =& 4D^2\{\delta(t_1 - t_2)\delta(t_3 - t_4) \\ &+ \delta(t_1 - t_3)\delta(t_2 - t_4) + \delta(t_1 - t_4)\delta(t_2 - t_3)\}\end{aligned} \tag{5.161}$$

which gives rise to a_4 of order $(\Delta t)^2$ in (5.148).

From (5.161) we see that $a_3, a_5, \ldots, a_{2n+1}$ are all zero and from (5.159) and (5.160)

$$a_{2n} \sim (\Delta t)^n \tag{5.162}$$

Hence

$$\lim_{\Delta t \to 0} \frac{1}{\Delta t} a_{2n} = 0 \,, \qquad n > 1 \tag{5.163}$$

However, if the driving stimulus is not white noise, higher-order terms must be included in the *Kramers-Moyal* expansion, (5.147), and one no longer has the Fokker–Planck equation.

We again emphasise with Wang and Uhlenbeck [592] in relation to (5.158) that (5.148)–(5.151) and (5.159)–(5.160) are *necessarily only approximations*. The basic equation is *always* Boltzmann's integral equation [123], [147]. These equations hold when in each collision the velocity (y, for example) of the particle can change very little so that the Boltzmann equation may be approximated by the diffusion (Fokker–Planck) equation (5.158).

Since in general we will be dealing with the multivariable form of the Fokker–Planck equation, it is necessary to quote the form of that equation for many dimensions characterised by a set of random variables $\{\boldsymbol{\xi}\} = \{\xi_1, \ldots, \xi_n\}$. The multivariable form of the Fokker–Planck equation [512] is with $W = W(\{\boldsymbol{y}\}, t|\{\boldsymbol{x}\})$, $\{\boldsymbol{y}\}$ denoting a set of realisations of the random variables $\{\boldsymbol{\xi}\}$:

$$\frac{\partial W(\boldsymbol{y}, t)}{\partial t} = -\sum_{i=1}^{n} \frac{\partial}{\partial y_i} \left[D_i^{(1)}(\boldsymbol{y}, t) W(\boldsymbol{y}, t) \right] + \frac{1}{2} \sum_{k=1}^{n} \sum_{l=1}^{n} \frac{\partial^2}{\partial y_k \partial y_l} \left[D_{k,l}^{(2)}(\boldsymbol{y}, t) W(\boldsymbol{y}, t) \right] \tag{5.164}$$

For simplicity, let us suppose that the process is characterised by a state vector $\boldsymbol{y}$ having only two components (y_1, y_2) (these, for example, could be the realisations of the position and velocity of a Brownian particle), and so the two variable Fokker–Planck equation written in full is

$$\frac{\partial W}{\partial t} = -\sum_{i=1}^{2} \frac{\partial}{\partial y_i} \left[D_i^{(1)} W \right] + \frac{1}{2} \sum_{k=1}^{2} \sum_{l=1}^{2} \frac{\partial^2}{\partial y_k \partial y_l} \left[D_{k,l}^{(2)} W \right] \tag{5.165}$$

or

$$\begin{aligned} \frac{\partial W}{\partial t} = &- \frac{\partial}{\partial y_1} \left[D_1^{(1)} W \right] - \frac{\partial}{\partial y_2} \left[D_2^{(1)} W \right] + \frac{1}{2} \frac{\partial^2}{\partial y_1^2} \left[D_{1,1}^{(2)} W \right] \\ &+ \frac{1}{2} \frac{\partial^2}{\partial y_1 \partial y_2} \left[D_{1,2}^{(2)} W \right] + \frac{1}{2} \frac{\partial^2}{\partial y_2 \partial y_1} \left[D_{2,1}^{(2)} W \right] + \frac{1}{2} \frac{\partial^2}{\partial y_2^2} \left[D_{2,2}^{(2)} W \right] \end{aligned} \tag{5.166}$$

In general, $D_{1,2}^{(2)} = D_{2,1}^{(2)}$ so that

$$\begin{aligned} \frac{\partial W}{\partial t} = &- \frac{\partial}{\partial y_1} \left[D_1^{(1)} W \right] - \frac{\partial}{\partial y_2} \left[D_2^{(1)} W \right] \\ &+ \frac{1}{2} \frac{\partial^2}{\partial y_1^2} \left[D_{1,1}^{(2)} W \right] + \frac{1}{2} \frac{\partial^2}{\partial y_2^2} \left[D_{2,2}^{(2)} W \right] + \frac{\partial^2}{\partial y_1 \partial y_2} \left[D_{1,2}^{(2)} W \right] \end{aligned} \tag{5.167}$$

where the various drift and diffusion coefficients are

$$D_i^{(l)} = \lim_{\Delta t \to 0} \frac{\overline{\Delta y_i}}{\Delta t} , \qquad D_{i,j}^{(2)} = \lim_{\Delta t \to 0} \frac{\overline{\Delta y_i \Delta y_j}}{\Delta t} , \quad (i, j = 1, 2) \tag{5.168}$$

We reiterate that we have assumed in writing our Fokker–Planck equation [referring to (5.158) for convenience] that

$$D^{(1)}(y, t) = \lim_{\Delta t \to 0} \frac{a_1(y, \Delta t)}{\Delta t} , \quad D^{(2)}(y, t) = \lim_{\Delta t \to 0} \frac{a_2(y, \Delta t)}{\Delta t} \tag{5.169}$$

and

$$D^{(n)}(y, t) = \lim_{\Delta t \to 0} \frac{a_n(y, \Delta t)}{\Delta t} = 0 \tag{5.170}$$

for $n > 2$. This allows us to truncate the Kramers-Moyal expansion (5.147). In the Fokker–Planck equation, these quantities (which express the fact that in small times Δt in the process under consideration, the only alteration in the random variable ξ is that due to the rapidly fluctuating Brownian force $F(t)$, which is the central idea underlying the theory of the Brownian motion) are to be calculated from the Langevin equation. The procedure emphasises again that the equation is the basic equation of the theory of the Brownian movement. We remark that the time Δt is of such short duration that (taking as an example **y** as the position and momentum of a particle) *the momentum does not significantly alter during the time Δt and neither does any external conservative force*. Nevertheless, Δt is supposed to be *sufficiently long that the chance that the rapidly fluctuating stochastic force $F(t)$ takes on a given value at time $t + \Delta t$ is independent of the value that force possessed at time t*. In other words, the Brownian force has no memory.

We shall now explicitly calculate the drift and diffusion coefficients in the Fokker–Planck equation for the simplest one-dimensional model, which is as follows. The Langevin equation for the process characterised by the one-dimensional random variable $\xi(t)$ (Figure 5.4), which describes, for example, the velocity of a particle of mass m undergoing one-dimensional Brownian motion, is

$$\dot{\xi}(t) + \beta \xi(t) = F(t)/m \tag{5.171}$$

where

$$\overline{F(t)} = 0 , \qquad \overline{F(t)F(t + \tau)} = 2\beta m k T \delta(\tau)$$

If we integrate this equation over a short time Δt, we have the integral equation with $\xi(t + \Delta t)$ being the solution of (5.171), which at time t has the sharp value y, so that

$$\xi(t + \Delta t) - y = -\int_t^{t+\Delta t} \beta \xi(t') \mathrm{d}t' + \frac{1}{m} \int_t^{t+\Delta t} F(t') \mathrm{d}t' \tag{5.172}$$

Thus, taking the statistical average of the realisations of ξ in a small time Δt, we can readily calculate the drift coefficient $D^{(1)}(y, t)$:

$$D^{(1)}(y, t) = \lim_{\Delta t \to 0} \frac{\overline{[\xi(t + \Delta t) - y(t)]}}{\Delta t} = -\beta y \tag{5.173}$$

To calculate the diffusion coefficient $D^{(2)}(y,t)$, we square $\xi(t+\Delta t)-y$ to obtain the integral equation

$$\begin{aligned}[\xi(t+\Delta t)-y]^2 =&\beta^2 y^2(\Delta t)^2 - 2\Delta t\beta y\frac{1}{m}\int_t^{t+\Delta t} F(t')\mathrm{d}t' \\ &+\frac{1}{m^2}\int_t^{t+\Delta t}\int_t^{t+\Delta t} F(t')F(t'')\mathrm{d}t'\mathrm{d}t''\end{aligned} \tag{5.174}$$

The first term on the right-hand side is of order $(\Delta t)^2$. The middle term vanishes because F and the sharp initial value y are statistically independent. The last term is on averaging $(2\beta kT/m)\Delta t$. Hence

$$D^{(2)}(y,t)=\lim_{\Delta t\to 0}\frac{\overline{[\xi(t+\Delta t)-y]^2}}{\Delta t}=2\beta kT/m \tag{5.175}$$

The third Kramers-Moyal coefficient $D^{(3)}(y,t)$ is calculated as follows. We form

$$\begin{aligned}\overline{[\xi(t+\Delta t)-y]^3} =&-\beta^2 y^3(\Delta t)^3+3y^2\beta^2(\Delta t)^2\frac{1}{m}\int_t^{t+\Delta t}F(t')\mathrm{d}t' \\ &-3y\beta\Delta t\left(\frac{1}{m}\int_t^{t+\Delta t}F(t')\mathrm{d}t'\right)^2+\left(\frac{1}{m}\int_t^{t+\Delta t}F(t')\mathrm{d}t'\right)^3\end{aligned} \tag{5.176}$$

The only term $\sim \Delta t$, which will contribute to the average in this equation, is the one involving the triple integral. However, this will vanish for a white noise driving force because by Isserlis' theorem, all odd values are zero. Thus, $D^{(3)}(y,t)=0$. Likewise we can prove that all the $D^{(n)}(y,t)=0$ for all $n\geq 3$.

Thus, the transition probability W satisfies the Fokker–Planck equation

$$\frac{\partial W}{\partial t}=\beta\frac{\partial}{\partial y}(yW)+\frac{\beta kT}{m}\frac{\partial^2 W}{\partial y^2} \tag{5.177}$$

corresponding to the Langevin equation (5.171). W must also satisfy, since it is a transition probability,

$$\lim_{t\to 0}W(y,t|x)=\delta(y-x)\,,\qquad \lim_{t\to\infty}W(y,t|x)=W(y) \tag{5.178}$$

where $W(y)$ denotes the stationary solution.

We shall now discuss how drift and diffusion coefficients may be evaluated in the most general case.

5.2.1 Drift and Diffusion Coefficients

The quantities $D^{(1)}$ and $D^{(2)}$ for the nonlinear Langevin equation may be calculated in the following way [512]. The most general Langevin equation in one stochastic variable ξ has the form [512]

$$\dot{\xi}(t) = h\,(\xi(t), t) + g\,(\xi(t), t)\,F(t) \tag{5.179}$$

If g is constant, (5.179) is called a Langevin equation with an *additive noise term*, while if g depends on ξ, (5.179) is called a Langevin equation with a *multiplicative noise term*. We shall consider only the multiplicative noise case since it is more general. We wish to evaluate [512]

$$D^{(1)}(y, t) = \lim_{\Delta t \to 0} \frac{\overline{\xi(t + \Delta t) - y}}{\Delta t}|_{\xi(t)=y} \tag{5.180}$$

and

$$D^{(2)}(y, t) = \frac{1}{2} \lim_{\Delta t \to 0} \frac{\overline{[\xi(t + \Delta t) - y]^2}}{\Delta t}|_{\xi(t)=y} \tag{5.181}$$

where $\xi(t + \Delta t)$ is a solution of (5.179), which at time t has a *sharp* value y such that

$$\overline{\xi(t)} = y \tag{5.182}$$

Following [512] we write the Langevin equation (5.179) in the integral form

$$\xi(t + \Delta t) - y = \int_t^{t+\Delta t} [h\,(\xi(t'), t') + g\,(\xi(t'), t')\,F(t')]\,\mathrm{d}t' \tag{5.183}$$

We now expand h and g as Taylor series about the sharp point $\xi = y$ so that on recalling that the increment during the interval (t, t') is $\xi(t') - y$ we obtain

$$h\,(\xi(t'), t') = h(y, t') + [\xi(t') - y]\,\frac{\partial h(y, t')}{\partial y} + \ldots \tag{5.184}$$

$$g\,(\xi(t'), t') = g(y, t') + [\xi(t') - y]\,\frac{\partial g(y, t')}{\partial y} + \ldots \tag{5.185}$$

where

$$\frac{\partial}{\partial \xi(t')} h\,(\xi(t'), t')\,|_{\xi(t)=y} = \frac{\partial h(y, t')}{\partial y} \quad \text{and} \quad \frac{\partial}{\partial \xi(t')} g\,(\xi(t'), t')\,|_{\xi(t)=y} = \frac{\partial g(y, t')}{\partial y}$$

Using these expansions in the integral equation (5.183), we have

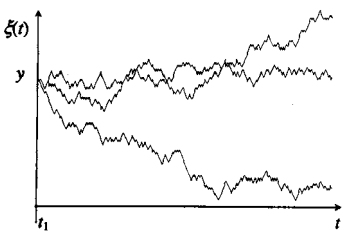

Fig. 5.4. Three typical realisations of a random variable $\xi(t)$ starting from a sharp initial point $\xi(t_1) = y$

$$\xi(t+\Delta t)-y=\int_t^{t+\Delta t}h(y,t')\mathrm{d}t'+\int_t^{t+\Delta t}[\xi(t')-y]\,\frac{\partial h(y,t')}{\partial y}\,\mathrm{d}t'+\cdots$$
$$+\int_t^{t+\Delta t}g(y,t')F(t')\mathrm{d}t'+\int_t^{t+\Delta t}[\xi(t')-y]\,\frac{\partial g(y,t')}{\partial y}F(t')\mathrm{d}t'+\cdots \tag{5.186}$$

We may now iterate for $\xi(t')-y$ in the integrand using (5.183) to get

$$\xi(t+\Delta t)-y=\int_t^{t+\Delta t}h(y,t')\mathrm{d}t'+\int_t^{t+\Delta t}\frac{\partial h(y,t')}{\partial y}\int_t^{t'}h(y,t'')\mathrm{d}t'\mathrm{d}t''$$
$$+\int_t^{t+\Delta t}\frac{\partial h(y,t')}{\partial y}\int_t^{t'}g(y,t'')F(t'')\mathrm{d}t'\mathrm{d}t''+\int_t^{t+\Delta t}g(y,t')F(t')\mathrm{d}t'$$
$$+\int_t^{t+\Delta t}\frac{\partial g(y,t')}{\partial y}\int_t^{t'}h(y,t'')F(t')\mathrm{d}t''\mathrm{d}t'$$
$$+\int_t^{t+\Delta t}\frac{\partial g(y,t')}{\partial y}\int_t^{t'}g(y,t'')F(t'')F(t')\mathrm{d}t''\mathrm{d}t'+O(\Delta t) \tag{5.187}$$

so that the last term involves a *product* of noises. Now we recall that

$$\overline{F(t)}=0\,,\qquad \overline{F(t')F(t'')}=2D\delta(t'-t'') \tag{5.188}$$

($D=\zeta kT$) and the property of the Dirac delta function [512]

$$\int_0^a f(t)\delta(t-a)\mathrm{d}t=\frac{1}{2}f(a) \tag{5.189}$$

Thus, we have from (5.187)

$$\overline{\xi(t+\Delta t)-y}=\int_t^{t+\Delta t}h(y,t')\mathrm{d}t'+2D\int_t^{t+\Delta t}\frac{\partial g(y,t')}{\partial y}\int_t^{t'}g(y,t'')\delta(t'-t'')\mathrm{d}t''\mathrm{d}t'+\ldots$$
$$=h(y,t+\Theta_1\Delta t)\Delta t+Dg(y,t+\Theta_2\Delta t)\frac{\partial g(y,t+\Theta_2\Delta t)}{\partial y}\Delta t+O(\Delta t) \tag{5.190}$$

($0\le\Theta_i\le 1$). Here, we have taken into account (5.189), i.e.,

$$2D\int_t^{t'}g(y,t'')\delta(t'-t'')\mathrm{d}t''=Dg(y,t') \tag{5.191}$$

Thus, we obtain

$$D^{(1)}(y,t)=\lim_{\Delta t\to 0}\frac{\overline{\xi(t+\Delta t)-y}}{\Delta t}=h(y,t)+D\frac{\partial g(y,t)}{\partial y}g(y,t) \tag{5.192}$$

Equation (5.192) may also be considered as an *evolution equation* for the sharp value y. This is the basis for the approach to the subject portrayed in this book; the sharp

initial condition corresponding to the delta function initial distribution in the Fokker–Planck picture so that in effect we are calculating the time dependence of the components of the transition probability when we impose the sharp initial condition on the Langevin equation. We emphasise that $\xi(t)$ in (5.179) and y in (5.192) have different meanings. $\xi(t)$ is a stochastic variable while $y = \xi(t)$ is a sharp (definite) value at time t. We have distinguished the sharp values from the stochastic variables by deleting the time argument. The last term in (5.192) is known as the *noise-induced drift*.

The other integrals in (5.187) have been ignored because [512], [587] they will either give a contribution of the form $(\Delta t)^n$ for $n = 2$ if there are $2n$ F's and by (5.163) they will vanish, or if there are $(2n + 1)$ F's they will vanish by Isserlis' theorem (5.160).

Similarly for $D^{(2)}(y, t)$, we have

$$\begin{aligned}[\xi(t + \Delta t) - y]^2 = &\int_t^{t+\Delta t} \int_t^{t+\Delta t} h(\xi, t')h(\xi, t'')\mathrm{d}t'\,\mathrm{d}t'' \\ &+ 2\int_t^{t+\Delta t} h(\xi, t')\mathrm{d}t' \int_t^{t+\Delta t} g(\xi, t')F(t')\mathrm{d}t' \\ &+ \int_t^{t+\Delta t} \int_t^{t+\Delta t} g(\xi, t')g(\xi, t'')F(t')F(t'')\mathrm{d}t'\,\mathrm{d}t''\end{aligned} \tag{5.193}$$

The first two terms of (5.193) will give contributions of the order $(\Delta t)^2$ and they vanish. Thus

$$\overline{[\xi(t + \Delta t) - y]^2} = 2D \int_t^{t+\Delta t} \int_t^{t+\Delta t} g(\xi, t')g(\xi, t'')2\delta(t' - t'')\,\mathrm{d}t'\,\mathrm{d}t'' \tag{5.194}$$

Therefore

$$D^{(2)}(y, t) = \frac{1}{2} \lim_{\Delta t \to 0} \frac{\overline{[\xi(t + \Delta t) - y]^2}}{\Delta t} = Dg^2(y, t) \tag{5.195}$$

Having illustrated the one-dimensional problem, we will now illustrate how the procedure is applied to obtain the drift and diffusion coefficients for the two-dimensional Fokker–Planck equation in phase space for a free Brownian particle. This equation is, as we have seen, often called the *Kramers* equation or *Klein-Kramers* equation [512]. In general, the Fokker–Planck equation in the context of a dynamical system, the motion of which in the absence of a heat bath is governed by Hamilton's equations with a *separable* and *additive* Hamiltonian comprising the sum of the kinetic and potential energies, is known as the Klein-Kramers equation.

We have seen that the Langevin equation for a free Brownian particle may be represented as the system

$$\dot{x} = v\,, \qquad \dot{v} = -\beta v + F(t)/m \tag{5.196}$$

with

$$\overline{F(t)} = 0\,, \qquad \overline{F(t_1)F(t_2)} = 2m\beta kT\delta(t_1 - t_2)$$

The corresponding Fokker–Planck equation for the transition probability density W in phase space with $x = y_1$, $v = y_2$ in (5.167) is

$$\frac{\partial W}{\partial t} = -\frac{\partial}{\partial x}\left[D_1^{(1)}(x,v)W\right] - \frac{\partial}{\partial v}\left[D_2^{(1)}(x,v)W\right] + \frac{1}{2}\frac{\partial^2}{\partial x^2}\left[D_{1,1}^{(2)}(x,v)W\right] + \frac{1}{2}\frac{\partial^2}{\partial v^2}\left[D_{2,2}^{(2)}(x,v)W\right] + \frac{\partial^2}{\partial x \partial v}\left[D_{1,2}^{(2)}(x,v)W\right] \tag{5.197}$$

Since $x = y_1$, $\Delta x = \Delta y_1$ and proceeding as in (5.169)

$$D_1^{(1)} = \lim_{\Delta t \to 0} \frac{\overline{\Delta y_1}}{\Delta t} = \lim_{\Delta t \to 0} \frac{\overline{\Delta x}}{\Delta t} = v \tag{5.198}$$

Now, the change in velocity in a small time Δt is

$$\Delta v \approx -\beta v \Delta t + \frac{1}{m}\int_t^{t+\Delta t} F(t')\,\mathrm{d}t'$$

Thus the drift coefficient $D_2^{(1)}$ is

$$D_2^{(1)} = \lim_{\Delta t \to 0} \frac{\overline{\Delta v}}{\Delta t} = -\beta v \tag{5.199}$$

Likewise, the diffusion coefficients $D_{1,1}^{(2)}(x,v)$ and $D_{1,2}^{(2)}(x,v)$ are

$$D_{1,1}^{(2)}(x,v) = \lim_{\Delta t \to 0} \frac{\overline{(\Delta x)^2}}{\Delta t} = \lim_{\Delta t \to 0} \frac{\overline{v^2(\Delta t)^2}}{\Delta t} = 0 \tag{5.200}$$

$$D_{1,2}^{(2)}(x,v) = \lim_{\Delta t \to 0} \frac{\overline{\Delta x \Delta v}}{\Delta t} = \lim_{\Delta t \to 0} \frac{\overline{v \Delta t \Delta v}}{\Delta t} = \lim_{\Delta t \to 0} \overline{-\beta v^2 \Delta t + v\int_t^{t+\Delta t} \frac{F(t')}{m}\mathrm{d}t'} = 0 \tag{5.201}$$

because $\overline{F(t)} = 0$. In order to evaluate

$$D_{2,2}^{(2)}(x,v) = \lim_{\Delta t \to 0} \frac{\overline{(\Delta v)^2}}{\Delta t} \tag{5.202}$$

consider

$$(\Delta v)^2 = \beta^2 v^2 (\Delta t)^2 - \frac{2\beta v \Delta t}{m}\int_t^{t+\Delta t} F(t')\mathrm{d}t' + \frac{1}{m^2}\int_t^{t+\Delta t}\int_t^{t+\Delta t} F(t')F(t'')\mathrm{d}t'\mathrm{d}t'' \tag{5.203}$$

The first term on the right-hand side of (5.203) is of order $(\Delta t)^2$, the second term vanishes on averaging, and

$$\int_t^{t+\Delta t}\int_t^{t+\Delta t} \overline{F(t')F(t'')}\mathrm{d}t'\mathrm{d}t'' = 2D\int_t^{t+\Delta t}\int_t^{t+\Delta t} \delta(t'-t'')\mathrm{d}t'\mathrm{d}t'' = 2D\Delta t$$

($D = \beta k T m$), whence the diffusion coefficient is

$$D^{(2)}_{2,2}(x, v) = 2kT\beta/m \tag{5.204}$$

Thus, we obtain

$$\frac{\partial W}{\partial t} + v\frac{\partial W}{\partial x} = \beta\left[\frac{\partial(vW)}{\partial v} + \frac{kT}{m}\frac{\partial^2 W}{\partial v^2}\right] \tag{5.205}$$

which is the desired Fokker–Planck equation. The Langevin and Fokker–Planck equations are often termed as arising out of a continuous diffusion and a jump-diffusion model, respectively.

We already considered a concrete example of the Fokker–Planck equation, for rotators, in Section 5.1. We now consider the thermally activated relaxation time of a single-domain ferromagnetic particle subjected to a uniform field at an oblique angle to the easy axis including comparison with experimental observations [137].

New asymptotes of the relaxation time of the magnetic moment of a single domain particle with a uniform magnetic field applied at an oblique angle to the easy axis (in excellent agreement with exact numerical results from the Fokker–Planck equation for the Néel–Brown model) are used to model the experimental angular variation of the switching field for individual Co and BaFeCoTiO particles. Good agreement is obtained, justifying the Néel–Brown (in effect, the Kramers) conception of the super-paramagnetic relaxation process and allowing one to deduce the value of the damping constant.

An accurate analytical expression for the prefactor of the greatest relaxation time τ due to thermal agitation of the magnetic moment $\mathbf{m}$ of single-domain nanoparticles subjected to a uniform external field $\mathbf{H}$ is necessary for modeling experiments and deducing other experimental parameters [230]. This problem is important in long-term stability [142], [597] of stored information and in [598] macroscopic quantum tunneling (MQT) of $\mathbf{m}$ (a mechanism of magnetization reversal suggested in [53]), as a knowledge of τ allows the separation of the different relaxation mechanisms. In all common particle assemblies, the easy directions $\mathbf{n}$ of the particles are randomized so that asymptotic τ for $\mathbf{H}$ at an arbitrary angle to $\mathbf{n}$ is required; this differs from the Brown [7] asymptote for axial symmetry; i.e., $\mathbf{H} \parallel \mathbf{n}$ because breaking the axial symmetry couples the transverse and longitudinal relaxation modes. Here we compare experimental and calculated τ as (i) the theory permits direct comparison with experiment (hitherto impossible), and (ii) accurate experiments on individual small particles are now available. Concerning the theory [133], [136] we have already presented exact numerical solutions and asymptotes of τ for a particle with uniaxial anisotropy with $\mathbf{H}$ in the x–z plane at an angle ψ to the easy direction z so that

$$vV(\vartheta) = vK\sin^2\vartheta - vM_sH(\cos\vartheta\cos\psi + \sin\vartheta\cos\varphi\sin\psi) \tag{5.206}$$

ϑ and φ are the polar angles of $\mathbf{m}$, K is the anisotropy constant, and M_s denotes the magnetization of a nonrelaxing particle of volume v.

Equation (5.206) is a *particular* nonaxially symmetric potential. In references [293], [136], we have shown that, for a *general* asymmetric bistable potential of free energy density $V = V(\mathbf{r})$ ($\mathbf{r} = \mathbf{M}/M_s$), with minima at $\mathbf{n}_1$ and $\mathbf{n}_2$ separated by a potential barrier containing a saddle point at $\mathbf{n}_0$ (with the $\mathbf{n}_i$ coplanar) that

$$\tau \approx \frac{2\tau_N}{\lambda_1} \tag{5.207}$$

where

$$\lambda_1 \approx \beta\left(\sqrt{c_1^{(1)}c_2^{(1)}}\mathrm{e}^{-\beta(V_0-V_1)} + \sqrt{c_1^{(2)}c_2^{(2)}}\mathrm{e}^{-\beta(V_0-V_2)}\right) \left[\frac{-c_1^{(0)} - c_2^{(0)} + \sqrt{\left(c_2^{(0)} - c_1^{(0)}\right)^2 - 4\alpha^{-2}c_1^{(0)}c_2^{(0)}}}{4\pi\sqrt{-c_1^{(0)}c_2^{(0)}}}\right] \tag{5.208}$$

verifying Brown's later calculation [293], [135]

$$\tau_N = \frac{\beta M_s(1+\alpha^2)}{2\gamma\alpha} \equiv \frac{\beta}{2b} \tag{5.209}$$

γ is the gyromagnetic ratio, $\beta = \nu/kT$:

$$\alpha = \eta\gamma M_s \tag{5.210}$$

is the dimensionless damping factor (η is the friction in Gilbert's equation [293]). Equation (5.208) is [136]

$$\tau^{-1} \approx \frac{\lambda_1}{2\tau_N} \approx \frac{\Omega_0}{2\pi\omega_0}\{\omega_1 \exp[-\beta(V_0 - V_1)] + \omega_2 \exp[-\beta(V_0 - V_2)]\} \tag{5.211}$$

ω_1 and ω_2 are the well angular frequencies; ω_0 and Ω_0 are the saddle and the damped saddle angular frequencies (V at the minima is denoted by $i = 1,\ 2$, respectively, and at the saddle point by 0). Equation (5.208) is the leading term in the asymptotic expansion of the smallest nonvanishing eigenvalue λ_1 of the Fokker–Planck equation (FPE);

$$\begin{aligned}\frac{\partial W}{\partial t} &= \frac{1}{\beta}\nabla^2 W + b\nabla^2 V \\ &\quad + b\left(\frac{\partial V}{\partial\theta}\frac{\partial W}{\partial\theta} + \frac{1}{\sin^2\theta}\frac{\partial V}{\partial\phi}\frac{\partial W}{\partial\phi}\right) \\ &\quad + \frac{b}{\alpha\sin\theta}\left(\frac{\partial V}{\partial\theta}\frac{\partial W}{\partial\phi} - \frac{\partial V}{\partial\phi}\frac{\partial W}{\partial\theta}\right)\end{aligned} \tag{5.212}$$

where W is the distribution of orientations of the magnetization $\mathbf{M}$ on the unit spherical surface (θ, ϕ). $c_1^{(i)}, c_2^{(i)}, i = 0, 1, 2$ in (5.208) are the coefficients in the truncated Taylor series [293], [134] of the potential at the well and saddle points. The α-values for which (5.208) is valid are discussed in [135], [358], where (5.208) is compared with the exact λ_1. Equation (5.208) approximates λ_1 if [135], [136]

$$\alpha\beta(V_0 - V_i) > 1\ , \quad \beta(V_0 - V_i) \gg 1 \tag{5.213}$$

and is called the intermediate- to high-damping (IHD) formula. Conversely, if α satisfies

$$\alpha\beta(V_0 - V_i) \ll 1\,, \quad \beta(V_0 - V_i) \gg 1 \tag{5.214}$$

so that the energy dissipated in one cycle of the motion is very small ($\ll kT$), then [136], [358]

$$\tau^{-1} \approx \frac{\alpha}{2\pi}\{\omega_1\beta(V_0 - V_1)\exp[-\beta(V_0 - V_1)] + \omega_2\beta(V_0 - V_2)\exp[-\beta(V_0 - V_2)]\} \tag{5.215}$$

This is the low damping (LD) limit in contrast to the intermediate- to high-damping (IHD) limit. The evaluation of $\Omega_0, \omega_i\,(i = 0, 1, 2)$ for (5.206) (involving numerical solution of a quartic equation) is described in [293], [134]. Experimentally, relaxation is observed only if τ is of the order of the measuring time of the experiment implying that $\beta(V_0 - V_2) \gg 1$ always (taking V_2 as the shallow minimum). Because of (5.213) and (5.214), we remark that little information about α for small particles is available so that α between 0.05 and 1 [229] is usually postulated; other values cannot be ruled out, however, meaning that in practice $\alpha\beta(V_0 - V_2)$ can be $\gg 1$, $\ll 1$, or ≈ 1; thus the distinction between (5.211) and (5.215) becomes important. Here, τ as a function of the field angle ψ is required. Such measurements can be made either on oriented particle assemblies where the easy axes are parallel or on an *individual* particle. We understand that data have not hitherto been available on an individual particle; however, accurate individual particle measurements are now available [597], [598], facilitating the comparison of theory and experiment.

In verifying (5.211) and (5.215) for the IHD and LD limits, we selected metallic Co particles synthesized by arc discharge [315] and insulating $BaFe_{10.4}Co_{0.8}Ti_{0.8}O_{19}$ particles (note that these are ferrimagnetic but the noncompensated magnetic moment is so large that they can be considered as ferromagnetic [598]) fabricated by a glass crystallization method [372]; each possesses strong uniaxial magnetocrystalline anisotropy. We used the results for a 20-nm sized Co particle [597] and a 10-nm sized BaFeO particle [598] gained by using planar Nb micro-SQUIDS allowing the study of the magnetization reversal of individual nanoparticles by waiting time and switching field experiments. The waiting-time measurements yield the switching probability. At a given temperature, the magnetic field **H** is increased to a waiting field near the switching field. Then the time elapsed until the magnetization switch is measured. This process is repeated several hundred times, yielding a waiting-time histogram. The integral of this histogram yields the switching probability. Regarding the switching field measurements, **H** is ramped at a given rate and the value stored when the sample magnetization switches. Next, the field ramp is reversed and the process repeated. After several hundred cycles, switching field histograms are established, yielding the mean switching fields $\langle H_{SW}\rangle$ and the width σ_{SW} (rms deviation). Both measurements can be studied as a function of ψ (the **H** direction). The number of decades for τ-values is limited for waiting-time experiments; short-time (milliseconds) experiments are limited by the inductance of the field coils and long-time (minutes) studies by the stability of the experimental setup. Furthermore, the total acquisition time is about a week; thus the more convenient switching field measurement is usually employed. Switching field measurements are equivalent to waiting-time measurements as the time scale for the sweeping rates is more than eight orders of magnitude greater than the time scale of the prefactor.

We shall demonstrate that the experimental results are in good agreement with the asymptotes, (5.211) and (5.215) [written as (5.222)]; moreover, one may determine α. Thus $\langle H_{SW}\rangle$ may be expressed [290] as

$$\langle H_{SW}\rangle = H_c\left\{1-\left[A^{-1}\ln\left(\frac{H_cB}{a(\mathrm{d}H/\mathrm{d}t)A^{1+b/e}}\right)\right]^{1/e}\right\} \tag{5.216}$$

and

$$\tau^{-1} = B\epsilon^{a+b-1}\mathrm{e}^{-A\epsilon^a} \tag{5.217}$$

with

$$\epsilon = 1-\frac{H}{H_c} \tag{5.218}$$

where $H = |\mathbf{H}|$ and $\mathrm{d}H/\mathrm{d}t$ is the rate of field ramping. For uniaxial anisotropy [133], [293],

$$\begin{aligned} H_c &= \frac{2K}{M_s}h_c = \frac{2K}{M_s}\left(\sin^{2/3}\psi+\cos^{2/3}\psi\right)^{3/2} \\ h_c &= \frac{M_sH_c}{2K} \end{aligned} \tag{5.219}$$

where K is the total anisotropy constant, and h_c is the reduced critical field where the bistable V structure vanishes. The particles have a large volume leading to high anisotropy barriers at low temperatures; thus, to observe relaxation, $\beta(V_0-V_2)$ must be about 25. The large volume implies small ϵ leading to $\beta(V_0-V_1)\gg\beta(V_0-V_2)$. Thus we neglect $\exp[-\beta(V_0-V_1)]$ in τ^{-1} and approximate (V_0-V_2) for $\epsilon\ll 1$ by [596]

$$\frac{V_0-V_2}{K} = 4\left(\frac{2}{3}\epsilon\right)^{3/2}\frac{|\cot\psi|^{1/3}}{1+|\cot\psi|^{2/3}} \tag{5.220}$$

[We checked (5.220) numerically against the exact solution [596], [351]; it is an excellent approximation for $5^\circ<\psi<85^\circ$ and $\epsilon<0.05$.] To determine the parameters in (5.216) and (5.217), let

$$\tau^{-1} = \frac{K\gamma}{M_s}P\exp[-\beta(V_0-V_2)] \tag{5.221}$$

where in IHD

$$\begin{aligned} P = P_{IHD} = \frac{M_s}{K\gamma}\frac{\Omega_0}{2\pi}\frac{\omega_2}{\omega_0} &= \frac{\alpha}{4\pi(1+\alpha^2)}\times\left(\frac{\sqrt{c_1^{(2)}c_2^{(2)}}}{-c_1^{(0)}c_2^{(0)}}\right) \\ &\times\left[-c_1^{(0)}+c_2^{(0)}+\sqrt{(c_1^{(0)}-c_2^{(0)})^2-4\alpha^{-2}c_1^{(0)}c_2^{(0)}}\right] \end{aligned} \tag{5.222}$$

while in LD

$$P = P_{LD} = \frac{M_s}{K\gamma}\frac{\alpha}{2\pi}\omega_2\beta(V_0-V_2) = \frac{\alpha}{2\pi}\sqrt{c_1^{(2)}c_2^{(2)}}\beta(V_0-V_2) \tag{5.223}$$

These can be fitted to

$$P_{IHD} = f_{IHD}(\psi, \alpha)\epsilon^{\delta_{IHD}} \tag{5.224}$$

and

$$\begin{aligned} P_{LD} &= \alpha f_{LD}(\psi)\beta(V_0 - V_2)\epsilon^{\delta_{LD}-3/2} \\ &= \alpha f_{LD}(\psi) \times \left[4\beta K \left(\frac{2}{3}\right)^{3/2} \frac{|\cot\psi|^{1/3}}{1+|\cot\psi|^{2/3}}\right] \epsilon^{\delta_{LD}} \end{aligned} \tag{5.225}$$

with ϵ given by (5.218). Equations (5.220)–(5.225) yield

$$\begin{aligned} a = \tfrac{3}{2} \qquad b = \delta - \tfrac{1}{2}\,, \qquad B = \tfrac{K\gamma}{M_s}\tfrac{P}{\epsilon^{\delta}} \\ A = 4\beta K \left(\tfrac{2}{3}\right)^{3/2} \tfrac{|\cot\psi|^{1/3}}{1+|\cot\psi|^{2/3}} \end{aligned} \tag{5.226}$$

In adjusting the theory to switching field measurements of individual nanoparticles, several conditions must be fulfilled: (i) the angular dependence of the switching field must obey the model of magnetization reversal by uniform rotation [570] (5.219), and (ii) the switching probability determined by waiting-time measurements must be an exponential function of the time ($\approx \exp[-t/\tau]$). These are satisfied by the metallic Co particle of [597] and the insulating BaFeCoTiO particle of [598].

Our comparison was accomplished as follows: (i) we chose IHD and guessed α; (ii) we adjusted the theory to the switching field measurements [597] at various ψ, knowing ν from scanning electron microscopy, γ and M_s from [315], [372], and K from H_c at $\psi = 90$ deg and (5.219); (iii) we compared the observed ψ of $f_{IHD}(\psi, \alpha)$, with the IHD formula (5.224); (iv) we altered the assumed α and repeated the adjustment of step (iii) until optimum agreement between theory and experiment is achieved; and (v) finally, where (5.213) is violated, we repeated the process using LD, i.e., we compared the results to $f_{LD}(\psi)$ of (5.225). Results for Co and BaFeCoTiO are presented in Figure 5.5. $f_{IHD}(\psi, \alpha)$, of the Co particle provides a good fit to IHD using $\alpha = 0.5 \pm 0.2$; likewise, $f_{LD}(\psi)$ of the BaFeCoTiO particle to LD with $\alpha = 0.035 \pm 0.005$. Both α fits are reasonable because (i) the damping in metallic particles is expected to be higher than in insulating particles in agreement with our experimental results and (ii) the values are close to the results of [230], [229]. Nevertheless, more detailed measurements should be carried out to substantiate these preliminary measurements. We emphasize that α is the *sole* fitting parameter causing us to reiterate that little information is available on α for fine particles; for γFe_2O_3 particles in a polymer, α ranges between 0.05 and 1 depending on the interparticle interaction strength [229]; again for interacting Fe particles in an alumina matrix [230] $\alpha \approx 1$ while, for bulk Fe, $\alpha \approx 0.01$. Furthermore, very low α-values are observed for particular compounds such as yttrium garnet. Also, in fine particles, α is a phenomenological constant in the Gilbert equation for the *entire* particle including *all* defects, in particular, the *surface* defects; thus one expects that the *smaller* the particle, the more pronounced will be the increase of α over its bulk value. The damping problem also plays an important role in the MQT of **m**. In general, dissipation due to, for example, conduction electrons strongly reduces quantum effects. This agrees

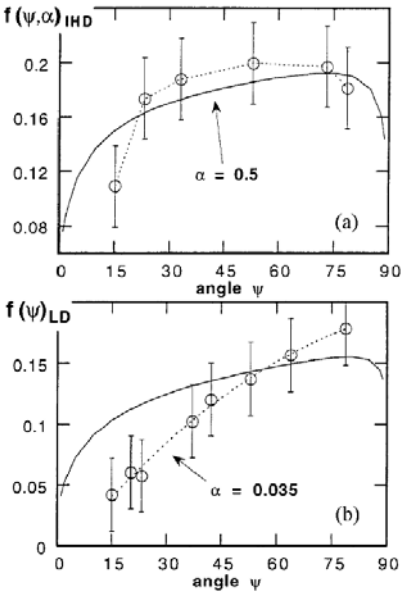

Fig. 5.5. Comparison of the (**a**) IHD and (**b**) LD formulae with measurements obtained on (a) a metallic Co particle [597] and (b) an insulating BaFeCoTiO particle [598]; $K\gamma/M_s = 5x10^{10}\ s^{-1}$ and $K\gamma/M_s = 6.9x10^{10}\ s^{-1}$, respectively, were used

with our measurements in that, for metallic Co particles, no quantum effects were found at low temperatures [597] whereas, for insulating BaFeCoTiO particles [598], strong deviations from the classical model exist below 0.4 K, which are quantitatively in agreement with the predictions of the MQT theory in the low dissipation regime [598].

We conclude that new asymptotes of τ of **m** of a nanoparticle with **H** at angle ψ with respect to **n** (in numerical agreement with the FPE [134], [136], [351]) reproduce the angular variation of the switching field of *individual* particles to a reasonable degree of accuracy, justifying the Néel–Brown (in effect, the Kramers) conception of the thermal relaxation process. Equations (5.211) and (5.215) are also valid for *any* nonaxially symmetric bistable potential with coplanar minima and saddle points allowing extension to other potentials, i.e., taking into account higher terms of the magnetocrystalline anisotropy. These asymptotes also pertain to the memoryless (white noise) limit (Ohmic damping). Nevertheless, as conjectured in [359] in the presence of long-time memory, they should hold with a reduced effective dissipation constant which influences, in particular [360], the LD prefactor. It is of course now standard practice [106] to generalize the classical Fokker–Planck equation to the quantum master equation

$$\frac{\partial W}{\partial t} = \left[-\frac{p}{M}\frac{\partial}{\partial x} + \frac{\mathrm{d}V}{\mathrm{d}x}\frac{\partial}{\partial p} + \frac{\partial}{\partial p}\left(\gamma p + D_{pp}\frac{\partial}{\partial p}\right) + D_{xp}\frac{\partial^2}{\partial x \partial p} + \sum_{s=1}^{\infty} \frac{(\mathrm{i}\hbar/2)^{2s}}{(2s+1)!} V^{(2s+1)} \frac{\partial^{2s+1}}{\partial p^{2s+1}} \right] W \tag{5.227}$$

The first three terms on the right-hand side, identfying $D_{pp} = \gamma M k_B T$, give the classical Klein–Kramers Fokker–Planck equation. The mixed diffusion term $D_{x,p}\partial^2/\partial x \partial p W$ is heuristically related to the colour of the quantum noise [145]. The s-series gives the quantum contribution to the unitary evolution of the closed system. Other generalizations are possible.

Other examples of the classical Fokker–Planck equation are given in Section 5.3 (albeit in fractal form) and Section 5.4.

5.3 Dieletric Relaxation, Anomalous Diffusion, Fractals, and After Effects

The inertia-corrected Debye model of rotational Brownian motion of polar molecules was generalized by Coffey et al. [138], [139], [140], [349], [141] to describe fractional dynamics and anomalous rotational diffusion. The linear-response theory of the normalized complex susceptibility was given in terms of a Laplace transform and as a function of frequency. The angular-velocity correlation function was parameterized via fractal Mittag–Leffler functions. Here we apply the latter method and complex-contour integral-representation methods to determine the original time-dependent amplitude as an inverse Laplace transform using both analytical and numerical approaches, as appropriate [199].

The fractional Klein–Kramers equation for anomalous rotational diffusion is

$$\frac{\mathrm{d}W}{\mathrm{d}\tau} = \frac{\partial W}{\partial \tau} + \dot{\phi}\frac{\partial W}{\partial \phi} \frac{-\mu E \sin\phi}{I} \frac{\partial W}{\partial \dot{\phi}} = {}_0D_t^{1-\alpha} L_{FP} W \tag{5.228}$$

Here, $W(\phi, \dot{\phi}, t)$ is the probability density function (pdf). The fractional Fokker–Planck (FP) operator has the property

$${}_0D_t^{1-\alpha} L_{FP} W = {}_0D_t^{1-\alpha} \frac{\tau^{1-\alpha}\zeta}{I} \times \left[\frac{\partial}{\partial \dot{\phi}}(\dot{\phi} W) + \frac{k_B T}{I}\frac{\partial^2 W}{\partial \dot{\phi}^2} \right] \tag{5.229}$$

where k_B is Boltzmann's constant, T is the temperature, ζ is the viscous damping coefficient of a dipole, I is the moment of inertia of the rigid dipole μ, ϕ is the azimuthal angle of the rigid rotator, t is the time, τ is the intertrapping time-scale, identifiable with the Debye relaxation time ($\zeta/(k_B T) \sim 10^{-11}$ s), and α is the anomalous exponent characterizing the fractal-time process. A weak uniform electric field E is suddenly switched off at time $t = 0$, when anomalous diffusion ensues. The fractal operator ${}_0D_t^{1-\alpha}$ is given by

$${}_0D_t^{1-\alpha} \equiv \frac{\partial}{\partial t}\,{}_0D_t^{-\alpha}$$

where we have, suppressing $\dot{\phi}$-dependence,

$$ {}_0D_t^{-\alpha} W(\phi, t) = \frac{1}{\Gamma(\alpha)} \int_0^t \frac{W(\phi, t')\mathrm{d}t'}{(t - t')^{1-\alpha}} \tag{5.230} $$

Here Γ is the gamma function. We may seek a solution of (5.228) as for normal diffusion, as

$$ W(\phi, \dot{\phi}, t) = \exp\left(-\eta^2 \dot{\phi}^2\right) \sum_{p=-\infty}^{+\infty} \sum_{n=0}^{\infty} c_{p,n}(t) \mathrm{e}^{\mathrm{i}p\phi} H_n(\eta\dot{\phi}) \tag{5.231} $$

where we define

$$ \eta = [I/(2k_B T)]^{1/2} $$

so that

$$ W(\phi, \dot{\phi}, 0) \approx \frac{1}{2\pi^{3/2}} \eta \mathrm{e}^{-\eta^2\dot{\phi}^2} \left[\frac{1 + \mu E \cos\phi}{k_B T}\right] \tag{5.232} $$

Linear-response ($p = 1$) theory requires the solution of the differential-recurrence relation:

$$ \frac{\mathrm{d}}{\mathrm{d}t} c_{1,n}(t) + \frac{\mathrm{i}}{2\eta} \left[2(n + 1)c_{1,n+1}(t) + c_{1,n-1}(t)\right] = -{}_0D_t^{1-\alpha} \tau^{1-\alpha} \frac{n\zeta}{I} c_{1,n}(t) \tag{5.233} $$

The usual Laplace operator L, given by

$$ L\{\{f(t)\} \equiv \tilde{f}(s) = \int_0^\infty \mathrm{e}^{-st} f(t)\mathrm{d}t $$

yields

$$ L\{{}_0D_{t^{1-\alpha}} f(t)\} = \begin{cases} s^{1-\alpha}\tilde{f}(s) - D_t^{-\alpha} f(t)|_{t=0} & \begin{pmatrix} 0 < \alpha < 1 \\ 1 < \sigma < 2 \end{pmatrix} \\ s^{1-\alpha}\tilde{f}(s) & \begin{pmatrix} 1 \le \alpha < 2 \\ 0 < \sigma \le 1 \end{pmatrix} \end{cases} $$

where we have introduced, for subsequent convenience, σ given by $\sigma = 2 - \alpha$. Transforming (5.233), we obtain

$$ \left[2\tau s + n(\gamma')^2(\tau s)^{1-\alpha}\right] \tilde{c}_{1,n}(s) + \mathrm{i}\gamma' \left[2(n + 1)\tilde{c}_{1,n+1}(s) + \tilde{c}_{1,n-1}(s)\right] = c_{1,n}(0) \tag{5.234} $$

where we have

$$ \gamma' = \frac{\tau}{\eta} = \zeta \sqrt{\frac{2}{(Ik_B T)}} \equiv \sqrt{\frac{b}{2}} $$

As shown by [138], (5.234) can be solved in terms of continued fractions to yield the normalized complex susceptibility, given by linear-response theory, namely

$$ \hat{\psi}(\omega) = 1 - \mathrm{i}\omega \frac{\tilde{c}_{1,0}(\mathrm{i}\omega)}{c_{1,0}(0)} \tag{5.235} $$

where ω is the angular frequency. In detail,

$$\hat{\psi}(\omega) = 1 - \frac{B(\mathrm{i}\omega\tau)^{\sigma}}{B(\mathrm{i}\omega\tau)^{\sigma} + \frac{B}{1+B(\mathrm{i}\omega\tau)^{\sigma}+\frac{2B}{2+B(\mathrm{i}\omega\tau)^{\sigma}+\frac{3B}{3+\cdots}}}} \tag{5.236}$$

and by comparison with

$$\frac{M(a,b,z)}{(b-1)M(a-1,b-1,z)} = \frac{1}{b-1-z+\frac{az}{b-z+\frac{az}{b-z+\frac{(a+1)z}{b+1-z+\cdots}}}} \tag{5.237}$$

based on the exact recurrence relation for the regular confluent hypergeometric function $M(A,B,C)$, namely

$$b(1-b+z)M(a,b,z) - azM(a+1,b+1,z) + b(b-1)M(a-1,b-1,z) = 0 \tag{5.238}$$

we obtain

$$\hat{\psi}(\omega) = 1 - \frac{1}{(1+(\mathrm{i}\tau\omega)^{-\sigma})}M(1,1+BC,B) \tag{5.239}$$

where

$$B = b(\mathrm{i}\omega\tau)^{2-2\sigma} \tag{5.240}$$

$$C = 1 + (\mathrm{i}\omega\tau)^{\sigma} \tag{5.241}$$

where

$$M(1,1+BC,B) = (BC)B^{-BC}\exp(B)\gamma(BC,B) \tag{5.242}$$

with the incomplete gamma function given by

$$\gamma(b,z) \equiv \int_0^z \mathrm{e}^{-t}t^{b-1}\mathrm{d}t \tag{5.243}$$

However, the question is: what is the time evolution of $c_{1,0}(t)$ or $F(t,\sigma)$ given by

$$F(t,\sigma)h(t) \equiv \frac{c_{1,0}(t)h(t)}{c_{1,0}(0)} = \frac{1}{2\pi\mathrm{i}}\int_{\gamma-\mathrm{i}\infty}^{\gamma+\mathrm{i}\infty}\mathrm{d}u\,\mathrm{e}^{ut}\tilde{c}_{1,0}(u) \tag{5.244}$$

Here, naturally enough, we have $h(t)$ the Heaviside step function and the Laplace transform

$$\tilde{c}_{1,0}(u) = \int_0^{\infty}\mathrm{e}^{-ut}c_{1,0}(t)\mathrm{d}t \tag{5.245}$$

Cancelling $h(t)$, it follows that

$$\frac{\tilde{c}_{1,0}(u=\mathrm{i}\omega)}{c_{1,0}(0)} = \int_0^{\infty}\mathrm{e}^{-\mathrm{i}\omega t}F(t,\sigma)\mathrm{d}t \tag{5.246}$$

where we have

$$F(t,\sigma) = \frac{c_{1,0}(t)}{c_{1,0}(0)} = \frac{1}{2\pi\mathrm{i}}\int_{\gamma-\mathrm{i}\infty}^{\gamma+\mathrm{i}\infty}\frac{\mathrm{d}u}{u}\frac{\mathrm{e}^{ut}}{1+(ut)^{-\sigma}}M(1,1+BC,B) \tag{5.247}$$

with B and C given by (5.240) and (5.241) with $\mathrm{i}\omega$ mapped to u. Can we now evaluate $F(t,\sigma)$?

Analytical Check

$$\mathrm{i}\omega\tilde{c}_{1,0}(\mathrm{i}\omega) = \mathrm{i}\omega \int_0^\infty \mathrm{e}^{-\mathrm{i}\omega t} F(t,\sigma)\mathrm{d}t \tag{5.248}$$

where

$$F(t,\sigma) = \frac{1}{2\pi\mathrm{i}} \int_{\gamma-\mathrm{i}\infty}^{\gamma+\mathrm{i}\infty} \mathrm{d}u\, \mathrm{e}^{ut} \int_0^\infty \mathrm{e}^{-uT} F(T,\tau)\mathrm{d}T \tag{5.249}$$

and setting $u = y + \mathrm{i}v$,

$$= \frac{1}{2\pi} \int_{-\infty}^{+\infty} \mathrm{d}v\, \mathrm{e}^{(\gamma+\mathrm{i}v)t} \int_0^\infty \mathrm{e}^{-(\gamma+\mathrm{i}v)T} F(T,\sigma)\mathrm{d}T \tag{5.250}$$

$$= \frac{1}{2\pi} \int_0^\infty \mathrm{d}T F(T,\sigma) \int_{-\infty}^{+\infty} \mathrm{d}v \mathrm{e}^{(\gamma+\mathrm{i}v)(t-T)} \tag{5.251}$$

$$= \int_0^\infty \mathrm{d}T F(T,\sigma) \mathrm{e}^{\gamma(t-T)} \delta(t-T) \tag{5.252}$$

$$= F(t,\sigma)h(t) \tag{5.253}$$

$$= F(t,\sigma) \qquad (t > 0 \;\Rightarrow\; h(t) = 1) \tag{5.254}$$

This completes our first check: consistency. Notice we may take ω to be $\mathrm{Re}\omega - \mathrm{i}\epsilon$ to speed up the convergence of the Fourier Integral. In effect, ϵ is γ.

Known Result for $\sigma = 1$

Equation (5.247) gives

$$F(t,1) = \frac{1}{2\pi\mathrm{i}} \int_{\gamma-\mathrm{i}\infty}^{\gamma+\mathrm{i}\infty} \frac{\mathrm{d}s\, \mathrm{e}^{st}}{\left(s + \frac{1}{\tau}\right)} \left[1 + \sum_{n=1}^{\infty} \frac{b^n}{(1+b+bs\tau)_n}\right] \tag{5.255}$$

where $(.)_n$ is the Pochhammer symbol. Thus we have, using partial fractions,

$$F(t,1) = \frac{1}{2\pi\mathrm{i}} \int_{\gamma-\mathrm{i}\infty}^{\gamma+\mathrm{i}\infty} \frac{\mathrm{d}s\, \mathrm{e}^{st}}{\left(s + \frac{1}{\tau}\right)} \times \left[1 + \sum_{n=1}^{\infty} b^n \sum_{r=1}^{n} \frac{\left(\prod_{q=1,q\neq r}^{n} \frac{1}{q-r}\right)}{r+b+bs\tau}\right] \tag{5.256}$$

Using gamma functions, their reflection formula, the Cauchy residue theorem and L'Hôspital's rule, we may show that

$$\prod_{q=1,q\neq r}^{n} \frac{1}{q-r} = \frac{(-1)^{r-1}}{(r-1)!(n-r)!} \tag{5.257}$$

Since there are simple poles on the negative real-s-axis at $s = -1/\tau$ and at

$$s = \frac{-(r+b)}{b\tau} < -\frac{1}{\tau} \qquad (1 \le r \le n) \tag{5.258}$$

it follows that

$$F(t,1) = \mathrm{e}^{-t/\tau} M(1,1,b) + \sum_{n=1}^{\infty} b^n \sum_{r=1}^{n} \frac{\frac{(-1)^{r-1}}{(r-1)!(r-n)!}\mathrm{e}^{-t(r+b)/b\tau}}{b\tau\left(-\frac{r}{b\tau} - \frac{1}{\tau} + \frac{1}{\tau}\right)} \tag{5.259}$$

$$= \mathrm{e}^{b-t/\tau} + \mathrm{e}^{-t/\tau} \sum_{n=1}^{\infty} \frac{b^n}{n!} \sum_{r=1}^{n} {}^{n}c_r \left(-\mathrm{e}^{-\frac{t}{b\tau}}\right)^r \tag{5.260}$$

$$= \mathrm{e}^{b-t/\tau} + \mathrm{e}^{-t/\tau} \sum_{n=1}^{\infty} \frac{b^n}{n!} \left[\left(1 - \mathrm{e}^{-\frac{t}{b\tau}}\right)^n - 1\right] \tag{5.261}$$

$$= \mathrm{e}^{b-\frac{t}{\tau}-b\exp(-t/b\tau)} \tag{5.262}$$

$$= E_{1,1}\left[-\frac{t}{\tau} + b - bE_{1,1}\left(-\frac{t}{b\tau}\right)\right] \tag{5.263}$$

in agreement with [121] and where we define the Mittag–Leffler function by

$$E_{\alpha,\beta}(z) \equiv \sum_{k=0}^{\infty} \frac{z^k}{\Gamma(\beta + \alpha k)} \tag{5.264}$$

([33], chapter 18, (19)), with the understanding that

$$E_{\alpha}(z) \equiv E_{\alpha,1}(z) \tag{5.265}$$

A complex-contour integral representation is given by

$$E_{\alpha,\beta}(z) = \frac{1}{2\pi\mathrm{i}} \int_{-\infty}^{(0+)} \frac{T^{\alpha-\beta}\exp(T)}{(T^{\alpha} - z)} \mathrm{d}T \tag{5.266}$$

which may be derived by using the Hankel transform for the reciprocal of the gamma function. In Appendix B.0.1, we show that an exact but normally divergent asymptotic series, valid for $|z| \gg 1$, is given by

$$E_{\alpha,\beta}(z) \cong -\frac{1}{z} E_{-\alpha,\beta-\alpha}\left(\frac{1}{z}\right) \tag{5.267}$$

The normal usage in asymptotic expansions, such as (5.267), is that one sums up to the smallest term, even if this is just the first term:

$$E_{\alpha,\beta}(z) \underset{|z| \to \infty}{\cong} -\frac{1}{z}\frac{1}{\Gamma(\beta - \alpha)} \tag{5.268}$$

This is an indication of the long-lasting fractal tail of such a function.

5.3.1 Numerical Calculation and Physical Understanding

For $0 \le t \le 2\tau$, we take

$$F(t, \sigma \neq 1) \equiv f_5(t) = \frac{1}{\pi}\left[\int_{-\infty}^{\gamma} \mathrm{d}x\, \mathrm{Im}\, \mathrm{e}^{\mathrm{ut}} \frac{\mathrm{C}-1}{\mathrm{C}} \mathrm{M}(1, 1+\mathrm{BC}, \mathrm{B}) + \int_{0}^{y_0} \mathrm{d}y\, \mathrm{Re}\, \mathrm{e}^{\mathrm{ut}} \frac{\mathrm{C}-1}{\mathrm{C}} \mathrm{M}(1, 1+\mathrm{BC}, \mathrm{B})\right] \tag{5.269}$$

where u is given, respectively, by $u = x - \mathrm{i}y_0$ and $u = \gamma + \mathrm{i}y$. This embraces an infinite rectangular contour with, typically, $\gamma \sim 0.1$ and $y_0 \sim 6.0$, so as to include any poles and the branch cut along the negative real-u-axis, with $\arg u$ assigned to zero on the positive real axis. Of course if $\sigma = 3/2$ then there are two poles at $u = \exp(\pm\pi\mathrm{i}/\sigma)$. We use numerical quadratures for the two integrals in (5.269), based on five-point Lobatto and internal subdivision to reach the required tolerance and accuracy. Typically $\sigma = 2 - \alpha = 1/2$, $\tau = 1.123$, and $\mathrm{Re}\,\omega = 0.1237$.

For $t \ge 2\tau$, we expand the M in (5.247) as an infinite sum over index n:

$$M(1, 1+BC, B) = \sum_{n=0}^{\infty} \frac{B^n}{(1+BC)_n} \tag{5.270}$$

Then we set

$$F(t, \sigma) = f_1 + f_2 + f_{33} + f_4 \tag{5.271}$$

Taking the term $n = 0$, we have ([33])

$$\begin{aligned} f_1 &= \frac{1}{2\pi\mathrm{i}} \int_{-\infty}^{(0+)} \frac{\mathrm{d}u}{u} \frac{\mathrm{e}^{ut}(u\tau)^{\sigma}}{1+(u\tau)^{\sigma}} \\ &= \frac{1}{2\pi\mathrm{i}} \int_{-\infty}^{(0+)} \frac{\mathrm{d}T}{T} \frac{\mathrm{e}^{T} T^{\sigma}}{T^{\sigma} + \left(\frac{t}{\tau}\right)^{\sigma}} \qquad (ut = T) \\ &= E_{\sigma}\left(-\left(\frac{t}{\tau}\right)^{\sigma}\right) \end{aligned} \tag{5.272}$$

$$\underset{t \gg \tau}{\cong} \frac{1}{\sqrt{\pi}} \left(\frac{\tau}{t}\right)^{\sigma} \tag{5.273}$$

The sum over $1 \le n \le \infty$, using partial fractions twice may be written as

$$\sum_{n=1}^{\infty} \frac{1}{2\pi\mathrm{i}} \int_{\gamma-\mathrm{i}\infty}^{\gamma+\mathrm{i}\infty} \frac{\mathrm{d}u}{u} \frac{\mathrm{e}^{ut}}{1+(u\tau)^{-\sigma}} b^n (u\tau)^{(2-2\sigma)n} \sum_{r=1}^{n} \frac{\frac{(-1)^{r-1}}{(r-1)!(n-r)!}}{r + b(u\tau)^{2-2\sigma} + b(u\tau)^{2-\sigma}} \tag{5.274}$$

and we have

$$\frac{1}{(1+(u\tau)^{-\sigma})(r + b(u\tau)^{2-2\sigma} + b(u\tau)^{2-\sigma})} = \frac{1/r}{1+(u\tau)^{-\sigma}} - \frac{\frac{b}{r}(u\tau)^{2-\sigma}}{\{r + b(u\tau)^{2-\sigma} + b(u\tau)^{2-2\sigma}\}} \tag{5.275}$$

The second term in (5.275) gives rise to f_{33} and f_4 of (5.271) while the first term creates

$$f_2 = \sum_{n=1}^{\infty} \frac{b^n}{n!} \sum_{r=1}^{n} {}^{n}c_r(-1)^{r-1} \frac{1}{2\pi \mathrm{i}} \int_{\gamma-\mathrm{i}\infty}^{\gamma+\mathrm{i}\infty} \frac{\mathrm{d}u}{u} \mathrm{e}^{ut} \frac{(u\tau)^{(2-2\sigma)n}}{1+(u\tau)^{-\sigma}} \tag{5.276}$$

$$= \sum_{n=1}^{\infty} \frac{b^n}{n!} \left(\frac{t}{\tau}\right)^{-2(1-\sigma)n} E_{\sigma,1-2(1-\sigma)n)} \left(-\left(\frac{t}{\tau}\right)^{\sigma}\right) \tag{5.277}$$

For $0 < \sigma < 1$, we see immediately why this is divergent for small t. Also, using the representation of the $E_{\alpha,\beta}(z)$ given by (5.264), with dummy summation index k, then for $\sigma = 1/2$ and for even k, the gamma function in the denominator has poles for $k > 2n - 2$. It follows that some care must be exercised in calling the NAG routine *s14aaf*(x, ifail). Regarding the second term in (5.275), we have

$$f_{33} + f_4 = b \sum_{n=1}^{\infty} \frac{b^n}{n!} \sum_{r=1}^{n} \frac{(-n)_r}{r!} \frac{1}{2\pi \mathrm{i}} \int_{\gamma-\mathrm{i}\infty}^{\gamma+\mathrm{i}\infty} \frac{\mathrm{d}u}{u} \frac{\mathrm{e}^{ut}(u\tau)^{(2-2\sigma)n+2-\sigma}}{\{r + b(u\tau)^{2-2\sigma} + b(u\tau)^{2-\sigma}\}} \tag{5.278}$$

For a given r, f_4 is obtained from the contributions of the conjugate pair of poles, which lie in the second and third quadrants of the u-plane. For $\sigma = 1/2$, say, a third pole lies on the next sheet ($\arg(u\tau) = \pm 2\pi \mathrm{i}$) and is inaccessible. Collapsing the contour in (5.278) onto the upper and lower lips of the branch cut along the negative real-u-axis, we have, since for $0 < \sigma < 1$, there are no poles on this line (unlike the $\sigma = 1$ case; see Section 5.3),

$$f_{33} = b \sum_{n=1}^{\infty} \frac{b^n}{n!} \sum_{r=1}^{n} \frac{(-n)_r}{r!} \frac{1}{2\pi \mathrm{i}} \int_{-\infty}^{(0+)} \frac{\mathrm{d}u}{u} \frac{\mathrm{e}^{ut}(u\tau)^{(2-2\sigma)n+2-\sigma}}{\{r + b(u\tau)^{2-2\sigma} + b(u\tau)^{2-\sigma}\}} \tag{5.279}$$

$$= \frac{b\tau^{2-\sigma}}{\pi} \int_0^{\infty} \mathrm{d}v \mathrm{e}^{-vt} v^{1-\sigma} \sum_{n=1}^{\infty} \frac{b^n}{n!} \tau^{2(1-\sigma)n} v^{2n(1-\sigma)}$$

$$\times \sum_{r=1}^{n} \frac{(-n)_r}{r!} \mathrm{Im} \frac{\mathrm{e}^{-(2n+1)\sigma\pi\mathrm{i}}}{[\mathrm{r} + \mathrm{b}(v\tau)^{2-\sigma}\mathrm{e}^{-\mathrm{i}\pi\sigma} + \mathrm{b}(v\tau)^{2-2\sigma}\mathrm{e}^{-2\mathrm{i}\pi\sigma}]} \tag{5.280}$$

where we have set $u = v\mathrm{e}^{\mathrm{i}\pi}$ on the upper lip and $u = v\mathrm{e}^{-\mathrm{i}\pi}$ on the lower. Once again the v-quadrature is performed using five-point Lobatto plus interval subdivision. Equation (5.279) could be expressed in terms of generalizations of the Mittag–Leffler functions, namely Wright functions ([33], section 18.1, p. 211, eq. (27)). However, this would not be numerically useful since the use of the binomial series on expansion of the denominator leads to divergence.

The conjugate pair of simple poles of the integrand in (5.278) is given by $z_\infty(r)$ and $z_\infty^*(r)$. Either is obtained iteratively using complex Newton–Raphson:

$$z_{n+1} = z_n - \frac{f(z_n)}{f'(z_n)} \tag{5.281}$$

where

$$f(z) \equiv \frac{r}{b} + z^{2-2\sigma} + z^{2-\sigma} \tag{5.282}$$

It was observed that $|\mathrm{Im} z_\infty(\mathrm{r})| < 6$ so that f_5 is consistent (for $0 \le t \le 2\tau$) and we have

$$f_4 = 2\tau \sum_{n=1}^{\infty} \frac{b^n}{n!} \sum_{r=1}^{n} \frac{(-n)_r}{r!} \mathrm{Re} \frac{e^{\frac{t}{\tau} z_\infty(\mathrm{r})} \{z_\infty(\mathrm{r})\}^{2(1-\sigma)n+\sigma}}{[(2-\sigma)\{z_\infty(\mathrm{r})\}^\sigma + 2(1-\sigma)]} \tag{5.283}$$

Clearly $z_\infty(r)$ and $z_\infty^*(r)$ are interchangeable in (5.283). In Figure 5.6, we present sample zeros of $f(z)$ in the second quadrant of the z-plane, where $z = u\tau$. Clearly they lie on a curve, which is very nearly a straight line.

Returning to (5.247) and (5.248), we calculate

$$\text{result } 1 = \frac{M(1, 1 + BC, B)}{1 + (\mathrm{i}\tau\omega)^{-\sigma}} \tag{5.284}$$

where B and C are given by (5.240) and (5.241) and

$$\text{result } 2 = \mathrm{i}\omega \int_0^\infty e^{-\mathrm{i}\omega t} F(t, \sigma) \mathrm{d}t \tag{5.285}$$

In Table 5.1, we present results 1 and 2 for $\sigma = 1/2$, $\tau = 1.123$, and $\mathrm{Re}\,\omega = 0.1237$. The $\mathrm{Im}\,\omega$ is given by ϵ. Clearly the results agree correct to three significant figures except for $\epsilon = -0.0$. For $0 \le t \le 2\tau$, we use $F(t, \sigma) = f(5)$ and for $2\tau \le t$, $F(t, \sigma) = f_1 + f_2 + f_{33} + f_4$. Because of the aymptotic property of the Mittag–Leffler functions, f_1 and f_2 fall off very slowly. Pragmatically, we took $t_{\max} \approx 500,000$ ($\epsilon = 0.0$) and took the first term of the asymptotic expansion (5.267) for f_1 for $t > 30$ and for f_2 for $t > 15$. Meanwhile both f_{33} and f_4 die off fairly quickly. For $0 \le t \le 2\tau$, we used f_5, since f_2 diverges.

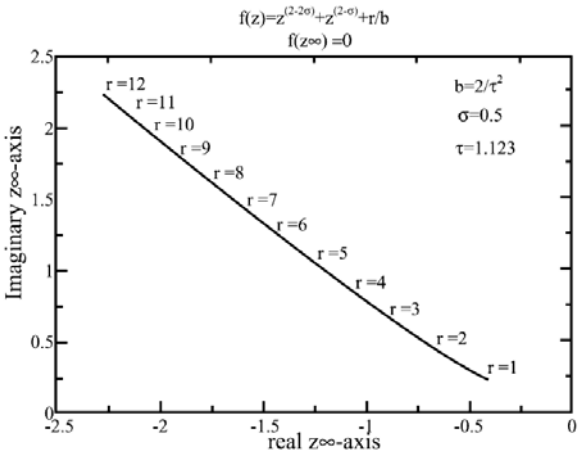

Fig. 5.6. We plot the complex zeros z of $f(z)$ as a function of $\mathrm{Re}\, z\infty$ and $\mathrm{Im}\, z\infty$ and of r, where $f(z)$, as a function of the integer r, is defined by (5.282). The values of b, s, and τ are inset

Table 5.1. For specimen numerical values of $\epsilon = \mathrm{Im}\,\omega$, $\sigma = 1/2$, and $r = 1.123$, we tabulate results 1 and 2, corresponding to (5.284) and (5.285)

ϵ	Result 1	Result 2
(a) -0.1	(0.3278, 0.1581)	(0.3278, 0.1585)
(b) -0.2	(0.4284, 0.1198)	(0.4285, 0.1193)
(c) -0.3	(0.5102, 0.0945)	(0.5100, 0.0940)
(d) -0.4	(0.2158, 0.2186)	(0.2156, 0.2143)

In conclusion, we find that our analysis is robust and reliable, but the theory of Mittag–Leffler functions requires numerical reinforcement, including the location of poles of the integrand.

In the case of $\sigma = 1/2$, our main consideration in this book, we have

$$ut + b(u\tau)^{2-2\sigma} = u(t + b\tau) \tag{5.286}$$

so that

$$f_1 + f_2 = f_{12} \equiv E_{\frac{1}{2},1}\left(-\left(\frac{t+b\tau}{\tau}\right)^{1/2}\right) \equiv \left(\frac{\tau}{t+b\tau}\right)^{1/2} E_{-\frac{1}{2},\frac{1}{2}}\left(-\left(\frac{\tau}{t+b\tau}\right)^{1/2}\right) \tag{5.287}$$

which provides an independent check on the work.

5.4 Nonlinear Response of Permanent Dipoles and After Effects

It is shown [144] how the existing theory of the dynamic Kerr effect and nonlinear dielectric relaxation based on the noninertial Brownian rotation of noninteracting rigid dipolar particles may be generalized to take into account interparticle interactions using the Maier–Saupe mean-field potential. The results available in simple closed form suggest that the frequency dependent nonlinear response provides a new method of measuring the Kramers escape rate (or the longest relaxation time). Similar considerations apply to the analogous problem of magnetic relaxation of fine single-domain ferromagnetic particles and their super-paramagnetic relaxation time.

The dielectric relaxation of assemblies of polar molecules with each constituent dipole having permanent electric moment $\boldsymbol{\mu}$ is usually studied by means of two apparently distinct models of the process. The first model is due to Debye [206], where the molecules are subject only to an external time-dependent applied field $\mathbf{E}(t)$ and thermal interactions with the surrounding heat bath. Here the molecules are very tightly bound to the bath (corresponding to large dissipative coupling meaning *inter alia* that the inertia of the molecule is ignored) so that orientation can only take place via the small-angle jumps characteristic of the Brownian motion. The underlying theory based on the Fokker–Planck equation is Einstein's treatment [239], [142] of the noninertial translational Brownian motion of a free particle as adapted to the orientational random walk of the tip of a typical dipole vector on the surface of the

unit sphere. The Fokker–Planck equation in this instance where inertial effects are ignored is known is the Smoluchowski equation. The same result may also be obtained from the Langevin equation for the time evolution of the dipole moment by averaging that equation over its realisations as shown in [142]. Such a model in the linear response approximation in the parameter ξ [which is the ratio of the applied field energy (Zeeman energy) to the thermal energy] always leads to a phase lag of the dipole moment in relation to the phase of the applied field leading to anomalous dispersion and absorption at microwave frequencies [206].

Similar considerations apply to a ferrofluid composed of a colloidal suspension of single-domain ferromagnetic particles [502], where the solid-state-like or Néel mechanism of orientation over the magnetocrystalline anisotropy barrier inside the particle is blocked. Thus the only possible mechanism of orientation is physical rotation of the single-domain ferrofluid particle. The sizes (in a real fluid there is always a distribution of sizes) of the particles, however, are now such that the magnetic susceptibility exhibits dissipative behavior in the low radio-frequency band. The Debye theory is expected to provide a better description of this magnetic dipole orientation process rather than electric dipole orientation due to the large average size of the ferrofluid particles so that they are true Brownian particles. In both cases the orientational behavior of the dipoles is described by the average of the dipole moment over its realisations.

The second model of dipolar orientation described by Debye [206] and much expanded upon by Fröhlich [142], [281], [139] is where a (rare) *energetic* dipole of the population in a potential well in a solid may relax by crossing, due to the shuttling action of the Brownian motion, the internal potential barriers in the solid. The model was also suggested by Néel [448] as an explanation of the magnetic (Néel) relaxation of unblocked single-domain ferromagnetic particles over their internal magnetocrystalline anisotropy barrier. In this magnetic mechanism the inertia of the particle of course plays no role.

The original approach of Debye followed a rate equation treatment combined with a discrete orientation approximation for a typical barrier crossing dipole whereby the dipole is either in a 0- or 180-degree orientation. Moreover, the Arrhenius law corresponding to transition-state theory as initiated by Eyring and later investigators was assumed for the rate of crossing over the potential barrier [79], [318]. Thus the time to cross the potential barrier is exponentially long. The model was later treated in the context of Néel relaxation by Brown [91] using the Einstein theory as modified for rotation to include a magnetocrystalline anisotropy potential and an external field potential. He took the underlying Langevin equation as the Larmor equation augmented by stochastic terms comprising a frictional retarding torque superimposed on which is a rapidly fluctuating (white noise) driving torque. This equation without the rapidly fluctuating noise term is usually known as the Landau–Lifshitz equation, yet another form of it is known as Gilbert's equation [142]. Thus Brown was able to write the exact Fokker–Planck equation for the density of magnetic moment orientations as in Einstein's theory. Brown's treatment, because it is based on a rotational diffusion equation, is no longer confined to the discrete-orientation approximation. Thus it has the merit that both orientation inside the wells of the potential and over-

barrier reorientation may be treated simultaneously. Moreover, the overbarrier relaxation process could be set firmly in the context of the theory of stochastic processes as formulated by Einstein, Smoluchowski, Langevin, Kramers, etc. [406] based on kinetic and stochastic differential equations. In particular, the Kramers [142], [318], [367] treatment of escape of particles over potential barriers as adapted to rotation could be used to obtain an asymptotic expression for the greatest relaxation time or time for a dipole to escape its potential well. Essentially the same model was used by Martin et al. [403] to study the orientational behavior of nematic liquid crystals in the high dissipative coupling limit where the inertia of the molecules can be ignored. Indeed, in most respects the theory of orientational behavior of nematics is a replica of the theory of magnetic relaxation over the magnetocrystalline anisotropy barrier of single-domain ferromagnetic particles. However, one should recall [142] that in Néel relaxation the Fokker–Planck equation for the density of magnetic moment orientations is *exact*, while in dielectric and ferrofluid relaxation, which involves physical rotation of the particles, the inertia is ignored leading to the *approximate* Smoluchowski equation. It is the purpose of this section to indicate how simple analytical formulae for the linear dielectric response and the dynamic Kerr effect response may be obtained for relaxation in a mean-field potential thus extending the existing Debye theory of dielectric and Kerr effect relaxation to relaxation in the presence of a mean field. In order to accomplish this we briefly describe the two principal models of dielectric relaxation, namely an assembly of noninteracting dipoles and an assembly of dipoles that may relax by crossing over a potential barrier.

5.4.1 Complex Susceptibility for the Debye and Debye-Fröhlich Models of Relaxation

The most important result of the original Debye model is that the mean electric dipole moment of a spherical assembly of N noninteracting dipoles with ϑ the polar (colatitude) angle of a typical dipole subjected to a field $\mathbf{E}(t) = \mathrm{Re}\left(\mathbf{E}_\mathrm{m}\mathrm{e}^{\mathrm{i}\omega t}\right)$ is given (in linear response) by

$$N\mu\langle\cos\vartheta\rangle_E(t) = \frac{N\mu^2}{3kT}\mathrm{Re}\left[\frac{\mathrm{E}_\mathrm{m}\mathrm{e}^{\mathrm{i}\omega t}}{1+\mathrm{i}\omega\tau_\mathrm{D}}\right] \tag{5.288}$$

Here $\tau_D = \zeta/(2kT)$ is the Debye relaxation (free rotational Brownian diffusion) time, and ζ is the viscous drag coefficient of a rotating dipole. The subscript E indicates that the average is taken in the presence of $E(t)$. In terms of the complex dielectric susceptibility $\chi(\omega) = \chi'(\omega) - \mathrm{i}\chi''(\omega)$, (5.288) may be written as

$$\chi(\omega) = \frac{\chi'(0)}{1+\mathrm{i}\omega\tau_D} \tag{5.289}$$

where $\chi'(0) = N\mu^2/(3kT)$ is the static susceptibility.

We may illustrate the second Debye model (or Debye–Fröhlich model for a continuous distribution of orientations) by considering dielectric relaxation in a

bistable potential representing the simplest uniaxial potential of the crystalline anisotropy [142], [403], viz.

$$V(\vartheta) = K \sin^2 \vartheta \tag{5.290}$$

where K is the anisotropy constant. Here the complex dielectric susceptibility is given by [142], [403]

$$\frac{\chi(\omega)}{\chi'(0)} = \sum_{k=1}^{\infty} \frac{\Delta_k}{1 + \mathrm{i}\omega/\lambda_k} \tag{5.291}$$

where the static susceptibility $\chi'(0)$ is defined as

$$\chi'(0) = \frac{N\mu^2}{3kT} (2\langle P_2 \rangle_0 + 1)$$

$\langle P_2 \rangle_0$ denotes the equilibrium average of the Legendre polynomial of order 2 in the absence of the applied field so that

$$\langle P_2 \rangle_0 = Z^{-1} \int_{-1}^{1} \mathrm{e}^{\sigma x^2} P_2(x) \mathrm{d}x \tag{5.292}$$

$Z = \int_{-1}^{1} \mathrm{e}^{\sigma x^2} \mathrm{d}x$ is the partition function, and $\sigma = K/(kT)$ is the dimensionless anisotropy constant. Here λ_k are the eigenvalues of the governing Fokker–Planck operator L_{FP}. The smallest nonvanishing eigenvalue λ_1 is associated with the slowest (overbarrier) relaxation mode. In the high barrier limit λ_1 may be approximated by the very high damping Kramers escape rate [142]. (We remark that in the application of the present model to single-domain ferromagnetic particles the anisotropy constant must be written in terms of the *magnetic* volume v_m of the particle [558], the magnetic moment is defined as $\mathbf{m} = \mathbf{M}(t)v_m$, where $\mathbf{M}$ is the magnetization, so that K must be redefined as the anisotropy constant per unit volume, that is $K \to K/v_m$.) Thus both solid-state-like and liquid-like relaxation models essentially have the *same* behaviour. However, for high barriers the longest relaxation times $\tau = 1/\lambda_1$ and the Debye relaxation time τ_D for isotropic diffusion *diverge* exponentially from each other.

Now, as demonstrated in [142], the spectra of $\chi(\omega)$ in (5.291) can be accurately described at all frequencies by a sum of two Lorentzians only, viz. [142], [348]

$$\frac{\chi(\omega)}{\chi'(0)} = \frac{\Delta_1}{1 + \mathrm{i}\omega/\lambda_1} + \frac{1 - \Delta_1}{1 + \mathrm{i}\omega\tau_W^{(1)}} \tag{5.293}$$

The two decay modes with relaxation times λ_1^{-1} and $\tau_W^{(1)}$ pertain respectively to the slow overbarrier (interwell) mode and a single (intrawell) mode representing the contribution of the infinity of the near degenerate decay modes inside the wells to the overall decay process. The first term in (5.293) is the overbarrier decay mode and λ_1 is the smallest nonvanishing eigenvalue of the Smoluchowski (Fokker–Planck) equation associated with the process. The intrawell relaxation time $\tau_W^{(1)}$ and the dimensionless parameter Δ_1 are determined [142], [143], [348] (see Appendix C) using

general (Tauberian) properties of the Fourier integral [599] from the asymptotic behaviour of the complex susceptibility at low and high frequencies.

In the high barrier limit, $\sigma \gg 1$, the most important case, the behavior of $\tau_W^{(1)}$ and Δ_1 is as follows [143] (see Appendix C): $\Delta_1 \approx 1 - \sigma^{-2}$ and $\tau_W^{(1)} \approx \tau_D/(2\sigma)$. Furthermore, from the Kramers theory of escape of particles over potential barriers, due to the shuttling action of the Brownian motion (as adapted to rotation [142], [91])

$$\lambda_1^{-1} \cong \tau \cong \tau_D \frac{\sqrt{\pi}}{2} \sigma^{-3/2} \mathrm{e}^{\sigma} , \quad \sigma \gg 1 \tag{5.294}$$

At low frequencies, $\omega/\lambda_1 \leq 1$, where the contribution of the second term is negligible, (5.293) can be further simplified to yield

$$\frac{\chi(\omega)}{\chi'(0)} = \frac{\Delta_1}{1 + \mathrm{i}\omega/\lambda_1} + 1 - \Delta_1 \tag{5.295}$$

Note that in dielectric relaxation this result, as is consistent with the Smoluchowski equation, holds only in the limit of very high dissipative coupling to the bath. In Néel relaxation on the other hand, (5.294) is *valid for all values of the dissipative coupling*. Here the underlying one-dimensional Fokker–Planck equation in the coordinate ϑ, arises from the symmetry of the problem as the gyromagnetic term drops out and not from the neglect of inertia and is *exact*, unlike the *approximate* Smoluchowski equation of the dielectric case. We remark that (5.293) may be obtained using the linear response theory equation [142]

$$\chi(\omega)/\chi'(0) = -\int_0^{\infty} \dot{\Phi}_{1,1}(t)\mathrm{d}t = 1 - \mathrm{i}\omega \int_0^{\infty} \Phi_{1,1}(t)\mathrm{e}^{-\mathrm{i}\omega t}\mathrm{d}t \tag{5.296}$$

by supposing that the equilibrium correlation function

$$\Phi_{1,1}(t) = \langle \cos\vartheta(0) \cos\vartheta(t)\rangle_0 / \langle \cos^2\vartheta(0)\rangle_0$$

(the subscript zero again denoting equilibrium averages) of the dipole moment as rendered by the after-effect solution (comprising an infinity of decaying exponentials) of the rotational Smoluchowski equation may be approximated by two exponentials only.

Finally for the purpose of practical calculations, if one is interested in all values of σ, λ_1 may be written as the simple empirical equation ([142], eq. (7.4.2.38)])

$$\lambda_1 \cong \frac{\sigma}{\tau_D\,(\mathrm{e}^{\sigma} - 1)} \left(2^{-\sigma} + \frac{2\sigma^{3/2}}{\sqrt{\pi}(1 + \sigma)} \right) \tag{5.297}$$

The foregoing results apart from λ_1^{-1} all apply to $\langle P_1 \cos\vartheta\rangle_E(t)$, namely the dipole moment in the linear approximation. Thus the relaxation in a symmetric mean-field potential is essentially similar to the relaxation in the absence of the potential; however, the corresponding relaxation times and static susceptibilities are altered.

5.4.2 Linear Dielectric Response

Referring to dielectric relaxation the cornerstone of all these calculations is the rotational diffusion or Smoluchowski (Fokker–Planck) equation for the density $W(\boldsymbol{\mu}, t)$ of orientations of dipoles $\boldsymbol{\mu}$ on the surface of the unit sphere:

$$\frac{\partial W}{\partial t} = [L_{FP} + L_{ext}(t)]\, W \tag{5.298}$$

where

$$L_{FP}W = \frac{1}{2\tau_D}\left[\nabla^2 W + \beta\nabla\cdot(W\nabla V)\right] \quad \text{and} \quad L_{ext}W = \frac{1}{2\tau_D}\beta\nabla\cdots(W\nabla V_{ext})$$

are the unperturbed Fokker–Planck operator and the external field operator, respectively. $\beta = (kT)^{-1}$, $V_{ext} = -\mu E(t)\cos\vartheta$, and V is given by (5.290). In our problem, the differential operator ∇ (the gradient on the surface of the unit sphere) contains only the polar angle ϑ due to the axially symmetric form of the potential.

Expansion of W in the basis of the Legendre polynomials $\{P_n\}$ and making use of their recurrence and orthogonality properties leads to the representation of the relaxation problem as the solution of the set of differential recurrence relations [142], [212] for the observables $f_n(t)$

$$\tau_D \dot{f}_n(t) + c_n f_{n-2}(t) + d_n f_n(t) + g_n f_n(t) = \xi(t) a_n [f_{n-1}(t) - f_{n+1}(t)] \tag{5.299}$$

where $\xi(t) = \beta\mu E(t)$, $f_n = \langle P_n \cos\vartheta\rangle(t) = 0$ for $n < 0$ and

$$a_n = \frac{n(n+1)}{2(2n+1)}, \qquad c_n = \frac{\sigma(n-1)n(n+1)}{(2n-1)(2n+1)}$$

$$d_n = \frac{n(n+1)}{2}\left(1 - \frac{2\sigma}{(2n-1)(2n+3)}\right), \qquad g_n = -\frac{\sigma n(n+1)(n+2)}{(2n+1)(2n+3)}$$

Equation (5.299) governs the exact solution of the problem. The exact solution of (5.299) can be obtained numerically using matrix continued fractions [212]. However, such a method precludes analytic formulae for the response. In order to obtain analytic formulae, one must reduce the five-term recurrence (5.299) to a driven three-term one. This is accomplished by treating the external field as a perturbation. As a first step we are only interested in solutions (the linear response) to first order in ξ. Hence in the general perturbation theory approximation viz.,

$$f_n(t) = f_n^{(0)} + f_n^{(1)}(t) + f_n^{(2)}(t) + f_n^{(3)}(t) + \cdots \tag{5.300}$$

with the superscripts denoting the relevant order in $E(t)$ we have for the observables in the mth order of perturbation theory

$$\tau_D \frac{\mathrm{d}}{\mathrm{d}t} f_n^{(m)}(t) + c_n f_{n-2}^{(m)}(t) + d_n f_n^{(m)}(t) + g_n f_{n+2}^{(m)}(t) = \xi(t) a_n \left[f_{n-1}^{(m-1)}(t) - f_{n+1}^{m-1}(t)\right] \tag{5.301}$$

Equation (5.301) for $m = 1$ can be written in the matrix form (Heisenberg-like representation)

$$\frac{\mathrm{d}}{\mathrm{d}t}\mathbf{f}^{(1)}(t) = \mathbf{L}_{FP}\mathbf{f}^{(1)}(t) + \mathbf{B}_0\mathbf{f}^{(0)}\xi(t) \tag{5.302}$$

where matrices $\mathbf{L}_{FP}$, $\mathbf{B}_0$, and the vectors $\mathbf{f}^{(1)}(t)$, $\mathbf{f}^{(0)}$ are defined as follows:

$$\mathbf{L}_{FP} = -\frac{1}{\tau_D}\begin{pmatrix} d_1 & 0 & g_1 & 0 & 0 & \cdots \\ 0 & d_2 & 0 & g_2 & 0 & \cdots \\ c_3 & 0 & g_3 & 0 & g_3 & \cdots \\ \vdots & \vdots & \vdots & \vdots & \vdots & \ddots \end{pmatrix} \tag{5.303}$$

$$\mathbf{B}_0 = \frac{1}{\tau_D}\begin{pmatrix} a_1 & 0 & -a_1 & 0 & 0 & 0 & \cdots \\ 0 & a_2 & 0 & -a_2 & 0 & 0 & \cdots \\ 0 & 0 & a_3 & 0 & -a_3 & 0 & \cdots \\ 0 & 0 & 0 & a_4 & 0 & -a_4 & \cdots \\ \vdots & \vdots & \vdots & \vdots & \vdots & \vdots & \ddots \end{pmatrix} \tag{5.304}$$

$$\mathbf{f}^{(1)}(t) = \begin{pmatrix} f_1^{(1}(t) \\ f_2(1)(t) \\ \vdots \end{pmatrix}, \quad \mathbf{f}^{(0)} = \begin{pmatrix} f_0^{(0)} \\ f_1(0) \\ f_2^{(0)} \\ \vdots \end{pmatrix} \tag{5.305}$$

The matrix elements of the column vector $\mathbf{f}^{(0)}$ obtained from the stationary solution in the absence of the probing field are the equilibrium ensemble averages of the Legendre polynomials. They may be calculated either from the equilibrium Maxwell–Boltzmann distribution in the absence of the ac field or by solving the time-independent version of (5.299) by continued fractions again in the absence of the driving field [142]. We remark that in the linear response only the Legendre polynomial averages of *odd* order occur in the response column vector $\mathbf{f}^{(1)}(t)$. On the other hand only the Legendre polynomial averages of *even* order contribute to the initial-value vector $\mathbf{f}^{(0)}$ in the driving-force term as only these differ from zero in the absence of an external field. These facts account for our definition of the driving-force matrix $\mathbf{B}_0$. A stationary solution of (5.302) is given by

$$\mathbf{f}^{(1)}(t) = \int_{-\infty}^{t} \exp\left[\mathbf{L}_{FP}(t-t')\right]\mathbf{B}_0\mathbf{f}^{(0)}\xi(t')\mathrm{d}t' \tag{5.306}$$

in the time domain. (For the steady-state ac response we assume stationary conditions, i.e., the ac field had been applied in the *infinite* past, hence all transient effects due to the sudden imposition of the ac field are ignored). This solution for a sinusoidal normalized driving field $\xi(t) = \xi_m \mathrm{e}^{\mathrm{i}\omega t}$ yields

$$\mathbf{f}^{(1)}(t) = \xi_m \mathrm{Re}\left[\chi(\omega)\mathbf{B}_0\mathbf{f}^{(0)}\mathrm{e}^{\mathrm{i}\omega t}\right] \tag{5.307}$$

where

$$\chi(\omega) = [\mathrm{i}\omega\mathbf{I} - \mathbf{L}_{FP}]^{-1} \tag{5.308}$$

is the one-sided Fourier transform of the transition matrix $\exp \mathbf{L}_{FP}t$, which is the Green function of the unperturbed Fokker–Planck equation [(5.298) with $\mathbf{L}_{ext} = 0$]

as originally suggested by Morita [438]; **I** is the unit matrix. Note that for $\sigma = 0$, $\mathbf{L}_{FP}$ is a pure diagonal matrix implying that the transition matrix is also purely diagonal, thus in the first Debye model *all* the matrix elements of $\mathbf{f}^{(1)}(t)$ *decouple* from each other. Extraction of the matrix element $f_1^{(1)}(t)$, or in practice its Fourier transform, yields the exact linear electric dipole orientation response [142]. This may also be accomplished using continued fraction methods [143] (see Appendix A and C).

5.4.3 Dynamic Kerr Effect

The quantities of interest in the present investigation are the *dynamic Kerr effect* and the *nonlinear dielectric effect*. These are, respectively, the response of the second Legendre polynomial (which always depends on the first approximation on the square of the applied field and so is inherently a nonlinear effect). The nonlinear dielectric effect is the cubic correction in the applied field to $\langle P_1 \cos\vartheta\rangle_E(t)$. The most important part to note about these two responses is that they are *nonlinear* thus no *unique* response function exists like (5.296) and the *response will always depend on the form of the stimulus*. The exact quadratic stationary solution for an arbitrary stationary stimulus is obtained as follows. Setting $m = 2$ in (5.301) and discarding all higher-order $f^{(m)}$ yields the stationary solution

$$\mathbf{f}^{(2)}(t) = \int_{-\infty}^{t} \exp\left[\mathbf{L}_{FP}(t-t')\right] \mathbf{B}\mathbf{f}^{(1)}(t')\xi(t')\mathrm{d}t' \tag{5.309}$$

where the driving force matrix **B** is now given by

$$\mathbf{B} = \frac{1}{\tau_D}\begin{pmatrix} 0 & -a_1 & 0 & 0 & \cdots \\ a_2 & 0 & -a_2 & 0 & \cdots \\ 0 & a_3 & 0 & -a_3 & \cdots \\ \vdots & \vdots & \vdots & \vdots & \ddots \end{pmatrix} \tag{5.310}$$

We remark that **B** differs from $\mathbf{B}_0$, (5.304), because $\mathbf{B}_0$ must operate on a vector containing $f_0^{(0)}$. Note that for higher-order responses $\mathbf{f}^{(m)}(t)$ one will always have **B** as the driving-force matrix. Substitution of the linear response solution $\mathbf{f}^{(1)}(t)$ from (5.306) into (5.309) yields

$$\begin{aligned}\mathbf{f}^{(2)}(t) = \int_{-\infty}^{t} \mathrm{d}t' \int_{-\infty}^{t'} \mathrm{d}t'' \exp\left[\mathbf{L}_{FP}(t-t')\right] \mathbf{B} \exp\left[\mathbf{L}_{FP}(t'-t'')\right] \\ \times \mathbf{B}_0\mathbf{f}^{(0)}(t')\xi(t')\xi(t'')\end{aligned} \tag{5.311}$$

The foregoing expression is the exact quadratic stationary Kerr effect response solution for a driving force, which may be expanded in a time Fourier series so that the two-sided Fourier transform exists. It is a generalization of the corresponding scalar result of Coffey and Paranjape [122] for noninteracting dipoles.

We remark that unlike the linear response, the odd and even time-dependent differential recurrence relations for the Legendre polynomial averages now *entangle*

as is predicted by the general nonperturbative solution, (5.299), which constitutes a five-term differential recurrence relation reducible to a matrix three-term recurrence relation. Equation (5.311) for arbitrary $\xi(t)$ has frequency domain representation as the convolution denoted by

$$\mathbf{F}^{(2)}(\omega) = \chi(\omega)\left\{\mathbf{B}\left[\chi(\omega)\mathbf{B}_0\mathbf{f}^{(0)}\xi_\omega\right] * \xi_\omega\right\} \tag{5.312}$$

For a driving field $\xi(t) = \xi_m \cos\omega_0 t$, we again have the time response in terms of the transition matrix (complex susceptibility matrix)

$$\mathbf{f}^{(2)}(t) = \frac{\xi_m^2}{2}\mathrm{Re}\left[\left(\chi(0) + \chi(2\omega_0)\mathrm{e}^{2\mathrm{i}\omega_0 \mathrm{t}}\right)\mathbf{B}\chi(\omega_0)\mathbf{B}_0\mathbf{f}^{(0)}\right] \tag{5.313}$$

The second-order solution for a single sinusoid demonstrates that the quadratic response vector consists of a frequency-dependent dc term superimposed on which is the second harmonic of the applied field. Thus the response is characteristically nonlinear as the form of the input stimulus is not reproduced (*the response depends on the precise form of the stimulus*). Such behavior, although illustrated for a single sinusoidal driving field, also carries over to any Fourier coefficient of an arbitrary periodic driving field, which may be expanded in a Fourier series. In this case, however, due to the square law characteristic of the response, cross terms involving sum and difference frequencies will also appear due to the nonlinear nature of the response. The frequency components present in the response for given ξ may always be inferred from the general square law characteristic $b\xi^2$. We further remark that *each* term of the linear response drives the Kerr effect response so that in general in order to calculate the Kerr effect response one requires *all* the matrix elements of the linear susceptibility column vector $f_n^{(1)}(t)$ with the exception of the first Debye model where all the matrix elements decouple from each other. The calculation of the second-order response may also be accomplished [143], [329] using continued fraction methods (see Appendix A and C).

5.4.4 Nonlinear Dielectric Relaxation

Just as in (5.311), we have for the third-order nonlinear dielectric effect

$$\begin{aligned}\mathbf{f}^3(t) = \int_{-\infty}^{t}\int_{-\infty}^{t'}\int_{-\infty}^{t''} &\exp\left[\mathbf{L}_{FP}(t-t')\right]\mathbf{B}\exp\left[\mathbf{L}_{FP}(t'-t'')\right] \\ &\times \mathbf{B}\exp\left[\mathbf{L}_{FP}(t''-t''')\right]\mathbf{B}_0\mathbf{f}^{(0)}(t')\xi(t')\xi(t'')\xi(t''')\mathrm{d}t'\mathrm{d}t''\mathrm{d}t'''\end{aligned} \tag{5.314}$$

Clearly, the mth order response can be written as an $(m-1)$-fold convolution. We remark that the nonlinear responses of odd order, namely $\mathbf{f}^{(3)}(t)$, $\mathbf{f}^{(5)}(t)$, etc., are also important in relaxation of the magnetic moment inside a single-domain ferromagnetic particle (Néel relaxation) because the Zeeman energy parameter is large enough in single-domain ferromagnetic particles to render the nonlinear susceptibilities significant [504]. For a cosinusoidal driving field $\xi(t) = \xi_m \cos\omega_0 t$, (5.314) yields

$$\mathbf{f}^{(3)}(t) = \frac{\xi^3}{4}\mathrm{Re}\,\{[(2\chi(\omega_0)\mathbf{B}\chi(0)\mathbf{B}\chi^*(\omega_0) + \chi(\omega_0)\mathbf{B}\chi(2\omega_0) \times\mathbf{B}\chi(\omega_0))\,\mathrm{e}^{-\mathrm{i}\omega_0 t} + \chi(3\omega_0)\mathbf{B}\chi(2\omega_0)\mathbf{B}\chi(\omega_0)\mathrm{e}^{-3\mathrm{i}\omega_0 t}]\,\mathbf{B}_0\mathbf{f}^{(0)}\} \tag{5.315}$$

Thus the third-order response to a pure sinusoid consists of a term at the fundamental frequency and the third harmonic term. The term at the fundamental frequency, which is more complicated than in the linear response, represents a cubic correction to the response at the fundamental frequency. Clearly the nonlinear dielectric relaxation acts as an odd harmonic generator just as the Kerr effect response acts as an even harmonic generator. Again sum and difference terms at the fundamental and third harmonic frequencies will appear in the response if a complex wave is applied. The behaviour of the dipole moment including linear response is in accordance with the response characteristic $b_1\xi + b_3\xi^3$. Equation (5.313) and (5.315) are purely formal *sui generis*; they cannot yield closed-form solutions for the response except in the particularly simple case of zero mean field potential and so are virtually useless for the purpose of comparison with experiment.

5.4.5 Approximate Analytical Formula for the Dynamic Kerr Effect for a Pure Cosinusoid

We have illustrated for the linear response [143] (see Appendix C) how the analytical equations (5.293) and (5.295) provide a good approximate to the exact solution. We now illustrate how a similar simple approximate closed-form solution may be obtained for the Kerr effect response.

The results of the investigation of the dynamic Kerr effect may be summarized as follows. For noninteracting dipoles, where all the system matrices are diagonal, Peterlin and Stuart [488], Benoit [65], [66], and Coffey and Paranjape [122] using the scalar version of (5.311) have shown that the exact quadratic response of the Legendre polynomial of order 2 for a driving field of the form $\mathbf{E}_m\cos\omega t = \mathrm{Re}\left(\mathbf{E}_\mathrm{m}\mathrm{e}^{\mathrm{i}\omega t}\right)$ is given by

$$\langle P_2(\cos\vartheta)\rangle_E(t) = \frac{\xi_m^2}{30}\left[\frac{1}{1+\omega^2\tau_D^2} + \frac{\cos(2\omega t-\varphi_2)}{(1+\omega^2\tau_D^2)^{1/2}(1+4\omega^2\tau_D^2/9)^{1/2}}\right] \tag{5.316}$$

where $\varphi_2 = \tan^{-1}\left[5\omega\tau_D(3-2\omega^2\tau_D^2)^{-1}\right]$. Equation (5.316) describes the exact quadratic dynamic Kerr effect for a pure cosinusoid for *noninteracting dipoles* and is the generalization of Debye's first model to the response of the Legendre polynomial of order 2. We remark that, as indicated by (5.316), the approximate solution [in accordance with the general solution (A.4)] consists of a frequency-dependent dc term superimposed on which is the second harmonic of the applied field. The behaviour is reminiscent of a rectifier or detector. We emphasise that the appearance of both these terms is indicative of the *nonlinear* nature of the Kerr effect response for permanent dipoles. The frequency-dependent dc term appears to have first been noted by Rocard [513] in his pioneering investigations of the role of inertial effect in dielectric relaxation.

In the present investigation, as far as relaxation in the mean-field potential of (5.290) is concerned, it may be shown [143] (see Appendix C) that the second-order response to an ac field of the form of (5.316) may be accurately represented by the simple analytic formula

$$\langle P_2(\cos\vartheta)\rangle_E(t) = \frac{\chi_2\xi_m^2}{2}\mathrm{Re}\left[\left(1+\frac{\mathrm{e}^{2\mathrm{i}\omega t}}{1+2\mathrm{i}\omega\tau_2^{\mathrm{eff}}}\right)\left(\frac{\Delta_2}{1+\mathrm{i}\omega/\lambda_1}+\frac{1-\Delta_2}{1+\mathrm{i}\omega\tau_W^{(2)}}\right)\right] \quad (5.317)$$

where λ_1 is the smallest nonvanishing eigenvalue of the Fokker–Planck operator [for all values of σ, λ_1 can be approximated by (5.297)], $\tau_W^{(2)}$ is the intrawell relaxation time, which can be evaluated numerically, and

$$\frac{\tau_2^{eff}}{\tau_D} = \frac{\langle P_2^2\rangle_0 - \langle P_2\rangle_0^2}{1+\langle P_2\rangle_0 - 2\langle P_2^2\rangle_0}\,, \qquad \chi_2 = \left(\langle P_2^2\rangle_0 - \langle P_2\rangle_0^2\right)/3$$

The low ($\sigma \le 1$) and high ($\sigma \gg 1$) barrier behaviors of the parameters Δ_2, τ_2^{eff}, and $\tau_W^{(2)}$ in (5.317) are given in [143] (see Appendix C). For the high barrier limit, $\sigma \gg 1$, the most important case, one has

$$\Delta_2 \approx 1+\frac{1}{2\sigma}+\frac{3}{4\sigma^2}+\cdots \quad \frac{\tau_2^{eff}}{\tau_D} \approx \frac{1}{2\sigma}\left(1+\frac{5}{2\sigma}+\frac{33}{4\sigma^2}\cdots\right), \quad \frac{T_W^{(2)}}{\tau_D} \approx -\frac{1}{2\sigma}-\frac{1}{4\sigma^2}+\cdots$$

For $\sigma \gg 1$, we are again justified in neglecting the frequency dependence of the second term in round braces of (5.317) (representing the effect of the near degenerate intrawell modes) so that

$$\langle P_2(\cos\vartheta)\rangle_E(t) = \frac{\chi_2\xi_m^2}{2}\mathrm{Re}\left[\left(1+\frac{\mathrm{e}^{2\mathrm{i}\omega t}}{1+2\mathrm{i}\omega\tau_2^{\mathrm{eff}}}\right)\left(\frac{\Delta_2}{1+\mathrm{i}\omega\tau}+1-\Delta_2\right)\right] \quad (5.318)$$

with $\tau = 1/\lambda_1$. Equation (5.318) is obviously of the same form as the zero mean-field result (5.316), the essential difference being in the relaxation times. For free diffusion ($\sigma = 0$), $\chi_2 = 1/15$, $\tau_2^{eff} = \tau_D/3$, $\lambda + 1 = 1/\tau_D$, and $\Delta_2 = 1$ so that (5.317) reduces to the zero mean field Peterlin and Stuart [488] (5.316).

We reiterate that as before the frequency-dependent dc component of the permanent dipole dynamic Kerr effect for a pure sinusoid in (5.318), viz.,

$$\langle P_2(\cos\vartheta)\rangle_{dc} = \frac{\chi_2\xi_m^2}{2}\left(\frac{\Delta_2}{1+(\omega\tau)^2}+1-\Delta_2\right) \quad (5.319)$$

has the same frequency dependence as the real part of the linear complex susceptibility, (5.295). Thus it is apparent that the correspondence that exists between the zero mean field, i.e., first Debye model, and the overbarrier relaxation or Debye–Fröhlich model for the dipole moment, that is, the Legendre polynomial of order one also effectively exists for quantities such as the dynamic Kerr effect for a pure sinusoid governed by the Legendre polynomial of order 2. Hence by measuring the spectrum of $\langle P_2(\cos\vartheta)\rangle_{dc}$ it is possible in principle to estimate the overbarrier relaxation time

$\tau = 1/\lambda_1$ (the Kramers escape rate) or in the terminology of liquid crystals, the retardation factor $g(\sigma) = \tau/\tau_D$ as a function of temperature ($\sigma \sim T^{-1}$). This simple theoretical result suggests the development of new experimental techniques for the measurement of the physical parameters of the system ($g(T)$, σ, τ_D) involving the dynamic Kerr effect just as in traditional dielectric spectroscopy (see, e.g., [588]).

We remark that the dependence of the dc component of the dynamic Kerr effect on $\tau = 1/\lambda_1$ is peculiar to permanent dipoles; no such behavior exists in the induced dipole dynamic Kerr effect. Here only the $\{f_{2n}(t)\}$ are involved in the response. The set $\{f_{2n}(t)\}$, which are now decoupled from the $\{f_{2n+1}(t)\}$, do not possess an exponentially small nonvanishing eigenvalue λ. Therefore the longest relaxation time $\tau = 1/\lambda_1$ is not involved in the induced dipole Kerr effect response truncated at terms quadratic in the field. It follows that none of the relaxation times associated with the induced dipole Kerr effect response have exponential behaviour.

We finally remark that our results based on rotational diffusion (that is, the diffusion limit of a random walk in which the rotator moves the mean square arc length in a fixed time) may also be extended to the fractional diffusion, i.e., the diffusion limit of a continuous time random walk [142], [425]. Here no mean waiting time exists, i.e., the random walk of the dipole can be interrupted by the dipole remaining trapped in a given orientation for an arbitrarily long period before making a jump. Such behaviour is typical of Cole–Cole [142], [348] dielectric relaxation, which has complex susceptibility at low frequencies of the form

$$\frac{\chi(\omega)}{\chi'(0)} = \frac{\Delta_1}{1 + (\mathrm{i}\omega\tau_D)^\alpha/(\tau_D\lambda_1)} + 1 - \Delta_1 \quad (0 < \alpha \leq 1) \tag{5.320}$$

All one has to do to generalize our time-ordered exponential solution to the fractional diffusion relaxation mechanism is to replace the transition matrix $\exp \mathbf{L}_{FP}t$ by the corresponding Mittag–Leffler function $E_\alpha(\mathbf{L}_{FP}t^\alpha)$ [349], [244]. Thus it is again possible to derive simple analytical approximations for the complex susceptibility, the dynamic Kerr effect response, etc. [142], [213].

A

Continued Fraction Solutions of Eq. (5.301)

Upon defining the Fourier transforms $F_n^{(1)}(\omega) = \int_{-\infty}^{\infty} f_n^{(1)}(t)\mathrm{e}^{\mathrm{i}\omega t}\mathrm{d}t$, we have an exact solution of (5.301) (details in [143], [329])

$$F_1^{(1)}(\omega) = \frac{\xi_\omega\,(1-\langle P_2\rangle_0)\,/3}{\mathrm{i}\omega\tau_D + 1 - 2\sigma[1-S_3(\omega)]/5} \times\left[1+\frac{2}{\sqrt{\pi}}\sum_{n=1}^{\infty}(-1)^n\frac{\Gamma(n+3/2)(f_{2n}^{(0)}-f_{2n+2}^{(0)})}{\Gamma(n+1)(1-\langle P_2\rangle_0)}\prod_{k=1}^{n}S_{2k+1}(\omega)\right] \tag{A.1}$$

where the infinite continued fractions $S_n(\omega)$ are defined by the recurrence relation

$$S_n(\omega) = c_n[\mathrm{i}\omega\tau_D - d_n - g_n S_{n+2}(\omega)]^{-1} \tag{A.2}$$

$$f_{2n}^{(0)} = \langle P_{2n}\rangle_0 = \frac{\sigma^n\Gamma(n+1/2)}{2\Gamma(2n+3/2)}\frac{M(n+1/2,2n+3/2,\sigma)}{M(1/2,3/2/\sigma)}$$

$$M(a,b,z) = \frac{\Gamma(b)}{\Gamma(a)}\sum_{n=0}^{\infty}\frac{\Gamma(a+n)z^n}{\Gamma(b+n)n!}$$

is the confluent hypergeometric (Kummer) function [1]. Equation (A.1) with ξ_ω omitted is, in fact, the complex susceptibility $\chi_1(\omega)$ associated with the matrix element $f_1^{(1)}(t)$, that is, the mean dipole moment. Equation (A.1) may be rewrittten as

$$\begin{aligned} F^{(1)}(0) = \;& \tfrac{\xi_\omega}{6}M(1,5/2,\sigma)\Big[\tfrac{M(1/2,5/2,\sigma)}{M(1/2,3/2,\sigma)} \\ & + \textstyle\sum_{n=1}^{\infty}\frac{(-1)^n(2n+1)(n+1)\Gamma(n+1/2)}{\Gamma(n+2)\Gamma(1/2)} \\ & \times\tfrac{\sigma^n\Gamma(n+1/2)}{\Gamma(2n+3/2)}\tfrac{M(n+1/2,2n+5/2,\sigma)}{2M(1/2,3/2,\sigma)} \\ & \times\tfrac{n!\sigma^n}{2^{2n}(5/4)_n(7/4)_n}\tfrac{M(n+1,2n+5/2,\sigma)}{M(1,5/2,\sigma)}\Big] \end{aligned} \tag{A.3}$$

Equation (A.3) can be further simplified by absorbing the first term within the square brackets into the infinite sum. On doing this we obtain using the properties of the Pochhammer symbol specifically

$$2^{2n}(5/4)_n(7/4)_n = (5/2)_{2n}$$

$$\frac{(3/2)_n}{(3/2)_{2n}} = \frac{\Gamma(n+3/2)}{\Gamma(2n+3/2)}$$

we get

$$F^{(1)}(0) = \frac{\xi_\omega}{6}\frac{1}{M(1/2,3/2,\sigma)}\sum_{n=0}^{\infty}\frac{(-1)^n(1/2)_n(3/2)_n\sigma^{2n}}{(3/2)_{2n}(5/2)_{2n}} \times M(n+1/2,2n+5/2,\sigma)M(n+1,2n+5/2,\sigma) \tag{A.4}$$

Equation (A.4) is still of reasonably complicated mathematical form as it involves infinite summations of products of infinite summations. This difficulty may be overcome by noting that from [499] vol. 3 (6.6.2) part 9:

$$\sum_{k=0}^{\infty}(-1)^k\frac{(a)_k(a')_k(b-1)_k}{k!(b-1)_{2k}(b)_{2k}}x^k y^k M(a+k,b+2k,x)M(a'+k,b+2k,y) = \Phi_2(a,a';b;x,y) \tag{A.5}$$

This is proven from first principles by changing the order of summations. Thus on making the substitutions

$$k = n\,, \quad x = y = \sigma\,, \quad a = 1/2\,, \quad a' = 1\,, \quad b = 5/2 \tag{A.6}$$

$$\sum_{n=0}^{\infty}(-1)^n\frac{(1/2)_n(1)_n(3/2)_n\sigma^{2n}}{n!(3/2)_{2n}(5/2)_{2n}}M\left(\frac{1}{2}+n,\frac{5}{2}+2n,\sigma\right) \times M\left(1+n,\frac{5}{2}+2n,\sigma\right) = \Phi_2\left(\frac{1}{2},1;\frac{5}{2};\sigma,\sigma\right)$$

so that the summation disappears and we have the simple relation

$$F_1^{(1)}(0) = \frac{\xi_\omega}{6M(1/2,3/2,\sigma_0)}\Phi_2\left(1,\frac{1}{2};\frac{5}{2};\sigma,\sigma\right) \tag{A.7}$$

where Φ_2 is the degenerate Appell function given by

$$\Phi_2(b,b';c;w,z) = \frac{\Gamma(c)}{\Gamma(b)\Gamma(b')\Gamma(c-b-b')} \iint u^{b-1}v^{b'-1}(1-u-v)^{c-b-b'-1}\mathrm{e}^{uw+vz}\mathrm{d}u\mathrm{d}v \tag{A.8}$$

where the double integral is performed subject to $u, v \geq 0$ and $u + v \leq 1$. Here it is assumed ([499], vol 3 p 451 (49)) that $\mathrm{Re}\{\mathrm{b}, \mathrm{b}', \mathrm{c} - \mathrm{b} - \mathrm{b}'\} > 0$. Accordingly the Φ_2 in (A.7) may be evaluated as a repeated integral given by

$$\frac{3}{4}\int_0^1 \mathrm{d}v\, v^{-1/2}\exp(\sigma v)\int_0^{1-v}\mathrm{d}u\exp(\sigma u) \tag{A.9}$$

$$= \frac{3}{4\sigma_0}\int_0^1 \mathrm{d}v\, v^{-1/2}[\exp(\sigma)-\exp(\sigma v)] \tag{A.10}$$

$$= \frac{3}{2\sigma_0}\int_0^1 \mathrm{d}x[\exp(\sigma)-\exp(\sigma x^2)]\,, \qquad (v=x^2) \tag{A.11}$$

$$= \frac{3}{2\sigma_0}[\exp(\sigma)-M(1/2,3/2,\sigma)] \tag{A.12}$$

$$= \frac{3}{2\sigma}\left[\mathrm{e}^{\sigma}-\frac{\sqrt{\pi}}{2\sqrt{\sigma}}erfi(\sqrt{\sigma})\right] \tag{A.13}$$

$$= M(3/2,5/2,\sigma) \tag{A.14}$$

where we have used (11) and (29) on pages 580–1 of Prudnikov et al., vol. 3 [499]. Thus (A.4) is reduced to the ratio of two hypergeometric functions

$$F_1^{(1)}(0) = \frac{\xi_\omega M(3/2,5/2,\sigma)}{6M(1/2,3/2,\sigma)} \tag{A.15}$$

and [130] the static susceptibility is given by

$$\chi(0) = 2\mu F_1^{(1)}(0) = \frac{\mu\xi_\omega}{3\sigma}\left[\frac{2\sqrt{\sigma}}{\pi}\mathrm{e}^{\sigma}\{erfi(\sqrt{\sigma})\}^{-1}-1\right] \tag{A.16}$$

This agrees, as it should, with the equation after equation (33) of [130], which is the static susceptibility as rendered by the equilibrium distribution, upon identifying the constants

$$\mu\xi_\omega = \frac{m^2N}{kT} \tag{A.17}$$

We remark, by linear response theory, that the matrix elements $f_{2n-1}^{(1)}(t)$ may also be expressed [558] in terms of the equilibrium correlation functions

$$\Phi_{1,2n-1}(t) = \langle\cos\vartheta(0)P_{2n-1}[\cos\vartheta(t)]\rangle_0/\langle\cos\vartheta(0)P_{2n-1}[\cos\vartheta(0)]\rangle_0$$

as

$$f_{2n-1}^{(1)}(t) = -\chi_{2n-1}\int_{-\infty}^{t}\dot{\Phi}_{1,2n-1}(t-t')\xi(t')\mathrm{d}t' \tag{A.18}$$

where $\chi_{2n-1} = \langle\cos\vartheta(0)P_{2n-1}[\cos\vartheta(0)]\rangle_0$. This is a useful representation of the solution as, in general, it is much easier to calculate $\Phi_{1,2n-1}(t)$, the after-effect solution rather than the ac response directly. The corresponding hierarchy of linear complex susceptibilities is

$$\chi_{2n-1}(\omega) = \chi_{2n-1}\left[1-\mathrm{i}\omega\int_0^\infty \Phi_{1,2n-1}(t)\mathrm{e}^{-\mathrm{i}\omega t}\mathrm{d}t\right]$$

so that in (5.293) $\chi(\omega)$ corresponds to $\chi_1(\omega)$.

It may also be shown by continued-fraction methods suitably adopted, how the matrix element $f_2^{(2)}(t)$ for a pure ω sinusoid $\xi(t) = \xi_m \cos \omega_0 t$ may be given (details in [143], [329], Appendix C)

$$f_2^{2)}(t) = \mathrm{Re}\left\{\mathrm{F}_0^{(2)}(\omega_0) + \mathrm{F}_2^{(2)}(2\omega_0)\mathrm{e}^{2\mathrm{i}\omega_0 \mathrm{t}}\right\} \tag{A.19}$$

where

$$\begin{pmatrix} F_0^{(2)}(\omega_0) \\ F_2^{(2)}(2\omega_0) \end{pmatrix} = \frac{3\sqrt{\pi}\xi_m^2}{8\sigma} \sum_{n=1}^{\infty} \frac{(-1)^{n+1}\Gamma(n+1)}{\Gamma(n+1/2)} \prod_{k=1}^{n} \begin{pmatrix} S_{2k}(0) \\ S_{2k}(2\omega_0) \end{pmatrix} \times [\chi_{2n-1}(\omega_0) - \chi_{2n+1}(\omega_0)] \tag{A.20}$$

and the continued fractions S_n are again defined by (A.2).

B

Mittag–Leffler Functions

B.0.1 Properties of Mittag–Leffler Functions

$$E_{\alpha,\beta}(z) = \frac{1}{2\pi \mathrm{i}} \int_{-\infty}^{(0+)} \frac{t^{\alpha-\beta} \mathrm{e}^t}{t^\alpha - z} \mathrm{d}t \tag{B.1}$$

$$= \frac{1}{2\pi \mathrm{i}} \int_{-\infty}^{(0+)} \mathrm{d}t\, t^{-\beta} \mathrm{e}^t \sum_{n=0}^{\infty} z^n t^{-\alpha n} \tag{B.2}$$

$$= \sum_{n=0}^{\infty} \frac{z^n}{\Gamma(\beta + \alpha n)} \qquad \text{(Hankel)} \qquad \text{(small } |z|\text{)} \tag{B.3}$$

Also, we have

$$E_{\alpha,\beta}(z) = \left(-\frac{1}{z}\right) \frac{1}{2\pi \mathrm{i}} \int_{-\infty}^{(0+)} \mathrm{d}t\, \mathrm{e}^t \sum_{n=0}^{\infty} \frac{t^{\alpha-\beta+\alpha n}}{z^n} \tag{B.4}$$

$$= -\frac{1}{z} \sum_{n=0}^{\infty} \frac{z^{-n}}{\Gamma(\beta - \alpha - \alpha n)} \qquad \text{(Hankel)} \tag{B.5}$$

$$= -\frac{1}{z} E_{-\alpha,\beta-\alpha}(1/z) \qquad \text{(large } |z|\text{)} \tag{B.6}$$

By the ratio test, in general (B.3) converges and (B.6) diverges ($0 < \alpha < 1$).

B.0.2 Asymptotics of Mittag–Leffler functions

$$E_\alpha(z) = \sum_{n=0}^{\infty} \frac{z^n}{\Gamma(1+\alpha n)} \tag{B.7}$$

$$= \sum_{n=0}^{\infty} \frac{z^n}{\alpha n \Gamma(\alpha n)} \tag{B.8}$$

$$= \sum_{n=0}^{\infty} \frac{z^n}{\alpha n} \sum_{l=1}^{\infty} c_l (\alpha n)^l \qquad ([1]\ (6.1.34))(\text{NB } c=1) \tag{B.9}$$

$$= 1 + \sum_{L=0}^{\infty} c_{L+1} \alpha^L \sum_{n=0}^{\infty} z^n n^L \qquad (l = L+1) \tag{B.10}$$

$$= 1 + \sum_{L=0}^{\infty} c_{L+1} \alpha^L \sum_{n=0}^{\infty} z^{n+1} (n+1)^L \qquad (n \to n+1) \tag{B.11}$$

$$= 1 + \frac{z c_1}{1-z} + z \sum_{L=1}^{\infty} c_{L+1} \alpha^L \sum_{n=0}^{\infty} z^n (n+1)^L \tag{B.12}$$

where

$$\sum_{n=0}^{\infty} z^{n+1} (n+1)^L = \frac{1}{z} \sum_{n=0}^{\infty} (n+1)^L z^{n+1} \tag{B.13}$$

$$= \frac{1}{z} \sum_{n=0}^{\infty} \left(z \frac{\mathrm{d}}{\mathrm{d}z} \right)^L z^{n+1} \tag{B.14}$$

$$= \frac{1}{z} \left(z \frac{\mathrm{d}}{\mathrm{d}z} \right)^L \left(\frac{z}{1-z} \right) \tag{B.15}$$

$$= -\frac{1}{z} \left(z \frac{\mathrm{d}}{\mathrm{d}z} \right)^L \frac{1}{z-1} \qquad (L \geq 1) \tag{B.16}$$

$$= -\frac{1}{z} \frac{\mathrm{d}^L}{\mathrm{d}t^L} f(g(t)) \tag{B.17}$$

where we have

$$z = \mathrm{e}^t \ , \ \ln z = t \ , \ g(t) = \mathrm{e}^t - 1 \tag{B.18}$$

and

$$f(g(t)) = \frac{1}{g(t)} = -\frac{1}{z} \sum_{m=0}^{L} f^{(m)}(g(t)) \sum (L; a_1 - a_L)' \prod_{j=1}^{L} \{ g^{(j)}(t) \}^{a_j} \tag{B.19}$$

using Faá di Bruno's formula ([1], p. 823) and summing over (see also [465])

$$a_1 + 2a_2 + \cdots + L a_L = L \tag{B.20}$$

$$a_1 + a_2 + \cdots + a_L = m \tag{B.21}$$

and where

$$\sum (L; a_1 - a_L)' \equiv S_L^{(m)} \tag{B.22}$$

namely a Stirling number of the second kind.

However,

$$g^{(j)}(t) = \mathrm{e}^t = z \qquad (1 \le j \le L) \tag{B.23}$$

$$\rightarrow \quad \prod_{j=1}^{L} \{g^{(j)}(t)\}^{a_j} = \mathrm{e}^{t(a_1+a_2+\cdots+a_L)} = \mathrm{e}^{mt} = z^m \tag{B.24}$$

$$\therefore \quad \sum_{n=0}^{\infty} z^n (n+1)^L = -\sum_{m=0}^{L} \frac{(-1)^m m!}{(z-1)^{m+1}} S_L^{(m)} z^m \tag{B.25}$$

since

$$f^{(m)}(g(t)) = \frac{(-1)^m m!}{\{g(t)\}^{m+1}} \tag{B.26}$$

$$\therefore \quad E_\alpha(z) = 1 + \frac{zc_1}{1-z} + \frac{1}{z}\sum_{L=1}^{\infty} c_{L+1}\alpha^L \sum_{m=0}^{L} m! \left(\frac{z}{1-z}\right)^{m+1} S_L^{(m)} \tag{B.27}$$

However

$$\sum_{m=0}^{L} (-1)^{L-m} m! S_L^{(m)} = 1 \qquad ([1]\ p.825\ IIB) \tag{B.28}$$

$$\therefore \quad E_\alpha(z) \underset{z\to\infty}{\cong} 1 + \frac{z}{1-z}\frac{-1}{z}\sum_{L=1}^{\infty} c_{L+1}(-\alpha)^L \tag{B.29}$$

$$= 1 + \frac{z}{1-z} + \frac{1}{z} + \frac{1}{\alpha z}\sum_{l=1}^{\infty} c_l(-\alpha)^l l \ (L = l-1) \tag{B.30}$$

$$= \frac{1}{1-z} + \frac{1}{z} + \frac{1}{\alpha z}\frac{1}{\Gamma(-\alpha)} \tag{B.31}$$

$$\cong -\frac{1}{z^2} - \frac{1}{z\Gamma(1-\alpha)} \cong \frac{-1}{z\Gamma(1-\alpha)} \tag{B.32}$$

Similarly, we have

$$E_{\alpha,\beta}(z)\ z \overset{\cong}{\rightarrow} \infty\ -\frac{1}{z\Gamma(\beta-\alpha)} \tag{B.33}$$

B.1 Check on Norm of $x^2(\tau)$

Check on equation (3.12) of [30], with

$$z = -\gamma t^\alpha \tag{B.34}$$

$$\langle x^2(\tau)\rangle = \frac{2kT}{m}\int_0^\tau \mathrm{d}t(\tau - t)E_\alpha(z) \tag{B.35}$$

$$= \frac{2kT}{m}\int_0^\tau \mathrm{d}t(\tau - t)\sum_{n=0}^{\infty}\frac{(-\gamma t^\alpha)^n}{\Gamma(1+\alpha n)} \tag{B.36}$$

$$= \frac{2kT}{m}\sum_{n=0}^{\infty}\frac{1}{\Gamma(1+\alpha n)}\times\left[\tau\frac{(-\gamma)^n t^{\alpha n+1}}{1+\alpha n} - \frac{(-\gamma)^n t^{\alpha n+2}}{2+\alpha n}\right]_{t=0}^{\tau} \tag{B.37}$$

$$= \frac{2kT}{m}\sum_{n=0}^{\infty}\frac{1}{\Gamma(1+\alpha n)}\times\left[\frac{\tau^{\alpha n+2}(-\gamma)^n}{1+\alpha n} - \frac{\tau^{\alpha n+2}(-\gamma)^n}{2+\alpha n}\right] \tag{B.38}$$

$$= \frac{2kT}{m}\sum_{n=0}^{\infty}\left[\frac{\tau^2(-\gamma\tau^\alpha)^n}{\Gamma(2+\alpha n)} - \frac{\tau^2(-\gamma\tau^\alpha)^n(1+\alpha n)}{\Gamma(3+\alpha n)}\right] \tag{B.39}$$

$$= \frac{2kT}{m}\sum_{n=0}^{\infty}\tau^2\frac{(-\gamma\tau^\alpha)^n[2+\alpha/n-1-\alpha/n]}{\Gamma(3+\alpha n)} \tag{B.40}$$

$$= \frac{2kT}{m}\tau^2 E_{\alpha,3}(-\gamma\tau^\alpha) \tag{B.41}$$

C

Nonlinear Response to Alternating Fields

A system in thermal equilibrium at temperature T disturbed by an external stimulus evolves to a new equilibrium (stationary) state. Moreover, if the energy stimulus is much lower than the thermal energy k_BT, *linear* in the stimulus) deviations of the expectation value of the relevant dynamical variable in the stationary state are sufficient to evaluate the generalized susceptibility (linear ac response) using appropriate equilibrium (stationary) correlation functions. The calculation of the nonlinear stationary (ac) response even for systems of noninteracting particles with a single coordinate is, however, much more difficult because no connection between the transient and the ac responses exists. If interactions are included the difficulties are compounded. Nonlinear dielectric relaxation and the dynamic Kerr effect of permanent dipoles in a mean field potential are naturally occurring examples.

In this context we remark that the orientational electric polarization of noninteracting permanent dipoles in an ac field $\mathbf{E}(t)$ treated by Debye [206] depends in the linear approximation in $\mathbf{E}(t)$ on the average over orientations of the Legendre polynomial $\langle P_1(\cos\vartheta)\rangle(t)$, ϑ being the polar angle of the electric dipole moment vector $\boldsymbol{\mu}$. Similar remarks apply to the magnetization of blocked noninteracting ferrofluid particles with magnetic dipole moment $\boldsymbol{\mu}$ in ac magnetic fields $\mathbf{H}(t)$ [504]. Subsequently [142]–[504] Debye's calculation was generalized to nonlinear responses. We mention $\langle P_2\rangle(t)$ governing the Kerr effect response (KER) [212]–[122] and the nonlinear dielectric effect (NLDE) [142], [567] amending $\langle P_1\rangle(t)$ to $O(E^3)$. The conclusions are [to $O(E^2)$)] for the KER for a pure sinusoid that the square law nonlinearity rectifies $\mathbf{E}(t)$, yielding a frequency-dependent dc response superimposed on which is the dephased second harmonic [65]. In the NLDE, additional terms in the fundamental and in the third harmonic appear in $\langle P_1\rangle(t)$. Experimental confirmation has been reported [567], [288]. The Debye theory may not be used for dense anisotropic dipolar systems, where intermolecular interactions occur, such as nematic liquid crystals. Here dielectric relaxation is usually interpreted using as a model the noninertial rotational Brownian motion of a rodlike particle in an external potential V (e.g., [142],[403], [460], [572]). This model was used in [132], where the exact linear ac response is calculated in terms of continued fractions (using linear response theory [373]) for the Maier–Saupe uniaxial anisotropy potential:

$$V = -K\cos^2\vartheta \tag{C.1}$$

where K is the anisotropy constant. Exact solutions for the nonlinear ac response in a uniaxial potential can also be obtained by matrix continued fractions without using perturbation theory [212], [142]. However, that approach cannot yield simple formulae for experimental comparison, and it cannot provide an exact evolution equation for the ac responses for perturbation purposes. Preliminary steps towards this were made in [504], [142], [501], [503], [91] for dielectric relaxation of dipolar systems and for magnetic relaxation (super-paramagnetism) of fine single-domain ferromagnetic particles (in most respects a replica of dielectric relaxation of nematics). Here we demonstrate how by calculating from perturbation theory the linear ac response in the presence of $\mathbf{E}(t)$ one may generate the KER and all higher-order nonlinear responses. The linear response comprising an infinity of relaxation modes may be accurately represented by two modes, that of low frequency arising from the slow barrier crossing of dipoles and that of high frequency representing the infinity of fast near-degenerate "intrawell" modes approximated as a single high-frequency mode. The analytical responses are obtained, utilizing the two-mode approximation for linear response combined with Morita's treatment [438] of nonlinear response, showing how the distribution function induced by a strong perturbing field may be calculated from the Green functions in the absence of the perturbation, with linear response theory as a special case.

The cornerstone of our calculation is the Smoluchowski (Fokker–Planck) equation for the density $W(\boldsymbol{\mu}, t)$ of orientations of dipoles $\boldsymbol{\mu}$ on the surface of the unit sphere [206], [437], [142]

$$\dot{W} = [L_{FP} + L_{ext}(t)]W \tag{C.2}$$

where $L_{FP}W = (2\tau_D)^{-1}[\Delta W + \beta\nabla\cdot(W\nabla V)]$ is the unperturbed Fokker—Planck operator while $L_{\text{ext}}W = (2\tau_D)^{-1}\beta\nabla\cdot(W\nabla V_{\text{ext}})$ is the Zeeman energy $V_{\text{ext}}W = -(\mathbf{E}\cdot\boldsymbol{\mu})$ contribution, and ∇ and Δ are the gradient and Laplacian on the surface of the unit sphere. Here $\beta = (k_BT)^{-1}$, $\tau_D = \beta\zeta/2$ is the Debye relaxation time for free diffusion, and ζ is the viscous drag coefficient. Expanding W in the $\{P_n\}$ yields [437], [142]

$$\tau_D\dot{f}_n(t) + c_n f_{n-2}(t) + d_n f_n(t) + g_n f_{n+2}(t) = \xi(t)a_n[f_{n-1}(t) - f_{n+1}(t)] \tag{C.3}$$

where $f_n(t) = \langle P_n(\cos\vartheta)\rangle(t)$ and $\xi(t) = \beta\mu E(t)$, and all the coefficients are given, e.g., in [437], [142]. One may write

$$f_n(t) = f_n^{(0)} + f_n^{(1)}(t) + f_n^{(2)}(t) + f_n^{(3)}(t) + \cdots$$

[with the superscripts denoting the relevant order in $\mathbf{E}(t)$] so that

$$\begin{aligned}\tau_D\dot{f}_n^{(m)}(t) + c_n f_{n-2}^{(m)}(t) + d_n f_n^{(m)}(t) + g_n f_{n+2}^{(m)}(t)\\ =\xi(t)a_n[f_{n-1}^{(m-1)}(t) - f_{n+1}^{(m-1)}(t)]\end{aligned} \tag{C.4}$$

Thus to calculate the matrix element $f_2^{(2)}(t)$, i.e., the lowest-order approximation to the KER, we first determine $\{f_{2n-1}^{(1)}(t)\}$ satisfying (C.4) with $m = 1$. The *exact* solutions of (C.4) for $f_{2n-1}^{(1)}(t)$ for the stationary response to $\xi(t) = \xi e^{i\omega t}$ are given by

continued fractions [212]. However, in order to obtain analytical approximations, we use another method. Suppose that a small probing field $\xi_1 = \beta\mu E_1 \ll 1$ applied along the polar axis at $t = -\infty$ is removed at $t = 0$. The step off [$\xi(t) = 0$ for $t > 0$] solution of (C.4) for $m = 1$ $f^{(1)}_{2n-1,off}(t)$, is

$$f^{(1)}_{2n-1,off}(t) = \xi_1 \chi_{2n-1} \Phi_{1,2n-1}(t) \tag{C.5}$$

where $\Phi_{1,2n-1}(t)$ are the normalized equilibrium correlation functions defined as

$$\Phi_{k,m}(t) = \frac{\langle P_k[\cos\vartheta(0)]P_m[\cos\vartheta(t)\rangle_0 - \langle P_k\rangle_0\langle P_m\rangle_0}{\langle P_k P_m\rangle_0 - \langle P_k\rangle_0\langle P_m\rangle_0} \tag{C.6}$$

$\langle P_n\rangle_0 = \langle P_n[\cos\vartheta(0)]\rangle_0$, and $\chi_{2n-1} = \langle P_1 P_{2n-1}\rangle_0$ are the static susceptibilities, which can be expressed as hypergeometric functions [132]. The Green functions $G_{2n-1}(t)$ of the unperturbed [$\xi(t) = 0$] (C.4) with $m = 1$ is $G_{2n-1}(t) = -\dot{\Phi}_{1,2n-1}(t)$ [373]. Thus

$$f^{(1)}_{2n-1}(t) = -\chi_{2n-1}\int_{-\infty}^{t} \dot{\Phi}_{1,2n-1}(t-t')\xi(t')\mathrm{d}t' \tag{C.7}$$

If $\xi(t) = \xi \mathrm{e}^{\mathrm{i}\omega t}$, (C.7) yields $f^{(1)}_{2n-1}(t) = \chi_{2n-1}(\omega)\xi\mathrm{e}^{\mathrm{i}\omega t}$, where $\chi_{2n-1}(\omega)$ are the generalized complex susceptibilities

$$\frac{\chi_{2n-1}(\omega)}{\chi_{2n-1}} = 1 - \mathrm{i}\omega\int_0^\infty \Phi_{1,2n-1}(t)\mathrm{e}^{-\mathrm{i}\omega t}\mathrm{d}t \tag{C.8}$$

The time domain behavior of $\Phi_{1,2n-1}(t)$ is characterized by the integral and effective relaxation times

$$\tau_{2n-1} = \int_0^\infty \Phi_{1,2n-1}(t)\mathrm{d}t\,, \qquad \tau^{eff}_{2n-1} = -1/\dot{\Phi}_{1,2n-1}(0) \tag{C.9}$$

Here τ^{eff}_{2n-1} is evaluated from (C.4) with $\xi(t) = 0$ using equilibrium averages as

$$\begin{aligned}\frac{\tau^{eff}_{2n-1}}{\tau_D} &= -\frac{f^{(1)}_{2n-1,off}(0)}{\tau_D \dot{f}^{(1)}_{2n-1,off}(0)} \\ &= \left\{ d_{2n-1} + c_{2n-1}\frac{\langle P_1 P_{2n-3}\rangle_0}{\langle P_1 P_{2n-1}\rangle_0} + g_{2n-1}\frac{\langle P_1 P_{2n+1}\rangle_0}{\langle P_1 P_{2n-1}\rangle_0}\right\}^{-1}\end{aligned}$$

and τ_{2n-1} is given by the mean first passage time approach of Szabo [577], which for the present problem yields

$$\begin{aligned}\tau_{2n-1} = \frac{2\tau_D}{Z\langle P_1 P_{2n-1}\rangle_0}\int_{-1}^{1}\mathrm{d}z\,\frac{\mathrm{e}^{-\sigma z^2}}{1-z^2}\int_{-1}^{z} x\mathrm{e}^{\sigma x^2}\mathrm{d}x \\ \times\int_{-1}^{z} P_{2n-1}(y)\mathrm{e}^{\sigma y^2}\mathrm{d}y\end{aligned}$$

where $Z = \int_{-1}^{1}\mathrm{e}^{\sigma z^2}\mathrm{d}z$ is the partition function and $\sigma = \beta K$ is the barrier height parameter. $\Phi_{1,2n-1}(t)$ may also be written as an eigensolution using the eigenvalues

$\{\xi_k\}$ of L_{FP}, viz., $\Phi_{1,2n-1}(t) = \sum_k c_k^n e^{-t\lambda_k}$, where $\sum_k c_k^n = 1$ and λ_1 (essentially the Kramers escape rate) is associated with the slowest relaxation mode and so with the long-time behavior of $\Phi_{1,2n-1}(t)$; the other λ_k characterize high-frequency intrawell modes. By (C.9) $\tau_{2n-1} = \sum_k c_k^n/\lambda_k$ and $\tau_{2n-1}^{eff} = 1/\sum_k c_k^n \lambda_k$. The behavior of λ_1, τ_{2n-1}, and τ_{2n-1}^{eff} is given, for $\sigma \leq 1$, by

$$\lambda_1 \tau_D = 1 - \frac{2}{5}\sigma + \cdots$$

$$\frac{\tau_{2n-1}}{\tau_D} = \frac{n! - (1/2)_n}{n(1/2)_n} + \sigma \frac{2 + 8n!/(3/2)_{n-2}}{3n(4n+1)} + \cdots$$

$$\frac{\tau_{2n-1}^{eff}}{\tau_D} = \frac{1}{n} + \frac{2\sigma}{4n^2 + n} + \cdots$$

[$(a)_n$ is the Pochhammer symbol] and, for $\sigma \gg 1$, by

$$\lambda_1 \tau_D \sim \frac{2\sigma^{3/2} e^{-\sigma}}{\sqrt{\pi}} \left(1 - \frac{1}{\sigma} - \frac{3}{4\sigma^2} + \cdots\right)$$

$$\frac{\tau_{2n-1}}{\tau_D} \sim \frac{\sqrt{\pi} e^{\sigma}}{2\sigma^{3/2}} \left(1 + \frac{1}{\sigma} - \frac{7 + n - 2n^2}{4\sigma^2} + \cdots\right)$$

$$\frac{\tau_{2n-1}^{eff}}{\tau_D} \sim \frac{2\sigma}{2n^2 - n} \left(1 - \frac{3}{2\sigma} + \cdots\right)$$

The spectra of $\chi_{2n-1}(\omega)$ can be accurately described at all frequencies (see Fig. C.1) by a sum of two Lorentzians, viz.,

$$\frac{\chi_{2n-1}(\omega)}{\chi_{2n-1}} = \frac{\Delta_{2n-1}}{1 + i\omega/\lambda_1} + \frac{1 - \Delta_{2n-1}}{1 + i\omega\tau_W^{2n-1}} \tag{C.10}$$

where Δ_{2n-1} and τ_{2n-1}^W are determineds to ensure the correct low- and high-frequency behavior of $\chi_{2n-1}(\omega)$, viz., $\chi_{2n-1}(\omega)/\chi_{2n-1} \approx 1 - i\omega\tau_{2n-1}$ as $\omega \to 0$ and $\chi_{2n-1}/\chi_{2n-1}(\omega) \sim i\omega\tau_{2n-1}^{eff}$ as $\omega \to \infty$, and are given by

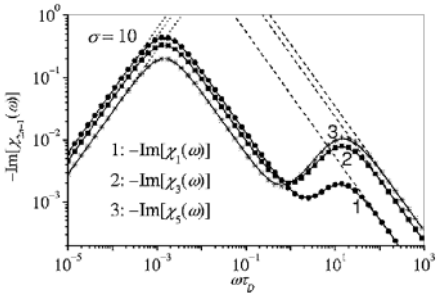

Fig. C.1. $-\mathrm{Im}\,[\chi_{2n-1}(\omega)]$ vs $\omega\tau_D$ (*solid lines*, (C.4) and (C.8) for $n = 1, 3, 5$); $\chi_{2n-1}\omega\tau_{2n-1}$ (*dotted lines*); $\chi_{2n-1}(\omega\tau_{2n-1}^{eff})^{-1}$ (*dashed lines*); symbols (C.10)

$$\Delta_m = \frac{\tau_m/\tau_m^{eff} - 1}{\lambda_1\tau_m - 2 + 1/(\lambda_1\tau_m^{eff})}\,, \qquad \tau_W^m = \frac{\lambda_1\tau_m - 1}{\lambda_1 - 1/\tau_m^{eff}} \tag{C.11}$$

In the time domain, the two-mode approximation (C.10) is equivalent to assuming that the relaxation function $\Phi_{1,2n-1}(t)$ (which in general comprises an *infinite number* of exponentials) may be approximated by *two* exponentials only. An interested reader can find a detailed description and various applications of this two-mode approximation in [142].

The second order response $\{f_{2n}^{(2)}(t)\}$ satisfies (C.4) with $m = 2$. The *exact* solution for the element $f_2^{(2)}(t)$ governing the KER, with $\xi(t) = \xi\cos\omega t$, is

$$f_2^{(2)}(t) = \xi^2 \mathrm{Re}[\mathrm{F}_0^{(2)}(\omega) + \mathrm{F}_2^{(2)}(\omega)\mathrm{e}^{2\mathrm{i}\omega t}] \tag{C.12}$$

where the frequency-dependent dc $F_0^{(2)}(\omega)$ and the second harmonic $F_2^{(2)}(\omega)$ terms are

$$\begin{pmatrix} F_0^{(2)}(\omega) \\ F_2^{(2)}(\omega) \end{pmatrix} = \frac{3\sqrt{\pi}}{4\sigma}\sum_{n=1}^{\infty}\frac{(-1)^{n+1}n!}{\Gamma(n+1/2)}\prod_{k=1}^{n}\begin{pmatrix} S_{2k}(0) \\ S_{2k}(2\mathrm{i}\omega) \end{pmatrix} \times [\chi_{2n-1}(\omega) - \chi_{2n+1}(\omega)] \tag{C.13}$$

and the continued fractions $S_n(\mathrm{i}\omega)$ are defined as $S_n(\mathrm{i}\omega) = c_n[\mathrm{i}\omega\tau_D - d_n - g_n S_{n+2}(\mathrm{i}\omega)]^{-1}$ [cf. [132], eq. (26)]. In order to obtain a simple analytic approximation for the KER, we notice that the normalized step-off solution of (C.4) with $m = 2$ is $f_{2,off}^{(2)}(t) = \xi^2\chi_2\Phi_{2,2}(t)$, where $\Phi_{2,2}(t)$ is the normalized second-rank equilibrium correlation function defined by (C.6) and $\chi_2 = (\langle P_2^2\rangle_0 - \langle P_2\rangle_0^2)/3$. As the overbarrier relaxation mode is not involved in the propagator of $f_2^{(2)}(t)$, one may use a single-mode approximation for $\Phi_{2,2}(t)$, viz.,

$$\Phi_{2,2}(t) \approx \mathrm{e}^{-t/\tau_2^{eff}} \tag{C.14}$$

with the effective relaxation time τ_2^{eff} given by

$$\frac{\tau_2^{eff}}{\tau_D} = -\frac{f_{2,off}^{(2)}(0)}{\tau_D\dot{f}_{2,off}^{(2)}(0)} = \frac{\langle P_2^2\rangle_0 - \langle P_2\rangle_0^2}{1 + \langle P_2\rangle_0 - 2\langle P_2^2\rangle_0}$$

The qualitative behavior of τ_2^{eff} is $\tau_2^{eff}/\tau_D = 1/3 + 2\sigma/189 + \cdots$ for $\sigma \le 1$ and $\tau_2^{eff}/\tau_D = \sigma^{-1}/2 + \sigma^{-2}5/4 + \cdots$ for $\sigma \gg 1$. Moreover, using the effective relaxation time means that (C.4) for $m = 2$ can be represented as

$$\tau_2^{eff}\dot{f}_2^{(2)}(t) + f_2^{(2)}(t) = -\chi_2\xi(t)\int_{-\infty}^{t}\dot{\Phi}^{(1)}(t - t')\xi(t')\mathrm{d}t'$$

with solution

$$f_2^{(2)}(t) = -\frac{\chi_2}{\tau_2^{eff}}\int_{-\infty}^{t}\xi(t')\mathrm{e}^{-(t-t')/\tau_2^{eff}}\int_{-\infty}^{t'}\dot{\Phi}^{(1)}(t' - t'')\xi(t'')\mathrm{d}t''\mathrm{d}t' \tag{C.15}$$

Here $\Phi^{(1)}(t)$ is the normalized $[\Phi^{(1)}(0) = 1]$ effective relaxation function, accounting for the driving functions $\{f^{(1)}_{2n-1}(t)\}$. As before, $\Phi^{(1)}(t)$ is characterized by the integral, τ, and effective, τ^{eff}, relaxation times, which can be estimated from the low- and high-frequency asymptotes of the dc KER $\tau = -\lim_{\omega\to 0} 2\,\mathrm{Im}\,[\mathrm{F}^{(2)}_0(\omega)]/(\omega\chi_2)$ and $\tau^{eff} = -\lim_{\omega\to\infty}\chi_2\{2\omega\,\mathrm{Im}\,[\mathrm{F}^{(2)}_0(\omega)]\}^{-1}$. The one-sided Fourier transform of $-\dot{\Phi}^{(1)}(t)$ may be represented in a two-mode approximation as

$$1 - \mathrm{i}\omega\tilde{\Phi}^{(1)} = \frac{\Delta_2}{1 + \mathrm{i}\omega/\lambda_1} + \frac{1 - \Delta_2}{1 + \mathrm{i}\omega\tau_W^2} \tag{C.16}$$

Here Δ_2 and τ_W^2 may be evaluated from (C.11) using λ_1, $\tau_m = \tau$, and $\tau_m^{eff} = \tau^{eff}$ (see Table C.1). For $\sigma < 1$ and $\sigma \gg 1$, their behavior is $\Delta_2 = 1 + \sigma/35 + \cdots$, $\tau_W^2/\tau_D = \sigma/70 + \cdots$, and $\Delta_2 = 1 + \sigma^{-1} + \cdots$, $\tau_W^2/\tau_D \sim -1/2\sigma + \cdots$, respectively. Thus, setting $\xi(t) = \xi\cos\omega t$, (C.15) yields

$$f^{(2)}_2(t) = \frac{\chi_2\xi^2}{2}\mathrm{Re}\left[\left(1 + \frac{\mathrm{e}^{2\mathrm{i}\omega t}}{1 + 2\mathrm{i}\omega\tau_2^{\mathrm{eff}}}\right)\left(\frac{\Delta_2}{1 + \mathrm{i}\omega/\lambda_1} + \frac{1 - \Delta_2}{1 + \mathrm{i}\omega\tau_{\mathrm{W}}^2}\right)\right] \tag{C.17}$$

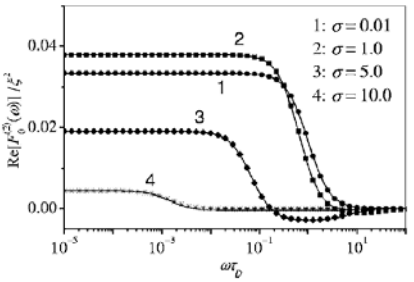

Fig. C.2. Exact $\mathrm{Re}\,[\mathrm{F}^{(2)}_0(\omega)]/\xi^2$ (C.13, *solid lines*) and approximate ((C.17), *symbols*) solutions

Apparently, the KER calculated from the approximate equation (C.17) is in excellent agreement with the exact equation (C.13); see Figures C.2 and C.3. The results suggest a method of measuring the overbarrier relaxation time $1/\lambda_1$, i.e., the inverse Kramers escape rate, using the dc component of the Kerr response. For free

Table C.1. Numerical values of $(\lambda_1\tau_D)^{-1}$, τ^{eff}/τ_D, and τ/τ_D

σ	0	1	2	3	4	5	6	8	10
$(\lambda_1\tau_D)^{-1}$	1.0	1.531	2.476	4.243	7.702	14.77	29.75	135.8	693.9
τ^{eff}/τ_D	-1.0	-2.169	83.37	2.411	1.352	1.021	0.881	0.805	0.826
τ/τ_D	1.0	1.582	2.655	4.713	8.788	17.09	34.43	153.2	757.9

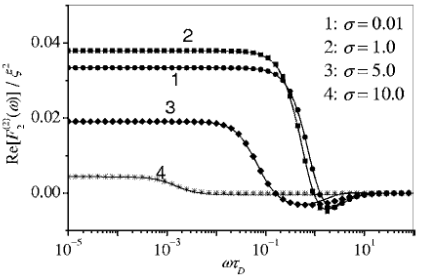

Fig. C.3. Exact Re $[F_2^{(2)}(\omega)]/\xi^2$ (C.13, *solid lines*) and approximate ((C.17), symbols) *symbols*

diffusion ($\sigma = 0$), $\chi_2 = 1/15$, $\tau_2^{eff} = \tau_D/3$, $\lambda_1 = 1/\tau_D$, and $\Delta_2 = 1$ so that (C.17) reduces to the known results [122], [124].

Finally as in [122], [124], $f_1^{(1)}(t)$, and $f_2^{(2)}(t)$ yield the NLDE $f_1^{(3)}(t)$. We have

$$f_1^{(3)}(t) = -\frac{1}{6}\left(\langle P_1^4\rangle_0 - 3\langle P_1^2\rangle_0^2\right)\int_{-\infty}^{t}\xi(t')\dot{\Phi}^{(3)}(t-t') \times \int_{-\infty}^{t'}\xi(t'')\dot{\Phi}_{2,2}(t'-t'') \times \int_{-\infty}^{t''}\dot{\Phi}^{(1)}(t''-t''')\xi(t''')\mathrm{d}t'''\mathrm{d}t''\mathrm{d}t' \tag{C.18}$$

representing the generalization of (21) of [122] or (14.21) of [124] to a mean field. $\Phi^{(3)}(t)$ contains the contribution of the matrix elements of the KER to $f_1^{(3)}(t)$ and is represented by a two-mode approximation as the propagator involves overbarrier relaxation.

We have described exact and approximate calculations of the nonlinear orientational ac response of permanent dipoles in the presence of a uniaxial potential (C.1). The approximate calculation accurately represents the relevant matrix elements of the exact time-ordered matrix exponential solution generated by perturbation theory using Picard's method [122], [124], [331]. Thus the approximate solution effectively generalizes the existing analytic results for noninteracting dipoles in ac driving fields to a mean field potential and has a similar mathematical form (C.17) (but with parameters given in terms of the barrier height parameter σ), so explaining the successful application of the known frequency-dependence of the KER for free diffusion to the analysis of experimental spectra of electric birefringence of nematics which was previously done without any theoretical justification (see, e.g., [532]). The results apply to both nonlinear dielectric relaxation and KER of nematics, and magnetic birefringence relaxation of ferrofluids. The solution of the problem citing, for example, the matrix element $f_2^{(2)}(t)$, clearly demonstrates that the dc component of a second-order nonlinear response contains information about the linear response function. This fact suggests possible methods of measurement of the overbarrier relaxation time (inverse Kramers rate) via the dc electric or magnetic birefringence. We have illustrated

the calculation for the simplest mean field potential and have ignored induced moments. The calculation may, however, be very easily extended to (a) nonstationary response, (b) induced moments, and (c) other mean field potentials such as biaxial anisotropy. Finally, the method may be extended to fractional Brownian motion resulting in anomalous relaxation as described in [142].

References

1. M. Abramowitz, I.A. Stegun: *Handbook of Mathematical Functions* (Dover, New York 1970)
2. R. Abrines R, I.C. Percival: Proc. R. Soc. A **88**, 861 (1966)
3. R. Abrines, I.C. Percival: Proc. Phys. Soc. London **88**, 873 (1966)
4. Y. Aharonov, J. Anandan: Phys. Rev. Lett. **58**, 1593 (1987)
5. A. Aharoni: Phys. Rev. **135**, 793 (1964)
6. A. Aharoni: Phys. Rev. **177**, 793 (1969)
7. A. Aharoni: *An Introduction to the Theory of Ferromagnetism* (Oxford University, London 1996)
8. N.I. Akhiezer: *Calculus of Variations* (Blaisdell, New York 1962)
9. L.H. Andersen, P. Hvelplund, H. Knudsen, S.P. Møller, J.O.P. Pedersen, S. Tang-Petersen, K. Elsener, E. Morenzoni: Phys. Rev. A **41**, 6536 (1990)
10. D. Andrick: J. Phys. B: At. Mol. Phys. **12**, L175 (1979)
11. R. Anholt et al: Phys. Rev. Lett. **53**, 234 (1984)
12. R. Anholt: Phys. Rev. A **31**, 3579 (1985)
13. R. Anholt, U. Becker: Phys. Rev. A **36**, 4628-4636 (1987)
14. H.A. Antosiewicz: *Handbook of mathematical functions* ch. 10 (Dover, New York 1965)
15. E.A.G. Armour, J.M. Carr: Nucl. Instrum. Meth. Phys. Res. B **143**, 218 (1998)
16. P. Ashley, J. Moxom, G. Laricchia: Phys. Rev. Lett. **77**, 1250 (1996)
17. Y.K. Bae, M.J. Coggiola, J.R. Peterson: Phys. Rev. A **28**, 3378 (1983)
18. Y.K. Bae, J.R. Peterson: Phys. Rev. A **37**, 3254 (1988)
19. A.J. Baltz, M.J. Rhoades-Brown, J. Wesener: Phys. Rev. A **44**, 5569 (1991)
20. A.J. Baltz, M.J. Rhoades-Brown, J. Wesener: Phys. Rev. A **48**, 2002 (1993)
21. A.J. Baltz, M.J. Rhoades-Brown, J. Wesener: Phys. Rev. A **50**, 4842 (1994)
22. A.J. Baltz, M.J. Rhoades-Brown, J. Wesener: Phys. Rev. E **54**, 4233 (1996)
23. D. Banks, K.S. Barnes, J.McB. Wilson: J. Phys. B **9**, L141-4 (1976)
24. A. Bárány: J. Phys. B **11**, L399 (1978)
25. A. Bárány: J. Phys. B **12**, 2841 (1979)
26. A. Bárány: J. Phys. B **13**, 147 (1980)
27. A. Bárány, D.S.F. Crothers: Physica Scripta **23**, 1096 (1981)
28. A. Bárány, D.S.F. Crothers: Proc. R. Soc. Lond. A **385**, 129 (1983)
29. A. Bárány et al: J. Phys. B: At. Mol. Phys. **19**, L427 (1986)
30. E. Barkai, R.J. Silbey: J. Phys. Chem. B **104**, 3866 (2000)
31. G. Basbas, W. Brandt, R. Laubert: Phys. Rev. A **7**, 983 (1973)

32. Bateman Manuscript Project: *Higher transcendental functions*, II (McGraw-Hill, New York 1953)
33. H. Bateman, A. Erdelyi, W. Magnus, F. Oberhettinger, F.G. Tricomi: *Higher Transcendental Functions, Bateman Manuscript Project*, vol 1 (McGraw-Hill, New York 1953)
34. D.R. Bates: Proc. Roy. Soc. A **247**, 294 (1958)
35. D.R. Bates: *Quantum theory*, Vol I (Academic Press, New York 1961)
36. D.R. Bates: *Atomic and Molecular Processes*, ed D.R. Bates (Academic, New York 1962)
37. D.R. Bates: Comments At Mol Phys **1**, 127 (1970)
38. D.R. Bates: Phys. Rep. **35** (4), 305 (1978)
39. D.R. Bates, D.A. Williams: Proc. Phys. Soc. A **83**, 245 (1964)
40. D.R. Bates, D.S.F. Crothers: Proc. Roy. Soc. Lond. A **315**, 465 (1970)
41. D.R. Bates, G. Griffing: Proc. Phys. Soc. A **66**, 961-71 (1953)
42. D.R. Bates, A.R.Holt: Proc. Roy. Soc. Lond. A **292**, 168 (1966)
43. D.R. Bates, H.S.W. Massey, A.L. Stewart: Proc. Roy. Soc. Lond. A **216**, 437 (1953)
44. D.R. Bates, R. McCarroll: Proc. Roy. Soc. A **245**, 175 (1958)
45. D.R. Bates, R. McCarroll: Adv. Phys. **11**, 39 (1962)
46. D.R. Bates, R.H.G. Reid: Adv. At. Mol. Phys. **4**, 13 (1968)
47. D.R. Bates, D. Sprevak: Chem. Phys. Lett. **10**, 428 (1971)
48. G. Baur: Phys. Lett. B **311**, 343 (1993)
49. G. Baur et al.: Phys. Lett. B **368**, 251 (1996)
50. J.E. Bayfield: Phys. Rev. **185**, 105-112 (1969)
51. J.E. Bayfield, G.A. Khayrallah: Phys. Rev. A **12**, 869 (1975)
52. J.E. Bayfield, E.E. Nikitin, A.I. Reznikov: Chem. Phys. Lett. **19**, 471 (1973) (Errata, **21**, 212)
53. C.P. Bean, J.D. Livingston: Suppl. J. Appl. Phys. **30**, 120S (1959)
54. U. Becker, N. Grün and W. Scheid: J. Phys. B **20**, 2075 (1987)
55. U. Becker: J. Phys. B **20**, 6563 (1987)
56. A. Belkacem, H. Gould, B. Feinberg, R.R. Bossingham, W.E. Meyerhof: Phys. Rev. Lett. **71**, 1514 (1993)
57. A. Belkacem, H. Gould, B. Feinberg, R.R. Bossingham, W.E. Meyerhof: Phys. Rev. Lett. **73**, 2432 (1994)
58. A. Belkacem, H. Gould, B. Feinberg, R.R. Bossingham, W.E. Meyerhof: Phys. Rev. A **50**, 4842 (1994)
59. A. Belkacem, H. Gould, B. Feinberg, R.R. Bossingham, W.E. Meyerhof: Phys. Rev. A **56**, 2806 (1997)
60. A. Belkacem, N. Claytor, T. Dinneen, B. Feinberg, H. Gould: Phys. Rev. A **58**, 1253 (1998)
61. D. Belkić: J. Phys. B: At. Mol. Phys. **10**, 3491 (1977)
62. D. Belkić: J. Phys. B: At. Mol. Phys. **11**, 3529 (1978)
63. D. Belkić: J. Phys. B: At. Mol. Phys. **12**, 337 (1979)
64. D. Belkić: *Principles of Quantum Mechanics* (Institute of Physics Publishing, London 2003)
65. H. Benoit: Ann. Phys. Paris **6**, 561 (1951)
66. H. Benoit: J. Chim. Phys. Paris **49**, 517 (1952)
67. K.H. Berkner, W.G. Graham, R.V. Pyle, A.S. Schlachter, J.W. Stearns: Phys. Rev. A **23**, 2891-904 (1981)
68. K.H. Berkner, W.G. Graham, R.V. Pyle, A.S. Schlachter, J.W. Stearns, R.E. Olson: J. Phys. B **11**, 875-85 (1978)
69. M.V. Berry: Proc. R. Soc. A **392**, 45 (1984)

70. M.V. Berry: Nature **326**, 277 (1987)
71. M.V. Berry: Proc. R. Soc. Lond. A **422**, 7 (1989)
72. M.V. Berry, K.E. Mount: Rep. Prog. Phys. **35**, 315 (1972)
73. C.A. Bertulani, G. Baur: Phys. Rep. **163**, 299 (1988)
74. C.A. Bertulani, G. Baur: Phys. Rev. D, 034005 (1998)
75. L. Bessais, L. Ben Jaffel, J.L. Dormann: Phys. Rev. B **45**, 7805 (1992)
76. H.A. Bethe, E.E. Salpeter: *Quantum Mechanics of One- and Two-Electron Atoms* (Academic, New York 1957)
77. E. Bichoutskaia, D.S.F. Crothers, D. Sokolovski: Proc. Roy. Soc. Lond. A **458**, 1399 (2002)
78. E. Bichoutskaia, D.S.F. Crothers: J. Phys. B **36**, 11 (2003)
79. G. Billing, K.V. Mikkelsen: *Molecular Dynamics and Chemical Kinetics*, (J. Wiley & Sons, New York 1996)
80. T. Bitter, D. Dubbers: Phys. Rev. Lett. **59**, 251 (1987)
81. G. Blanford, D.C. Christian, K. Gollwitzer, M. Mandelkern, C.T. Munger, J. Schlutz, G. Zioulas: Phys. Rev. Lett. **80**, 3037 (1998)
82. J. Bradley, S.F.C. O'Rourke, D.S.F. Crothers: Phys. Rev. A **71**, 032706 (2005)
83. J. Bradley, S.F.C. O'Rourke, D.S.F. Crothers: J. Phys. B **38**, 1695 (2005)
84. J. Bradley, S.F.C. O'Rourke, D.S.F. Crothers: to be published (2007)
85. B.H. Bransden: Adv. At. Mol. Opt. Phys. **1**, 85 (1965)
86. B.H. Bransden: Rep. Prog. Phys **35**, 949 (1972)
87. L. Brillouin: C. R. Acad. Sci. Paris **183**, 24 (1926)
88. D.M. Brink: *Semi-classical methods for nucleus-nucleus scattering*, (Cambridge, London 1985)
89. H.C. Brinkman, H.A. Kramers: Proc. Acad. Soc. Amsterdam **33**, 973 (1930)
90. W.F. Brown Jr: J. Appl. Phys. Suppl. **30**, 130S (1959)
91. W.F. Brown Jr: Phys. Rev. **130**, 1677 (1963)
92. S.J. Brotton, S. Cvejanovic, F.J. Currel, N.J. Bowring, F.H. Read: Phys. Rev. A. **55**, 318 (1997)
93. G.J.N. Brown, D.S.F. Crothers: J. Phys. B **27**, 5309 (1994)
94. G.J.N. Brown, D.S.F. Crothers: Phys. Rev. Lett. **76**, 392 (1996)
95. G.J.N. Brown, D.S.F. Crothers, *The Physics of Electronic and Atomic collisions, XX International Conference Progress Report: Invited talks of XXth Int. Conf. on Photonic, Electronic and Atomic collsions, Vienna, Austria, July 1997*, edited by F. Aumayr and H. Winter, (World Scientific, 1997), p525
96. J.N.H. Brunt, G.C. King, F.H. Read: J. Phys. B: At. Mol. Phys. **10**, 433 (1977)
97. V.E. Bubelev, D.H. Madison: J. Phys. B **26**, 3541 (1993)
98. S.J. Buckman, P. Hammond, F.H. Read, G.C. King: J. Phys. B: At. Mol. Phys. **16**, 4039 (1983)
99. S.J. Buckman, D.S. Newman: J. Phys. B: At. Mol. Phys. **20**, L711 (1987)
100. K.G. Budden: *The Propagation of Radio Waves*, (Cambridge Univ Press 1961)
101. K.G. Budden: *Radio Waves in the Ionosphere*, (Cambridge Univ Press 1985)
102. A.V. Bunge, C.F. Bunge: Phys. Rev. A **19**, 452 (1979)
103. P.G. Burke, W.T. Robb: Adv. Atom. Molec. Phys. **11**, 144 (1975)
104. W.D. Burns, D.S.F. Crothers: J. Phys. B **9**, 2479-2498 (1976)
105. V.K. Bykovskii, E.E. Nikitin, M.Ya. Ovchinnikova: Sov. Phys.-JETP **20**, 500 (1965)
106. O.A. Caldeira, A.J. Leggatt: Physica A **121**, 587 (1983)
107. D.R.J. Carruthers, D.S.F. Crothers: J. Phys. B: At. Mol. Phys. **24**, L199 (1991)
108. D.R.J. Carruthers, D.S.F. Crothers: Z. Phys. D **23**, 365 (1992)

109. M.C. Charlton: Phys. Atom. Nucei **61**, 1625 (1998)
110. M. Chassid, M. Horbatsch: Phys. Rev. A **66**, 012714 (2002)
111. J.C.Y. Chen, K.M. Watson: Phys. Rev. **174**, 152 (1968)
112. I.M. Cheshire: Proc. Phys. Soc. London **84**, 89 (1964)
113. This name dates from [I.M. Cheshire, Proc. Phys. Soc. **84**, 89 (1964)] and should not be confused with 'charge-density waves' as used in solid-state physics.
114. R.Y. Chiao, Y.S. Wu: Phys. Rev. Lett. **57**, 933 (1986)
115. M.S. Child: Molec. Physics **20**, 171 (1971)
116. M.S. Child: *Molecular Collision Theory* (Academic Press, London 1974)
117. P. Chocian, W. Ihra, P.F. O'Mahony: Phys. Rev. A **57**, 3583 (1998)
118. Y.P. Chong, W.L. Fite: Phys. Rev. A **16**, 933-942 (1977)
119. M.F. Ciappina, W.R. Cravero, C.R. Garibotti: J. Phys. B **36**, 3775 (2003)
120. W.T. Coffey, D. de Cogan, P.J. Cregg, D.S.F. Crothers, K.P. Quinn, C.N. Scully (private communication)
121. W.T. Coffey, A. Morita: J. Phys. D **9**, 47 (1976)
122. W.T. Coffey, B.V. Paranjape: Proc. R. Ir. Acad. Sect. A **78**, 17 (1978)
123. W.T. Coffey: Development and Application of the Theory of Brownian Motion. In: *Dynamical Processes in Condensed Matter, Adv. Chem. Phys.* **63**, 69, ed by M.W. Evans, Series eds I. Prigogine, S. Rice (Wiley, New York 1985)
124. W.T. Coffey: Adv. Chem. Phys. **63**, 69 (1985)
125. W.T. Coffey, D.S.F. Crothers, Yu.P. Kalmykov, E.S. Massawe, J.T. Waldron: J. Magn. Magn. Mat. **127**, L254 (1993)
126. W.T. Coffey, P.J. Cregg, Yu.P. Kalmykov: Adv. Chem. Phys. **83**, 263 (1993)
127. W.T. Coffey, Yu.P. Kalmykov, E.S. Massawe: Phys. Rev. E: **48**, 669 (1993)
128. W.T. Coffey, Yu.P. Kalmykov, E.S. Massawe, J.T. Waldron: J. Chem. Phys. **99**, 4011 (1993)
129. W.T. Coffey, Yu.P. Kalmykov, E.S. Massawe: The effective eigenvalue method and its application to stochastic problems in conjunction with the non-linear Langevin equation. In: *Modern Non-linear Optics*, *Advances in Chemical Physics*, vol 85, part 2, ed by I. Prigogine, S.A. Rice and M.W. Evans (Wiley-Interscience, New York 1993) p 667
130. W.T. Coffey, D.S.F. Crothers, Yu.P. Kalmykov, E.S. Massawe, J.T. Waldron: Phys. Rev. E **49**, (3) 1869 (1994)
131. W.T. Coffey, D.S.F. Crothers, J.T. Waldron: Physica A **203**, 600 (1994)
132. W.T. Coffey, D.S.F. Crothers, Yu.P. Kalmykov, J.T. Waldron: Physica A **213**, 551 (1995)
133. W.T. Coffey et al: Phys. Rev. B **52**, 15 951 (1995)
134. W.T. Coffey, D.S.F. Crothers, J.L. Dormann, L.J. Geoghegan, E.C. Kennedy: Phys. Rev. B **58**, 3249 (1998)
135. W.T. Coffey: Adv. Chem. Phys. **103**, 259 (1998)
136. W.T. Coffey, D.S.F. Crothers, J.L. Dormann, L.J. Geoghegan, E.C. Kennedy, W. Wernsdorfer: J. Phys. Cond. Matter **10**, 9093 (1998)
137. W.T. Coffey, J.L. Dormann, Yu.P. Kalmykov, E.C. Kennedy, W. Wernsdorfer: Phys. Rev. Lett **80**, 5655 (1998)
138. W.T. Coffey, Yu.P. Kalmykov, S.V. Titov: Phys. Rev. E **65**, 032102 (2002)
139. W.T. Coffey: J. Mol. Liq. **114**, 5 (2004)
140. W.T. Coffey, Yu.P. Kalmykov, S.V. Titov: J. Mol. Liq. **114**, 35 (2004)
141. W.T. Coffey, Yu.P. Kalmykov, S.V. Titov, J.K.Vij: Phys. Rev. E **72**, 011103 (2005)
142. W.T. Coffey, Yu. P . Kalmykov, J.T. Waldron: *The Langevin Equation*, 2edn (World Scientific Publishing, Singapore 2004)
143. W.T. Coffey, D.S.F. Crothers, Yu.P. Kalmykov, P.M. Déjardin: Phys. Rev. E **71**, 062102 (2005); Appendix C

144. W.T. Coffey, D.S.F. Crothers, Yu.P. Kalmykov: J. Non-Crystalline Solids **352**, 4710 (2006)
145. D. Cohen: Phys. Rev. Lett. **78**, 2878 (1997)
146. D.S. Condren, J.F. McCann, D.S.F. Crothers: J. Phys. B: At. Mol. Opt. Phys. **39**, 3639 (2006)
147. P.I. Cootner: *The Random Character of Stock Market Prices* (The M.I.T. Press, Cambridge, Mass. 1964)
148. F.B.M. Copeland, D.S.F. Crothers: J. Phys. B: At. Mol. Opt. Phys. **27**, 2039 (1994)
149. F.B.M. Copeland, D.S.F. Crothers: J. Phys. B: At. Mol. Opt. Phys. **28**, L763 (1995)
150. F.B.M. Copeland, D.S.F. Crothers: Atomic and Nuclear Data Tables **65**, 273 (1997)
151. P.M. Corcoran, W.T. Coffey: Chem. Phys. Lett. **144**, 2 (1988)
152. P.V. Coveney, M.S. Child, A. Bárány: J. Phys. B: At. Mol. Phys. **18**, 4557 (1985)
153. P.V. Coveney, D.S.F. Crothers, J.H. Macek: J. Phys. B: At. Mol. Phys. **21**, L165 (1988)
154. T.E. Cravens: Astrophys. J. **532**, L153 (2000)
155. H.J. Crawford: Ph.D. Thesis, University of California (1979)
156. R.J. Cross: J. Chem. Phys. **47**, 3724 (1967)
157. D.S.F. Crothers: Ph.D. Thesis, Queens University Belfast (1966)
158. D.S.F. Crothers, A.R. Holt: Proc. Phys. Soc. **88**, 75, (1966)
159. D.S.F. Crothers, R.P. McEachran: J Phys. B **3**, 976 (1970)
160. D.S.F. Crothers: Adv. Phys. **20**, 405 (1971)
161. D.S.F. Crothers: J. Phys. A. **5**, 256 (1972)
162. D.S.F. Crothers: J. Phys. B: At. Mol. Phys. **6**, 1418 (1973)
163. D.S.F. Crothers: J. Phys. B: At. Mol. Phys. **8**, L442 (1975)
164. D.S.F. Crothers: J. Phys. B: At. Mol. Phys. **9**, 635 (1976)
165. D.S.F. Crothers: J. Phys. B: At. Mol. Phys. **10**, L557 (1977)
166. D.S.F. Crothers, J.G. Hughes: J. Phys. B: At. Mol. Phys. **10**, L557 (1977)
167. D.S.F. Crothers: J. Phys. B: At. Mol. Phys. **11**, 1025 (1978)
168. D.S.F. Crothers, J.G. Hughes: Proc. R. Soc. Lond. A **359**, 345-363 (1978)
169. D.S.F. Crothers, N.R. Todd: J. Phys. B: At. Mol. Phys. **11**, L663 (1978)
170. D.S.F. Crothers: J. Phys. B: At. Mol. Phys. **12**, 775 (1979)
171. D.S.F. Crothers, J.G. Hughes: J.Phys. B **12**, L567-570 (1979)
172. D.S.F. Crothers, J.G. Hughes: Phys. Rev. Lett. **43**, 1584-1587 (1979)
173. D.S.F. Crothers, J.G. Hughes: Philos. Trans. R. Soc. **292**, 539-561 (1979)
174. D.S.F. Crothers, N.R. Todd: J. Phys. B: At. Mol. Phys. **13**, 547 (1980)
175. D.S.F. Crothers: *Advances in atomic molecular physics*, vol 17, pp 55 (Academic Press, New York 1981)
176. D.S.F. Crothers, N.R. Todd: J. Phys. B **14**, 2233-2249 (1981)
177. D.S.F. Crothers, N.R. Todd: J. Phys. B **14**, 2251-2258 (1981)
178. D.S.F. Crothers: J. Phys. B: At. Mol. Phys. **15**, 2061 (1982)
179. D.S.F. Crothers: Physica Scripta **T3**, 236 (1983)
180. D.S.F. Crothers, J.F. McCann: J. Phys. B: At. Mol. Phys. **16**, 3229-3242 (1983)
181. D.S.F. Crothers, J.G. Hughes: Comments At. Mol. Phys. **15**, 15-28 (1984)
182. D.S.F. Crothers, J.F. McCann: J. Phys. B: At. Mol. Phys. **17**, L177 (1984)
183. D.S.F. Crothers: Math. Rev. **85j** No 34121, 4428 (1985)
184. D.S.F. Crothers: J. Phys. B **18**, 2879 (1985)
185. D.S.F. Crothers: J. Phys. B **18**, 2893 (1985)
186. D.S.F. Crothers: J. Phys. B: At. Mol. Phys. **19**, 463 (1986)
187. D.S.F. Crothers: Nucl. Instrum. Meth. Phys. Res. B **27**, 555 (1987)
188. D.S.F. Crothers, K.M. Dunseath: J. Phys. B: At. Mol. Phys. **20**, 4115 (1987)

189. D.S.F. Crothers, R. McCarroll: J. Phys. B **20**, 2835 (1987)
190. D.S.F. Crothers, D.J. Lennon: J. Phys. B: At. Mol. Phys. **21**, L409 (1988)
191. D.S.F. Crothers, L.J. Dubé: J. Phys. B: At. Mol. Opt Phys. **22**, L609 (1989)
192. D.S.F. Crothers, L.J. Dub*é*: Adv. At. Mol. Opt. Phys. **30** 287, (1993)
193. D.S.F. Crothers, S.F.C. ORourke: J. Phys. B: At. Mol. Phys. **26**, L547 (1993)
194. D.S.F. Crothers: *Barriers, thresholds and Negative Ions* in Physics World **12**, 21 (1999)
195. D.S.F. Crothers, A.M. Loughan: Phil. Trans. R. Soc. A **357**, 1391 (1999)
196. D.S.F. Crothers: *Relativistic Heavy Particle Collision Theory* (Kluwer Academic/Plenum Publishers, New York 2000)
197. D.S.F. Crothers, D.M. McSherry, S.F.C. O'Rourke, C. McGrath, M.B. Shah, H.B. Gilbody: Phys. Rev. Lett. **88**, 053201 (2002)
198. D.S.F. Crothers, P.G. Mulligan: Phase-Integral Derivation of Parabolic-Model Stokes Constants, Chapter 8, 93-123, in *Nonadiabatic transitions in quantum systems*, ed Osherov, Ponomarev (Chernogolovka, Russia 2004)
199. D.S.F. Crothers, D. Holland, Yu.P. Kalmykov, W.T. Coffey: J. Mol. Liq. **114**, 27 (2004)
200. D.S.F. Crothers, F.B.M. McCausland, J.T. Glass, J.F. McCann, S.F.C. O'Rourke, R.T. Pedlow: Continuum Distorted Wave and Wannier Methods CH 52 in *Springer Handbook of Atomic, Molecular and Optical Physics*, ed G.W.F. Drake (Springer, New York 2006)
201. N.C. Deb, D.S.F. Crothers; J. Phys. B: At. Mol. Opt. Phys **23**, L799 (1990)
202. N.C. Deb, D.S.F. Crothers: J. Phys. B: At. Mol. Opt. Phys. **33**, L623 (2000)
203. N.C. Deb, D.S.F. Crothers: J. Phys. B: At. Mol. Opt. Phys. **34**, 143 (2001)
204. N.C. Deb, D.S.F. Crothers: Phys. Rev. A **63**, 034701 (2001)
205. N.C. Deb, D.S.F. Crothers: J. Phys. B: At. Mol. Phys. **35**, L85 (2002)
206. P. Debye: *Polar Molecules*, (Chemical Catalog, New York 1929) (Reprinted by: Dover, New York)
207. F. Decker: Phys. Rev. A **41**, 65524 (1990)
208. F. Decker, J. Eichler: J. Phys. B: At. Mol. Phys. **26**, 2081 (1993)
209. G.R. Deco, R.D. Rivarola: J. Phys. B **21**, 1229 (1988); J. Phys. B **21**, 1861 (1988); J. Phys. B **21**, L299 (1988)
210. G.R. Deco, R.D. Rivarola: J. Phys. B **22**, 1043 (1989)
211. G.R. Deco, N. Grün: J. Phys. B **22**, 1357 (1989)
212. J.L. Déjardin, Yu.P. Kalmykov, P.M. Déjardin: Adv. Chem. Phys. **117**, 275 (2001)
213. J.L. Déjardin, J. Jadzyn: J. Chem. Phys. **122**, 074502 (2005)
214. D. Delande, A. Buchleitner: Adv. At. Mol. Opt. Phys. **34**, 85 (1994)
215. J.B. Delos: Phys. Rev. A **9**, 1626 (1974)
216. J.B. Delos, W.R. Thorson: Phys. Rev. Lett. **28**, 647 (1972)
217. J.B. Delos, W.R. Thorson: Phys. Rev. A **6**, 720 (1972)
218. J.B. Delos, W.R. Thorson: Phys. Rev. A **6**, 728 (1972) (Errata: A **9**, 1026)
219. J.B. Delos, W.R. Thorson: Phys. Rev. A **9**, 1026 (1974)
220. J.B. Delos, W.R. Thorson, S.K. Knudson: Phys. Rev. A **6**, 709 (1972)
221. Yu.N. Demkov: Soviet Physics JETP **18**, 138 (1964)
222. Yu.N. Demkov, M. Kunicke: Vestn. Leningr. Univ. No. **16**, 39 (1969)
223. K. Dettmann, K.G. Harrison, M.W. Lucas M W: J. Phys B **7**, 269-187 (1974)
224. A. Devdariani, E. Bichoutskaia, E. Tchesnokov, T. Bichoutskaia, D.S.F. Crothers, E. Leboucher-Dalimier, P. Sauvan, P. Angelo: J. Phys. B: At. Mol. Opt. Phys. **35**, 2469 (2002)
225. M.S. Dimitrijevic, P.V. Grujic, N.S. Simonovic: J. Phys. B **27**, 5717 (1994)
226. R.B. Dingle: *Asymptotic Expansions: their derivations and interpretation* (Academic Press, London 1973)

227. I.R. Dodd, K.R. Greider: Phys. Rev. **146**, 675 (1966)
228. M. Domke, K. Schulz, G. Remmers, G. Kaindl: Phys. Rev. A. **53**, 1424 (1996)
229. J.L. Dormann et al: Phys. Rev. B **53**, 14 297 (1996)
230. J.L. Dormann, D. Fiorani, E. Tronc: Adv. Chem. Phys. **98**, 283 (1997)
231. R.M. Drisko PhD Thesis, Carnegie Institute of Technology (1955)
232. G.V. Dubrovskiy: Soviet Phys. J.E.T.P. **19**, 591 (1964)
233. O. Dulieu, C. Le Sech: Europhys. Lett. **3**, 975 (1987)
234. K.M. Dunseath: PhD Thesis, Queen's University Belfast (1990)
235. K.M. Dunseath, D.S.F. Crothers: J. Phys. B **24**, 5003 (1991)
236. J. Eades: Comments At. Mol. Phys **31**, 51 (1995)
237. J. Eichler: Phys. Rep. **193**, 165 (1990)
238. J. Eichler: Phys. Rev. Lett. **75**, 3653 (1995)
239. A. Einstein: Ann. Phys. **17**, 549 (1905), reprinted in 'Investigations on the Theory of the Brownian Motion', R. Fürth (Ed.), (Dover Publications, New York 1954)
240. A. Einstein: *Dynamical Theories of Brownian Motion* (Princetom University Press, Princeton 1967)
241. D. Elizaga et al: J. Phys. B: At. Mol. Opt. Phys. **32**, 857(1999)
242. W.D. Ellison, S. Borowitz: In *Atomic collision processes* ed. M.R.C. McDowell, pp790 (Amsterdam, North-Holland 1964)
243. H. Enge: *Introduction to Nuclear Physics* (Addison-Wesley, Reading, Mass., 1978)
244. A. Erdélyi et al: *Higher Transcendental Functions, Bateman Manuscript Project*, (McGraw-Hill, New York 1953)
245. L.F. Errea, J.M. Gómez-Llorente, L. Méndez, A. Riera: Phys. Rev. A **32**, 2158 (1985)
246. L.F. Errea, J.M. Gómez-Llorente, L. Méndez, A. Riera: Phys. Rev. A **35**, 4060 (1987)
247. L.F. Errea, C. Harel, C. Illescas, H. Jouin, L. Méndez, B. Pons, A. Riera: J. Phys. B: At. Mol. Opt. Phys. **31**, 3199 (1998)
248. L.F. Errea, C. Harel, H. Jouin, J.M. Maidagan, L. Méndez, B. Pons, A. Riera: Phys. Rev. A **46**, 5617 (1992)
249. L.F. Errea, C. Harel, H. Jouin, J.M. Maidagan, L. Méndez, B. Pons, A. Riera: J. Phys. B: At. Mol. Opt. Phys. **27**, 3603 (1994)
250. L.F. Errea, J.M. Maidagan, L. Méndez, A. Riera: J. Phys. B: At. Mol. Opt. Phys. **24**, L387 (1991)
251. L.F. Errea, L. Méndez, A. Riera: J. Phys. B: At. Mol. Opt. Phys. **15**, 101 (1982)
252. L.F. Errea, L. Méndez, A. Riera: Phys. Lett. A **92**, 231-234 (1982)
253. L.F. Errea, L. Méndez, A. Riera: Phys. Rev. A **37**, 2404 (1989)
254. L.F. Errea, L. Méndez, A. Riera: J. Phys. B: At. Mol. Opt. Phys. **28**, 907 (1995)
255. B.D. Esry, Z. Chen, C.D. Lin, R.D. Piacentini: J. Phys. B **26**, 1579-1586 (1993)
256. B.C. Eu: *Semiclassical Theories of Molecular Scattering* (Springer-Verlag, Berlin 1984)
257. Europhysics news **29**, 6, 190 Nov/Dec (1998)
258. H. Exton: *Handbook of Hypergeometric Integrals* (Halsted Press, New York 1978)
259. P.D. Fainstein, V.H. Ponce, R.D. Rivarola: Phys. Rev. A **36**, 3639 (1987)
260. P.D. Fainstein, V.H. Ponce, R.D. Rivarola: J. Phys. B **21**, 287 (1988)
261. P.D. Fainstein, V.H. Ponce, R.D. Rivarola: J. Phys. E: At. Mol. Opt. Phys. **21**, 2989 (1988)
262. P.D. Fainstein, V.H. Ponce, R.D. Rivarola: J. Phys. B **24**, 3091 (1991)
263. U. Fano: Phys. Rev. A **22**, 2660 (1980)
264. J.M. Feagin, J. Macek: J. Phys. B: At. Mol. Phys. **17**, L245 (1984)
265. A.F. Ferguson: Proc. R. Soc. A **264**, 540 (1961)
266. A.F. Ferguson, R. McCarroll: Proc. R. Soc. A **547** (1961)

267. J. Fiol, R.E. Olson: Nucl. Instrum. Methods Phys. Res. B **205**, 474 (2003)
268. O.B. Firsov: Zh. Eksp. Teor. Fiz. **21**, 1001 (1951)
269. D. Fischer, R. Moshammer, M. Schulz, J. Ullrich: J. Phys. B **36**, 3555 (2003)
270. W.L. Fite, A.C.H. Smith, R.F. Stebbing: Proc. R. Soc. A **268**, 527 (1962)
271. M.R. Flannery: American Journal of Physics, **73** (3),265 (2005)
272. W.C. Fon, K.A. Berrington, P.G. Burke, A.E. Kingston: J. Phys. B **22**, 3939 (1989)
273. M. Foster, D.H. Madison, J.L. Peacher, J. Ullrich: J. Phys. B **37**, 3797 (2004)
274. W. Fritsch, C.D. Lin: J. Phys. B **15**, 1255 (1982)
275. W. Fritsch, C.D. Lin: Phys. Rev. A **16**, 762 (1982)
276. W. Fritsch, C.D. Lin: Phys. Rev. A **26**, 762-769 (1982)
277. W. Fritsch, C.D. Lin: Phys. Scripta **T3**, 241-243 (1983)
278. W. Fritsch, C.D. Lin: Phys. Rev. A **41**, 4776 (1990)
279. W. Fritsch, C.D. Lin: Phys. Rep. **202**, 1 (1991)
280. W. Fritsch: J. Phys. B **27**, 3461-3474 (1994)
281. H. Fröhlich: *Theory of Dielectrics*, 2nd edn, (Oxford University Press, Oxford 1958)
282. N. Fröman, P.O. Fröman: *J.W.K.B. - approximation, contributions to the theory* (Amsterdam, North-Holland 1965)
283. N. Fröman, S. Yngve: Phys. Rev. D **22**, 1375 (1980)
284. N. Fröman, P.O. Fröman, B. Lundborg: *Phase-integral method: allowing nearlying transition points*, Chapter 5 (Springer-Verlag, New York 1996)
285. H. Fukuda, N. Koyama, M. Matsuzawa: J. Phys. B: At. Mol. Phys. **20**, 2959 (1987)
286. A.T. Fuller: *Nonlinear Stochastic Control Systems* (Taylor & Francis, London 1970)
287. W.H. Furry: Phys. Rev. **71**, 360 (1947)
288. T. Furukawa, K. Matsumoto: Jpn. J. Appl. Phys., Part 1 **31**, 840 (1992)
289. R. Gans: Ann. Phys. Lpz. **47**, 709 (1915)
290. A. Garg: Phys. Rev. B **51**, 15 592 (1995)
291. C.R. Garibotti, J.E. Miraglia: Phys. Rev. A **21**, 572-80 (1980)
292. R. Gayet: J. Phys. B **5**, 483-91 (1972)
293. L.J. Geoghegan, W.T. Coffey, B. Mulligan: Adv. Chem. Phys. **100**, 475 (1997)
294. T.L. Gilbert: Phys. Rev. **100**, 1243 (1955)
295. H.B. Gilbody: Adv. At. Mol. Opt. Phys. **22**, 143 (1986)
296. H.B. Gilbody: Adv. At. Mol. Opt. Phys. **33**, 149 (1994)
297. G.H. Giliespie: J. Phys. B **15**, L729-32 (1982)
298. G.H. Giliespie: Phys. Lett. **93A**, 327-32 (1983)
299. J.T. Glass, J.F. McCann, D.S.F. Crothers: J. Phys. B **25**, L541 (1992); J. Phys. B **27**, 3975 (1994)
300. J.T. Glass, J.F. McCann, D.S.F. Crothers: J. Phys. B **27**, 3445 (1994); J. Phys. B **27**, 3975 (1994)
301. J.E. Golden, J.H. McGuire: Phys. Rev. Lett. **32** 1218-21 (1974)
302. J.E. Golden, J.H. McGuire: Phys. Rev. A **12**, 80-4 (1975)
303. J.E. Golden, J.H. McGuire: Phys. Rev. A **15**, 499-507 (1977)
304. T.A. Green: Proc. Phys. Soc. **86**, 1017-1029 (1965)
305. T.A. Green: Phys. Rev. A **23**, 519-531 (1981)
306. T.A. Green: Phys. Rev. A **23**, 532-545 (1981)
307. T.A. Green, R.E. Johnson: Phys. Rev. **152**, 9 (1966)
308. T.A. Green, E.J. Shipsey, J.C. Browne: Phys. Rev. A **23**, 546-561 (1981)
309. T.A. Green, E.J. Shipsey, J.C. Browne: Phys. Rev. A **25**, 1364-1373 (1982)
310. P.T. Greenland: Contemp. Phys. **38**, 181 (1997)
311. W. Greiner: *Relativistic Quantum Mechanics Wave Equations*, 2nd ed (Springer-Verlag, Berlin 1997)

312. J. Grifone, Z. Muzsnay: *Variational Principles for Second-Order Differential Equations* (World Scientific, Singapore 2000)
313. P.V. Grujić, N.S. Simonović: J. Phys. B: At. Mol. Opt. Phys. **28**, 1159 (1995)
314. M. Gryziński: Phys. Rev. **138**, A336 (1965)
315. C. Guerret-Piécourt et al: Nature (London) **372**, 761 (1994)
316. L. Gulyás, P.D. Fainstein, A. Salin: J. Phys. B **28**, 245 (1995)
317. J. Haansen et al: J. Phys. B: At. Mol. Phys. **15**, 4043 (1964)
318. P. Hänggi, P. Talkner, M. Borkovec: Rev. Mod. Phys. **62**, 251 (1990)
319. D.J. Hardie: PhD thesis, University of Newcastle-upon-Tyne (1981)
320. C. Harel, H. Jouin, B. Pons: At. Data Nucl. Data Tables **68**, 279 (1998)
321. C. Harel, H. Jouin, B. Pons, L.F. Errea, L. Méndez, A. Riera: Phys. Rev. A **55**, 287 (1997)
322. G.J. Hatton et al: J. Phys. B: At. Mol. Phys. **12**, L571 (1979)
323. C. Haritos, Th. Mercouris, C.A. Nicolaides: J. Phys. B: At. Mol. Phys. **31**, L783 (1998)
324. J. Heading: *An Introduction to Phase-Integral Methods* (London: Methuen 1962)
325. P.J. Hicks, J. Cromer: J. Phys. B: At. Mol. Phys. **8**, 1866 (1975)
326. J. Hill, J. Geddes, H.B. Gilbody: J. Phys. B: At. Mol. Phys. **12**, L341-344 (1979)
327. Y.K. Ho: Phys. Rev. A. **34**, 4402 (1986)
328. Y.K. Ho, J. Calloway: Phys. Rev. A. **34**, 130 (1986)
329. D. Holland, Ph.D. Thesis, The Queen's University of Belfast (2005)
330. E. Holøien, J. Midtdal: Proc. Phys. Soc. A **68**, 815 (1955)
331. K. Hosokawa et al: J. Chem. Phys. **110**, 4101 (1999)
332. M.P. Hughes, J. Geddes, H.B. Gilbody: J. Phys. B: At. Mol. Opt. Phys. **27**, 1143 (1994)
333. W.J. Humphries, B.L. Moiseiwitsch: J. Phys. B: At. Mol. Phys, **17**, 2655 (1984)
334. W.J. Humphries, B.L. Moiseiwitsch: J. Phys. B: At. Mol. Phys. **18**, 2295 (1985)
335. Y.J. I'Haya, T. Morikawa: Adv. Quant. Chem. **12**, 43-63 (1980)
336. W. Ihra, J.H. Macek, F. Mota-Furtado, P.F. OMahony: Phys. Rev. Lett. **78**, 4027 (1997)
337. W. Ihra, F. Mota-Furtado, P.F. O'Mahony: Phys. Rev. A **55**, 4263 (1997)
338. D.C. Ionescu, J. Eichler: Phys. Rev. A **54**, 4960 (1996)
339. A. Jain, T.G. Winter: : J. Phys. B: At. Mol. Opt. Phys. **29**, 4675 (1996)
340. I. Jakushina, S. Linnaeus: J. Phys. A: Math. Gen. **28**, 1727 (1995)
341. R.K. Janev, J.J. Smith: Nucl. Fusion (Suppl.) **4**, 1 (1993)
342. H. Jeffreys: Proc. Lond. Math. Soc. **23**, 428 (1923)
343. H. Jeffreys, B.S. Jeffreys: *Methods of Mathematical Physics*, 2nd edn (Cambridge Univ. Press, Cambridge 1950)
344. B.R. Johnson: Chem. Phys. Lett. **27**, 373 (1974)
345. S. Jones, D.H. Madison, MK. Srivastava: J. Phys. B: At. Mol. Opt. Phys. **25**, 1899 (1992)
346. S. Jones, D.H. Madison: Phys. Rev. Lett. **81**, 2886 (1998)
347. S. Jones, D.H. Madison: Phys. Rev. A **62**, 042701 (2000)
348. Yu.P. Kalmykov, W.T. Coffey, S.V. Titov: Phys. Rev. E **69**, 021105 (2004)
349. Yu.P. Kalmykov, W.T. Coffey, D.S.F. Crothers, S.V. Titov: Phys. Rev. E **70**, 041103 (2004)
350. W.C. Keever, E. Everhart: Phys. Rev. **150**, 43 (1966)
351. E.C. Kennedy, Ph.D. thesis, The Queen's University of Belfast (1997)
352. M. Kimura, C.D.0 Lin: Phys. Rev. A **32**, 1357 (1985); Phys. Rev. A **34**, 176 (1986)
353. M. Kimura, W.R. Thorson: Phys. Rev. A **24**, 1780-1792 (1981)
354. M. Kimura, W.R. Thorson: Phys. Rev. B **24**, 3019-3031 (1981)
355. M. Kimura, W.R. Thorson: J. Phys. B **16**, 1471-1479 (1983)
356. T. Kirchner, L. Gulyás, R. Moshammer, M. Schulz, J. Ullrich: Nucl. Instrum. Methods Phys. Res. B **205**, 479 (2003)

357. H. Klar: J. Phys. B: At. Mol. Phys. **14**, 4165 (1981)
358. I. Klik, L. Gunther: J. Stat. Phys. **60**, 473 (1990)
359. I. Klik, L. Gunther: J. Appl. Phys. **67**, 4505 (1990)
360. M. Klosek-Dygas et al: SIAM J. Appl. Math. **48**, 425 (1988)
361. H. Knudsen, L. Brun-Nielsen, M. Charlton, M.R. Poulsen: J. Phys. B: At. Mol. Opt. Phys. **23** 3955 (1990)
362. S.K. Knudson, W.R. Thorson: J. Phys. **48**, 313-329 (1970)
363. W. Kohn: Phys. Rev. **74**, 1763 (1948)
364. Y. Komninos, M. Chrysos, C.A. Nicolaides: J. Phys. B: At. Mol. Phys. **20**, L791 (1987)
365. T. Kondow, R.J. Girnius, Y.P. Chong, W.L. Fite: Phys. Rev. A **10**, 1167-1176 (1974)
366. H.A. Kramers: Z. Phys. **39**, 828 (1926)
367. H.A. Kramers: Physica **7**, 284 (1940)
368. H.F. Krause, C.R. Vane, S. Datz, P. Grafström, H. Knudsen, C. Scheidenberger, R.H. Schuch: Phys. Rev. Lett. **80** 1190 (1998)
369. S.D. Kravis, M. Abdallah, C.L. Cocke, C.D. Lin, M. Stockli, B. Walch, Y.D. Wang, R.E. Olson, V.D. Rodrguez, W. Wu, M. Pieksma, N. Watanabe: Phys. Rev. A **54**, 1394 (1996)
370. O.J. Kroneisen, H.J. Lüdde, T. Kirchner, R.M. Dreizler: J. Phys. A:Math. Gen. **32**, 2141 (1999)
371. J. Kuang, C. D. Lin: J. Phys. B **29**, 5443 (1996)
372. O. Kubo, T. Ido, H. Yokoyama: IEEE Trans. Magn. **23**, 3140 (1987)
373. R. Kubo et al: *Statistical Physics II: Non-Equilibrium Statistical Mechanics*, 2nd ed (Springer-Verlag, Berlin 1991)
374. H. Kuratsuji, I. Iida: Phys. Lett. **111A**, 220 (1985)
375. H. Kuratsuji, I. Iida: Phys. Rev. Lett. **5**, 1003 (1986)
376. L. Landau: Phys. Z. Sowjet. **2**, 46 (1932)
377. L.D. Landau, E.M. Lifshitz: *Quantum Mechanics* (Pergamon Press, Oxford 1965)
378. R.E. Langer: Phys. Rev. **51**, 669 (1937)
379. J.I. Lauritz Jr, R. Zwanzig: Adv. Molec. Rel. Interact. Proc. **5**, 339 (1973)
380. R.J.S. Lee, J.V. Mullan, J.F. McCann, D.S.F. Crothers: Phys. Rev. A **64**, 062712 (2001)
381. C.D. Lin: Comments At. Mol. Phys. **11**, 261-269 (1982)
382. C.D. Lin, S. Watanabe: Phys. Rev. A **35**, 4499 (1987)
383. W. Lindinger, A. Hansel, Z. Herman: Adv. At. Mol. Opt. Phys. **43**, 243 (2000)
384. G.J. Lockwood, E. Everhart: Phys. Rev. **125**, 567-572 (1962)
385. A.M. Loughan: Adv. Chem. Phys. **114**, 311 (2000)
386. A.M. Loughan, D.S.F. Crothers: Phys. Rev. Lett. **79**, 4996 (1997)
387. A.M. Loughan, D.S.F. Crothers: J. Phys. B: At. Mol. Opt. Phys. **31**, 2153 (1998)
388. P.O. Löwdin: Ark. Mat. Astron Fys. **35A**, 9-18 (1947)
389. P.O. Löwdin: J. Chem. Phys. **18**, 365-375 (1950)
390. H.J. Lüdde, R.M. Dreizler: J. Phys. B **14**, 2191-2201 (1981)
391. H.J. Lüdde, R.M. Dreizler: J. Phys. B **15**, 2703-2711 (1982)
392. H.J. Lüdde, R.M. Dreizler: J. Phys. B **16**, 1009-1016 (1983)
393. J.H. Macek, S.G. Alston: Phys. Rev. A **26** 250 (1982)
394. A. Maćias, A. Riera, M. Yáñez: Phys. Rev. A: **27**, 206-212 (1983)
395. A. Maćias, A. Riera, M. Yáñez: Phys. Rev. A: **27**, 213-219 (1983)
396. R.P. Madden, K. Codling: Phys. Rev. Lett. **10**, 516 (1963)
397. J. Maddox: Nature **323**, 199 (1986)
398. C.F. Maggi, I.D. Horton, H.P. Summers: Plasma Phys. Control. Fusion. **42**, 669 (2000)
399. W. Magnus, F. Oberhettinger: *Special Functions of Mathematical Physics* (Chelsea, New York 1949)

400. O. Makarov, K.B. MacAdam: Phys. Rev. A **60**, 2131 (1999)
401. H. Margenau, G.M. Murphy: *The Mathematics of Physics and Chemistry*, (van Nostrand, New York 1956)
402. P.J. Martin, D.M. Blankenship, T.J. Krale, E. Redd, J.L. Peacher, J.T. Park: Phys. Rev. A **23**, 3357 (1981)
403. A.J. Martin, G. Meier and A. Saupe: Symp. Faraday Soc. **5**, 119 (1971)
404. H.S.W. Massey, C.B.O. Mohr: Proc. R. Soc. A **140**, 613-36 (1933)
405. H.S.W. Massey, R.A. Smith: Proc. R. Soc. A **142**, 142 (1933)
406. R. Mazo: *Brownian Motion: Fluctuations, Dynamics & Applications*, (Oxford University Press, Oxford 2002)
407. C. McCaig: PhD Thesis Queens University, Belfast (1998)
408. C. McCaig, D.S.F. Crothers: J. Phys. B: At. Mol. Opt. Phys. **33**, 3555 (2000)
409. J.F. McCann: J. Phys. B: At. Mol. Phys. **16**, 3229 (1983)
410. J.F. McCann, D.S.F. Crothers: J. Phys. B: At. Mol. Phys. **19**, L399 (1986)
411. J.F. McCann, J.T. Glass, D.S.F. Crothers: J. Phys. B: At Mol Opt. Phys. **29**, 6155 (1996)
412. R. McCarroll: Proc. R. Soc. A **264**, 547 (1961)
413. R. McCarroll, D.S.F. Crothers: Adv. At. Mol. Opt. Phys. **32**, 253-278 (1994)
414. R. McCarroll, R.D. Piacentini: J. Phys. B **4**, 1026-1039 (1971)
415. R. McCarroll, A. Salin: J. Phys. B **1**, 163 (1968)
416. C. McGrath et al: J. Phys. B: At. Mol. Opt. Phys. **33**, 3693 (2000)
417. J.H. McGuire: Phys. Rev. A **26**, 143-7 (1982)
418. J.H. McGuire: Phys. Rev. A **36**, 1114 (1987)
419. J.H. McGuire: Adv. At. Mol. Opt. Phys. **29**, 217 (1992)
420. D.M. McSherry, S.F.C. O'Rourke, C. McGrath, M.B. Shah, D.S.F. Crothers: CP576, Application of Accelerators in Research and Industry - 16th International Conference (ed J.L. Duggan, I.L. Morgan)
421. D.M. McSherry, S.F.C. ORourke, D.S.F. Crothers: Comput. Phys. Commun. **155**, 144 (2003)
422. H. Meier, Z. Halabuka, K. Hencken, D. Trautmann, G. Baur: Eur. Phys. J. C. **5**, 287 (1998)
423. A. Messiah: *Quantum Mechanics II* (Amsterdam, North-Holland 1965)
424. A. Messiah: *Quantum mechanics* (North-Holland Publishers 1986), chapter 19
425. R. Metzler, J. Klafter: Phys. Rep. **339**, 1 (2000); R. Metzler, J. Klafter: Adv. Chem. Phys. **116**, 223 (2001)
426. R.E. Meyer, J.F. Painter: SIAM J. Math. Anal. **14**, 450 (1983)
427. W.H. Miller: J. Chem. Phys. **62**, 1899 (1975)
428. S.C. Miller, R.H. Good: Phys. Rev. **91**, 174 (1953)
429. Modern Computing Methods ch 13 (H.M.S.O, London 1961)
430. B.L. Moiseiwitsch, S.G. Stockman: J. Phys. B: At. Mol. Phys, **13**, 2975 (1980)
431. B.L. Moiseiwitsch, S.G. Stockman: J. Phys. B: At. Mol. Phys, **13**, 4031 (1980)
432. B.L. Moiseiwitsch: J. Phys. B: At Mol. Opt. Phys. **21**, 603 (1988)
433. B.L. Moiseiwitsch: Phys. Rev. A **39**, 5609 (1989)
434. B.L. Moiseiwitsch: J. Phys. B: At Mol Opt. Phys. **25**, 3015 (1992)
435. T.J. Morgan, J. Geddes, H.B. Gilbody: J. Phys. B **6**, 2118-2138 (1973)
436. T.J. Morgan, J. Stone, R. Mayo: Phys. Rev. A **22**, 1460-1466 (1980)
437. A. Morita, S. Watanabe: Adv. Chem. Phys. **56**, 255 (1984)
438. A. Morita: Phys. Rev. A **34**, 1499 (1986)
439. G. Moro, P.L. Nordio: Molec. Phys. **56**, 255 (1985)
440. P.M. Morse, H. Feshbach: *Methods of Theoretical Physics* vol II (McGraw–Hill, New York 1953)

441. R. Moshammer et al: Phys. Rev. Lett. **73**, 3371 (1994)
442. N.F. Mott: Proc. Camb. Phil. Soc. **27**, 553 (1931)
443. N.F. Mott, H.S.W. Massey: *Theory of atomic collisions* (3rd ed), (Clarendon Press, Oxford 1965)
444. P.G. Mulligan, D.S.F. Crothers: Phys. Scripta **70**, 17 (2004)
445. J. Muller, X. Yang, J. Burgdorfer: Phys. Rev. A. **49**, 2470 (1994)
446. J.G. Murphy, K.F. Dunn, H.B. Gilbody: J. Phys. B: At. Mol. Opt. Phys. **27**, 3687 (1994)
447. H. Nakamura: *Nonadiabatic Transitions* (World Scientific, New York 2002)
448. L. Néel: Ann. Géophys. **5**, 99 (1949)
449. R.K. Nesbet: J. Phys. B: At. Mol. Phys. **11**, L21 (1978)
450. B.S. Nesbitt, S.F.C. O'Rourke, D.S.F. Crothers: J. Phys. B: At. Mol. Opt. Phys. **29**, 2515 (1996)
451. B.S Nesbitt, M.B. Shah, S.F.C. ORourke, C. McGrath, J. Geddes, D.S.F. Crothers: J. Phys. B: At. Mol. Opt. Phys. **33**, 637 (2000)
452. C.W. Newby: J. Phys. B: At. Mol. Phys. **18**, 1781 (1985)
453. E.E. Nikitin: Opt. Spectr. **13**, 431 (1962)
454. E.E. Nikitin: Discuss. Faraday Soc. **33**, 14 (1962)
455. E.E. Nikitin: Opt. Spectr. **18**, 431 (1965)
456. E.E. Nikitin: Adv. Quantum Chem. **5**, 135 (1970)
457. E.E. Nikitin, M.Ya. Ovchinnikova: Soviet Phys. Usp. **14**, 394 (1972)
458. E.E. Nikitin, A.I. Reznikov: J. Phys. B **11**, L659 (1978)
459. E.E. Nikitin, S.Ya. Umanskii: *Theory of Slow Atomic Collisions* (Springer Verlag, Berlin 1984)
460. P.L. Nordio, P. Busolin: J. Chem. Phys. **55**, 5485 (1971)
461. A. Nordsieck: Phys. Rev. A **93**, 785 (1954)
462. W.L. Nutt et al: J. Phys. B: At. Mol. Phys. **11**, 163 (1978)
463. H. O'Hara, F.J. Smith: Comput. J. **12**, 179 (1969)
464. P.C. Ojha, D.S.F. Crothers: J. Phys. B **17**, 4797 (1984)
465. K.B. Oldham, J. Spanier: *The Fractional Calculus* (Academic Press, New York and London 1974)
466. J.R. Oppenheimer: Phys. Rev. **31**, 349 (1928)
467. S.F.C. O'Rourke, D.S.F. Crothers: Proc. R. Soc. Lond. A **438**, 1 (1992)
468. S.F.C. O'Rourke, D.S.F. Crothers: J. Phys. B: At. Mol. Opt. Phys. **27**, 2497 (1994)
469. S.F.C. O'Rourke, D.S.F. Crothers: J. Phys. B: At. Mol. Phys. **30**, 2443 (1997)
470. S.F.C. O'Rourke, R. Moshammer, J. Ullrich: J. Phys. B: At. Mol. Phys. **30**, 5281 (1997)
471. S.F.C. O'Rourke, I. Shimamura, D.S.F. Crothers: Proc. Roy. Soc. Lond. A **452**, 176 (1996)
472. S.F.C. O'Rourke et al: Adv. Chem. Phys. **103**, 217 (1998)
473. S.F.C. O'Rourke, D.M. McSherry, D.S.F. Crothers: Int. J. Qu. Chem. **99**, 569 (2004)
474. R.E. Olsen, A. Salop: Phys. Rev. A **16**, 531 (1977)
475. R.E. Olson, J. Fiol: J. Phys. B **36**, L365 (2003)
476. F.W.J. Olver: J. Res. Nat. Bur. Standards, **63B** 131 (1959)
477. F.W.J. Olver: *Asymptotic and Special Functions* (Academic Press, New York 1974)
478. F.W.J. Olver: Phil. Trans. R. Soc. Lond. A **289**, 501 (1978)
479. D. Oza: Phys. Rev. A. **33**, 824 (1986)
480. C. Pan, A.F. Starace: Phys. Rev. Lett. **67**, 185 (1991)
481. J.T. Park, J.E. Aldag, J.M. George, J.L. Peacher, J.H. McGuire: Phys. Rev. **15**, 508-16 (1977)
482. T. Pattard, J.M. Rost: Physica Scripta T **80**, B 295 (1999)

483. R.T. Pedlow: Ph.D. Thesis, Queens University Belfast (2005) unpublished
484. R.T. Pedlow, S.F.C. ORourke, D.S.F. Crothers: Phys. Rev. A **72**, 062719 (2005)
485. A. Perico, R. Pratolongo, K.F. Freed, R.W. Pastor, A. Szabo: J. Chem. Phys. **98**, 564 (1993)
486. R.K. Peterkop: J. Phys. B: At. Mol. Phys. **4**, 513 (1971)
487. R.K. Peterkop: *Theory of Ionization of Atoms by Electron Impact* (Boulder, Colorado University Press 1977); Russian edn (Riga, Zinatne, 1975)
488. A. Peterlin, H. Stuart: Hand-und-Jahrbuch der Chemischen Physik, vol. 8, Leipzig, 1943
489. S. Pfeiffer, J.D. Garcia: J. Phys. B **15**, 1275-1287 (1982)
490. R.D. Piacentini, A. Salin: J. Phys. B: At. Mol. Phys. **7**, 1666 (1974)
491. R.D. Piacentini, A. Salin: J. Phys. B: At. Mol. Phys. **10**, 1515 (1977)
492. H.T.H. Piaggio: *Differential Equations*, (Bell, London 1958)
493. P. Pluvinage: Ann. Phys., NY **5**, 145 (1950)
494. P. Pluvinage: J. Phys. Radium **12**, 789 (1951)
495. V.H. Ponce: J. Phys. B: At. Mol. Phys. **12**, 3731 (1979)
496. L.I. Ponomarev, T.P. Puzynina: Sov. Phys. - JETP 25 846 (1967)
497. J.D. Power: Phil. Trans. Roy. Soc. A **274** (1246), 663 (1973); Quantum Chemistry Program Exchange, 233
498. E. Praestgaard, N.G. van Kampen: Mol. Phys. **43**, 33 (1981)
499. A.P. Prudnikov, Y.A. Brychkov, O.I. Marichev: *Integrals and Series*, Vols 1-3, (Gordon and Breach, New York 1983)
500. Yu.L. Raĭkher, M.I. Shliomis: Zh. Eksp. Teor. Fiz. **67**, 1060 (1974) [Sov. Phys. JETP **40**, 526 (1975)]
501. Y.L. Raĭkher et al: J. Colloid Interface Sci. **144**, 308 (1991)
502. Yu.L. Raĭkher, M.I. Shliomis: Adv. Chem. Phys. **87**, 595 (1994)
503. Y.L. Raĭkher, V.I. Stepanov: Phys. Rev. B **66**, 214406 (2002)
504. Yu.L. Raĭkher, V.I. Stepanov: Adv. Chem. Phys. **129**, 419 (2004)
505. A.R.P. Rau: Phys. Rev. A **4**, 207 (1971)
506. M. Razavy: *Quantum Theory of Tunneling* (World Scientific, London 2005)
507. H. Risken: *The Fokker–Planck Equation*, 2nd edn (Springer-Verlag, Berlin 1989)
508. P.J. Redmond: (unpublished) as discussed in L. Rosenberg, Phys. Rev. D **8**, 1833 (1973)
509. A. Ronveauax: *Heun Differential Equations* (Oxford Science Publications, 1997)
510. A. Riera, A. Salin: J. Phys. B**9**, 2877-2891 (1976)
511. M.E. Riley, T.A. Green: Phys. Rev. A **4**, 619 (1971)
512. H. Risken: *The Fokker-Planck Equation*, 2edn 1989 (Springer, Berlin 1984)
513. Y. Rocard: J. Phys. Radium Paris **4**, 247 (1933)
514. M. Rødbro, F.D. Andersen: J. Phys. B **12**, 2883-903 (1979)
515. V.D. Rodríguez: J. Phys. B **29**, 275 (1996)
516. V.D. Rodríguez: Nucl. Instrum. Methods Phys. Res. B **205**, 498 (2003)
517. M.E. Rose: *Elementary Theory of Angular Momentum* (Dover, New York 1995)
518. T. Rösel, J. Róder, L. Frost, K. Jung, H. Ehrhardt, S. Jones, D.H. Madison: Phys. Rev. A **46** 2539-52 (1992)
519. N. Rosen, C. Zener: Phys. Rev. **40**, 502 (1932)
520. J.M. Rost: J. Phys. B: At. Mol. Opt. Phys. **28**, 3003 (1995)
521. J.M. Rost, J.S. Briggs: J. Phys. B: At. Mol. Phys. **21**, L233 (1988)
522. J.M. Rost, J.S. Briggs: J. Phys. B: At. Mol. Phys. **22**, 3587 (1989)
523. J.M. Rost, E. Heller: Phys. Rev. A **49**, R4289 (1994)
524. J.M. Rost, T. Pattard: Phys. Rev. A **55**, R5 (1997)
525. T.A. Roth: Phys. Rev. A **5** 476 (1972)

526. H. Ryufuku: Phys. Rev. A **25**, 720-36 (1982)
527. H.R. Sadeghpour et al: J. Phys. B: At. Mol. Opt. Phys. **33**, R93 (2000)
528. S. Sahoo, K. Roy, N.C. Sil, S.C. Mukherjee: Phys. Rev. A **59**, 275-281 (1999)
529. A. Salin: Phys. Rev. A **36**, 5471 (1987)
530. M. San Miguel, L. Pesquera, M.A. Rodrigues, A. Hernández-Machado: Phys. Rev. A **354**, 208 (1987)
531. B.K.P. Scaife, *Principles of Dielectrics*, (Oxford Univ. Press, Oxford 1989)
532. M. Schadt: J. Chem. Phys. **67**, 210 (1977)
533. L.I. Schiff, *Quantum mechanics*, 3rd ed. (New York; London, McGraw-Hill 1968)
534. E.W. Schmid: Z. Phys. A **311**, 67-70 (1983)
535. W. Schmitt, R. Moshammer, S.F.C. O'Rourke, H. Kollmus, L. Sarkadi, R. Mann, S. Hagmann, R.E. Olson, J. Ullrich: Phys. Rev. Lett. **81**, 4337 (1998)
536. S.B. Schneidermann, A. Russek: Phys. Rev. **181**, 311 (1969)
537. M. Schulz, L An, R.E. Olson: J. Phys. B: At. Mol. Opt. Phys. **33**, L629 (2000)
538. M. Schulz, R. Moshammer, A.N. Perumal, J. Ullrich: J. Phys. B **35**, L161 (2002)
539. C.N. Scully, P.J Cregg, D.S.F. Crothers: Phys. Rev. B **45**, 474 (1992)
540. J. Segert: J. Math. Phys. **28**, 2102 (1987)
541. P. Selles, A. Huetz, J. Mazeau: J. Phys. B: At. Mol. Phys. **20**, 5195 (1987)
542. M.B. Shah, D.S. Elliot, H.B. Gilbody: J. Phys. B **20**, 2481-2485 (1987)
543. M.B. Shah, D.S. Elliot, P. McCallion, H.B. Gilbody: J. Phys. B **21**, 2455-2458 (1988)
544. M.B. Shah, H.B. Gilbody: J. Phys. B: At. Mol. Phys. **11**, 121 (1978)
545. M.B. Shah, H.B. Gilbody: J. Phys. B: At. Mol. Phys. **14**, 2361-77 (1981)
546. M.B. Shah, H.B. Gilbody: J. Phys. B: At. Mol. Phys. **14**, 2831-41 (1981)
547. M.B. Shah, H.B. Gilbody: J. Phys. B: At. Mol. Phys. **15**, 413-21 (1982)
548. M.B. Shah, H.B. Gilbody: J. Phys. B: At. Mol. Phys. **16**, L449-51 (1983)
549. M.B. Shah, H.B. Gilbody: J. Phys. E: At. Mol. Phys. **18**, 899 (1985)
550. M.B. Shah, P. McCallion, H.B. Gilbody: J. Phys. B: At. Mol. Opt. Phys. **22**, 3037 (1989)
551. L.F. Shámpine, M.K. Gordon: *Computer Solution of Ordinary Differential Equations* (1975)
552. N. Shimakura, H. Inouye, F. Koike, T. Watanabe: J. Phys. B **14**, 2203-2214 (1981)
553. N. Shimakura, H. Sato, M. Kimura, T. Watanabe: J. Phys. B: At. Mol. Phys. **20**, 1801 (1987)
554. R. Shingal: Bull. Am. Phys. Soc. **35**, 1778 (1990)
555. R. Shingal, C.D. Lin: J. Phys. B: At. Mol. Opt. Phys. **24**, 251 (1991)
556. R. Shingal, C.D. Lin: J. Phys. B: At. Mol. Opt. Phys. **24**, 963 (1991)
557. E.J. Shipsey, T.A. Green, J.C. Browne: Phys. Rev. A **27**, 821-832 (1983)
558. M.I. Shliomis, V.I. Stepanov: Adv. Chem. Phys. textbf87, 1 (1994)
559. E.Y. Sidky, C.D. Lin: Phys Rev. A **65**, 012711 (2001)
560. N.C. Sil: Proc. Phys. Soc. London **75**, 194 (1960)
561. B. Simon: Phys. Rev. Lett. **51**, 2167 (1983)
562. L.J. Slater: *Confluent Hypergeometric Functions* (Cambridge University Press 1960)
563. L.J. Slater: *Generalized Hypergeometric Functions* (Cambridge University Press, New York 1966)
564. H.A. Slim, E.L. Heck, B.H. Bransden, D.R. Flower: J. Phys. B: At. Mol. Opt. Phys. **23**, L611 (1990)
565. H.A. Slim, E.L. Heck, B.H. Bransden, D.R. Flower: J. Phys. B: At. Mol. Opt. Phys. **24**, 1683 (1991)
566. H.A. Slim, E.L. Heck, B.H. Bransden, D.R. Flower: J. Phys. B: At. Mol. Opt. Phys. **24**, L421 (1991)

567. K. De Smet et al: Phys. Rev. E **57**, 1384 (1998)
568. I.N. Sneddon: *Special Functions of Mathematical Physics and Chemistry*, (Oliver & Boyd, Edinburgh 1961)
569. E.O. Steinborn; *ETO Multicenter Molecular Integrals*, ed C.A. Weatherford, H.W. Jones (London, Reidel 1982) pp.7-27
570. E.C. Stoner, E.P. Wohlfarth: Philos. Trans. R. Soc. London A **240**, 599 (1948)
571. B.A. Storonkln: Theor. Math. Phys. **41**, 1098 (1979)
572. B.A Storonkin, Kristallografiya: Sov. Phys. Crystallogr. **30**, 489 (1985)
573. N. Stolterfoht, R.D. DuBois, R.D. Rivarola: *Electron Emission in Heavy-Ion Atom Collsions*, Vol. 20 (Springer-Verlag, Berlin 1997)
574. E.C.G. Stueckelberg: Helv. Phys. Acta. **5**, 369 (1932)
575. O. Sueoka, B. Jin, A. Hamada: Appl. Surf. Sci. **85**, 59 (1995)
576. R.A. Swainson, G.W.F. Drake: J Phys. B **23**, 1079 (1990)
577. A. Szabo: J. Chem. Phys. **72**, 4620 (1980)
578. A. Temkin: Phys. Rev. Lett. **49**, 365 (1982)
579. A. Temkin: J. Phys. B: At. Mol. Phys. **15**, L301 (1982)
580. L.H. Thomas: Proc. Camb. Phil. Soc. **23**, 713 (1927)
581. W.R. Thorson, M. Kimura, J.H. Choi, S.K. Knudson: Phys. Rev. A **24**, 1768-1779 (1981)
582. A. Tomita, R.Y. Chiao: Phys. Rev. Lett. **57**, 937 (1986)
583. N. Toshima: Phys. Rev. A **50**, 3940 (1994)
584. N. Toshima, J. Eichler: Comments At. Mol. Phys **31**, 109 (1995)
585. N. Toshima, T. Nakagawa: Phys. Rev. A **60**, 2182 (1999)
586. H.C. Tseng, C.D. Lin: Phys. Rev. A **58**, 1966 (1966)
587. G.E. Uhlenbeck, L.S. Ornstein: Phys. Rev. **36**, 823 (1930)
588. S. Urban, D. Büsing, A. Würflinger, B. Gestblom: Liq. Cryst. **25**, 253 (1998)
589. J. Vaaben, K. Taulbjerg: J. Phys. B: At. Mol. Phys. **14**, 1815 (1981)
590. N.G. van Kampen: *Stochastic Processes in Physics and Chemistry*, 2edn (North-Holland Physics Publishing, Amsterdam 1992)
591. P.B. Visscher: Phys. Rev. B **13**, 3272 (1976)
592. M.C. Wang, G.E. Uhlenbeck: Rev. Mod. Phyd. **17**, 323 (1945)
593. G.H. Wannier: Phys. Rev. **90**, 817 (1953)
594. G.N. Watson: *Theory of Bessel Functions*, 2nd edn (Cambridge Univ. Press, Cambridge 1944)
595. G. Wentzel: Z. Phys **38**, 518 (1926)
596. W. Wernsdorfer: Ph.D. thesis, Joseph Fourier University, Grenoble (1996)
597. W. Wernsdorfer et al: Phys. Rev. Lett. **78**, 1791 (1997)
598. W. Wernsdorfer et al: Phys. Rev. Lett. **79**, 4014 (1997)
599. N. Wiener: *The Fourier Integral*, (Cambridge University Press, Cambridge 1933)
600. E.P. Wigner: Phys. Rev. **73**, 1002 (1948)
601. L. Wilets, S.J. Wallace: Phys. Rev. **169**, 84 (1968)
602. T.G. Winter: Phys. Rev. A **37**, 4656 (1988)
603. T.G. Winter: Phys. Rev. A **43**, 4727 (1991)
604. T.G. Winter: Phys. Rev. A **44**, 4353 (1991)
605. T.G. Winter: Phys. Rev. A **49**, 1767 (1994)
606. T.G. Winter: Phys. Rev. A **56**, 2903 (1997)
607. T.G. Winter: Phys. Rev. A **69**, 042711 (2004)
608. T.G. Winter, G.J. Hatton: Phys. Rev. A **21**, 793 (1980)
609. T.G. Winter, N.F. Lane: Phys. Rev. A **17**, 66 (1978)
610. T.G. Winter, C.D. Lin: Phys. Rev. A **29**, 567 (1984)
611. C. Zener: Proc. Roy. Soc. Lond. A **137**, 696 (1932)
612. Zhu: PhD thesis, Institute for Molecular Science, Okazaki (unpublished) (1993)
613. M. Zubek, G.C. King, P.M. Rutter, F.H. Read: J. Phys. B: At. Mol. Phys. **22**, 3411 (1989)
614. A. Zwaan: Arch. Neerland, Ser. IIIA **12**, 1 (1929)

Index